Abstract

Hepatitis C virus (HCV) is a leading cause of chronic liver disease. Identification of key host cellular factors involved in the HCV replication cycle is important for understanding disease pathogenesis and identifying novel antiviral therapeutic targets.

The objective of this study was to identify novel host factors with important roles in the HCV replication cycle. Two approaches were used to select factors to test as potential HCV cofactors. The first approach investigated factors previously shown to facilitate the replication of other RNA viruses. This included Rab GTPases and the RNA binding proteins, Staufen, TIAL1 and TIA1. The second approach investigated factors observed to be upregulated during HCV infection following microarray expression profiling of HCV (JFH-1 clone) infected Huh7 hepatoma cells. Host genes controlling innate immunity, proliferation, lipid and protein metabolism and intracellular transport were observed to increase in expression, whilst genes controlling oxidative stress and cytoskeletal regulation decreased in expression. The expression patterns observed also indicated that HCV associated pathogenesis may be caused by HCV-induced gene expression changes. Further investigation into the upregulation of lipid synthesis genes observed during HCV infection demonstrated that intracellular lipid abundance also increased significantly, and may contribute to the development of hepatic steatosis in chronically infected patients.

Host gene silencing by siRNA knockdown was used to investigate the potential cofactor role of the selected candidate host factors. Factors shown to be essential for effective HCV replication and secretion included those involved in lipid metabolism (TXNIP, CYP1A1 and CIDEC), intracellular transport (RAB2B, RAB4A, RAB11B, RAB27A/B, RAB33B and ABLIM3), and mRNA regulation (Staufen1). It was also shown that TXNIP may control lipid metabolite abundance during HCV replication, and Staufen1 may colocalise with HCV replication complexes to control HCV genome translation, replication or trafficking. Further investigation into the potential HCV cofactors identified should now be performed to improve understanding of the HCV replication cycle and enable identification of novel factors for antiviral targeting.

Table of Contents

Abstract 3
Table of Contents 5
Table of Figures 11
Table of Tables 14
Abbreviations 15
Publications and Presentations 22
Acknowledgements 23
Declaration 24
Chapter 1: General Introduction 25
1.1 The pathogenesis, treatment and classification of Hepatitis C virus 27
1.1.1 Pathogenesis of HCV infection 27
1.1.2 Treatment of HCV infection 27
1.1.3 Classification of HCV infection 29
1.2 The HCV RNA genome 30
1.3 The HCV replication cycle 31
1.3.1 HCV entry 31
1.3.2 Genome translation and replication 33
1.3.3 Virus particle assembly and secretion 34
1.4 The role of virus proteins in the HCV replication cycle 40
1.4.1 The structural HCV proteins 40
1.4.2 The non-structural HCV proteins 42
1.5 The role of cellular host factors in the HCV replication cycle 47
1.5.1 Host factors with a role in genome translation and replication 47
1.5.2 Host factors with a role in assembly and secretion 50
1.5.3 Host factors involved in the production of HCV-essential metabolites 53
1.5.4 The role of the cellular cytoskeleton in the HCV replication cycle 54

1.6 *In vitro* and *in vivo* systems for studying the HCV replication cycle 54
1.6.1 In vitro systems for studying the HCV replication cycle 54
1.6.2 In vivo systems for studying the HCV replication cycle 58
1.7 Experimental approaches used to study the HCV replication cycle 59
1.7.1 Protein capture assays 59
1.7.2 Genomic studies of HCV infection 60
1.7.3 Proteomic studies of HCV infection 63
1.7.4 Host factors involved in the replication of other related RNA viruses 65
1.8 Hypothesis and Project Aims 77
Chapter 2: Materials and Methods 79
2.1 Cell culture 81
2.2 Production of infectious JFH-1 virus stocks 81
2.3 Affymetrix microarray profiling of host expression during JFH-1 infection 85
2.4 Quantitative PCR analysis of host expression during JFH-1 infection 86
2.5 Generation of genotype 2a (GT2a) replicon expressing cell lines 91
2.6 Generation of JFH-1 core expressing Huh7 cells 93
2.7 Western blot analysis of host proteins during JFH-1 infection 96
2.8 Triglyceride quantification assay 99
2.9 Cholesterol quantification assay 101
2.10 Lipid droplet staining and quantification 102
2.11 Glucose quantification assay 104
2.12 siRNA transfection of Huh7 and Huh7.5 cells 104
2.13 Alamar blue cell viability assay 110
2.14 Quantitative PCR expression analysis of interferon stimulated genes 111
2.15 Immunofluorescent staining of host proteins 112
2.16 Statistical Analysis of Results 113

Chapter 3: The Effect of HCV Infection on Host Gene Expression 115
Chapter 3: Introduction 117
Chapter 3: Results 119
3.1 The JFH-1 cell culture system 119
3.1.1 Production of infectious JFH-1 virus 119
3.1.2 A high-titre production line for JFH-1 virus 119
3.1.3 JFH-1 infectivity in Huh7 and Huh7.5 cells 120
3.2 Why study the effect of HCV infection on host gene expression? 121
3.3 Expression profiling of factors involved in the replication of other viruses .. 121
3.4 Identification of host factors upregulated during HCV infection 123
3.4.1 Microarray gene expression profiling of JFH-1 infected Huh7 cells 123
3.4.2 Intracellular JFH-1 RNA abundance in the JFH-1 infected Huh7 cells . 124
3.4.3 Gene ontology analysis of the microarray expression data 124
3.4.4 JFH-1 infection alters the expression of cellular defence genes 126
3.4.5 JFH-1 infection alters the expression of metabolism and transport genes 127
3.4.6 The biological significance of HCV induced gene expression patterns 129
3.4.7 Validation of the microarray expression data by quantitative PCR 131
3.4.8 Comparing host cell response to infection: Huh7 versus Huh7.5 cells . 134
3.5 Gene expression profiling of cells expressing a subgenomic replicon 137
3.5.1 Generating cells that express a genotype 2a subgenomic replicon 137
3.5.2 Quantitative PCR analysis of subgenomic replicon expressing cells ... 140
3.5.3 Intracellular replicon RNA abundance in the replicon expressing cells 143
3.5.4 The effect of JFH-1 infection on cholesterol biosynthesis gene expression 143
3.6 Gene expression profiling of cells expressing the JFH-1 core protein 144
3.6.1 Expression of JFH-1 core using the Semliki Forest Virus replicon 145

3.6.2 Expression of JFH-1 core using the pIRES expression vector 146

3.7 Quantification of host protein abundance during JFH-1 infection..... 147

3.8 Quantification of intracellular lipid metabolites during JFH-1 infection 151

3.8.1 Optimisation of cholesterol and triglyceride quantification assays..... 151

3.8.2 Cholesterol and triglyceride levels in JFH-1 infected cells..... 152

3.8.3 Cholesterol and triglyceride levels in replicon expressing cells 152

3.9 Quantification of intracellular lipid droplets during JFH-1 infection..... 154

3.9.1 Lipid droplet abundance in JFH-1 infected cells..... 154

3.9.2 Lipid droplet abundance in the subgenomic replicon expressing cells . 157

3.9.3 Lipid droplet abundance in JFH-1 core expressing cells 160

Chapter 3: Discussion 163

Chapter 3: Conclusions 182

Chapter 4: Identifying Novel Host Proteins with a Role in the HCV Replication Cycle using siRNA Knockdown 185

Chapter 4: Introduction 187

Chapter 4: Results..... 197

4.1 Optimisation of an siRNA knockdown assay to test the role of host factors in the HCV replication cycle..... 197

4.1.1 Optimising siRNA transfection of Huh7 cells 197

4.1.2 Optimisation of the siRNA knockdown assay using a HCV siRNA 198

4.1.3 Optimisation of the siRNA knockdown assay using RAB1B siRNA molecules 201

4.2 The effect of host gene knockdown on JFH-1 replication and secretion 204

4.2.1 Silencing host genes with a role in the replication of other RNA viruses..... 204

4.2.2 Silencing host genes upregulated during JFH-1 infection 208

4.2.3 The effect of individual siRNA molecules on JFH-1 replication and secretion..... 211

4.3 Testing siRNA molecules for non-specific effects on JFH-1 replication 213

4.3.1 Cellular viability analysis 213

4.3.2 Quantitative PCR analysis of the dsRNA interferon response 216

4.4 Quantification of JFH-1 proteins following host gene knockdown 221

Chapter 4: Discussion 229

Chapter 4: Conclusions 241

Chapter 5: Characterising the Role of the Thioredoxin Interacting Protein (TXNIP) and Staufen1 (STAU1) in the HCV Replication Cycle 243

Chapter 5: Introduction 245

Chapter 5: Results 255

5.1 Identifying transcription factors that induce TXNIP expression 255

5.1.1 The expression of TXNIP transcription factor genes during JFH-1 infection 255

5.1.2 Quantification of intracellular glucose levels in JFH-1 infected cells 256

5.1.3 The expression of glucose metabolism genes during JFH-1 infection . 257

5.1.4 Knockdown of transcription factors controlling TXNIP expression 258

5.1.5 TXNIP expression following knockdown of MLX complexes 260

5.2 Investigating the role of alpha arrestins in the HCV replication cycle 261

5.3 The effect of TXNIP knockdown on the transcriptional activity of PPARα .. 263

5.3.1 PPARα target gene expression following TXNIP knockdown 263

5.3.2 ACSL3 gene expression following TXNIP knockdown 266

5.4 Investigating the localisation of Staufen1 during JFH-1 infection 267

Chapter 5: Discussion 271

Chapter 5: Conclusions 280

Chapter 6: General Discussion and Future Work 281

6.1 Introduction 283

6.2 The host cell response to HCV infection 283

6.3 Host cell factors involved in the HCV replication cycle 289

6.4 Conclusions 296

Bibliography and Appendix 299
Appendix 329
A.1 Quantitative real-time PCR primer sequences 329
A.2 pCR2.1 vector sequencing primers 330
A.3 pIRES vector core protein PCR primers 330
A.4 PCR cycling conditions 331
A.5 DNA and RNA molecular weight ladders 332
A.6 DNA plasmid maps 333
A.7 siRNA molecule sequences 334
A.8 Fold change expression values on a log2 scale as represented in the heat map diagrams 336
A.9 Functional role of host genes regulated by JFH-1 infection 347
A.10 Microarray confidence interval values at 48 hours post-infection 351
A.11 Microarray confidence interval values for the time-course infection 356
A.12 *In vitro* RNA transcription of the genotype 2a replicon RNA 359
A.13 *In vitro* RNA transcription of the SFV replicon (JFH-1 core) RNA 360
A.14 Cloning the JFH-1 core sequence into the pIRES vector 361
A.15 qRT-PCR GAPDH curves for JFH-1 and mock infected samples 362
A.16 NS2 protein sequence homology of JFH-1 and J6 HCV clones 363
A.17 Knockdown of Staufen2 expression by siRNA silencing 364
A.18 siRNA transfection does not alter cell viability or ISG expression 365
A.19 Expression of MLX target genes at 48 hours post-infection 366

Table of Figures

Figure 1.1 HCV genome organisation 31

Figure 1.2 The HCV replication cycle 39

Figure 1.3 HCV subgenomic replicon gene organisation 56

Figure 1.4 Regulators of Rab GTPase protein activity and localisation 67

Figure 1.5 Intracellular localisation of the Rab GTPase proteins 68

Figure 3.1 JFH-1 infected Huh7.5 cells stain positively for the HCV core protein 119

Figure 3.2 Media passage generates higher JFH-1 virus titres 120

Figure 3.3 Infectivity of Huh7 and Huh7.5 cells with JFH-1 virus 120

Figure 3.4 Fold change in host gene expression during JFH-1 infection 122

Figure 3.5 Intracellular JFH-1 RNA levels increase throughout infection 124

Figure 3.6 JFH-1 infection significantly alters host gene expression 125

Figure 3.7 Genes regulating sphingolipid metabolism and cholesterol biosynthesis alter in expression during JFH-1 infection 130

Figure 3.8 Comparison of microarray and qRT-PCR gene expression data collected for Huh7 cells infected with JFH-1 for 48 hours 132

Figure 3.9 Temporal regulation of host expression during JFH-1 infection 133

Figure 3.10 qRT-PCR expression profiling of JFH-1 infected Huh7.5 cells 136

Figure 3.11 Replicon cells stain positively for NS3, NS5A and dsRNA 139

Figure 3.12 The genotype 2a replicon alters Huh7 cell gene expression 141

Figure 3.13 The genotype 2a replicon alters Huh7.5 cell gene expression 142

Figure 3.14 Replicon RNA levels in replicon expressing Huh7 and Huh7.5 cells 143

Figure 3.15 JFH-1 infection alters cholesterol synthesis gene expression 144

Figure 3.16 JFH-1 core expression using the Semliki Forest Virus replicon 146

Figure 3.17 Comparison of HCV core protein expression in pIRES(core) and SFV(core) RNA transfected Huh7 cells 147

Figure 3.18 Western blot optimisation of antibodies recognising HCV NS3, HCV core, tubulin, TXNIP and PGC1α 149

Figure 3.19 JFH-1 infection increases TXNIP and PGC1α protein levels 150
Figure 3.20 Optimisation of cholesterol and triglyceride quantification assays ... 151
Figure 3.21 JFH-1 infection increases intracellular cholesterol and triglyceride . 152
Figure 3.22 The HCV replicon increases cholesterol and triglyceride levels 153
Figure 3.23 JFH-1 infection increases lipid droplet abundance 156
Figure 3.24 The subgenomic replicon increases lipid droplet abundance 159
Figure 3.25 HCV core protein expression increases lipid droplet abundance 162
Figure 4.1 Huh7 cells are efficiently transfected using Lipofectamine 2000 197
Figure 4.2 The HCV siRNA reduces JFH-1 replication and secretion 199
Figure 4.3 Transfection of the HCV siRNA does not affect cellular viability..... 200
Figure 4.4 RAB1B siRNAs reduce RAB1B mRNA without altering cell viability.. 202
Figure 4.5 RAB1B knockdown reduces HCV replication 203
Figure 4.6 The effect of host gene silencing on JFH-1 RNA and virus titres 1.... 207
Figure 4.7 The effect of host gene silencing on JFH-1 RNA and virus titres 2.... 209
Figure 4.8 The effect of host gene silencing on JFH-1 RNA and virus titres 3.... 210
Figure 4.9 The effect of individual siRNAs on JFH-1 RNA and virus titres 212
Figure 4.10 Pools of target siRNAs do not significantly alter cell viability 214
Figure 4.11 Individual siRNAs do not significantly alter cellular viability 215
Figure 4.12 IFNα and poly (I:C) treatment induces ISG expression 217
Figure 4.13 Target specific siRNAs do not significantly alter ISG expression 220
Figure 4.14 Host gene knockdown alters JFH-1 protein abundance 222
Figure 4.15 TXNIP protein knockdown reduces JFH-1 NS3 protein abundance 224
Figure 4.16 Staufen1 protein knockdown reduces JFH-1 protein abundance 226
Figure 4.17 Anti-Staufen1 antibody does not detect Staufen1 isoforms 227
Figure 5.1 JFH-1 infection alters the expression of cellular transcription factors 255
Figure 5.2 JFH-1 infection does not alter intracellular glucose levels 256

Figure 5.3 JFH-1 infection alters the expression of glucose metabolism genes. 257

Figure 5.4 The effect of transcription factor knockdown on TXNIP expression and the JFH-1 replication cycle. 259

Figure 5.5 Knockdown of MLX, MLXIP and MLXIPL reduces TXNIP expression 260

Figure 5.6 ARRDC4 is upregulated during JFH-1 infection but is not required for effective JFH-1 replication or secretion 262

Figure 5.7 TXNIP knockdown alters the expression of PPARα target genes 265

Figure 5.8 TXNIP knockdown reduces ACSL3 mRNA during JFH-1 infection ... 266

Figure 5.9 An anti-Staufen1 antibody detects a protein at the nuclear periphery 268

Figure 5.10 The intracellular localisation of Staufen1 during JFH-1 infection 270

Table of Tables

Table 1.1 Host factors involved in the HCV replication cycle 52

Table 1.2 Rab GTPase localisation and function 70

Table 3.1 Total number of gene probesets regulated during JFH-1 infection 123

Table 5.1 PPARα target genes in human hepatocytes 250

Table 6.1 Summary of siRNA knockdown data 291

Abbreviations

ABLIM3	Actin binding LIM protein family, member 3
ACADL	Acyl-Coenzyme A dehydrogenase long-chain
ACC	Acetyl-CoA carboxylase alpha
ACOX1	Acyl-CoA oxidase 1, palmitoyl
ACSL3	Acyl-CoA synthetase long-chain family member 3
AHR	Aryl hydrocarbon receptor
ALiX	ALG-2 interacting protein X
AMPK	AMP-activated protein kinase
ANOVA	Analysis of variance
ANXA2	Annexin A2
APOB/E	Apolipoprotein B/E
ARRDC	Arrestin domain containing
ARF1	ADP-ribosylation factor 1
ARF-P	Alternative reading frame protein
Atg5	Autophagy protein 5
BMV	Brome Mosaic Virus
BSA	Bovine serum albumin
Ca.	Circa (approximately)
C-terminal/us	Carboxy terminal/us
cDNA	Complementary DNA
CENPE	Centromere protein E
CERT	Ceramide transfer protein
CHMP	Chromatin modifying protein
CIDE	Cell death-inducing DFFA-like effector
CKIα/II	Casein kinase Iα/II
CLDN1	Claudin 1
COPI	Coat protein complex I
COPII	Coat protein complex II
CPT1A	Carnitine palmitoyltransferase 1A

CPT2	Carnitine palmitoyltransferase 2
CT	Cycle threshold
CYP1A1	Cytochrome P450, family 1, subfamily A, polypeptide 1
CYP1B1	Cytochrome P450, family 1, subfamily B, polypeptide 1
CXCL	Chemokine (C-X-C motif) ligand
DAPI	4,6-diamidino-2-phenylindole
DFF	DNA fragmentation factor,
DGAT1	Diacylglycerol O-acyltransferase 1
DMEM	Dulbecco's modified Eagles medium
DNA	Deoxyribonucleic acid
dsRNA	Double stranded RNA
DV	Dengue Virus
EBP	Emopamil binding protein
ECH1	Enoyl CoA hydratase 1
EEA1	Early endosome antigen 1
EET	Epoxyeicosatrienoic acid
EIF2A	Eukaryotic translation initiation factor 2A
ELOVL4	ELOVL member 4, elongation of long chain fatty acids
ELOVL7	ELOVL member 7, elongation of long chain fatty acids
EMCV	Encephalomyocarditis virus
ER	Endoplasmic reticulum
ESCRT	Endosomal sorting complex required for transport
FABP3	Fatty acid binding protein 3
FASN	Fatty acid synthase
FBL2	F-box and leucine-rich repeat protein 2
FBP	Far upstream element (FUSE) binding protein 1
FDFT1	Farnesyl-diphosphate farnesyltransferase 1
FDPS	Farnesyl diphosphate synthase
FFU	Focus forming units
FOXO1	Forkhead box O1

FXR	Farnesoid X receptor
xg	G force (relative centrifugal force)
G3BP1	GTPase activating protein (SH3 domain) binding protein 1
G6P	Glucose 6 phosphate
GAP	GTPase activating protein
GAPD	Glyceraldehyde-3-phosphate
GAPDH	Glyceraldehyde-3-phosphate dehydrogenase
GBF1	Golgi brefeldin A resistant guanine nucleotide exchange factor 1
GDF	GDI displacement factor
GDI	Rab GDP dissociation inhibitor
GEF	GDP-GTP exchange factor
GFP	Green fluorescent protein
GGPS1	Geranylgeranyl diphosphate synthase 1
GGT	Geranylgeranyl transferase
GLUT4	Glucose transport receptor 4
GT2A	Genotype 2a
HCV	Hepatitis C Virus
HETE	Hydroxyeicosatetraenoic acid
HDL	High density lipoprotein
HIF1α	Hypoxia inducible factor 1, alpha subunit
HIV	Human Immunodeficiency Virus
HK2	Hexokinase 2
HMCV	Human Cytomegalovirus
HMGCR	3-hydroxy-3-methylglutaryl-CoA reductase
HNF4α	Hepatocyte nuclear factor 4, alpha
HPV8	Human Papilloma Virus 8
HRP	Horseradish peroxidase
HSC70	Heat shock 70kDa protein 8
HuR	Hu-antigen R
IFNα	Interferon alpha

IFNβ	Interferon beta
IGF2BP1	Insulin-like growth factor 2 binding protein 1
IL8	Interleukin 8
IPS-1	Inositol pyrophosphate synthase 1 (also known as MAVS, CARDIF and VISA)
IRES	Internal ribosomal entry site
ISG	Interferon stimulated gene
ISG15	ISG15 ubiquitin-like modifier
JFH-1	Japanese fulminant Hepatitis-1
Kb	Kilobase
KDSR	3-ketodihydrosphingosine reductase
KLF6	Kruppel-like factor 6
La	La autoantigen
LASS1	LAG1 homolog, ceramide synthase 1
LB	Luria Bertani
LD	Lipid droplet
LDL	Low density lipoprotein
LMP7	Large multifunctional peptidase 7
LXR	Liver X receptor
MDA5	Melanoma differentiation associated protein-5
MEV	MultiExperiment Viewing software
miRNA	Micro RNA
miR122	Micro RNA 122
MI	Mock infected
MLX	MAX-like protein X
MLXIP	MLX interacting protein (also known as MondoA)
MLXIPL	MLX interacting protein-like (also known as Chrebp)
M-MLV	Moloney murine leukemia virus
MOI	Multiplicity of infection
mRNA	Messenger RNA
MTSS1	Metastasis suppressor 1

MTT	3-(4,5-Dimethylthiazol-2-yl)-2,5-diphenyltetrazolium bromide)
MTTP	Microsomal triglyceride transfer protein
MVB	Multivesicular body
MVD	Mevalonate (diphospho) decarboxylase
MX1	Myxovirus (influenza virus) resistance 1
N-terminal/us	Amino terminal/us
NASH	Non alcoholic steatohepatitis
nM	Nanomolar
NMD	Nonsense-mediated decay
NMR	Nuclear magnetic resonance
npt	Neomycin phosphotransferase
NS	Non-structural
NTR	Non-translated region
OAS	2',5'-oligoadenylate synthetase
OSBP	Oxysterol binding protein
PBS	Phosphate buffered saline
PCK2	Phosphoenolpyruvate carboxykinase 2
PCR	Polymerase chain reaction
PDK4	Pyruvate dehydrogenase kinase, isozyme 4
PEG	Polyethylene glycol
PEPCK	Phosphoenolpyruvate carboxykinase 2
PGC1A	Peroxisome proliferator-activated receptor gamma coactivator 1α
PI3K	Phosphotidylinositol 3 kinase
PI4K	Phosphotidylinositol 4 kinase
PIP2	Phosphotidylinositol (4,5) bisphosphate
PI4P	Phosphatidylinositol 4 phosphate
PKD	Protein kinase D1
PKR	Protein kinase RNA-activated (Protein kinase R)
Poly (I:C)	Polyriboinosinic:polyribocytidylic acid

PLD	Phospholipase D1
PRK2	Protein-kinase C-related kinase 2
PPAP2B	Phosphatidic acid phosphatase type 2B
PPARα	Peroxisome proliferator activated receptor alpha
PPARγ	Peroxisome proliferator activated receptor gamma
PTB	Polypyrimidine tract binding protein 1
qRT-PCR	Quantitative reverse-transcription PCR
RAB	Rab GTPase protein
RABIP4	Rab4-interacting protein
REP	Rab escort protein
RIG-I	Retinoic acid-inducible gene 1 protein
RIP140	Receptor interacting protein 140
RISC	RNA induced silencing complex
RNA	Ribonucleic acid
RPLPO	Large ribosomal protein
RPM	Revolutions per minute
SCID	Severe combined immunodeficiency
SD	Standard deviation
SDS	Sodium dodecyl sulphate
SFV	Semliki Forest Virus
SGMS2	Sphingomyelin synthase 2
SGPL1	Sphingosine-1-phosphate lyase 1
SGPP1	Sphingosine-1-phosphate phosphatase 1
siRNA	Small interfering RNA
SLC27A2	Solute carrier family 27 (fatty acid transporter), member 2
SMD	Staufen-mediated decay
SNARE	Soluble NSF attachment protein receptor
SOCS	Suppressor of cytokine
SPT	Serine palmitoyltransferase
SPTLC1	Serine palmitoyltransferase, long chain base subunit 1

SR-BI	Scavenger receptor class B, member 1
SREBF1	Sterol regulatory element binding transcription factor 1
SQLE	Squalene epoxidase
STAT1	Signal transducer and activator of transcription 1
STAT3	Signal transducer and activator of transcription 3
SVR	Sustained virological response
STAU1	Staufen1
TBC1D20	TBC1 domain family, member 20
TCDD	2, 3, 7, 8-Tetrachlorodibenzodioxin
TIA1	T cell restricted intracellular antigen 1
TIAL1	TIA1 protein like 1
TICAM1	Toll-like receptor adaptor molecule 1 (also known as TRIF)
TGFβ	Transforming growth factor, beta 1
TLR3	Toll-like receptor 3
TRIB3	Tribbles homolog 3
tRNA	Transfer RNA
TSG101	Tumour susceptibility gene 101
TXNIP	Thioredoxin interacting protein
TUBB2A	Tubulin, beta 2A
UPA	Urokinase plasminogen activator
UPF	Up-frameshift suppressor 1
UTR	Untranslated region
VAP-A	Vesicle associated protein A
VAP-B	Vesicle associated protein B
VPS4	Vacuolar protein sorting 4 homolog
VLDL	Very low density lipoprotein
v/v	Volume / volume
w/v	Weight / volume
WNV	West Nile Virus

Publications and Presentations

Publications

May 2010: Gene expression profiling indicates the roles of host oxidative stress, apoptosis, lipid metabolism, and intracellular transport genes in the replication of hepatitis C virus. Blackham S et al, Journal of Virology, 2010 May;84(10):5404-14.

Oral Presentations

September 2010: The Transcriptional Regulation of Lipid Metabolism and Transport in the HCV Replication Cycle. 17th International Symposium on Hepatitis C Virus and Related Viruses, Yokohama, Japan.

May 2010: Transcriptional Regulation of Lipid Metabolism and Transport During Hepatitis C Virus Infection. 8th UK Meeting on the Biology and Pathology of Hepatitis C Virus, Ambleside, UK.

April 2010: The Effect of HCV Infection on Host Gene Expression. Society for General Microbiology Spring 2010 Meeting, Edinburgh, UK.

May 2009: Analysis of Host Gene Expression During HCV Infection. 7th UK Meeting on the Biology and Pathology of Hepatitis C Virus, Ambleside, UK.

Poster Presentations

October 2009: Changes in Host Cell Gene Expression During HCV Infection. 16th International Symposium on Hepatitis C Virus and Related Viruses, Nice, France.

Acknowledgements

I would like to thank my supervisor, Dr Michael McGarvey, for his support and encouragement during this project, and the rest of the team in the department for their help and friendship over the past three years. I would also like to thank Beverley, John, Emma and Johnny for their support throughout the duration of my postgraduate studies.

Declaration

The data presented in this thesis is the result of my own work and in no way forms part of any other thesis, except where indicated. This work was carried out in the Department of Hepatology and Gastroenterology, Faculty of Medicine, Imperial College under the supervision of Dr. Michael McGarvey.

Chapter 1: General Introduction

1.1 The pathogenesis, treatment and classification of Hepatitis C virus

1.1.1 Pathogenesis of HCV infection

Current estimates suggest that 170 million people worldwide are infected with the Hepatitis C Virus (HCV): a blood-borne hepatotrophic virus that causes chronic liver disease. The most common route of HCV transmission is through the use of contaminated syringes by intravenous drug users or medical professionals in developing countries, where the use of contaminated blood during transfusion also contributes significantly to the spread of the virus. Other less common routes of transmission include sexual and perinatal, where infection passes from mother to child [1, 2].

Infection with HCV usually begins with a relatively mild acute phase which progresses to a persistent chronic infection in 60-85% of infected individuals. The severity of pathogenesis associated with chronic HCV infection varies between infected individuals, with some having only minor symptoms, whilst others develop severe liver damage including liver fibrosis, steatosis, cirrhosis and occasionally hepatocellular carcinoma [1]. Additional extra-hepatic complications also occur in chronically infected patients including an increased risk for the development of type 2 diabetes, cryoglobulinemia vasculitis, lymphoproliferative disorders, renal disease and rheumatoid arthritis-like polyarthritis [3]. The rate at which these pathogenic symptoms develop is usually slow and it often takes between 20 to 30 years for the signs of infection to appear [1].

1.1.2 Treatment of HCV infection

At present, there is no approved vaccine available for the prevention of HCV infection, although several promising vaccination strategies are currently in clinical development [4]. Instead treatment is administered retrospectively and includes the use of pegylated interferon-α (IFNα) and ribavirin, which has proven successful at resolving infection in around 41-52% of patients infected with genotype 1 HCV [1]. IFNα treatment works by inducing a cellular antiviral response that in some patients is able to successfully eliminate infection in the HCV infected hepatocytes. The modification of IFNα through the addition of polyethylene glycol (PEG) facilitates the slow release of IFNα into the body allowing less frequent dosing [5]. Incorporation of ribavirin further improves the success rates of treatment possibly

through its ability to stimulate increased expression of antiviral interferon stimulated genes e.g. IRF7 and IRF9 [1, 6].

In order to achieve a sustained virological response (SVR) in patients, treatment with IFNα and ribavirin is often prolonged, which can lead to the development of severe side effects; including anemia, cytopenias, neutropenia and thrombocytopenia, and more frequently headaches, nausea, fatigue and vomiting [1, 2]. Another drawback to the prolonged treatment program required is that treatment-resistant infections can develop as mutations accumulate in the virus genome to generate virus strains that are no longer sensitive to interferon treatment [7].

As a result of the limitations associated with the current treatment strategy, the development of more effective anti-HCV therapies is an important objective at present. One approach being developed is the use of inhibitors that target the enzymatic activity of key virus proteins such as the NS3 protease (including linear and macrocyclic inhibitors) and the NS5B RNA polymerase (including nucleos(t)ide and non-nucleoside inhibitors). These inhibitors provide a much more effective targeted approach to antiviral therapy. Some of the most promising inhibitors developed to date include: Telaprevir and Boceprevir, which are linear NS3 active site inhibitors currently in phase 3 clinical trials; the NS5B nucleotide inhibitor, PSI-7977 and the NS5B non-nucleoside inhibitor, Filibuvir, both of which are currently in phase 2 clinical trials. Alongside the development of NS3 and NS5B inhibitors, compounds targeting the NS5A protein have also recently been generated, including BMS-790052, which is currently in phase 2 clinical trials [8]. In comparison to the standard IFNα treatment regimen used, much greater antiviral activity is observed when these inhibitors are also incorporated into the treatment program. For example, treatment of genotype 1 infected patients with Telaprivir / IFNα / ribavirin combination therapy has been observed to induce a 72-75% SVR compared to IFNα / ribavirin combination therapy alone, which induced a 44% SVR [8]. However, despite the high antiviral activity of these inhibitors, since the focus of these treatments remains directed against the virus, treatment resistant infections are still a major problem, as the virus genome can mutate rapidly to generate treatment resistant virus strains [7, 8]. To overcome the issues faced by the development of HCV resistance, it is anticipated that many of the antiviral inhibitors developed will be used in combination [8].

Alongside the development of antivirals that target the virus directly, an alternative approach involves the development of antivirals that target the host, in particular the proteins that are required for effective entry, replication and secretion of HCV. Approaches that target the host rather than the virus should facilitate the development of a more broad-spectrum treatment, to which the patient is unlikely to develop resistance, as the mutation rates of host genes are low [7]. HCV encodes only a small number of virus proteins in its genome, and there is significant evidence to suggest that it relies heavily upon interactions with host proteins for many aspects of its replication cycle. As a result, there are likely to be many potential host factors that may be targetable for the development of antiviral therapy. Some examples of host factors recently identified for antiviral targeting are the cell surface host proteins required for HCV entry. The efficacy of antivirals targeting these host factors has been demonstrated using a variety of small molecule compounds and antibodies, which have been shown to successfully block cell surface host proteins (e.g. SR-B1, CDB1 and CLDN1) to reduce virus entry into liver hepatocytes [9]. As our understanding of the HCV replication cycle continues to grow, it is likely that more host factors will be identified for antiviral targeting allowing significant increase in the range of effective therapeutic options available for the treatment of chronically infected patients. Alongside the targeting of host factors involved directly in the HCV replication cycle, antivirals targeting the host immune response are also being developed, such as the toll-like receptor (TLR) agonists that stimulate TLR7 (e.g. Isatoribine and resiquimod) and TLR9 (e.g. CPG10101), which induce immune activation against HCV infection [1, 10, 11].

1.1.3 Classification of HCV infection

HCV is an enveloped positive-stranded RNA virus that belongs to the *Hepacivirus* genus of the *Flaviviridae* family. Other genera of this family include the *Flaviviridae* (e.g. West Nile Virus, Dengue Virus and Yellow Fever Virus) and the *Pestiviridae* (e.g. Bovine Viral Diarrhea Virus and Classical Swine Fever Virus) [12]. HCV can be divided into 7 different genotypes, some of which have several subtypes e.g genotype 1a, 1b and 1c [13, 14]. The geographical distribution of the different HCV genotypes is varied; genotypes 1 – 3 are the most predominant in Europe, the USA and Japan; genotypes 4 and 5 in Africa and the Middle East; genotypes 2, 3 and 6 in Asia; and genotype 7 in central Africa [1, 14]. These different genotypes

vary in their responsiveness to IFNα / ribavirin therapy, as a sustained virological response is observed in 41-52% of patients infected with genotype 1 and 4 HCV, compared to 76-82% of patients infected with genotype 2 and 3 HCV [1]. The different genotypes also display varying degrees of pathogenic severity. For example, patients infected with genotype 3 HCV consistently develop liver steatosis and liver fibrosis at a much higher rate than patients infected with other HCV genotypes [15, 16].

1.2 The HCV RNA genome

The HCV genome is an uncapped 9.6 Kb RNA molecule that encodes a single polypeptide within a central open reading frame, and is flanked at the 5' and 3' ends by highly structured non-translated regions (NTRs) (**Fig. 1.1**). The 5' NTR contains an internal ribosomal entry site (IRES) that is necessary for cap-independent translation of the viral RNA. The 5'NTR also contains cis-acting sequences that are important for virus RNA replication [17]. The 3' NTR contains a short variable region, a poly U/UC tract and a series of conserved stem loop structures, known as the X tail, which are also essential for genome replication [17, 18]. Several host cell proteins have been shown to interact with the cis-acting sequences and secondary structures of the NTRs to control genome translation and replication; examples include the polypyrimidine tract binding protein (PTB), La autoantigen and the hu antigen R protein (HuR) [19-21].

When the single polypeptide chain encoded by the genome is translated, a series of co- and post-translational cleavage events take place to produce the individual virus proteins. Host cell peptidase enzymes (signal peptidase and signal peptide peptidase) cleave the polypeptide to generate the viroporin p7 protein and the HCV structural proteins including the 'core' capsid protein and envelope proteins, E1 and E2. The non-structural proteins are cleaved from the polypeptide by two virus encoded proteases: the NS2-NS3 cysteine protease, which cleaves the NS2/NS3 junction, and the NS3-NS4A serine protease, which cleaves the rest of the polypeptide into the remaining non-structural proteins: NS3, NS4A, NS4B, NS5A and NS5B [17, 18]. An additional protein (ARF-P) is also generated from the sequence of the core protein by translation of an alternative reading frame or through ribosomal frameshifting. At present, there is no known function for this protein and it is not required for replication of HCV in cell culture [18] (**Fig. 1.1**).

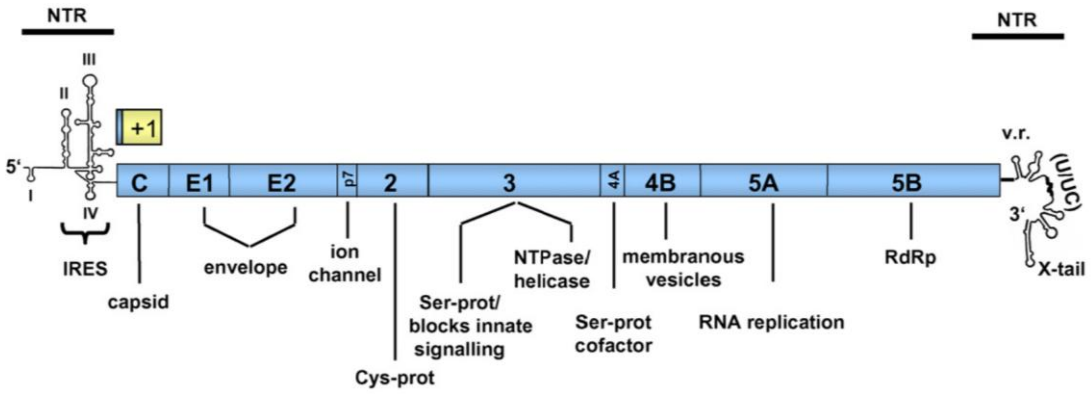


Figure 1.1 HCV genome organisation [18]

HCV genome organisation and protein function. The HCV genome coding region is shown in blue with vertical lines indicating polypeptide cleavage positions. The coding region is translated to generate the structural proteins: core (C) and envelope proteins 1 and 2 (E1 and E2); the viroporin p7 (p7); and the non-structural proteins: NS2 (2), NS3 (3), NS4A (4A), NS4B (4B), NS5A (5A) and NS5B (5B). An additional protein, ARF-P is also translated from the core protein coding region and is indicated in yellow (+1). Non-translated regions (NTR) of the genome include the 5'NTR, which contains stem loop structures I, II, III and IV and encodes the IRES, and the 3'NTR, which contains a variable region (v.r), a poly U/UC tract (U/UC) and three stem loop structures (X tail). HCV protein functions are indicated beneath each gene in the genome and the abbreviations used are as follows: cys-prot (cysteine-protease); ser-prot (serine-protease) and RdRp (RNA dependent RNA polymerase).

1.3 The HCV replication cycle

1.3.1 HCV entry

Infection of human hepatocytes with HCV occurs following the binding of HCV particles to host receptors present on the hepatocyte cell surface. Initial attachment at the cell surface occurs through low affinity binding of glycosaminoglycans (e.g. heparin sulphate); and possibly the LDL receptor, which may interact with HCV associated lipoproteins (e.g. LDL and VLDL) [22]. Once the virus particle has docked at the cell surface, specific entry factors including CD81, Scavenger Receptor Class B Type I (SR-BI), Claudin-1 and Occludin provide higher affinity attachments which enable the virus to undergo clathrin-dependent receptor-mediated endocytosis. Direct binding has been observed to occur between the HCV envelope protein, E2, SR-BI and CD81, which form a ternary complex; and between CD81 and Claudin, which form a co-receptor complex. Additional interactions may also form between SR-BI and HCV associated lipoproteins, which may mimic typical SR-BI ligands, such as HDL (high density

lipoprotein) and oxidised LDL [23]. These findings indicate that HCV entry may occur following the formation of a tightly orchestrated HCV entry factor complex [9, 22]. Alongside the role of Claudin-1 in the HCV entry process, Claudin-6 and 9 have also been observed to facilitate HCV entry into hepatoma cells and may also form part of the HCV entry complex [9]. Once the HCV particle has been endocytosed, it enters into the early endosomal pathway and localises within RAB5-positive early endosomes [9]. Inside the early endosome, the HCV particle is exposed to an acidic pH. This causes the virus particle envelope to fuse with the endosomal membrane and releases the virus genome into the cytosol, where it is translated at the rough endoplasmic reticulum [9, 22].

Hepatocyte cells in the liver are polarised and have two distinct cell surface environments known as the apical and basolateral surfaces. The apical surfaces provide contact points between adjacent hepatocyte cells via a series of tight junction complexes. In contrast, the basolateral surfaces are in contact with the blood supply delivered through the sinusoidal vessels from the hepatic artery. Two of the HCV host entry factors, Occludin and Claudin1, are key components of the tight junction complexes that connect adjacent cells, and are localised to the apical surfaces of hepatocytes. However, exposure of the polarised hepatocytes to HCV occurs via the blood supply at the basolateral surface. This selective distribution of HCV entry factors to the hepatocyte apical surface raises the important question of how the HCV particles present in the bloodstream are able to access these factors for virus entry [24, 25]. One possibility is that HCV binds loosely to the basolateral surface and migrates laterally along the membrane to the tight junction where the remaining entry factors complete the process of virus entry [25]. However, many studies investigating HCV entry do not support this mechanism; instead they indicate that entry occurs at a location that is not restricted to the tight junction complex, but is most likely localised at the basolateral surface of the cells [26]. This is supported by evidence indicating that the tight junction protein, Claudin1 has been observed to colocalise with CD81 and SR-BI at the basolateral surface in both HCV infected and normal liver tissue [22, 24, 26]. The tight junction protein, Occludin has also been observed to localise to the basolateral surface when it is first synthesised by the cell before being transported to the apical surface for formation of tight junction complexes [25]. This evidence indicates that there are likely to be areas of the hepatocyte basolateral surface where all the HCV entry factors colocalise allowing the HCV particles present in the bloodstream to enter

the cells for initiation of infection. Further evidence to support the idea that HCV entry may occur outside of the tight junction includes the observation that HCV can successfully infect the Huh7.5 hepatoma cell line, which does not form functional tight junction complexes [27].

1.3.2 Genome translation and replication

Once the HCV genome is released into the cytosol it localises to the host ribosomes, which are present at the surface of the endoplasmic reticulum (ER), allowing genome translation to take place. The HCV polypeptide produced is transported co-translationally into the lumen of the ER, where the individual HCV proteins are cleaved from the single polypeptide. As virus proteins accumulate in the ER, replication complexes required for virus genome replication are assembled upon cytoplasmic membranes which rearrange to form a vesicular structure, containing double membrane vesicles, termed the 'membranous web' [18, 28]. These structures provide a stable and confined environment for viral RNA synthesis, protecting against cellular nucleases and proteases, and preventing host immune response proteins from recognising the virus genome [29]. Replication complexes colocalise with markers from the ER, the Golgi body, early endosomes and autophagosomes indicating that multiple intracellular compartments may contribute to the 'membranous web' structure [28, 30-32]. Replication complexes actively engaged in RNA synthesis also cofractionate with detergent-resistant 'lipid raft' regions of the membrane that are enriched in cholesterol and sphingolipids [32]. The membrane of the ER does not contain lipid raft structures, unlike the Golgi body which has an abundance of cholesterol and sphingolipid molecules enabling lipid raft formation. This selective distribution of lipid rafts has led several studies to suggest that replication complexes may initially assemble in the ER, but relocate to the Golgi body for activation of replication. This is supported by the observation that RNA replication activity is observed predominantly in the Golgi-localised replication complexes [32]. However, there is some discrepancy about the accuracy of this replication model, as other studies have not been able to show colocalisation of replication complexes with the Golgi body [30]. In addition, this model does not account for the colocalisation observed between replication complexes and the markers of early endosomes (EEA1 and Rab5) [30] and autophagosomes (Atg5) [28, 31]. Therefore, at present the mechanism of membranous web formation is unclear,

but may involve the recruitment of membrane or membrane components that are usually found in the ER, Golgi body, early endosomes and autophagosomal compartments.

The assembly of the HCV replication complex is dependent on the HCV non-structural proteins NS3, NS4A, NS4B, NS5A and NS5B, which provide all the necessary virus components for HCV genome replication [33]. Several host cell proteins also participate in the formation and activation of replication complexes and the membrane rearrangements that take place (**Table 1.1**). An excess of non-structural proteins has been observed in the replication complex structure. Many of these excess proteins do not participate in RNA synthesis, but instead they may be required as structural components of the membranous web or they may have other functional roles within the cell [29]. Numerous studies have reported the interaction of HCV non-structural proteins with host cellular proteins, such as those involved in apoptosis, cell proliferation and innate immune responses. A well-studied example is the interaction of NS3 with components of the Toll-like receptor 3 (TLR3) and retinoic acid-inducible gene I (RIG-I) pathways that are involved in antiviral innate immune signalling. NS3 proteolytic cleavage of cellular proteins acting downstream of TLR3 and RIG-I results in the inhibition of an interferon response and enables HCV to establish a persistent infection [34, 35].

Once HCV replication complexes have assembled, RNA synthesis takes place allowing amplification of positive-stranded RNA genomes via negative-stranded templates. Newly synthesised RNA genomes can either be used in translation, as templates for negative-strand synthesis, or they can be incorporated into nucleocapsids during the formation of nascent virus particles [18]. Several host proteins been have shown to bind directly to the 5’ and 3’ NTR regions of the HCV genome to facilitate initiation of genome replication, and control whether the RNA template is used for translation or replication [36, 37].

1.3.3 Virus particle assembly and secretion

The processes of genome translation and replication generate abundant supplies of the HCV RNA genome and the HCV structural proteins, which are necessary for the production of nascent virus particles. Following genome translation, the structural proteins initially insert into or anchor at the ER membrane until virus

particle assembly takes place, and the proteins relocalise for the final stages of the HCV replication cycle [17].

The process of virus assembly initiates with oligomerisation of the core capsid protein to generate the nucleocapsid structure into which the RNA genome is packaged. Encapsidation of the genome is dependent upon an interaction that forms between the core protein and the HCV genome [38]. There is accumulating evidence to indicate that nucleocapsid formation may occur at the surface of lipid droplets, which are the dynamic intracellular organelles responsible for storage of neutral lipids. Lipid droplets are formed using membrane and lipids derived from the ER and are able to migrate on microtubules to deliver lipids and proteins to other intracellular organelles [39]. Studies have demonstrated that during infection, replication complexes and newly synthesised virus RNA localise to the lipid droplet surface using NS5A, which interacts with the lipid droplet localised core protein [39-41]. Through these interactions, it is thought that lipid droplets may become embedded within the HCV membranous web structure for efficient delivery of the virus genome from replication complexes to virus assembly sites. Alongside this model, an alternative mechanism has also been proposed whereby nucleocapsid formation takes place at the ER membrane, and requires lipid droplets to function as a HCV core protein transport vehicle, trafficking core from the site of translation to the site of virus assembly [42].

Once the HCV genome has been packaged into a nucleocapsid, virus particles undergo budding to acquire an outer envelope containing the envelope glycoproteins, E1 and E2, which are embedded into a lipid bilayer structure. At present, it is not clear where the process of virion budding takes place. However, NS2 may play a key structural role in this process, as it is able to form HCV protein complexes that localise adjacent to the core coated lipid droplets and contain replicase components (NS3 and NS5A), the viroporin p7 and the envelope proteins (E1 and E2) [43, 44]. Recent studies suggest it is possible that virus particle budding may occur in specialised lipid rich microdomains of the ER that are located near to the core localised lipid droplets and are involved in the process of VLDL synthesis [45, 46]. This is based on the observation that the assembly, maturation and secretion of nascent HCV virus particles appears to be dependent on the process of VLDL synthesis [42, 47].

The role of VLDL synthesis in the secretion of HCV was first suggested following the observation that HCV particles isolated from the serum of chronically infected patients are often found in a low density configuration in association with components of secreted VLDL (including triglyceride, Apolipoprotein B100 (ApoB) and Apolipoprotein E (ApoE)), and are commonly referred to as 'lipoviroparticles' [42, 48]. Typically, VLDL production initiates following the fusion of the ER protein, ApoB, with lipid droplet derived triglyceride and cholesterol ester molecules in the lumen of the ER using the microsomal triglyceride transfer protein (MTTP) [42, 47]. This process results in the formation of a pre-VLDL particle, which can either be directly secreted or further lipidated using another lipoprotein, ApoE, which facilitates the fusion of the pre-VLDL particle with lumenal lipid droplets generating a triglyceride rich VLDL particle [42, 48]. The exact location and mechanism of pre-VLDL lipidation is still unclear, but most likely occurs within the ER or Golgi body. Mature VLDL particles are then secreted from the cell using ER derived COPII (coat protein complex II) dependent transport vesicles, which are thought to traffic through the Golgi body to exit the cell [45].

The key role of lipid droplets in the VLDL synthesis pathway indicates that a mechanism may exist whereby HCV components localised at the lipid droplet surface are delivered to the VLDL synthesis machinery for the process of HCV assembly, maturation and secretion [40]. In support of this potential mechanism, studies have demonstrated that knockdown of ApoB and ApoE and inhibition of MTTP activity significantly reduces the intracellular and extracellular titres of infectious HCV produced [45-47, 49]. Other host proteins involved in VLDL synthesis have also recently been shown to be essential for the process of HCV particle secretion including ACSL3, which controls production of phospholipids for VLDL synthesis [50] and ARF1 GTPase (ARF1), which controls lipidation of the pre-VLDL particle [51]. However, despite the significant evidence indicating the key role of VLDL synthesis in the HCV replication cycle, other studies have been unable to demonstrate the requirements for ApoB and MTTP during HCV assembly and secretion. Instead, these studies have demonstrated that ApoE alone is essential for both HCV assembly and secretion and interacts directly with NS5A [49, 52]. These findings suggest a specific role for ApoE in the HCV replication cycle and indicate that NS5A may facilitate the switch from HCV replication to assembly. Because of these disparities, further studies need to be performed to clarify the exact role of VLDL synthesis during HCV infection [42].

Future studies will also need to focus on the differences observed in the assembly and secretion of HCV taking place in hepatoma cells (Huh7 cells) compared to primary human hepatocytes. The VLDL secretory pathway in Huh7 cells has been shown to be defective, as ApoB VLDL precursors cannot fuse with ApoE rich lipid droplets to form mature VLDL particles [23]. This results in the production of HCV particles that are enriched in ApoE, but not ApoB, making them different to the ApoB and ApoE rich lipoviroparticles usually found in chronically infected patients [23, 42].

Alongside, the evidence that suggests a key role for VLDL synthesis in the assembly, maturation and secretion of HCV particles, proteins controlling endosomal cargo sorting have also recently been shown to be important for the process of HCV virion release [53]. Endosomal cargo sorting is controlled by a series of ESCRT (endosomal sorting complexes required for transport) protein complexes. These complexes facilitate the sorting of ubiquitinated endocytosed cargo into intralumenal vesicles that form within endosomes to create a multivesicular body (MVB). This MVB then undergoes fusion with lysosomes allowing the degradation of the intralumenal vesicles and their cargo. ESCRT complexes 0-II control the process of cargo sorting and the recruitment of ESCRTIII, which controls the process of membrane scission required during intralumenal vesicle formation. ESCRTIII complex disassembly and recycling is controlled by the ATPase protein, Vps4, which is required for correct functioning of the sorting and degradation process [53, 54]. Recently, several components of the ESCRT pathway have been shown to be essential for the release of infectious HCV virions; including the ESCRT complex binding proteins, TSG101 and ALiX [55]; ESCRT III complex proteins, CHMP1A, 2A, 3, 4B, 5 and 6; and the ATPase, VPS4 [53, 55]. However, further investigation is required to confirm the role of TSG101 and ALiX, as only one out of the two studies performed has demonstrated a requirement for these factors during HCV secretion [55]. Further evidence for a role of the ESCRT pathway in the HCV secretion process was also recently observed, as HCV core was shown to interact directly with the ESCRT III complex protein, CHMP4B [55].

There is significant evidence demonstrating that the processes of VLDL synthesis and endosomal cargo sorting are required for the assembly and secretion of HCV particles. However, the mechanism involved is likely to require an even wider

range of host cellular factors, as the oxysterol binding protein (OSBP), the ceramide transfer protein (CERT) [56], Annexin A2 (ANXA2) [57] and the heat shock cognate protein 70 (HSC70) [44] have also been shown to facilitate the processes of HCV particle assembly and secretion (**Table 1.1**).

A summary of the HCV replication cycle including the processes of virus entry, genome translation and replication, and virion assembly and secretion is shown in **Fig. 1.2**.

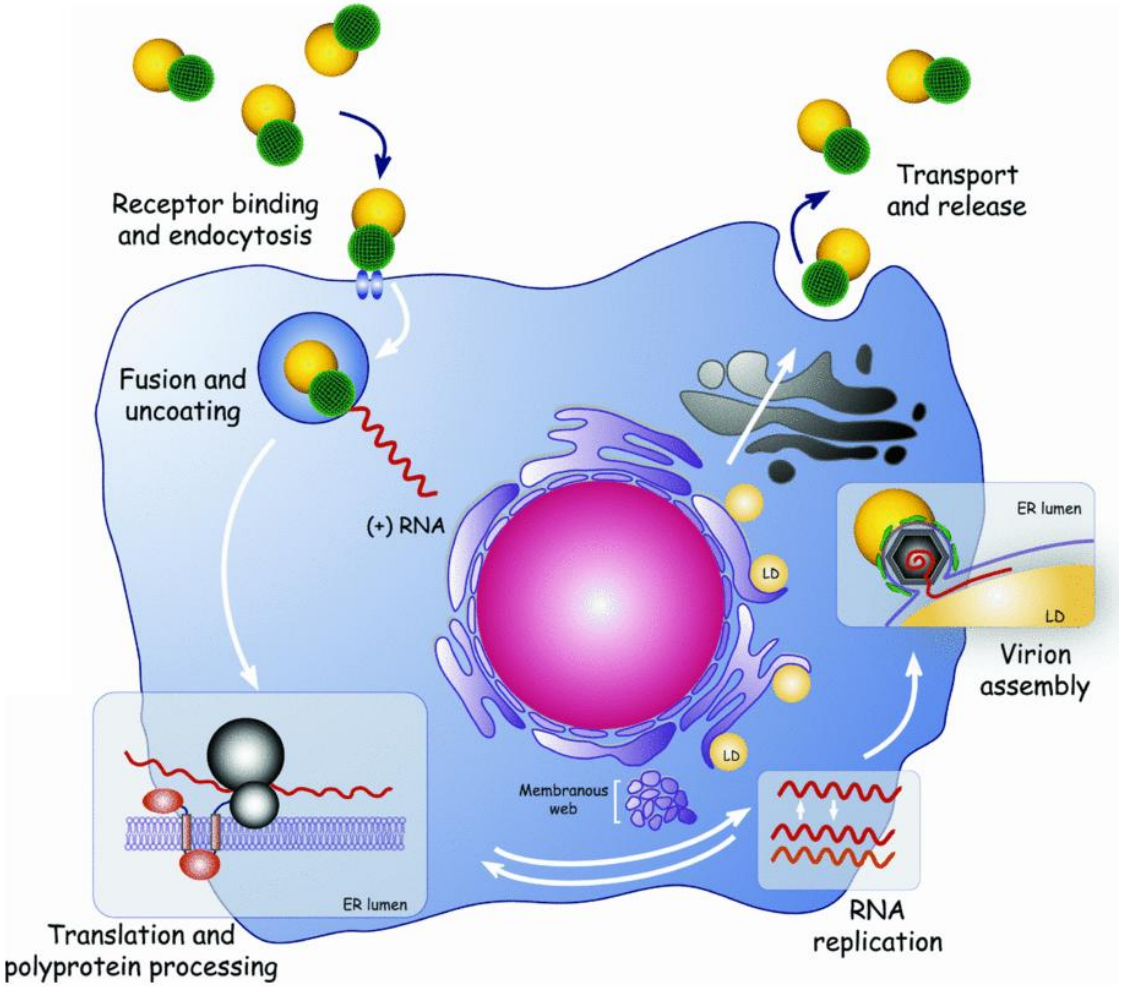


Figure 1.2 The HCV replication cycle [58]

HCV virus particles (green spheres) associated with lipoproteins (yellow spheres) enter the liver hepatocytes by clathrin-dependent receptor mediated endocytosis following interaction with cell surface factors (heparin sulphate, LDLR, CD81, SR-B1, Claudin-1 and Occludin). The HCV particle is endocytosed into an early endosome and the virus envelope fuses with the endosomal membrane. The HCV genome is released into the cytosol and translated at the rough endoplasmic reticulum. Polyprotein processing takes place at the endoplasmic reticulum (ER) to produce the individual HCV proteins. The non-structural HCV proteins assemble into HCV replication complexes localised to a membranous web structure that assembles from intracellular membrane components (e.g. ER and Golgi body derived membrane). Replication of the HCV genome takes place within HCV replication complexes via a negative-sense RNA template. The newly synthesised HCV genome is incorporated into a nucleocapsid structure at the lipid droplet surface (LD) and may bud through the ER membrane. Nascent HCV particles are secreted from the cell in conjunction with lipoproteins (e.g. VLDL particles), which may exit the cell through the Golgi body.

1.4 The role of virus proteins in the HCV replication cycle

1.4.1 The structural HCV proteins

Core is the RNA-binding capsid protein responsible for encapsulating the HCV genome into the virus nucleocapsid structure. It is the first protein to be cleaved from the amino terminus (N terminus) of the polypeptide chain at the ER membrane. The host cell protease enzyme, signal peptidase initially cleaves the core-E1 boundary at a signal peptide sequence. Further cleavage of the core protein by the signal peptide peptidase enzyme removes the remaining signal peptide from the immature core protein to produce a mature core protein. Once processing of the core protein is complete, it relocalises from the ER to the lipid droplet surface [40]. This process has recently been shown to occur in conjunction with diacylglycerol acyltransferase 1 (DGAT1), the ER localised triglyceride synthesising enzyme responsible for formation of cytosolic lipid droplets [59]. Once the core protein is localised at the surface of cytosolic lipid droplets, it has been shown to recruit the HCV genome for nucleocapsid formation by binding to the NS5A protein allowing delivery of HCV replication complexes that contain the HCV genome [41], and by binding directly to the HCV genome itself [38]. Binding of HCV core to lipid droplets also induces relocalisation of the droplets from a cytoplasmic to a perinuclear location allowing close association with the ER [60], where other cellular components required for HCV assembly and secretion can be found (e.g. VLDL synthesis machinery). The mature core protein is composed of two functional domains: domain 1 (D1), at the N terminus of the protein, is responsible for mediating HCV RNA binding and protein-protein interactions; and domain 2 (D2), at the carboxy terminus (C-terminus) of the protein, is responsible for mediating lipid droplet association (valine position 147) [40, 45].

Alongside the key role of HCV core protein at the lipid droplet surface, core has also been shown to localise to the outer membrane of mitochondria during HCV infection [61, 62]. The purpose of this localisation is unclear; however, it may contribute to the induction of mitochondrial-mediated apoptosis that has been observed to occur as a result of HCV infection [62]. The core protein has also been shown to interact directly with several host cellular proteins resulting in disruption of key signalling pathways including cellular proliferation and survival (e.g. signal transducer and activator of transcription 3 (STAT3) [63]), RNA interference pathways (e.g. Dicer [64]) and mRNA metabolism (e.g. hnRNPK [65]).

The expression of the HCV core protein is also associated with alterations in intracellular lipid metabolism including increased expression and activity of adipogenic genes such as the sterol regulatory element binding protein 1 (SREBF1) and the peroxisome proliferator activated receptor γ (PPARγ) [66, 67]; decreased expression of the peroxisome proliferator activated receptor α (PPARα), which controls fatty acid oxidation and degradation [68]; and inhibition of the MTTP protein involved in VLDL synthesis [69]. As a result of these effects on lipid metabolism, the HCV core protein is thought to contribute significantly to the development of hepatic steatosis in chronically infected patients. In support of these observations, variation in the protein sequence of core has been shown to be responsible for the predisposition of genotype 3 HCV infected patients to liver steatosis [70].

E1 and E2 are transmembrane proteins that anchor into the envelope membrane surrounding the HCV nucleocapsid. Both proteins contain a C-terminal transmembrane domain for membrane localisation and a highly N-glycosylated N-terminal ectodomain that gives the virus particle a protective glycan coat [61, 71]. In order to recognise the HCV cell surface entry factors, E1 and E2 form large covalent complexes stabilised by disulphide bonding. This organisation differs from that observed when the envelope proteins are expressed in the host cell and a non-covalent heterodimer is formed between E1 and E2 in the ER membrane [71]. The two envelope proteins have been shown to play different roles in the virus entry process. E1 is required to promote pH dependent fusion of the virus envelope with the early endosomal membrane, following clathrin mediated endocytosis of the HCV particle [72]. E2 plays a direct role in virus particle docking at the host cell surface by binding, via its N-terminal ectodomain, to the cellular entry receptors CD81, SR-B1 and heparin sulphate [61]. Fusion peptides have also been identified in the E2 sequence [72] indicating that it may participate alongside E1 in the process of membrane fusion. The observation that both E1 and E2 are heavily glycosylated with complex glycans provides evidence to indicate that HCV virion secretion most likely occurs through the Golgi body, where glycosylation enzymes are localised [71]. This supports the data suggesting that HCV virion secretion occurs in conjunction with VLDL secretion, which is also thought to traffic through the Golgi body [45].

P7 is a small viroporin protein that oligomerises to form a hexameric or heptameric ion channel in host cell membranes [73-75]. P7 monomers have two transmembrane domains, which both anchor into the membrane to orient the C and N-termini of the protein towards the ER lumen [74]. During HCV infection, p7 has been detected within the membrane of the ER and the mitochondria [61], and in NS2 containing HCV protein complexes that localise adjacent to cytosolic lipid droplets for structural organisation of HCV virus assembly [43, 76]. The expression of p7 is not required during genome replication, but is essential for the formation and release of virus particles from infected cells. The channel formed by the p7 oligomer acts as a proton (H^+) conductor and is thought to prevent the acidification of secretory vesicles that transport pH sensitive intracellular HCV particles out of the cell [77]. The p7 oligomer has additional functions in the HCV replication cycle unrelated to its ion channel function and is able to regulate the intracellular localisation and membrane topology of HCV NS2 during HCV infection [43, 78].

1.4.2 The non-structural HCV proteins

NS2 is a transmembrane protein involved in the early stages of virus replication. It forms part of the NS2/NS3 cysteine protease that cleaves the NS2/NS3 boundary of the HCV polyprotein. The NS2 protein is composed of two functional domains, with an N-terminal membrane binding domain and a C-terminal globular and protease subdomain [76]. Structural analysis of the protease has demonstrated that NS2 forms a dimer with proteolytic activity, whilst NS3 acts as a cofactor promoting formation of an active NS2 protease [79]. After its initial role in the HCV replication cycle, NS2 is not required for HCV genome replication, but is instead involved in the latter stages of infection during the assembly of virus particles [43, 76]. NS2 is able to bind to both structural and non-structural proteins including the envelope proteins (E1 and E2), p7, NS3 and NS5A. Through these interactions, NS2 acts as a linker between the HCV proteins involved in genome replication and those involved in virus particle assembly. During the switch from genome replication to virus assembly, the NS5A protein localises to the surface of intracellular lipid droplets by interacting with the HCV core protein [41]. The docking of these proteins at the lipid droplet surface is thought to facilitate recruitment of HCV replication complexes and delivery of the viral RNA genome for nucleocapsid formation. The ability of NS2 to interact with NS5A means that NS2 is also able to localise near to the lipid droplet surface. Once nucleocapsid

formation has taken place, NS2 may direct formation of the virus envelope by binding and recruiting the envelope proteins to the nucleocapsid structure at the lipid droplet surface [43, 76]. NS2 and NS5A may also play an additional role in a late stage assembly process, as inhibition of the interaction between NS2 and NS5A was also shown to disrupt a post-particle assembly step in virus production [43]. During this process, p7 has been shown to control the membrane topology of NS2 regulating its ability to interact with other HCV proteins [43]. Alongside a direct role in the HCV replication cycle, NS2 has also been shown to induce ER stress and inhibit protein translation in cells, possibly as a mechanism to limit virus replication and facilitate establishment of a persistent infection [80].

NS3 is a cytosolic protein with N-terminal serine protease activity and C-terminal NTPase/ RNA helicase activity. Both the helicase and protease activities of NS3 are dependent on the binding of the NS4A cofactor. The protease activity of NS3 in the NS3/NS4A complex is responsible for proteolytic processing of the HCV polypeptide downstream of NS3 in the ER membrane. Initially the NS3/NS4A protease cleaves the NS3/NS4A boundary in *cis* followed by *trans* cleavage of the NS5A/NS5B boundary to form a NS4A-NS5A intermediate. Cleavage of the NS4A/NS4B boundary then takes place to release an NS4B/NS5A precursor, after which the NS4B/NS5A boundary is cleaved [81]. The NS3 serine protease domain has a chymotrypsin-like fold with two β-barrel subdomains and a catalytic triad active site (histidine 57, aspartic acid 81 and serine 139) [81]. The presence of NS4A in the NS3/NS4A protease is required for activation of the NS3 protease and for localisation of the complex to the ER membrane where polyprotein processing takes place [61]. Alongside the proteolytic cleavage of the HCV polypeptide, protease activity of NS3/NS4A is also used for proteolytic digestion of host proteins including the phosphate starvation-1 adaptor protein (IPS-1) (also known as MAVS, CARDIF and VISA) and the toll-like receptor adaptor molecule 1 (TICAM1) (also known as TRIF). IPS-1 and TICAM1 are involved in the RIG-I and TLR3 pathways, respectively, and are responsible for stimulating the expression of interferon β in response to dsRNA [34, 35]. The cleavage of these proteins reduces antiviral signalling in the infected cells to facilitate the replication of HCV.

The second enzymatic function of the NS3 protein is the NTPase/ RNA helicase, which is a member of the 2 DExH / D-box helicase superfamily. The NS3 helicase uses ATP hydrolysis to perform dsRNA unwinding and is important for the

structural organisation of HCV RNA during genome replication [81, 82]. The NS3 helicase has been proposed to perform dsRNA unwinding through a ratchet like fashion [81]. Similar to NS3 protease, the NS3 helicase is dependent on the binding of NS4A, which facilitates activation of the ATPase required for helicase function [83].

Alongside the key role of NS3 in HCV genome replication, NS3 may also be required during HCV virus assembly, as it forms interactions with other HCV proteins involved in this process (e.g. NS2) [43, 76, 84]. In addition, NS3 has also been shown to bind to a number of cellular host proteins including those involved in cellular proliferation and apoptosis (e.g. p53 [85]) and innate immune signalling (e.g. the large multifunctional protease 7 (LMP7) [86]). Through these interactions and the cleavage of key cellular antiviral proteins, NS3 is able to promote cellular survival to facilitate establishment of a persistent HCV infection.

NS4A is a small transmembrane protein, which acts as a cofactor for NS3 stimulating its protease and helicase enzymatic activities [61]. The N terminus of NS4A comprises a transmembrane α helix for membrane localisation, the centre portion of NS4A facilitates folding of the NS3 protease in the NS3/NS4A complex and the C terminus of NS4A has been shown to interact with other replicase components and may be involved in the process of HCV RNA synthesis and virus particle assembly [81]. In addition to its role as a cofactor, NS4A has been shown to accumulate on the mitochondrial outer membrane and may contribute to the mitochondrial dysfunction and cellular apoptosis that occurs during HCV infection [87].

NS4B is a highly hydrophobic transmembrane protein that independently associates with membrane lipid rafts and HCV non-structural proteins to drive the assembly of the membranous web and structurally organise the HCV replication complex [61]. NS4B contains four central transmembrane domains, two N-terminal amphipathic helices and two C-terminal helices, one of which is also amphipathic. Other than the four transmembrane domains, the second amphipathic helix at the N-terminus also traverses the membrane, whilst the first N-terminal helix is localised towards the lumenal side of membranous web and the two C-terminal helices are oriented towards the cytosol [88].

NS4B is able to oligomerise into a higher order structure, which may facilitate induction of membrane curvature and drive membranous web formation. Oligomerisation may occur as a result of homotypic and heterotypic interactions that have been observed to form between the membrane-localised N-terminal and C-terminal amphipathic helices of adjacent NS4B proteins [89]. Insertion of NS4B into cellular membranes is first thought to occur in the ER following the processing of the HCV polypeptide. However, the precise location at which NS4B directs membranous web formation is not clear, as replication complexes colocalise with markers of the ER, Golgi body, early endosomes and autophagosomes [28, 30, 32]. In addition to the central role of NS4B in membranous web formation, it has also been implicated in virus assembly, and possesses NTPase activity that can hydrolyse both ATP and GTP. NS4B interacts with several cellular host proteins including those involved in the ER stress response and lipid metabolism, such as the SREBF1 transcription factor that controls expression of genes involved in lipid synthesis [88, 90].

NS5A is an RNA-binding phosphoprotein that has been shown to play a key role in both HCV RNA replication and virus particle assembly. NS5A is composed of three distinct domains (domain 1, 2 and 3) separated by low complexity sequences, with an N-terminal amphipathic α-helix that anchors the protein into the ER membrane [91]. Domains 1 and 2 have largely been implicated in the regulation of HCV genome replication, whilst domain 3 has been shown to be important during virus particle assembly [91, 92]. However, residues in domain 3 have been shown to influence the process of replication [93] and proteins required during virus particle assembly have also been shown to bind to NS5A domain 1 [94].

NS5A is an essential component of the HCV replication complex and has been implicated in the regulation of RNA replication and targeting of the virus genome to the replication complex [61]. To perform these functions, NS5A interacts directly with the 3'NTR and 5'NTR regions of the HCV RNA genome and the 3'NTR of the negative sense HCV RNA strand [91, 95]. Studies investigating HCV RNA binding activity of NS5A have demonstrated that although all three domains of NS5A were observed to bind to the 3'NTR of the HCV genome, domains 1 and 2 demonstrated much higher affinity binding than domain 3 [91]. NS5A also contributes to the regulation of HCV genome replication by binding to the NS5B

protein, enhancing its RNA polymerase activity [96], and interacting with a range of host cellular factors that control the formation and functioning of the HCV replication complex. These include: vesicle associated proteins A and B (VAP-A and VAP-B) [97], Cyclophilin A and B [98] and phosphatidylinositol 4 kinase (PI4K) [99].

In addition to its role in the HCV replication complex, NS5A also colocalises with HCV core protein at the surface of intracellular lipid droplets and is required during virus particle assembly [39-41]. Domain 3 of the NS5A protein has been shown to mediate interaction with the HCV core protein at the lipid droplet surface, although NS5A is also able to localise independently to lipid droplets via domain 1 [100]. Through its ability to bind the HCV replication complex, the HCV genome and lipid droplets, NS5A may control the switch from genome replication to virus assembly by facilitating the transport of the HCV genome from replication complexes to the lipid droplet surface. The phosphorylation status of NS5A may be an important factor that determines the timing of this switch, as NS5A can either be found in a basally phosphorylated form (56KDa), or a hyperphosphorylated form (58KDa) [95]. Hyperphosphorylation of NS5A blocks its interaction with VAP-A, and inhibits the function of the HCV replication complex. This indicates that hyperphosphorylation of NS5A may signal a switch from HCV replication to HCV assembly, and enable trafficking of NS5A and the HCV genome to lipid droplets for initiation of assembly [95]. Several serine and threonine residues have been identified as potential phosphorylation sites in the NS5A protein; however the exact position and number of these sites is still unclear [101]. A variety of kinase enzymes have been shown to phosphorylate the NS5A protein; including casein kinase II (CKII), which is responsible for basal phosphorylation of residues located in domain 2 and 3; and casein kinase Iα (CKIα), which is responsible for hyperphosphorylation of residues in domain 2 [95, 101].

Alongside the role of NS5A in the regulation of genome replication and virus assembly, it has also been shown to interact with host proteins involved proliferation, apoptosis and stress response pathways; including p53 [102], phosphatidylinositol 3 kinase (PI3K) [103] and protein kinase R (PKR) [104].

NS5B is a membrane-associated protein that acts as the RNA-dependent RNA polymerase during HCV infection, synthesising positive and negative HCV RNA strands. It uses a de-novo mechanism to initiate RNA synthesis, and prefentially

replicates the positive RNA strand to facilitate accumulation of the viral genome for rapid production of nascent virus particles [61, 105]. It is not clear whether NS5B acts as a monomer or a higher-order oligomer during RNA synthesis; however, a recent study demonstrated that NS5B is likely to act as a dimer, which undergoes a conformational change for activation [106]. The activity of the polymerase enzyme is tightly regulated by the binding of both virus and cellular proteins. HCV proteins that control NS5B activity include the uncleaved form of the NS2/NS3 protease, which inhibits polymerase activity in a negative feedback mechanism [107]; NS3, which controls dsRNA unwinding during template replication [105]; and NS5A, which stimulates initiation of replication for the positive RNA strand, and promotes the elongation phase of RNA synthesis [96]. NS4B has also been shown to negatively regulate the activity of NS5B by interacting with NS3 to inhibit its NTPase activity and block helicase function [105]. NS5B polymerase activity can also be modulated by the binding of cellular proteins. These include: nucleolin, an RNA chaperone [108]; Atg5, an autophagy protein which may facilitate initiation of viral replication [31]; p68, an RNA helicase which is required for negative strand synthesis [109]; and VAP-A and B, which control structural organisation of the replication complex [97]. The phosphorylation status of NS5B has also been shown to control polymerase function, as phosphorylation at the N-terminus of NS5B by protein kinase C-related kinase 2 (PRK2) is essential for HCV genome replication [110].

1.5 The role of cellular host factors in the HCV replication cycle

The HCV genome encodes only a small number of virus proteins, and as a result the HCV replication cycle is heavily dependent on a range of cellular host factors that perform both structural and functional roles. Some examples of factors involved in the HCV replication cycle include:

1.5.1 Host factors with a role in genome translation and replication

La Autoantigen (La)

La autoantigen is an RNA-binding phosphoprotein that protects the 3'UUU-OH tails on newly synthesised RNA polymerase III transcripts. In HCV infected cells, La has been shown to interact with the 5' and 3' NTR regions of the HCV genome to stimulate its translation and replication. Binding at the 5'NTR occurs via stem loop IV at the AUG initiation codon and binding at the 3'NTR occurs via the poly

U/UC tract [111]. Further investigation into the expression of La protein during HCV infection has demonstrated that the expression of La is upregulated following JFH-1 infection of Huh7.5 cells [112]

Vesicle associated proteins A and B (VAP-A and VAP-B)

VAP proteins localise to the ER and Golgi body membrane to regulate the processes of vesicular trafficking and membrane fusion. VAP-A and VAP-B can interact with each other to form homo- and heterodimers, and can also interact directly with NS5A and NS5B. These interactions mediate indirect binding between NS5A and NS5B and are essential for structural formation of the HCV replication complex [97].

Autophagy related proteins (Atgs)

Autophagy is the process responsible for degradation of unwanted cellular components, bacterial inclusions and unfolded proteins, which become encapsulated in a double membrane compartment (autophagosome) that is targeted for lysosomal degradation. During HCV infection, an increase is observed in the formation of autophagosomes [113], which have been shown to colocalise with HCV proteins (e.g NS4B and NS5B) and the HCV membranous web [28, 31]. Direct interaction has also been observed between the autophagy protein, Atg5 and HCV NS5B [31]. These findings indicate that the vesicles formed by autophagosomes may contribute to the HCV membranous web [28], and the proteins regulating autophagosome formation may be directly involved in HCV genome replication. This is further supported by the observation that knockdown of key autophagy proteins reduces replication and translation of the HCV genome [31, 113]. However, these proteins are required only for the initiation of HCV replication and translation, as silencing of autophagy proteins in cells containing pre-established replication complexes does not alter HCV genome replication or translation [113]. Furthermore, colocalisation of Atg5 and NS5B was observed during the early stages of infection (2 days post-infection), but not at the later stages of infection (5 days post-infection) [31].

Phosphatidylinositol 4 Kinase Type 3 alpha (PI4KIIIα)

PI4KIII*α* is an ER-localised kinase that phosphorylates the membrane phospholipid, phosphatidylinositol to phosphatidylinositol 4 phosphate (PI4P). Further kinase action by other enzymes results in the generation of

phosphatidylinositol 4,5 bisphosphate and phosphatidylinositol 3,4,5 triphosphate. Together these phospholipids act as substrates for the initiation of intracellular signalling cascades, and as docking points for other cellular proteins [99]. Through siRNA silencing experiments, PI4KIIIα has been to shown to play an essential role in HCV genome replication [99, 114-116]. Its kinase activity is stimulated through interaction with HCV NS5A (via domain 1), which recruits PI4KIIIα to the site of HCV genome replication and induces an increase in the production of PI4P [99]. This has been shown to be important for maintaining the correct formation of the HCV membranous web structure, which may be dependent on the creation of phospholipid docking sites that recruit cellular and viral proteins required during membranous web formation [115]. One example of a key host cellular protein recruited to PI4P that is also an essential HCV cofactor is the oxysterol binding protein (OSBP) [99]. Other studies have demonstrated that PI4KIIIβ is also required for membranous web formation, and that PI4KIIIα and PI4KIIIβ may both play an additional role in HCV entry [117].

MicroRNA 122 (miR122)

Alongside the role of cellular proteins as cofactors in the HCV replication cycle, other host cellular molecules, such as RNA, have also been implicated. One example is miR122, a liver-specific microRNA that regulates host gene expression by targeting specific mRNA molecules for degradation. In the HCV replication cycle, miR122 adopts an unusual role and directly simulates the translation and replication of the HCV genome following binding at the 5'NTR. Two miR122 binding sites have been identified within the 5'NTR and are localised between stem loops I and II [118]. Alongside the direct binding of the HCV genome, miR122 also regulates the availability of lipid metabolites required during HCV infection, as it stimulates the expression of genes involved in the synthesis of fatty acids and cholesterol [119]. These lipid molecules are required for production of lipid droplets, intracellular membrane and VLDL particles and are important for efficient HCV replication and secretion. MiR122 is thought to stimulate the expression of these lipid synthesis genes through downregulation of host factors that usually inhibit gene transcription [119]. However, despite the regulation of lipid metabolism by miR122, this function is not responsible for the key role of miR122 in the HCV replication cycle, which is primarily associated with the binding of miR122 to the HCV genome [120]. Recently, Ago2, an argonaute protein present in the RNA induced silencing complex (RISC), was identified as a potential factor involved in

miR122 mediated stimulation of HCV genome translation and HCV RNA accumulation. These findings indicate that miR122 may facilitate recruitment of an Ago2 containing complex to the HCV genome during the HCV replication cycle [121].

1.5.2 Host factors with a role in assembly and secretion

Annexin A2 (ANXA2)

ANXA2 is a cytosolic protein that localises to membranous lipid rafts following calcium dependent binding of negatively charged membrane phospholipids (e.g. phosphatidylinositol (4,5) bisphosphate (PIP2)). ANXA2 can also bind directly to F-actin allowing lipid raft regions of the membrane to be connected with the actin cytoskeleton. As a result of these interactions, ANXA2 has been shown to play a role in the trafficking of membrane during MVB biogenesis, recycling of plasma membrane receptors and calcium induced exocytosis of secretory granules. During the HCV replication cycle, ANXA2 colocalises with HCV NS5A (domain 3), and is required for assembly of nascent virus particles. This may depend on the ability of ANXA2 to link to virus assembly sites with the actin cytoskeleton or it may reflect the role of ANXA2 in membrane organisation, which may be required for virion morphogenesis [57].

ADP Ribosylation factor 1 (ARF1)

ARF1 is a small GTPase protein that localises to the Golgi body to control membrane trafficking during intra-Golgi transport and VLDL synthesis. Membrane localised effector proteins activated by ARF1 include phospholipase D1 (PLD), the COPI complex (coat protein complex I), and PI4K. Inactive GDP-bound ARF1 has also been shown to localise to the surface of intracellular lipid droplets. ARF1 activity is required during HCV infection to control genome replication, virus assembly and virus secretion [51]. The role of ARF1 in HCV replication may be associated with its ability to activate COPI [114], and PI4K [99, 115], both of which have recently been identified as essential HCV replication cofactors. In addition, golgi brefeldin A resistant guanine nucleotide exchange factor 1 (GBF1), an ARF1 guanine exchange factor protein, has also recently been shown to control the activity of HCV replication complexes [122]. ARF1 may also play a role in the assembly and secretion of HCV particles by controlling the distribution of HCV proteins between the Golgi body and the lipid droplet surface. HCV NS5A has been shown to increase the abundance of inactive GDP-bound ARF1, which

promotes the trafficking of NS5A to lipid droplets for virus assembly [51]. This indicates that NS5A may play an essential role in the switch from HCV genome replication to assembly. The ability of ARF1 to control HCV assembly and secretion may also be associated with its role in VLDL synthesis, which is required for HCV assembly and secretion [47, 51].

Oxysterol binding protein (OSBP) and Ceramide transfer protein (CERT)

OSBP is a cytosolic lipid-binding protein that localises to the *trans* golgi network (TGN) to control trafficking of cholesterol and hydroxycholesterol from the ER. To perform its trafficking function, OSBP binds to both the VAP-A protein present in the ER and the phosphatidylinositol 4-phosphate (PI4P) membrane phospholipid in the TGN membrane allowing the two membrane sites to be connected for lipid transfer. CERT is functionally homologous to OSBP and is responsible for trafficking of ceramide from the ER to the TGN facilitating sphingolipid synthesis at the TGN membrane [56]. The functions of both OSBP and CERT have been shown to be essential for the secretion of HCV particles [56], and OSBP has been shown to bind directly to the HCV NS5A protein (domain 1) at the Golgi body [94]. Further support for the role of OSBP and CERT in the secretion of HCV was observed recently, as HCV infection was also shown to inhibit the activity of the protein kinase D (PKD) enzyme, which phosphorylates and inactivates OSBP and CERT. Furthermore, knockdown of PKD protein by shRNA transfection or enzymatic inhibition of PKD function enhanced the secretion of HCV particles from infected cells further supporting the observation that OSBP and CERT are key host factors involved in the HCV replication cycle [56]. The observation that Golgi localised proteins are important for the HCV secretory process provides further evidence to indicate that HCV particles may be co-secreted with VLDL particles, which are also thought to be secreted via the Golgi body [94].

In addition to the role that these factors play in the HCV replication cycle, there are many other examples of host factors shown to be essential for HCV infection. Some of these are summarised in **Table 1.1**.

Host factors with a role in genome translation and replication		
Host protein	**HCV interaction partner/s**	**Role in the HCV replication cycle**
hnRNPA1 /Septin 6	HCV RNA (5' and 3'NTR) and NS5B	HCV genome replication. May facilitate NS5B localisation on the HCV RNA [123].
RNA helicase A / NFAR1/ NFAR2 / NF45	HCV RNA (5' and 3'NTR) and NS5A (NFAR1 only)	Looping of HCV RNA at 5' and 3' NTRs. May coordinate translation and replication [36].
PTB	HCV RNA (5' and 3' NTR), NS3 and NS5B	Regulation of HCV genome translation and replication [20, 111].
HuR	HCV RNA (3' NTR) / HCV antisense RNA (5' NTR)	Required for HCV genome translation [21, 124].
Complex of p54, LSm1 and PatL1	HCV RNA (5' and 3' NTR)	Required for HCV genome replication and translation [37].
IGF2BP1	HCV RNA (5' and 3'NTR)	Required for HCV genome translation. Recruits the eIF3 translation initiation factor [125].
Cyclophilin A and B	NS5A and NS5B	Required for HCV genome replication. May facilitate folding of NS5A and NS5B [98].
FBL2	NS5A	Required for HCV genome replication [126].
FBP	HCV RNA (3'NTR) and NS5A	Required for HCV genome replication. May regulate replication to translation switch [127].
TBC1D20 (RAB1B GAP)	NS5A	TBC1D20 and RAB1B both required for effective HCV genome replication. May regulate membranous web formation [128].
Rab GTPase 5	NS4B	Potential role in membranous web formation [30].
G3BP1	NS5B	Potential component of the HCV replication complex controlling genome replication [129].
Human Butyrate Transcript 1	NS5A	Complexes with FKBP8, Hsp90 and NS5A to facilitate HCV replication [130].

Host factors with a role in assembly and secretion		
Host protein	**HCV interaction partner/s**	**Role in the HCV replication cycle**
DGAT1	Core	Trafficking of HCV core to lipid droplets [59]
HSC70	Core and E2	May participate in virus particle assembly, budding or secretion [44]. Potential virion component.

Table 1.1 Host factors involved in the HCV replication cycle

1.5.3 Host factors involved in the production of HCV-essential metabolites

Several of the host factors shown to be essential for HCV infection do not play a direct structural or functional role in the HCV replication cycle. Instead, they play an important role in the synthesis and modification of the cellular metabolites that are required during HCV infection. Examples include the enzymes involved in the metabolism of intracellular lipids, which are essential for many aspects of the HCV replication cycle.

Serine palmitoyltransferase (SPT)

SPT catalyses the first step in the biosynthesis of sphingolipids allowing condensation of L-serine and palmitoyl CoA [131]. Sphingolipids are key components of the intracellular membrane localising to lipid raft regions of the Golgi body and plasma membrane to control membrane fluidity. The replication complexes of HCV have been shown to colocalise predominantly with lipid raft regions of membrane, which assemble into the membranous web structure [32]. Inhibitors of SPT activity reduce the production of key cellular sphingolipids including ceramide and sphingomyelin, and significantly reduce the replication of HCV due to inhibition of membranous web formation [131].

3-hydroxy-3-methylglutaryl coenzyme A reductase (HMGCR)

HMGCR catalyses the rate limiting step in the mevalonate cholesterol biosynthesis pathway, in which HMG-CoA is converted to mevalonic acid. This pathway is responsible for the production of cholesterol, geranylgeranyl and farnesyl lipids. Studies have demonstrated that inhibition of this enzyme significantly reduces HCV replication [131, 132]. A key role of HMGCR in the HCV replication cycle is associated with the production of geranylgeranyl lipids, which are used to post-translationally modify cellular host proteins facilitating membrane localisation [132]. A number of key host proteins required during the HCV replication cycle are modified by geranylgeranylation, including FBL2 [126] and Rab GTPase proteins [30, 128]. HMGCR inhibition may also reduce HCV replication because of the key role that cholesterol plays in the formation of the membranous lipid rafts that generate the HCV membranous web [32], and in the formation of the lipid metabolite, cholesterol ester, which is used for production of lipid droplets and VLDL particles, both of which play essential roles in HCV assembly and secretion [39, 47, 132].

Long chain acyl-CoA synthetase 3 (ACSL3)

ACSL3 catalyses the addition of CoenzymeA to long chain fatty acids producing fatty acyl-CoA esters, which are used to generate triglycerides, phospholipids and cholesterol esters. ACSL3 has been shown to play an essential role in VLDL synthesis through the production of the phospholipid, phophatidylcholine, which is a major component of the VLDL particle. VLDL synthesis is required for the assembly and secretion of HCV and through its direct role in VLDL synthesis, ACSL3 has been shown to be an important cofactor of the HCV replication cycle [50].

1.5.4 The role of the cellular cytoskeleton in the HCV replication cycle

Microtubule and actin filaments are cytoskeletal components of the cell which form a series of intracellular transport networks. Microtubule filaments are responsible for transporting membranous organelles and various proteins to specific cellular locations. Actin filaments are involved in regulating the processes of cell adhesion, cell motility, endocytosis and exocytosis [133]. As a result of these functions, microtubule and actin filaments play an essential role in many aspects of the HCV replication cycle. The HCV core protein is able to bind directly to microtubule filaments, which facilitates trafficking of the virus particle during entry [134] and enables relocalisation of core-coated lipid droplets during virus assembly [60]. The NS3/4A complex and NS5A protein also interact with microtubule and actin filaments to enable trafficking of HCV replication complexes during the switch from genome replication to assembly [133].

1.6 *In vitro* and *in vivo* systems for studying the HCV replication cycle

1.6.1 In vitro systems for studying the HCV replication cycle

Molecular cloning of the HCV genome

In vitro studies investigating the cellular mechanisms involved in the HCV replication cycle were limited for many years because of an inability to culture serum derived virus in the laboratory. Obtaining the first consensus sequence of the HCV genome enabled studies to be performed that investigated the functional properties of the individual virus proteins. Additional consensus genomes for other HCV isolates were also obtained allowing comparison of the proteins encoded by different virus strains. However, despite numerous efforts and the observation that the HCV clones generated produced infectious virus particles in chimpanzee,

transfection of *in vitro* cultured cells with the RNA genome of these clones did not permit virus replication or production of infectious particles at a detectable level. Thus, for many years research was limited to studying the HCV proteins in isolation, with no possible way of investigating the different processes of the HCV replication cycle [18].

The first system developed which enabled observation of HCV genome translation and replication was the subgenomic replicon [33]. Subgenomic replicons are RNA molecules containing the HCV non-structural genes (NS2-NS5B), HCV NTRs, and a selectable marker gene (e.g. neomycin resistance (neomycin-phosphotransferase) gene), which replaces the structural genes in the genome (**Fig. 1.3**). Protein expression from the replicon allows the assembly of replication complexes and replication of the replicon RNA. The presence of the selectable marker gene (e.g. neomycin resistance) means that stable cell lines expressing the replicon construct can be generated by selecting for replicon expressing cells in the presence of a selection agent (e.g. neomycin (Geneticin)). Occasionally, replicon constructs may also contain a reporter gene (e.g. luciferase gene) alongside or in place of the selectable marker gene, allowing replication of the replicon RNA to be directly quantified through analysis of the luciferase signal [18]. To date, several different subgenomic replicons have been developed for HCV clones that represent genotype 1a, 1b and 2a HCV strains. For almost all of the subgenomic replicons developed, cell culture adaptive mutations have been observed to occur in the sequence of the replicon RNA. These mutations are thought to facilitate adaptation of the virus proteins to function effectively in tissue culture, the conditions of which differ to those found in the liver [18]. Although subgenomic replicons allowed HCV genome translation and replication to be studied for the first time, the processes of virus assembly and budding do not occur, and it is not possible to generate infectious virions. Attempts were made to clone the sequences of the cell culture adapted subgenomic replicons back onto the full genome with the original structural proteins. However, infectious virions could not be generated with the full-length genomes created, either in tissue culture, or in chimpanzee even though the genome was observed to undergo active replication [18].



Figure 1.3 HCV subgenomic replicon gene organisation [18]

*In the HCV subgenomic replicon, the HCV structural proteins of the full-length genome (**Fig. 1.1**) are replaced with a gene coding for neomycin resistance (neomycin phosphotransferase (npt)) followed by the IRES of the encephalomyocarditis virus (EMCV IRES). The 5' and 3'NTR regions of the HCV genome are positioned at either end of the replicon. The 5'NTR HCV IRES directs translation of the npt gene and the EMCV IRES drives translation of the non-structural HCV proteins; including NS2 (2), NS3 (3), NS4A (4A), NS4B (4B), NS5A (5A) and NS5B (5B). The presence of both 5' and 3' NTR regions of the HCV genome ensures that the replicon RNA molecule is efficiently replicated.*

A breakthrough occurred in HCV research with the discovery of JFH-1 (Japanese fulminant hepatitis 1), a genotype 2a HCV isolate. The clone of this isolate demonstrated the capacity to replicate at high levels in cell culture to produce high titres of infectious virions without developing cell culture adapted mutations [135]. The discovery of JFH-1 meant that the complete HCV replication cycle, including the processes of virus entry, assembly and secretion, could finally be studied for the first time in cell culture. The ability of JFH-1 to produce infectious virions has been attributed to the unique capacity of the clone to replicate *in vitro* without the need for cell culture adapted mutations. Studies have now shown that it was the presence of these mutations in the genome of other HCV clones that interfered with their abilities to produce infectious virions [18, 136]. Since the discovery of JFH-1, other full-length HCV clones with the capacity to produce infectious virions have also been generated. These include: H77S, a genotype 1a clone, which produces infectious virions at a much lower rate than JFH-1 [137]; and Jc1, a chimeric virus that was generated using sequences from JFH-1 and another genotype 2a virus known as J6 [138]. In comparison to JFH-1, Jc1 produces even higher titres of infectious virions and is often used in studies investigating the HCV replication cycle [18].

Cell culture systems that support efficient HCV propagation

To study the role of virus and host proteins during the HCV replication cycle, several different immortalised human hepatoma cell lines are currently available. The most widely used is the Huh7 cell line, which has been shown to successfully

support HCV replication and production of infectious virions [135]. Derivatives of this cell line have been produced following interferon-α curing of Huh7 cells containing HCV subgenomic replicons [139]. These derivatives display enhanced permissiveness to the replication of HCV RNA and production of infectious virions in comparison to the parental Huh7 cell line. One of the most frequently used Huh7 cell derivatives is the Huh7.5 cell line, which was generated following curing of Huh7 cells containing a genotype 1b replicon [139]. The increased permissiveness of Huh7.5 cells has been attributed to a mutation identified in the RIG-I gene, which controls the intracellular pathway responsible for inducing interferon β expression in response to viral dsRNA [140]. The mutation present in the RIG-I gene of Huh7.5 cells inactivates the RIG-I protein and prevents activation of the RIG-I antiviral pathway. As a result, Huh7.5 cells are less able to produce interferon in response to viral infection and this facilitates a higher level of HCV replication. Huh7.5 cells have also been shown to express high levels of the HCV entry receptor, CD81, which further increases the permissiveness of the cells to HCV infection [141].

Whilst the majority of studies investigating the HCV replication cycle have been performed using Huh7 cells and their derivatives, several studies have recently been performed to investigate the ability of alternative cell lines to support HCV replication. Some examples of immortalised cell lines shown to support active replication of the JFH-1 genome include other hepatic cell lines such as HepG2 and IMY-N9 cells [142], and non-hepatic cell lines such as the osteosarcoma U20S cell line [143] and neuroepithelioma cells [144]. Some of these cell lines, namely the HepG2 and IMY-N9 cells [142], have also been shown to support production of infectious JFH-1 virions. Although these cell lines have been shown to support JFH-1 replication, the rate at which replication takes place is much lower than that observed in the parental Huh7 cells and the Huh7 cell derivatives, which continue to be the most effective cell line used for studying the process of HCV infection [142-144].

The use of immortalised cell lines for investigation of the HCV replication cycle provides a simple cell culture system that is easy to use and allows continuous propagation of cells. The drawback to this type of system is that the cells used are de-differentiated, non-polarised and grow in a monolayer. This is different to the environment observed in the liver where hepatocytes grow as differentiated,

polarised, non-dividing cells in a complex 3-dimensional structure [145]. The use of primary human hepatocytes isolated from patients is one way in which it is possible to achieve an infectious cell culture system that better reflects the characteristics of *in vivo* infection [145]. Techniques for culturing primary human hepatocytes have significantly improved in recent years. Studies have demonstrated that these cells can be successfully infected with both serum derived [146, 147] and cell culture grown HCV [145] resulting in replication of the virus genome and secretion of infectious virions. Despite the improved biological significance of using cultured primary hepatocytes, most laboratories still do not routinely use these cells, as they are difficult to obtain, costly and non-dividing preventing them being used for long-term culture. As a result, Huh7 cells and their derivatives remain the most widely used cell culture system for studying the HCV replication cycle.

1.6.2 In vivo systems for studying the HCV replication cycle

The *in vitro* cell culture systems used in HCV research are useful for providing an initial insight into the processes involved in the virus replication cycle. However, these systems will always be limited by their inability to provide a true representation of *in vivo* infection. Furthermore, they do not permit investigation of the complex interactions between the immune system of the host and the infected liver hepatocytes. To facilitate characterisation of the complete HCV replication cycle and the host immune response to infection, several different approaches are used to study the process of HCV infection in its *in vivo* environment [148].

One of the most widely used approaches involves the analysis of liver biopsy material isolated from chronically infected patients. Biopsy material is often used to investigate host response to infection by quantifying changes at the mRNA or protein level and comparing host factor expression with that observed in uninfected individuals [149, 150]. Although these experiments provide a direct insight into the events occurring in HCV infected patients, they are often difficult to perform because of the heterogeneous nature of biopsy tissue, the complexity of identifying well matched uninfected controls and the limited amount of biopsy material available for use.

One solution to these problems is the use of animal models that can be readily infected with HCV allowing controlled experiments to be performed. Unfortunately,

there is no small animal model available that can be naturally infected with HCV and the only laboratory animal with permissiveness to HCV infection is the chimpanzee [148], which is now rarely used due to ethical concern and high costs [148, 151]. Instead, significant advances have been made in the development of mouse models that can be infected with HCV. One model developed is the UpA/SCID (urokinase-type plasminogen activator / severe combined immunodeficient) mouse, which is transplanted with human hepatocytes that can be readily infected with HCV [148, 151, 152]. Although the human hepatocytes can be successfully infected with HCV, the mice are immunocompromised to prevent immune rejection of the human liver transplant, and this prevents studies investigating the host immune response to HCV infection [148, 153]. A more recently developed mouse model for HCV infection overcomes this problem by creating a humanised mouse with a functional human immune system (AFC8-hu HSC/Hep) in addition to the grafting of human hepatocytes [153]. These latest developments in generating an immunocompetent animal model for HCV infection means that complete *in vivo* studies of the host cell response to infection can now be performed.

1.7 Experimental approaches used to study the HCV replication cycle

A wide range of different *in vitro* and *in vivo* systems are available for studying the processes involved in the HCV replication cycle. Using these systems, a number of different approaches have been adopted to investigate the specific roles of virus and host proteins in the HCV replication cycle. These include:

1.7.1 Protein capture assays

Protein capture assays, such as the yeast 2 hybrid system and co-immunoprecipitation experiments, were some of the first techniques used to investigate the interactions that form between HCV and the host cell. These assays focus upon the identification of host proteins capable of interaction either with individual virus proteins [97], HCV replication complexes [154] or the HCV RNA genome [155, 156]. As a result of these studies, many host proteins with a role in HCV replication have been identified. Some well-known examples include: VAP-A and VAP-B, which interact with NS5A and NS5B [97]; FBL2, which interacts with NS5A [126]; and HuR, which interacts with the HCV RNA genome [124]. Nowadays, these techniques are routinely used to further investigate host

cell-virus interactions that have been identified by other genome-wide studies of the HCV replication cycle.

1.7.2 Genomic studies of HCV infection

The advent of the genomic era in recent years has introduced a new approach to studying the HCV replication cycle; instead of focusing on individual host factors, the whole genome content of a cell can be studied. As a result, it has been possible to study the effect of HCV infection or the presence of HCV proteins on the entire mRNA expression profile of the host cell. Microarray hybridisation technology is routinely used to characterise the gene expression profile of the complete human transcriptome in mammalian cells. This technology has been used to investigate the effect of HCV proteins on cellular gene expression in a wide range of samples; including cells transfected with individual virus proteins [157, 158], cells transfected with subgenomic replicons [159, 160] and liver biopsies from chronically infected HCV patients [149] and HCV infected chimpanzee [161-163]. Due to the recent development of the infectious HCV cell culture system, several studies investigating the gene expression profile of cells infected with full-length HCV have also been performed [149, 164, 165].

Microarray analysis of cells expressing the HCV genome or parts of the genome may facilitate identification of host factors involved in the HCV replication cycle. This is because genes encoding host factors that are required for effective replication of HCV may increase in expression as a result of the HCV replication cycle. These gene expression changes may occur as a result of feedback mechanisms, if the demand for a host factor or host metabolite increases during HCV infection. Alternatively, proteins encoded by HCV may be able to directly alter gene transcription through interactions that form with cellular transcription factors. Analysis of gene expression patterns induced by the HCV replication cycle can also provide insight into host genes involved in cellular antiviral responses, and genes that contribute to HCV-associated liver pathology.

A comparison of genomic studies performed to date indicates that a common set of intracellular pathways are affected during the HCV replication cycle. Key cellular pathways observed to be significantly regulated include:

- **Lipid metabolism.** Host genes controlling intracellular lipid synthesis have been shown to increase in expression in the presence of HCV proteins. HCV

NS4B [90] and core [66] have been shown to increase the expression of SREBF1; and NS5A has been shown to increase the expression of PPARγ [166]. Both of these genes encode transcription factors that control the expression of lipid synthesis genes. An increase in the expression of cholesterol synthesis genes and SREBF1 has also been observed in cells transfected with genotype 1b and 2a subgenomic replicons [159]. The HCV replication cycle relies heavily upon intracellular lipids, particularly those involved in the formation of membranous lipid rafts [32] and intracellular lipid droplets [39], and in the process of VLDL synthesis [47]. Increases in the expression of genes controlling lipid metabolite abundance may be a mechanism that HCV uses to promote virus replication and production of nascent virus particles. These gene expression patterns may also provide an explanation as to why chronically infected patients often develop liver steatosis [167].

- **Cellular immunity.** Genes involved in host innate immune responses increase in expression in the presence of HCV proteins. An increase in the expression of genes controlling the interferon response and cytokine expression was observed in Huh7.5 cells infected with Jc1 (e.g. interferon stimulated gene 15 (ISG15), interleukin 8 (IL8) and chemokine (c-x-c motif) ligand 1 (CXCL1)) [149]. Induction of an interferon response during HCV infection has also been observed in the livers of acutely infected chimpanzee, which involved an increase in the expression of ISG15, 2'-5' oligoadenylate synthase 1 and 2 (OAS1, OAS2), myxovirus resistance 1 (MX1), and signal transducer and activator of transcription 1 (STAT1) [163]. The ability of HCV to stimulate the expression of these proinflammatory genes indicates that the high levels of inflammation observed in chronically infected patients [168] may occur as a result of the host cell response induced in the HCV infected hepatocytes.
- **Proliferation and apoptosis.** HCV proteins have been shown to alter the expression of genes regulating cellular proliferation and apoptosis to control cellular survival of HCV infected cells. In Huh7.5 cells infected with Jc1, perturbations in the expression of genes controlling p53 activation, cell cycle progression, mitochondrial cytochrome c release and transforming growth factor β (TGFβ) signalling were observed [149], leading to increased rates of cell cycle arrest and apoptosis. These observations indicate that chronically

infected patients may suffer from significant liver destruction as a result of increased hepatocyte apoptosis induced by HCV infection. However, conflicting results have been observed in studies investigating the effects of individual HCV proteins, which instead alter host gene expression to promote an increase in cellular proliferation and survival. One example is the increase observed in the expression of the transcription factor, STAT3, when the HCV core protein is overexpressed in primary human hepatocytes [157]. STAT3 controls the expression of genes promoting cellular proliferation; therefore, induction of STAT3 signalling by HCV core may promote survival of HCV infected cells to facilitate establishment of a persistent infection.

- **Molecular transport.** Several studies have demonstrated that HCV proteins can alter the expression of genes controlling intracellular transport and regulation of the actin and microtubule cytoskeleton networks. Transfection of a full-length genotype 1b HCV genome into Huh7 cells induced an increase in the expression of tubulin beta 2A (TUBB2A), a key component of microtubule filaments; centromere protein E (CENPE), a microtubule binding protein; and metastasis suppressor 1 (MTSS1), an actin binding protein [169]. Both actin and microtubule filaments have been shown to be essential for trafficking of virus components during the HCV replication cycle [60, 133, 134]. Increased expression of genes controlling the function of these filaments indicates that these factors may be important for correct functioning of cytoskeleton transport during HCV infection.

From these published genomic studies it is possible to gain insight into the mechanisms that may contribute to HCV-associated pathogenesis. HCV induced expression patterns have been observed that may contribute to the development of hepatic steatosis [167] and inflammation [168], and hepatocyte destruction [170]. The expression patterns observed also facilitate identification of host factors that may be required during the HCV replication cycle. This includes host genes that regulate the synthesis of key intracellular lipid metabolites and the functioning of the intracellular cytoskeleton, which are both processes that have previously been shown to be essential for the HCV replication cycle. Although there is good consistency in the overall cellular pathways affected by HCV protein expression, there is often little overlap in the host genes that alter in expression between different genomic studies. These differences most likely reflect variation in the

experimental systems used, as comparisons have been made between the expression profiles observed in patient biopsy tissue, HCV infected primary hepatocytes and HCV infected hepatoma cell lines.

Many of the genomic studies performed to date investigate the host response to either individual HCV proteins [157, 158] or subgenomic replicons [159, 160]. Whilst these studies provide an interesting insight into the HCV replication cycle, the biological significance of gene expression patterns identified is less clear since the full virus replication cycle, including the processes of viral entry, assembly and exit, does not take place. Several studies have recently been described that overcome these limitations by investigating the effect of the complete HCV replication cycle on host gene expression [149, 164, 165]. Comparison of the findings from these studies to those investigating only part of the HCV replication cycle demonstrates that many more host genes are regulated when the complete HCV replication cycle takes place; this indicates that the processes of virus entry, assembly and secretion have many additional effects on host gene expression. Much more detailed analysis of the effects that the complete HCV replication cycle has on host gene expression is now required to enable characterisation of the full host response to infection and facilitate a greater understanding of the complex interactions between HCV and the host cell.

1.7.3 Proteomic studies of HCV infection

In addition to identifying the gene expression patterns associated with HCV infection, it is also important to investigate the effect of HCV protein expression on the abundance of intracellular host proteins. This is because changes at the mRNA level are not always reflected at the protein level due to the actions of additional post-transcriptional and post-translational regulatory mechanisms [150].

Proteomic profiling has been performed for cells transfected with HCV subgenomic replicons [171], cells transfected [172] or infected with full-length HCV [150, 164], and for liver biopsies isolated from chronically infected patients [150]. Consistent with the findings of genomic studies, HCV proteins have been shown to regulate the expression of host proteins involved in antiviral responses, and cellular pathways that regulate key processes required for efficient HCV replication. To date, two studies have been performed that investigate the effect of Jc1 infection on host protein expression in Huh7.5 cells. Both studies demonstrated that

proteins involved in lipid and carbohydrate metabolism, and oxidative stress significantly altered in abundance as a result of infection [150, 164]. Another study investigating Huh7 cells transfected with a genotype 1b HCV genome, observed alterations in the abundance of proteins that regulate the host cell cytoskeleton, intracellular trafficking, molecular chaperones, apoptosis, protein degradation, oxidative and ER stress, cell cycle progression, antigen presentation, and calcium homeostasis [172]. Studies have also been performed to investigate the proteomic profile of specific subcellular fractions in the presence of HCV proteins. For example, one study investigating the lipid raft proteome of HCV replicon cells demonstrated that 150 proteins out of 1036 proteins altered in abundance as a result of HCV protein expression. Proteins observed to increase in abundance included those involved in: vesicular trafficking, cellular signalling and apoptosis, protein processing and protein biosynthesis [173].

Comparison of the data observed through genomic and proteomic studies of HCV infected cells will facilitate accurate characterisation of the host cell response to infection. Further investigation of host factors consistently affected in both studies may facilitate identification of novel host factors involved in the HCV replication cycle and enable an increased understanding of the mechanisms contributing to the pathogenesis of infection.

Alongside investigations into the abundance of host proteins during HCV infection, it is also important to consider the effects that HCV infection might have on the post-translational modification of host proteins. It is possible that there are many host proteins which display altered activity levels during HCV infection due to alterations in their post-translational modification patterns rather than alterations in their mRNA or protein expression level. Little work has been done to characterise the effect of HCV infection on global post-translational modification; however, there are several examples of individual host proteins which display altered modification patterns during HCV infection. For example, the phosphorylation pattern of AMP activated protein kinase (AMPK), a global regulator of ATP production, has been observed to alter significantly during the HCV replication cycle [174]. In cells expressing either a HCV subgenomic replicon or a full-length HCV genome, a decrease was observed in the phosphorylation of the AMPK threonine 172 residue, usually required to activate AMPK activity, whilst an increase was observed in the phosphorylation of AMPK serine 485, usually

required to inhibit AMPK activity. This resulted in an overall decrease in AMPK activity during the HCV replication cycle [174]. This example demonstrates how important it is to analyse the effect of HCV infection on host protein post-translational modification in addition to analysing the host gene and protein expression profiles. Recent developments in the methods for analysing post-translational modification on a global scale will hopefully facilitate studies that investigate the effect of HCV infection on the protein modification patterns of the entire cell [175].

1.7.4 Host factors involved in the replication of other related RNA viruses

The protein capture assays, genomic studies and proteomic studies widely used to investigate the HCV replication cycle often adopt a random screening approach to gain insight into the cellular processes and host factors involved in the HCV replication cycle. An alternative approach, that is much more focused, specifically selects candidate host factors that have previously been shown to play a role in the replication of other RNA viruses to identify potential cofactors involved in the HCV replication cycle. This approach is based on the observation that the replication cycles for different RNA viruses are often similar with overlapping processes for virus replication and secretion [12]. One example is the mechanism used by many viruses for genome replication, which involves the assembly of virus replication complexes inside a protective membranous web structure that is synthesised using cellular organelle membrane components [12]. There is growing evidence to indicate that a common set of host factors may be used by viruses to assemble these structures and perform genome replication. For example, Arf GTPase proteins, which were originally shown to direct membrane reorganisation during poliovirus replication [176], were recently implicated in the replication of the HCV genome and production of infectious virions [51]. Furthermore, proteins regulating the 5'-3' deadenylation dependent mRNA decay pathway have been shown to regulate genome translation and replication for the brome mosaic virus (BMV), which replicates in the yeast *Saccharomyces cerevisiae* model system [177]. Mammalian homologs of these yeast proteins (LSm1-7, PatL1 and p54) have also been shown to regulate translation and replication of the HCV genome [37].

These examples demonstrate how investigation of the host factors shown to be involved in the replication of other RNA viruses may facilitate the identification of

novel factors involved in the replication of RNA viruses with an unknown mechanism. To facilitate the identification of novel host factors involved in the HCV replication cycle, several host factors can be chosen from the replication cycles of other related RNA viruses. Examples of host factors with significant evidence that indicates they might be involved in the HCV replication cycle include: Rab GTPase proteins and RNA binding proteins such as the T cell restricted antigen-1 protein (TIA1), TIA1 protein like-1 (TIAL1) and Staufen1.

Rab GTPase Proteins: Intracellular localisation and function

Rab GTPase proteins are members of the Ras GTPase superfamily that regulate global membrane trafficking in eukaryotic cells. In humans there are over 60 Rab proteins, which localise to specific cellular membrane compartments to facilitate the formation, trafficking, tethering and fusion of intracellular transport vesicles [178, 179]. The function of each Rab protein is dependent on its ability to switch between active GTP-bound and inactive GDP-bound forms at a specific membrane surface. To ensure precise regulation of Rab protein function in cells, several host factors have been identified to control Rab protein activity e.g. GTPase-activating proteins (GAP) and guanine nucleotide exchange factors (GEF); and Rab protein intracellular membrane localisation e.g. the Rab escort protein (REP), geranylgeranyl transferase enzyme (GGT), Rab GDP dissociation inhibitor proteins (GDI) and Rab GDI displacement factors (GDF) (**Fig 1.4**) [179]. Once activated, GTP-bound Rab proteins are able to bind to specific effector proteins such as tethering factors, sorting adaptors and motor proteins. Many of the Rab proteins identified to date have been mapped to a specific cellular location, which is usually associated either with the membrane of a particular intracellular organelle, or trafficking vesicle; this enables each Rab protein to regulate a specific aspect of membrane trafficking within the cell. Examples of membrane trafficking events regulated by Rab GTPase proteins include regulation of endocytosis and exocytosis, protein sorting, protein degradation and the formation of autophagosomes, lipid droplets and melanosomes (**Fig. 1.5 and Table 1.2**) [179]. To facilitate the regulation of these different processes, Rab GTPase proteins have been shown to act in a coordinated fashion through complex regulatory networks. For example, Rab effector proteins can link different Rab proteins by binding to more than one Rab at a time. Rab proteins are also

able to crosstalk by activating or inhibiting the GAP and GEF proteins of other neighbouring Rabs to establish a cascade of Rab protein activity [179].

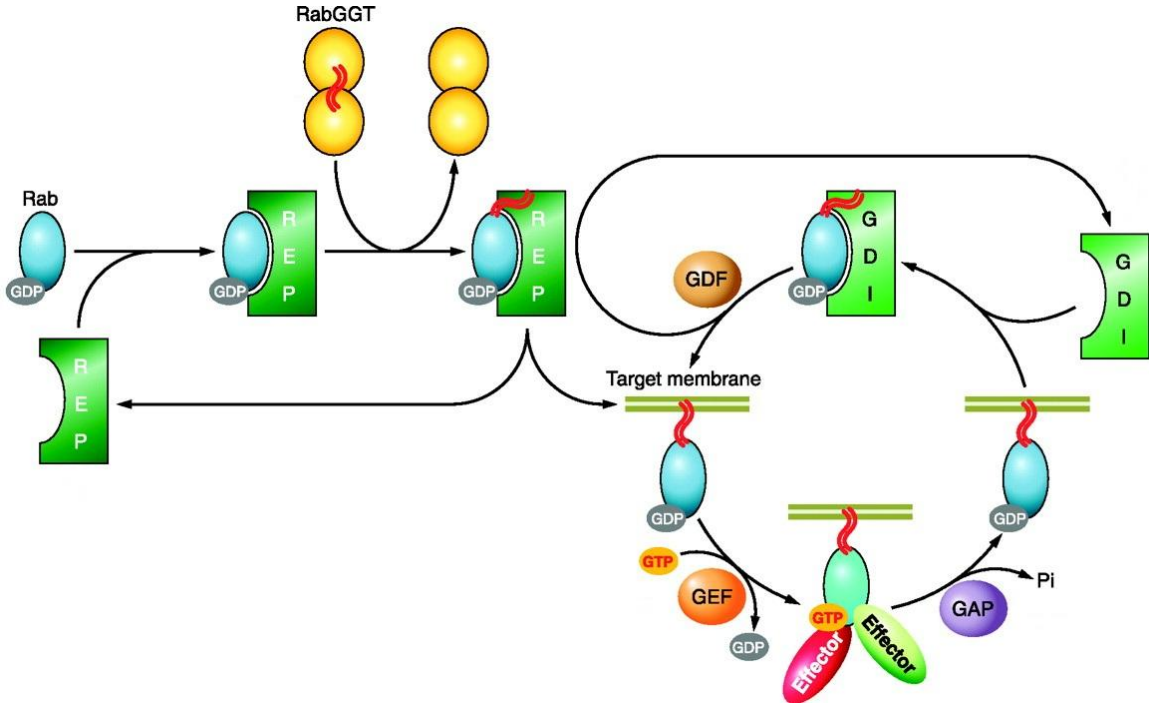


Figure 1.4 Regulators of Rab GTPase protein activity and localisation (adapted from Hutagalung et al) [180]

To ensure that Rab GTPase protein function is tightly controlled, several host proteins are required for the regulation of Rab protein activity and membrane localisation. When a Rab protein is first translated, the Rab escort protein (REP) delivers the GDP-bound Rab to a geranylgeranyl transferase enzyme (RabGGT), which transfers a geranylgeranyl motif (red wavy lines) to one or two C-terminal cysteine residues of the Rab protein. The geranylgeranylated GDP-bound Rab protein is then delivered to the target membrane by the REP protein. A guanine nucleotide exchange factor (GEF) catalyses activation of the Rab protein by exchanging GDP for GTP. The GTP-bound Rab protein is able to bind to its specific effector proteins such as tethering factors, sorting adaptors and motor proteins to perform its membrane trafficking function. The activated GTP-bound Rab then interacts with a GTPase-activating protein (GAP), which catalyses the hydrolysis of GTP to GDP by the Rab GTPase protein. This results in the release of inorganic phosphate (Pi) and prevents association of the Rab protein with its effectors. The inactive GDP-bound Rab is removed from the membrane by interacting with a Rab GDP dissociation inhibitor protein (GDI), which binds specifically to GDP-bound Rab proteins and extracts them from the membrane. The GDI-bound Rab protein can be re-inserted into target membrane by interacting with a Rab GDI displacement factor (GDF), which recognises specific GDI bound Rab proteins and releases the GDI protein from the GDP-bound Rab. The membrane localised GDP-bound Rab is re-activated through interaction with a GEF protein and the Rab activation cycle begins again. Alongside the role of GDF factors in the displacement of GDI for membrane localisation of GDP-bound Rabs, they can also facilitate REP directed membrane insertion of newly translated GDP-bound Rab proteins.

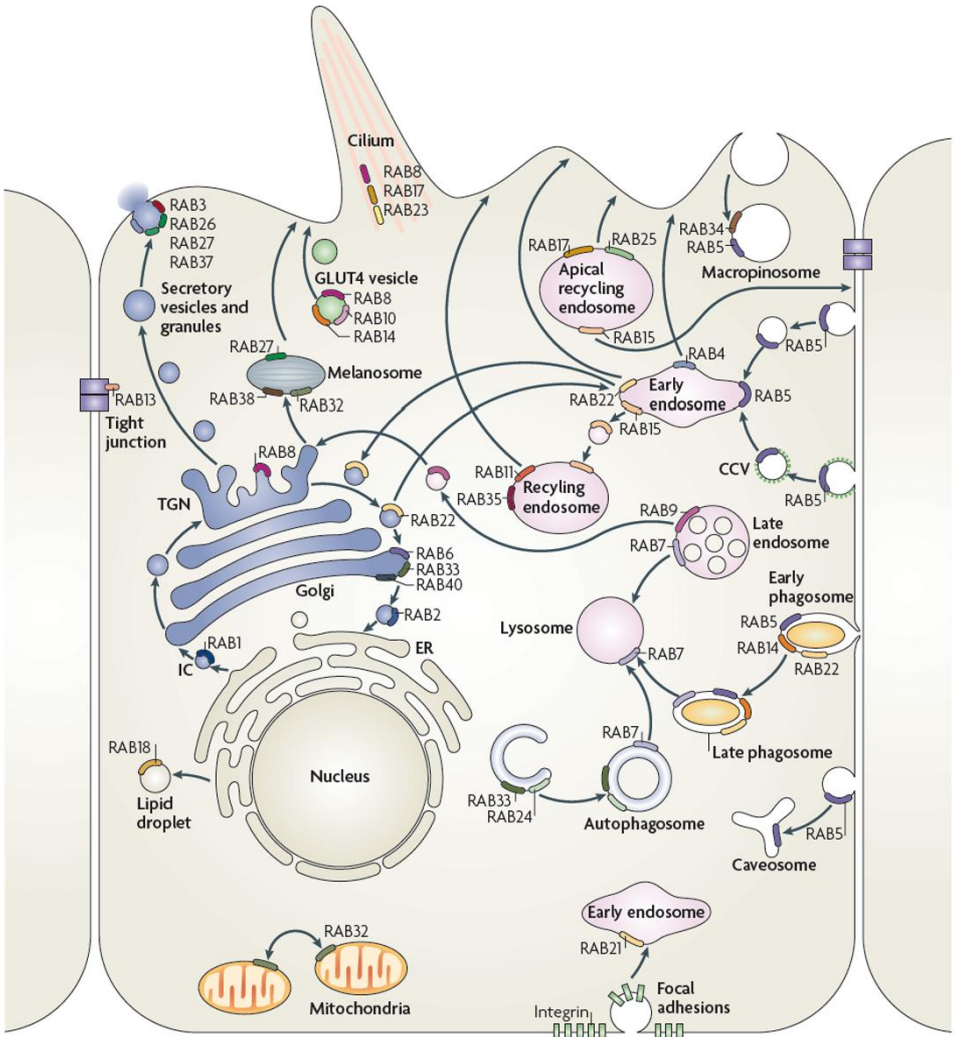


Figure 1.5 Intracellular localisation of the Rab GTPase proteins [179]

The Rab protein regulated vesicular transport pathways in a typical epithelial cell. Pathways include those controlling transport of proteins around the cell, e.g. sorting of proteins by trafficking through the endoplasmic reticulum (ER), Golgi intermediate compartment (IC) and trans-Golgi network (TGN) (RAB1 (ER to Golgi), RAB2 (Golgi to ER), RAB6, 33 and 40 (intra-Golgi)); constitutive biosynthetic trafficking from the TGN to the plasma membrane (RAB8), trafficking between the TGN and early endosomes (RAB22); regulated exocytosis via secretory granules or vesicles (RAB3, 26, 27 and 37); translocation of melanocytes to the cellular periphery (RAB27); GLUT4 vesicle translocation to the plasma membrane (RAB8,10 and 14); endocytosis and endosome fusion of clathrin-coated vesicles (RAB5); integrin endocytosis (RAB21); macropinocytosis (RAB5 and RAB34); maturation of early phagosomes (RAB5, 14 and 22); slow endocytic recycling through recycling endosomes (RAB11 and RAB35); rapid endocytic recycling from early endosomes (RAB4); trafficking from early endosomes to recycling endosomes (RAB15), trafficking from recycling endosomes to plasma membrane (RAB15, 17 and 25); maturation of late endosomes and phagosomes and their fusion with lysosomes (RAB7); and trafficking of late endosomes to the TGN (RAB9). Pathways regulated by Rab GTPase proteins also include those controlling organelle biogenesis and cell structural organisation, e.g. melanosome biogenesis (RAB32 and RAB38); mitochondrial fission (RAB32); lipid droplet formation (RAB18); ciliogenesis (RAB8, 17 and 23); autophagosome formation (RAB24 and RAB33) and tight junction assembly (RAB13).

Rab Group	Rab GTPase	Cellular localisation	Functional role
13	RAB1A/B	ER and Golgi body	ER to Golgi and Intra-Golgi transport
11	RAB2A/B	ER, ER-Golgi intermediate compartment and Golgi body	Golgi to ER transport
13	RAB3A/B/C/D	Synaptic/secretory vesicles and plasma membrane	Exocytosis and neurotransmitter release
11	RAB4A/B/C	Early endosome	Protein recycling to plasma membrane
9	RAB5A/B/C	Plasma membrane, clathrin coated vesicles, early endosomes and phagosomes	Endocytosis and early endosome fusion
8	RAB6A/A'/B/C	Golgi	(A/A') Endosome to Golgi, intra-Golgi and Golgi to ER transport, (B) intra-Golgi transport (neuronal cells)
5	RAB7A/B	(A) Late endosomes, lysosomes, phagosomes and melanosomes. (B) Lysosomes.	Maturation of late endosomes and phagosomes and their fusion with lysosomes. Lysosome biogenesis
13	RAB8A/B	(A) Cell membrane, vesicles and primary cilia. (B) Cell membrane and vesicles	Exocytosis, transport from trans-Golgi network and recycling endosomes to plasma membrane. GLUT4 vesicle translocation and ciliogenesis
5	RAB9A/B/C	(A) Late endosomes. (B) Late endosomes and Golgi.	Endosome to Golgi transport.
13	RAB10	Golgi, basolateral sorting endosomes and GLUT4 vesicles	Exocytosis, transport from trans-Golgi network and recycling endosomes to basolateral plasma membrane
11	RAB11A/B	Golgi, recycling endosomes and early endosomes	Transport from trans-Golgi network/ recycling endosomes to plasma membrane
13	RAB12	Golgi and secretory vesicles	Exocytosis
13	RAB13	Tight junctions, trans-Golgi network and recycling endosomes	Transport from trans-Golgi network and recycling endosomes to plasma membrane and tight junction biogenesis.
11	RAB14	Golgi, early endosomes and GLUT4 vesicles	Transport from trans-Golgi network and recycling endosomes to plasma membrane
13	RAB15	Early and recycling endosomes	Transport from early endosomes to recycling endosomes. Transport from recycling endosomes (apical) to plasma membrane (basolateral)
9	RAB17	Apical recycling endosomes	Transcytosis. Transport from recycling endosomes (apical) to plasma membrane (apical) and ciliogenesis

Rab Group	Rab GTPase	Cellular localisation	Functional role
10	RAB18	Golgi and lipid droplets	Lipid droplet formation
9	RAB20	Golgi and endosome	Apical membrane recycling
9	RAB21	Early endosomes	Integrin endocytosis
9	RAB22A/B and RAB31	(A) Early endosomes. (B and RAB31) Endosomes and trans-Golgi network	Transport between trans-Golgi network and early endosomes
1	RAB23	Plasma membrane and endosomes	Transport/recycling to the plasma membrane and ciliogenesis
9	RAB24	ER	Autophagosome formation
11	RAB25	Recycling endosomes	Transport of recycling endosomes (apical) to plasma membrane (apical)
14	RAB26	Secretory granules	Exocytosis
14	RAB27A/B	Melanosomes	Exocytosis
2	RAB32	Mitochondria and melanosomes	Trans-Golgi network to melanosome transport and mitochondrial fission
12	RAB33A/B	(A)Golgi and dense core vesicles. (B) Golgi	Retrograde Golgi transport to ER. Autophagosome formation
7	RAB34	Golgi and macropinosomes	Intra-Golgi transport and peri-Golgi positioning of lysosomes. Formation of macropinosomes
14	RAB37	Secretory granules	Exocytosis. Mast cell degranulation
2	RAB38	Melanosomes	Trans-Golgi network to melanosome transport
13	RAB40A/B/C	Golgi and recycling endosomes	Endosome transport
12	RAB43	ER, Golgi	ER to Golgi transport

Table 1.2 Rab GTPase localisation and function [178, 180]

Rab GTPase protein intracellular localisation and function. Where multiple isoforms exist for a Rab GTPase protein, these are indicated as A, B, C and D. Each Rab protein belongs to a Rab family group, which is predicted using comparative sequence analysis and dendrogram clustering. Predicted Rab protein groupings are as follows: group 1 (RAB23), group 2 (RAB29, 32 and 38), group 3 (RABL2, L3 and L5), group 4 (Ran), group 5 (RAB7 and RAB9), group 6 (RAB28 and RABL4), group 7 (RAB34 and RAB36), group 8 (RAB6 and RAB41), group 9 (RAB5, 7, 20, 21, 22A, 31 and 24), group 10 (RAB18), group 11 (RAB2, 4, 11, 14, 25, 39 and 42), group 12 (RAB19, 30, 33 and 43), group 13 (RAB1, 3, 8, 10, 12, 13, 15 and 40) and group 14 (RAB26, 27, 37 and 44). Only the Rab proteins with known cellular functions are shown in the table.

Rab GTPase Proteins: Rab effector protein function

To control membrane trafficking in the cell, Rab GTPase proteins are able to activate a wide range of effector proteins, which can act as tethering and sorting factors or motor proteins in the cell. Some well studied examples of Rab effector proteins include:

- *Tethering factors that promote membrane fusion*. RAB5 localises to the plasma membrane, and the membrane of early endosomes and phagosomes to facilitate endocytosis and endosomal fusion of clathrin-coated vesicles. Activation of RAB5 results in the recruitment of two effector proteins: rabenosyn 5 and early endosome antigen1 (EEA1). These effector proteins can bind directly to endosomal soluble NSF attachment protein receptors (SNAREs), including syntaxin 6, 7 and 13. These SNARE proteins are then able to interact directly with a set of opposing SNARE proteins localised at the target membrane surface allowing the process of membrane docking and fusion to take place [179].

- *Sorting factors that package cargo into transport vesicles*. RAB4 localises to the surface of early endosomes, and has been shown to play a role in the 'rapid' recycling of endocytosed cell surface receptors back to the plasma membrane. One of the effector proteins shown to be recruited by activated RAB4 is Rab interacting protein 4 (RABIP4). Activated RABIP4 has been shown to bind to the glucose transport receptor 4 protein (GLUT4), and is responsible for its recycling to the plasma membrane following endocytosis [181].

- *Motor proteins that traffic intracellular vesicles*. RAB27A localises to the membranes of melanosomes in melanocytes to facilitate their trafficking to the cellular periphery. Activation of RAB27A results in the recruitment of melanophilin, an adaptor protein that can bind directly to the actin motor protein, myosin Va. Once myosin Va has been successfully recruited, the RAB27A positive melanosomes can traffic along actin filaments moving towards the cellular periphery [179].

Rab GTPase Proteins: The role of Rab proteins in virus infection

As a result of the major role that Rab proteins play in the regulation of intracellular trafficking and in the formation and functioning of cellular organelles, many viruses

have evolved to incorporate Rab proteins into their replication cycles. So far, Rab proteins have been implicated in the processes of virus entry, assembly and exit and the rearrangement of intracellular membrane during the formation of membrane-associated virus replication complexes. Two highly-related flaviviruses, West Nile virus (WNV) and Dengue virus (DV), have both been shown to utilise RAB5-positive early endosomes during virus entry [182]. This was demonstrated using RAB5 silencing which significantly reduced WNV and DV infection of HeLa cells. RAB11 has been identified as a key factor involved in the assembly and budding of several different viruses, including the Human Cytomegalovirus, Hantavirus, Respiratory Syncytial virus and Influenza A virus. In cells infected with these viruses, RAB11 silencing has been shown to reduce the extracellular titres of virus generated [183]. It is thought that RAB11 may be important for virus budding by controlling either the separation of virus and cellular membrane during envelope formation, or for the recruitment of additional cellular factors that are required during budding and exit [183].

Recently, studies investigating the HCV replication cycle have also demonstrated that Rab proteins may be important during HCV replication. Silencing the expression of RAB1B [128] and RAB5 [30] significantly reduced the replication of HCV observed in cells expressing a full-length HCV genome. Staining for the RAB5B protein in HCV replicon (subgenomic and full-length) expressing cells also indicated that RAB5B colocalises directly with the NS4B and NS5A proteins present at the HCV replication complex. In these cells, colocalisation was also observed to occur between the HCV replication complex and RAB4 [30]. The preliminary data from these studies indicates that Rab proteins present in the ER and Golgi body (e.g. RAB1B) and early endosomes (e.g. RAB4 and 5) may be involved in the formation and/or functioning of HCV replication complexes. There is no evidence at present to indicate that HCV utilises Rab proteins either during virus entry, assembly or exit.

Given the evidence from the replication cycles of other RNA viruses, and some preliminary data on the HCV replication cycle, it is possible that Rab proteins may play an important role during HCV infection. Rab proteins that might be interesting to study for their potential role in the HCV replication cycle include those that regulate membrane trafficking at the ER, Golgi body and early endosome such as RAB2, 4 and 6 [178, 180], as there is significant evidence to indicate that

membrane from these locations contributes to the HCV membranous web structure [30, 32]. RAB11 may also be an interesting factor to study because of the key role that this protein has been shown to play in the budding and secretion of other RNA viruses [183]. Finally, RAB18, which localises to the surface of intracellular lipid droplets, may also be an interesting host factor to further investigate due to key role that lipid droplets have been shown to play in the process of HCV assembly [39]. RAB18 is involved in regulating the association of lipid droplets with the ER and, therefore, may be important for linking the processes of HCV replication, assembly and secretion [184, 185].

RNA binding proteins: T cell restricted antigen-1 (TIA1) /TIA1 protein like-1 (TIAL1)

TIA1 and TIAL1 are RNA-binding proteins that shuttle between the nucleus, where they play a role in alternative mRNA splicing; and the cytosol, where they control the levels of mRNA translation during conditions of high cellular stress [186]. Cellular stresses such as UV irradiation, heat shock, oxidative stress and ER stress result in a block on global mRNA translation. This occurs following formation of an inhibited initiation complex on mRNA molecules when the eukaryotic translation initiation factor 2A (EIF2A) becomes phosphorylated by PKR. The TIA1 and TIAL1 proteins bind to this inhibited initiation complex, as well as multiple polyadenylated mRNAs, and are able to self aggregate resulting in the formation of stress granules in the cytosol [187]. Stress granules act as a temporary store for untranslated mRNA molecules, which are released once the cell returns to normal conditions to facilitate rapid recovery of protein expression. In addition to their role in stress granule formation, TIA1 and TIAL1 are also able to bind to and block the translation of specific mRNA molecules containing AU-rich sequences, CU-rich sequences or hairpin consensus motifs at their 3’ UTRs [186].

As a result of their RNA binding activity, TIA1 and TIAL1 have both been implicated in the replication of the positive stranded RNA viruses, WNV and DV [187]. TIA1 and TIAL1 were observed to relocalise during WNV and DV infection to accumulate in the perinuclear region of infected cells, where virus replication complexes assemble. TIA1 and TIAL1 were also observed to colocalise directly with dsRNA and the NS3 protein present in WNV and DV replication complexes [187]. Furthermore, direct interaction has been observed to occur between TIA1 and TIAL1 and the 3’ terminal stem loop of the negative-stranded RNA template generated during WNV genome replication. Knockdown of TIAL1 significantly

reduced the replication of WNV, whilst knockdown of TIA1 delayed the time required to reach maximum replication levels. This indicates that TIAL1 (and perhaps TIA1) may be required for synthesis of the WNV RNA genome [188]. Alongside the potential role of TIA1 and TIAL1 in the replication of WNV and DV, a reduction in the formation of stress granules was also observed to occur during WNV and DV infection. This was attributed to the sequestration of TIA1 and TIAL1, which are stress granule promoting factors, to the virus replication complexes. Reduced abundance of stress granule promoting factors may further stimulate virus replication by promoting an increase in global mRNA translation [187].

Considering the role that TIA1 and TIAL1 may play in the replication of positive-stranded RNA during WNV and DV infection, a similar role may also exist in the HCV replication cycle. Other stress granule promoting factors, such as Ras-Gap-SH3 domain binding protein (G3BP1), have already been shown to be recruited from stress granules to the core coated lipid droplets to play a key role in the HCV replication cycle [129, 189]. In addition, TIA1 has been observed to bind to the 5'NTR of the HCV negative RNA strand [156] and the 3'NTR of the HCV positive RNA strand [155] indicating a potential role for this protein in the replication of the HCV genome.

RNA binding proteins: Staufen1

Staufen is a dsRNA-binding protein originally identified in Drosophila, where it is involved in the trafficking and translation of cellular mRNAs during embryonic development. In mammalian cells, two homologs of Staufen (Staufen1 and Staufen2) have been identified with 51% homology at the amino acid level. These proteins have been shown to bind specific motifs on cellular mRNA molecules to facilitate the formation of ribonucleoprotein complexes that control mRNA trafficking, translation and degradation [190]. Although the two mammalian Staufen homologs are thought to have similar intracellular functional roles, their expression patterns differ significantly, as Staufen1 is expressed ubiquitously, whilst Staufen2 expression is restricted to neurons [190, 191]. In addition, several different protein isoforms have been observed for both Staufen homolog genes as a result of alternative splicing. These include the 55KDa and 63KDa isoforms generated for Staufen1 and the 52KDa, 56KDa, 59KDa and 62KDa isoforms generated for Staufen2. These isoforms have been shown to differ in their mRNA

binding specificity and are thought to form distinct ribonucleoprotein complexes in cells [190].

As a result of the role that Staufen proteins play in the trafficking, translation and degradation of mRNA molecules, Staufen1 and 2 have been shown to localise to the rough endoplasmic reticulum in ribonucleoprotein complexes associated with ribosomes. The only exception is the Staufen2 62KDa isoform, which is found in ribosome free ribonucleoprotein complexes [190]. Staufen1 and 2 have also been observed to traffic between the nucleus and the cytosol to control the localisation of newly synthesised mRNA [192]. To enable the trafficking function of Staufen proteins, Staufen1 has been shown to contain a tubulin-binding domain and is able to form complexes with cytoskeletal filament proteins (tubulin and actin), cytoskeletal control proteins (CDC42 and RAC1) and cytoskeletal motor proteins (myosin and kinesin) [193]. Staufen2 has also been shown to traffic along microtubule filaments towards the dendrites of neurons in conjunction with mRNA molecules and can bind directly to α and β tubulin [191].

Alongside, the role of Staufen1 and 2 in mRNA trafficking, Staufen1 has also been shown to play a major role in the translation and degradation of cellular mRNA molecules. Binding of Staufen1 to the 3'UTR of cellular mRNAs targets them for degradation through a process termed 'staufen-mediated decay' (SMD) [194]. This relies on the recruitment of the up-frameshift suppressor 1 protein (UPF1), a cellular host factor usually involved in the process of nonsense-mediated decay (NMD), which degrades mRNAs containing incorrect translation termination sequences. Conversely, the binding of Staufen1 to the 5'UTR of cellular mRNAs enhances the efficiency of their translation [195]. Staufen1 is able to further increase the translational activity of a cell through its ability to control the balance between polysomes, which perform cellular mRNA translation; and stress granules, which translationally repress cellular mRNAs during times of cellular stress [196].

Staufen1 has been implicated in the replication cycles of several RNA viruses including the Human Immunodeficiency virus (HIV) and the Influenza A virus. In the HIV replication cycle, Staufen1 has been shown to bind to the HIV Gag precursor protein ($Pr55^{Gag}$) and the HIV RNA genome and is present in the HIV virion particle. These interactions facilitate multimerisation of the Gag precursor protein and enable encapsidation of the HIV RNA during the assembly of nascent

HIV particles [196, 197]. As part of its role in virus assembly, Staufen1 has been shown to relocalise, in conjunction with the HIV Gag protein and HIV RNA, to lipid raft domains of the plasma membrane where HIV assembly takes place [197]. Staufen1 has also been shown to play a separate role in the HIV replication cycle controlling the rate at which HIV Gag protein is translated [196]. In the replication cycle of Influenza A, Staufen1 has been detected as part of a viral ribonucleoprotein complex containing viral RNA, viral polymerase and nucleoprotein. Its presence in this complex is thought to facilitate encapsidation of the viral RNA genome into nascent virus particles, as silencing Staufen1 expression reduces Influenza virus particle production without affecting virus replication or the level of virus protein expression. An additional interaction has been identified between Staufen1 and the Influenza A non-structural protein, NS1; although the precise function of this interaction is not clear at present [198]. Alongside the evidence demonstrating that Staufen1 is involved in the replication cycle of both HIV and Influenza A, several studies have demonstrated that Staufen1 is able to bind directly to the 3'NTR of the HCV genome and the 5'NTR of the negative HCV RNA strand [155, 156]. This indicates that Staufen1 may also be involved in the HCV replication cycle and may control processes such as genome replication or encapsidation during the assembly of nascent virus particles.

1.8 Hypothesis and Project Aims

1.8.1 Hypothesis

The recent development of a full-length infectious JFH-1 clone alongside significant advances in genome-wide profiling techniques provides an excellent opportunity to investigate the processes involved in the HCV replication cycle. Using these latest developments, this study aims to investigate the effect of HCV infection on host gene expression to characterise the host cell response to the complete HCV replication cycle. By characterising the host cell response to HCV infection, it is hypothesised that it may be possible to identify cellular host factors as potential cofactors involved in the HCV replication cycle. It may also be possible to identify HCV-induced biological changes that contribute to the pathogenesis of infection. Alongside the use of gene expression profiling techniques to facilitate identification of potential HCV cofactors, host factors shown to be involved in the replication of other RNA viruses will also be tested for their role in the HCV replication cycle. Rab GTPase family members and RNA binding proteins involved in the translation, transport and degradation of cellular mRNA molecules are promising candidates that will be tested for their role in the HCV replication cycle. By using these two approaches to select host factors for investigation as potential HCV cofactors, it should be possible to gain greater understanding of the cellular host factors that are involved in the HCV replication cycle.

1.8.2 Project aims

1. To investigate the host cell response to HCV infection using microarray gene expression profiling.

    - Huh7 cells infected with JFH-1 will be characterised by microarray expression profiling.
    - Microarray expression patterns observed will be further explored using quantitative PCR, western blotting and cell metabolite quantification assays.
    - To determine whether specific HCV proteins contribute to the expression patterns observed, quantitative PCR will also be used to investigate host expression in cells expressing a genotype 2a subgenomic replicon and the JFH-1 core protein.

2. To investigate the function of potential HCV cofactors in the JFH-1 replication cycle using siRNA silencing.

    - Potential HCV cofactors to be tested will include:

        - Host factors significantly upregulated during HCV infection, identified through microarray expression profiling.

        - Host factors involved in the replication cycle of other RNA viruses including Rab GTPase proteins and RNA binding proteins (Staufen1, TIA1 and TIAL1).

3. To characterise the structural or functional role of novel HCV cofactors shown to be required during the JFH-1 replication cycle.

    - The intracellular localisation of HCV cofactors will be characterised to investigate whether HCV infection alters cofactor trafficking. The ability of cofactors to colocalise with HCV proteins will also be determined.

    - The effect of host factor silencing on relevant signalling pathways will be investigated to determine the role that potential cofactors may play in the HCV replication cycle.

Chapter 2: Materials and Methods

2.1 Cell culture

Huh7 and Huh7.5 cells were grown in Dulbecco's modified Eagles medium (DMEM) supplemented with 10% (v/v) foetal calf serum, 100U/ml penicillin and 100µg/ml streptomycin at 37°C, 5% CO_2. Growth medium was additionally supplemented with 500µg/ml Geneticin (Invitrogen) for the Huh7 and Huh7.5 cells transfected with a genotype 2a HCV subgenomic replicon, and with 10µg/ml Blasticidin (Invitrogen) for the Huh7 cells transfected with the pIRES(core) or pIRES(empty) plasmid DNA. Cells were passaged by trypsinisation every 4 days. All cells were cultured in the following volumes of growth medium: 8-well chamber slide (250µl), 24-well plate (500µl), 6-well plate (2ml), 25cm^2 flask (5ml) and 75cm^2 flask (15ml). When culturing cells for Lipofectamine 2000 mediated siRNA, RNA or plasmid DNA transfection, cells were grown in DMEM medium that did not contain penicillin or streptomycin. Huh7 cells were generously donated by Dr John Monjardino, Imperial College London [199] and the Huh7.5 cells were generously donated by Dr Charles Rice, Rockefeller University [139].

2.2 Production of infectious JFH-1 virus stocks

2.2.1 Preparation of the pJFH-1 plasmid DNA

Copies of the pJFH-1 plasmid were produced by DNA transformation of Library Efficiency DH5α *E. coli* (Invitrogen). A transformation mix was assembled using 10ng of pJFH-1 plasmid DNA and 50µl of *E. coli.* The transformation mix was incubated on ice for 30 minutes, heat shocked at 42°C for 45 seconds, incubated on ice for a further 2 minutes and added to 250µl SOC medium (Invitrogen). The bacteria were shaken at 200rpm/37°C for 1 hour and plated onto Luria Bertani (LB) agar containing 100µg/ml ampicillin (Sigma) for overnight incubation at 37°C. The following day, transformed bacterial colonies were picked and grown overnight at 37°C in 5ml LB medium containing 100µg/ml ampicillin. pJFH-1 plasmid DNA was then prepared from the transformed DH5α cultures using the Plasmid Mini Kit (Qiagen). Plasmid preparation was performed according to the manufacturer's instructions. The pGEM-T easy plasmid construct containing the JFH-1 sequence (pJFH-1) was generously donated by Dr Takaji Wakita, Tokyo Metropolitan Institute for Neuroscience [135, 200]. A plasmid map for pJFH-1 can be found in the Appendix section A.6. All plasmid maps were created using pDRAW32 DNA analysis software. Preparation of the pJFH-1 plasmid DNA, as described, was performed by Andrew Baillie, Imperial College London [201].

2.2.2 In vitro RNA transcription of the JFH-1 RNA genome

16µg of pJFH-1 plasmid DNA was linearised with 1µl of XbaI (100 units/µl) (NEB), 5µl of 10x NEBuffer 2 (NEB), 0.5µl of 100x BSA and nuclease-free water in a final volume of 50µl, and was incubated at 37˚C for 2 hours. Complete plasmid digestion was confirmed by agarose gel electrophoresis on a 1% (w/v) agarose gel stained with SYBR safe (Invitrogen). The linearised DNA was purified using phenol-chloroform extraction and ethanol precipitation. The 50µl restriction digestion was mixed with 50µl TE buffer (10mM Tris-HCl, 1mM EDTA, pH8.0). 100µl of 25:24:1 phenol: chloroform: isoamyl alcohol (Sigma) was added, the mixture was shaken vigorously, and centrifuged in a Sorvalc Biofuge Fresco microcentrifuge at 11,200rpm (ca.12,000xg) for 15 minutes. The upper aqueous phase was transferred to a new 1.5ml eppendorf tube, and 100µl of chloroform was added. Samples were shaken vigorously and centrifuged at 11,200rpm (ca.12,000xg) for 5 minutes. The upper aqueous phase was transferred to a new 1.5ml eppendorf tube, 0.1 volume 3M sodium acetate and 2.5 volumes of ethanol were added, the samples were mixed and incubated for 20 minutes at -80˚C. DNA was pelleted by centrifugation at 11,200rpm (ca.12,000xg) (4˚C) for 20 minutes, and the supernatant was removed. The pellet was washed by adding 0.5ml of 75% (v/v) ethanol/H_2O and centrifuging at 11,200rpm (ca.12,000xg) (4˚C) for 15 minutes. The supernatant was removed and the pellet was air-dried and resuspended in 43µl of nuclease-free water. To remove 3’ overhanging DNA, the DNA was digested in a total reaction volume of 50µl, with 2µl of Mung Bean nuclease (10 units/µl) (NEB) and 5µl of 10x Mung bean nuclease buffer for 30 minutes at 30˚C. The 50µl digestion mix was treated with 10µl of 10% (w/v) SDS, 2µl of Proteinase K (20µg/µl) (Invitrogen) and nuclease-free water in a final volume of 200µl. The reaction was incubated for one hour at 50˚C, after which the DNA was extracted using 200µl of 25:24:1 phenol: chloroform: isoamyl alcohol and 200µl of chloroform, and was precipitated with 3M sodium acetate and ethanol, as detailed above. The DNA pellet was resuspended in 20µl of nuclease-free water. DNA concentration was measured using a Nanodrop 1000 spectrophotometer.

The JFH-1 RNA genome was transcribed from the linearised pJFH-1 plasmid using the T7 MEGAscript *in vitro* RNA transcription kit (Ambion). RNA transcription was performed using 1µg of linearised plasmid DNA in a 20µl T7 MEGAscript *in vitro* RNA transcription reaction, containing 2µl of rATP, 2µl of rCTP, 2µl of rGTP, 2µl of rUTP, 2µl of 10x kit reaction buffer, 2µl of T7 polymerase enzyme mix and

nuclease-free water. Transcription reactions were incubated at 37°C for 6 hours. The JFH-1 RNA transcript was incubated with 1µl DNase enzyme (2 units/µl) for 15 minutes at 37°C. The RNA was purified using the RNeasy Mini kit (Qiagen). Transcription reactions were made up to 100µl total volume with nuclease-free water and 350µl of RLT kit buffer (Qiagen) was added. The samples were processed according to the manufacturer's instructions and final RNA samples were eluted in 30µl of nuclease-free water. RNA transcript concentration was measured using a Nanodrop 1000 spectrophotometer. The RNA sample was also run on a 0.8% (w/v) non denaturing agarose gel stained with SYBR safe for assessment of RNA quality and size. Preparation of the JFH-1 RNA transcript, as described, was performed by Andrew Baillie, Imperial College London [200, 201].

2.2.3 Transfection of the JFH-1 RNA genome into Huh7.5 cells

Huh7.5 cells were seeded in a 6-well tissue culture plate at a density of $6x10^5$. The following day, growth medium was replaced with 2ml of OptiMEM medium (Invitrogen). A transfection mix was assembled by combining 250µl of OptiMEM containing 10µl of Lipofectamine 2000 (Invitrogen) and 250µl of OptiMEM containing 5µg of the JFH-1 RNA genome. The transfection mix was incubated at room temperature for 20 minutes and added to the cells. After a 6 hour incubation period, the transfection medium was replaced with 2ml of growth medium and the cells were incubated overnight. The following day, the transfected cells were passaged into a $25cm^2$ tissue culture flask for JFH-1 virus production. Transfection of Huh7.5 cells with the JFH-1 RNA transcript was optimised by Andrew Baillie, Imperial College London [201]

2.2.4 Harvesting stocks of the JFH-1 virus

Growth medium was collected from the Huh7.5 cells 4 days after transfection of the JFH-1 RNA transcript. The medium was clarified by centrifugation in a Mistral 3000 Benchtop centrifuge (MSE) at 2000rpm (670xg) for 10 minutes, after which, the supernatant was filtered through 0.45µm 150ml filter units (Millipore). Virus particles in the filtered medium were concentrated through Amicon Ultra-15 filtration units (Millipore) by centrifugation in a Mistral 3000 Benchtop centrifuge (MSE) at 3600rpm (2173xg) (4°C) for 25 minutes. Concentrated JFH-1 stocks were collected and stored at -20°C.

2.2.5 Titration of JFH-1 virus stocks

Huh7.5 cells were seeded into 8-well chamber slides at a density of $0.8x10^5$. The concentrated JFH-1 virus stocks, diluted by 1 in 10 (0.1µl), 1 in 100 (0.01µl) and 1 in 1000 (0.001µl) in DMEM growth medium, were used to infect the Huh7.5 cells in duplicate. At 48 hours post-infection, the chamber slides were stained for HCV core protein (see 2.2.6), and foci were counted using a Nikon Eclipse TE2000S fluorescence microscope. Focus forming units per ml (ffu/ml) of virus stock was calculated from the total numbers of foci counted for each well.

2.2.6 Immunofluorescent staining of the HCV core protein

JFH-1 infected cells were fixed in 4% (w/v) paraformaldehyde / phosphate buffered saline (PBS) for 30 minutes, washed in PBS for 10 minutes, and permeabilised in 0.1% (v/v) Triton X-100/PBS for 10 minutes. The cells were incubated for 1 hour at room temperature in a humidity chamber with a mouse anti-core antibody (Abcam C7-50), diluted 1 in 400 in 1% (w/v) bovine serum albumin (BSA)/PBS. The cells were washed in PBS for 5 minutes, three times and incubated for 1 hour at room temperature in a humidity chamber with an AlexaFluor 594-conjugated donkey anti-mouse antibody (Invitrogen), diluted 1 in 1000 in 1% (w/v) BSA/PBS. The cells were washed in PBS for 5 minutes, three times, and incubated in a humidity chamber with 20µg/ml 4,6-diamidino-2-phenylindole (DAPI) (Invitrogen) for 10 minutes. The cells were washed three times with PBS, once with water and mounted using Mowiol 4-88 mounting medium (Sigma) [202]. Core protein staining was analysed using a Nikon Eclipse TE2000S fluorescence microscope.

2.2.7 Production of high-titre JFH-1 stocks (media-passage method)

Huh7.5 cells were seeded in $75cm^2$ tissue culture flasks at a density of $2x10^6$. Concentrated JFH-1 virus stocks were used to infect the Huh7.5 cells at a multiplicity of infection (MOI) of 0.1 ($2x10^5$ ffu). Infected Huh7.5 cells were incubated for 4 days and the growth medium was collected and clarified. 1.5ml (~$2x10^5$ ffu) of the infectious clarified medium was passaged onto a fresh batch of naive Huh7.5 cells seeded in $75cm^2$ tissue culture flasks. The remaining clarified medium was concentrated and stored at -20°C. Infectious clarified medium, isolated from the infected Huh7.5 cells, was serially passaged onto naive Huh7.5 cells every 4 days to provide a continuous supply of high titre JFH-1 stocks. Every 2 months, JFH-1 production was re-started from an original concentrated stock of

JFH-1 virus to avoid the accumulation of genetic mutations in the virus genome. The JFH-1 stock used was harvested at passage 3 post-pJFH-1 transfection and had a virus titre of $1x10^6$ ffu/ml. 200µl of the concentrated virus stock ($2x10^5$ ffu) was used to infect a single 75cm^2 tissue culture flask seeded at a density of $2x10^6$ to achieve an MOI of 0.1.

2.3 Affymetrix microarray profiling of host expression during JFH-1 infection

Huh7 cells were seeded into 25cm^2 culture flasks at a density of $5x10^5$. The following day, the cells were either infected with JFH-1 at an MOI of 3, or mock infected with an equal volume of concentrated conditioned growth medium, produced using growth medium collected from uninfected Huh7.5 cells. At 6, 12, 18, 24 and 48 hours post-infection, cells were washed once in ice cold PBS and cellular RNA was extracted using 3ml of TRIzol reagent (Invitrogen). TRIzol lysates were homogenised by pipetting and transferred to cryovials and stored at -80˚C. All mock and JFH-1 infections were performed in triplicate. Infection of Huh7 cells for microarray analysis was performed by Andrew Baillie, Imperial College London [201]. Trizol lysates were shipped to Expression Analysis (NC, USA) where RNA was purified, quality tested using the Agilent Bioanalyser and hybridised onto Human U133 Plus 2.0 Affymetrix microarray chips for fluorescence data acquisition. One genechip array was used for each JFH-1 infected or mock infected sample extract. Raw microarray expression data was analyzed by Katja Remlinger (GlaxoSmithKline, NTC, USA) with Array Studio software (Omicsoft, USA) using the microarray data default settings and the RMA signal extraction method. Two samples (Mock_6hrs_1 and JFH-1_6hrs_1) did not pass the data quality control measures (principal component analysis and correlation based quality control), and were excluded from the analysis. Data was analyzed on the $\log_2$ scale, using analysis of variance (ANOVA), followed by pre-specified contrast statements. Fold change in host gene expression was calculated using the estimated least squares mean differences between the triplicate JFH-1 infected and mock infected samples at each time-point. Host genes demonstrating at least a 2 fold change in expression and a significant differential expression at a raw p-value level of 0.05 were selected for further investigation. The microarray data was submitted to the GEO (Gene Expression Omnibus) database and can be found under the accession number GSE20948.

Gene Ontology programs used to identify expression patterns in the data included Ingenuity pathway analysis [203] and PANTHER Classification [204]. Heat maps representing the microarray data were generated using MultiExperiment Viewing (MEV) software available within the TM4 Microarray Software Suite. Hierarchical clustering by Pearson Correlation was used to cluster the genes in each heat map [205]. The $\log_2$ expression data represented in the heat maps can be found in Appendix section A.8.

In addition to the heatmap diagrams, the microarray gene expression data observed was also plotted onto graphs representing mean fold change in expression (Figures 3.8, 3.9, 5.1, 5.3, 5.6, 5.7 and A.19). The 95% confidence interval values representing the range of mean fold change values observed for the triplicate repeat infection samples can be found in Appendix A.10 and A.11. For some of the genes analysed by the Affymetrix microarray genechip, several probe sets were available (probe set = 11 different probe pairs for a given gene). For those genes with multiple gene probe sets on the microarray genechip, the mean fold change microarray gene expression data was plotted with error bars to represent the range of mean fold change values observed for the different gene probe sets.

Each probe set has an Affymetrix ID, which indicates the nature of probe sequences in the set. Probe sets ending in '_at' indicate that the probes represent a unique transcript sequence; probe sets ending in '_s_at' indicate that the probes represent multiple transcript splice variants; and probe sets ending in '_x_at' indicate that the probes represent two or more similar sequences e.g. highly similar transcripts.

2.4 Quantitative PCR analysis of host expression during JFH-1 infection

2.4.1 Acute JFH-1 infection of Huh7 and Huh7.5 cells

Huh7 cells and Huh7.5 cells were seeded in 25cm^2 tissue culture flasks at a density of 5x10^5. The following day, the cells were either infected with JFH-1 at an MOI of 3, or mock infected with an equal volume of concentrated conditioned growth medium. At 6, 12, 18, 24 and 48 hours post-infection, cells were washed once in ice cold PBS and cellular RNA was extracted from the Huh7 cells, and at 48 hours post-infection, cellular RNA was extracted from the Huh7.5 cells for qRT-PCR analysis. All mock and JFH-1 infections were performed in triplicate.

Note: The Huh7 cell RNA used for qRT-PCR validation of the microarray expression data and quantification of the intracellular JFH-1 RNA levels was generated in a separate experiment to the RNA used for microarray analysis. The same stock of JFH-1 virus was used to infect Huh7 and Huh7.5 cells for qRT-PCR analysis as was used for the microarray experiment.

2.4.2 Extraction of total cellular RNA

Total cellular RNA from JFH-1 infected and mock infected cells was extracted by adding 3ml of TRIzol reagent (Invitrogen) to each 25cm^2 flask. The flasks were incubated for 5 minutes at room temperature and samples were homogenised by pipetting and transferred to cryovials for storage at -80˚C. When all time-point samples had been collected, each 3ml sample was split into 3 x 1ml aliquots in 1.5ml eppendorf tubes. 200µl of chloroform was added to each tube and the samples were shaken vigorously for 15 seconds and incubated at room temperature for 3 minutes. The samples were centrifuged in a Sorvalc Biofuge Fresco microcentrifuge at 11,200rpm (ca.12,000xg) (4˚C) for 15 minutes. The upper aqueous phase was transferred to a new 1.5ml eppendorf and 500µl isopropanol was added to each tube. The samples were mixed and incubated at room temperature for 10 minutes to precipitate the RNA, after which the samples were centrifuged at 11,200rpm (ca.12,000xg) (4˚C) for 10 minutes to pellet the RNA. The supernatant was removed from the tube and the RNA pellet was washed with 1ml of 75% (v/v) ethanol/H_2O. The samples were centrifuged at 8,800rpm (ca.7500xg) (4˚C) for 5 minutes. The supernatant was removed from the tube and the RNA pellet was air-dried and resuspended in 20µl of nuclease-free water. The 3 RNA aliquots for each sample were recombined and the RNA concentration was measured using a Nanodrop 1000 spectrophotometer.

Purified RNA samples were treated with DNA-free Turbo DNAse (Ambion) to remove possible contaminating genomic DNA. 8µg of RNA was treated with 1µl of DNA-free Turbo DNase (2 units/µl), 2µl of 10x DNase buffer and nuclease-free water in a 20µl total reaction volume. The samples were incubated at 37˚C for 30 minutes. To inactivate and remove the Turbo DNase, 2µl of kit inactivation reagent (0.1 volumes) was added and the samples were incubated at room temperature for 5 minutes. The samples were centrifuged in a Sorvalc Biofuge Fresco microcentrifuge at 10,200rpm (ca.10,000xg) for 1.5 minutes and the supernatant

was transferred to a new 1.5ml eppendorf tube. The RNA concentrations of DNase treated RNA samples were measured using a Nanodrop 1000 spectrophotometer.

2.4.3 Real time quantitative reverse-transcription PCR (qRT-PCR)

Relative quantification

Relative quantification by qRT-PCR was used to calculate fold change in host gene expression between the JFH-1 infected and mock infected cellular RNA extracts [206]. Relative quantification qRT-PCR reactions were performed using the Quantitect PCR SYBR green kit (Qiagen) and Lightcycler equipment (Roche). Reactions were performed in a final volume of 10µl using 1µg of cDNA (~1µl), 0.5µM reverse primer, 0.5µM forward primer, 5µl of 2x Quantitect SYBR green PCR mastermix and nuclease-free water. cDNA was synthesised by incubating 2µg of cellular RNA with 1µg oligo d(T) primers (Invitrogen) in a total reaction volume of 12.5µl. Samples were incubated at 70˚C for 5 minutes and placed on ice for 2 minutes. A further 12.5µl reaction mix added to the RNA samples consisting of 1µl of M-MLV reverse transcriptase (200 units/µl) (Promega), 5µl of 5x M-MLV reverse transcriptase reaction buffer, 0.625µl of Recombinant RNasin ribonuclease inhibitor (40 units/µl) (Promega), 1.25µl of dATP (10mM), 1.25µl of dCTP (10mM), 1.25µl of dGTP (10mM) 1.25µl of dTTP (10mM) (Promega) and 0.875µl of nuclease-free water. RNA samples were incubated at 42˚C for 60 minutes and the concentration of cDNA generated was measured using a Nanodrop 1000 spectrophotometer.

To calculate fold change in expression, the cycle threshold (CT) values obtained following qRT-PCR analysis of the mock and JFH-1 infected samples were used in the ΔΔCT equation [207].

The ΔΔCT equation:

CT target gene – CT reference gene = ΔCT
ΔCT JFH-1 infected sample – ΔCT mock infected sample = ΔΔCT
Fold change in gene expression = $2^{-\Delta\Delta CT}$

To normalise the gene expression data, GAPDH was used as the reference gene for most experiments, although normalisation was also performed using the genes encoding the large ribosomal protein (RPLPO) [208] and beta actin, where indicated.

Fold change in host gene expression (calculated using the ΔΔCT equation) was plotted as a value between 0 and 1 for those genes that decreased in expression in the JFH-1 infected samples compared to the mock infected samples (which have a reference fold change value of 1). Genes with expression fold change values of 0.5 and 0.25 represent genes showing a 2-fold and 4-fold decrease in expression as a result of JFH-1 infection. By comparison, genes increasing in expression as a result of JFH-1 infection were observed to have expression fold change values greater than 1.

Primers for qRT-PCR were designed using Primer 3 software to amplify a product between 100bp and 150bp in size. The annealing temperature used for all primer pairs was 58°C. Sequences for all qRT-PCR primers and the PCR cycle conditions used can be found in the Appendix section A.1 and A.4 respectively.

Absolute quantification

Absolute quantification was used to calculate the intracellular JFH-1 RNA levels present in the JFH-1 infected Huh7 and Huh7.5 cellular RNA extracts. Absolute quantification qRT-PCR reactions were performed using the one-step Quantitect RT-PCR SYBR green kit (Qiagen) and Lightcycler equipment (Roche). Reactions were performed in a final volume of 10µl, with 250ng of total RNA (~1µl), 0.1µl of reverse-transcription enzyme, 1µM of reverse primer, 1µM of forward primer, 5µl of 2x Quantitect SYBR green RT-PCR mastermix and nuclease-free water. The one-step qRT-PCR cycle conditions used can be found in the Appendix section A.4. To calculate the absolute amount of JFH-1 RNA present in cellular mRNA extracts, a JFH-1 RNA standard curve was included in the qRT-PCR reaction. Genome copies of JFH-1 RNA present in each sample were calculated from the absolute quantification data using the equation:

$$\text{Genome copies} = \text{X grams JFH-1 RNA} / [\text{transcript length nucleotides} \times \text{MWT nucleotide}]) \times (6.023 \times 10^{23})$$

Genome copies = genome copies in 250ng total RNA
X grams JFH-1 RNA = grams of JFH-1 PCR product quantified in 250ng of total RNA
Transcript length = 280 nucleotides (56xA, 82xG, 81xC and 61xU)
Molecular weight of nucleotides (MWT) (g/mol) = A (347.2), G (363.2), C (323.2) and U (324.2)
Transcript length nucleotides x MWT nucleotide = 95340

The JFH-1 template RNA used in the standard curve was generated by *in vitro* RNA transcription using the T7 MEGAscript *in vitro* RNA transcription kit (Ambion). Template DNA used in the transcription reaction corresponded to the cloned PCR

product generated by the JFH-1 qRT-PCR primer pair. Template DNA was PCR amplified from 50ng of pJFH-1 plasmid DNA in a final reaction volume of 50µl using 5µl of 10x NH_4 buffer (Bioline), 2µl of 50mM $MgCl_2$ solution, 0.5µl of 100mM dNTP mix, 0.5µM of forward qRT-PCR primer, 0.5µM of reverse qRT-PCR primer, 1µl of Red Taq polymerase (1 unit/µl) (Bioline) and nuclease-free water. PCR cycle conditions used can be found in the Appendix A.4. The correct size PCR product was confirmed using agarose gel electrophoresis with a 1% (w/v) agarose gel stained using SYBR safe and was gel extracted using the QIAquick gel extraction kit (Qiagen), according to the manufacturer's instructions. The PCR product was then ligated into the pCR2.1 vector using the TA cloning kit (Invitrogen). A 10µl ligation reaction was performed using 50ng of pCR2.1 vector, 0.5µl of the gel extracted PCR product, 1µl of 10x kit ligation buffer, 1µl (4 Weiss units) of T4 DNA ligase and nuclease-free water. Reactions were incubated overnight at 14˚C. Bacterial transformation was performed using 2µl of the ligated pCR2.1 vector to generate a high concentration plasmid DNA preparation (see 2.2.1). Sequencing of plasmid DNA preparations was performed using M13 forward and reverse primers at the Imperial College Genomics Core Facility. 10µl sequencing reactions were performed using 500ng plasmid DNA, 1µl of forward or reverse M13 primer (3.2pmole/µl) and nuclease-free water. The plasmid preparation containing the correct DNA sequence was identified using BioEdit software and selected for use in the transcription reaction.

The pCR2.1 vector containing the cloned JFH-1 qRT-PCR product was linearised by HindIII digestion (NEB). 10µg of pCR2.1 (qRT-PCR-JFH-1) plasmid was digested using 1µl HindIII (100 units/µl) (NEB) and 5µl of 10x NEBuffer 2 (NEB) in a final volume of 50µl. The digestion reaction was incubated at 37˚C for 2 hours. Complete plasmid digestion was confirmed by agarose gel electrophoresis on a 1% agarose gel stained with SYBR safe. The linearised DNA was added to 50µl of TE buffer and purified using phenol-chloroform extraction and ethanol precipitation (see 2.2.2). The air-dried DNA pellet was resuspended in 20µl of nuclease-free water. RNA transcription was performed using 1µg of linearised plasmid DNA in a 20µl T7 MEGAscript *In vitro* RNA transcription reaction (Ambion) incubated at 37°C for 6 hours, according to the manufacturer's instructions (see 2.2.2). The JFH-1 RNA transcript generated was purified using the RNeasy Mini kit (Qiagen) (see 2.2.2). The RNA sample was run on a 0.8% non denaturing agarose gel for assessment of RNA quality and size. The RNA transcript concentration was

measured using a Nanodrop 1000 spectrophotometer and was diluted to generate a standard curve ranging from 1ng/µl to 100fg/µl. 1µl of each RNA standard was used in the one step qRT-PCR reaction to generate the JFH-1 RNA standard curve. Sequences for the qRT-PCR primers and M13 sequencing primers can be found in Appendix section A.1 and A.2, respectively.

2.5 Generation of genotype 2a (GT2a) replicon expressing cell lines

2.5.1 Preparation of the pGT2a(NS2-NS5B) plasmid DNA

The pGT2a(NS2-NS5B) plasmid DNA was used in *E.coli* bacterial transformation to generate enough plasmid DNA for *in vitro* RNA transcription (see 2.2.1). The pGT2a(NS2-NS5B) plasmid DNA (clone N3126-17-56) was generously donated by Cindy Richards (GlaxoSmithKline, USA) and consists of the J6 (genotype 2a) NS2 gene sequence fused to the JFH-1 (genotype 2a) sequences for NS3 to NS5B. The plasmid also encodes a luciferase reporter gene and neomycin resistance selection gene. A plasmid map for pGT2a(NS2-NS5B) can be found in the Appendix section A.6.

2.5.2 In vitro RNA transcription of subgenomic replicon RNA

The genotype 2a subgenomic replicon RNA was transcribed from 1µg of linearised pGT2a(NS2-NS5B) plasmid DNA with the T7 MEGAscript *in vitro* RNA transcription kit (Ambion) (see 2.2.2). To prepare linearised DNA for the reaction, 16µg of plasmid DNA was digested with XbaI, treated with Mung bean nuclease and Proteinase K and purified using phenol-chloroform extraction and ethanol precipitation (see 2.2.2).

2.5.3 Transfection of the subgenomic replicon RNA into Huh7 and Huh7.5 cells

Huh7 and Huh7.5 cells were transfected with 5µg of the GT2a subgenomic replicon RNA using Lipofectamine 2000 (see 2.2.3). At 24 hours post-transfection, Geneticin (Invitrogen) was added to the growth medium at a final concentration of 500µg/ml. A week later, the transfected cells were passaged into a 25cm^2 tissue culture flask with growth medium containing 500µg/ml Geneticin. After five weeks of passaging the transfected Huh7 and Huh7.5 cells in the presence of Geneticin, the cells were tested for the expression of the HCV NS3 and NS5A proteins and dsRNA by immunofluorescent staining (see 2.5.4). Intracellular subgenomic replicon RNA levels were also quantified by qRT-PCR using absolute

quantification, which was performed using the same primers and RNA standard curve that was used for quantification of the full-length JFH-1 genome (see 2.4.3).

2.5.4 Immunofluorescent staining of HCV NS3, HCV NS5A and dsRNA

Huh7 and Huh7.5 cells expressing the subgenomic replicon were seeded onto coverslips in a 24-well tissue culture plate at a density of $1x10^5$. The following day, the cells were fixed, permeabilised and stained for HCV NS3, HCV NS5A and dsRNA (see 2.2.6). The antibodies used for staining included: a mouse anti-NS3 antibody (Virogen), diluted 1 in 200 in 1% (w/v) BSA/PBS; a rabbit anti-NS5A antibody (Virogen), diluted 1 in 200 in 1% (w/v) BSA/PBS and a mouse anti-dsRNA antibody (Scicons, Hungary), diluted 1 in 200 in 1% (w/v) BSA/PBS. Detection of the bound primary antibodies was performed using an Alexa Fluor 488-conjugated goat anti-rabbit antibody and an Alexa Fluor 594-conjugated donkey anti-mouse antibody (Invitrogen), both of which were diluted 1 in 1000 in 1% (w/v) BSA/PBS.

2.5.5 Interferon-α curing of the subgenomic replicon expressing Huh7 and Huh7.5 cells

Geneticin was removed from the growth medium of the Huh7 and Huh7.5 cells expressing the subgenomic replicon, and the cells were grown in normal DMEM for one week. Growth media was then supplemented with 100IU/ml of interferon-α (IFNα) (Sigma) for eight weeks, after which the cells were grown in normal DMEM. During this time, the cells were tested every 2 weeks for the expression of HCV NS3 using immunofluorescent staining (see 2.5.4) and the presence of the subgenomic replicon RNA using qRT-PCR (see 2.4.3).

2.5.6. Investigating host gene expression in the subgenomic replicon expressing Huh7 and Huh7.5 cells

Wild type Huh7 cells, cured Huh7 cells and Huh7 cells expressing the subgenomic replicon (p10 post-transfection) were seeded in triplicate in $25cm^2$ tissue culture flasks at a density of $5x10^5$. The cells were incubated for 48 hours in normal DMEM growth medium, after which intracellular RNA was extracted using 3ml of TRIzol reagent (see 2.4.2) for qRT-PCR analysis of host gene expression (see 2.4.3). Fold change in host gene expression was calculated by comparing the replicon expressing and cured cells to the wild type cells using relative quantification, with GAPDH as the normalising control reference gene. The same

procedure was used to investigate host gene expression in wild type Huh7.5 cells, cured Huh7.5 cells and Huh7.5 cells expressing the subgenomic replicon (p10 post-transfection). Intracellular replicon RNA levels were also quantified in the extracted RNA samples by qRT-PCR using absolute quantification (see 2.4.3). The qRT-PCR primers and RNA standard curve used to quantify intracellular JFH-1 RNA levels were also used to quantify the GT2a replicon RNA. Sequences for all qRT-PCR primers can be found in the Appendix section A.1.

2.6 Generation of JFH-1 core expressing Huh7 cells

2.6.1 Preparation of the pSFV(core) and pSFV(empty) plasmid DNA

Plasmids containing the sequence for the Semliki Forest virus (SFV) replicon alone or in combination with the JFH-1 core protein were generously donated by Dr John McLauchlan (University of Glasgow Centre for Virus Research) [60]. The pSFV(core) and pSFV(empty) plasmid DNAs were used in *E.coli* bacterial transformation to generate enough DNA for *in vitro* RNA transcription (see 2.2.1). Plasmid maps for pSFV(core) and pSFV(empty) can be found in the Appendix section A.6.

2.6.2 In vitro RNA transcription of the SFV(core) and SFV(empty) RNA

The SFV(core) and SFV(empty) replicon RNA molecules were transcribed from the pSFV(core) and pSFV(empty) plasmid DNA using the SP6 RiboMAX *in vitro* RNA transcription kit (Promega). 10µg of pSFV(core) and pSFV(empty) plasmid DNA was linearised using 5µl of SapI (10 units/µl) (NEB), 5µl of 10x NEBuffer 4 (NEB) and nuclease-free water in a total reaction volume of 50µl. The digestion reaction was incubated at 37˚C for 1 hour. Complete plasmid digestion was confirmed by agarose gel electrophoresis on a 1% (w/v) agarose gel stained with SYBR safe. The linearised DNA was added to 50µl of TE buffer and purified using phenol-chloroform extraction and ethanol precipitation (see 2.2.2). Plasmid DNA concentration was measured using a Nanodrop 1000 spectrophotometer. RNA transcription was performed using 1µg of linearised plasmid DNA in a 25µl SP6 RiboMAX *in vitro* RNA transcription reaction, containing 5µl of 5x SP6 transcription buffer, 5µl rNTPs (25mM rATP, 25mM rCTP, 25mM rUTP and 12.5mM rGTP), 1.8µl Ribo m7G cap analogue (40mM) (Promega), 2.5µl SP6 polymerase enzyme mix and nuclease-free water. Transcription reactions were incubated at 37°C for 2 hours and the RNA transcript was purified using the RNeasy Mini kit (Qiagen).

Transcription reactions were made up to 100µl total volume with nuclease-free water and 350µl of RLT kit buffer (Qiagen) was added. The samples were processed according to the manufacturer's instructions and final RNA samples were eluted in 30µl of nuclease-free water. The RNA transcript concentration was measured using a Nanodrop 1000 spectrophotometer. Purified RNA samples were treated with DNA-free Turbo DNAse (Ambion) to remove all remaining plasmid DNA (see 2.4.2). The DNase treated RNA transcript was re-quantified using a Nanodrop 1000 spectrophotometer and was run on a 0.8% (w/v) non-denaturing agarose gel stained with SYBR safe for assessment of RNA quality and size.

2.6.3 Transfection of SFV(core) and SFV(empty) replicon RNA into Huh7 cells

Huh7 cells were seeded onto coverslips in a 24-well tissue culture plate at a density of $0.8x10^5$. The following day, growth medium was replaced with 500µl of OptiMEM medium. A transfection mix was assembled by combining 50µl of OptiMEM containing 2µl of Lipofectamine 2000 and 50µl of OptiMEM containing either 1µg or 2µg of the SFV(core) RNA and SFV(empty) RNA. The transfection mix was incubated at room temperature for 20 minutes and added to the cells, which were incubated for a total of 24 hours and stained for the HCV core protein (see 2.2.6).

2.6.4 Cloning the JFH-1 core sequence into the pIRES vector

PCR amplification of the JFH-1 core sequence from the pSFV(core) plasmid DNA was performed using Red Taq DNA polymerase (Bioline). PCR was performed using 50ng of pSFV(core) plasmid DNA in a final reaction volume of 50µl with 5µl of 10x NH_4 buffer (Bioline), 2µl of 50mM $MgCl_2$ solution, 0.5µl of 100mM dNTP mix, 0.5µM of forward core primer, 0.5µM of reverse core primer, 1µl of Red Taq polymerase (1 unit/µl) (Bioline) and nuclease-free water. PCR cycle conditions used can be found in the Appendix A.4. The PCR product was confirmed using agarose gel electrophoresis with a 1% (w/v) agarose gel stained using SYBR safe and was gel extracted using the QIAquick gel extraction kit (Qiagen), according to the manufacturer's instructions. The PCR product was then ligated into the pCR2.1 vector using the TA cloning kit (Invitrogen) (see 2.4.3). Bacterial transformation was performed using the ligated pCR2.1 vector to generate a high concentration plasmid DNA preparation (see 2.2.1). Sequencing of plasmid DNA preparations was performed using M13 forward and reverse primers at the Imperial College Genomics Core Facility (see 2.4.3). The plasmid preparation

containing the correct template DNA sequence was identified using BioEdit software.

The core PCR primers used to clone the core gene were designed to amplify a 607bp product, with the restriction enzyme cutting sites for NheI and MluI added at the 5' and 3' ends, respectively. This was to ensure directional cloning of the JFH-1 core sequence into the empty pIRES vector, which contains both NheI and MluI restriction enzyme sites in its multiple cloning site (Appendix A.6). Double digestion of the pCR2.1(JFH-1 core) plasmid and the empty pIRES plasmid (Clonetech) was performed using NheI and MluI (Promega). 5µg of plasmid DNA was digested in a total reaction volume of 50µl, with 5µl of NEBuffer 2 (NEB), 1µL of NheI (10 units/µl) (NEB), 1µl MluI (10 units/µl) (NEB), 0.5µl of 100x BSA and nuclease-free water. The digestion reactions were incubated at 37˚C for 3 hours. The digested JFH-1 core insert and the digested empty pIRES plasmid were run on a 1% agarose gel and were extracted using the QIAquick gel extraction kit (Qiagen), according to the manufacturer's instructions. Ligation of the digested pIRES and core insert was performed using the Rapid DNA ligation kit (Roche). Ligation was performed by diluting 50ng of digested pIRES and 5ng of digested JFH-1 core insert (1:1 vector to insert molar ratio) in 10µl of 1x DNA dilution buffer. 10µl of T4 DNA ligation buffer and 1µl of T4 DNA ligase was added to the diluted DNA sample. The ligation reaction was incubated for 30 minutes at room temperature. Bacterial transformation was performed using 5µl of the ligated pIRES vector with 50µl of competent cells to generate a high concentration plasmid DNA preparation (see 2.2.1). Sequencing of plasmid DNA preparations was performed using core forward and reverse primers at the Imperial College Genomics Core Facility (see 2.4.3).

Diagnostic PCR was performed using 50ng of the pIRES(core) plasmid DNA in a final reaction volume of 50µl, with 5µl of 10x NH_4 buffer (Bioline), 2µl of 50mM $MgCl_2$ solution, 0.5µl of 100mM dNTP mix, 0.5µM of forward core primer, 0.5µM of reverse core primer, 1µl of Red Taq polymerase (1 unit/µl) (Bioline) and nuclease-free water. PCR cycle conditions used can be found in the Appendix A.4. The PCR product was confirmed using agarose gel electrophoresis with a 1% (w/v) agarose gel stained using SYBR safe. A no-template control was included in the PCR reaction to test for DNA contamination and 50ng of pSFV(core) plasmid DNA was used as a positive control for the PCR reaction. Diagnostic restriction digestion

was also performed on the pIRES(core) and pIRES(empty) plasmid DNA preparations using BamHI (Promega). 500ng of plasmid DNA was digested in a 20µl final reaction volume, with 2µl of 10x NEBuffer 3, 0.5µl of BamHI (20 units/µl), 0.2µl of 100x BSA and nuclease-free water. Digestion reactions were incubated for 2 hours at 37˚C and run on a 1% agarose gel stained with SYBR safe. Correct digestion of the pIRES(core) plasmid generated fragments of: 525bp, 1215bp, 2279bp and 3178bp. Correct digestion of the pIRES(empty) plasmid generated fragments of: 525bp, 2279 and 3813bp.

Sequences for the core PCR primers and a map of the pIRES(core) and pIRES(empty) plasmids can be found in the Appendix sections A.3 and A.6, respectively. The pIRES bicistronic plasmid containing a Blasticidin resistance gene in the second multiple cloning site of the vector was generously donated by Dr Marco Purbhoo (Imperial College London).

2.6.5 Transfection of the pIRES(core) and pIRES(empty) plasmids into Huh7 cells

Huh7 cells were transfected either with 5µg of the pIRES(core) plasmid or 5µg of the pIRES(empty) plasmid using Lipofectamine 2000 (see 2.2.3). At 24 hours post-transfection, Blasticidin (Invitrogen) was added to the growth medium at a final concentration of 10µg/ml. A week later, the transfected cells were passaged into a 25cm^2 tissue culture flask with growth medium containing 10µg/ml Blasticidin. After four weeks of passaging the transfected Huh7 cells in the presence of Blasticidin, 1x10^5 of the pIRES(core) and pIRES(empty) transfected cells were seeded onto coverslips in a 24-well tissue culture plate. The cells were tested for the expression of the HCV core protein by immunofluorescent staining (see 2.2.6).

2.7 Western blot analysis of host proteins during JFH-1 infection

2.7.1 Western blot analysis of TXNIP and PGC1α during JFH-1 infection

Huh7 cells were seeded in a 6-well tissue culture plate at a density of 2.5x10^5. The following day, the cells were either infected with JFH-1 at a MOI of 3, or mock infected with an equal volume of concentrated conditioned growth medium. At 24, 36 and 48 hours post-infection, the cells were washed in PBS and harvested in 50µl of 0.5% Triton X-100 lysis buffer (20mM Tris-HCl pH7.6, 150mM NaCl, 0.5% (v/v) Triton X-100, 1mM EDTA and 1x protease inhibitors (100x stock Pierce Biosciences)). Cell lysates were incubated at 4˚C for 30 minutes, centrifugation was performed in a Sorvalc Biofuge Fresco microcentrifuge at 12,100rpm

(ca.14000xg) for 20 minutes and the supernatant was collected and stored at -20˚C. Protein quantification was performed using the Bradford reagent (Sigma) by incubating 5µl of protein lysate (diluted by 1 in 10 in deionised water), with 250µl of Bradford reagent in a 96-well flat bottom microplate. The cell lysates were incubated for 5 minutes at room temperature and absorbance was measured at 595nm using a Versamax Plus microplate reader. A BSA standard curve (1.5, 1.25, 1, 0.75, 0.5 and 0.25 mg/ml) was included to allow protein concentration to be estimated. 50µg of each protein lysate was run on a 10% (v/v) acrylamide gel in a total sample reaction volume of 35µl. (Note: An 8% (v/v) acrylamide gel was used for the analysis of PGC1α due to the high molecular weight of the PGC1α protein). Each sample was made up to 17.5µl with 0.5% Triton X-100 lysis buffer and added to 17.5µl of 2x sample loading buffer (125mM Tris HCl, 4% (w/v) SDS, 10% (v/v) β-mercaptoethanol, 20% (v/v) glycerol and 0.004% (v/v) bromophenol blue, pH6.8). Samples were incubated at 100˚C for 5 minutes and loaded onto the gel which was run at 200V for 30 minutes in 1x Tris-glycine running buffer (25mM Tris Base, 190mM glycine and 0.1% SDS, pH8.3). The gel was transferred onto nitrocellulose membrane in 1x Tris-glycine running buffer with 20% (v/v) methanol. Transfer was performed at 100V for 60 minutes (4˚C). When transferring proteins for PGC1α analysis, transfer was performed in 1x Tris-glycine running buffer with 10% (v/v) methanol for 80 minutes (4˚C). The membrane was blocked using 4% (w/v) skimmed milk powder / PBST (0.1% (v/v) Tween20 / PBS) for 1 hour at room temperature. The membrane was probed using 5ml of primary antibody diluted in 4% (w/v) BSA/PBST and incubated overnight at 4˚C. Primary antibodies used to detect host proteins included: mouse anti-TXNIP antibody, diluted 1 in 1000 (MBL International JY2 clone); mouse anti-PGC1α antibody, diluted 1 in 400 (Santa Cruz sc-13067) and mouse anti-α-tubulin antibody, diluted 1 in 10,000 (Sigma clone B512). Primary antibodies used to detect HCV proteins included: mouse anti-core antibody, diluted 1 in 1000 (Abcam C750 clone); and mouse anti-NS3 antibody, diluted 1 in 1000 (Virogen). Following incubation with primary antibody, the membrane was washed in 25ml of PBST for 10 minutes, three times. For detection of the bound primary antibody, the membrane was probed for 1 hour at room temperature with 5ml of horseradish peroxidase (HRP) conjugated goat anti-mouse polyclonal antibody (Millipore), diluted 1 in 2000 in 4% (w/v) BSA/PBST. The membrane was washed in 25ml of PBST for ten minutes, three times, and developed using a chemiluminescent ECL substrate (Pierce Bioscience

Supersignal West Pico Substrate). 2.5ml of Stable Peroxide solution was mixed with 2.5ml of Luminol Enhancer solution and the 5ml solution was added to the membrane for 5 minutes. The chemiluminescent signal was detected by X-ray film. Exposure times varied depending on the antibody. Approximate timings used were: 30 seconds (Tubulin), 60 seconds (TXNIP and NS3), 5 minutes (core) and 20 minutes (PGC1α). 10µl of prestained protein ladder (Invitrogen) was included alongside the protein samples on each protein gel. To investigate the abundance of several proteins on one western blot, the membrane was stripped by incubating it in 10ml of commercial blot stripping buffer (Restore Plus Western blot stripping buffer Thermo Scientific) for 20 minutes. The membrane was then washed in 25ml of PBST for 20 minutes, three times.

2.7.2 Quantification of western blot protein bands

Quantification of western blot protein bands was performed using ImageJ. The mean intensity of each protein band was quantified and normalised using the band intensities quantified for the α-tubulin protein. Fold change in protein abundance was calculated by comparing the normalised band intensities quantified for the JFH-1 infected samples to those quantified for the mock infected samples at each time-point. Fold change data shown is based on the data obtained from two independent western blots performed for PGC1α and TXNIP.

2.7.3 Optimisation of TXNIP and PGC1α antibodies for western blot analysis

The anti-TXNIP antibody was optimised using 50µg of protein lysate obtained from Huh7 cells that had been JFH-1 or mock infected for 48 hours (see 2.7.1), and 50µg of protein lysate obtained from the K562 cell line. K562 cells were seeded at a density of $2.5x10^5$ in a 6-well plate and incubated for 48 hours. All cells were harvested in 50µl of 0.5% Triton X-100 lysis buffer and used for western blot analysis with the anti-TXNIP antibody (see 2.7.1). The anti-PGC1α antibody was optimised using 25µg and 50µg of protein lysates obtained from PGC1α expressing HEK293T cells. HEK293T cells were seeded into a 6-well plate at a density of $6x10^5$. The following day, the cells were transfected with 5µg of a pcDNA3.1D/V5-His-TOPO plasmid that contained the human PGC1α gene sequence using Lipofectamine 2000 (see 2.2.3). The transfected cells were incubated for 48 hours, harvested in 50µl of 0.5% Triton X-100 lysis buffer and used for western blot analysis with the anti-PGC1α antibody (see 2.7.1). The

pcDNA3.1D/V5-His-TOPO PGC1α plasmid was generously donated by Dr Mark Christian (Imperial College London).

2.7.4 Testing an anti-Staufen1 antibody in western blot analysis

An anti-Staufen1 antibody was tested using 75µg of protein lysate isolated from Huh7 cells that had been JFH-1 or mock infected for 48 hours (see 2.7.1), and 75µg of protein lysate from a HepG2 cell line (the recommended positive control). HepG2 cells were seeded into a 6-well plate at a density of $5x10^5$ and incubated for 48 hours. All cells were harvested in 50µl of 0.5% Triton X-100 lysis buffer and used for western blot analysis (see 2.7.1). Protein lysates were run on a 10% (v/v) acrylamide gel and transferred to a nitrocellulose membrane (see 2.7.1). The blot was probed using a rabbit anti-Staufen1 antibody (Abcam ab50914), diluted 1 in 500 in 4% (w/v) BSA/PBST; this was detected using a HRP-conjugated goat anti-rabbit antibody, diluted 1 in 2000 in 4% (w/v) BSA/PBST (Millipore).

The anti-Staufen1 antibody was also tested using 75µg of protein lysate isolated from Huh7 cells transfected with Staufen1 siRNA molecules. Huh7 cells were seeded into a 12 well plate at a density $2x10^5$. The following day, growth medium was replaced with 1ml of OptiMEM medium. A transfection mix was assembled by combining 100µl of OptiMEM containing 2µl Lipofectamine 2000 and 100µl of OptiMEM containing 3µl of 10µM STAU1-1 siRNA (25nM) and 3µl of STAU1-2 siRNA (25nM). Negative control samples were prepared using 6µl of 10µM negative control non-targeting siRNA (50nM). The transfection mixes were incubated at room temperature for 20 minutes and added to the cells. After an 8 hour incubation period, the transfection medium was replaced with 1ml of growth medium. At 48 hours post-transfection, the cells were harvested in 20µl of 0.5% Triton X-100 lysis buffer and used for western blot analysis with the anti-Staufen1 and anti-Tubulin antibodies (see above and 2.7.1).

2.8 Triglyceride quantification assay

2.8.1 Quantification of intracellular triglyceride in JFH-1 infected cells

Huh7 cells were seeded in triplicate in a 6-well tissue culture plate at a density of $2.5x10^5$. The following day, the cells were either infected with JFH-1 at an MOI of 3, or mock infected with an equal volume of concentrated conditioned growth medium. At 24, 48 and 72 hours post-infection, the cells were washed in PBS, trypsinised in 50µl of 1x trypsin/EDTA, pelleted by centrifugation in a Mistral 3000

Benchtop centrifuge (MSE) at 1300rpm (283xg) and washed twice in PBS. After the second PBS wash, the cells were pelleted again and lysis was performed in 50µl of 5% (v/v) Triton X-100 / H_2O. The cell lysates were heated slowly in a water bath at 90˚C for 5 minutes, cooled slowly at room temperature, and heated again in a water bath at 90˚C for 5 minutes. The cell lysates were centrifuged in a Sorvalc Biofuge Fresco microcentrifuge at 12,100rpm (ca.14000xg) for 5 minutes and the supernatant was collected. The protein concentration for each lysate was estimated using the Bradford protein quantification assay (see 2.7.1). 25µg of each cell lysate was diluted in a total volume of 10µl using the 5% Triton X-100 lysis buffer. Cell lysate samples were then added to 38µl of triglyceride kit assay buffer with 2µl of lipase enzyme, and incubated at room temperature for 20 minutes. To each of the 50µl samples, 46µl of triglyceride kit assay buffer, 2µl of triglyceride probe, and 2µl of triglyceride enzyme mix was added. The samples were incubated for 30 minutes at room temperature, and absorbance at 570nm was measured using a Versamax Plus microplate reader. A standard curve was included in the assay for absolute quantification of triglyceride, and was generated using 2, 4, 5, 6, 8 and 10nmol of the triglyceride standard reagent. All reagents for quantification of intracellular triglyceride were provided by the triglyceride quantification kit (Abcam). Fold change in triglyceride levels at each time-point was calculated by comparing the absolute triglyceride quantified for the JFH-1 infected samples to the mock infected samples. Samples for quantification of triglyceride were extracted in duplicate for each time-point and the experiment was performed three times. The triglyceride quantification assay described was optimised by testing the kit with uninfected Huh7 cell protein lysate.

2.8.2 Quantification of intracellular triglyceride in replicon expressing cells

Wild type, cured and subgenomic replicon expressing (p10 post-transfection) Huh7 cells were seeded in triplicate in a 6-well tissue culture plate at a density of $2.5x10^5$. The cells were incubated in normal DMEM growth medium for 48 hours, after which, the cells were trypsinised, washed twice in PBS and lysed using 5% Triton X-100 / H_2O. Cell lysates were processed and intracellular triglyceride levels were quantified using the triglyceride quantification kit (Abcam) (see 2.8.1). Fold change in triglyceride levels was calculated by comparing the absolute triglyceride quantified for the replicon expressing and cured cells to the wild type cells. Samples for quantification of triglyceride were extracted in triplicate for each cell type and the experiment was performed twice.

2.9 Cholesterol quantification assay

2.9.1 Quantification of intracellular cholesterol in JFH-1 infected cells

Huh7 cells were seeded in triplicate in a 6-well tissue culture plate at a density of $2.5x10^5$. The following day, the cells were either infected with JFH-1 at an MOI of 3, or mock infected in triplicate with an equal volume of concentrated conditioned growth medium. At 24, 48 and 72 hours post-infection, the cells were washed in PBS, trypsinised in 50µl of 1x trypsin/EDTA, pelleted by centrifugation in a Mistral 3000 Benchtop centrifuge (MSE) at 1300rpm (283xg) and washed twice in PBS. After the second PBS wash, the cells were pelleted again and lysis was performed in 50µl of 0.5% Triton X-100 lysis buffer (20mM Tris-HCl pH7.6, 150mM NaCl, 0.5% (v/v) Triton X-100, 1mM EDTA and 1x protease inhibitors (100x stock Pierce Biosciences)). Cell lysates were incubated at 4˚C for 30 minutes, and the supernatant was harvested by centrifugation in a Sorvalc Biofuge Fresco microcentrifuge at 12,100rpm (ca.14000xg) (4˚C) for 20 minutes. The protein concentration for each lysate was estimated using the Bradford protein quantification assay (see 2.7.1). 25µg of each cell lysate was diluted in a total volume of 10µl using the 0.5% Triton X-100 lysis buffer; samples were then added to 40µl of the cholesterol kit reaction buffer. To each of the 50µl samples, 0.75µl Amplex Red reagent, 0.5µl HRP, 0.5µl cholesterol oxidase, 0.5µl cholesterol esterase and 48.2µl of the cholesterol kit reaction buffer was added. For the quantification of 'free cholesterol', cholesterol esterase was omitted from the reaction mix. Samples were incubated for 30 minutes at 37˚C and absorbance at 560nm was measured using a Versamax Plus microplate reader. A standard curve was also included in the assay for absolute quantification of cholesterol, and was generated using 0.5, 1, 2, 3, 4 and 8 µg/ml of the cholesterol standard reagent. All reagents for quantification of intracellular cholesterol were provided by the Amplex Red cholesterol quantification kit (Invitrogen). Fold change in cholesterol levels at each time-point was calculated by comparing the absolute cholesterol quantified for the JFH-1 infected samples to the mock infected samples. Samples for quantification of cholesterol were extracted in duplicate for each time-point and the experiment was performed three times. The cholesterol quantification assay described was optimised by testing the kit with uninfected Huh7 cell protein lysate.

2.9.2 Quantification of intracellular cholesterol in replicon expressing cells

Wild type, cured and subgenomic replicon expressing (p10 post-transfection) Huh7 cells were seeded in triplicate in a 6-well tissue culture plate at a density of $2.5x10^5$. The cells were incubated in normal DMEM growth medium for 48 hours, after which, the cells were trypsinised, washed twice in PBS and lysed using 0.5% Triton X-100 lysis buffer. Cell lysates were processed and intracellular cholesterol levels were quantified using the Amplex Red cholesterol quantification kit (Invitrogen) (see 2.9.1). Fold change in cholesterol levels was calculated by comparing the absolute cholesterol quantified for the replicon expressing and cured cells to the wild type cells. Samples for quantification of cholesterol were extracted in triplicate for each cell type and the experiment was performed twice.

2.10 Lipid droplet staining and quantification

2.10.1 Lipid droplet staining in JFH-1 infected cells

Huh7 cells were seeded into an 8-well chamber slide at a density of $0.2x10^5$. The following day, the cells were either infected with JFH-1 at an MOI of 3, or mock infected with an equal volume of concentrated conditioned growth medium. At 48 hours post-infection, the cells were fixed and stained for the HCV core protein (see 2.2.6). Once staining for the HCV core protein was complete, the cells were incubated for 1 hour at room temperature with 50µg/ml BODIPY 493/503 (Invitrogen), diluted in PBS. The cells were then washed in PBS for 5 minutes, three times; stained with DAPI and mounted in Mowiol. Images were captured using a Nikon Eclipse TE2000S fluorescence microscope. The same exposure time and gain settings were used for image acquisition to allow accurate image comparison.

2.10.2 Quantification of lipid droplet abundance in JFH-1 infected cells

Huh7 cells were seeded into an 8-well chamber slide at a density of $0.2x10^5$. The following day, the cells were infected with JFH-1 at an MOI of 0.5. At 48 hours post-infection, the cells were stained for the HCV core protein and intracellular lipid droplets (see 2.2.6 and 2.10.1). Images were captured using a Nikon Eclipse TE2000S fluorescence microscope. Quantification of BODIPY staining was performed using Image J. Fold change in BODIPY staining during JFH-1 infection was calculated by comparing the mean BODIPY fluorescence quantified for the HCV core-positive cells to the HCV core-negative cells, captured in the same

image. Quantification of BODIPY fluorescence was performed for a total of 15 HCV core-positive cells and 15 HCV core-negative cells.

2.10.3 Quantification of lipid droplet abundance in replicon expressing cells

Wild type, cured and subgenomic replicon expressing Huh7 cells were seeded onto coverslips in a 24-well tissue culture plate at a density of $0.8x10^5$. The cells were incubated in normal DMEM growth medium for 48 hours. The cells were fixed and stained for the HCV NS3 protein and intracellular lipid droplets (see 2.5.4 and 2.10.1). Images were captured using a Nikon Eclipse TE2000S fluorescence microscope. The same exposure time and gain settings were used for image acquisition to allow accurate image comparison. Quantification of BODIPY staining was performed using Image J. Fold change in BODIPY staining was calculated by comparing the mean BODIPY fluorescence quantified for the replicon expressing Huh7 cells that stained positively for NS3 and the replicon expressing Huh7 cells that did not stain for NS3, captured in the same image. Quantification of BODIPY fluorescence was performed for a total of 15 NS3-positive replicon Huh7 cells and 15 NS3-negative replicon Huh7 cells. Replicon expressing cells from passage 4 post-transfection were used to ensure that a mix of transfected (NS3 positive) and non-transfected (NS3 negative) cells were present.

2.10.4 Quantification of lipid droplet abundance in cells expressing JFH-1 core

Huh7 cells seeded onto coverslips in a 24-well tissue culture plate were transfected with 1µg of the SFV(core) RNA, 1µg of the SFV(empty) RNA, or transfection medium alone (see 2.6.3). The transfected cells were incubated for 24 hours and stained for the HCV core protein and intracellular lipid droplets (see 2.2.6 and 2.10.1). Images were captured using a Nikon Eclipse TE2000S fluorescence microscope. The same exposure time and gain settings were used for image acquisition to allow accurate image comparison. Quantification of BODIPY staining was performed using Image J. Fold change in BODIPY staining was calculated by comparing the mean BODIPY fluorescence quantified for the Huh7 cells transfected with SFV(core) RNA that stained positively for HCV core and the Huh7 cells transfected SFV(core) RNA that did not stain for the HCV core protein, captured in the same image. Quantification of BODIPY fluorescence was performed for a total of 15 core-positive cells and 15 core-negative cells.

2.11 Glucose quantification assay

Quantification of intracellular glucose in JFH-1 infected cells

Huh7 cells were seeded in 25cm^2 tissue culture flasks at a density of 0.8x10^6. The following day, the cells were either infected with JFH-1 at an MOI of 3, or mock infected with an equal volume of concentrated conditioned growth medium. At 48 hours post-infection, the cells were washed in PBS, trypsinised in 500µl of 1x trypsin/EDTA, pelleted by centrifugation in a Mistral 3000 Benchtop centrifuge (MSE) at 1300rpm (283xg) and washed twice in PBS. After the second PBS wash, the cells were pelleted again and lysis was performed in 100µl of 0.5% Triton X-100 lysis buffer (20mM Tris-HCl pH7.6, 150mM NaCl, 0.5% (v/v) Triton X-100, 1mM EDTA and 1x protease inhibitors (100x stock Pierce Biosciences)). Cell lysates were incubated at 4˚C for 30 minutes and the supernatant was harvested by centrifugation in a Sorvalc Biofuge Fresco microcentrifuge at 12,100rpm (ca.14000xg) (4˚C) for 20 minutes. The protein concentration for each lysate was estimated using the Bradford protein quantification assay (see 2.7.1). 75µg of each cell lysate was diluted in a total volume of 20µl using the 0.5% Triton X-100 lysis buffer and added to 30µl of the glucose kit reaction buffer. To each of the 50µl samples, 0.5µl Amplex Red reagent, 1µl HRP, 1µl glucose oxidase and 47.5µl of glucose kit reaction buffer was added. Samples were incubated for 30 minutes at room temperature and absorbance at 560nm was measured using a Versamax Plus microplate reader. A standard curve was included in the assay for absolute quantification of glucose, and was generated using 2.5, 12, 25 and 50µM of the glucose standard reagent. All reagents for quantification of intracellular glucose were provided by the Amplex Red glucose quantification kit (Invitrogen). Fold change in glucose levels was calculated by comparing the absolute glucose quantified for the JFH-1 infected cells to the mock infected cells. Samples for quantification of glucose were extracted in triplicate for each sample and the experiment was performed twice. The glucose quantification assay described was optimised by testing the kit with uninfected Huh7 cell protein lysate.

2.12 siRNA transfection of Huh7 and Huh7.5 cells

2.12.1 Optimisation of siRNA transfection using a GAPDH-targeting siRNA

Huh7 cells were seeded in a 24-well tissue culture plate at a density of 0.8x10^5. The following day, growth medium was replaced with 500µl of OptiMEM medium.

A transfection mix was assembled by combining 50µl of OptiMEM containing 1µl Lipofectamine 2000 and 50µl of OptiMEM containing 3µl of 10µM GAPDH siRNA stock (50nM). Negative control samples were prepared using 3µl of 10µM negative control non-targeting siRNA (50nM). The transfection mixes were incubated at room temperature for 20 minutes and added to the cells. After an 8 hour incubation period, the transfection medium was replaced with growth medium. At 48 hours post-transfection, the cells were washed in ice-cold PBS and intracellular RNA was harvested using 200µl of TRIzol reagent. RNA was extracted using 40µl chloroform, precipitated using 100µl isopropanol and washed in 1ml of 75% (v/v) ethanol/H_2O (see 2.4.2). The RNA pellet was air-dried and resuspended in 8µl of nuclease-free water. RNA was treated with Turbo DNA-free DNase in a total reaction volume of 10µl, with 1µl Turbo DNA-free DNase buffer and 1µl of Turbo DNA-free DNase. 2µl of DNase inactivation reagent was used to inactivate and remove the DNase (see 2.4.2). RNA concentration was measured using a Nanodrop 1000 spectrophotometer. The efficiency of GAPDH gene knockdown was investigated by one-step qRT-PCR using the ΔΔCT equation (see 2.4.3). To perform qRT-PCR, the extracted RNA samples were used directly in a one-step qRT-PCR reaction. Reactions were performed in a final volume of 10µl, with 250ng of total RNA, 0.1µl of reverse-transcription enzyme, 1µM reverse primer, 1µM forward primer, 5µl of 2x Quantitect SYBR green RT-PCR mastermix and nuclease-free water. The one-step qRT-PCR cycle conditions used can be found in the Appendix section A.4. CT values obtained were used directly in the ΔΔCT equation to calculate fold change in GAPDH expression, comparing the cells transfected with the GAPDH siRNA to the cells transfected with the non-targeting siRNA. Fold change in GAPDH expression was plotted as a value between 0 and 1, with the negative control siRNA having a fold change value of 1. The expression data was normalised using Beta actin (see 2.4.3). Comparison was also made to cells transfected with Lipofectamine 2000 only and transfection medium only. The GAPDH and non-targeting siRNA molecules were transfected in duplicate and the transfection experiment was performed twice.

2.12.2 Optimisation of the siRNA knockdown assay using a HCV siRNA

Huh7 cells seeded into 24-well tissue culture plates were transfected with siRNA molecules using Lipofectamine 2000 (see 2.12.1). Transfection was performed using a single siRNA targeting the HCV genome [209], which was tested at 10, 50 and 100nM (0.6µl, 3µl and 6µl of a 10µM siRNA stock). Negative control samples

were also transfected using 10, 50 and 100nM of a negative control non-targeting siRNA. The transfected cells were incubated for 48 hours, and infected with JFH-1 at an MOI of 3. At 4 hours post-infection, the cells were washed twice in PBS and incubated with DMEM growth medium. At 48 hours post-infection, growth medium for each sample was collected and stored at -20˚C, the cells were washed in ice-cold PBS and the intracellular RNA was extracted using 200µl of TRIzol reagent (see 2.12.1 and 2.4.2). RNA was treated with Turbo DNA-free DNase and concentration was measured using a Nanodrop 1000 spectrophotometer (see 2.12.1 and 2.4.2). The effect of siRNA transfection on the intracellular levels of JFH-1 genomic RNA was investigated by one-step qRT-PCR using the ΔΔCT equation (see 2.12.1 and 2.4.3). Fold change in JFH-1 RNA abundance was calculated by comparing the cells transfected with the HCV siRNA to the cells transfected with the non-targeting siRNA. The expression data obtained for intracellular JFH-1 RNA abundance was normalised using GAPDH. The HCV and non-targeting siRNA molecules were transfected in duplicate for all three siRNA concentrations and the transfection experiment was performed twice.

To investigate the effect of siRNA transfection on JFH-1 virus secretion, the titres of JFH-1 virus in the media collected at 48 hours post-infection were quantified. Huh7.5 cells were seeded in a 96-well plate at a density of $1x10^4$. The following day, growth medium was removed from the cells and was replaced with 100µl of the medium collected for each transfection reaction, which had been diluted by 1 in 100 in DMEM growth medium. At 48 hours post-infection, the cells were stained for the HCV core protein (see 2.2.6). Core staining was visualised using a Nikon Eclipse TE2000S fluorescence microscope. The numbers of core-positive foci were counted for each sample. A comparison was made between the foci numbers counted for the HCV siRNA transfected cells to the foci numbers counted for the cells transfected with the negative control non-targeting siRNA. Each media sample was analysed in duplicate, and all samples from the two transfection experiments were tested.

HCV core protein staining was also performed to test the effect of HCV siRNA transfection on JFH-1 replication. Huh7 were cells seeded onto coverslips in a 24-well tissue culture plate. The cells were transfected with 50nM of HCV siRNA or a negative control non-targeting siRNA using Lipofectamine 2000 for 48 hours, followed by infection with JFH-1 at a MOI of 3 (see above). At 48 hours post-

infection, the cells were stained for HCV core protein (see 2.2.6). Core staining was visualised using a Nikon Eclipse TE2000S fluorescence microscope. The same exposure time and gain settings were used for image acquisition to allow accurate image comparison.

2.12.3 Optimisation of the siRNA knockdown assay using RAB1B siRNAs

Huh7 cells seeded into 24-well tissue culture plates were transfected with siRNA molecules using Lipofectamine 2000 and infected with JFH-1 at an MOI of 3 (see 2.12.1 and 2.12.2). Three different siRNAs for RAB1B were transfected individually at a final concentration of 50nM [128]. Negative control samples were also transfected using 50nM of a negative control non-targeting siRNA. At 48 hours post-infection, the intracellular RNA for each sample was extracted using 200µl of TRIzol reagent (see 2.12.1 and 2.4.2). RNA was treated with Turbo DNA-free DNase and concentration was measured using a Nanodrop 1000 spectrophotometer (see 2.12.1 and 2.4.2). The effects of RAB1B siRNA transfection on the intracellular levels of JFH-1 genomic RNA and target RAB1B mRNA were investigated by one-step qRT-PCR using the ΔΔCT equation (see 2.12.1 and 2.4.3). Fold change in JFH-1 RNA and RAB1B mRNA abundance was calculated by comparing the cells transfected with the RAB1B siRNA molecules to the cells transfected with the non-targeting siRNA; the expression data obtained was normalised using GAPDH. The RAB1B and non-targeting siRNA molecules were transfected in duplicate and the transfection experiment was performed three times.

The efficiency of RAB1B knockdown following RAB1B siRNA transfection was investigated using a time-course transfection experiment. Huh7 cells were transfected with RAB1B siRNAs or a negative control non-targeting siRNA for 24, 48, 72 or 96 hours (see 2.12.1). The effects of RAB1B siRNA transfection on the intracellular levels of RAB1B mRNA were investigated by one-step qRT-PCR using the ΔΔCT equation (see 2.12.1 and 2.4.3). The RAB1B and non-targeting siRNA molecules were transfected in duplicate and the transfection experiment was performed twice.

2.12.4 The siRNA knockdown assay: Investigating the effect of host gene silencing on JFH-1 replication and secretion

Huh7 and Huh7.5 cells seeded into 24-well tissue culture plates were transfected with siRNA molecules using Lipofectamine 2000 and infected with JFH-1 at an MOI of 3 (see 2.12.1 and 2.12.2). When testing the effects of the RAB2A/B, RAB4A/B, RAB6A, RAB11A/B, RAB18, Staufen1, TIA1, TIAL1, RAB27A/B, RAB33B, RAB37, TXNIP, CYP1A1 and ABLIM3 siRNA molecules, cells were transfected either with a 50nM pool of two siRNAs for each target (1.5µl of 10µM siRNA 1 + 1.5µl of 10µM siRNA 2) or 25nM of individual siRNAs (1.5µl of 10µM siRNA). When testing the effects of the PGC1α, RIP140, CIDEB, CIDEC, FOXO1, KLF6, MLX, MLXIP, MLXIPL and ARRDC4 siRNA molecules, cells were transfected with 50nM of a single siRNA for each target. Negative control samples were transfected either with 25nM or 50nM of a negative control non-targeting siRNA. At either 24 or 48 hours post-infection, growth medium for each sample was collected and stored at -20˚C and the intracellular RNA was extracted using 200µl of TRIzol reagent (see 2.12.1 and 2.4.2). RNA was treated with Turbo DNA-free DNase and concentration was measured using a Nanodrop 1000 spectrophotometer (see 2.12.1 and 2.4.2). The effects of siRNA transfection on target gene expression and the intracellular level of JFH-1 genomic RNA were investigated by one-step qRT-PCR using the ΔΔCT equation (see 2.12.1 and 2.4.3). Fold change in target mRNA and JFH-1 RNA abundance was calculated by comparing the cells transfected with a target-specific siRNA molecule to the cells transfected with a non-targeting siRNA; the expression data obtained was normalised using GAPDH. To investigate the effect of siRNA transfection on JFH-1 virus secretion, the titres of JFH-1 virus in the media collected at 48 hours post-infection were quantified (see 2.12.2). The numbers of core-positive foci were counted for each sample. A comparison was made between the foci numbers counted for medium from the target-specific siRNA transfections to the foci numbers counted for the medium from the negative control non-targeting siRNA transfections. Each media sample was analysed in duplicate, and all samples from the three transfection experiments were tested.

To investigate the effect of host siRNA knockdown on JFH-1 protein abundance, Huh7 cells were transfected with siRNA and infected with JFH-1 as detailed above. Cells were transfected with 25nM of individual siRNAs targeting RAB2B, RAB4A, RAB11B, RAB27B, CYP1A1, STAU1 and TXNIP and 50nM of the

individual siRNA targeting STAU2. The siRNA molecules targeting Staufen1 and TXNIP were also transfected as a pool of two siRNAs at a final concentration of 50nM. Negative control samples were transfected with either 25nM or 50nM of negative control non-targeting siRNA. In some of the transfection experiments, cells were also transfected with 50nM of the HCV siRNA as a positive control. At 48 hours post-infection, the cells were washed in PBS and harvested in 20µl of 0.5% Triton X-100 lysis buffer. Cell lysates were processed for western blotting and protein concentration was measured using the Bradford protein quantification assay (see 2.7.1). 25µg of each protein lysate was run on a 10% acrylamide gel and transferred onto nitrocellulose membrane, which was probed using an anti-core antibody (Abcam), an anti-NS3 antibody (Virogen) and an anti-α-tubulin antibody (Sigma) (see 2.7.1). Quantification of the western blot protein bands was performed using ImageJ (see 2.7.2). Fold change values shown are based on the data obtained from a single western blot analysing cells transfected with RAB2B, RAB4A, RAB11B, RAB27B, CYP1A1 and Staufen1 siRNA molecules, and from two independent western blots analysing cells transfected with TXNIP siRNA molecules.

The sequences for all the qRT-PCR primers and siRNA molecules used can be found in the Appendix sections A.1 and A.7, respectively. The siRNA molecules targeting RAB27A and RAB33B were generously donated by Dr Gill Elliott (Imperial College London).

2.12.5 PPARα target gene expression following TXNIP gene knockdown

Huh7 cells seeded into a 24-well tissue culture plate were transfected with 50nM of a pool of TXNIP siRNAs (1.5µl of 10µM siTXNIP-1 + 1.5µl of 10µM siTXNIP-2) or 50nM of a negative control non-targeting siRNA using Lipofectamine 2000 (see 2.12.1). At 48 hours post-transfection, the cells were either processed for RNA extraction and gene expression analysis (see 2.12.1, 2.4.2 and 2.4.3), or the cells were infected with JFH-1 at an MOI of 3, incubated for a further 48 hours and then processed for RNA extraction and gene expression analysis (see 2.12.2, 2.4.2 and 2.4.3). The expression of PPARα target genes in the cellular RNA extracts was investigated by one-step qRT-PCR using the ΔΔCT equation (see 2.12.1 and 2.4.3). Fold change in host gene expression was calculated by comparing the cells transfected with the TXNIP siRNA molecules to the cells transfected with a non-targeting siRNA; the expression data was normalised using GAPDH. In both

experiments, the TXNIP and non-targeting siRNA molecules were transfected in triplicate in one experiment. The expression of PPARα target genes in Huh7 cells infected with JFH-1 for 48 hours was also investigated by microarray and qRT-PCR analysis (see 2.3 and 2.4). Sequences for the primers used in qRT-PCR can be found in the Appendix section A.1.

To further investigate the effect of TXNIP silencing on ACSL3 expression, Huh7 cells seeded in a 24 well plate were also transfected in triplicate with 25nM of individual TXNIP siRNAs (siTXNIP-1, siTXNIP-2 and siTXNIP-3) or 25nM of non-targeting siRNA and infected with JFH-1 (MOI = 3) (see 2.12.1 and 2.12.2). Intracellular RNA was extracted using 200µl TRIzol reagent (see 2.12.1 and 2.4.2). RNA was treated with Turbo DNA-free DNase and concentration was measured using a Nanodrop 1000 spectrophotometer (see 2.12.1 and 2.4.2). TXNIP and ACSL3 expression was investigated using one-step qRT-PCR and the ΔΔCT equation (2.12.1 and 2.4.3).

2.13 Alamar blue cell viability assay

Huh7 and Huh7.5 cells were seeded in a 96-well tissue culture plate at a density of $2x10^4$. The following day, growth medium was replaced with 100µl of OptiMEM medium. Transfection mixes were assembled by combining 25µl of OptiMEM containing 0.25µl Lipofectamine 2000 and 25µl of OptiMEM containing either 25nM of individual siRNAs (3.75µl of 1µM siRNA), 50nM of individual siRNAs (7.5µl of 1µM siRNA), or 50nM of an siRNA pool (3.75µl of 1µM siRNA1 + 3.75µl of 1µM siRNA-2). Negative control samples included: cells transfected with a negative control non-targeting siRNA at a concentration of either 25nM or 50nM, cells transfected with Lipofectamine 2000 only and cells transfected with transfection medium only. The transfection mixes were incubated at room temperature for 20 minutes and added to the cells. After an 8 hour incubation period, the transfection medium was replaced with 100µl of growth medium. At 20 hours post-transfection, 10µl of the alamar blue reagent (Invitrogen) was added to each well. Several controls were also added to the plate including: media only (blank) (100µl growth medium), oxidised alamar blue (100µl growth medium with 10µl alamar blue) and reduced alamar blue (100µl growth medium with 10µl alamar blue, reduced by autoclaving for 15 minutes). At 24, 48 and 72 hours post-transfection, the absorbance of the wells was measured at 570nm (reduced alamar blue) and 600nm (oxidised alamar blue) using a Versamax Plus microplate

reader. Absorbance values were used to calculate the percentage of reduced alamar blue in each well, which correlates to the metabolic activity of the cells present.

The following calculations were used to calculate percentage of reduced alamar blue:

1. 570nm absorbance values for samples and controls – 570nm absorbance media only
2. 600nm absorbance values for samples and controls – 600nm absorbance media only
3. Correction factor = Absorbance oxidised control 570nm/Absorbance oxidised control 600nm
4. % reduced alamar = (Absorbance 570nm – (Absorbance 600nm x correction factor)) x 100

Note: The correction factor is required to correct for the small overlap observed in the absorbance of oxidised and reduced alamar blue (see manufacturer's instructions for further details). The viability of the siRNA transfected cells was calculated by comparing the levels of reduced alamar blue quantified for target specific siRNA transfected cells to the non-targeting siRNA transfected cells [210]. Each siRNA molecule was tested for its effects on cell viability in triplicate in two separate transfection experiments.

2.14 Quantitative PCR expression analysis of interferon stimulated genes

2.14.1 Optimisation of the IFNα and poly (I:C) positive controls

Huh7 and Huh7.5 cells were seeded into a 24-well tissue culture plate at a density of $0.8x10^5$. The following day, the cells were treated with 5, 10, 50, 100 and 200 IU/ml of IFNα (Sigma), which was added directly to the DMEM growth medium. Negative control cells were incubated in DMEM growth medium that did not contain IFNα (0 IU/ml IFNα). The cells were also transfected with 1, 10, 50 and 100ng of poly (I:C) (Sigma) using Lipofectamine 2000. The cells were incubated in 500µl of OptiMEM medium and transfection mixes were prepared by combining 50µl of OptiMEM containing 1µl Lipofectamine 2000 and 50µl of OptiMEM containing 1, 10, 50 and 100ng poly (I:C) (equivalent to 0.1µl, 1µl, 5µl and 10µl of 10µg/ml poly (I:C) / PBS.) The transfection mixes were incubated at room temperature for 20 minutes and added to the cells. Negative control samples included cells transfected with Lipofectamine 2000 reagent only and cells transfected with the transfection medium only (0ng poly (I:C)). The cells were incubated for 48 hours and intracellular RNA was extracted using 200µl of TRIzol reagent (see 2.12.1 and 2.4.2). RNA was treated with Turbo DNA-free DNase and

concentration was measured using a Nanodrop 1000 spectrophotometer (see 2.12.1 and 2.4.2). The expression of the interferon stimulated genes (ISG), PKR and MX1, was investigated by one-step qRT-PCR using the ΔΔCT equation (see 2.12.1 and 2.4.3). Fold change in ISG expression was calculated by comparing the cells treated with IFNα and poly (I:C) to the negative control cells; expression data was normalised using GAPDH. All samples were tested in triplicate in a single experiment. Sequences for the primers used in qRT-PCR can be found in the Appendix section A.1

2.14.2 Quantitative PCR analysis of ISG expression following siRNA transfection

Huh7 and Huh7.5 cells seeded in 24-well tissue culture plates were transfected with siRNA molecules targeting host genes using Lipofectamine 2000 (see 2.12.1). The siRNA molecules were either transfected individually at a final concentration of 25nM (TXNIP, CYP1A1 and STAU1 siRNAs) or 50nM (PGC1α, RIP140, CIDEB, CIDEC, FOXO1, KLF6, MLX, MLXIP, MLXIPL and ARRDC4 siRNAs), or in a pool at a final concentration of 50nM. Negative control samples included: cells transfected with 25nM or 50nM of a negative control non-targeting siRNA, cells transfected with Lipofectamine 2000 only and cells transfected with transfection medium only. Positive control samples included cells treated with 100IU/ml IFNα and cells transfected with 100ng poly (I:C). The cells were incubated for 48 hours and intracellular RNA was extracted using 200µl of TRIzol reagent (see 2.12.1 and 2.4.2). RNA was treated with Turbo DNA-free DNase and concentration was measured using a Nanodrop 1000 spectrophotometer (see 2.12.1 and 2.4.2). The expression of PKR and MX1 was investigated by one-step qRT-PCR using the ΔΔCT equation (see 2.12.1 and 2.4.3). Fold change in ISG expression was calculated by comparing the cells transfected with target-specific siRNA molecules to cells transfected with a negative control non-targeting siRNA. Expression data was normalised using GAPDH. The target-specific siRNA molecules were transfected in triplicate and the transfection experiment was performed twice.

2.15 Immunofluorescent staining of host proteins

2.15.1 Immunofluorescent staining of Staufen1 in untreated Huh7 cells

Huh7 cells were seeded onto coverslips in a 24-well tissue culture plate at a density of $1.5x10^5$. The following day, the cells were fixed, permeabilised and stained for Staufen1 using a rabbit anti-Staufen1 antibody (Abcam), diluted 1 in

200 in 1% (w/v) BSA/PBS (see 2.2.6). Detection of the bound primary antibody was performed using an Alexa Fluor 488-conjugated goat anti-rabbit antibody (Invitrogen), diluted 1 in 1000 in 1% (w/v) BSA/PBS. Before incubation with the Staufen1 antibody, the cells were blocked for 1 hour at room temperature in 1% BSA/PBS. Images were captured using a Nikon Eclipse TE2000S fluorescence microscope

2.15.2 Immunofluorescent staining of Staufen1 following STAU1 gene knockdown

Huh7 cells seeded onto coverslips in a 24-well tissue culture plate were transfected with 50nM of Staufen1 siRNAs (25nM of siSTAU1-1 + 25nM of siSTAU1-2) and 50nM of a negative control non-targeting siRNA using Lipofectamine 2000 (see 2.12.1). At 48 hours post-transfection the cells were stained for the Staufen1 protein (see 2.15.1). Images were captured using a Nikon Eclipse TE2000S fluorescence microscope. The same exposure time and gain settings were used for image acquisition to allow accurate image comparison.

2.15.3 Immunofluorescent staining of Staufen1 during JFH-1 infection

Huh7 cells were seeded onto coverslips in a 24 well tissue culture plate at a density of $0.8x10^5$. The following day, the cells were infected with JFH-1 at an MOI of 0.5 and incubated for 48 hours. The cells were stained for HCV core, HCV NS3, dsRNA and the Staufen1 protein (see 2.2.6, 2.5.4 and 2.15.1). Images were captured using a Nikon Eclipse TE2000S fluorescence microscope. The same exposure time and gain settings were used for image acquisition to allow accurate image comparison.

2.16 Statistical Analysis of Results

Calculations to determine the statistical significance of all fold change data were performed using a two-tailed unpaired T test with Prism Graphpad software. Data points with a p value of less than 0.05 were considered statistically significant. Results graphs representing fold change data were generated using Graphpad Prism software and display error bars that represent mean values +/- standard deviation (SD) (with the exception of fold change in protein abundance calculated for western blotting experiments, which display error bars that represent mean and replicate range).

Chapter 3: The Effect of HCV Infection on Host Gene Expression

Chapter 3: Introduction

To identify novel host factors involved in the HCV replication cycle, two approaches were used in this study to investigate:

- Host factors involved in the replication cycle of other RNA viruses.
- Host factors upregulated during HCV infection.

Host factors involved in the replication cycle of other RNA viruses

To try and identify host factors that may be involved in the HCV replication cycle, several host genes with a role in the replication of other RNA viruses were chosen for analysis including members of the Rab protein family (e.g. RAB 2, 4, 6, 11 and 18), and the RNA binding proteins, TIA1, TIAL1 and Staufen1. Before investigating the requirements for these host genes in the HCV replication cycle, it was important to determine whether each gene was actively transcribed during HCV infection. In order to do this, several experimental methods were optimised; including the production of JFH-1 virus, the protocol used to infect Huh7 and Huh7.5 host cell lines, and the method for quantitative reverse-transcription PCR, which is routinely used to investigate host gene expression. The following chapter summarises work optimising these assays and investigates whether JFH-1 infection alters the expression of the selected candidate genes.

Host factors upregulated during HCV infection

It may also be possible to identify potential HCV cofactors by investigating host genes upregulated during HCV infection. This approach was based on the idea that HCV infection may alter host gene expression to adapt the host cell for maximum replication and secretion of virus. Host genes that increase in expression as a result of infection may, therefore, provide an essential cellular function required for HCV infection.

To identify host genes that alter in expression as a result of infection, microarray analysis was used to investigate host gene expression in Huh7 cells infected with JFH-1. Gene ontology analysis of the expression data was performed to provide insight into the cellular pathways significantly altered by infection. Upregulated host factors involved in pathways that may be important during HCV infection were selected for further testing as potential cofactors. Furthermore, microarray data

was analysed to identify HCV induced gene expression patterns that may contribute to HCV associated pathogenesis. The following chapter summarises the data obtained from this microarray experiment and presents additional validation data to support the gene expression patterns observed. Validation assays performed included quantitative reverse-transcription PCR, western blot analysis and metabolic quantification of intracellular lipids. These were used to investigate the effect of JFH-1 infection on host gene expression, host protein abundance and host cellular metabolism. Data is also presented from a study performed to investigate which HCV proteins were responsible for the gene expression patterns and metabolic data observed. This included analysis of host gene expression and lipid metabolism in Huh7 and Huh7.5 cells expressing a genotype 2a (GT2a) subgenomic replicon, and analysis of lipid metabolism in Huh7 cells expressing the JFH-1 core protein.

The experiments presented in this chapter were performed using both the Huh7 and Huh7.5 hepatoma cell lines. The Huh7.5 cell line has a defective RIG-I antiviral signalling pathway and is highly permissive to HCV infection. As a result, Huh7.5 cells were the preferred cell line for production of high-titre JFH-1 virus stocks. However, when performing microarray gene expression profiling, Huh7 cells were used because they have an intact RIG-I antiviral signalling pathway and may respond to HCV infection through mechanisms that better reflect the characteristics of *in vivo* infection. For many of the experiments performed a comparison was made between the effects of JFH-1 infection in both Huh7 and Huh7.5 cells to investigate the extent to which the host cell responses were affected by RIG-I signalling.

Chapter 3: Results

3.1 The JFH-1 cell culture system

3.1.1 Production of infectious JFH-1 virus

Full-length infectious JFH-1 virus was produced using the permissive Huh7.5 cell line. Transfection of Huh7.5 cells with JFH-1 genomic RNA was optimised by Andrew Baillie (Imperial College London), a former PhD student in Dr McGarvey's laboratory [201]. JFH-1 virus produced by the transfected Huh7.5 cell line was used to infect naive Huh7.5 cells for establishment of a high titre JFH-1 virus production line. HCV core protein staining of JFH-1 infected Huh7.5 cells was performed to identify cells expressing the JFH-1 genome (**Fig. 3.1**).

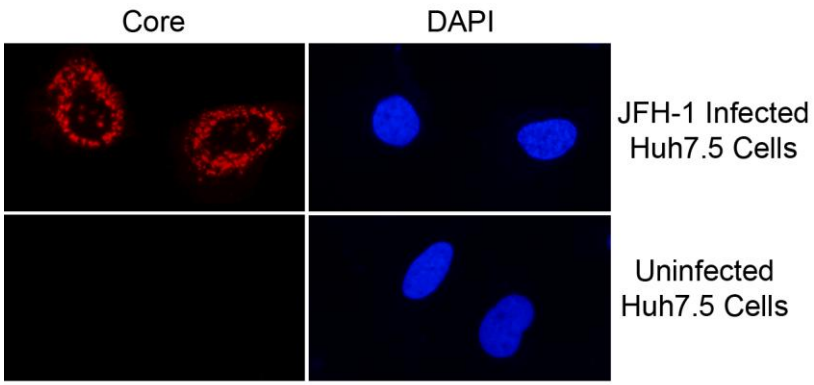


Figure 3.1 JFH-1 infected Huh7.5 cells stain positively for the HCV core protein

HCV core protein staining of JFH-1 infected Huh7.5 cells. Huh7.5 cells producing infectious JFH-1 virus particles were stained for HCV core protein using a mouse anti-core antibody (red staining). Cell nuclei were also stained with DAPI (blue staining). Core protein staining in the infected cells was compared to uninfected Huh7.5 cells. Images were captured using a Nikon Eclipse TE2000S fluorescence microscope at a magnification of 60x.

3.1.2 A high-titre production line for JFH-1 virus

To produce high titre JFH-1 stocks for *in vitro* experiments, infectious culture medium containing JFH-1 was serially passaged onto naive Huh7.5 cells every four days. This method of passaging infectious medium generated much higher virus titres compared to an original method, in which chronically infected Huh7.5 cells were passaged [200, 201] (**Fig. 3.2**).

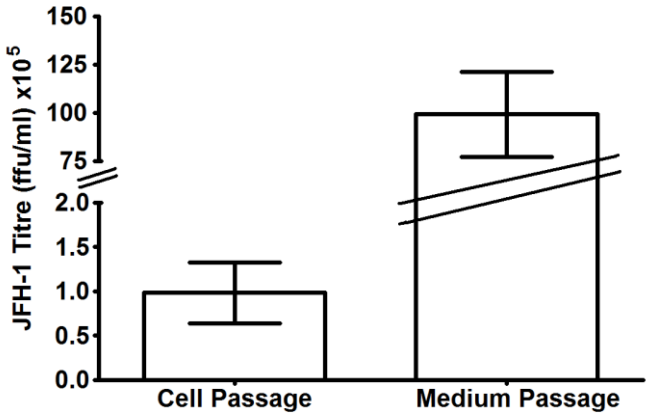


Figure 3.2 Media passage generates higher JFH-1 virus titres

The JFH-1 virus titres (ffu/ml) obtained by passage of infectious medium were compared to the titres obtained by the passage of chronically infected cells. The virus titre values shown represent the mean (±SD) of 5 different rounds of media and cell passage.

3.1.3 JFH-1 infectivity in Huh7 and Huh7.5 cells

Titration of infectious JFH-1 virus on both Huh7 and Huh7.5 cells was previously performed by Andrew Baillie (Imperial College London) to demonstrate that a multiplicity of infection (MOI) of 3 was required to achieve complete cell infection [201]. HCV core protein staining was performed on Huh7 and Huh7.5 cells infected with JFH-1 at an MOI of 3 to confirm that total cellular infection was achieved (**Fig. 3.3**).

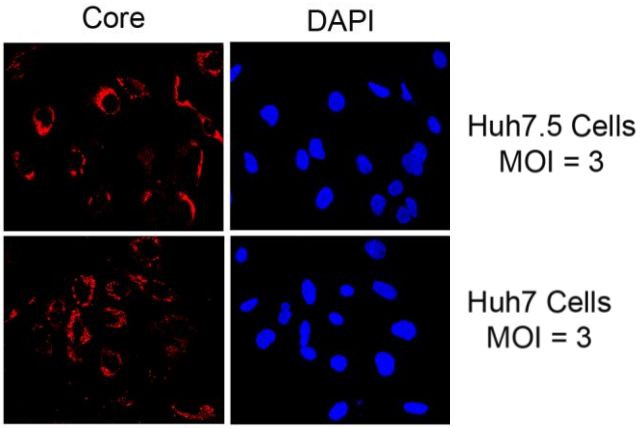


Figure 3.3 Infectivity of Huh7 and Huh7.5 cells with JFH-1 virus

HCV core protein staining of JFH-1 infected Huh7 and Huh7.5 cells. Huh7 and Huh7.5 cells were infected with JFH-1 at a MOI of 3. At 48 hours post-infection, the cells were stained for HCV core using a mouse anti-core antibody (red staining). Cell nuclei were also stained with DAPI (blue staining). Images were captured using a Nikon Eclipse TE2000S fluorescence microscope at a magnification of 40x.

3.2 Why study the effect of HCV infection on host gene expression?

In this study two approaches were used to identify potential HCV cofactors; in both cases it was important to investigate the effect of HCV infection on host gene expression. In the first approach, it was important to determine whether the expression of the selected candidate host genes was affected by HCV infection. In the second approach, host genes significantly upregulated by infection were identified to enable selection of host candidates for testing as potential HCV cofactors.

3.3 Expression profiling of factors involved in the replication of other viruses

Host proteins involved in the replication of other RNA viruses that were chosen for further investigation included members of the Rab GTPase protein family (RAB2, RAB4, RAB6, RAB11 and RAB18), TIA1, TIAL1 and Staufen1. Before investigating whether these proteins participate in the HCV replication cycle, it was important to determine whether transcription of the genes encoding these proteins was affected by HCV infection.

The expression level of the selected candidate host genes was investigated in Huh7 cells infected with JFH-1 at an MOI of 3 for 48 hours. Host gene expression was also investigated in negative control cells that had been mock infected for 48 hours to identify gene expression changes occurring as a result of JFH-1 infection. Quantitative reverse-transcription PCR (qRT-PCR) was used to determine the mRNA levels of the candidate host genes in the JFH-1 and mock infected Huh7 cells. Relative quantification was performed to calculate fold change in host gene expression using the cycle threshold (CT) values obtained, which were analysed using the ΔΔCT equation (see section 2.4) [206, 207]. To normalise the gene expression data observed, the expression of the GAPDH reference gene was quantified in each sample tested. To investigate whether GAPDH was an accurate reference gene to use in HCV infected samples, a second reference gene, encoding the large ribosomal protein (RPLPO), was also quantified [208]. Fold change in host gene expression was calculated using the ΔΔCT equation with either GAPDH or RPLPO as the normalising control reference gene (**Fig. 3.4**). Very similar gene expression patterns were observed when either reference gene was used; this indicated that GAPDH was an accurate reference gene for normalisation of gene expression data in HCV infected samples. Little effect was

observed on the expression of host genes as a result of JFH-1 infection. The largest change in expression was seen for RAB6A which increased by 1.6 fold. Other genes which also increased in expression include RAB2B, RAB11A, RAB18 and TIA1. Several of the genes investigated showed a decrease in expression; including RAB4A, RAB4B and Staufen1.

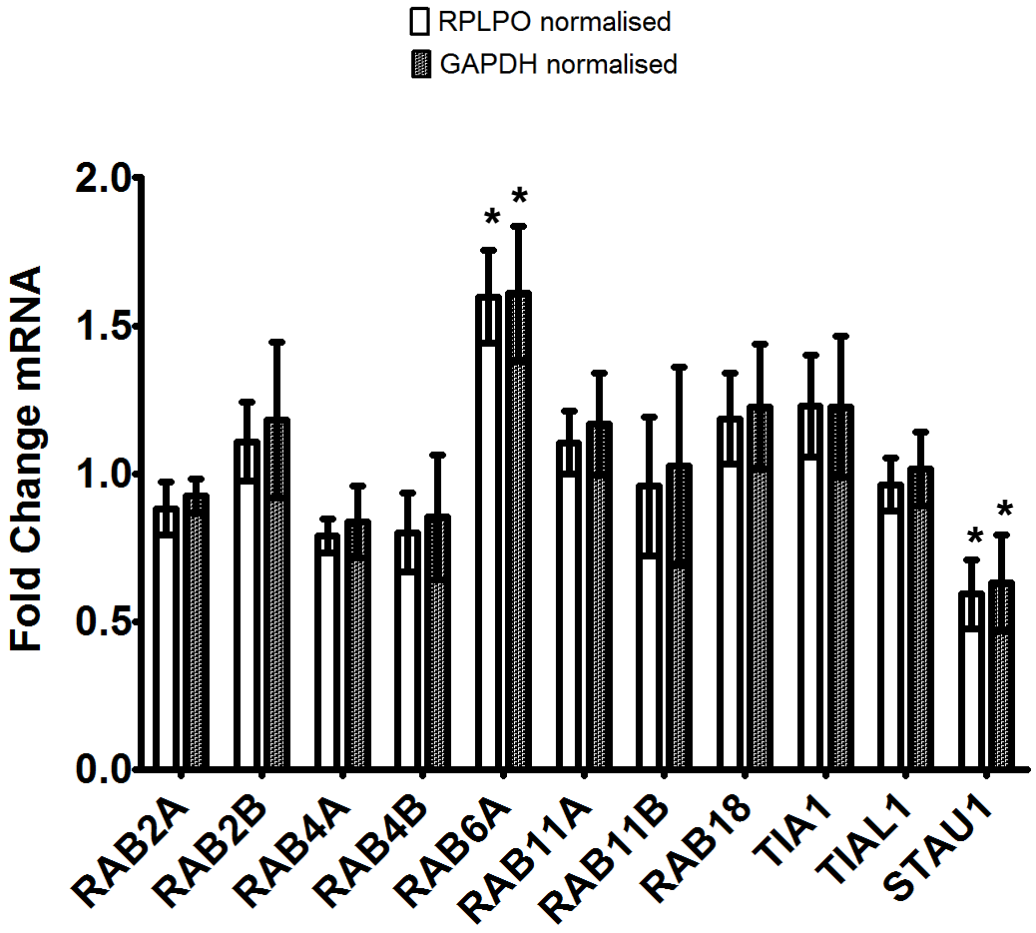


Figure 3.4 Fold change in host gene expression during JFH-1 infection

Fold change in the expression of candidate host genes (Rab GTPase genes, TIA1, TIAL1 and Staufen1) during JFH-1 infection, normalised using either RPLPO (white bars) or GAPDH (grey bars). Huh7 cells were infected with JFH-1 (MOI = 3) or mock medium for 48 hours. Intracellular RNA was extracted for qRT-PCR analysis of host gene expression by relative quantification. Fold change data represents mean (±SD) calculated for one experiment with repeat infections performed in triplicate. Host genes with a statistically significant change in expression in the JFH-1 infected cells compared to the mock infected cells (p value ≤ 0.05) are indicated by an asterisk (*). P values were calculated using a two-tailed unpaired T test in Graphpad Prism.

3.4 Identification of host factors upregulated during HCV infection

3.4.1 Microarray gene expression profiling of JFH-1 infected Huh7 cells

The characterisation of novel host factors involved in the HCV replication cycle may also be facilitated by studies that identify host genes significantly upregulated during infection. To enable such studies to be performed, the effect of HCV infection on host gene expression was investigated using Huh7 cells infected with JFH-1 (MOI = 3) or mock medium for 6, 12, 18, 24 and 48 hours. Total RNA extracted from the JFH-1 and mock infected cells was hybridised to Affymetrix Human U133 Plus 2.0 GeneChips for gene expression analysis of the entire human transcriptome (54,000 gene probe sets representing 38,500 genes). The gene expression data collected was compared between the JFH-1 and mock infected samples to calculate fold change in expression at each time-point. Gene probe sets showing at least a 2 fold change in expression and greater than 95% probability of being differentially expressed ($p \leq 0.05$) were considered to be significantly regulated by infection. These selection criteria were chosen to enable a comparison of the results obtained to those observed in previous HCV microarray studies, which also use these cut-off values [149, 157, 160, 165]. A large number of probe sets were observed to significantly alter in expression as a result of infection; the total number of which increased over time (**Table 3.1**).

Hours post-infection	Fold change = ≥ + 2	Fold change = ≤ - 2
6	74	165
12	270	117
18	146	232
24	617	383
48	1275	870

Table 3.1 Total number of gene probesets regulated during JFH-1 infection

The total number of microarray gene probe sets shown to significantly alter in expression as a result of JFH-1 infection; including those that increase in expression by at least 2 fold (≥+2) and those that decrease in expression by at least 2 fold (≤-2). Huh7 cells were infected in triplicate with JFH-1 (MOI = 3) or mock medium for 6, 12, 18, 24 and 48 hours. Intracellular RNA was extracted and used for microarray analysis (Affymetrix Human U133 Plus 2.0 GeneChip) to identify host genes transcriptionally regulated by infection. Microarray gene probe sets significantly regulated by infection were identified to have at least a 2 fold change in expression nd greater than 95% probability of being differentially expressed (p value ≤ 0.05) in the JFH-1 infected cells compared to the mock infected cells.

3.4.2 Intracellular JFH-1 RNA abundance in the JFH-1 infected Huh7 cells

The intracellular JFH-1 RNA levels at each time-point were quantified using qRT-PCR. An increase was observed in the abundance of JFH-1 RNA throughout the course of infection (**Fig. 3.5**).

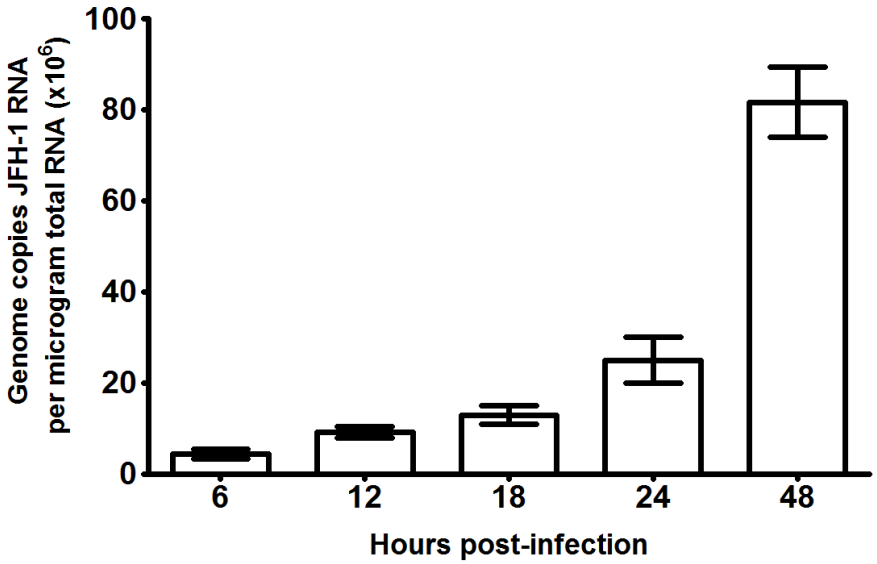


Figure 3.5 Intracellular JFH-1 RNA levels increase throughout infection

Intracellular JFH-1 RNA levels in Huh7 cells infected with JFH-1 for 6, 12, 18, 24 and 48 hours. The intracellular RNA extracts from a replicate time-course infection experiment were used to quantify JFH-1 RNA levels by qRT-PCR using absolute quantification. Quantification data represents mean (±SD) of triplicate infections performed for each time-point.

3.4.3 Gene ontology analysis of the microarray expression data

To facilitate interpretation of the microarray expression data, gene ontology analysis was performed using the PANTHER classification program and Ingenuity Pathway Analysis. These programs indicated that the host genes altering in expression during JFH-1 infection were involved in a range of biological processes; including host defence mechanisms (e.g. inflammation, oxidative stress and apoptosis), host metabolism (e.g. lipid and protein metabolism) and intracellular transport (e.g. vesicle trafficking and cytoskeleton transport) (**Fig. 3.6**). Some of the host genes significantly regulated by infection were also involved in processes such as vision, taste and embryogenesis. These processes were not considered relevant to the study and were excluded from further analysis.

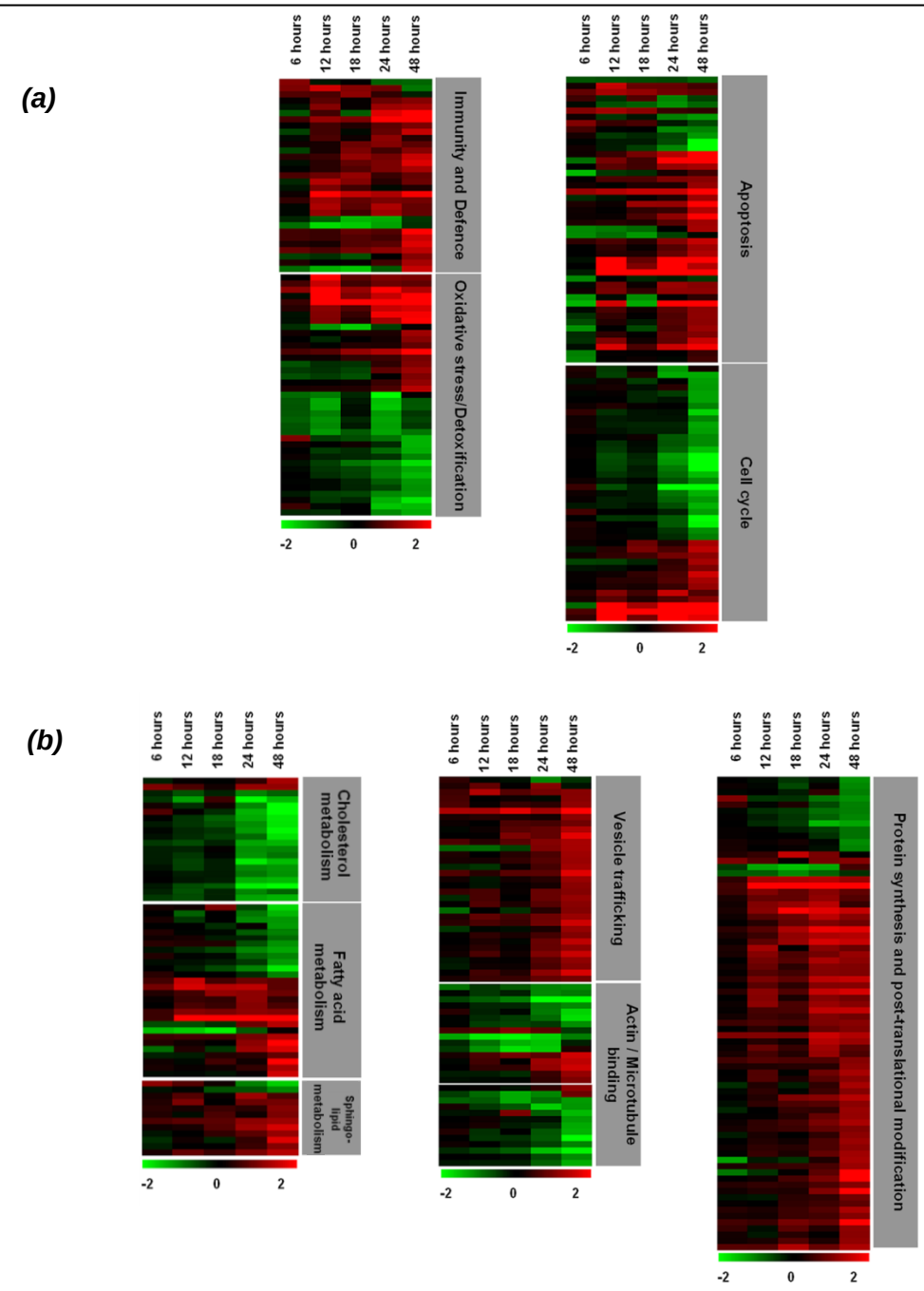


Figure 3.6 JFH-1 infection significantly alters host gene expression

Heat-map representation of the gene expression patterns observed during JFH-1 infection in the pathways regulating ***(a)*** *cellular defence and* ***(b)*** *cellular metabolism and intracellular transport. The expression profile of host genes significantly regulated (≥ 2 fold, p value ≤ 0.05) following infection of Huh7 cells with JFH-1 was characterised using microarray analysis, comparing gene expression in JFH-1 infected cells to mock infected cells at 6, 12, 18, 24 and 48 hours post-infection. Boxes coloured in red represent upregulated gene probe sets, boxes coloured in green represent downregulated gene probe sets and boxes coloured in black represent gene probe sets that did not alter in expression. Each row represents expression data for a single gene probe set. Expression profiles are represented on a log_2 fold change scale and were calculated from an average of the expression values collected for triplicate samples at each time point. Where multiple probe sets exist for a gene, the data from a representative probe set was chosen. Log_2 fold change values can be found in Appendix A.8.*

3.4.4 JFH-1 infection alters the expression of cellular defence genes

Many of the genes regulated following infection were involved in host defence mechanisms that protect the cell against infection and oxidative stress, and in turn determine the fate of cellular survival. The expression profile for the cellular defence genes regulated by JFH-1 infection is represented by heat-map diagrams as shown in **Fig. 3.6a**.

(i) JFH-1 infection stimulates the expression of pro-inflammatory antiviral genes

Genes involved in innate immune signalling increased in expression following JFH-1 infection including those involved in type I and II interferon responses (e.g. IRF1, IRF9, MX1), the complement cascade (e.g. MBL2 and MASP1) and the production of pro-inflammatory chemokines and cytokines (e.g. IL8 and CXCL1, 2, 3, 5, 6 and 16). Increased expression of genes encoding negative regulators of the interferon response was also observed including several members of the suppressor of cytokine signalling (SOCS) gene family (e.g. SOCS2 and 3).

(ii) JFH-1 infection regulates the expression of cellular antioxidant genes

The expression of genes involved in cellular antioxidant responses decreased following infection including the genes transcribed following NRF2 activation (e.g. CAT and NQO1), members of the metallothionein gene family, the glutathione-s-transferase enzymes (e.g. GSTM1-4) and other key antioxidants (e.g. ATOX1 and GLRX). Expression patterns promoting an increase in intracellular reactive oxygen species were also observed as genes involved in the inhibition of antioxidant proteins (e.g. TXNIP) and the production of reactive oxygen species (e.g. AOX1) significantly increased in expression. Alongside the decreased expression of genes involved in cellular antioxidant pathways, an increase was observed in the expression of genes controlling detoxification and xenobiotic metabolism (e.g. NNMT, UGT2B4, AHR, CYP1A1 and CYP1B1).

(iii) JFH-1 infection regulates the expression of genes controlling cellular survival

The genes controlling apoptosis and cell cycle arrest significantly altered in expression during infection. Transcriptional changes that promoted apoptosis and cell cycle arrest were observed; these included an increase in the expression of genes that induce apoptosis such as those involved in p53 and TGFβ signalling (e.g. NEDD9, SIRT1, PMAIP and TP53BP2), an increase in the expression of pro-apoptotic transcription factors (e.g. FOXO3 and ATF4) and an increase in the

expression of genes promoting cell cycle arrest (e.g. INHBE). A decrease in the expression of genes required for cell cycle progression (e.g. CCNB1, CCNE1 and SKP2), cytokinesis (e.g. CP110 and SPC24) and S phase DNA synthesis (e.g. RFC3 and RFC5) was also observed. At the same time genes promoting apoptosis and inhibition of the cell cycle also decreased in expression (e.g. BCL2L11, DFFB, CDKN3 and CDKN2C) and genes promoting cellular survival, cell cycle progression and cytokinesis increased in expression (e.g. CCNH, TUBE1, CDK6 and MIS12) demonstrating that conflicting transcriptional changes occur following infection.

3.4.5 JFH-1 infection alters the expression of metabolism and transport genes

A second class of host genes significantly regulated by JFH-1 infection were those involved in more general housekeeping functions of the cell including cellular metabolism and intracellular transport. The expression profile of the genes involved in these processes is represented by heat-map diagrams in **Fig. 3.6b**.

(i) JFH-1 infection regulates the expression of genes controlling lipid metabolism

Host genes involved in the biosynthesis, degradation and transport of intracellular lipids were significantly regulated following infection. Genes involved in the VLDL secretory pathway (e.g. MTTP and APOB) and the cholesterol biosynthesis pathway (e.g. SQLE and HMGCR) decreased in expression following infection. However, genes regulating the transfer of geranyl moieties from the mevalonate cholesterol pathway onto cellular proteins actually increased in expression (e.g. GGPS1 and PGGT1B), indicating that the different branches of the cholesterol synthesis pathway are differentially regulated during infection. Genes involved in the synthesis of cellular sphingolipids (e.g. SGPP1, SPTLC1 and LASS1) and phospholipids (e.g. CHKA and ACSL3) increased in expression following infection. The expression of genes involved in fatty acid and triglyceride metabolism was also significantly regulated following infection; including a decrease in the expression of genes involved in the degradation and oxidation of fatty acids (e.g. ACADSB, ACADVL, CES2 and CPT2). The expression of PPARα, a key transcription factor regulating fatty acid oxidation was also decreased, whilst the expression of TXNIP, a potential PPARα inhibitor, significantly increased following infection. Conversely, genes involved in the uptake and elongation of fatty acids and the synthesis of triglycerides significantly increased in expression (e.g. FABP3, ELOVL4/7 and ACSL3). Increased expression was also observed for

transcription factors and coactivators that control the expression of genes involved in lipid metabolism and the production of triglyceride-rich lipid droplets (e.g. SREBF1 and PGC1α).

(ii) JFH-1 infection regulates the expression of genes involved in host protein synthesis, degradation and post-translational modification

The expression of genes involved in host protein synthesis and protein processing increased following infection. Increased expression was observed for the genes that control amino acid metabolism (e.g. PSAT1 and BCAT1), tRNA synthesis (e.g. AARS, SARS, GARS and WARS), production of ribosomes (e.g. RPL13 and RPL37), pre-mRNA processing and splicing (e.g. HNRNPH3 and QKI), protein translation (e.g. eIF-4E and eIF4EBP1) and post-translational modification of proteins by glycosylation (e.g. MGAM) and sulphation (e.g. SULT2A1). In addition to promoting increased rates of protein synthesis, there may also be a decrease in the rate of protein degradation as host genes involved in the poly-ubiquitination of proteins and the function of the proteasome and lysosome decreased in expression (e.g. UBE3B, PSMAI and CTSC) and genes promoting the disassembly of poly-ubiquitin increased in expression (e.g. USP15 and OTUD1).

(iii) JFH-1 infection regulates genes controlling intracellular protein transport and vesicle trafficking

The expression of genes involved in protein sorting and vesicle trafficking increased following infection. This included the genes responsible for regulating endosomal vesicle trafficking (e.g. SNX12, SNX16 and PICALM), trafficking between the ER and Golgi body (e.g. RAB6B, RAB7L1, RAB33B and ARF-GEF1) and trafficking of secretory vesicles to the plasma membrane (e.g. RAB27A, RAB27B and RAB37).

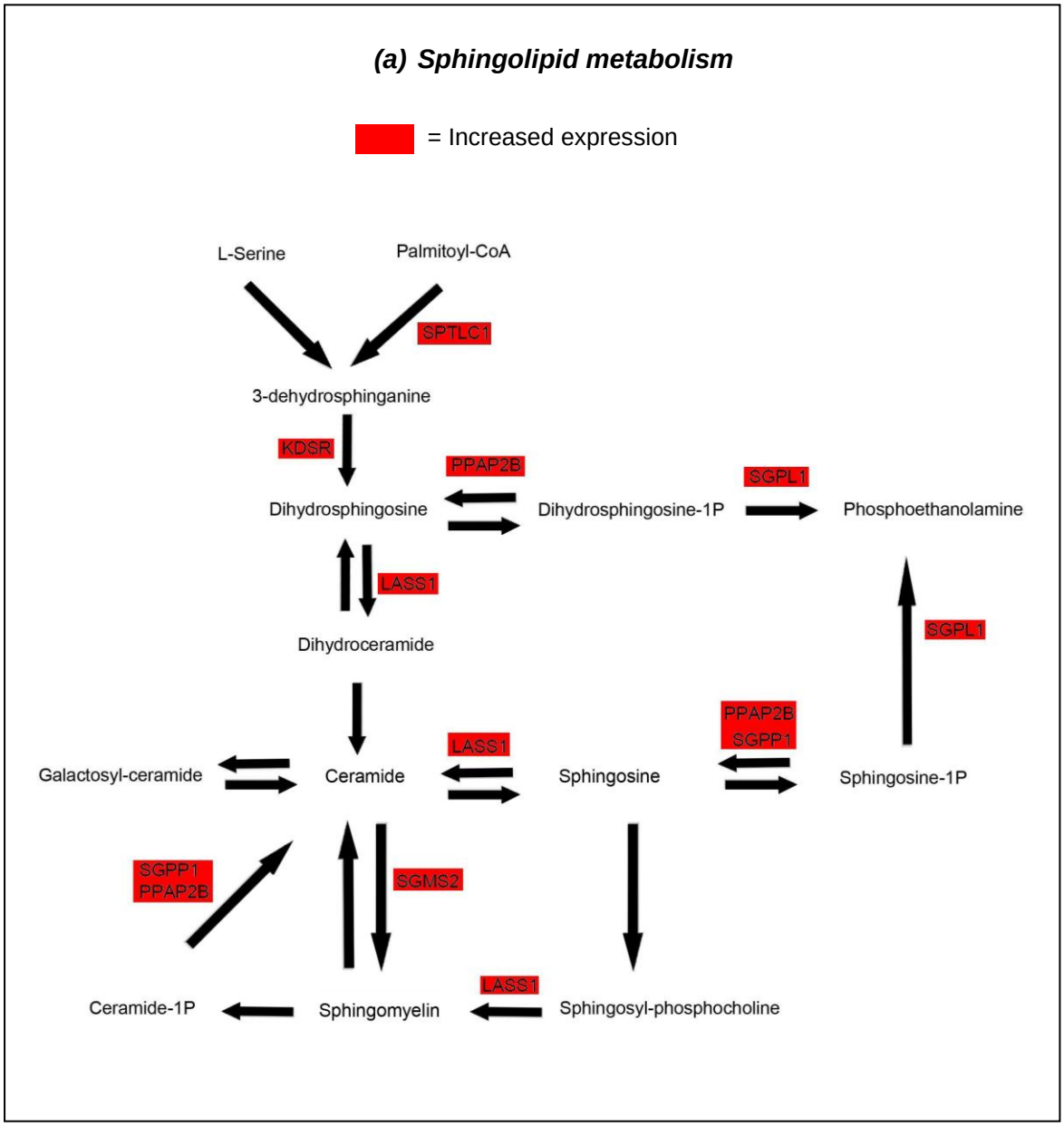
(iv) JFH-1 infection regulates the expression of genes encoding actin and microtubule binding proteins

Genes that control the function of actin and microtubule cytoskeleton filaments were also significantly regulated by infection. A large proportion of the genes encoding actin and microtubule binding proteins decreased in expression (e.g. KIF20A, MICAL2, TAGLN and MYL9). A small number of genes encoding actin binding proteins also increased in expression (e.g. ABLIM3).

Details of the genes regulated by JFH-1 are shown in the Appendix A.8 and A.9.

3.4.6 The biological significance of HCV induced gene expression patterns

For some of the pathways regulated by JFH-1 infection, almost all of the genes involved were observed to alter in expression. By highlighting the gene expression changes observed on diagrams representing these pathways, it is possible to see the extent of the changes that take place. Two pathways significantly altered by infection were sphingolipid metabolism (**Fig. 3.7a**) and cholesterol biosynthesis (**Fig. 3.7b**). Despite the significant decreases observed in the expression of cholesterol synthesis genes between 6 and 48 hours post-infection, further experiments demonstrated the occurrence of a biphasic mechanism of gene regulation, as significant increases in cholesterol synthesis gene expression were observed at 72 hours post JFH-1 infection (**Fig. 3.15**).



(b) Cholesterol biosynthesis

= Decreased expression

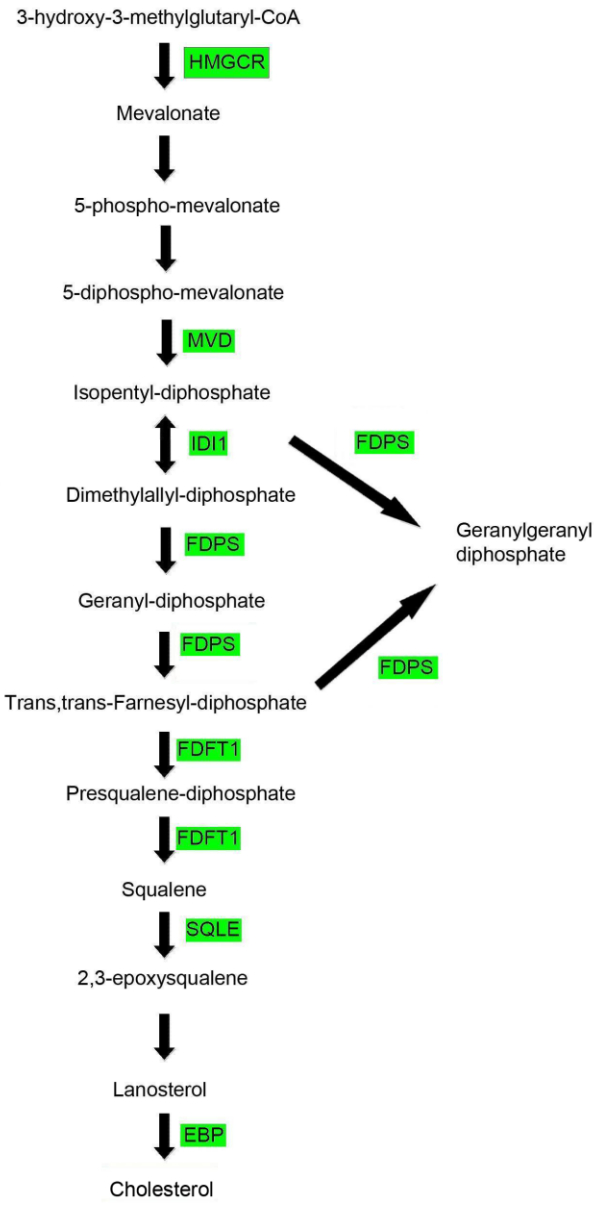


Figure 3.7 Genes regulating sphingolipid metabolism and cholesterol biosynthesis alter in expression during JFH-1 infection

*Host genes involved in **(a)** sphingolipid metabolism and **(b)** cholesterol biosynthesis that altered in expression at 48 hours post-JFH-1 infection. Host genes that altered in expression during JFH-1 infection are highlighted either in green if the gene decreased in expression, or in red if the gene increased in expression. Metabolic pathway diagrams shown were produced using pathway information obtained following Ingenuity pathway analysis of the microarray gene expression data.*

3.4.7 Validation of the microarray expression data by quantitative PCR

As a result of microarray analysis, several interesting gene expression patterns were observed following JFH-1 infection. To validate these expression changes, qRT-PCR was used to investigate gene expression in JFH-1 and mock infected Huh7 cells. The expression of genes involved in sphingolipid metabolism, cholesterol synthesis, fatty acid metabolism, lipid droplet production, xenobiotic metabolism and intracellular transport was investigated using RNA extracted at 48 hours post-infection (**Fig. 3.8**). Focus was placed on host genes involved in cellular processes closely linked with HCV replication and secretion to facilitate identification of novel genes involved in HCV replication. The qRT-PCR expression data was consistent with the microarray data, although larger fold change values were observed with qRT-PCR for the majority of the genes tested.

Because the microarray experiment was observed to be less sensitive than qRT-PCR, several host genes that did not fall within the 2 fold expression change criteria were also investigated using qRT-PCR. This included genes encoding CIDEB, CIDEC and RIP140, key regulators of lipid droplet formation alongside PGC1α; and PPARγ, a key lipid metabolism transcription factor alongside PPARα and SREBF1. Several of these genes, including CIDEB, RIP140 and PPARγ, were observed to be upregulated during infection when tested by qRT-PCR. The expression of CIDEA, another gene regulating lipid droplet formation alongside CIDEB and CIDEC, was also tested; however, no primer pairs were identified to amplify the CIDEA transcript. The microarray data obtained for these genes is summarised in Appendix A.8.

For some of the genes upregulated by JFH-1 infection, qRT-PCR was also used to investigate expression at 6, 12, 18 and 24 hours post-infection (**Fig. 3.9**). Different patterns were observed in the transcription of host genes following JFH-1 infection. For example, TXNIP was consistently transcribed at a high level from 12 to 48 hours post-infection (**Fig. 3.9a**). By comparison, ABLIM3 was expressed at increasing levels between 6 and 18 hours post-infection. However, at 18 hours post-infection the transcription of ABLIM3 reached a maximum level and returned to normal levels of expression by 48 hours (**Fig. 3.9f**). Other genes, such as RAB27A, did not show any change in expression until a later stage of infection when gene expression increased to reach a maximum level at 48 hours post-infection (**Fig. 3.9d**).

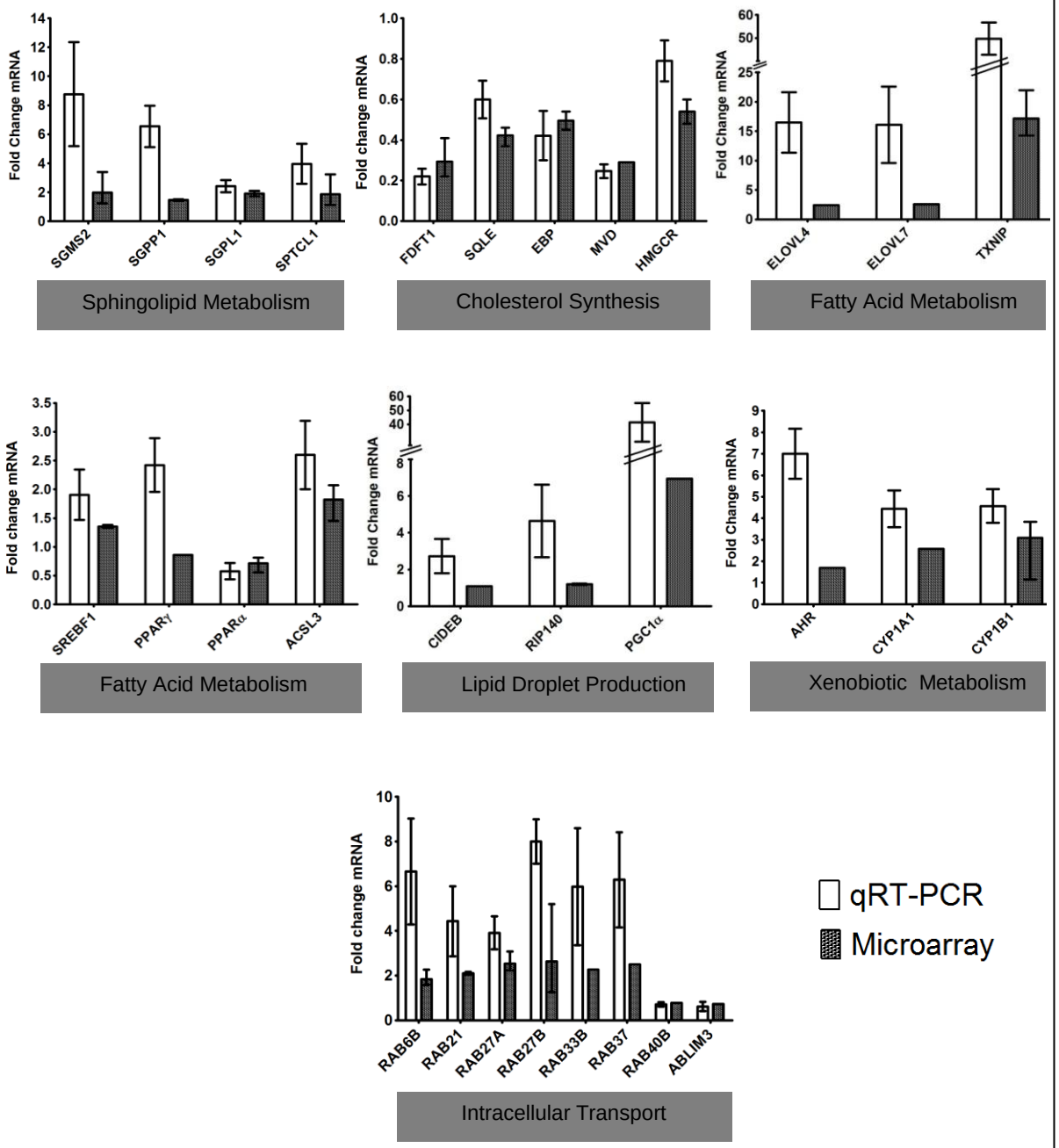


Figure 3.8 Comparison of microarray and qRT-PCR gene expression data collected for Huh7 cells infected with JFH-1 for 48 hours

Fold change in Huh7 cell host gene expression at 48 hours post-JFH-1 infection, quantified using microarray analysis and qRT-PCR. Huh7 cells were infected with JFH-1 (MOI = 3) or mock medium for 48 hours. Intracellular RNA was extracted and used for qRT-PCR analysis of host gene expression using relative quantification. The qRT-PCR data shown represents the mean (±SD) of triplicate infection samples (white bars). The corresponding microarray gene expression data is also shown (grey bars) and represents the mean fold change value calculated for triplicate infections at 48 hours post-infection. Confidence interval values calculated for the triplicate infection sample repeats of the microarray experiment can be found in the Appendix A.10. For some of the host genes investigated multiple probe sets were available on the microarray genechip, thus error bars are displayed for some of the microarray datapoints (grey bars) to represent the range of mean fold change values observed for different gene probe sets.

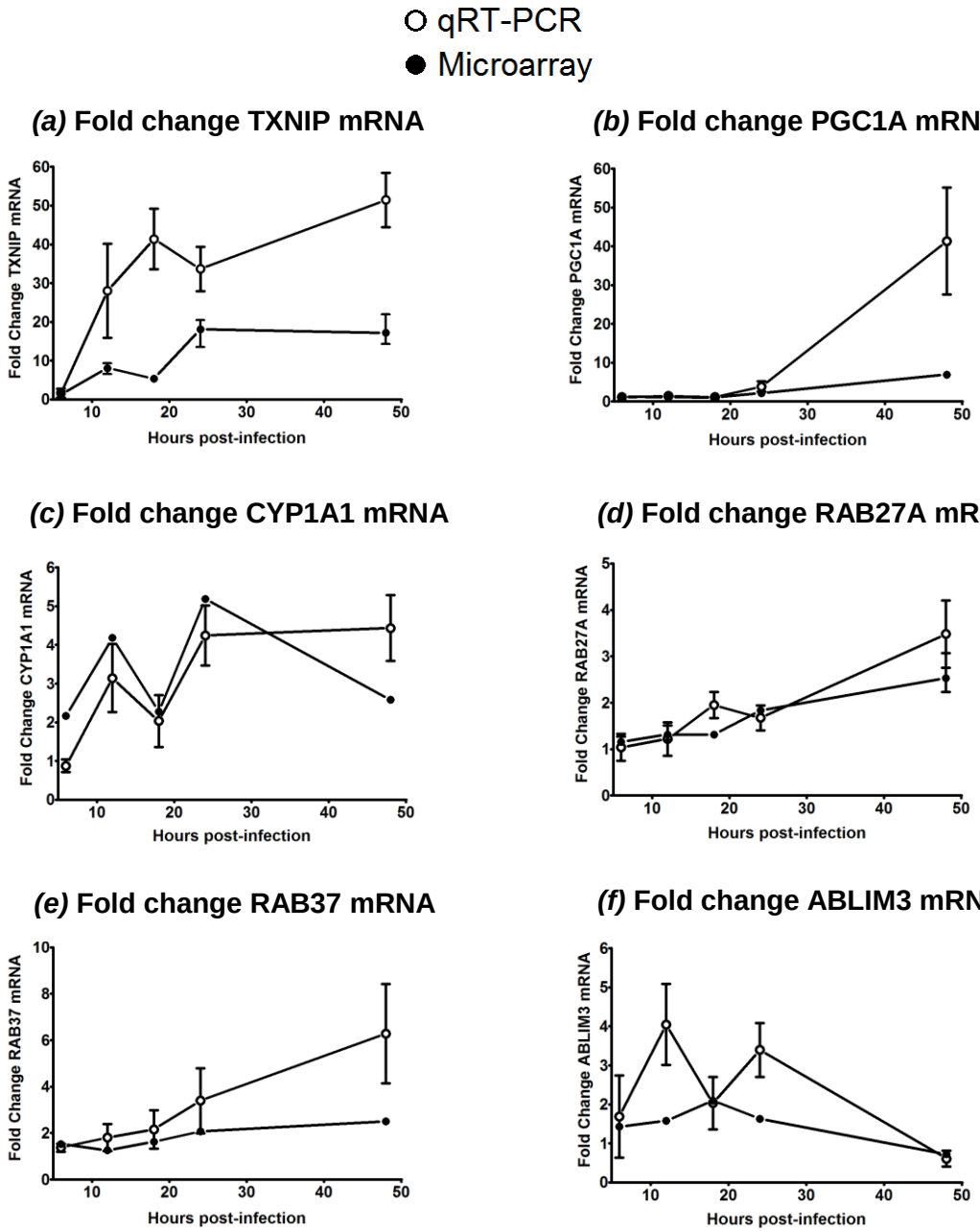


Figure 3.9 Temporal regulation of host expression during JFH-1 infection

Fold change in Huh7 cell host gene expression at 6, 12, 18, 24 and 48 hours post-JFH-1 infection, quantified using microarray analysis and qRT-PCR; including genes encoding ***(a)*** *TXNIP,* ***(b)*** *PGC1α,* ***(c)*** *CYP1A1,* ***(d)*** *RAB27A,* ***(e)*** *RAB37 and* ***(f)*** *ABLIM3. Huh7 cells were infected with JFH-1 (MOI = 3) or mock medium. Intracellular RNA was extracted and used for qRT-PCR analysis of host gene expression using relative quantification. The qRT-PCR data shown represents the mean (±SD) of triplicate infections for each time-point (open symbols). The corresponding microarray gene expression data is also shown (closed symbols) and represents the mean fold change values calculated for triplicate infections at each time-point. Confidence interval values calculated for the triplicate infection sample repeats of the microarray experiment can be found in the Appendix A.11. For the genes encoding TXNIP and RAB27A, multiple probe sets were available on the microarray genechip, thus error bars are displayed for the microarray datapoints (closed symbols) of these genes to represent the range of mean fold change values observed for the different gene probe sets.*

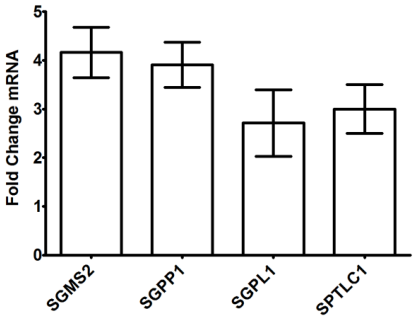
3.4.8 Comparing host cell response to infection: Huh7 versus Huh7.5 cells

To determine whether the RIG-I mutation present in the Huh7.5 cell line had a significant effect on the host cell response to HCV infection qRT-PCR was also used to investigate host gene expression in Huh7.5 cells infected with JFH-1 for 48 hours. The expression of genes involved in sphingolipid metabolism, cholesterol synthesis, fatty acid metabolism, lipid droplet production, xenobiotic metabolism and intracellular transport was investigated (**Fig. 3.10a**).

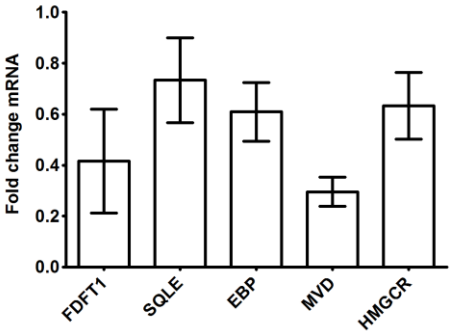
The effect of JFH-1 infection on Huh7.5 cell gene expression was largely consistent with that observed for the JFH-1 infected Huh7 cells (**Fig. 3.8**), as the genes controlling sphingolipid metabolism, fatty acid metabolism, xenobiotic metabolism and intracellular transport increased in expression following infection, whilst the genes controlling cholesterol synthesis decreased in expression. The degree to which gene expression was affected by JFH-1 infection was also consistent between the two cell lines, as the cholesterol synthesis genes showing the greatest decrease in expression in both Huh7 and Huh7.5 cells were FDFT1 and MVD, and the sphingolipid metabolism genes showing the greatest increase in expression in both Huh7 and Huh7.5 cell lines were SGMS2 and SGPP1.

Despite these similarities, the overall fold change expression values observed for JFH-1 infected Huh7.5 cells were lower than those observed for the JFH-1 infected Huh7 cells. For example, ELOVL4 and ELOVL7 demonstrated a 16 fold increase in expression in the JFH-1 infected Huh7 cells compared to the 3 to 3.5 fold increase observed in the JFH-1 infected Huh7.5 cells. Quantification of the intracellular JFH-1 RNA levels demonstrated that these differences did not reflect a higher level of infection in the JFH-1 infected Huh7 cells, as the abundance of intracellular JFH-1 RNA present in the JFH-1 infected Huh7 cells was lower than the abundance quantified in the JFH-1 infected Huh7.5 cells (**Fig. 3.10b**).

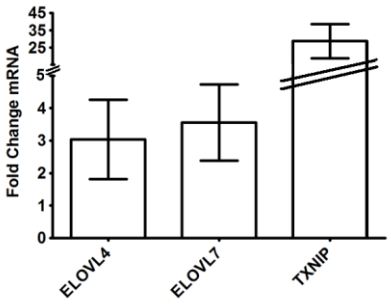
(a)



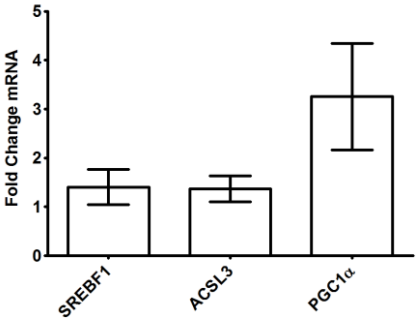
Sphingolipid Metabolism



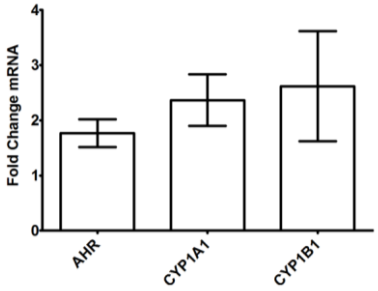
Cholesterol Synthesis



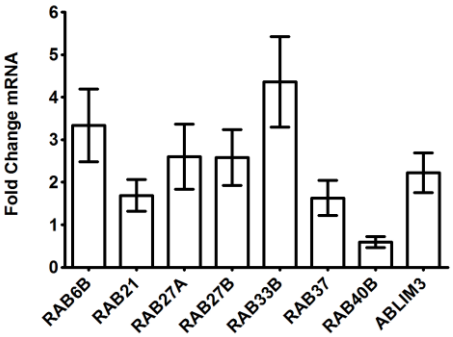
Fatty Acid Metabolism



Fatty Acid Metabolism



Xenobiotic Metabolism



Intracellular Transport

(b)

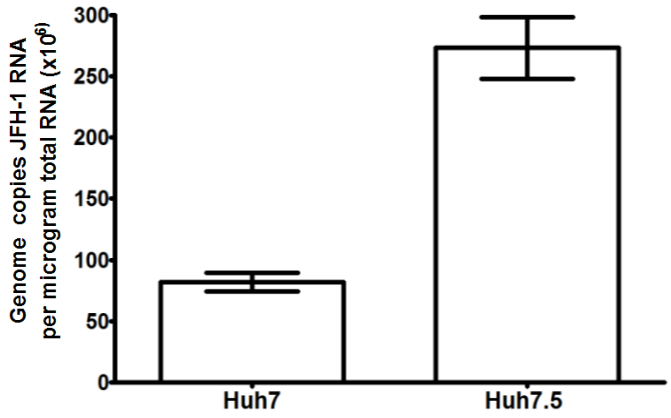


Figure 3.10 qRT-PCR expression profiling of JFH-1 infected Huh7.5 cells

(a) *Fold change in Huh7.5 cell host gene expression at 48 hours post-JFH-1 infection, quantified using qRT-PCR. Huh7.5 cells were infected with JFH-1 (MOI = 3) or mock medium for 48 hours. Intracellular RNA was extracted and used for qRT-PCR analysis of host gene expression using relative quantification. The qRT-PCR data shown represents the mean (±SD) of triplicate infection samples.* ***(b)*** *Intracellular JFH-1 RNA levels quantified for Huh7 and Huh7.5 cells infected with JFH-1 (MOI = 3) for 48 hours. Intracellular RNA was extracted from the infected cells for qRT-PCR analysis of JFH-1 RNA levels using absolute quantification. JFH-1 RNA titre data shown represents the mean (±SD) of triplicate infections for both Huh7 and Huh7.5 cells.*

3.5 Gene expression profiling of cells expressing a subgenomic replicon

According to Figures 3.8-3.10, several interesting gene expression patterns were observed to occur as a result of JFH-1 infection. To determine whether these expression patterns were caused by specific HCV proteins or processes in the HCV replication cycle, the effect of a genotype 2a (GT2a) subgenomic replicon on host gene expression was also investigated. Cells transfected with subgenomic replicon RNA express only the non-structural HCV proteins, which direct the assembly of HCV genome replication complexes allowing continuous replication of the HCV genome. Therefore, investigation of host gene expression in cells that express the subgenomic replicon enabled determination of the effects that HCV genome translation and replication have on host gene expression.

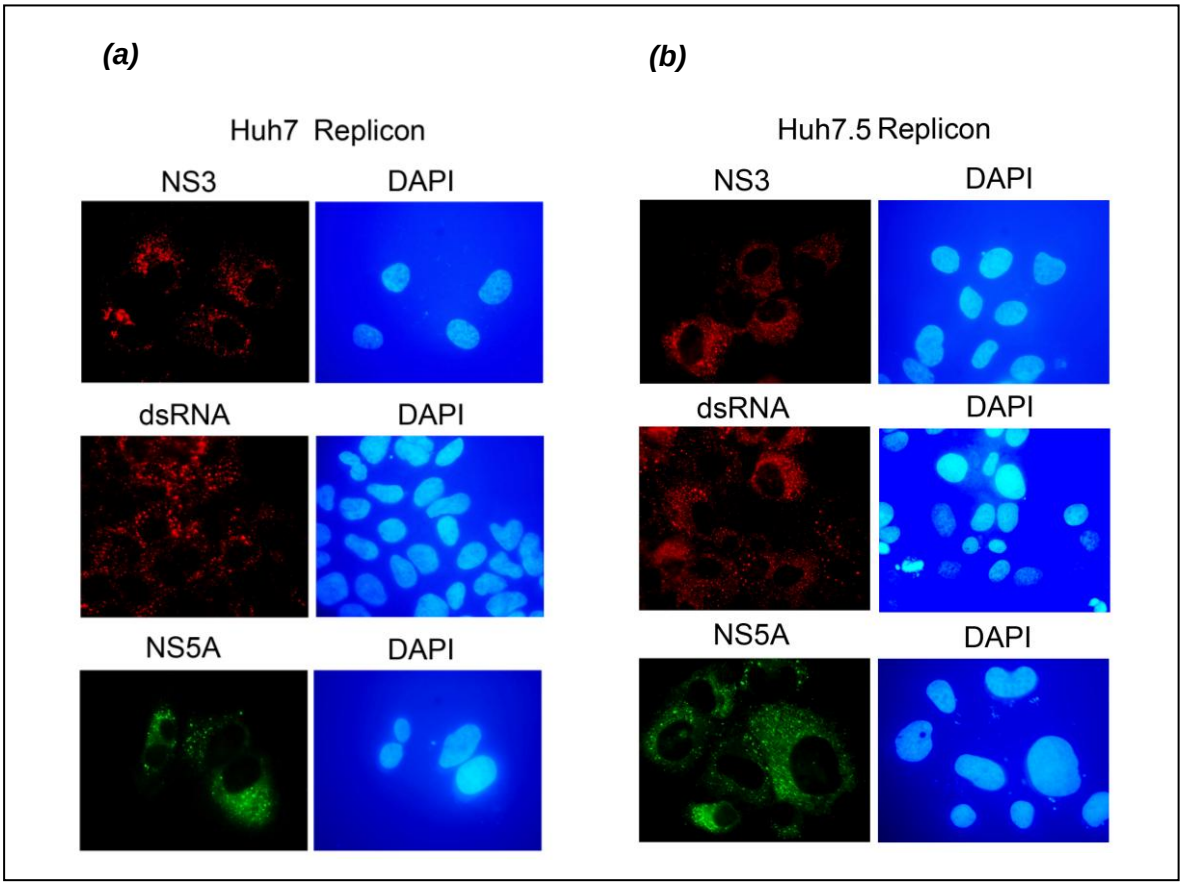
3.5.1 Generating cells that express a genotype 2a subgenomic replicon

Stable cell lines expressing a subgenomic replicon were generated using both Huh7 and Huh7.5 cells. Subgenomic replicon RNA was synthesised by *in vitro* transcription using a linearised DNA plasmid, pGT2a(NS2-NS5B), which contained the sequence for the J6 NS2 gene fused to the JFH-1 NS3-NS5B genes, and a gene coding for Geneticin resistance (**Appendix A.12**). The subgenomic replicon RNA transcript produced was transfected into Huh7 and Huh7.5 cells, which were grown in the presence of Geneticin until all the cells stained positively for the non-structural HCV proteins, NS3 and NS5A, and dsRNA (the replicative intermediate of the HCV genome) (**Fig. 3.11a and b**). Both of the transfected cell lines showed 100% positive staining for HCV proteins and dsRNA after five weeks of selection in Geneticin.

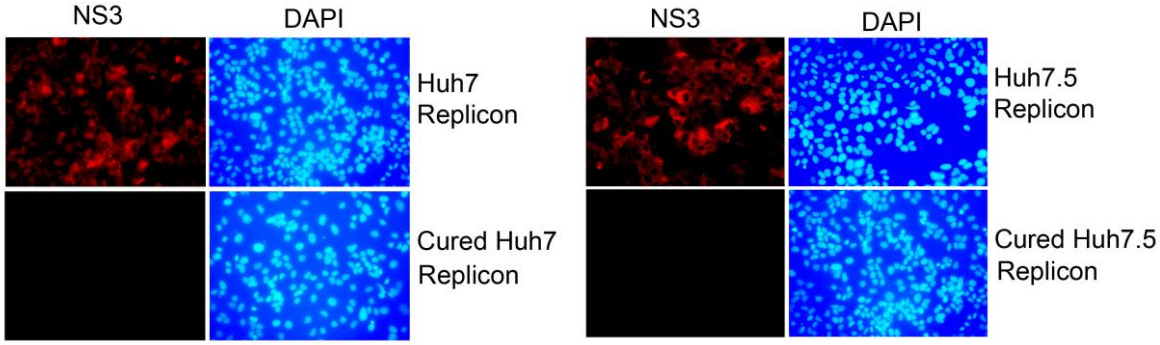
The replicon expressing cell lines were produced for use in a gene expression profiling study and it was important that an appropriate negative control cell line was generated for these experiments. The process of selecting cell lines with Geneticin can result in the selection of a narrow range of cell clones compared to the heterogeneous population of cells in the wild type cell line. This is because some cell clones in the heterogeneous mix of cells are likely to have phenotypes that better support the replication of the HCV genome and are therefore able to grow more rapidly in the presence of Geneticin. To identify whether the replicon expressing cell lines generated represented a smaller selection of cell clones compared to the original wild type cell line, replicon RNA was eliminated from the

transfected cells by treatment with interferon-α (IFNα). Both Huh7 and Huh7.5 replicon cells were treated with IFNα until the replicon RNA and the HCV protein, NS3, was no longer detected; at this stage the cell lines were considered to be 'cured' (**Fig. 3.11c and d**). Comparison of the gene expression profile for these 'cured' cells to the replicon expressing and wild type cells allowed us to determine whether the gene expression patterns observed were due to the direct presence of the HCV non-structural proteins and the HCV genome, or whether the expression patterns resulted from the selection of cell clones that support a high level of HCV genome replication.

In order to cure the replicon expressing cells, treatment with 100IU/ml of IFNα was performed. The success of treatment was assessed by investigating both the expression of HCV NS3 through immunofluorescent staining and the abundance of replicon RNA through qRT-PCR. Although the positive signal for NS3 staining was lost after four weeks of IFNα treatment, it took much longer for the replicon RNA levels to decrease. Cells were treated for a total of eight weeks before the replicon RNA could no longer be detected by qRT-PCR in both the Huh7 and Huh7.5 replicon expressing cells (**Fig. 3.11e**).



(c) ***(d)***



(e)

IFNα treatment	Replicon expressing Huh7 cells		Replicon expressing Huh7.5 cells	
	NS3 protein	Replicon RNA	NS3 protein	Replicon RNA
Week 0	Positive	Positive	Positive	Positive
Week 2	Positive	Positive	Positive	Positive
Week 4	Negative	Positive	Negative	Positive
Week 6	Negative	Positive	Negative	Positive
Week 8	Negative	Negative	Negative	Negative

Figure 3.11 Replicon cells stain positively for NS3, NS5A and dsRNA

(a/b) *Immunofluorescent staining of HCV NS3, HCV NS5A and dsRNA in* ***(a)*** *replicon expressing Huh7 cells and* ***(b)*** *replicon expressing Huh7.5 cells. Huh7 and Huh7.5 cells were transfected with the GT2a subgenomic replicon RNA transcript and selected using Geneticin for five weeks. The replicon expressing cells were stained with anti-NS3 antibody (red staining 1st row), anti-dsRNA antibody (red staining 2nd row) and anti-NS5A antibody (green staining). Cell nuclei were stained with DAPI (light blue staining). Images were captured using a Nikon Eclipse TE2000S fluorescence microscope at a magnification of 60x.* ***(c/d)*** *Immunofluorescent staining of HCV NS3 in* ***(c)*** *replicon expressing and cured Huh7 cells and* ***(d)*** *replicon expressing and cured Huh7.5 cells. IFNα treatment was performed on the replicon expressing Huh7 and Huh7.5 cells for eight weeks to generate cured cell lines. Replicon expressing and cured cell lines were stained using an anti-NS3 antibody (red staining). Cell nuclei were stained with DAPI (light blue staining). Images were captured using a Nikon Eclipse TE2000S fluorescence microscope at a magnification of 20x.* ***(e)*** *Detection of HCV NS3 protein and GT2a replicon RNA in replicon expressing Huh7 and Huh7.5 cells treated with IFNα. Huh7 and Huh7.5 cells transfected with the GT2a replicon were treated with IFNα at 100IU/ml for a period of eight weeks. Every two weeks, the cells were tested for the presence of NS3 protein by immunofluorescent staining with a mouse anti-NS3 antibody and for the presence of intracellular GT2a replicon RNA by qRT-PCR.*

3.5.2 Quantitative PCR analysis of subgenomic replicon expressing cells

qRT-PCR was used to investigate host gene expression in the replicon expressing Huh7 cells (**Fig. 3.12**) and replicon expressing Huh7.5 cells (**Fig. 3.13**). Host gene expression in the replicon expressing cells was compared to the gene expression profile observed for both the cured and wild type cells. The expression of genes involved in sphingolipid metabolism, cholesterol synthesis, fatty acid metabolism, lipid droplet production, xenobiotic metabolism and intracellular transport was investigated.

Comparison of the expression patterns observed for the replicon expressing cells and the JFH-1 infected cells demonstrated that several host genes increased in expression in both conditions including genes involved in sphingolipid metabolism (SGPP1 and SPTLC1), lipid droplet production (PGC1α), xenobiotic metabolism (CYP1A1 and CYP1B1) and intracellular transport (ABLIM3). Several of the host genes that increased in expression during JFH-1 infection showed little change in expression in the replicon expressing cells; this included genes involved in fatty acid metabolism (SREBF1, PPARγ, ACLS3, ELOVL4, ELOVL7 and TXNIP), lipid droplet production (RIP140 and CIDEB) and intracellular transport (RAB27B, RAB33B and RAB37). Some of the host genes tested altered in expression in opposite directions in the JFH-1 infected cells compared to the replicon expressing cells, such as the host genes involved in cholesterol biosynthesis, which decreased in expression in the JFH-1 infected cells, but increased in expression in the replicon expressing cells (FDFT1, SQLE, EBP, MVD and HMGCR).

For the majority of genes tested, little difference in gene expression was observed between the cured and wild type cells. However, some of the genes tested did increase in expression in the cured cells compared to the wild type cells. This included PGC1α, which increased in expression in both Huh7 and Huh7.5 cured cell lines and ABLIM3, which increased in expression in the Huh7 cured cells only. These findings indicate that during the process of selecting for replicon transfected cells, cell clones with elevated levels of PGC1α and ABLIM3 expression may have supported a higher level of replicon RNA replication and may have been positively selected above other cellular clones in the wild type cell lines.

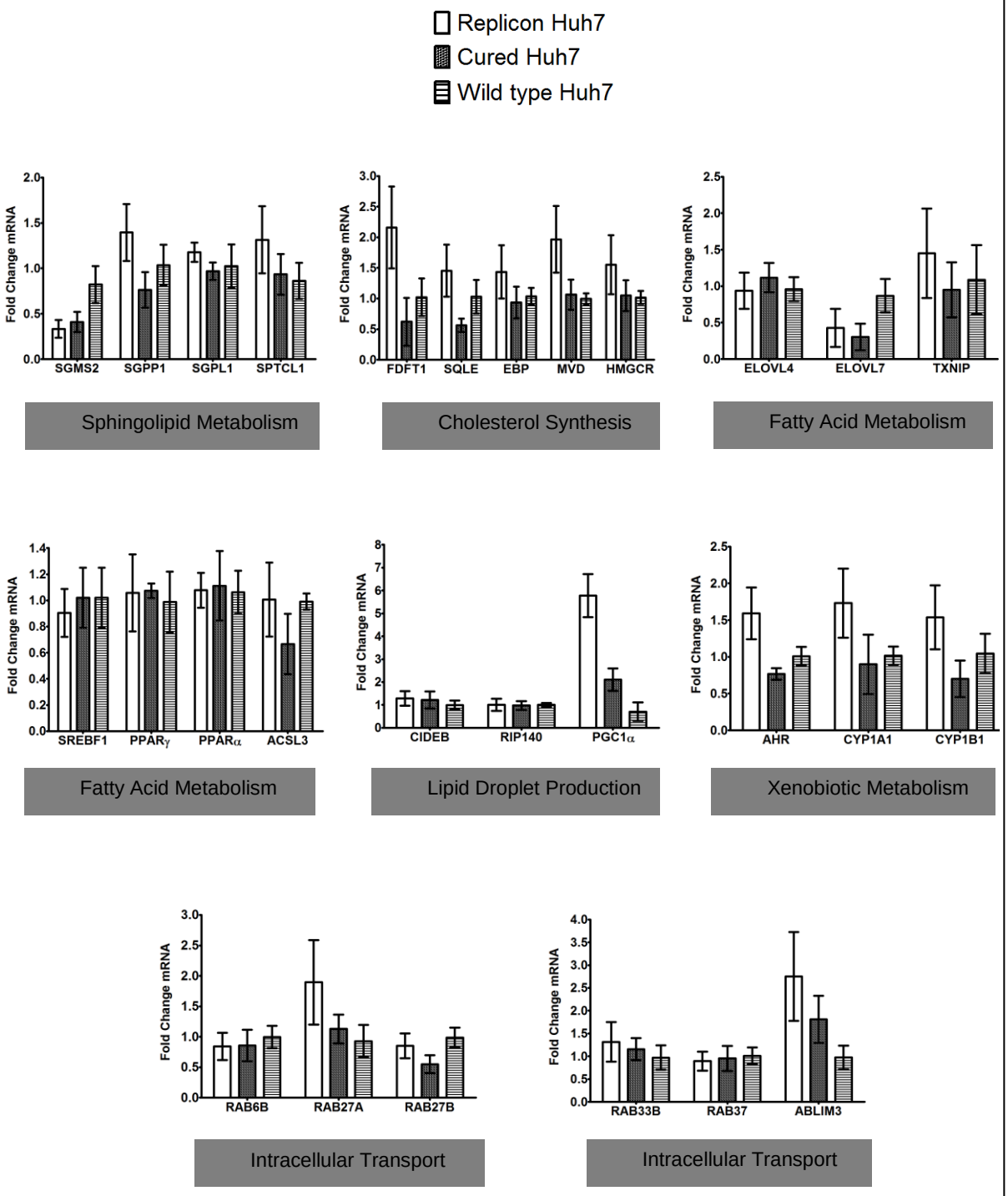


Figure 3.12 The genotype 2a replicon alters Huh7 cell gene expression

Fold change in Huh7 cell host gene expression following transfection of the genotype 2a subgenomic replicon. Intracellular RNA was extracted from the replicon expressing (white bars), IFNα cured (grey bars) and wild type (striped bars) Huh7 cells. RNA extracts were used for qRT-PCR analysis of host gene expression using relative quantification. The qRT-PCR data shown represents the mean (±SD) of a single experiment with each cell line seeded and extracted in triplicate.

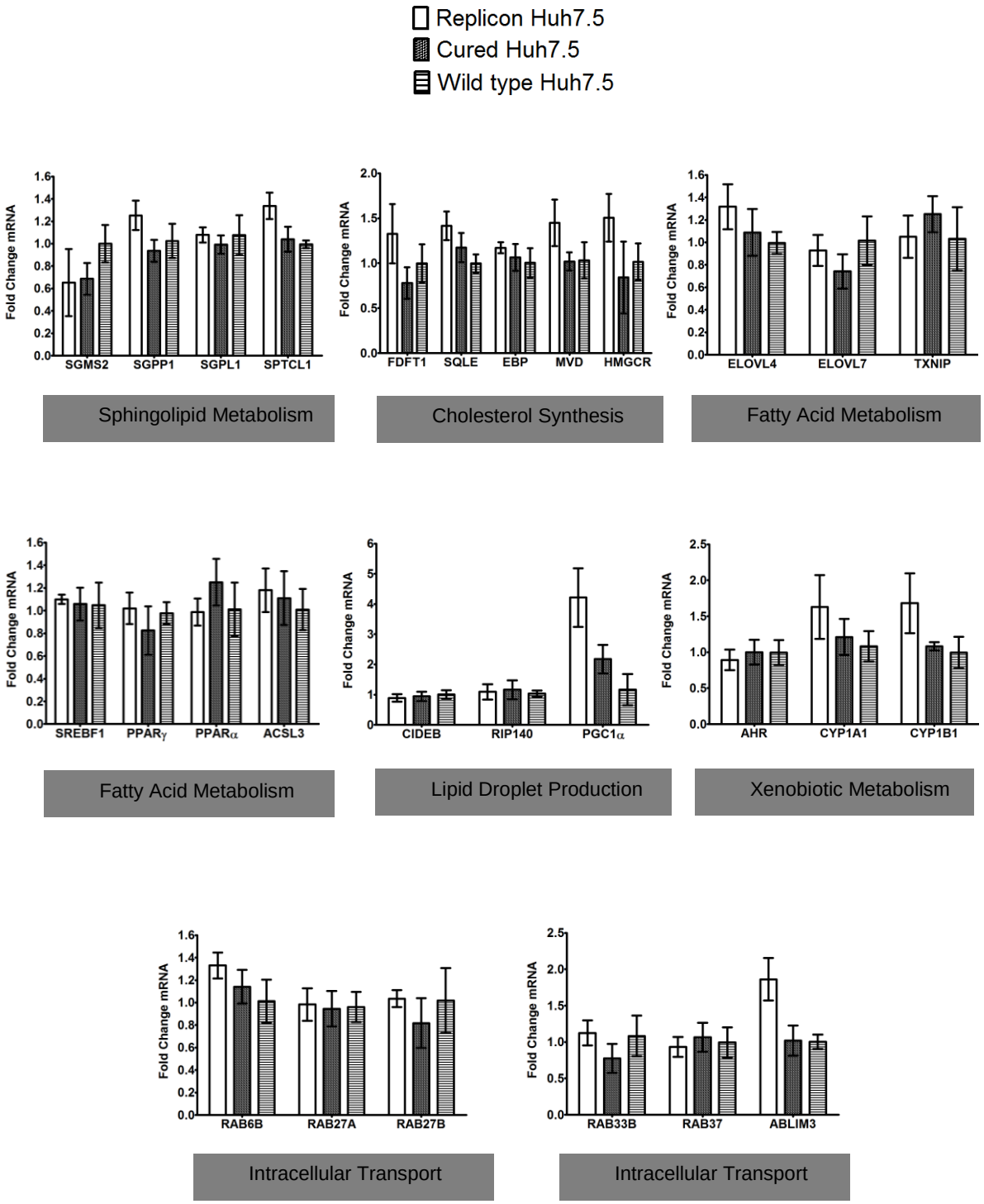


Figure 3.13 The genotype 2a replicon alters Huh7.5 cell gene expression

Fold change in Huh7.5 cell host gene expression following transfection of the genotype 2a subgenomic replicon. Intracellular RNA was extracted from the replicon expressing (white bars), IFNα cured (grey bars) and wild type (striped bars) Huh7.5 cells. RNA extracts were used for qRT-PCR analysis of host gene expression using relative quantification. The qRT-PCR data shown represents the mean (±SD) of a single experiment with each cell line seeded and extracted in triplicate.

3.5.3 Intracellular replicon RNA abundance in the replicon expressing cells

The intracellular replicon RNA levels in the replicon expressing cells were quantified by qRT-PCR using absolute quantification (**Fig. 3.14**). Higher levels of the replicon RNA were observed in the replicon expressing Huh7.5 cells compared to the replicon expressing Huh7 cells. This finding reflected the differences observed in JFH-1 RNA levels between the JFH-1 infected Huh7 and Huh7.5 cells, although the fold difference observed was smaller (**Fig. 3.10**). The overall levels observed in the replicon expressing cells were also lower than those during infection (**Fig. 3.10**).



Figure 3.14 Replicon RNA levels in replicon expressing Huh7 and Huh7.5 cells

Intracellular genotype 2a replicon RNA levels quantified for the replicon expressing Huh7 and Huh7.5 cells. Intracellular RNA was extracted from the replicon expressing Huh7 and Huh7.5 cells at passage 10 post-transfection. qRT-PCR was used to quantify replicon RNA levels by absolute quantification. The RNA quantification data shown represents the mean (±SD) of samples seeded and extracted in triplicate.

3.5.4 The effect of JFH-1 infection on cholesterol biosynthesis gene expression

As observed in Figures 3.8, 3.10, 3.12 and 3.13, host genes controlling cholesterol biosynthesis were differentially regulated in the JFH-1 infected and replicon expressing cells. To try and understand these differences, the effect of JFH-1 infection on the expression of cholesterol biosynthesis genes was further investigated. In addition to investigating host gene expression in cells infected for 24 and 48 hours, expression was also investigated in cells infected for 72 hours (**Fig. 3.15**). The expression of genes controlling cholesterol biosynthesis was observed to vary at different times post infection. At 24 and 48 hours post infection, a decrease was observed in the expression of the cholesterol biosynthesis genes; however, at 72 hours post infection the expression of these

genes increased, consistent with the expression pattern observed in the replicon expressing cells (Fig. 3.12 and Fig. 3.13).

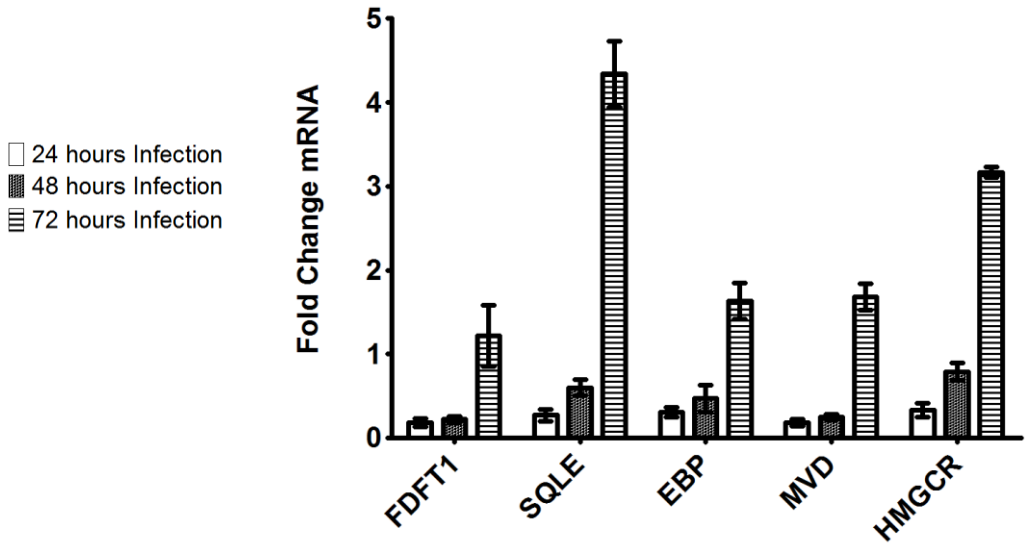


Figure 3.15 JFH-1 infection alters cholesterol synthesis gene expression

Fold change in the expression of cholesterol synthesis genes in Huh7 cells infected with JFH-1 for 24, 48 and 72 hours. Huh7 cells were infected with JFH-1 (MOI = 3) or mock medium for 24 (white bars), 48 (grey bars) and 72 (striped bars) hours. Intracellular RNA was extracted and used for qRT-PCR analysis of host gene expression using relative quantification. The qRT-PCR data shown represents the mean (±SD) of triplicate infections for each time point.

3.6 Gene expression profiling of cells expressing the JFH-1 core protein

Comparison of the host gene expression patterns observed for JFH-1 infected and replicon expressing cells provided insight into whether the HCV non-structural proteins were responsible for transcriptionally regulating host gene expression during JFH-1 infection. However, many of the genes shown to alter in expression during infection did not alter in expression in the replicon expressing cells. To further investigate whether other HCV proteins were responsible for transcriptional regulation of these genes, Huh7 cells expressing the JFH-1 core protein were generated to investigate the effect of the HCV core protein on Huh7 cell gene expression. Two different approaches were used to generate Huh7 cells expressing the JFH-1 core protein; however, neither approach was successful in generating a cell line where all the cells expressed the core protein.

3.6.1 Expression of JFH-1 core using the Semliki Forest Virus replicon

The first approach used to generate core expressing Huh7 cells involved the use of the Semliki Forest Virus (SFV) replication system, which typically enables a high level of target protein expression in cells in conjunction with the assembly of SFV replication complexes. Transfection of *in vitro* transcribed RNA encoding the SFV replicase components and a target gene of interest results in the expression of SFV replicase and target proteins. The SFV replication complexes that assemble from the replicase proteins permit replication of the input RNA resulting in high levels of protein expression for the target gene encoded [211]. Plasmids containing the sequence for the SFV replication complex with and without the JFH-1 core gene were generously donated by Dr John McLauchlan (University of Glasgow Centre for Virus Research) [60].

To express core protein from the pSFV(core) plasmid, RNA molecules were transcribed using *in vitro* RNA transcription from a SapI linearised form of the plasmid. Negative control RNA transcripts were also generated from pSFV(empty) SapI linearised plasmid DNA (**Appendix A.13**). Huh7 cells transfected with the SFV(core) RNA were stained for the HCV core protein at 24 hours post-transfection (**Fig. 3.16**), as replication of the SFV genome is known to have a pro-apoptotic effect on cells within around 24 to 48 hours post-transfection [211]. To optimise the transfection of Huh7 cells with the SFV(core) RNA, cells were transfected with 1µg and 2µg of the RNA transcript. The efficiency of transfection was increased in the cells transfected with 2µg of RNA; however, even with this large amount of RNA, the numbers of cells successfully transfected was still too low for accurate gene expression profiling to be performed.

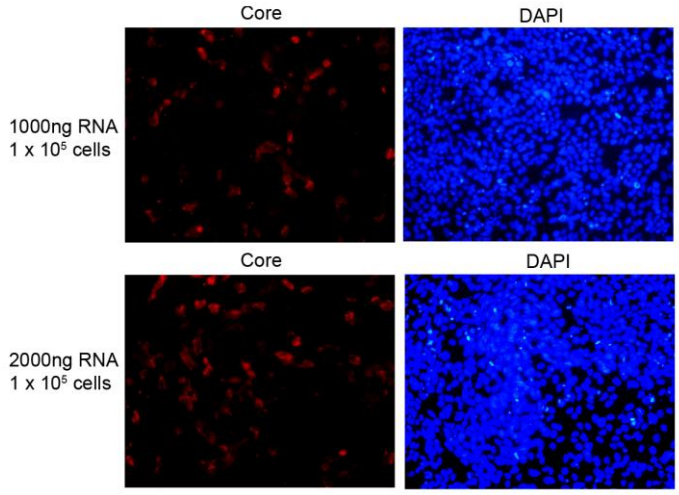


Figure 3.16 JFH-1 core expression using the Semliki Forest Virus replicon

Core protein staining of Huh7 cells transfected with the SFV(core) RNA transcript for 24 hours. $1x10^5$ Huh7 cells were transfected with 1µg and 2µg of the SFV(core) RNA transcript. At 24 hours post-transfection, the cells were stained using an anti-core antibody (red staining). Cell nuclei were also stained with DAPI (blue staining). Images were captured using a Nikon Eclipse TE2000S fluorescence microscope at a magnification of 20x.

3.6.2 Expression of JFH-1 core using the pIRES expression vector

The second approach used to generate core expressing cells involved the production of a stable core expressing cell line using a pIRES bicistronic expression vector. A bicistronic pIRES plasmid containing a Blasticidin resistance gene was generously donated by Dr Marco Purbhoo (Imperial College London). The JFH-1 core sequence was PCR amplified out of the pSFV(core) plasmid and cloned into the pIRES-Blasticidin vector (**Appendix A.14a**). To verify the ligation of the JFH-1 core sequence with the pIRES vector, diagnostic PCR and diagnostic restriction enzyme digestion was performed (**Appendix A.14b and c**). Huh7 cells were transfected with the pIRES(core) and pIRES(empty) plasmid DNA and were grown in the presence of Blasticidin. The cells were tested for core protein expression every week for a total of 8 weeks. Although the levels of core expressing cells increased during this time, many core-negative cells remained in the transfected cell population at 8 weeks post-transfection (**Fig 3.17**). In addition, comparison of core protein staining between the pIRES(core) transfected cells and the SFV(core) RNA transfected cells also demonstrated that HCV core protein expression was much weaker with the pIRES expression system than with the pSFV expression system (**Fig. 3.17**).

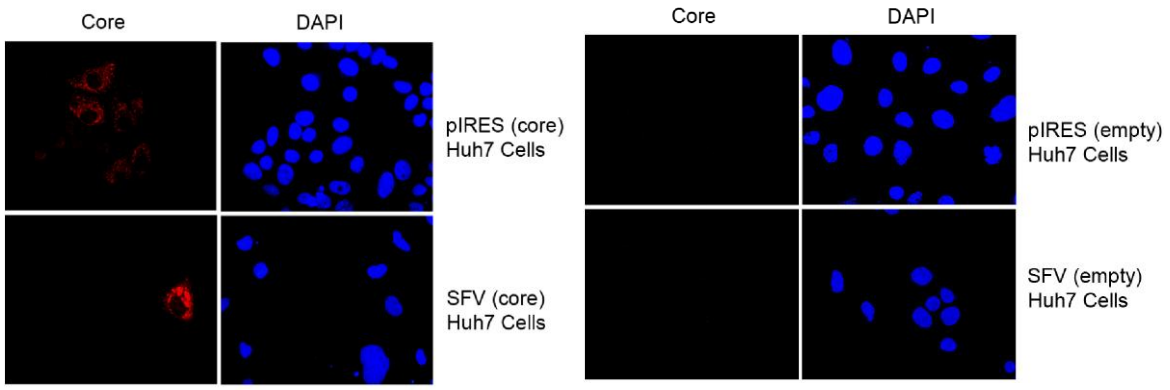


Figure 3.17 Comparison of HCV core protein expression in pIRES(core) and SFV(core) RNA transfected Huh7 cells

Core protein staining in Huh7 cells transfected with pIRES(core) DNA, pIRES(empty) DNA, SFV(core) RNA and SFV(empty) RNA. Huh7 cells were transfected with pIRES(core) and pIRES(empty) plasmid DNA and selected in the presence of Blasticidin (10µg/ml) for 8 weeks. Huh7 cells were also transfected with 2µg of SFV(core) and SFV(empty) RNA transcripts for 24 hours. All transfected cells were stained for the JFH-1 core protein using an anti-core antibody (red staining). Cell nuclei were also stained with DAPI (blue staining). Images were captured using a Nikon Eclipse TE2000S fluorescence microscope at a magnification of 60x. Images were captured using equal exposure time and gain settings.

3.7 Quantification of host protein abundance during JFH-1 infection

In addition to validating the microarray gene expression data by qRT-PCR, it was also important to determine whether alterations in mRNA abundance had an effect on host protein expression. Two host factors chosen from the microarray study for further investigation were the thioredoxin interacting protein (TXNIP) and the peroxisome proliferator activated receptor gamma alpha protein (PGC1α). The genes encoding both of these proteins showed large increases in expression as a result of JFH-1 infection (**Fig. 3.8**). Before investigating the effect of JFH-1 infection on host protein expression, the antibodies recognising TXNIP, PGC1α, HCV NS3, HCV core and tubulin proteins were optimised for use in western blotting with cell lysates generated from JFH-1 and mock infected Huh7 cells (**Fig. 3.18**). A protein lysate obtained from K562 cells was also used to test the activity of the anti-TXNIP antibody, as this cell line expressed a high level of TXNIP protein. To test the activity of the anti-PGC1α antibody, protein lysates were generated from HEK293T cells that had been transiently transfected with a pcDNA3.1D/V5-His-TOPO plasmid expressing the PGC1α protein. This plasmid was generously donated by Dr Mark Christian (Imperial College London). All the

antibodies tested detected a product of the correct molecular weight for each protein. Most of antibodies were also very specific detecting only a single protein product. One exception was the anti-core antibody, which detected an additional smaller protein (14KDa) in the JFH-1 infected sample alongside a protein of the correct size (21KDa) (**Fig. 3.18b**). The anti-TXNIP antibody also detected a series of very large molecular weight proteins in addition to the 50KDa TXNIP protein. It is likely that these additional bands resulted from non-specific binding of the TXNIP antibody (**Fig. 3.18d**).

Having optimised the antibodies for western blotting, the effect of JFH-1 infection on the expression of TXNIP and PGC1α was investigated in Huh7 cells infected either with JFH-1 or mock medium (**Fig. 3.19a and b**). The abundance of both TXNIP and PGC1α proteins was elevated in JFH-1 infected cells compared to the mock infected cells. Successful infection of the cells was confirmed by the detection of either HCV NS3 or HCV core proteins in the JFH-1 infected cells. To determine fold change in protein abundance during infection, quantification of the blot band intensities was performed (**Fig. 3.19c and d**). Band intensities for the tubulin protein bands were used to normalise the signal from the TXNIP and PGC1α protein bands. Although the fold change in gene expression for both TXNIP and PGC1α was relatively large (e.g. 50 fold), the fold change in protein expression was much smaller by comparison.

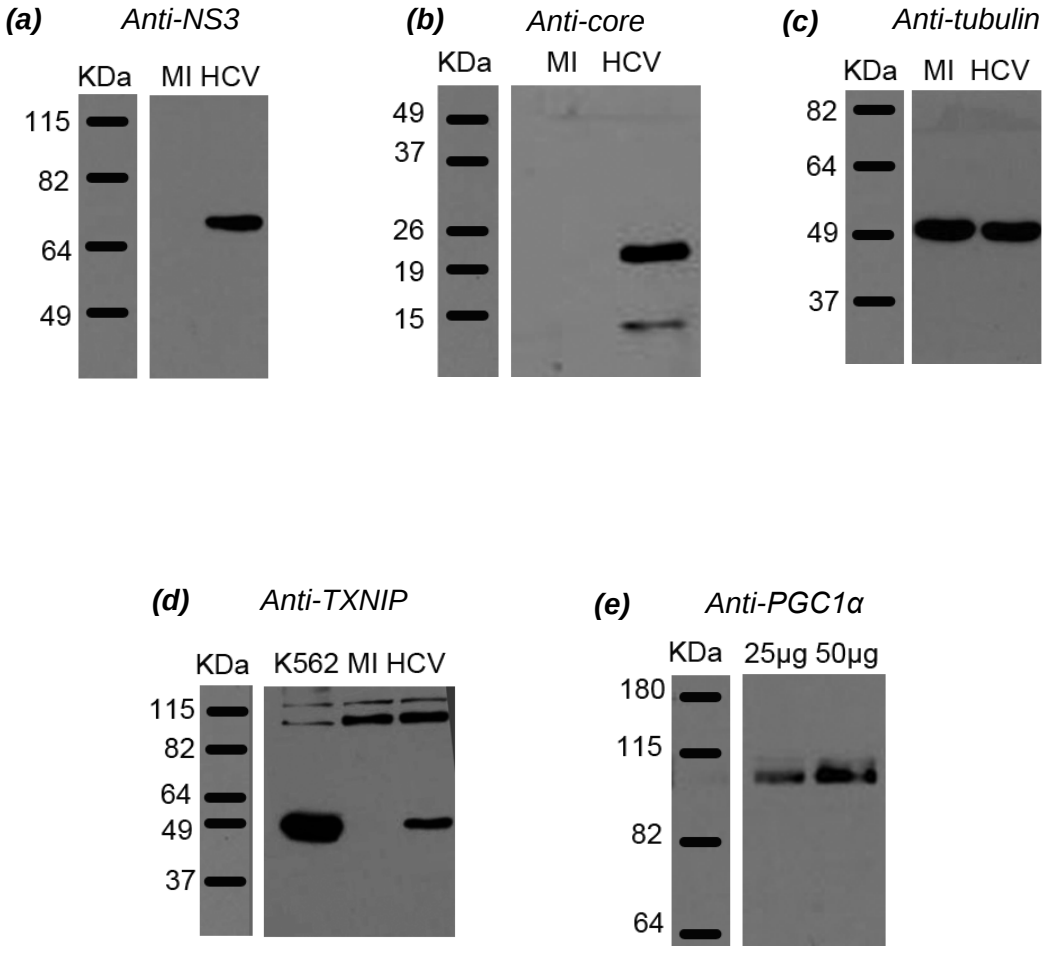


Figure 3.18 Western blot optimisation of antibodies recognising HCV NS3, HCV core, tubulin, TXNIP and PGC1α

(a-d) *Western blotting of JFH-1 infected and mock infected Huh7 cell lysates with antibodies that recognise HCV NS3, HCV core, tubulin and TXNIP. Huh7 cells were infected with JFH-1 (HCV) (MOI = 3) or mock medium (MI) for 48 hours. Cells were lysed using 0.5% Triton X-100 lysis buffer and 50µg of protein was run on a 10% acrylamide gel. Blotting of the gel was performed onto nitrocellulose membrane which was probed with* ***(a)*** *anti-NS3 antibody,* ***(b)*** *anti-core antibody,* ***(c)*** *anti-tubulin antibody and* ***(d)*** *anti-TXNIP antibody. 50µg of a protein cell lysate from K652 cells was also run on the blot testing the anti-TXNIP antibody.* ***(e)*** *Western blotting of HEK293T cells transiently transfected with a PGC1α expression plasmid using an antibody that recognises PGC1α. HEK293T cells were transfected for 48 hours with a PGC1α expression plasmid. Cells were lysed in 0.5% Triton X-100 lysis buffer; 25µg and 50µg of the cell lysate was run on an 8% acrylamide gel. Blotting of the gel was performed onto nitrocellulose membrane which was probed with anti-PGC1α antibody. Antibodies are expected to identify proteins of the following molecular weights: NS3 (70KDa), core (21KDa), tubulin (50 KDa), TXNIP (50 KDa) and PGC1α (90KDa).*

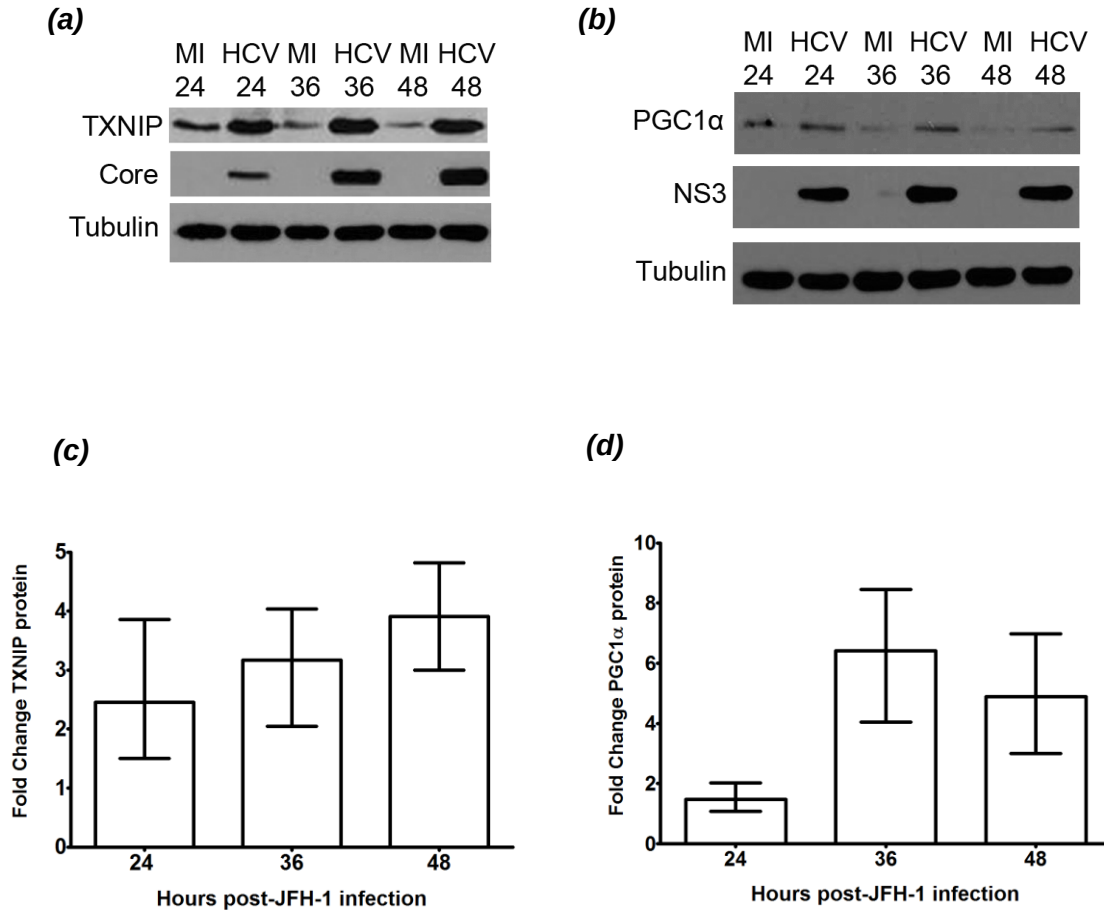


Figure 3.19 JFH-1 infection increases TXNIP and PGC1α protein levels

(a) *TXNIP protein expression following JFH-1 infection of Huh7 cells. Huh7 cells were infected either with JFH-1 (HCV) (MOI = 3) or mock medium (MI) for 24, 36 and 48 hours. Cells were lysed in 0.5% Triton X-100 lysis buffer and 50µg of protein was run on a 10% acrylamide gel. Blotting of the gel was performed onto nitrocellulose membrane which was probed with anti-TXNIP, anti-core and anti-tubulin antibodies.* ***(b)*** *PGC1α protein expression following JFH-1 infection of Huh7 cells. Huh7 cells were infected either with JFH-1 (HCV) (MOI = 3) or mock medium (MI) for 24, 36 and 48 hours. Cells were lysed in 0.5% Triton X-100 lysis buffer and 100µg of protein was run on an 8% acrylamide gel. Blotting of the gel was performed onto nitrocellulose membrane which was probed with anti-PGC1α, anti-NS3 and anti-tubulin antibodies.* ***(c)*** *Fold change in TXNIP protein at 24, 36 and 48 hours post-infection and* ***(d)*** *fold change in PGC1α protein at 24, 36 and 48 hours post-infection. Fold change was calculated by quantifying the intensity of each protein band on the TXNIP and PGC1α blots, and comparing the intensities calculated for the JFH-1 infected and mock infected samples at each time-point. Protein band intensities were calculated using ImageJ and normalisation was performed using tubulin. Fold change data plotted represents mean fold change (and replicate range) at each time-point post-infection calculated from the single protein bands observed on two repeat TXNIP and PGC1α blots (N=2). Note: only one representative blot for TXNIP and PGC1α is shown here.*

3.8 Quantification of intracellular lipid metabolites during JFH-1 infection

Gene expression profiling of JFH-1 infected cells demonstrated that several pathways controlling intracellular lipid synthesis were upregulated during infection. These expression patterns indicate that HCV infection may increase the rate of intracellular lipid synthesis providing potential insight into why chronically infected patients frequently develop hepatic steatosis. To investigate whether the expression patterns observed may contribute to the development of steatosis and to further validate the expression data observed, the effect of JFH-1 infection on intracellular lipid abundance was investigated.

3.8.1 Optimisation of cholesterol and triglyceride quantification assays

To quantify intracellular cholesterol and triglyceride abundance, colorimetric absorbance assays were used. Initially, the assays were optimised using protein lysate from untreated Huh7 cells (**Fig. 3.20**). The optimal amount of protein lysate chosen for both cholesterol and triglyceride quantification was 25µg.

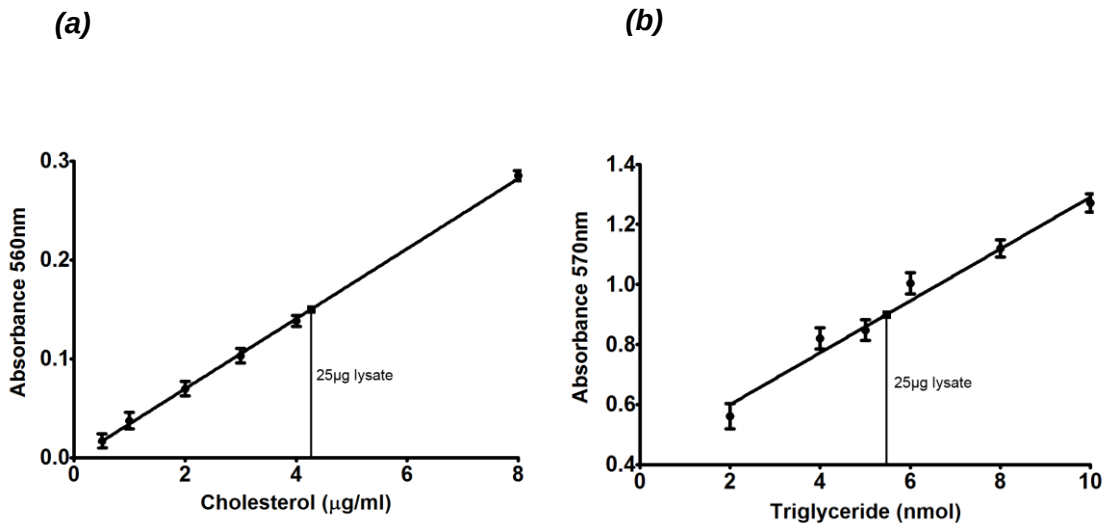


Figure 3.20 Optimisation of cholesterol and triglyceride quantification assays

(a) *Optimisation of the cholesterol quantification assay using 25µg of Huh7 cell protein lysate. Huh7 cells lysed in 0.5% Triton X-100 lysis buffer were tested alongside a cholesterol standard curve (0.5, 1, 2, 3, 4 and 8 µg/ml cholesterol) in the Amplex Red cholesterol quantification assay.* ***(b)*** *Optimisation of the triglyceride quantification assay using 25µg of a Huh7 cell protein lysate. Huh7 cells lysed in 5% Triton X-100 / H_20 were tested alongside a triglyceride standard curve (2, 4, 5, 6, 8 and 10 nmol triglyceride) in the triglyceride quantification assay. All standard curve absorbance readings represent the mean (±SD) of triplicate standard curve assays.*

3.8.2 Cholesterol and triglyceride levels in JFH-1 infected cells

The effect of JFH-1 infection on the intracellular levels of cholesterol and triglyceride was investigated using Huh7 cells infected with JFH-1 or mock medium for 24, 48 and 72 hours (**Fig. 3.21a and b**). An increase in both cholesterol and triglyceride was observed as a result of infection, with the largest fold change being observed at 72 hours post-infection.

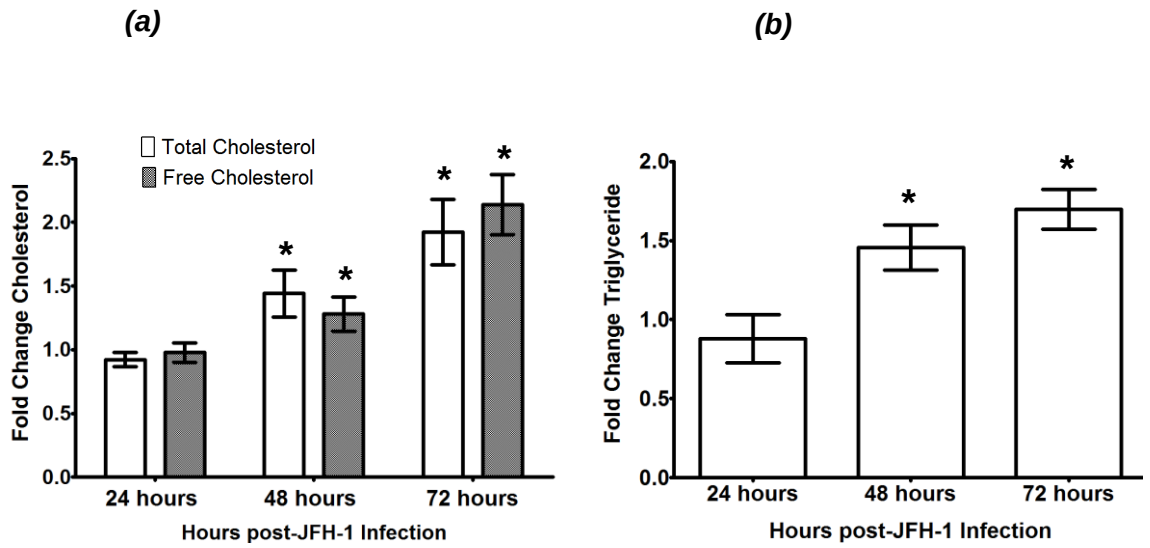


Figure 3.21 JFH-1 infection increases intracellular cholesterol and triglyceride

(a) *Fold change in total and free cholesterol levels during JFH-1 infection. Huh7 cells infected with JFH-1 (MOI = 3) or mock medium for 24, 48 and 72 hours were lysed in 0.5% Triton X-100 lysis buffer and the intracellular cholesterol levels were quantified using the Amplex red cholesterol quantification kit. Each sample was analysed in the presence and absence of the cholesterol esterase enzyme for quantification of total cholesterol (white bars) and free cholesterol (grey bars), respectively.* ***(b)*** *Fold change in triglyceride levels during JFH-1 infection. Huh7 cells infected with JFH-1 (MOI = 3) or mock medium for 24, 48 and 72 hours were lysed in 5% Triton X-100 / H_20 and the intracellular triglyceride levels were quantified using the triglyceride quantification kit. Metabolite quantification data displayed represents the mean (±SD) of three independent experiments, each containing repeat infections performed in duplicate (N=6). Triglyceride and cholesterol levels with a statistically significant increase in abundance in JFH-1 infected cells compared to mock infected cells (p value ≤ 0.05) are indicated by an asterisk (*). P values were calculated using a two-tailed unpaired T test in Graphpad Prism.*

3.8.3 Cholesterol and triglyceride levels in replicon expressing cells

Many of the lipid metabolism genes upregulated in the JFH-1 infected cells were also upregulated in the replicon expressing cells (**Fig. 3.12 and 3.13**). To investigate whether the increased expression of these genes also induced an

increase in the intracellular lipid levels of the replicon expressing cells, the abundance of cholesterol and triglyceride was quantified in the replicon expressing, cured and wild type Huh7 cells (**Fig. 3.22**).

Increases were observed in the intracellular cholesterol levels of the replicon expressing cells compared to the cured and wild type cell lines, and in the triglyceride levels of the replicon expressing cells compared to the wild type cells. An increase was also observed in the triglyceride levels quantified in the cured Huh7 cells compared to the wild type Huh7 cell line. Comparison of the fold increase observed for cholesterol and triglyceride in the replicon expressing cells to that observed for the JFH-1 infected cells indicated that cells exposed to the full HCV replication cycle accumulated a greater level of intracellular lipid metabolites (**Fig. 3.21 and 3.22**).

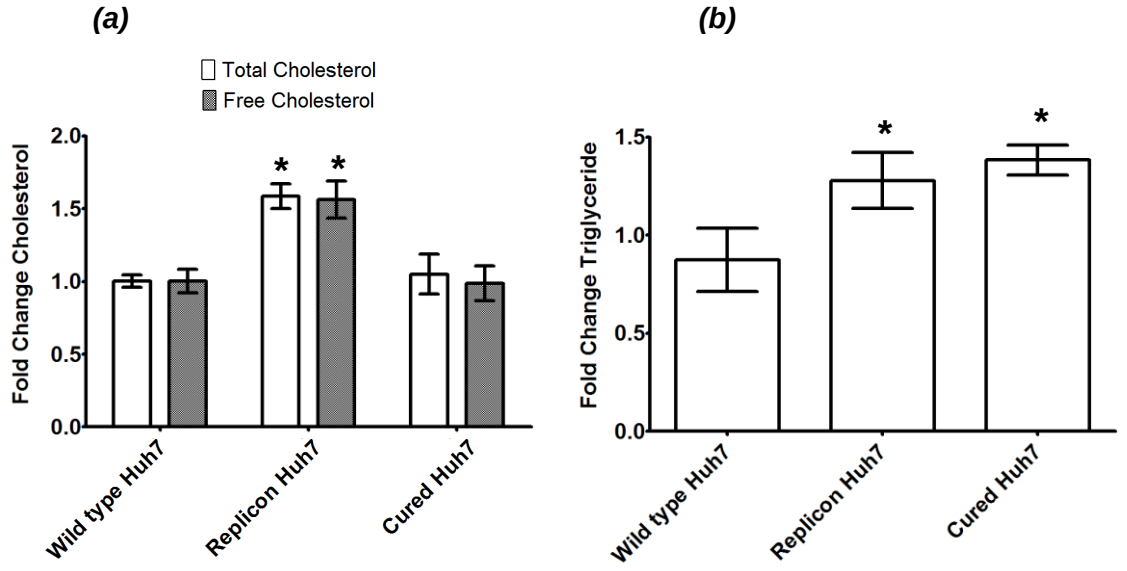


Figure 3.22 The HCV replicon increases cholesterol and triglyceride levels

(a) *Fold change in total and free cholesterol levels in the replicon expressing, cured and wild type Huh7 cells. All cells were lysed in 0.5% Triton X-100 lysis buffer and the intracellular cholesterol levels were quantified using the Amplex red cholesterol quantification kit. Each sample was analysed in the presence and absence of the cholesterol esterase enzyme for quantification of total cholesterol (white bars) and free cholesterol (grey bars), respectively.* ***(b)*** *Fold change in triglyceride levels in the replicon expressing, cured and wild type Huh7 cells. All cells were lysed in 5% Triton X-100 / H_20 and the intracellular triglyceride levels were quantified using the triglyceride quantification kit. Metabolite quantification data displayed represents the mean (±SD) of two independent experiments with each cell line seeded and extracted in triplicate (N=6). Triglyceride and cholesterol levels with a statistically significant increase in abundance in replicon cells and cured cells compared to wild type cells (p value ≤ 0.05) are indicated by an asterisk (*). P values were calculated using a two-tailed unpaired T test in Graphpad Prism.*

3.9 Quantification of intracellular lipid droplets during JFH-1 infection

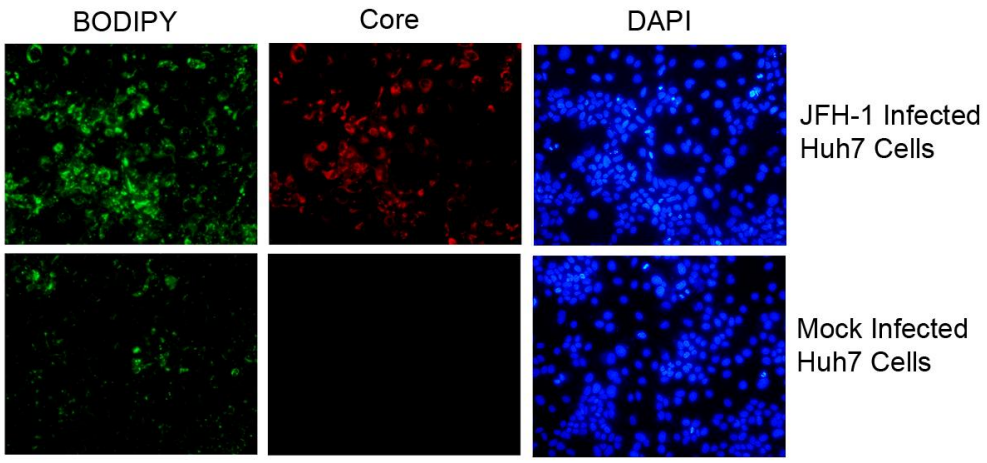
According to Figures 3.21 and 3.22, an increase was observed in the triglyceride and cholesterol levels of both JFH-1 infected cells and replicon expressing cells. Previous published studies have demonstrated that JFH-1 infection alters the accumulation and positioning of intracellular lipid droplets, which are the lipid storage organelles synthesised from excess triglyceride and cholesterol ester molecules [60, 212]. To investigate whether the increased triglyceride and cholesterol levels in the JFH-1 infected and replicon expressing cells also correlated with an accumulation of lipid droplets, the intracellular abundance of lipid droplets in these cells was investigated.

3.9.1 Lipid droplet abundance in JFH-1 infected cells

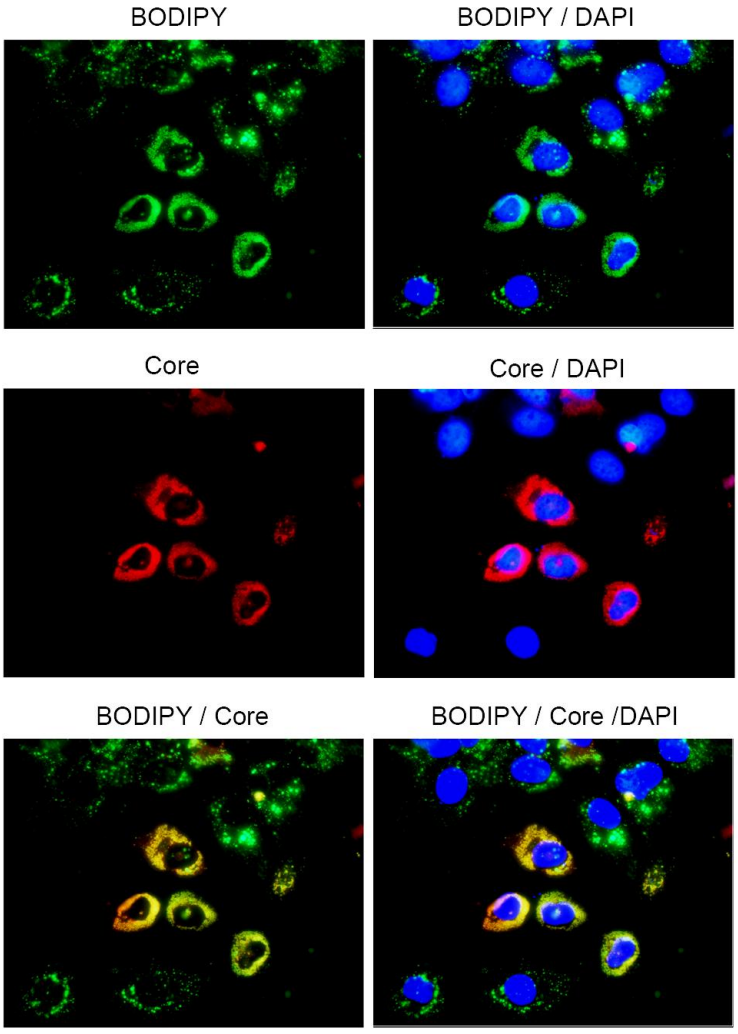
To investigate lipid droplet abundance during infection, a lipid droplet specific fluorescent dye, BODIPY 493/503, was used to stain Huh7 cells that had been JFH-1 infected (MOI = 3) or mock infected for 48 hours (**Fig. 3.23a**). Core protein staining was also performed to indicate which cells had been successfully infected. A significant increase was observed in the intensity of BODIPY staining in the JFH infected cells compared to the mock infected cells. Consistent with the ability of the HCV core protein to bind to the surface of lipid droplets, significant overlap of the BODIPY and core protein staining was also observed in the JFH-1 infected cells (**Fig. 3.23a, b and c**).

Staining of the core protein and lipid droplets was also performed for Huh7 cells infected with JFH-1 at a lower MOI of 0.5. This ensured that only a proportion of the cells became infected and allowed the intensity of the BODIPY signal to be compared between JFH-1 infected cells (core positive) and non infected cells (core negative) that had been captured in the same image (**Fig. 3.23b, c and d**). Comparison of the BODIPY signal quantified for these cells demonstrated that a 3 fold increase was observed in lipid droplet abundance during JFH-1 infection (**Fig. 3.23e**).

***(a)** Huh7 cells infected with JFH-1 (MOI=3) or mock media*



***(b)** JFH-1 infected Huh7 cells (MOI=0.5)*



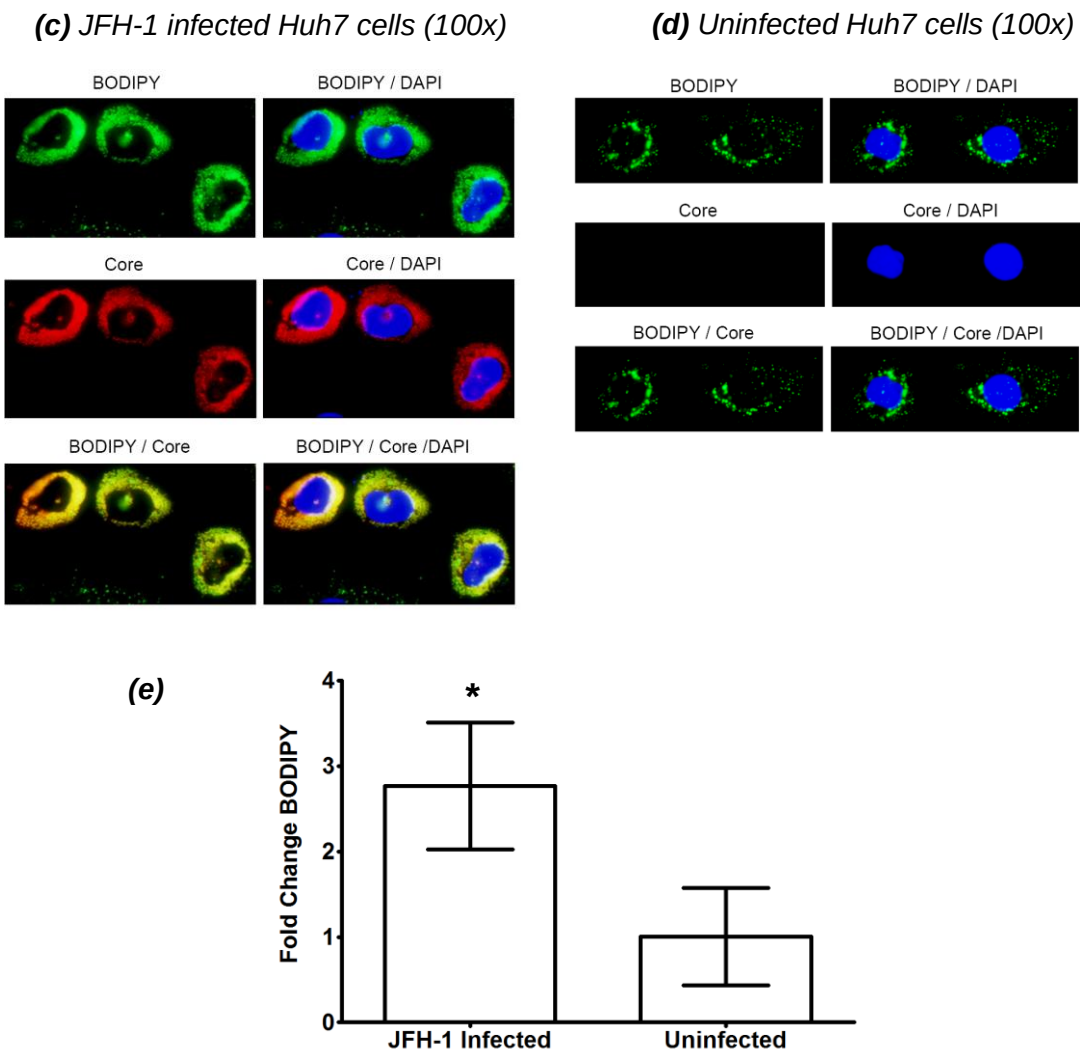


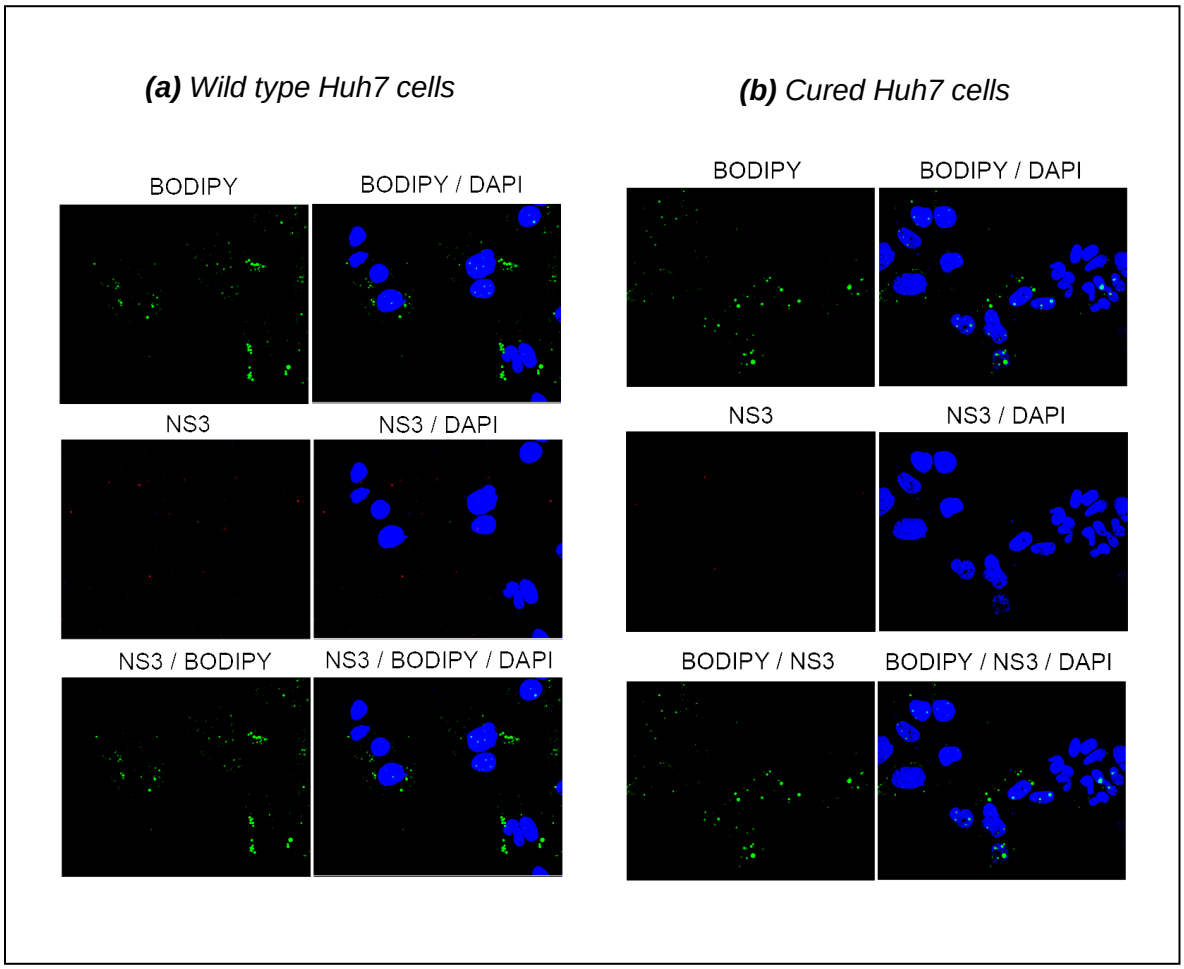
Figure 3.23 JFH-1 infection increases lipid droplet abundance

(a) *Lipid droplet staining of JFH-1 infected and mock infected Huh7 cells. Huh7 cells were infected with JFH-1 (MOI=3) or mock medium for 48 hours. Cells were stained using anti-core antibody (red staining) and 50µg/ml BODIPY 493/503 (green staining). Cell nuclei were also stained with DAPI (blue staining). Images were captured using a Nikon Eclipse TE2000S fluorescence microscope at a magnification of 20x.* ***(b)*** *Lipid droplet staining of Huh7 cells infected with a low MOI of JFH-1. Huh7 cells were infected with JFH-1 (MOI=0.5) for 48 hours and stained using anti-core antibody (red staining) and 50µg/ml BODIPY 493/503 (green staining). Cell nuclei were also stained with DAPI (blue staining). Images were using a Nikon Eclipse TE2000S fluorescence microscope at a magnification of 60x.* ***(c/d)*** *High magnification images of* ***(c)*** *JFH-1 infected Huh7 cells and* ***(d)*** *uninfected Huh7 cells taken at a magnification of 100x. All images were taken using the same exposure time and gain settings.* ***(e)*** *Fold change in BODIPY staining for JFH-1 infected and uninfected Huh7 cells. Fold change was calculated by comparing the BODIPY fluorescence quantified for JFH-1 infected (core positive) and uninfected (core negative) Huh7 cells using Image J. BODIPY quantification data displayed represents the mean (±SD) of 15 different cell counts for the infected and uninfected cells. The fold change in lipid droplet abundance during infection was statistically significant with a p value < 0.001 (indicated by an asterisk (*)). P values were calculated using a two-tailed unpaired T test in Graphpad Prism.*

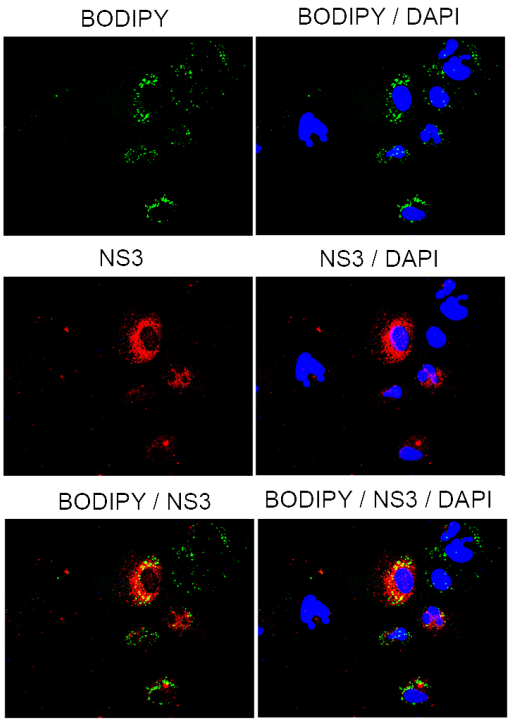
3.9.2 Lipid droplet abundance in the subgenomic replicon expressing cells

Lipid droplet staining was also performed using the replicon expressing, cured and wild type Huh7 cells to determine whether the non-structural HCV proteins also altered lipid droplet abundance (**Fig. 3.24**). The cells were stained for the HCV NS3 protein to identify the presence of replicon expressing cells. Unlike the HCV core protein, NS3 did not co-localise with lipid droplets in the replicon expressing cells.

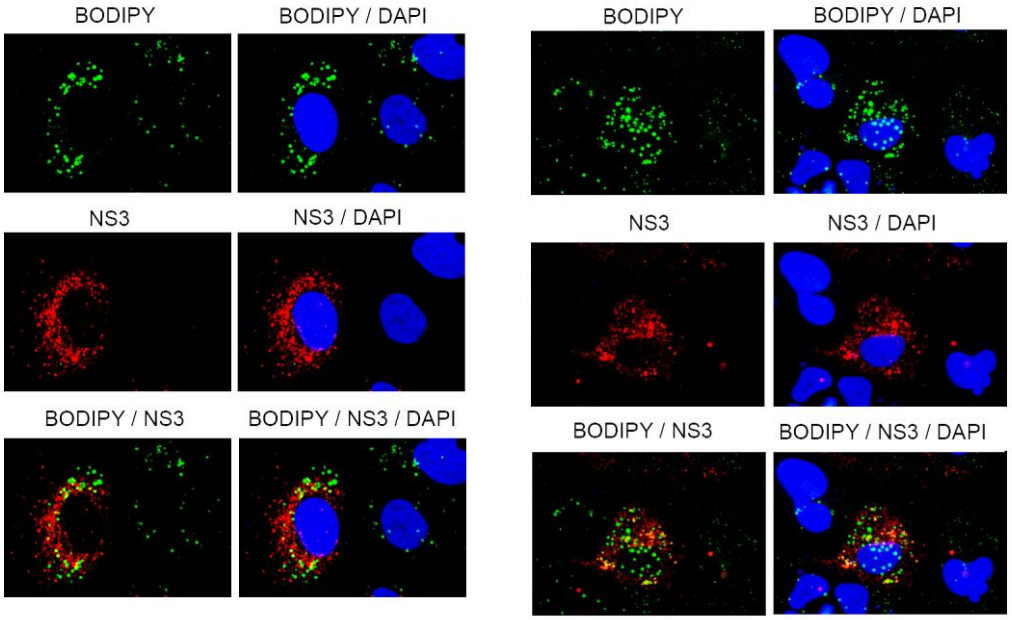
Comparison of the lipid droplet staining observed for the replicon expressing (**Fig. 3.24c and d**), cured (**Fig. 3.24b**) and wild type Huh7 cells (**Fig. 3.24a**) demonstrated that the expression of the non-structural HCV proteins increased lipid droplet abundance. A 1.5 fold increase in BODIPY staining was observed when comparing the cells that stained positively for NS3 to the cells that stained negatively for NS3 in the replicon expressing cell line (**Fig. 3.24e**). Comparison of the lipid droplet abundance quantified for the replicon expressing cells to the JFH-1 infected cells indicated that cells exposed to the full HCV replication cycle accumulated a greater level of intracellular lipid droplets.



(c) *Replicon expressing Huh7 cells*



(d) *Replicon expressing Huh7 cells (100x)*



(e)

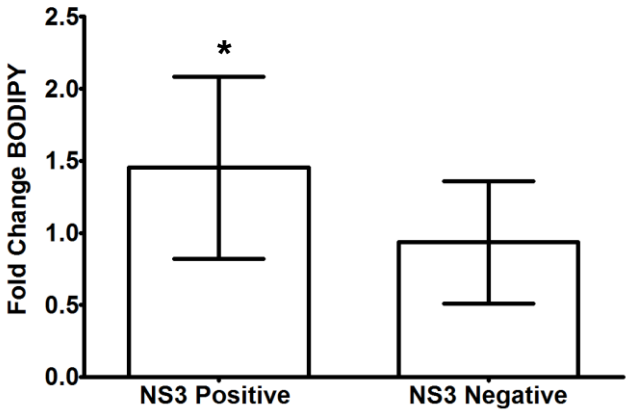


Figure 3.24 The subgenomic replicon increases lipid droplet abundance

(a-d) *Comparison of lipid droplet staining observed for* ***(a)*** *wild type,* ***(b)*** *cured and* ***(c and d)*** *replicon expressing Huh7 cells (p=4). Lipid droplets were stained using 50µg/ml of BODIPY 493/503 (green staining). The HCV NS3 protein was stained using an anti-NS3 antibody (red staining) and cell nuclei were stained with DAPI (blue staining). Images were captured using a Nikon Eclipse TE2000S fluorescence microscope at a magnification of 60x* ***(a, b and c)*** *and 100x* ***(d)****. All images were taken using the same exposure time and gain settings.* ***(e)*** *Fold change in BODIPY staining for NS3 positive and NS3 negative replicon expressing Huh7 cells. Fold change was calculated by comparing the BODIPY fluorescence quantified for the NS3 positive and NS3 negative replicon expressing cells using Image J. BODIPY quantification data displayed represents the mean (±SD) of 15 different cell counts for the NS3 positive and negative replicon expressing cells. The fold change in lipid droplet abundance in the NS3 positive cells compared to the NS3 negative cells was statistically significant with a p value < 0.007 (indicated by an asterisk (*)). P values were calculated using a two-tailed unpaired T test in Graphpad Prism.*

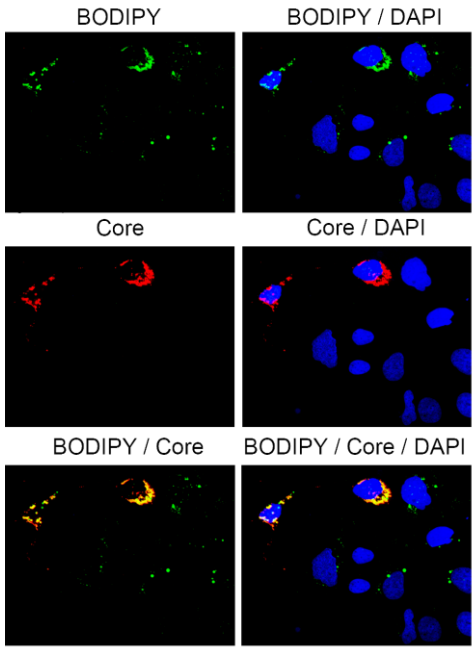
3.9.3 Lipid droplet abundance in JFH-1 core expressing cells

The accumulation of lipid droplets observed was greater in the JFH-1 infected cells than in the replicon expressing cells. This may have occurred because the intracellular JFH-1 levels were higher in the infected cells compared to the replicon cells, which may have resulted in greater upregulation of lipid droplet abundance. It may also have occurred because the structural proteins, which were present in the JFH-1 infected cells and absent in the replicon expressing cells, may have had additional effects on lipid droplet abundance.

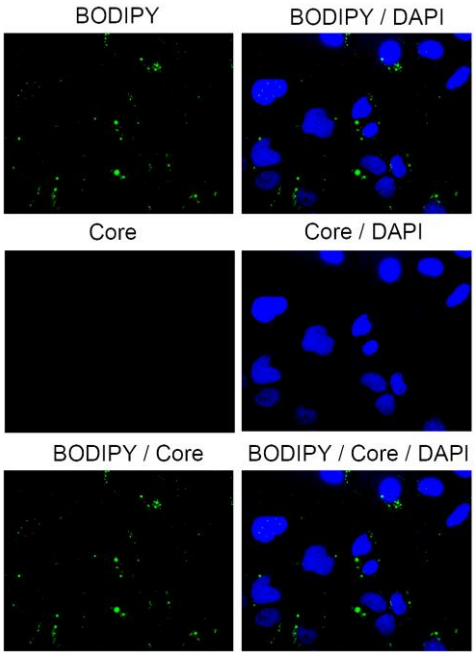
There is already significant published evidence to suggest that HCV core induces lipid accumulation during HCV infection [66, 212]. To test whether JFH-1 core contributed to the accumulation of lipid droplets during JFH-1 infection, lipid droplet staining of core expressing Huh7 cells was performed. To induce high level expression of JFH-1 core, the SFV replicon expression system was used. Huh7 cells transfected with the SFV(core) and SFV(empty) RNA transcripts were stained for the HCV core protein and lipid droplets (**Fig. 3.25a and b**). Staining of non-transfected Huh7 cells was also performed to determine whether the SFV replication complex had additional effects on lipid droplet abundance (**Fig. 3.25c**).

An increase in BODIPY staining was observed for the Huh7 cells transfected with the SFV(core) RNA transcript that stained positively for the HCV core protein (**Fig. 3.25a and d**) compared to the cells transfected with the SFV(empty) RNA transcript (**Fig. 3.25b**), non-transfected cells (**Fig. 3.25c**) and cells transfected with the SFV(core) RNA transcript which did not stain positively for the HCV core protein (**Fig. 3.25a and d**). Little difference was observed in the BODIPY staining of the SFV(empty) transfected cells and the non-transfected cells indicating that the SFV replication complexes did not significantly alter lipid droplet abundance. Comparison of the BODIPY signal intensity quantified for Huh7 cells that stained positively and negatively for the HCV core protein indicated that a 2.5 fold increase in BODIPY staining was observed as a result of core protein expression (**Fig. 3.25e**). This increase was greater than that observed for the replicon expressing cells indicating that the HCV core protein may play a more significant role in lipid droplet accumulation than the non-structural HCV proteins (**Fig. 3.24**). Consistent with previous studies, lipid droplets also appeared to accumulate around the edge of the nucleus in the presence of the HCV core protein, which co-localised directly with the lipid droplet surface (**Fig. 3.25d**).

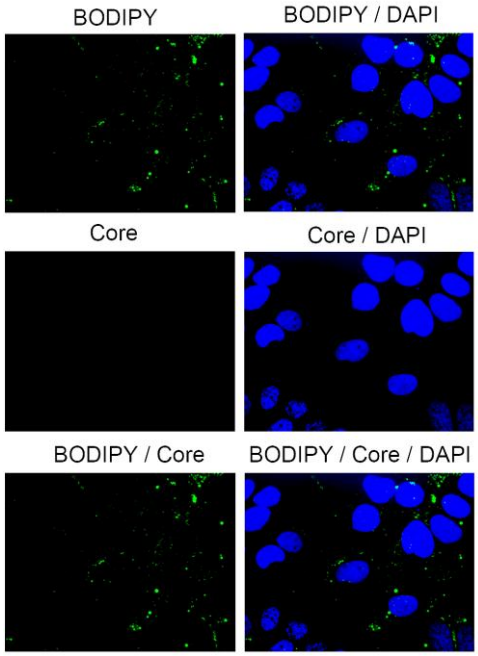
(a) *SFV(core) Huh7 Cells*



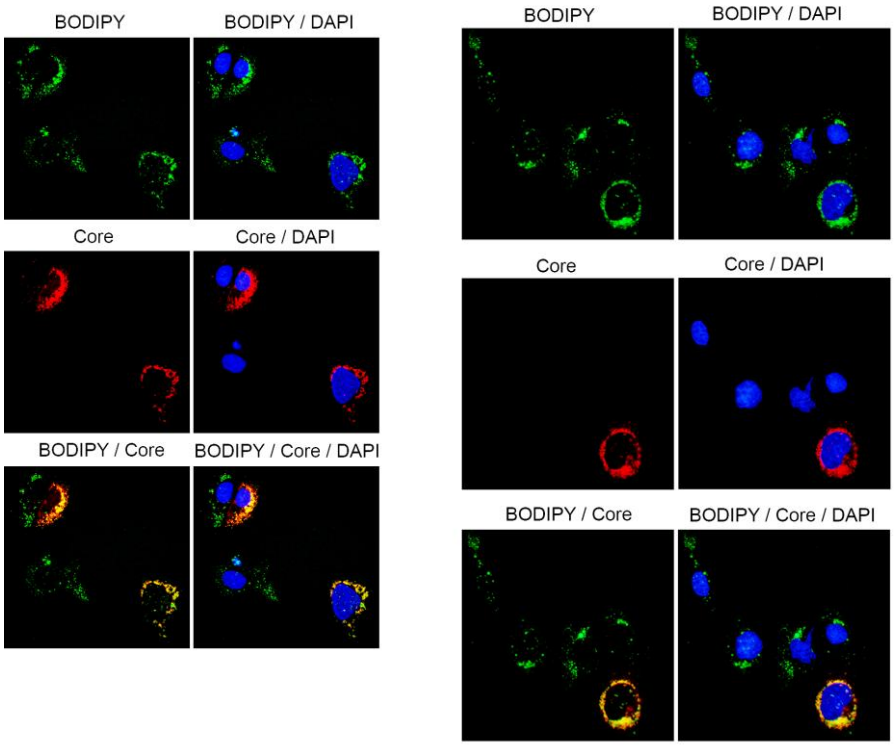
(b) *SFV(empty) Huh7 Cells*



(c) *Non-transfected Huh7 Cells*



(d) *SFV(core) Huh7 cells (100x)*



(e)

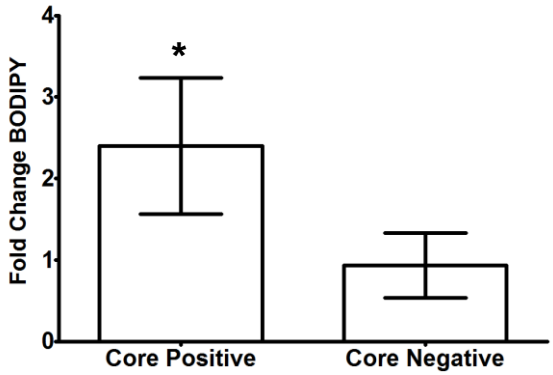


Figure 3.25 HCV core protein expression increases lipid droplet abundance

(a-d) *Comparison of the lipid droplet staining observed for Huh7 cells transfected with* ***(a/d)*** *SFV(core) RNA,* ***(b)*** *SFV(empty) RNA and* ***(c)*** *transfection medium only. The transfected cells were incubated for 24 hours and stained with the anti-core antibody (red staining) and 50µg/ml BODIPY 493/503 (green staining). Cell nuclei were also stained with DAPI (blue staining). Images were captured using a Nikon Eclipse TE2000S fluorescence microscope at a magnification of 60x* ***(a, b and c)*** *or 100x* ***(d)****. All images were taken using the same exposure time and gain settings.* ***(e)*** *Fold change in BODIPY staining for the core positive and negative cells transfected with SFV(core) RNA. Fold change was calculated by comparing the BODIPY fluorescence quantified for the core positive and core negative cells using Image J. BODIPY quantification data displayed represents the mean (±SD) of 15 different core positive and negative cells. The fold change in lipid droplet abundance in the core positive cells compared to the core negative cells was statistically significant with a p value < 0.001 (indicated by an asterisk (*)). P values were calculated using a two-tailed unpaired T test in Graphpad Prism.*

Chapter 3: Discussion

The JFH-1 cell culture system

Stocks of high titre JFH-1 virus were produced when infectious culture medium was serially passaged onto naive Huh7.5 cells. This method of JFH-1 production increased the yield of virus compared to the passage of chronically infected cells (**Fig. 3.2**). Recent reports suggest that HCV infection has direct cytopathic effects on cells, leading to cell cycle arrest and apoptosis [149]. It is likely that the reduced virus production observed with passage of infected cells was due to reduced growth rates and increased cell death of the chronically infected cells.

Host gene expression during HCV infection

Expression profiling of host factors involved in the replication of other RNA viruses

Before investigating the potential role of the selected candidate host genes in the HCV replication cycle, it was important to determine whether the expression of these genes was affected by HCV infection. Relative quantification of host gene expression in JFH-1 infected cells indicated that only minor changes were observed in the expression of the candidate host genes during infection (**Fig. 3.4**). This confirmed that all of the candidate host genes were still actively transcribed during HCV infection and could still be tested for their involvement in the HCV replication cycle.

To ensure accurate quantification of host gene expression in the HCV infected samples, a comparison was made between the expression data generated when GAPDH and RPLPO [208] were used for expression normalisation. Both reference genes generated consistent gene expression data indicating that either gene could be used to accurately perform relative quantification of host gene expression in HCV infected samples. GAPDH was chosen as the reference gene for all gene expression studies performed, as this gene has frequently been used for gene expression normalisation in other published qRT-PCR studies [149, 160, 169].

Identification of host factors upregulated during HCV infection

A second approach used to select host factors for testing as potential cofactors in the HCV replication cycle involved the identification of host genes that increased in expression during HCV infection. Microarray analysis of JFH-1 infected Huh7 cells was performed to facilitate identification of cellular pathways significantly regulated

during infection. Upregulated host genes for investigation as potential HCV cofactors were selected from the pathways most significantly associated with the HCV replication cycle.

Results from the microarray study demonstrated that a significant number of host genes altered in expression during the course of infection (**Table 3.1**). The total number of genes regulated by infection increased over time which may correspond to the increasing viral RNA levels observed (**Fig. 3.5**). Gene ontology analysis of the expression data demonstrated that many of the genes which altered in expression were involved in a small number of cellular pathways. These pathways included those regulating cellular defence mechanisms, cellular metabolism and intracellular transport (**Fig. 3.6**). For several of the metabolic pathways that were regulated during infection, almost all of the enzymes involved altered in expression e.g. sphingolipid metabolism, cholesterol synthesis and the production of tRNA molecules. The high level of coordination in the expression of genes in these pathways indicates that the expression changes observed were likely to be biologically significant.

qRT-PCR expression analysis was used to validate the microarray experiment (**Fig. 3.8**). Although the patterns of gene expression were consistent between the qRT-PCR and microarray experiments, the fold change values calculated by qRT-PCR were generally larger than those calculated in the microarray experiment. These differences may be due to the use of different RNA samples for the qRT-PCR and microarray experiments. However, variation is more likely to have occurred because of differences in the sensitivities of the two techniques, as microarray expression analysis is known to be less sensitive than qRT-PCR [149, 213].

When performing qRT-PCR, upregulated host genes selected for investigation were chosen because of their role either in lipid metabolism or intracellular transport. Accumulating evidence indicates that these cellular processes are very important during the HCV replication cycle and the upregulated host genes involved were, therefore, very good candidates as potential HCV cofactors [30, 39, 47, 97, 128, 132, 214]. Host genes upregulated during infection may be required to provide essential lipid metabolites that participate in the HCV replication cycle or they may control intracellular transport mechanisms that facilitate HCV trafficking during virus entry and exit. qRT-PCR quantification of host genes involved in

cellular defence was also performed by other members of Dr McGarvey's laboratory: Andrew Baillie (Imperial College London) [201] and Fadhil Al-Hababi (Imperial College London) [215, 216]. Validating the expression patterns observed for cellular defence genes was less of a priority for this project, as they were less likely to encode proteins that play a functional or structural role in the HCV replication cycle. However, analysis of the expression patterns observed for the cellular defence genes still provided an interesting insight into the potential mechanisms underlying HCV associated pathogenesis.

JFH-1 infection alters the expression of host genes involved in cellular defence

Many of the genes shown to be regulated by JFH-1 infection were involved in cellular defence mechanisms (**Fig. 3.6a**). An increase in the expression of genes that encode pro-inflammatory cytokines and chemokines was observed supporting prior evidence that infected hepatocytes may act as a major source of inflammation in the liver [149]. In particular, CXCL chemokines (1, 2, 3, 5, 6 and 8) which act via CXCR1 and CXCR2 receptors and are known to stimulate the chemotaxis and respiratory burst activity of neutrophils [217] as well the induction of hepatocyte proliferation [218] all had elevated levels of their mRNAs. Increased expression was also observed for several suppressor of cytokines (SOCS) genes, which act as negative feedback regulators of cytokine function [219]. This has been observed previously in studies investigating HCV infected and core expressing cells and may contribute to the interferon alpha resistance that can develop in HCV patients [149, 220, 221]. An increase in the expression of fibrosis-promoting complement factors, MASP1 and MBL2 was also observed, indicating that they may be in part responsible for the liver fibrosis that frequently occurs in HCV infected patients [222].

HCV infection is known to stimulate the production of reactive oxygen species which promote oxidative stress induced damage in patients [164, 223]. A significant reduction in the expression of genes that function in multiple antioxidant pathways was observed (e.g. metallothionein genes, glutathione peroxidase and catalase) indicating that damage caused by oxidative stress may be amplified by the absence of a functional antioxidant response. Decreased expression of antioxidant genes (e.g. catalase) has been shown to occur following cytokine stimulation [224]. The increased expression of cytokines observed in this study may, therefore, have been responsible for the changes observed in antioxidant

expression. Decreased expression of anti-oxidant proteins during virus infection has also been observed in other studies investigating HCV and Respiratory Syncytial virus infections [149, 225, 226].

In addition to observing a decrease in many antioxidant responses, there was also evidence to suggest that some protective pathways were switched on during infection, as genes involved in the aryl hydrocarbon receptor (AHR) pathway for xenobiotic metabolism increased in expression. CYP1A1 and CYP1B1 are two key AHR target enzymes involved in xenobiotic metabolism that increased in expression during infection. These enzymes have also been shown to play a role in lipid metabolism and the processing of long chain fatty acids during the production of eicosanoids [227, 228]. Furthermore, stimulation of AHR transcription factor activity has been shown to induce hepatic steatosis in mice [229]. Increased expression of these genes may, therefore, have several implications during the HCV replication cycle and may contribute to the development of hepatic steatosis that frequently occurs in chronically infected patients.

Genes controlling cellular proliferation and apoptosis were also significantly regulated during JFH-1 infection supporting evidence from recent studies indicating that HCV infection stimulates apoptosis and growth arrest [149, 230]. These findings indicate that the hepatocyte cell death frequently observed in patients may result from a virally driven process of apoptosis in addition to the pro-apoptotic actions of cytotoxic immune cells [231].

JFH-1 alters the expression of host genes involved in metabolism and transport

Intracellular lipid metabolism

One of the pathways most highly regulated by JFH-1 infection was intracellular lipid metabolism (**Fig. 3.6b**). This was a particularly interesting observation because of the key role that intracellular lipids have been shown to play in the HCV replication cycle. Cholesterol, sphingolipids and phospholipids are key components of the membranous web structure upon which HCV replication complexes assemble [32], triglyceride rich lipid droplets have been identified as the site of virus particle assembly [39], and the VLDL secretory pathway facilitates the exit of nascent HCV particles from the cell [47, 132]. Furthermore, upregulation of cellular pathways controlling intracellular lipid metabolism indicates that HCV-

induced alterations in the expression of lipid synthesis genes may contribute significantly to the development of hepatic steatosis, which develops in approximately 73% of patients infected with genotype 3 HCV and 50% of patients infected with other HCV genotypes [45].

Consistent with the high demand for cellular lipid metabolites in the HCV replication cycle, host genes involved in the synthesis and transport of sphingolipids, phospholipids and triglycerides and the production of intracellular lipid droplets increased in expression following infection. SREBF1 and PPARγ are key transcription factors that control the expression of many lipid synthesis genes [232-234]. An increase in the expression of these genes was also observed and may have been responsible for increasing the expression of lipid metabolism genes during infection. Previous gene expression studies of HCV infection including those performed using hepatocytes isolated from HCV infected chimpanzee and chronically infected patients [161, 163, 235], hepatoma cells infected by HCV *in vitro* [164] and HCV replicon expressing cells [159] have also demonstrated increased expression of genes involved in fatty acid metabolism and triglyceride synthesis. The expression of individual HCV proteins in hepatoma cell lines including NS4B [90], NS5A [166] and core [66, 236] has also been shown to increase the expression and activity of key lipid metabolism transcription factors such as SREBF1, SREBF2 and PPARγ. This indicates that the transcriptional regulation of lipid metabolism may have resulted from the direct effects of individual HCV proteins including both non-structural proteins and the HCV core structural protein. Recent studies investigating microRNA expression during HCV infection have also demonstrated decreased abundance of several microRNAs that repress the expression of fatty acid metabolism genes upregulated in this study (**Fig. 3.8**), e.g. miR15a/b and miR181a, which repress ACSL1 expression [165]. This indicates that HCV induced alterations in microRNA abundance may also have been responsible for the alterations in lipid metabolism gene expression observed during HCV infection.

Alongside an increase in the pathways producing intracellular lipids, decreased expression was also observed in the genes involved in lipid catabolism including those responsible for the degradation and oxidation of fatty acids. A decrease was observed in the expression of the peroxisome proliferator activated receptor α (PPARα) transcription factor, which controls the expression of many fatty acid

oxidation genes [237]. Recent studies investigating the effects of PPARα and PPARγ agonists on HCV replication have demonstrated that stimulating PPARα activity reduces the rate of HCV replication, whilst stimulating PPARγ activity increases the rate of HCV replication [159]. This data supports the observations that JFH-1 infection increased the expression of PPARγ and decreased the expression of PPARα in this study (**Fig. 3.8**). Other studies investigating gene expression in liver biopsy tissue isolated from chronically infected patients and hepatoma cells expressing the HCV core protein have also observed a decrease in PPARα expression as a result of HCV protein expression [68, 238]. Interestingly, an increase was also observed in the expression of a potential PPARα inhibitor known as the thioredoxin interacting protein (TXNIP) [239]. Increased expression of TXNIP has previously been observed in Huh7 cells that support a high level of HCV genome replication indicating that the increased expression of this gene may be an important mechanism for controlling lipid metabolism during HCV infection [240].

Although increased expression was observed for genes involved in the synthesis of many intracellular lipids, almost all of the genes controlling cholesterol synthesis decreased in expression between 6 and 48 hours post-infection. The only exception was the increase observed in the expression of genes involved in the geranylgeranylation of host proteins; consistent with the key role of geranylgeranylated proteins in HCV replication [126]. These findings do not support the observations of other gene expression studies performed using HCV infected cells [164], replicon expressing cells [159] and liver biopsy material from chronically infected patients [235], which have instead demonstrated an increase in the expression of cholesterol synthesis genes. Furthermore, investigation of host gene expression in Huh7 and Huh7.5 cells expressing a genotype 2a subgenomic replicon also demonstrated an increase in the expression of cholesterol synthesis genes as a result of JFH-1 genome translation and replication (**Fig. 3.12 and 13**). These findings led to a re-investigation into the effects of JFH-1 infection on the expression of cholesterol synthesis genes. To gain further insight into the regulation of gene expression, the maximum time period of infection performed was extended from 48 to 72 hours. As observed in the initial study, the expression of cholesterol synthesis genes was again decreased at 24 and 48 hours post infection. However, at 72 hours post infection, the expression patterns reversed and all of the cholesterol synthesis genes tested

increased in expression (**Fig. 3.15**). These findings demonstrated that the host response to HCV can rapidly alter throughout the course of infection. The gene expression patterns observed may reflect the changes in cellular signalling that occur as virus proteins accumulate in the infected cell. For example, during the early stages of JFH-1 infection, when the virus protein levels were low, the host cell may have responded to infection through the production of interferon-β (IFNβ). IFNβ has been shown to block the expression of the microRNA, miR122 [241], which has been shown to positively regulate the transcription of genes involved in cholesterol synthesis [119]. Thus, these changes may have contributed to the decreased expression of cholesterol synthesis genes observed during the early stages of JFH-1 infection. To support this possibility, other studies investigating microRNA expression during HCV infection have demonstrated decreased levels of miR122 as a result of HCV replication [242, 243]. However, as the course of HCV infection progressed and the abundance of HCV proteins accumulated, a reduction in the interferon response may have occurred as a result of the actions of HCV proteins that are known to inhibit antiviral signalling, such as the NS3 protein which has been shown to block the RIG-I and TLR3 pathways [35, 244]. A reduction in cellular interferon signalling may have enabled the expression of miR122 to resume, resulting in activation of cholesterol synthesis gene transcription. In addition, the expression of the cholesterol synthesis genes may also have been directly stimulated by the actions of the HCV proteins, which have been shown to directly regulate the expression of key transcription factors involved in cholesterol synthesis [66, 90, 166, 236]. Together these effects may have been responsible for the increased expression observed in the cholesterol synthesis genes at 72 hours post-infection.

Host protein synthesis, degradation and post-translational modification

Alongside the transcriptional regulation of lipid metabolism during infection, significant effects were also observed in the expression of genes controlling protein metabolism (**Fig. 3.6b**). This included the genes involved in protein synthesis, protein turnover and post-translational protein modification. Similar findings were also observed in a recently published gene expression study of JFH-1 infected Huh7.5 cells, which demonstrated that multiple tRNA synthetase genes were upregulated during infection [165]. Furthermore other viruses such as HIV have been shown to boost protein synthesis during the early stages of virus infection and utilise protein sulphation for virus protein modification [245, 246]. An

increase in the expression of genes controlling protein synthesis and post-translational modification is consistent with the reliance of HCV on host cellular machinery for virus protein expression and modification [17]. The coordinated regulation of functionally related genes such as the tRNA synthetases and eukaryotic translation initiation factors also indicates that key transcription factors regulating these pathways may have been activated during JFH-1 infection.

Intracellular protein transport and vesicle trafficking

Recent studies have demonstrated that host proteins regulating intracellular transport and vesicle trafficking are important for the HCV replication cycle. These proteins have been shown to play either structural roles in the HCV replication complex (e.g. VAP-A/B) [97] or functional roles in trafficking and membrane organisation during replication complex formation (e.g. ARF1, Rab1 GTPase and Rab5 GTPase) [30, 51, 128]. In this study, host genes regulating vesicle trafficking between the ER, Golgi body and plasma membrane were upregulated indicating that the proteins encoded may be important for viral entry and exit, or the reorganisation of intracellular membrane during virus replication and assembly (**Fig. 3.6b**). Examples of genes that increased in expression included those involved in the regulation of endocytosis (STON2 [247] and PICALM [248]), which may facilitate HCV entry, and those involved in retrograde transport from the Golgi body to the ER (RAB6B and RAB33B), which may facilitate the accumulation of virus proteins in the ER for replication complex formation [249-251]. RAB33B has also been shown to play a role in autophagy, a cellular process recently shown to be essential for the replication of HCV [31, 113, 252]. RAB6B has previously been shown to increase in expression in cells that are highly permissive to HCV infection suggesting that it may be an important host cell protein required during HCV replication [240].

Other host genes that increased in expression were involved in the regulation of vesicle trafficking within the Golgi body including: Rab7L1, which was previously identified through siRNA silencing as an essential protein required for HCV replication [253]; and ARFGEF1, which controls the activity of the ARF1 protein that has recently been implicated in the replication and assembly of HCV [51]. An increase in the expression of genes that regulate the trafficking of secretory vesicles was also observed (RAB27A, RAB27B and RAB37) [178] indicating that

these factors may be important for the secretion of nascent virus particles from infected cells.

Actin and microtubule binding proteins

The cytoskeleton network generated from actin and microtubule filaments has been implicated in many aspects of the HCV replication cycle. This includes the process of virus entry [254], trafficking of HCV replication complexes during translation and assembly [133], and trafficking of lipid droplets towards the perinuclear region of the cell for virus assembly and virion morphogenesis [60]. In this study, JFH-1 infection modulated the expression of genes encoding several actin and microtubule binding proteins that regulate cytoskeleton function (**Fig. 3.6b**). The majority of genes decreased in expression with the exception of several actin binding proteins which significantly increased in expression. One example was ABLIM3, a scaffold protein that connects adherens junctions to the actin cytoskeleton providing tensile strength in epithelial and endothelial cell layers [255]. Increased expression of this gene may be important for controlling the function of the actin cytoskeleton during HCV trafficking.

It is not clear why HCV infection reduced the overall expression of the genes encoding cytoskeletal binding proteins; however, the abundance of cytoskeleton binding proteins has been shown to decrease during oncogenesis [256, 257]. Another virus shown to reduce the expression of cytoskeleton binding proteins is the Human Papilloma Virus type 8 (HPV8). HPV8 is known to result in oncogenic transformation of cells and is frequently associated with the development of non-melanoma skin cancer [258]. Decreased expression of these genes may, therefore, be one mechanism by which chronic HCV infection can promote the development of hepatocellular carcinoma.

Temporal changes in host gene expression

By investigating host gene expression in Huh7 cells infected with JFH-1 for 6, 12, 18, 24 and 48 hours, the microarray data obtained has provided insight into the temporal regulation of gene expression during HCV infection. A range of different expression patterns were observed for the host genes regulated during infection as demonstrated by the genes encoding TXNIP, ABLIM3 and RAB27A (**Fig. 3.9**). The differences in temporal regulation observed for these genes may indicate whether gene transcription was altered directly by the HCV replication cycle, when

gene expression altered during the early stages of infection, or indirectly through secondary effects on cellular signalling, when gene expression altered in the latter stages of infection.

A particularly interesting example of temporal change in gene expression was observed for the genes involved in cholesterol synthesis, many of which showed an initial decrease in expression during early infection followed by significant increases in expression at 72 hours post infection (**Fig. 3.15**). These observations indicate that HCV replication can have rapid and opposing effects on host gene expression throughout the course of infection.

Several groups of related genes also showed identical expression patterns in response to infection. This included genes that belong to the same family (e.g. tRNA synthetases and eukaryotic translation initiation factors) or genes that participate in the same cellular pathway (e.g. sphingolipid metabolism and cholesterol synthesis). The expression of these genes may be co-regulated by a common mechanism or transcription factor that is altered during HCV infection.

Comparing host cell responses to JFH-1 infection: Huh7 versus Huh7.5 cells

Most of the published microarray studies investigating the host cell response to HCV infection have been performed in Huh7.5 cells [149, 164, 165]. These cells support a high level of HCV replication as a result of a mutation in the RIG-I gene [139, 140]. For the purpose of this microarray study, the Huh7 cell line was selected instead of the Huh7.5 cell line because it has an intact RIG-I pathway and may respond to HCV infection through mechanisms that better reflect the characteristics of *in vivo* infection.

When comparing the findings of this microarray experiment to previously published studies performed in Huh7.5 cells, several overlapping expression patterns were observed. These included the regulation of genes involved in proliferation and apoptosis, cytokine and chemokine production, lipid metabolism, tRNA production and cytoskeleton regulation [149, 159, 160, 164, 165]. However, many of the expression patterns observed in this study were novel and have not been observed in previous studies of HCV infection. This included the regulation of genes involved in sphingolipid metabolism, protein synthesis, protein degradation, post-translational modification and vesicular trafficking. These differences may reflect the cell type or virus genotype used and the period of time for which the

cells were infected. To determine whether the expression patterns observed in this study were cell type specific, host gene expression was also investigated in JFH-1 infected Huh7.5 cells using qRT-PCR. Host genes involved in lipid metabolism, xenobiotic metabolism and vesicle trafficking that increased in expression in the infected Huh7 cells were also upregulated in the infected Huh7.5 cells; indicating that the expression patterns observed were not cell type specific and were not affected by alterations in the RIG-I pathway.

Despite the overlap in expression patterns for the infected Huh7 and Huh7.5 cells, there were significant differences in the expression fold change values observed for most of the host genes tested, with Huh7.5 cells showing much smaller fold changes in expression than the Huh7 cells. These differences did not correlate with the level of virus replication taking place, as Huh7.5 cells had significantly higher intracellular JFH-1 RNA levels than the Huh7 cells (**Fig. 3.10**); reflecting the increased permissiveness of these cells to HCV infection [139-141]. The elevated level of JFH-1 RNA observed in the infected Huh7.5 cells is unlikely to be responsible for the fold change differences observed between the Huh7 and Huh7.5 cells, as the overall abundance of viral RNA present in JFH-1 infected cells was relatively low in comparison to the total RNA population [29, 259, 260]. This is supported by the observation that the CT values observed for GAPDH expression in the Huh7 and Huh7.5 cell lines were consistent for both the JFH-1 infected and mock infected samples (**Appendix A.15**). This indicates that the quality and quantity of cDNA synthesised for these samples was equivalent and was not affected by the presence of JFH-1 RNA in the JFH-1 infected cells compared to the mock infected cells, or by the elevated levels of JFH-1 RNA in the JFH-1 infected Huh7.5 cells compared to the JFH-1 infected Huh7 cells.

There are already several known differences between Huh7 and Huh7.5 cells; including differences in the RIG-I signalling pathway and the abundance of cell surface host entry receptors (e.g. CD81 and SR-BI) [140, 141, 261]. In addition to these differences between the two cell lines, there may be other differences in cellular signalling that may account for the variation observed in the fold change expression response to JFH-1 infection.

Gene expression profiling of cells expressing the genotype 2a replicon

The data obtained through microarray analysis of JFH-1 infected cells has provided excellent insight into the cellular pathways that may be important for the HCV replication cycle and the HCV-induced changes that may contribute to pathogenesis. To further explore the expression patterns observed and investigate whether specific HCV proteins were responsible for transcriptionally regulating host genes, expression profiling was also performed in Huh7 and Huh7.5 cells expressing a genotype 2a subgenomic replicon (**Fig. 3.12 and 13**). In order to accurately investigate host gene expression in these cells, the Huh7 and Huh7.5 replicon expressing cells were cured by IFNα treatment. This enabled the production of replicon-cured cell lines that had a similar clonal population of cells as the replicon expressing cells, but lacked the presence of the HCV non-structural proteins (**Fig. 3.11**) [139, 160].

To completely eradicate the replicon RNA from the replicon expressing cells, as analysed by qRT-PCR, eight weeks of IFNα treatment was required. However, only two weeks of treatment was required before the cells no longer stained positively for the HCV proteins (**Fig. 3.11e**). This difference most likely occurred as a result of variation in the sensitivity of the detection methods used, as qRT-PCR is a very sensitive technique compared to immunofluorescent staining of proteins. After two weeks of IFNα treatment, the replicon RNA levels may have decreased sufficiently so that level of HCV protein expression was below the detection limit of the staining protocol used. Several previously published studies which performed IFNα treatment to 'cure' replicon cells did not investigate replicon RNA abundance in the cells, but relied upon detection of HCV protein expression as a measure of IFNα treatment effectiveness. Treatment strategies in these studies generally lasted for around two weeks before the cells were considered cured [159]. As a result, these studies may have used cells with low levels of replicon expression rather than completely cured cell lines. This must be taken into consideration when comparing the results obtained in this study to those observed in previous studies investigating host expression in replicon expressing and cured cell lines.

Analysis of the host gene expression profiles observed for the replicon expressing, cured and wild type cells demonstrated that several of the genes regulated by infection were also significantly regulated by the genotype 2a replicon. This included the genes involved in sphingolipid metabolism and cholesterol synthesis

and the genes encoding PGC1α, ABLIM3, CYP1A1 and CYP1B1; indicating that the non-structural HCV proteins may have regulated the expression of these genes during infection. Increased expression of genes controlling cholesterol synthesis and expression of the CYP1A1 protein has been observed previously in cells expressing HCV subgenomic replicons [159, 262].

Although several genes were observed to be upregulated in both the replicon expressing and JFH-1 infected cells, many of the genes upregulated by infection did not alter in expression in the presence of the subgenomic replicon. The upregulation of these genes during infection most likely occurred as a result of specific processes taking place in the full replication cycle or as a result of the presence of the HCV structural proteins. It is also possible that differences in the regulation of gene expression may have arisen due to the use of different NS2 gene sequences in the JFH-1 infected cells (JFH-1 NS2) and replicon expressing cells (J6 NS2). The proteins encoded by these genes were very similar with 86% homology (**Appendix A.16**); however, it is possible that they may have had slightly different effects on host gene expression.

To determine whether the expression patterns observed in the replicon expressing cells resulted from the direct effects of HCV protein expression or from the selection of cellular clones that supported a high level of replicon RNA replication, host gene expression was compared between the cured and wild type cells. For the majority of the genes tested, little difference was observed between the cured and wild type cells, with the exception of the genes encoding PGC1α and ABLIM3, which were expressed at higher levels in the cured cells compared to the wild type cells. This observation indicates that cells with a higher expression level of the PGC1α and ABLIM3 genes may have supported higher rates of replicon replication. This would have produced greater quantities of the Geneticin resistance marker and would have allowed the cells to grow more rapidly in the presence of Geneticin. Other studies comparing gene expression between cured and wild type cells have also identified host genes that are expressed at a higher level in the cured cells compared to the wild type cells; examples include the genes involved in sphingolipid and cholesterol synthesis [159]. In this study, the expression of cholesterol and sphingolipid metabolism genes was increased in the replicon expressing cells, but not in the cured or wild type cells. The differences observed between these studies may have resulted from the protocols used to

generate the cured cells, as this study used a prolonged IFNα treatment protocol lasting eight weeks compared to the previously published study, which treated the cells with IFNα for two weeks only [159].

Although the replicon expressing Huh7 and Huh7.5 cells demonstrated almost identical host gene expression patterns, slightly larger fold change expression values were observed for the replicon expressing Huh7 cells compared to the replicon expressing Huh7.5 cells. This reflected the fold change gene expression differences observed when comparing JFH-1 infected Huh7 and Huh7.5 cells, although in this case the differences observed were much less significant. As before, these differences did not correlate with viral RNA levels, as the replicon expressing Huh7.5 cells had higher levels of intracellular replicon RNA than the replicon expressing Huh7 cells (**Fig. 3.14**).

Gene expression profiling of cells expressing the JFH-1 core protein

Alongside investigations analysing host gene expression in the presence of non-structural proteins, it was also important to investigate the effect that HCV structural proteins have on host gene expression. Focus was placed on investigating the effects of the HCV core protein because there was significant evidence indicating that this protein alters host gene expression, in particular the genes involved in lipid metabolism [66, 263]. To investigate the effect of HCV core on host gene expression, cells expressing the JFH-1 core protein were generated. Two different approaches were used to express the core protein in Huh7 cells, neither of which enabled the generation of a cell line that expressed the core protein in 100% of the cells. If the effect of the core protein on host gene expression was to be accurately determined, a cell line in which all the cells express the HCV core was needed. Although the pSFV replicon transfected cells enabled a very high level of core protein expression in the cells that were transfected, the transfection efficiency of cells with the pSFV RNA was limited (**Fig. 3.16**). It was also not possible to create a stable cell line using this vector as the cells underwent apoptosis as a result of SFV replicon replication [211].

The HCV core protein was also expressed using a pIRES vector, which introduced a Blasticidin resistance marker into transfected cells allowing stable cell lines to be established. The level of core protein expression achieved in these cells was much lower than that obtained with the pSFV replicon system, and despite the selection

of transfected cells with Blasticidin, Huh7 cells that did not stain positively for the HCV core protein still survived in the presence of Blasticidin (**Fig. 3.17**). Based on the bicistronic construction of the pIRES vector, the transfected cells should have expressed the Blasticidin resistance protein only in conjunction with the core protein. The pIRES vector was designed to transcribe the Blasticidin resistance gene and HCV core gene as a single transcript that would be translated as two separate proteins. Therefore, it is unlikely that the vector would have integrated into the genome in such a way that the Blasticidin resistance protein was expressed without the core protein. However, it is possible that different cells expressed the vector at different levels depending on the genome integration site of the plasmid DNA. Some cells may have expressed the vector at low levels so that the amount of core protein being produced was below the detection limit of the staining protocol used. These cells may have been able to survive in the Blasticidin due to expression of the Blasticidin resistance protein, but they may not have stained positively for the HCV core protein as the protein level may have been too low. One future way around this problem may involve the selection of single cell clones that express the pIRES vector at a high level. Once a cell line has been generated from a cell clone that expresses high levels of the core protein, it should be possible to investigate the effect of core protein expression on host gene expression.

Quantification of host protein abundance during JFH-1 infection

To determine whether the host gene expression patterns observed during HCV infection correlated with changes in host protein expression, the effect of JFH-1 infection on TXNIP and PGC1α protein expression was investigated. These proteins were of particular interest as potential HCV cofactors due to the key role that they have been shown to play in lipid metabolism.

Western blotting for these proteins confirmed the gene expression data obtained, although in both cases the fold change in protein abundance was much smaller than that observed for gene expression (**Fig. 3.19**). To determine whether the cells had been successfully infected, the cell lysates were also blotted for the HCV core and NS3 proteins. Investigation into core protein abundance was performed for the TXNIP blot since the samples were run on a 10% acrylamide gel, which allowed detection of low molecular weight proteins. When blotting for the PCG1α protein, samples were run on an 8% acrylamide gel to allow resolution of PGC1α, which is

a high molecular weight protein. Blotting was performed for the NS3 protein instead of the HCV core protein, which was too small to be detected on the blot.

When blotting for the HCV core protein, two protein bands were specifically observed in the JFH-1 infected samples. These included one protein band at the correct molecular weight for the HCV core protein (21KDa), and one protein band for a much smaller and less abundant protein (14KDa) (**Fig. 3.18**). There is evidence to suggest that the HCV core transcript contains an alternative translation initiation site which results in the production of several smaller core protein variants that range in size from 8KDa to 14KDa [264]. The smaller protein band detected may correspond to one of these smaller core protein variants generated through alternative translation of the genome.

Quantification of intracellular lipid metabolites during JFH-1 infection

Cholesterol and triglyceride levels in JFH-1 infected cells

Investigation into cellular metabolite levels during JFH-1 infection demonstrated that both triglyceride and cholesterol levels significantly increased throughout the course of infection (**Fig. 3.21**). These observations demonstrated that the gene expression patterns identified through microarray analysis were biologically significant. They also provided further evidence to indicate that HCV-induced alterations in the expression of lipid synthesis genes may contribute directly to the development of hepatic steatosis in chronically infected patients [167]. Further support for these observations was recently observed in a study investigating the effect of Jc1 HCV infection on Huh7.5 cell metabolism, which demonstrated an increase in the expression of lipid synthesis genes and an increase in the abundance of intracellular cholesterol and free fatty acids [164].

The rate at which lipid metabolite levels increased during infection was much more rapid for intracellular triglyceride than cholesterol (**Fig. 3.21**). For example, at 48 hours post-infection, triglyceride levels had increased substantially whilst little change was observed in the cholesterol levels until 72 hours post-infection. These observations supported the gene expression data, which demonstrated that the expression of genes controlling fatty acid metabolism and triglyceride synthesis increased as early as 12 hours post-infection (**Fig. 3.6b**), whilst the expression of cholesterol synthesis genes was reduced until 72 hours post-infection, when a rapid increase was observed in the expression of these genes (**Fig. 3.15**).

Considering that the expression of the cholesterol synthesis genes was decreased at both 24 and 48 hours post-infection, it was surprising to find that the cholesterol levels quantified at these time points were not reduced. One possible explanation for these findings is that the abundance of cholesterol in Huh7 cells is controlled not only by cholesterol synthesis, but also by the rate at which cholesterol is exported from the cell in VLDL particles. Several genes involved in the VLDL synthesis pathway were shown to decrease in expression in the microarray study, including MTTP and ApoB. Decreased expression of these genes may have reduced the efficiency of the VLDL secretory pathway preventing export of cholesterol from the cells. Therefore, despite a decrease in the expression of cholesterol synthesis genes during the initial stages of infection, a simultaneous reduction in the export of cholesterol from the cells may have prevented the intracellular cholesterol levels from falling. Previous studies investigating the effect of HCV infection on VLDL secretion have also demonstrated a reduction in the activity of the VLDL pathway during infection. This has been shown to occur following a reduction in the expression of MTTP during infection and inhibition of MTTP protein activity as a result of its interaction with the HCV core protein [69].

Cholesterol and triglyceride levels in the genotype 2a replicon expressing cells

The abundance of intracellular lipid metabolites was also investigated in the replicon expressing Huh7 cells. Higher levels of both cholesterol and triglyceride were observed in the replicon expressing cells compared to the wild type Huh7 cells (**Fig. 3.22**). This supported the increased expression observed for lipid synthesis genes in the replicon expressing cells including those involved directly in cholesterol synthesis, fatty acid metabolism and the transcription of lipid synthesis genes. Comparison of the cholesterol and triglyceride levels observed for the cured and wild type cells also supported the gene expression patterns observed, as no differences were observed in the expression of cholesterol synthesis genes or the abundance of cholesterol detected in the cured cells compared to the wild type cells. Whilst, increased abundance was observed for intracellular triglyceride in the cured Huh7 cells compared to the wild type cells, which may reflect the increased expression observed for lipid metabolism genes (e.g. PGC1α) in the cured cells. A recent study investigating lipid droplet accumulation in the presence of HCV subgenomic replicons also demonstrated an increase in lipid droplet abundance in both replicon expressing and cured Huh7 cells compared to the wild

type cell line [159]. This suggests that the selection process used to generate replicon expressing cells may have selected for Huh7 cell clones with higher levels of intracellular triglyceride, as these cells may have supported a higher level of replicon replication.

Whilst these findings indicate that the non-structural HCV proteins contributed to the accumulation of lipids observed during HCV infection, it is likely that these proteins were not the only contributing factor. Comparison of the fold change in triglyceride and cholesterol abundance observed for the JFH-1 infected and replicon expressing cells demonstrated that the JFH-1 virus induced much greater lipid accumulation than the subgenomic replicon. This reflected the gene expression data collected as JFH-1 infection induced much larger fold changes in host gene expression compared to the subgenomic replicon. These findings may result from differences in the abundance of HCV proteins present as higher HCV RNA levels were observed in the infected cells compared to the replicon expressing cells (**Fig. 3.10 and 3.14**). However, the greater accumulation of lipids observed during infection may also have occurred because of additional effects that the structural proteins may have had on lipid metabolism. The HCV core protein has been shown to significantly increase the expression of lipid synthesis genes and induce an accumulation of lipids in cells [66, 236, 263]. Specific polymorphisms in the sequence of the core protein from genotype 3 HCV have also been associated with increased lipid accumulation in cells and increased liver steatosis [70]. Unfortunately, it was not possible to quantify intracellular triglyceride and cholesterol in the core expressing cells, as only a proportion of the core expressing cells generated were positive for the JFH-1 core protein.

Quantification of intracellular lipid droplets during JFH-1 infection

To further investigate the contribution of the different HCV proteins to the accumulation of lipid metabolites during HCV infection, lipid droplet abundance in the presence of the different HCV proteins was also investigated. When quantifying the differences between lipid droplet abundance in cells, comparison was made between infected and uninfected cells, NS3-positive (replicon expressing) and NS3-negative (non-replicon expressing) cells and core-positive and core-negative cells captured in the same image. This was to ensure the most accurate comparison of lipid droplet staining, as bleaching of the BODIPY signal was rapid.

Comparison of the lipid droplet staining quantified for the different HCV protein expressing cell lines indicated that an increase was observed in the abundance of lipid droplets in the JFH-1 infected, NS3-positive (replicon expressing) and core-positive Huh7 cells compared to the uninfected, NS3-negative (non-replicon expressing) and core-negative Huh7 cells, respectively (**Fig. 3.23-25**). Fold change in lipid droplet abundance observed for the JFH-1 infected and core-positive cells was greater than that observed for the NS3-positive replicon expressing cells indicating that the structural HCV proteins, in particular the HCV core protein, may have had a greater effect on cellular lipid accumulation than the non-structural HCV proteins.

Previous studies investigating the effect of HCV proteins on lipid droplet staining have also demonstrated significant increases in lipid droplet abundance in cells infected with HCV [90, 174], cells expressing HCV subgenomic replicons [159, 174] and cells expressing individual HCV proteins including NS4B [90], NS5A [166] and core [236]. Comparison of the effects that individual HCV proteins have on the expression of the fatty acid synthase (FASN) protein has indicated that the HCV core protein induces a greater increase in FASN abundance than the NS4B protein [90]. This supports the observation that the HCV core protein induced greater lipid accumulation than the non-structural HCV proteins. In addition, the HCV core protein has also been shown to inhibit the MTTP protein involved in VLDL synthesis, reducing the export of lipids from core expressing cells [69]. This may also have contributed to the greater accumulation of lipid droplets observed in the presence of the HCV core protein compared to the presence of the non-structural HCV proteins.

Chapter 3: Conclusions

Through the work presented in this chapter, the host cell response to HCV infection has been successfully characterised. Detailed analysis of the expression patterns observed has enabled identification of cellular pathways that may be important for the HCV replication cycle and may contribute to HCV associated pathogenesis.

Microarray and qRT-PCR analysis of JFH-1 infected Huh7 cells demonstrated that many host genes involved in lipid metabolism and intracellular trafficking were significantly upregulated during JFH-1 infection. These expression patterns were shown to be biologically significant as JFH-1 infection also increased the abundance of the proteins encoded by these genes and induced an increase in the lipid metabolites synthesised by the upregulated synthetic pathways. Furthermore, gene expression profiling of cells expressing a genotype 2a subgenomic replicon demonstrated that the non-structural HCV proteins may have been responsible for the transcriptional regulation of some of the genes identified. Out of all the host genes shown to increase in expression during infection, a small selection of candidate genes was chosen for further investigation as potential HCV cofactors. These included: RAB27A/B, RAB33B, RAB37, TXNIP, CYP1A1, ABLIM3, PGC1α, RIP140 and CIDEB. The decision to focus on these genes was based on the cellular functions of the proteins encoded and evidence from previous studies that indicate a potential role for these proteins in the HCV replication cycle. The proteins encoded by these genes either play a role in intracellular vesicle trafficking, membrane organisation or lipid metabolism, and it is possible that increased expression of these genes during infection may be important for adaptation of the host cell during HCV replication and secretion.

Alongside the use of the microarray gene expression data to identify potential HCV cofactors, several host factors were also chosen for investigation because of the role that they have been shown to play in the replication cycle of other RNA viruses. These included: Rab GTPase proteins (RAB2, 4, 6A, 11 and 18), TIA1, TIAL1 and Staufen1. The investigation of host gene expression in HCV infected cells presented in this chapter demonstrated that the expression of genes encoding most of these proteins was not significantly affected during HCV infection.

In addition to facilitating the identification of potential HCV cofactors, microarray analysis of HCV infected cells has also provided insight into the HCV induced expression patterns that may contribute to HCV associated pathogenesis. Expression patterns of particular interest include the genes that increased in expression with a role in: apoptosis and cell-cycle arrest, which may promote hepatocyte cell destruction; production of inflammatory cytokines and chemokines, which may promote increased liver inflammation; and lipid synthesis, which may promote development of hepatic steatosis. In addition, genes that decreased in expression were also of interest including those encoding anti-oxidant proteins, which may contribute to oxidative-stress induced hepatocyte damage; and cytoskeletal binding proteins, which may reduce the structural organisation of cells in the liver facilitating development of hepatocellular carcinoma. One of the most significant effects on host gene expression in the HCV infected cells was the upregulation of genes involved in lipid synthesis. Considering the potential contribution of this expression pattern to HCV associated pathogenesis and the potential cofactor role of lipid synthesis genes in the HCV replication cycle, the biological significance of the gene expression patterns observed was tested. Cells expressing the entire JFH-1 genome, a genotype 2a subgenomic replicon and the JFH-1 core protein were all shown to increase the intracellular abundance of lipid metabolites. These findings provided further evidence to indicate that HCV proteins may be directly responsible for the development of hepatic steatosis in chronically infected patients.

Chapter 4: Identifying Novel Host Proteins with a Role in the HCV Replication Cycle using siRNA Knockdown

Chapter 4: Introduction

To identify novel host factors involved in the HCV replication cycle, several candidate proteins were chosen for testing as potential cofactors. These included host factors chosen based on their role in the replication of other RNA viruses such as the Rab GTPase proteins (RAB2A/B, 4A/B, 6A, 11A/B and 18), TIA1, TIAL1 and Staufen1. Details of the cellular functions of these proteins and the potential roles that they may play in the HCV replication cycle can be found in **Chapter 1: Introduction**. Host factors with an increase in expression during HCV infection were also chosen following microarray analysis of JFH-1 infected Huh7 cells. Host genes selected from the microarray study for further investigation included genes involved in the regulation of intracellular vesicle trafficking (RAB27A/B, RAB33B and RAB37), genes encoding actin binding proteins (ABLIM3) and genes involved in the regulation of lipid metabolism (TXNIP, CYP1A1, PGC1α, RIP140, CIDEB and CIDEC). Although the expression of CIDEC did not increase during JFH-1 infection, it was still chosen for further investigation because of the key role that it plays, alongside CIDEB, in the formation of intracellular lipid droplets. By analysing the normal cellular function for each of these factors it is possible to predict how these proteins might participate in the HCV replication cycle.

Rab GTPase proteins

RAB27A and RAB27B:

RAB27 is a regulator of secretory vesicle trafficking involved in the exocytosis of protein products from cells. Two isoforms of RAB27 exist including RAB27A and RAB27B. RAB27A is the predominant isoform; it is widely expressed and controls a broad range of exocytic activities including the release of lytic granules from cytotoxic T lymphocytes, the release of insulin from pancreatic beta cells and the trafficking of melanosomes to the periphery of melanocytes. RAB27B is expressed much less frequently and is restricted to the pituitary gland, platelets, mast cells and the digestive tract, where it regulates pituitary hormone secretion from the pituitary gland, zymogen secretion from the pancreatic acinar cells, amylase secretion from the parotid acinar cells and controls the process of mast cell degranulation [265]. Studies investigating the nature of the exocytic particles controlled by RAB27 isoforms have demonstrated that particles originate from two

distinct cellular membrane populations in different cell types. These include secretory granules that are derived from the Golgi body (e.g. zymogen, amylase and insulin containing granules) and lysosome related organelles that are derived from the endosomal system (e.g. melanocyte melanosomes, T cell lytic granules, platelet dense granules and mast cell basophilic granules) [265, 266].

A wide range of effector proteins have been identified that bind to activated RAB27A/B to coordinate vesicle trafficking during exocytosis. Some of the effector proteins are able to bind to the actin cytoskeleton, allowing RAB27 coated vesicles to traffic along actin filaments towards the cellular periphery e.g. melanophilin in the trafficking of melanosomes. Other effector proteins mediate the docking of RAB27 bound vesicles at the plasma membrane by binding to the SNARE proteins involved in membrane fusion e.g. granuphilin, which binds to the syntaxin 1a SNARE protein at the plasma membrane during insulin secretion [267].

The expression of both RAB27A and RAB27B was significantly elevated during JFH-1 infection. Given the key role that these proteins play in the trafficking of secretory vesicles to the plasma membrane, it is possible they are important for exporting nascent HCV particles from the cell. At present, HCV secretion has been shown to rely upon the VLDL secretory pathway, which may facilitate co-assembly or co-secretion of VLDL and HCV [47], and the ESCRT pathway, which may facilitate release of virus particles [53]. Very little is known about the processes controlling trafficking between the virus assembly site and the plasma membrane and it is possible that RAB27 coated vesicles are important.

RAB37:

RAB37 is also a regulator of secretory vesicle trafficking belonging to same functional group as other secretory Rab proteins including RAB3, 26 and 27 [268]. Little work has been done to characterise the specific cargo that is transported by RAB37 bound vesicles, although it has been implicated in the regulation of mast cell degranulation [269]. The increased expression of RAB37 observed during JFH-1 infection indicates that this protein might also be important for mediating trafficking of HCV virus particles during viral exit. It is intriguing that several secretory Rab proteins are simultaneously upregulated by infection, and indicates that the mechanisms regulating the expression of these genes may be linked.

RAB33B:

RAB33B is a regulator of retrograde trafficking within the Golgi body, where it functions alongside RAB6 to target Golgi and ER resident proteins to their correct organelle location [249]. RAB33B has also been implicated in the process of autophagy facilitating autophagosome formation through interaction with the autophagy inducing protein, Atg16L [252].

An increase in the expression of RAB33B during JFH-1 infection may have several implications in the HCV replication cycle because of its multitude of cellular functions. The role of RAB33B in the process of retrograde trafficking may facilitate accumulation of HCV proteins in the ER following genome translation, which may be important for assembly of HCV replication complexes. The role of RAB33B in the process of autophagy may also be important for the assembly of replication complexes, as membrane derived from the autophagosome vesicle is thought to contribute to the HCV membranous web [28]. An increase in the rate of autophagosome formation has been observed during HCV infection and an increase in the expression of RAB33B may contribute to this process [113].

Actin binding proteins

Actin binding LIM protein family, member 3 (ABLIM3):

ABLIM3 is an actin-binding protein that localises to adherens junctions present in epithelial and endothelial cell layers. Adherens junctions are responsible for providing connections between adjacent cells within cellular layers. Proteins present at the adherens junction bind directly to the actin cytoskeleton to provide high tensile strength for the cell to cell contacts making the epithelial and endothelial layers durable. Recent studies investigating ABLIM3 have demonstrated that it is localised to the adherens junctions of epithelial layers lining the liver, lung and pancreas and endothelial layers found in the diaphragm, the heart and skeletal muscle tissue [255].

The localisation of ABLIM3 to the adherens junctions found specifically within the liver indicates that ABLIM3 may potentially be one of the liver specific host factors involved in the HCV replication cycle. To date, several host factors that localise to the tight junctions of hepatocytes have been identified as HCV entry factors including Claudin1 and Occludin [22]. It is unlikely that ABLIM3 acts as an entry factor, as it is not localised to the cell surface of the junctional complex. However,

the ability of ABLIM3 to bind directly to the actin cytoskeleton indicates that it may facilitate the actin-mediated trafficking events that take place during and after endocytosis of the virus particle [254].

Lipid metabolism regulators

The thioredoxin interacting protein (TXNIP):

TXNIP is a cellular signalling protein ubiquitously expressed in cells. Its expression is upregulated during conditions of cellular stress, including UV irradiation, heat-shock, exposure to H_2O_2 and high intracellular concentrations of glucose [270]. Biological pathways regulated by the expression of TXNIP include those involved in cellular defence responses. TXNIP is an inhibitor of the anti-oxidant protein, thioredoxin, and an increase in the expression of TXNIP significantly increases the levels of intracellular oxidative stress [271]. Increased expression of TXNIP has also been shown to induce cell cycle arrest and cellular apoptosis by increasing the stability and expression of cell cycle regulators, such as CDKN1B [272], and by activating mitochondrial-mediated apoptosis [270]. TXNIP expression also promotes increased inflammation through activation of the NLRP3 inflammasome [273], and is involved in the differentiation and function of natural killer cells [274].

In addition to the role of TXNIP in the regulation of cellular defence pathways, it has also been widely implicated in the regulation of intracellular lipid and glucose metabolism. TXNIP is a negative regulator of glucose uptake into fat and muscle tissue and is required for gluconeogenesis in the liver [275]. TXNIP is also involved in the regulation of lipid metabolism and has been shown to negatively regulate the activity of the PPARα transcription factor, which controls the expression of genes involved in fatty acid oxidation [239].

Through its ability to control PPARα activity and its role in hepatic gluconeogenesis, TXNIP may be able to regulate the availability of lipid metabolites and glucose required during the HCV replication cycle. Furthermore, the high level of oxidative stress, apoptosis and inflammation induced by the overexpression of TXNIP may contribute significantly to the pathogenesis of HCV infection, which is widely associated with an increase in these biological processes [149, 223, 231].

Cytochrome P450 Family 1 Member A1 (CYP1A1):

CYP1A1 is a haem-containing enzyme involved in the metabolism of synthetic toxic chemicals and naturally occurring cellular metabolites. Typically, CYP1A1 expression is induced following activation of AHR, a ligand-activated transcription factor that enters the nucleus for initiation of mRNA transcription following ligand binding. Ligands shown to stimulate CYP1A1 expression include xenobiotics (e.g. environmental pollutants such as 2,3,7,8-Tetrachlorodibenzodioxin (TCDD)) and endogenous compounds (e.g. eicosanoids) [276].

Alongside CYP1A1, the activation of AHR also results in the expression of another related detoxification enzyme, CYP1B1. Interestingly, the genes encoding CYP1A1, CYP1B1 and AHR were all upregulated as a result of JFH-1 infection in the microarray study performed (**Fig. 3.8**). Further investigation into host gene expression during HCV replication demonstrated that these genes were also upregulated in the cells expressing a genotype 2a subgenomic replicon (**Fig. 3.12 and 13**), indicating that non-structural HCV proteins may play a role in the regulation of their expression. A previous study investigating host gene expression in Huh7 cells expressing a genotype 1b HCV subgenomic replicon also observed a ten-fold increase in the expression of CYP1A1 indicating that upregulation of CYP1A1 during HCV infection is not restricted to genotype 2a HCV [262].

In addition to AHR, another transcription factor recently shown to regulate CYP1A1 expression was the fatty acid metabolism transcription factor, PPARα [277]. This factor has also been shown to induce the expression of other detoxification genes including CYP1B1, CYP1A2, CYP2 and CYP3 [237]. Further evidence to indicate that CYP1A1 may be involved in the regulation of lipid metabolism includes the observation that exposure of mice to the AHR activating ligand, 3-methylcholanthrene (3MC), results in an increase in the levels of hepatic steatosis [229]. This indicates that the upregulation of AHR, CYP1A1 and CYP1B1 observed during JFH-1 infection may contribute significantly to the development of hepatic steatosis in patients and the accumulation of lipids quantified in the JFH-1 infected cells (**Fig. 3.21 and 3.23**).

One of the key functions for CYP1A1 is the role that it plays in the production of intracellular eicosanoids (lipid derived hormones and signalling molecules) from long-chain fatty acids. CYP1A1 has been shown to metabolise the membrane

localised fatty acid, arachidonic acid, to produce arachidonic acid epoxides such as hydroxyeicosatetraenoic acid (e.g. 16, 17, 18 and 19-HETE) and epoxyeicosatrienoic acid (e.g. 14 and 15-EET) [228]. Studies investigating arachidonic acid epoxides have demonstrated that these molecules can act as ligands for PPAR transcription factors. Interestingly, 14 and 15-EET have both been observed to specifically stimulate the transcriptional activity of PPARγ [278]. The ability of CYP1A1 to produce ligands that activate PPARγ indicates that its function may be important for controlling the abundance of lipid metabolites during HCV infection. Furthermore, recent studies investigating the effect of polyunsaturated fatty acids on the replication of HCV have indicated that arachidonic acid significantly inhibits HCV genome replication [279]. Therefore, it is possible that CYP1A1 may also facilitate the replication of HCV by reducing the intracellular abundance of arachidonic acid present in the HCV infected cells.

The peroxisome proliferator activated gamma coactivator alpha1 protein (PGC1α):

PGC1α is a transcriptional coactivator protein that stimulates the activity of ligand activated transcription factors, including PPARα, PPARγ, LXRα, FXRα and HNF4α. Through the regulation of these factors, PGC1α is able to control the expression of genes involved in cholesterol catabolism, fatty acid oxidation, glucose metabolism and ketogenesis [280]. Due to its role in these processes, the expression of PGC1α is restricted to tissues with high metabolic activity including adipose tissue, liver, brain, heart and skeletal muscle [281].

The cellular effect of PGC1α activation varies between different tissue types depending on the transcription factors present and the metabolic status of the tissue. Overexpression of PGC1α in adipocyte cells has recently been shown to upregulate the expression of a lipid droplet protein, cell-death inducing DFFA-like effector A protein (CIDEA), which is responsible for inducing an increase in the accumulation of intracellular lipid droplets [282]. In the liver, PGC1α also induces an increase in the expression of a liver specific lipid droplet CIDE protein, CIDEB. However, alongside the role of CIDEB in lipid droplet production, expression of CIDEB in the liver is also associated with the production of VLDL particles. As a result, a reduction in the abundance of triglyceride was observed in hepatoma cells when CIDEB expression was increased, as the secretion of VLDL was stimulated [280]. There may also be occasions when PGC1α activity in the liver stimulates an increase in triglyceride abundance, as the expression of PPARγ, a

key PGC1α activated transcription factor, has been observed to contribute to the development of hepatic steatosis in mice [283].

In the JFH-1 infected Huh7 cells, an increase was observed in the expression of CIDEB and PPARγ (**Fig. 3.8**), and in the abundance of intracellular triglyceride, cholesterol and lipid droplets (**3.21 and 3.23**). Based on the multiple roles that PGC1α protein has been shown to play in controlling lipid droplet abundance and lipid metabolism, it is possible that increased expression of this protein during HCV infection is important for mediating these changes. Previous studies have demonstrated that the HCV NS5A protein induces an increase in the expression of PPARγ, and promotes an interaction between PGC1α and PPARγ to stimulate the transcription of adipogenic genes [166]. Increased abundance of PGC1α during HCV infection may ensure that sufficient coactivator protein is available for activation of PPARγ and stimulation of intracellular lipid synthesis.

The cell death inducing DFF45-like effector (CIDE) gene family:

The CIDE gene family consists of three gene members: CIDEA, CIDEB and CIDEC. These genes share homology with the DNA fragmentation factor (DFF) family including DFF40 and DFF45, which induce apoptosis through DNA fragmentation. Consistent with the homology observed between the CIDE and DFF gene families, expression of CIDE proteins has also been shown to induce apoptosis in a number of cell lines. In addition, a more recent role for the CIDE genes is associated with the regulation of intracellular lipid metabolism [284]. Due to their roles in lipid metabolism, the expression of CIDE genes is restricted to metabolically active tissues, with CIDEA and CIDEC being predominantly expressed in white adipose tissue, and CIDEB being expressed in the liver and small intestine. In the cells of these tissues, CIDE proteins have been shown to localise to the surface of lipid droplets and, in the case of CIDEA and CIDEB, to the ER membrane. As a result of lipid droplet localisation, overexpression of CIDEA and CIDEC are able to induce an accumulation of lipid droplets in cells. The localisation of CIDEC to lipid droplets in adipocytes is also essential for adipocyte differentiation [284]. As described earlier, CIDEB has been shown to play a role in VLDL particle synthesis. This is due to its ability to bind to the lipid droplet surface and the ER-localised ApoB protein, which facilitates the delivery of lipids from the lipid droplet to the VLDL synthesis machinery present within the ER [280, 285]. CIDEB has also been shown to control the expression of SREBF1c, a

key transcription factor controlling adipogenesis [284]. Interestingly, the HCV NS2 protein was shown to interact directly with CIDEB to inhibit its ability to induce mitochondrial-mediated apoptosis [286]. This indicates that CIDEB may act as a potential link between HCV components on intracellular lipid droplets and the VLDL secretory pathway, which is required for co-assembly and/or co-secretion of HCV particles [47].

Given the key role of the CIDE family in the metabolism of lipids and the synthesis of lipid droplets, it is possible that these proteins are important cofactors for the HCV replication cycle. CIDEB is a particularly interesting target to study because of its predominant expression in the liver, its upregulation during JFH-1 infection and its ability to bind to HCV NS2.

Receptor Interacting Protein-140 (RIP140):

RIP140 is a coregulator protein that can alter the activity of several transcription factors including peroxisome proliferator activated receptors (PPARα, PPARβ and PPARγ), thyroid hormone receptors (TRα and TRβ) and estrogen related receptors (ERRα and ERRβ). For the majority of these factors, RIP140 acts as a corepressor modulating the expression of genes involved in glucose uptake, glycolysis, oxidative phosphorylation, fatty acid oxidation and mitochondrial biogenesis. RIP140 is particularly important for regulating the activity of these transcription factors in metabolically active tissues including adipose tissue, liver, skeletal muscle and the heart [287]. In the liver, RIP140 has been shown to have both corepressor and coactivator activities. For example, the binding of RIP140 to the liver x receptor (LXR) transcription factor represses its ability to transcribe genes involved in gluconeogenesis (e.g. phosphoenolpyruvate carboxykinase (PEPCK)), but stimulates its ability to transcribe genes involved in lipid synthesis (e.g. SREBF-1c and FASN) [287].

Due to its ability to stimulate the expression of genes involved in lipid synthesis and repress the expression of genes involved in fatty acid oxidation, RIP140 may be an important cofactor required during the HCV replication cycle. An increase in the expression of RIP140 during HCV infection may facilitate the synthesis of essential lipid metabolites required during infection and may contribute to the accumulation of lipids observed in the JFH-1 infected cells (**Fig. 3.21 and 3.23**).

Investigating the role of potential HCV cofactors in the HCV replication cycle

A range of candidate host genes with roles in lipid metabolism, intracellular transport and RNA processing were selected as potential HCV cofactors. To investigate whether these genes are required during HCV infection, the effect of host gene silencing on the replication and secretion of JFH-1 was tested. This chapter summarises the assays used to optimise an siRNA knockdown experiment using positive control siRNAs that target either the HCV genome directly [209] or the RAB1B GTPase gene, which has previously been implicated in the HCV replication cycle [128]. The optimised siRNA knockdown assay was used to investigate the effect of candidate host gene silencing on the replication and secretion of JFH-1. A summary of the results obtained following siRNA knockdown of the selected candidate genes is presented, alongside a series of validation assays that test for non-specific effects of siRNA transfection. A study was also performed to investigate whether siRNA molecules that reduce JFH-1 replication and secretion can also reduce JFH-1 protein expression.

Several of the candidate genes chosen for further investigation belong to the Rab GTPase gene family and may be important for controlling vesicle trafficking and membrane organisation during the HCV replication cycle. For many of the Rab GTPase proteins chosen, multiple isoforms, with high levels of amino acid sequence homology, exist e.g. RAB2A and RAB2B (82% homology [288]), RAB4A and RAB4B (87% homology [289]), RAB11A and RAB11B (91% homology [290]) and RAB27A and RAB27B (72% homology [291]). Classification of Rab GTPase proteins into different subgroups containing isoforms was originally performed based on sequence homology, and overlap in protein localisation and function [292]. As a result, many Rab GTPase isoforms are often assumed to have the same or similar functional role in cells. However, as our knowledge of Rab GTPase proteins grows, it is becoming more apparent that there may be high levels of functional variation between different Rab isoforms. One recent study performed to characterise novel Rab GTPase effector proteins identified several examples of single effector proteins that bound specifically to individual Rab GTPase isoforms, for example the effector proteins GMCL1 and GAR1, were observed to bind only to RAB2B and not RAB2A [293]. Other studies investigating the function of the Rab GTPase isoforms tested in this study also indicate functional diversity between different isoform proteins. A recent study investigating

the role of Rab27 isoforms in exosome secretion demonstrated that RAB27A and RAB27B play different and non-redundant roles in the process of exosome secretion and localise to distinct locations within cells [294]. RAB11A and RAB11B isoforms have also been shown to localise to distinct vesicular compartments in epithelial cells [295], and have been shown to colocalise with different cargo proteins including the acid-base transporter, V-ATPase, which was observed to colocalise with RAB11B, but not RAB11A [296]. As a result of the increasing evidence that Rab GTPase isoforms play functionally distinct intracellular roles, the siRNA knockdown experiment described in this chapter analysed the effects of the Rab isoform siRNAs individually, allowing isoform specific effects on the HCV replication cycle to be determined.

Chapter 4: Results

4.1 Optimisation of an siRNA knockdown assay to test the role of host factors in the HCV replication cycle

4.1.1 Optimising siRNA transfection of Huh7 cells

The efficiency of Huh7 cell siRNA transfection was investigated using a positive-control GAPDH siRNA, which was transfected using Lipofectamine 2000. At 48 hours post-transfection, intracellular RNA was extracted and used for qRT-PCR analysis of GAPDH expression (**Fig. 4.1**). A 70% reduction in GAPDH was observed in the cells transfected with 50nM GAPDH siRNA (siGAPDH) compared to the cells transfected with 50nM of a negative control non-targeting siRNA (siNegative). Little effect was observed on the expression of GAPDH when comparing cells transfected with the negative control siRNA to cells transfected with Lipofectamine 2000 only (Lipofectamine 2000) or transfection medium only (no transfection).

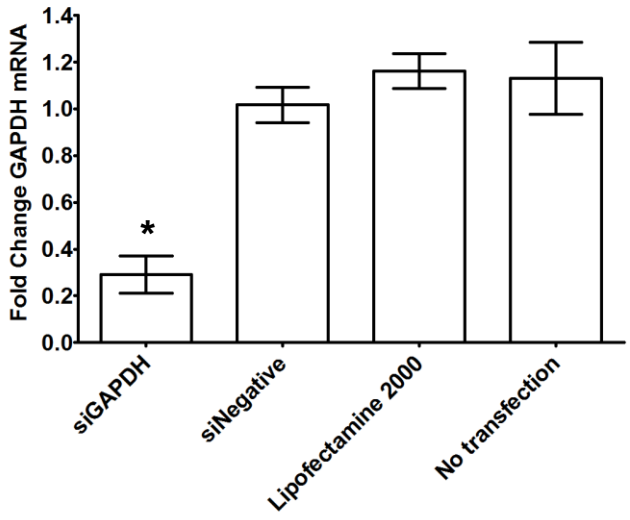


Figure 4.1 Huh7 cells are efficiently transfected using Lipofectamine 2000

Fold change in GAPDH expression in Huh7 cells transfected with a GAPDH siRNA using Lipofectamine 2000. Huh7 cells were transfected for 48 hours with 50nM GAPDH siRNA, 50nM negative control non-targeting siRNA, Lipofectamine 2000 only or transfection medium only. Intracellular RNA was extracted and used for qRT-PCR analysis of GAPDH expression. Fold change expression data displayed represents the mean (±SD) of two independent experiments, each containing repeat siRNA transfections performed in duplicate (N=4). The knockdown of GAPDH expression achieved with the GAPDH siRNA compared to the negative control siRNA was statistically significant with a p value ≤ 0.005 (indicated by an asterisk (*)). P values were calculated using a two-tailed unpaired T test in Graphpad Prism.

4.1.2 Optimisation of the siRNA knockdown assay using a HCV siRNA

The effect of HCV siRNA transfection on the replication and secretion of JFH-1

An siRNA that directly targets the HCV genome was tested for its ability to disrupt the replication and secretion of the full-length JFH-1 virus. Huh7 cells were transfected with 10, 50 and 100nM of the HCV siRNA and infected with JFH-1 (MOI = 3). At 48 hours post-infection, intracellular RNA was extracted and the levels of JFH-1 RNA were quantified using qRT-PCR to compare cells transfected with the HCV siRNA to cells transfected with a negative control non-targeting siRNA. To investigate the effect of HCV siRNA transfection on JFH-1 secretion, medium was also collected from the transfected, JFH-1 infected cells and was used to infect naïve Huh7.5 cells. At 48 hours post-infection, the cells were stained for the HCV core protein and the number of core-positive foci was counted to calculate the extracellular JFH-1 virus titres in each sample. A comparison was made between the titres quantified for the HCV siRNA transfected cells to the titres quantified for the cells transfected with the negative control non-targeting siRNA (**Fig. 4.2a**).

The HCV siRNA significantly reduced both intracellular JFH-1 RNA and extracellular JFH-1 virus titres in the infected Huh7 cells. The level of JFH-1 knockdown observed correlated directly with the amount of siRNA transfected. When 100nM of the siRNA was transfected, intracellular JFH-1 RNA was reduced by 90% and extracellular JFH-1 titres were reduced by 92%. By comparison, when 10nM of the siRNA was transfected, intracellular JFH-1 RNA was reduced by 60% and extracellular JFH-1 virus titres were reduced by 68% (**Fig. 4.2a**).

The effect of the HCV siRNA on JFH-1 protein expression was also investigated by staining the siRNA transfected, JFH1 infected Huh7 cells for the HCV core protein (**Fig. 4.2b**). The proportion of cells staining positive for HCV core was significantly reduced in the Huh7 cells transfected with the HCV siRNA compared to the cells transfected with the negative control non-targeting siRNA.

.

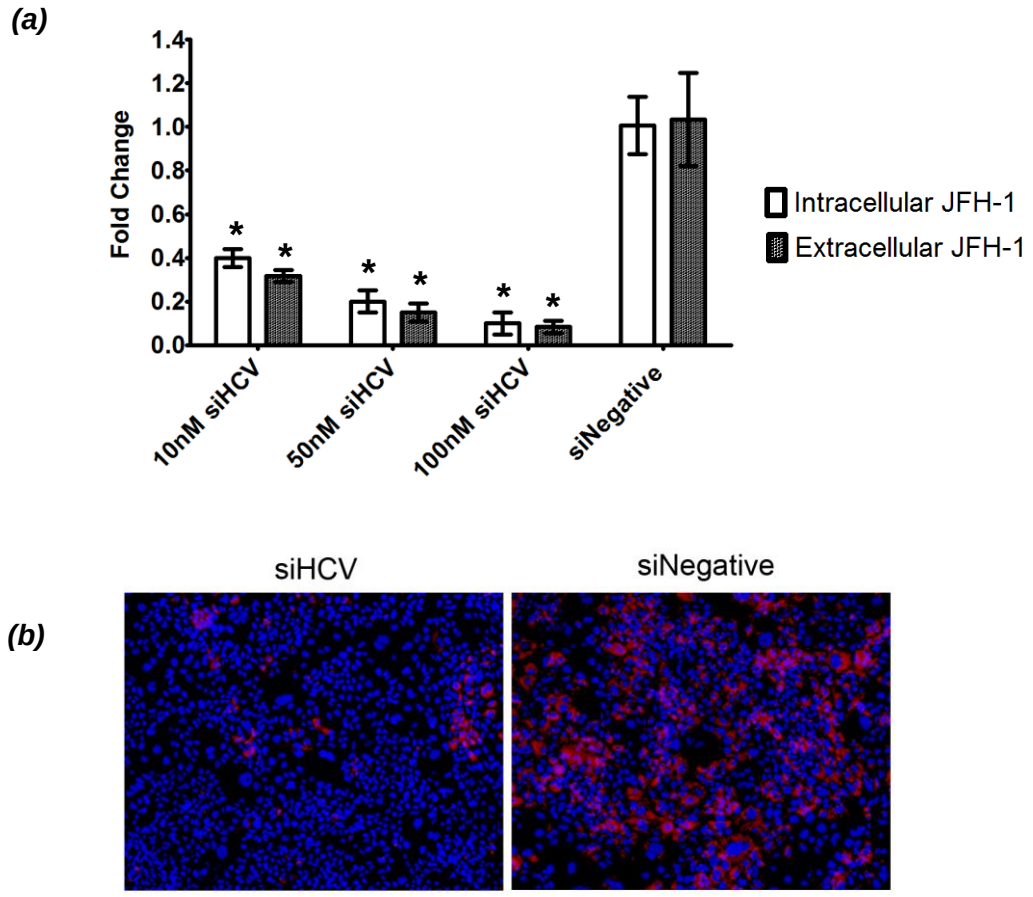


Figure 4.2 The HCV siRNA reduces JFH-1 replication and secretion

(a) *Fold change in the intracellular JFH-1 RNA (white bars) and extracellular JFH-1 virus titres (grey bars) in infected Huh7 cells transfected with an siRNA targeting the HCV genome. Huh7 cells were transfected for 48 hours with 10, 50 and 100nM of the HCV siRNA or 10, 50 and 100nM of a negative control non-targeting siRNA. The transfected cells were infected with JFH-1 at an MOI of 3 and incubated for 48 hours. Intracellular RNA was extracted and used for qRT-PCR quantification of JFH-1 RNA. Media was also collected from the transfected, JFH-1 infected cells for quantification of JFH-1 virus titres. The data presented for the negative control siRNA is an average of the data collected for cells transfected with 10, 50 and 100nM of negative control siRNA. Fold change expression data displayed represents the mean (±SD) of two independent experiments, each containing repeat siRNA transfection performed in duplicate (N=4). The knockdown of JFH-1 RNA and virus titres achieved with the HCV siRNA compared to the negative control siRNA was statistically significant with a p value ≤ 0.05 (indicated using an asterisk (*)). P values were calculated using a two-tailed unpaired T test in Graphpad Prism.* ***(b)*** *Core protein staining of JFH-1 infected Huh7 cells transfected with the HCV siRNA. Huh7 cells transfected with 50nM of the HCV siRNA and the negative control non-targeting siRNA for 48 hours were infected with JFH-1 at an MOI of 3. At 48 hours post-infection, the cells were stained for the HCV core protein using an anti-core antibody (red staining).Cell nuclei were also stained using DAPI (blue staining). Images were captured using a Nikon Eclipse TE2000S fluorescence microscope at a magnification of 20x*.

Cell viability analysis of cells transfected with the HCV siRNA molecule

To determine whether the HCV siRNA had any non-specific effects on the viability of cells, the effect of siRNA transfection on Huh7 cell viability was investigated using the alamar blue assay (**Fig. 4.3**). The alamar blue reagent is non-toxic, which means that the effect of siRNA transfection on the viability of cells can be monitored over time. Cell viability was measured at 24 and 48 hours post-transfection in Huh7 cells transfected with the HCV siRNA, the non-targeting negative control siRNA and transfection medium only. Little difference was observed in the percentage viability of Huh7 cells transfected with the HCV siRNA compared to cells transfected with the negative control non-targeting siRNA and transfection medium only.

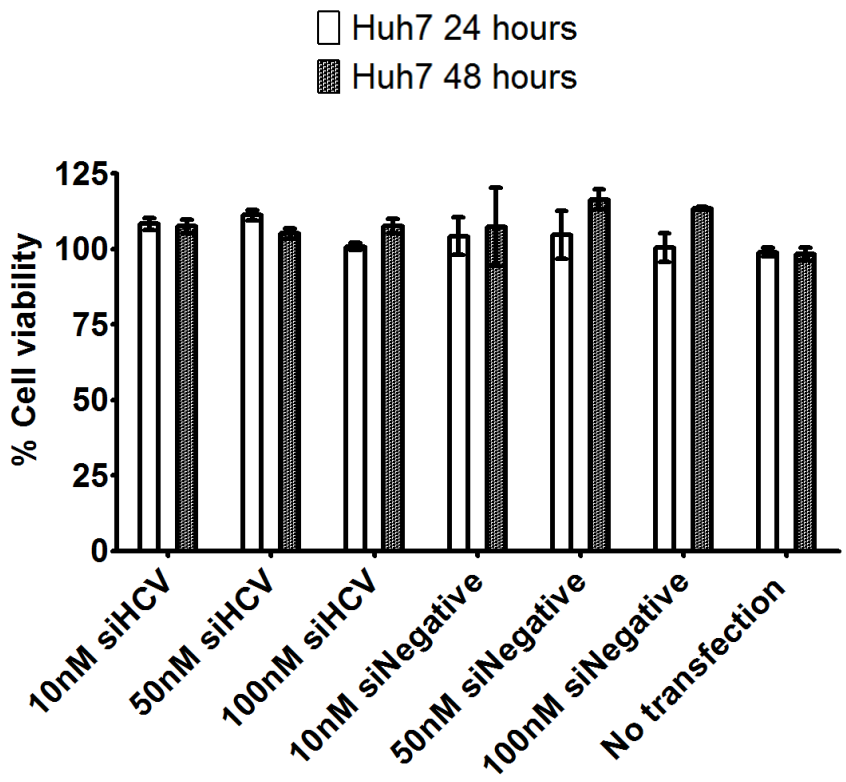


Figure 4.3 Transfection of the HCV siRNA does not affect cellular viability

Percentage viability of Huh7 cells transfected with the HCV siRNA. Huh7 cells were transfected with 10, 50 and 100nM of the HCV siRNA, 10, 50 and 100nM of the negative control non-targeting siRNA, and transfection medium only. Cell viability was measured using the alamar blue assay at 24 (white bars) and 48 hours (grey bars) post-transfection. Percentage cell viability data displayed represents the mean (±SD) of two independent experiments, each containing repeat siRNA transfections performed in duplicate (N=4).

4.1.3 Optimisation of the siRNA knockdown assay using RAB1B siRNA molecules

Recently published data demonstrated that siRNA knockdown of RAB1B GTPase caused an 85% reduction in the replication of Jc1 (JFH-1/J6) [128]. To test whether the siRNA knockdown assay established enabled identification of HCV cofactors, the effect of RAB1B knockdown on JFH-1 virus replication was investigated.

RAB1B knockdown in Huh7 cells

The efficiency of RAB1B silencing in Huh7 cells transfected with three different RAB1B siRNA molecules was investigated at 24, 48, 72 and 96 hours post-transfection using qRT-PCR. Maximum RAB1B knockdown was observed using siRAB1B-2 and siRAB1B-3, which reduced RAB1B expression by 80% to 90%. Less efficient RAB1B silencing was observed with siRAB1B-1, which reduced RAB1B expression by 45% to 60% (**Fig. 4.4a**).

The cell viability of RAB1B siRNA transfected cells was investigated using the alamar blue assay (**Fig. 4.4b**). The viability of the RAB1B siRNA transfected cells was reduced by 20% at 24 hours post-transfection, but returned to normal at 48 hours post-transfection. Overall, there was no major difference between the viability of cells transfected with RAB1B siRNAs and the negative control cells.

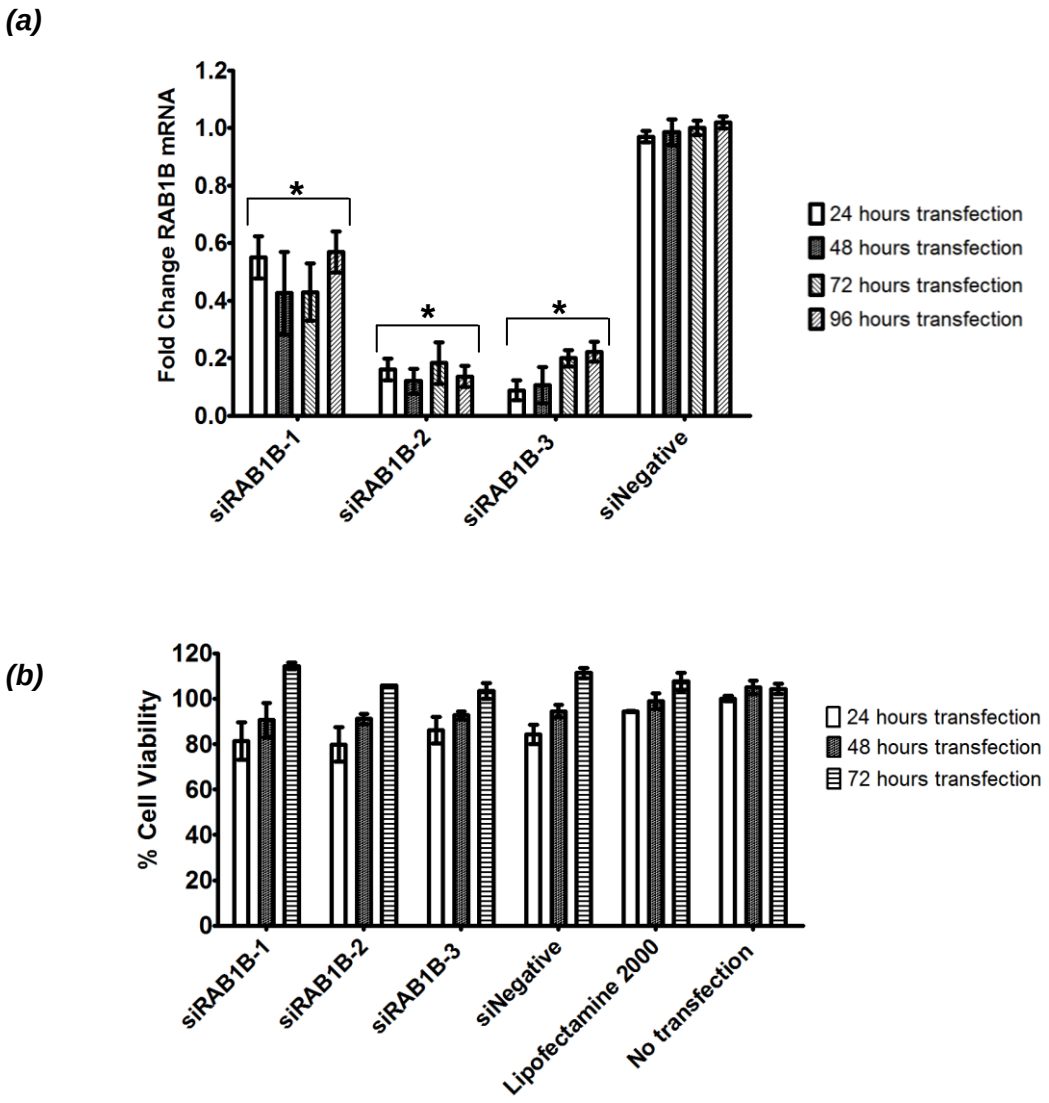


Figure 4.4 RAB1B siRNAs reduce RAB1B mRNA without altering cell viability

(a) *Fold change in RAB1B expression in Huh7 cells transfected with RAB1B siRNA molecules. Huh7 cells were transfected with 50nM of siRNAs targeting RAB1B (siRAB1B-1, siRAB1B-2, siRAB1B-3) and a negative control non-targeting siRNA for 24, 48, 72 and 96 hours. Intracellular RNA was extracted and used for qRT-PCR quantification of RAB1B expression. Fold change expression data displayed represents the mean (±SD) of two independent experiments, each containing repeat siRNA transfections performed in duplicate (N=4). The knockdown of RAB1B expression achieved with the RAB1B siRNAs compared to the negative control siRNA was statistically significant with a p value ≤ 0.05 (indicated by an asterisk (*)). P values were calculated using a two-tailed unpaired T test in Graphpad Prism.* ***(b)*** *Percentage viability of Huh7 cells transfected with RAB1B siRNAs. Huh7 cells were transfected with 50nM of RAB1B siRNAs, a negative control non-targeting siRNA, Lipofectamine 2000 only and transfection medium only. Cell viability was measured using the alamar blue assay at 24, 48 and 72 hours post-transfection. Percentage cell viability data displayed represents the mean (±SD) of two independent experiments, each containing repeat siRNA transfections performed in triplicate (N=6).*

Quantification of JFH-1 RNA abundance following RAB1B knockdown

The effect of RAB1B knockdown on JFH-1 genome replication was investigated using Huh7 cells that were transfected with RAB1B siRNAs and infected with JFH-1 virus (MOI = 3). At 48 hours post-infection intracellular RNA was extracted and used in qRT-PCR analysis to quantify intracellular JFH-1 RNA and RAB1B mRNA. RAB1B knockdown reduced the intracellular levels of RAB1B mRNA and JFH-1 RNA (**Fig. 4.5**). The level of JFH-1 knockdown observed correlated roughly with the efficiency of RAB1B knockdown. For example, JFH-1 RNA levels were reduced by 22% in the cells transfected with siRAB1B-1, which reduced RAB1B expression by 53%. By comparison, the JFH-1 RNA levels were reduced by 50% in the cells transfected with siRAB1B-3, which reduced RAB1B expression by 86%.

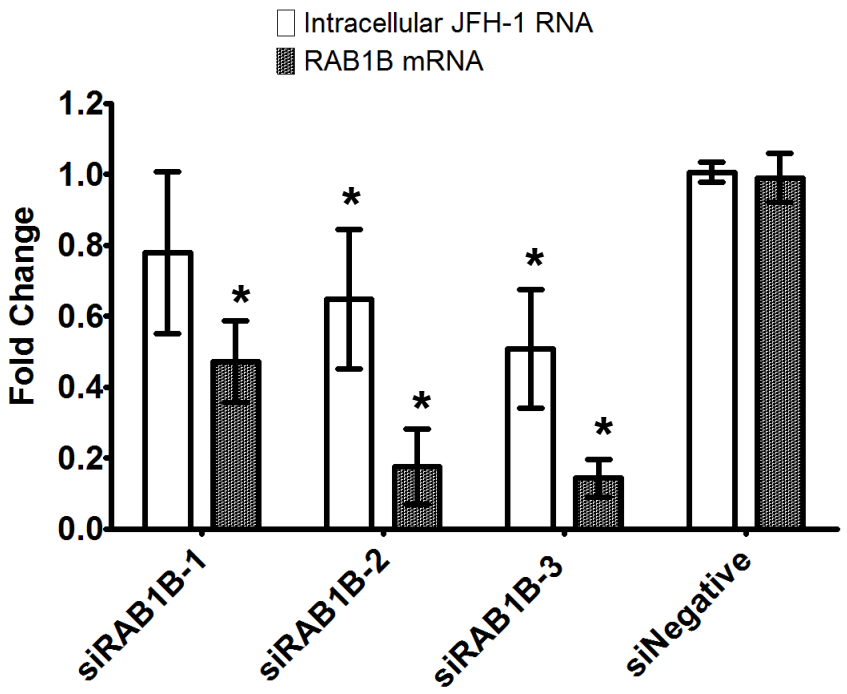


Figure 4.5 RAB1B knockdown reduces HCV replication

Fold change in RAB1B expression and JFH-1 RNA abundance in Huh7 cells transfected with RAB1B siRNAs. Huh7 cells were transfected with 50nM of RAB1B siRNAs and a negative control non-targeting siRNA for 48 hours. The transfected cells were infected with JFH-1 (MOI = 3) for 48 hours. Intracellular RNA was extracted and used for qRT-PCR quantification of RAB1B expression (grey bars) and JFH-1 RNA abundance (white bars). Fold change expression data displayed represents the mean (±SD) of three independent experiments, each containing repeat siRNA transfections performed in duplicate (N=6). The knockdown of RAB1B mRNA and JFH-1 RNA achieved with the RAB1B siRNAs compared to the negative control siRNA was statistically significant with a p value ≤ 0.05 (indicated by an asterisk (*)). P values were calculated using a two-tailed unpaired T test in Graphpad Prism.

4.2 The effect of host gene knockdown on JFH-1 replication and secretion

Through analysis of siRNA molecules targeting the HCV genome and the expression of RAB1B, an assay has been established to test the effect of host gene knockdown on the replication and secretion of JFH-1. This assay was used to investigate whether the selected candidate host genes identified in **Chapter 3** are required during the HCV replication cycle. The targets chosen for investigation included genes involved in the replication of other RNA viruses (e.g. Rab GTPase proteins (RAB2, 4, 6A, 11 and 18), TIA1, TIAL1 and Staufen1) and genes significantly upregulated during HCV infection (e.g. RAB27A/B, RAB33B, RAB37, TXNIP, CYP1A1, ABLIM3, PGC1α, CIDEB and RIP140).

To investigate the effect of host gene silencing on JFH-1 replication and secretion, each host gene was silenced using a pool of two siRNA molecules. However, some of the host genes (e.g. PGC1α, CIDEB, CIDEC and RIP140) were targeted only with a single siRNA. For the majority of targets tested, transfection was performed in both Huh7 and Huh7.5 cells, which were infected with JFH-1 for either 24 or 48 hours. Intracellular RNA was extracted from the cells and the abundance of JFH-1 RNA was quantified using qRT-PCR to determine the effect of host gene silencing on the replication of the JFH-1 genome. To investigate the effect of host gene silencing on JFH-1 secretion, media from the transfected cells (infected for 48 hours) was collected and used for quantification of JFH-1 virus titres. To control for variation in transfection efficiency, the HCV siRNA was also included as a positive control.

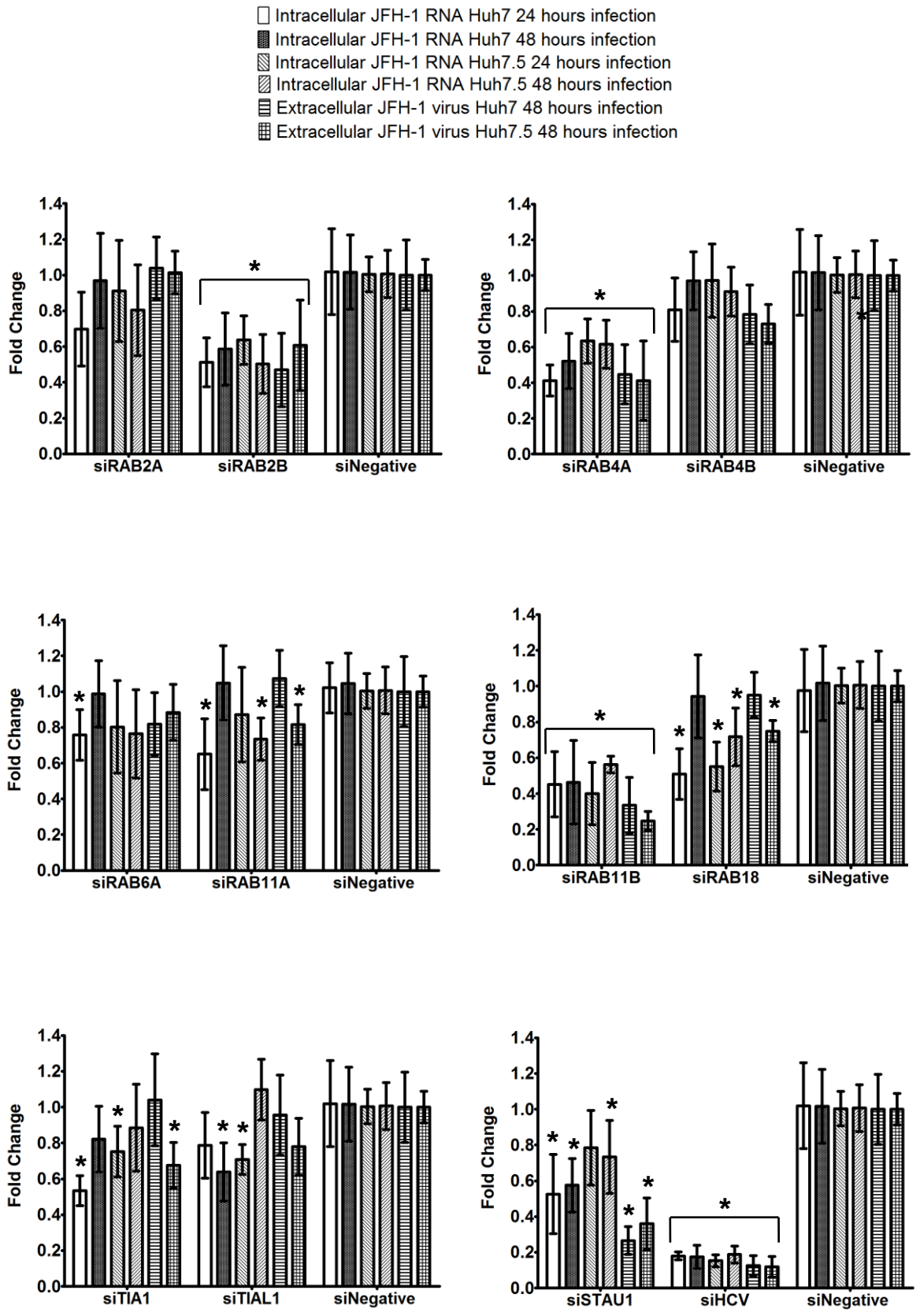
4.2.1 Silencing host genes with a role in the replication of other RNA viruses

Pools of siRNA molecules targeting the expression of RAB2A/B, RAB4A/B, RAB6A, RAB11A/B, RAB18, TIA1, TIAL1 and Staufen1 were tested for their effects on JFH-1 replication and secretion in Huh7 and Huh7.5 cells (**Fig 4.6a**). Silencing the expression of RAB2B, RAB4A, RAB11B and Staufen1 had significant effects on JFH-1 RNA levels and JFH-1 virus titres in both Huh7 and Huh7.5 cells. For example, RAB2B silencing reduced JFH-1 RNA levels by 42% and JFH-1 virus titres by 55% in Huh7 cells infected with JFH-1 for 48 hours. In Huh7.5 cells infected for 48 hours, RAB2B silencing reduced JFH-1 RNA levels by 50% and JFH-1 virus titres by 40%. Silencing the expression of Staufen1 had more significant effects on the extracellular virus titres than the intracellular RNA

levels compared to RAB2B, RAB4A and RAB11B silencing, which reduced JFH-1 RNA and virus levels to a similar extent. For example, Staufen1 silencing reduced JFH-1 RNA levels by 42% and JFH-1 virus titres by 73% in Huh7 cells infected with JFH-1 for 48 hours. In Huh7.5 cells infected for 48 hours, Staufen1 silencing reduced JFH-1 RNA levels by 27% and JFH-1 virus titres by 65%. siRNA molecules targeting other host factors had much less significant or inconsistent effects on JFH1 replication and secretion including RAB2A, RAB4B, RAB6A, RAB11A, RAB18, TIA1 and TIAL1. Silencing the expression of these host genes generally reduced the JFH-1 RNA and virus levels by around 10% to 25% in both Huh7 and Huh7.5 cells. The HCV siRNA was also included in the assay as a positive control and reduced the JFH-1 RNA and JFH-1 virus titres by 80% to 90% in both Huh7 and Huh7.5 cells.

The efficiency of host target mRNA knockdown was also investigated by qRT-PCR (**Fig. 4.6b**). Host gene knockdown of around 80% was observed for most of the targets in cells infected for either 24 or 48 hours. Silencing of TIA1 and TIAL1 was less efficient and was limited to around 60% knockdown. Data represented contains an average of the knockdown observed for both the Huh7 and Huh7.5 cells at either 24 or 48 hours post-infection.

(a) *Fold change in intracellular JFH-1 RNA and extracellular JFH-1 virus titres*



***(b)** Fold change in target mRNA*

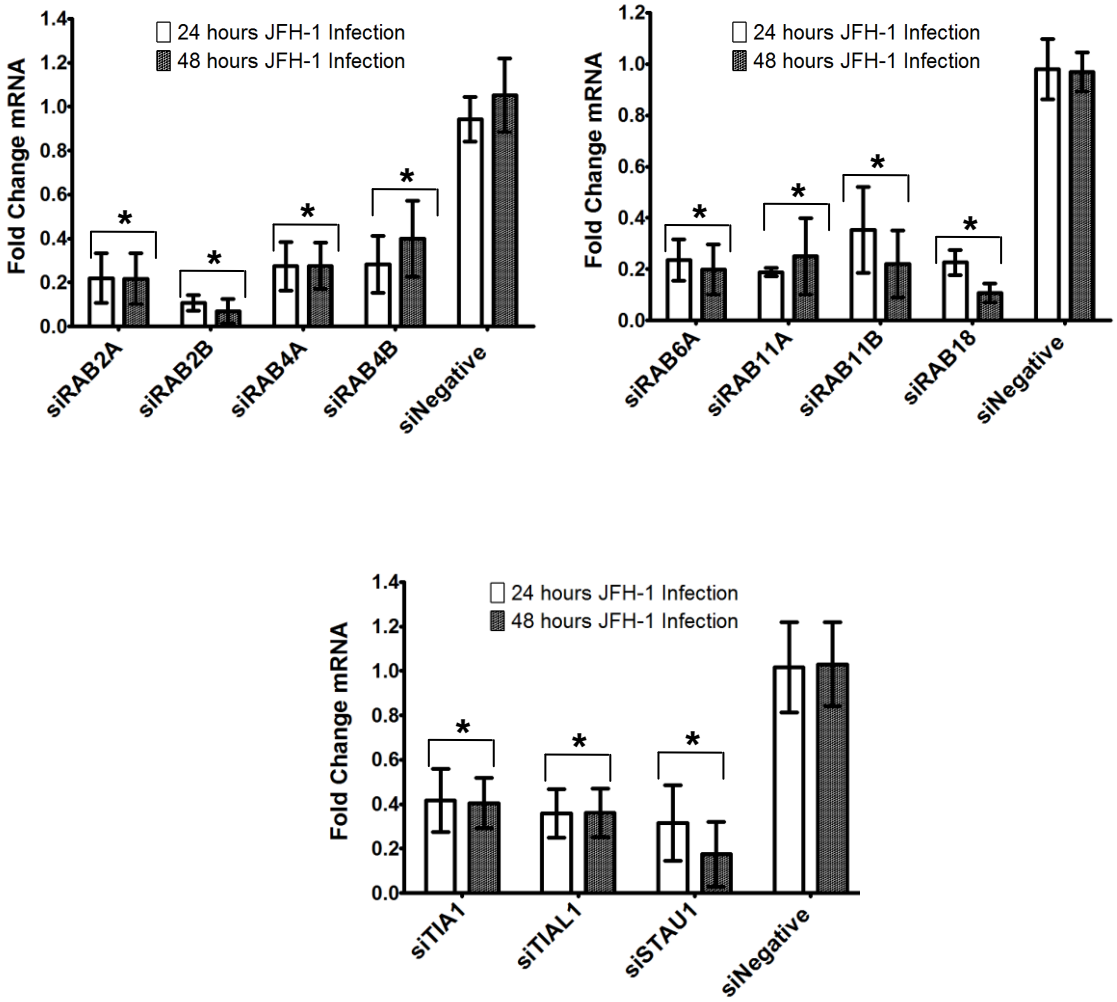


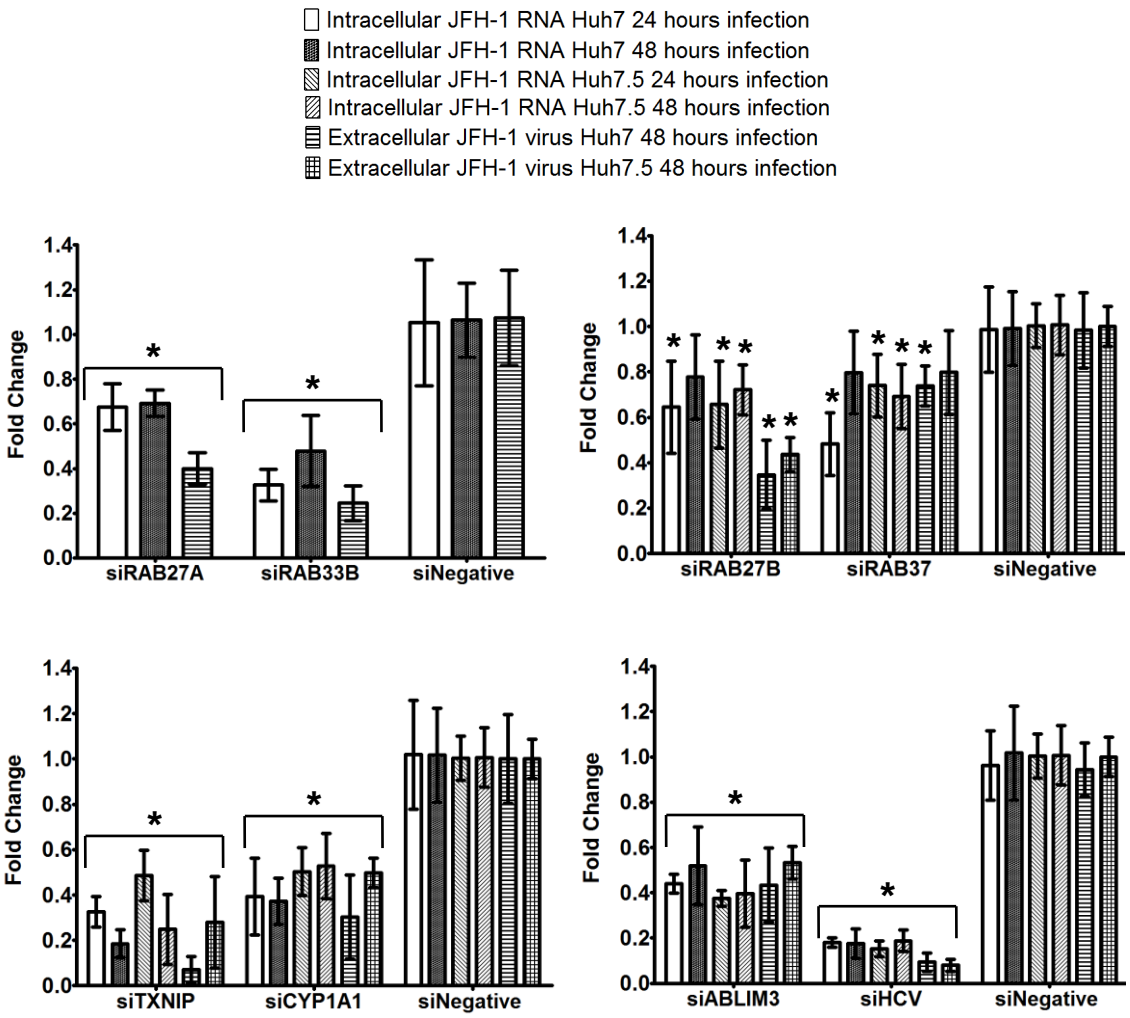
Figure 4.6 The effect of host gene silencing on JFH-1 RNA and virus titres 1

*Fold change in JFH-1 RNA abundance, JFH-1 virus titres and host gene expression following host gene knockdown in JFH-1 infected Huh7 and Huh7.5 cells. Huh7 and Huh7.5 cells were transfected with 50nM of target specific siRNA (25nM siRNA1 and 25nM siRNA2), 50nM of a negative control non-targeting siRNA and 50nM of a positive control siRNA targeting the HCV genome. At 48 hours post-transfection, the cells were infected with JFH-1 (MOI = 3) for either 24 or 48 hours. Intracellular RNA was extracted from the cells for qRT-PCR quantification of **(a)** JFH-1 RNA and **(b)** target mRNA. Media was also collected from the transfected cells (infected for 48 hours) for quantification of JFH-1 virus titres. Fold change data displayed represents the mean (±SD) of three independent experiments, each containing repeat siRNA transfections performed in duplicate (N=6). The target specific siRNAs causing a statistically significant knockdown (p value ≤ 0.05) of JFH-1 RNA, JFH-1 virus titres and target gene expression in comparison to the negative control siRNA are indicated by an asterisk (*). P values were calculated using a two-tailed unpaired T test in Graphpad Prism.*

4.2.2 Silencing host genes upregulated during JFH-1 infection

Pools of siRNA molecules targeting the expression of RAB27B, RAB37, TXNIP, CYP1A1 and ABLIM3 were tested for their effects on JFH-1 replication and secretion in Huh7 and Huh7.5 cells. Pools of siRNAs targeting the expression of RAB27A and RAB33B were transfected into Huh7 cells only (**Fig. 4.7a**). Silencing the expression of RAB33B, ABLIM3, TXNIP and CYP1A1 had the most significant effect on both JFH-1 RNA levels and virus titres. For example, silencing TXNIP expression reduced JFH-1 RNA levels by 82% and JFH-1 virus titres by 90% in the Huh7 cells infected with JFH-1 for 48 hours. In Huh7.5 cells infected for 48 hours, TXNIP silencing reduced JFH-1 RNA by 75% and JFH-1 virus titres by 72%. Silencing the expression of CYP1A1 reduced JFH-1 RNA levels by 63% and JFH-1 virus titres by 70% in the Huh7 cells infected with JFH-1 for 48 hours. In Huh7.5 cells infected for 48 hours, CYP1A1 silencing reduced JFH-1 RNA by 50% and JFH-1 virus titres by 49%. Other siRNA molecules tested had a more significant effect on the levels of secreted virus than the levels of intracellular JFH-1 RNA including RAB27A and RAB27B. For example, RAB27B silencing reduced JFH-1 RNA levels by only 23%, yet reduced JFH-1 virus titres by 65% in Huh7 cells infected with JFH-1 for 48 hours. In Huh7.5 cells infected for 48 hours, RAB27B silencing reduced JFH-1 RNA levels by 28% and reduced JFH-1 virus titres by 57%. Compared to RAB27A/B, RAB33B, TXNIP, CYP1A1 and ABLIM3, silencing the expression of RAB37 had a less significant effect on the JFH-1 replication cycle and only reduced JFH-1 RNA levels by 20% and JFH-1 virus titres by 27% in Huh7 cells infected with JFH-1 for 48 hours. In Huh7.5 cells infected for 48 hours, RAB37 silencing reduced JFH-1 RNA levels by 30% and reduced JFH-1 virus titres by 20%. The efficiency of host target mRNA knockdown with each siRNA was also investigated by qRT-PCR (**Fig. 4.7b**). Efficient knockdown of at least 80% was observed for RAB27A/B, RAB37, RAB40B and TXNIP. Less efficient target knockdown was observed for RAB33B, CYP1A1 and ABLIM3. Data represented contains an average of the knockdown observed for Huh7 and Huh7.5 cells at 24 or 48 hours post-infection. Comparing both sets of silencing data (**Fig. 4.6 and 4.7**), the effects of host gene silencing on JFH-1 replication and secretion was often greater in cells infected for 24 hours than in cells infected for 48 hours. These differences did not reflect the efficiency of host gene knockdown, as the cells infected for 48 hours often had a greater reduction in host gene expression than the cells infected for 24 hours.

***(a)** Fold change in intracellular JFH-1 RNA and extracellular JFH-1 virus titres*



***(b)** Fold change in target mRNA*

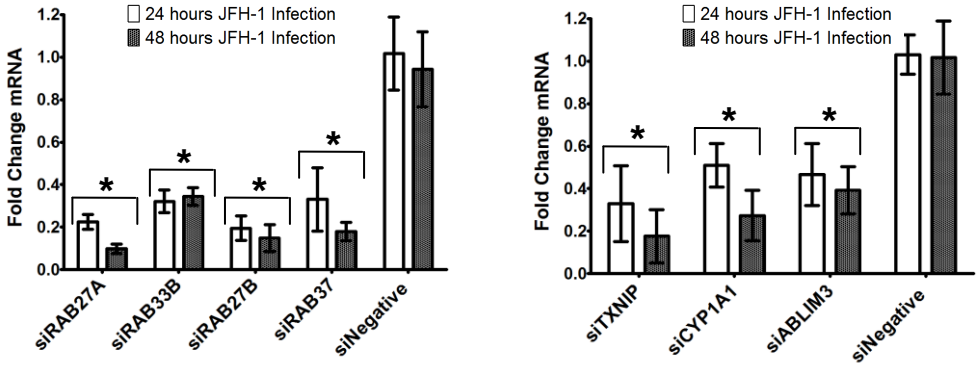


Figure 4.7 The effect of host gene silencing on JFH-1 RNA and virus titres 2

Refer to Figure 4.6 for description. When targeting RAB27A and RAB33B, transfection was performed using 50nM of an siRNA pool in Huh7 cells only. All other siRNAs were transfected according to the protocol given in Figure 4.6. Fold change data displayed represents the mean (±SD) of three independent experiments, each containing repeat siRNA transfections performed in duplicate (N=6) (except siRAB27A and siRAB33B, which were analysed in two independent experiments with repeat transfections performed in duplicate (N=4).

To test whether PGC1α, CIDEB, CIDEC and RIP140 are required for the JFH-1 replication cycle, individual siRNA molecules targeting host gene expression were tested for their effects on JFH-1 replication and secretion in Huh7 cells infected with JFH-1 for 48 hours (**Fig. 4.8**). The siRNA molecules silencing the expression of both PGC1α and RIP140 had very little effect on either JFH-1 RNA levels or JFH-1 virus titres. Silencing CIDEB reduced JFH-1 RNA levels by 40% with relatively little effect on JFH-1 virus titres. Silencing CIDEC only reduced JFH-1 RNA levels by 20% but reduced JFH-1 virus titres by 60% (**Fig. 4.8a**). Efficient host target knockdown of at least 80% was observed for PGC1α, RIP140 and CIDEB. Less efficient knockdown was observed for CIDEC, which was reduced by 63% only (**Fig. 4.8b**).

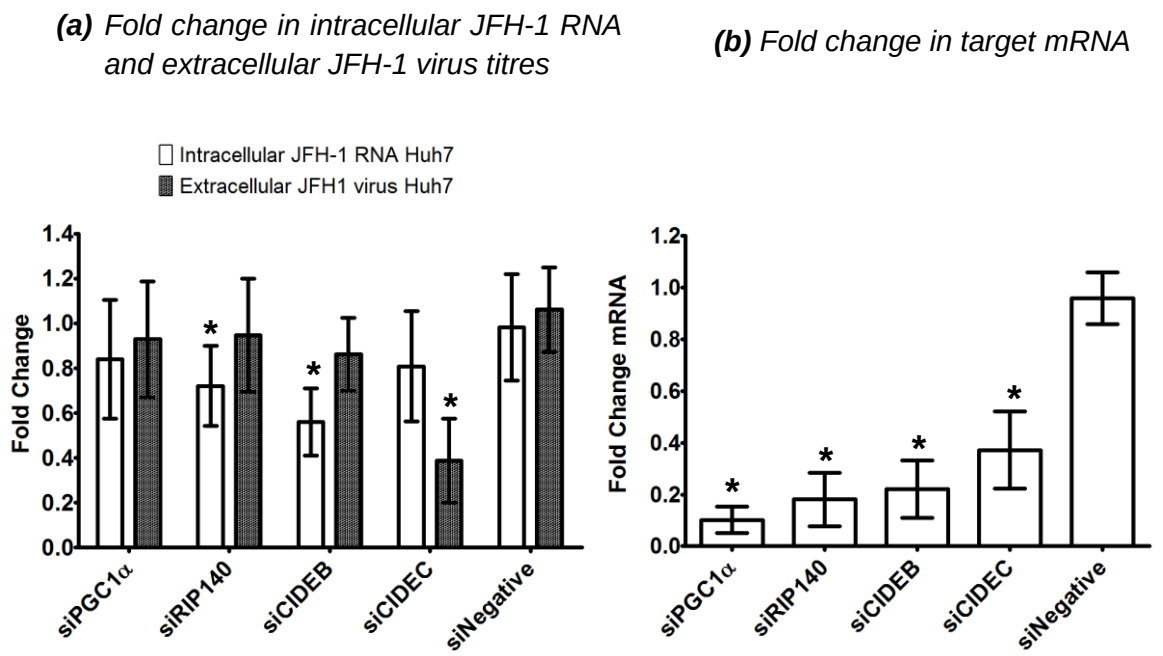


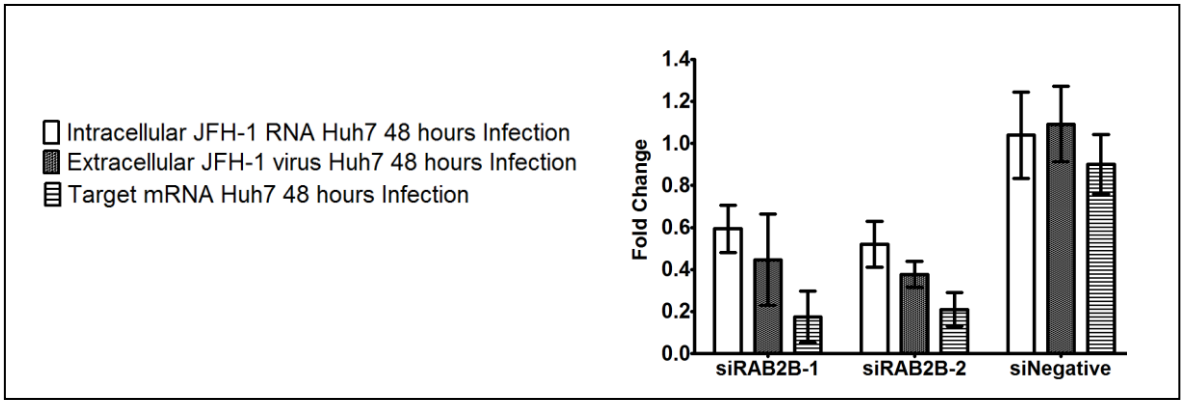
Figure 4.8 The effect of host gene silencing on JFH-1 RNA and virus titres 3

*Fold change in JFH-1 RNA abundance, JFH-1 virus titres and host gene expression following host gene knockdown in Huh7 cells. Huh7 cells were transfected with 50nM of target specific siRNA and 50nM of a negative control non-targeting siRNA for 48 hours. Cells were infected with JFH-1 (MOI = 3) for 48 hours. Intracellular RNA was extracted from the cells for qRT-PCR quantification of **(a)** JFH-1 RNA and **(b)** target mRNA**.** Media was also collected from the transfected cells for quantification of JFH-1 virus titres. Fold change data displayed represents the mean (±SD) of three independent experiments, each containing repeat siRNA transfections performed in duplicate (N=6). The target specific siRNAs causing a statistically significant knockdown (p value ≤ 0.05) of JFH-1 RNA, JFH-1 virus titres and target gene expression in comparison to the negative control siRNA are indicated by an asterisk (*). P values were calculated using a two-tailed unpaired T test in Graphpad Prism.*

4.2.3 The effect of individual siRNA molecules on JFH-1 replication and secretion

Investigating the effect of host gene knockdown on JFH-1 replication and secretion enabled identification of host factors that may be required during the JFH-1 replication cycle (**Fig. 4.6, 4.7 and 4.8**). In the assays performed, host factors were silenced using a pool of siRNA molecules. To investigate whether the effects observed were reproducible, the siRNA molecules were also transfected individually at a final concentration of 25nM. Individual siRNA molecules targeting the expression RAB2B, RAB4A, RAB11B, Staufen1, TXNIP, CYP1A1 and RAB27B were tested for their effects on the replication and secretion of JFH-1 in Huh7 cells infected for 48 hours (**Fig. 4.9**). An additional third siRNA was also tested against TXNIP and Staufen, as knockdown of these targets had significant effects on JFH-1 replication and secretion.

For the majority of the host factors targeted, each of the individual siRNAs tested had a similar effect on the JFH-1 replication cycle. For example, silencing RAB2B and RAB4A reduced JFH-1 RNA levels by 40% to 50% and JFH-1 virus titres by 55% to 60% with either of the individual siRNAs tested. Silencing Staufen1 with the individual siRNAs consistently reduced JFH-1 RNA levels by 30% to 40% and JFH-1 virus titres by 65% to 70%. However, for some of the individual siRNAs tested, greater variation was observed. For example, the TXNIP targeting siRNAs had variable effects on the JFH-1 replication cycle, with siTXNIP-1 reducing the JFH-1 RNA levels by 60% compared to the 45% reduction observed with siTXNIP-2 and siTXNIP-3. The RAB11B targeting siRNAs also had variable effects, as siRAB11B-1 reduced JFH-1 RNA levels by 40% compared to the 65% reduction observed with siRAB11B-2. This variation may be partially explained by differences in the efficiency of target gene knockdown, as siTXNIP-1 reduced TXNIP expression to a greater extent than siTXNIP-2 and siTXNIP-3, and siRAB11B-2 reduced RAB11B expression to a greater extent than siRAB11B-1.



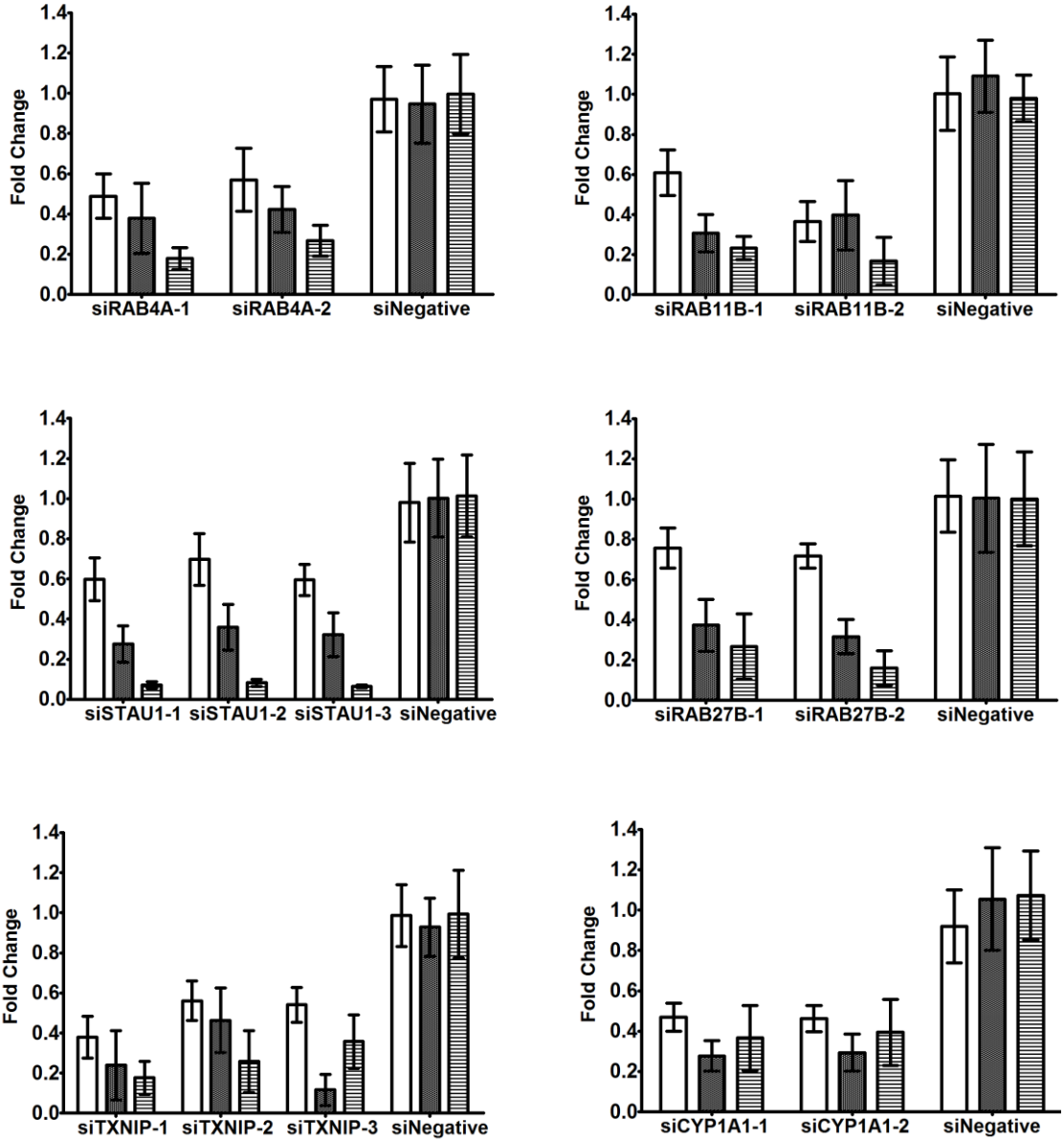


Figure 4.9 The effect of individual siRNAs on JFH-1 RNA and virus titres

Fold change in JFH-1 RNA abundance, JFH-1 virus titres and host gene expression following host gene knockdown in Huh7 cells. Huh7 cells were transfected with 25nM of individual target specific siRNAs and 25nM of a negative control non-targeting siRNA for 48 hours. Cells were infected with JFH-1 (MOI = 3) for 48 hours. Intracellular RNA was extracted from the cells for qRT-PCR quantification of JFH-1 RNA and target mRNA. Media was also collected from the transfected cells for quantification of JFH-1 virus titres. Fold change data displayed represents the mean (±SD) of three independent experiments, each containing repeat siRNA transfections performed in duplicate (N=6). The knockdown of JFH-1 RNA abundance, JFH-1 virus titres and target gene expression achieved with all the target-specific siRNAs was statistically significant with a p value ≤ 0.05, calculated using a two-tailed unpaired T test in Graphpad Prism.

4.3 Testing siRNA molecules for non-specific effects on JFH-1 replication

Before continuing to investigate the effects observed through siRNA target knockdown, several essential control assays were performed to check whether any of the siRNA molecules could interfere non-specifically with the JFH-1 replication cycle. These assays tested for effects of siRNA transfection on the viability of cells, as significant reduction in cellular viability may impair JFH-1 replication and secretion. In addition, the effect of siRNA transfection on the dsRNA interferon pathway was also tested, as transfection of siRNA molecules can induce an antiviral interferon response in cells [297].

4.3.1 Cellular viability analysis

The effect of host target knockdown on cellular viability was investigated using the alamar blue assay. Huh7 and Huh7.5 cells were transfected with pools of target specific siRNA molecules, the negative control non-targeting siRNA, Lipofectamine 2000 reagent only or transfection medium only. Alamar blue was used to investigate the viability of transfected cells at 24, 48 and 72 hours post-transfection (**Fig. 4.10**). None of the siRNAs tested had a significant effect on the viability of either Huh7 or Huh7.5 cells when compared to the negative control cells.

In addition to testing the effects of pooled siRNA molecules on cellular viability, the effect of individual siRNAs on the viability of Huh7 cells was also tested including the multiple siRNAs used to target CYP1A1, Staufen1 and TXNIP (**Fig. 4.11a**) and the single siRNAs used to target PGC1α, RIP140, CIDEB, CIDEC (**Fig. 4.11b**). Little effect was observed on Huh7 cell viability as a result of transfection, with the exception of the siRNAs targeting Staufen1, TXNIP and CIDEB, which reduced cell viability by 20% at all the time-points tested.

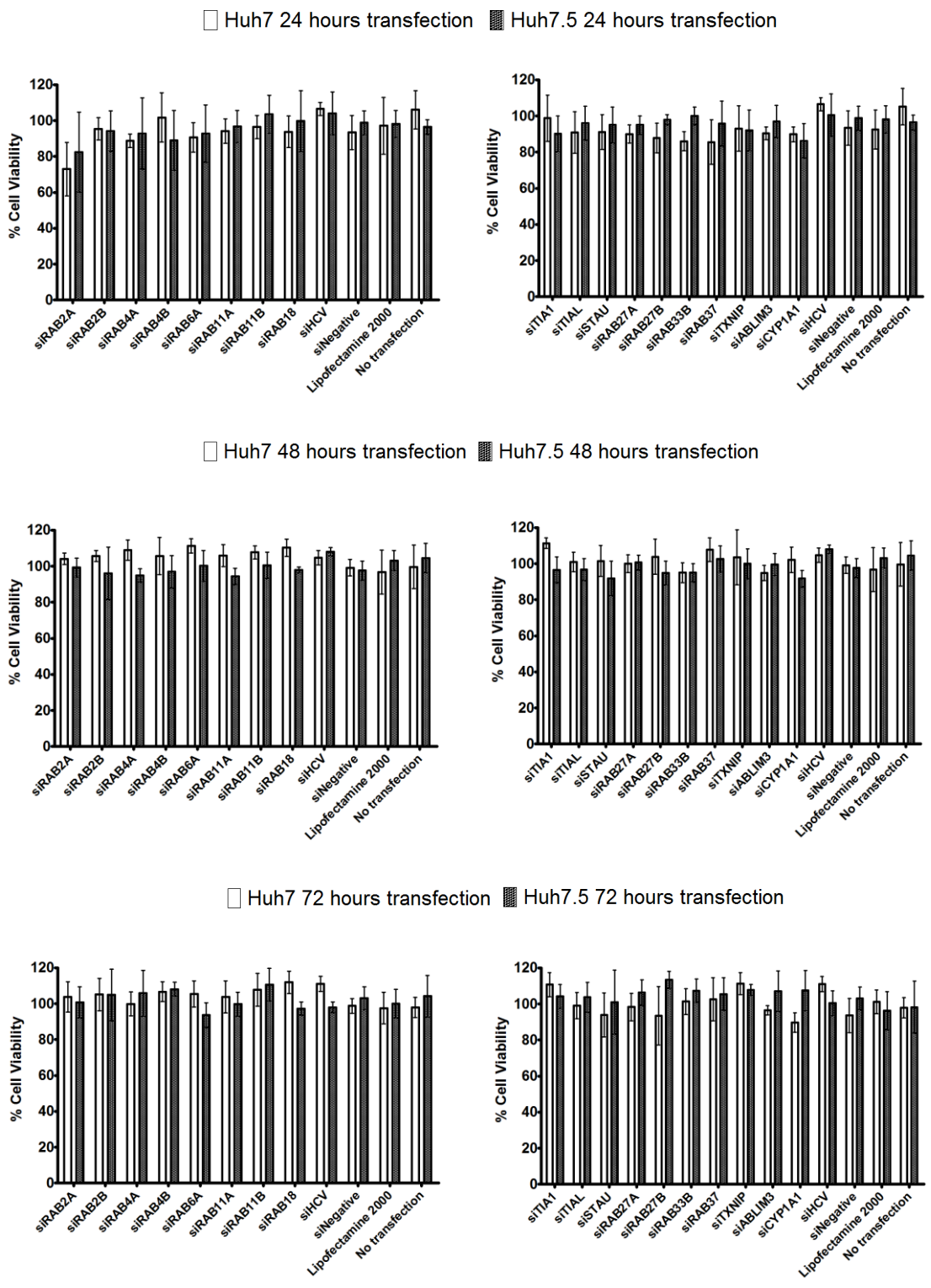


Figure 4.10 Pools of target siRNAs do not significantly alter cell viability

Percentage viability of cells transfected with pools of target specific siRNA molecules. Huh7 (white bars) and Huh7.5 cells (grey bars) were transfected with 50nM pools of target specific siRNA (25nM siRNA-1 and 25nM siRNA-2),50nM of a negative control non-targeting siRNA, Lipofectamine 2000 reagent only or transfection medium only. Cell viability was measured using the alamar blue assay at 24, 48 and 72 hours post-transfection. Percentage cell viability data displayed represents the mean (±SD) of two independent experiments, each containing repeat siRNA transfections performed in triplicate (N=6).

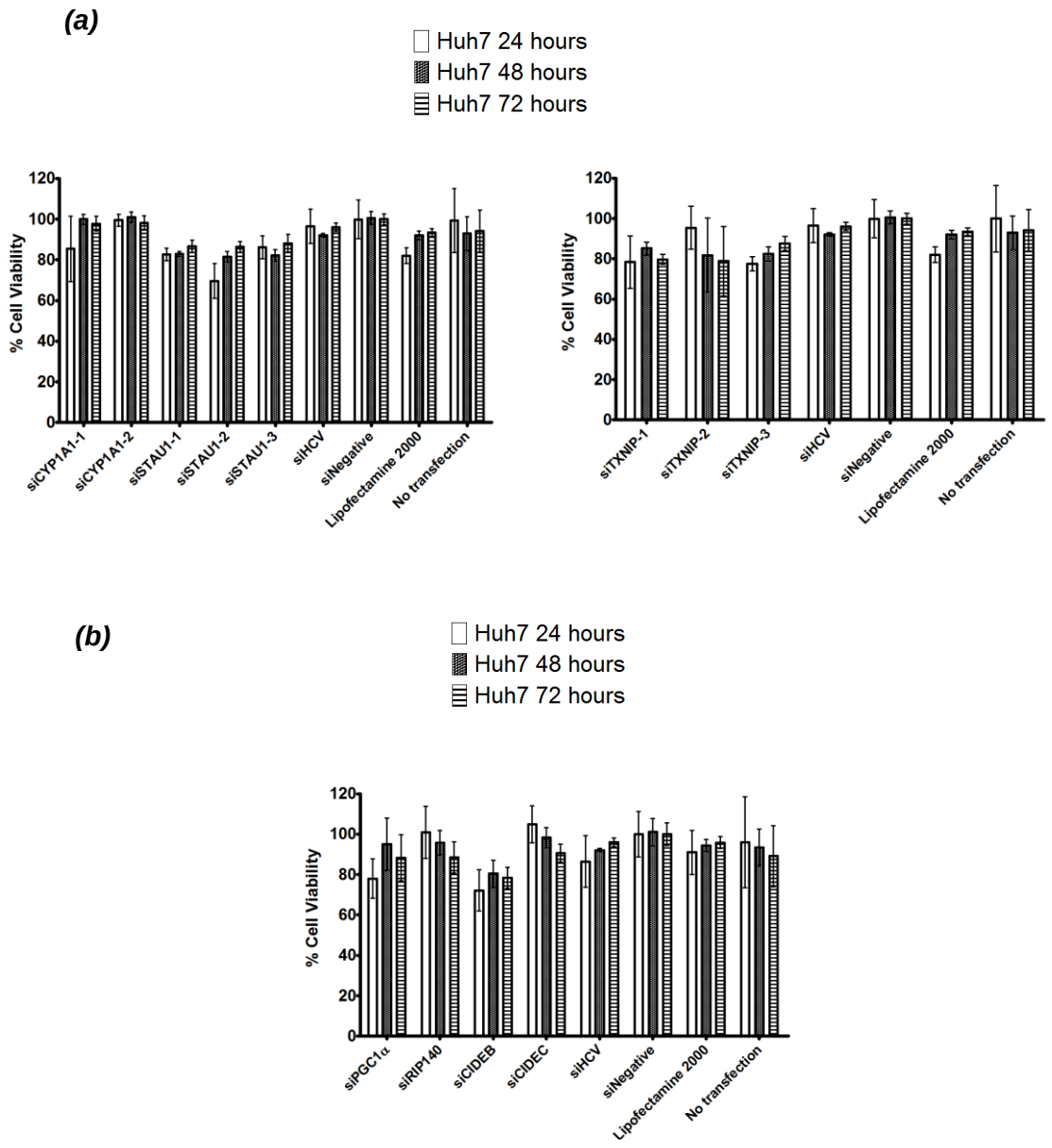


Figure 4.11 Individual siRNAs do not significantly alter cellular viability

Percentage viability of cells transfected with individual target specific siRNA molecules. Huh7 cells were transfected with individual target specific siRNAs, a negative control non-targeting siRNA, Lipofectamine 2000 reagent only or transfection medium only. Target specific siRNAs included: ***(a)*** *25nM of individual siRNAs targeting CYP1A1, STAU1 and TXNIP and* ***(b)*** *50nM of individual siRNAs targeting PGC1α, RIP140, CIDEB and CIDEC. Cell viability was measured at 24 (white bars), 48 (grey bars) and 72 hours (striped bars) post-transfection using the alamar blue assay. Percentage cell viability data displayed represents the mean (±SD) of two independent experiments, each containing repeat siRNA transfections performed in triplicate (N=6).*

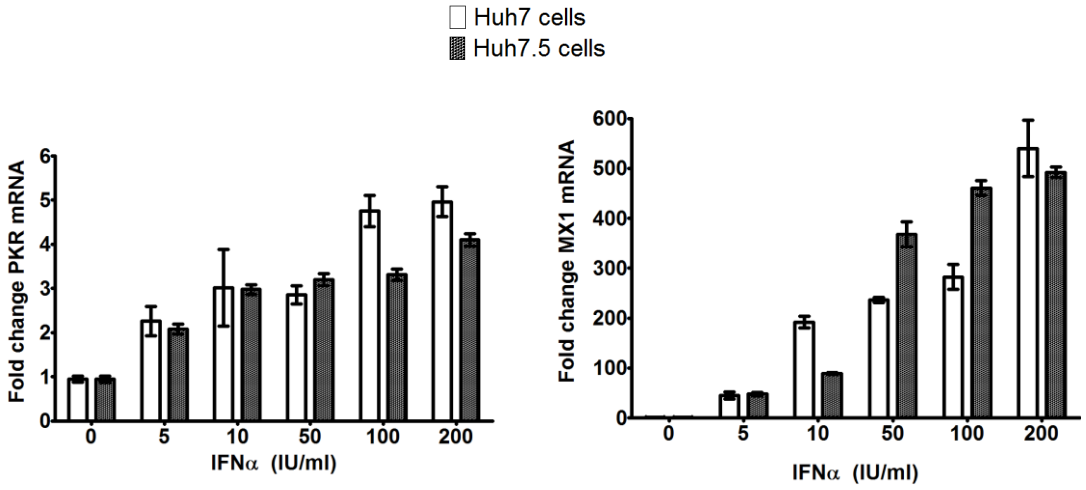
4.3.2 Quantitative PCR analysis of the dsRNA interferon response

To investigate whether transfection of the target specific siRNA molecules resulted in activation of a double-stranded RNA (dsRNA) interferon response, siRNA molecules were tested for their ability to upregulate the expression of interferon stimulated genes (ISG), including PKR (protein kinase R) and MX1 (myxovirus resistance 1) [298].

Before testing the target specific siRNAs, Huh7 and Huh7.5 cells were stimulated with IFNα or transfected with poly (I:C) (a dsRNA analogue) to determine the nature of the interferon response in these cells [299, 300]. Investigation of ISG expression was performed at 48 hours post-treatment using qRT-PCR, comparing the cells treated with IFNα to untreated cells; and the cells transfected with poly (I:C) to cells transfected with Lipofectamine 2000 only and transfection medium only (**Fig. 4.12**).

Treatment of cells with IFNα induced the largest interferon response in both cell types. For example, Huh7 cells treated with 200IU/ml of IFNα had a 5 fold increase in PKR expression and a 500 fold increase in MX1 expression (**Fig. 4.12a**). By comparison, Huh7 cells transfected with 100ng of poly (I:C) had a 2.5 fold increase in PKR expression and a 45 fold increase in MX1 expression (**Fig. 4.12b**). In Huh7.5 cells, IFNα treatment induced a similar ISG response as the Huh7 cells, with a 4 fold increase in PKR expression and a 450 fold increase in MX1 expression (**Fig. 4.12a**). However, Huh7.5 cells demonstrated little response to poly (I:C) treatment, as the expression of PKR did not alter and the expression of MX1 was upregulated by 2 fold in the Huh7.5 cells transfected with 100ng poly (I:C) (**Fig. 4.12b**). These findings indicate that although the Huh7 and Huh7.5 cells had a similar ISG transcriptional response to IFNα, the Huh7.5 cells had a much weaker response to poly (I:C) treatment than the Huh7 cells.

***(a)** Interferon alpha (IFNα) treatment of Huh7 and Huh7.5 cells*



***(b)** Poly (I:C) treatment of Huh7 and Huh7.5 cells*

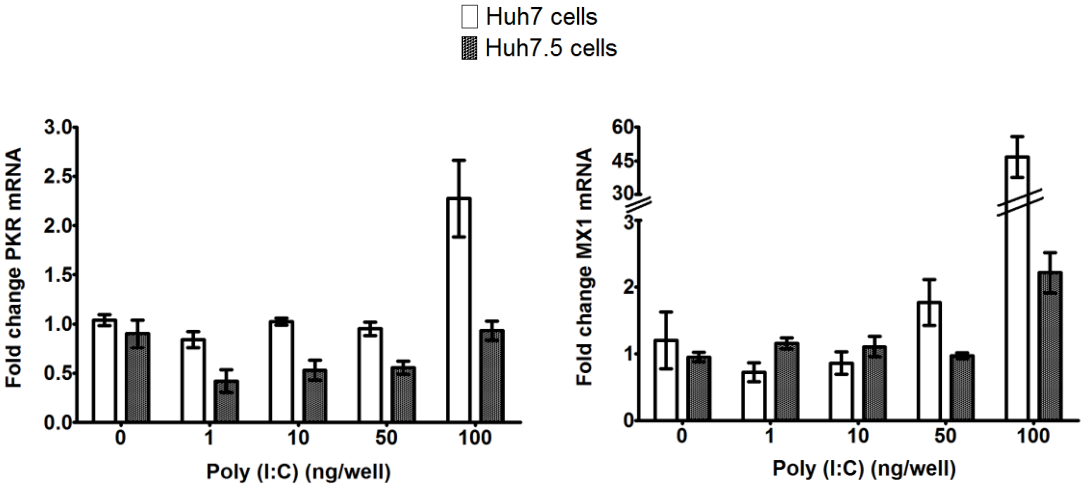


Figure 4.12 IFNα and poly (I:C) treatment induces ISG expression

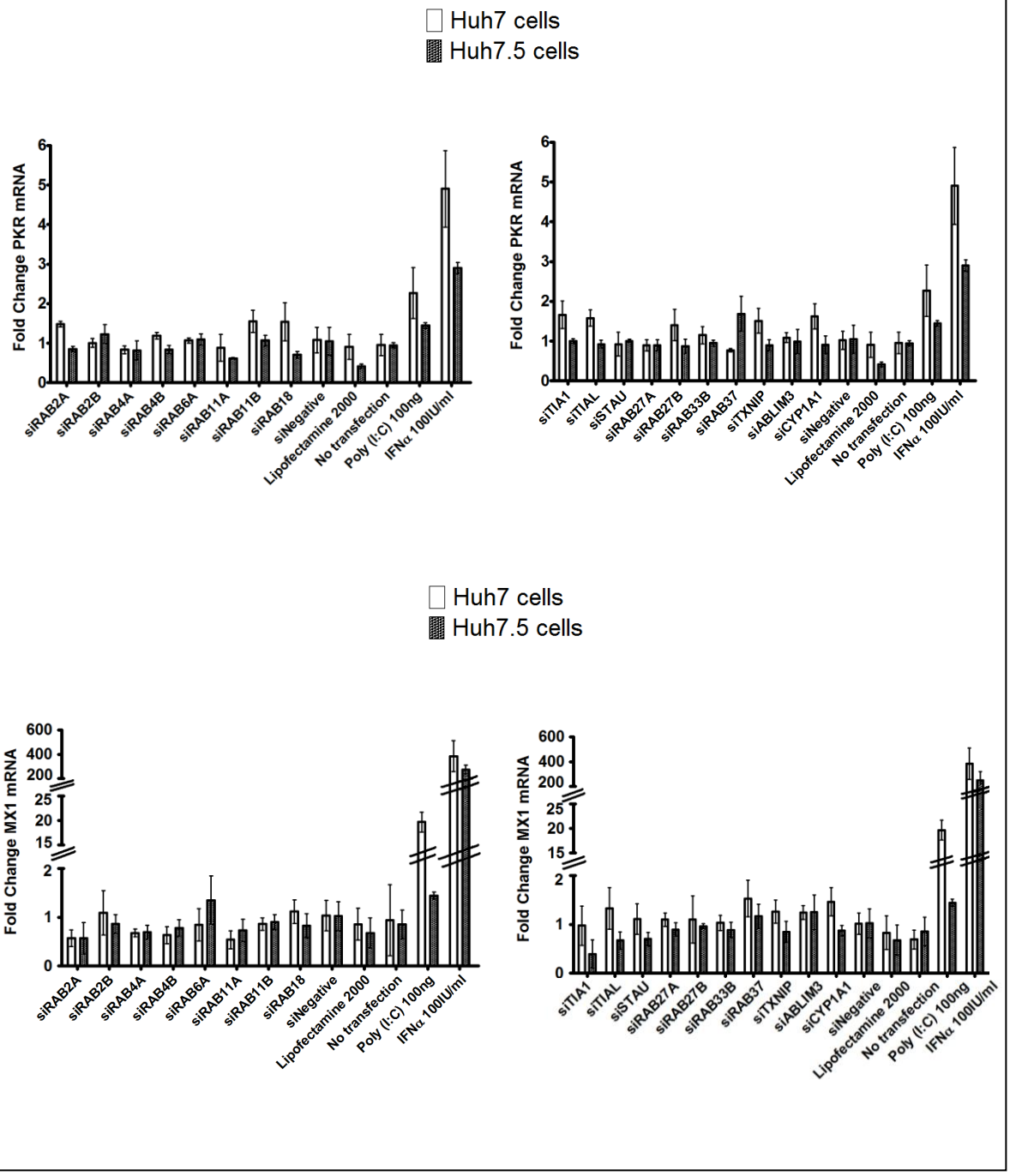
***(a)** Fold change in ISG expression following treatment of Huh7 and Huh7.5 cells with IFNα. Huh7 (white bars) and Huh7.5 cells (grey bars) were treated with 5, 10, 50, 100 and 200IU/ml of IFNα for 48 hours. Negative control cells (0 IU/ml IFNα) were incubated in DMEM growth medium that did not contain IFNα. Intracellular RNA was extracted from the cells for qRT-PCR quantification of PKR and MX1 mRNA. **(b)** Fold change in ISG expression following transfection of Huh7 (white bars) and Huh7.5 cells (grey bars) with poly (I:C). Huh7 and Huh7.5 cells were transfected with 1, 10, 50 and 100ng poly (I:C) per well (600µl total volume) using Lipofectamine 2000 for 48 hours. Negative control cells (0ng poly (I:C)) were transfected with Lipofectamine 2000 alone and transfection medium alone. Intracellular RNA was extracted from the cells for qRT-PCR quantification of PKR and MX1 mRNA. An average of the data collected for the cells transfected with Lipofectamine 2000 only or transfection medium only was used to generate the 0ng poly (I:C) data point. Fold change expression data displayed represents the mean (±SD) of a single experiment with repeat treatments performed in triplicate (N=3).*

Having demonstrated that stimulation of an interferon response can be successfully detected through qRT-PCR analysis of ISG expression. The siRNA molecules were tested for their ability to stimulate a dsRNA interferon response. Target specific siRNA molecules were transfected either as a pool in both Huh7 and Huh7.5 cells, or individually in Huh7 cells for 48 hours. The effect of siRNA transfection on ISG expression was compared to that observed in cells transfected with a negative control non-targeting siRNA, Lipofectamine 2000 reagent only and transfection medium only. Cells were also treated with 100IU/ml IFNα and 100ng poly (I:C) as positive controls for the experiment.

Target specific siRNAs transfected as a pool included those targeting the expression of RAB2A/B, RAB4A/B, RAB6A, RAB11A/B, RAB18, TIA1, TIAL, Staufen1, RAB27A/B, RAB33B, RAB37, TXNIP, ABLIM3 and CYP1A1 (**Fig. 4.13a**). None of the siRNA pools tested had a major effect on the expression of PKR or MX1. On the occasions where an siRNA pool did increase ISG expression, the effect was not consistent for both the ISGs tested. For example, the pool of siRNAs targeting TXNIP expression caused a 1.5 fold increase in PKR expression, but only a 1.2 fold increase in MX1 expression in Huh7 cells. The changes in ISG expression were also very small in comparison to the effects of the positive control treatments, as IFNα treatment induced a 5 fold increase in PKR expression and a 400 fold increase in MX1 expression, whilst poly (I:C) treatment induced a 2.2 fold increase in PKR expression and a 20 fold increase in MX1 expression in Huh7 cells.

Target specific siRNAs transfected individually included those targeting the expression of PGC1α, RIP140, CIDEB, CIDEC, TXNIP, CYP1A1 and Staufen1 (**Fig. 4.13b**). Little effect was observed on ISG expression when testing the PGC1α, RIP140, CIDEB and CIDEC siRNAs. Greater fluctuation was observed when testing individual siRNAs targeting TXNIP, CYP1A1 and Staufen1. None of the siRNAs caused significant effect on the expression of the ISGs, although siSTAU1-1 and siSTAU1-3 did consistently upregulate ISG expression by around 1.8 fold. Again, these effects were minimal when compared to the effects of IFNα and poly (I:C) on the expression of ISGs.

(a) *The effect of siRNA pools on ISG expression in Huh7 and Huh7.5 cells*



***(b)** The effect of individual siRNAs on ISG expression in Huh7 cells*

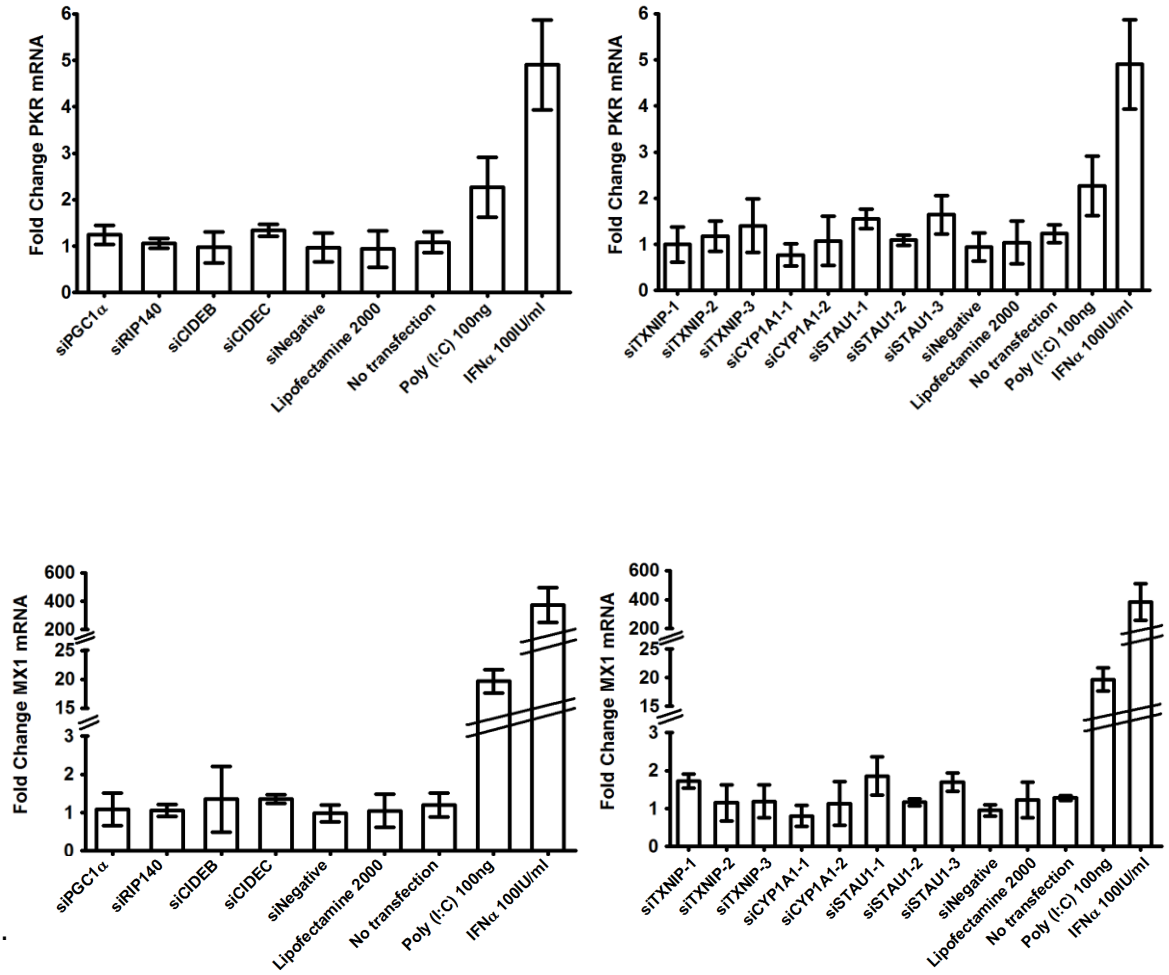


Figure 4.13 Target specific siRNAs do not significantly alter ISG expression

*Fold change in ISG expression following transfection of Huh7 and Huh7.5 cells with target specific siRNA molecules. Transfection was performed on **(a)** Huh7 (white bars) and Huh7.5 cells (grey bars) using pools of target specific siRNAs (25nM siRNA1 and 25nM siRNA2), 50nM of a negative control non-targeting siRNA, Lipofectamine 2000 reagent only and transfection medium only, and **(b)** Huh7 cells with 25nM of individual target specific siRNAs (TXNIP, CYP1A1 and STAU1), 50nM of individual target specific siRNAs (PGC1α, RIP140, CIDEB and CIDEC), 25nM and 50nM of a negative control non-targeting siRNA, Lipofectamine 2000 reagent only and transfection medium only. Cells were also treated with 100IU/ml IFNα and 100ng/well poly (I:C) as positive controls. At 48 hours post-transfection, intracellular RNA was extracted from the cells for qRT-PCR quantification of PKR and MX1 mRNA. Fold change data displayed represents the mean (±SD) of two independent experiments, each containing repeat siRNA transfections performed in triplicate (N=6).*

4.4 Quantification of JFH-1 proteins following host gene knockdown

To further investigate the results obtained from the siRNA silencing screen, the effect of host gene knockdown on JFH-1 protein abundance was investigated. Huh7 cells transfected with target specific siRNAs were infected with JFH-1 for 48 hours and protein lysates were extracted for western blot analysis of JFH-1 core and NS3 proteins. Each blot was also tested for the presence of the host protein, tubulin, which was used to normalise the blot quantification data.

The effect of host gene silencing on the intracellular abundance of JFH-1 proteins was investigated for the genes encoding RAB2B, RAB4A, RAB11B, RAB27B and CYP1A1 (**Fig. 4.14a-c**). Huh7 cells transfected with individual siRNAs targeting the expression of RAB2B, RAB11B and CYP1A1 had reduced intracellular levels of JFH-1 core and NS3 proteins compared to cells transfected with a negative control non-targeting siRNA (NT). By comparison, the fold reduction observed in core and NS3 protein abundance was much smaller in the Huh7 cells transfected with siRNAs targeting the expression of RAB4A and RAB27B. Overall, the effects observed were consistent with the results obtained for the siRNA knockdown assay investigating the effect of host gene silencing on JFH-1 RNA abundance and JFH-1 virus titres (**Fig. 4.9**). One exception was the effect of RAB4A silencing, which reduced the levels of JFH-1 RNA and JFH-1 virus titres significantly, but had a much less significant effect on the abundance of JFH-1 proteins.

For the siRNAs targeting RAB2B and CYP1A1, a more significant reduction was observed in the abundance of HCV core protein than the abundance of HCV NS3. For example, an 80% reduction was observed in core protein abundance when silencing RAB2B compared to a 30% reduction in NS3 abundance. When silencing CYP1A1, a 60% to 70% reduction was observed in core protein abundance, whilst a 30% to 40% reduction was observed in NS3 abundance.

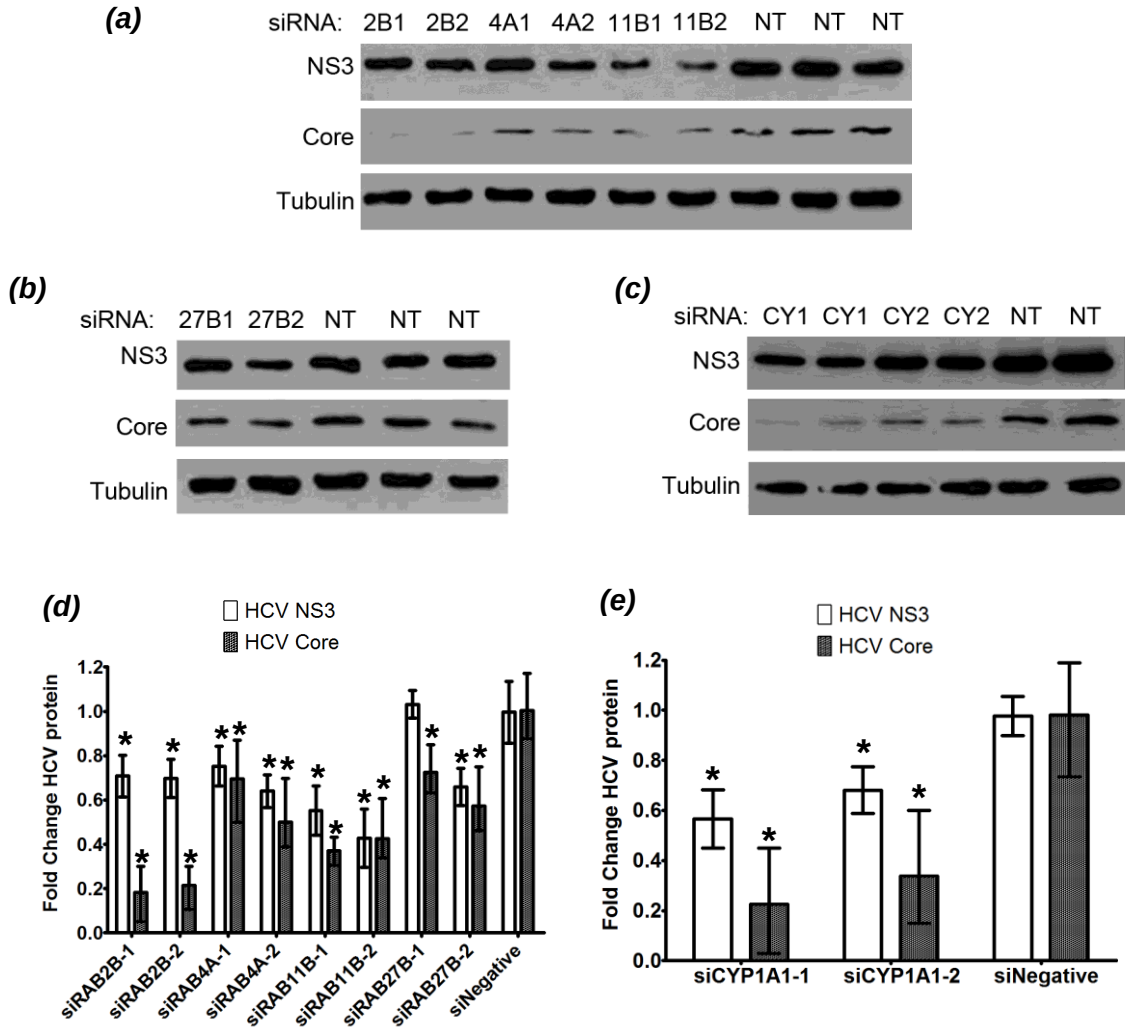


Figure 4.14 Host gene knockdown alters JFH-1 protein abundance

(a-c) *Western blot analysis of JFH-1 core and NS3 proteins following transfection of JFH-1 infected Huh7 cells with target specific siRNAs. Huh7 cells were transfected with 25nM of individual siRNAs targeting* ***(a)*** *RAB2B (2B1 and 2B2), RAB4A (4A1 and 4A2) and RAB11B (11B1 and 11B2)* ***(b)*** *RAB27B (27B1 and 27B2) and* ***(c)*** *CYP1A1 (CY1 and CY2) for 48 hours. Negative control cells were transfected with 25nM of a negative control non-targeting siRNA (NT). The transfected cells were infected with JFH-1 (MOI = 3) for 48 hours and lysed using 0.5% Triton X-100 lysis buffer. Western blot analysis was performed with 25µg of each protein lysate. Blots shown are representative of the results obtained from a single transfection experiment.* ***(d/e)*** *Fold change in core and NS3 protein abundance following host gene silencing in JFH-1 infected cells. Fold change was calculated by comparing protein band intensities quantified for JFH-1 infected Huh7 cells transfected with siRNAs targeting* ***(d)*** *RAB2B, RAB4A, RAB11B and RAB27B and* ***(e)*** *CYP1A1 to JFH-1 infected Huh7 cells transfected with a negative control siRNA. Protein band intensities were quantified using Image J, and normalised using tubulin. Fold change in protein abundance shown represents mean fold change (and replicate range) calculated using repeat band intensity quantifications of single bands (siRAB2B-1/-2, siRAB4A-1/-2, siRAB11B-1/-2 and siRAB27B-1/-2) or duplicate bands (siCYP1A1-1/-2). All target specific siRNAs caused a statistically significant knockdown (p value ≤ 0.05) of JFH-1 protein abundance (indicated by an asterisk (*)) with the exception of siRAB27B-1.*

Quantification of JFH-1 NS3 protein abundance following TXNIP knockdown

To investigate the effect of TXNIP silencing on JFH-1 protein expression, western blotting was used to investigate JFH-1 NS3 protein abundance in JFH-1 infected Huh7 cells transfected with TXNIP siRNAs either in a pool (e.g. siTXNIP-1 and siTXNIP-2) (**Fig. 4.15a**) or individually (e.g. siTXNIP-1, siTXNIP-2 or siTXNIP-3) (**Fig. 4.15b**). The HCV siRNA targeting the JFH-1 genome was included as a positive control for the experiment. In addition, blotting for the TXNIP protein was also performed to determine the efficiency of TXNIP knockdown; this was performed using the mouse anti-TXNIP antibody optimised in **Figure 3.18**.

Quantification of protein abundance was performed to determine the fold change in TXNIP and JFH-1 NS3 proteins as a result of TXNIP knockdown (**Fig. 4.15c**). Efficient silencing of TXNIP protein expression was observed following transfection of Huh7 cells with TXNIP siRNAs when they were used either as a pool or individually. Silencing the expression of TXNIP with the individual and pooled siRNAs caused a reduction in the abundance of JFH-1 NS3. The HCV siRNA caused complete inhibition of JFH-1 genome translation, as no JFH-1 NS3 was detected in the siHCV transfected cells (**Fig. 4.15a**).

When using the individual siRNAs slight variation was observed in the extent to which TXNIP silencing reduced JFH-1 protein abundance. For example, an 80% reduction was observed in the abundance of NS3 protein when TXNIP was silenced using siTXNIP-1, compared to the 60% and 55% reduction observed when using siTXNIP-2 and siTXNIP-3, respectively. These results reflect the findings observed when the individual siRNAs were tested for their effects on JFH-1 RNA abundance and virus titres (**Fig. 4.9**). There was no obvious difference in the efficiency of TXNIP protein silencing between the three siRNAs that might explain the differences in their effects on JFH-1 NS3 abundance.

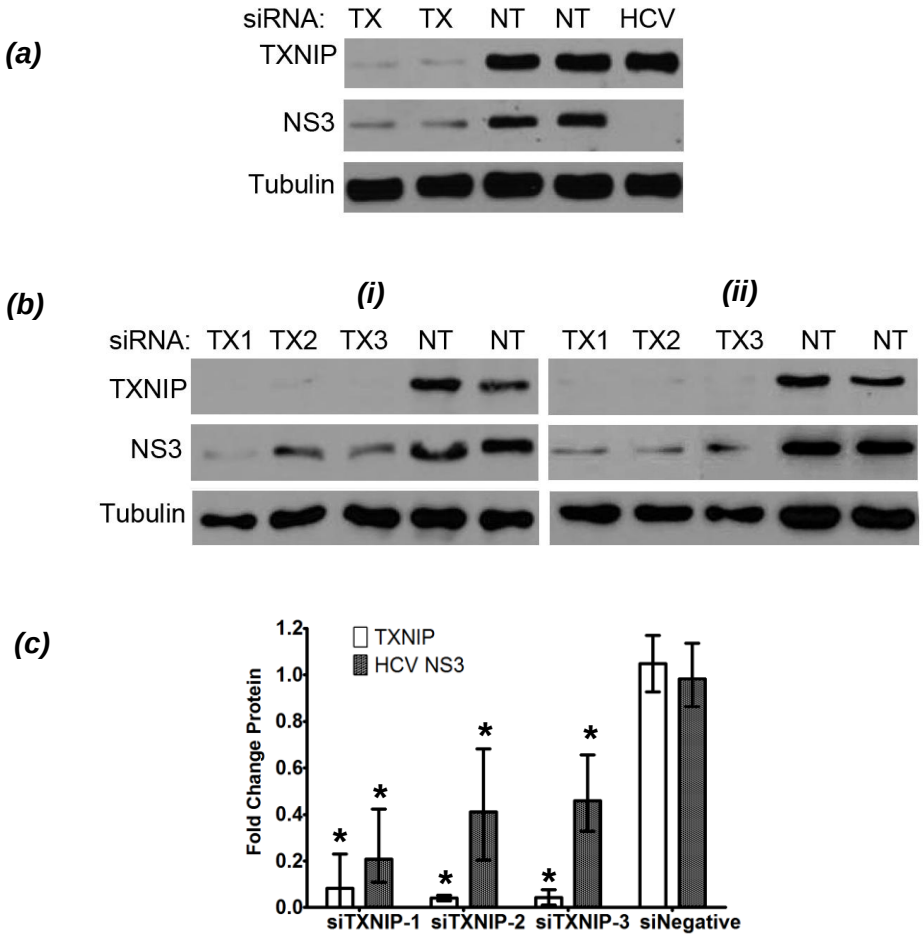


Figure 4.15 TXNIP protein knockdown reduces JFH-1 NS3 protein abundance

(a) *Western blot analysis of TXNIP and JFH-1 NS3 proteins following transfection of JFH-1 infected Huh7 cells with TXNIP siRNAs. Huh7 cells were transfected with 50nM of pooled TXNIP siRNAs (TX) (siTXNIP-1 and siTXNIP-2), 50nM of a negative control non-targeting siRNA (NT) and 50nM of the HCV siRNA (HCV) for 48 hours. Transfected cells were infected with JFH-1 (MOI = 3) for 48 hours and lysed using 0.5% Triton X-100 lysis buffer. Western blot analysis was performed with 25µg of each protein lysate.* ***(b)*** *Western blot analysis of TXNIP and JFH-1 NS3 proteins following transfection of JFH-1 infected Huh7 cells with individual TXNIP siRNAs. Huh7 cells were transfected with 25nM of TXNIP siRNAs (siTXNIP-1 (TX1), siTXNIP-2 (TX2) or siTXNIP-3 (TX3)) and 25nM of a negative control non-targeting siRNA (NT) for 48 hours. Transfected cells were infected with JFH-1 (MOI = 3) for 48 hours and lysed using 0.5% Triton X-100 lysis buffer. Western blot analysis was performed with 25µg of each protein lysate. Blots (i) and (ii) represent the results obtained in two transfection experiments.* ***(c)*** *Fold change in TXNIP and NS3 protein abundance following TXNIP knockdown in JFH-1 infected cells. Fold change was calculated by comparing protein band intensities quantified for JFH-1 infected Huh7 cells transfected with individual TXNIP siRNAs to JFH-1 infected Huh7 cells transfected with a negative control siRNA. Protein band intensities were quantified using Image J, and normalised using tubulin. Fold change in protein abundance represents mean fold change (and replicate range) calculated using repeat band intensity quantifications of the protein bands on blots i and ii. TXNIP siRNAs caused a statistically significant knockdown (p value ≤ 0.05) of JFH-1 protein abundance (indicated by an asterisk (*)). P values were calculated using a two-tailed unpaired T test in Graphpad prism.*

Quantification of JFH-1 protein abundance following Staufen1 knockdown

To investigate the effect of Staufen1 silencing on JFH-1 protein expression, western blotting was used to investigate JFH-1 core and NS3 protein abundance in JFH-1 infected Huh7 cells transfected with Staufen1 siRNAs either in a pool (e.g. siSTAU1-1 and siSTAU1-2) (**Fig. 4.16a**) or individually (e.g. siSTAU1-1, siSTAU1-2 or siSTAU1-3 (**Fig. 4.16b**). The effect of Staufen2 silencing on JFH-1 protein abundance was also tested to determine whether the gene homolog of Staufen1 was also required during the JFH-1 replication cycle (**Fig. 4.16a**).

Quantification of protein abundance was performed to determine the fold change in JFH-1 core and NS3 proteins as a result of Staufen1 knockdown (**Fig. 4.16c**). Silencing the expression of Staufen1 with the individual and pooled siRNAs reduced the abundance of JFH-1 core and NS3 proteins. Conversely silencing the expression of Staufen2 had no effect on JFH-1 NS3 protein abundance, indicating that it is unlikely to play a role in the JFH-1 replication cycle. Staufen2 mRNA abundance following transfection of the STAU2 siRNA was significantly reduced in comparison to cells transfected with a non-targeting siRNA (**Appendix A.17**). Similar to the results observed following knockdown of RAB2B and CYP1A1 (**Fig. 4.14d**), the fold reduction of JFH-1 core protein caused by Staufen1 silencing was much more significant than the fold reduction observed for the JFH-1 NS3 protein. For example, 95% reduction was observed in core with the siSTAU1-1 siRNA compared to 45% reduction observed in NS3. These differences were most significant with the siSTAU1-1 and siSTAU1-2 siRNA molecules (**Fig. 4.16c**).

To investigate the efficiency of Staufen1 protein knockdown, an anti-Staufen1 antibody was used in western blotting. The antibody was tested using a HepG2 cell lysate (the recommended positive control for the antibody), and lysates obtained from JFH-1 and mock infected Huh7 cells (**Fig. 4.17a**). In both HepG2 and Huh7 cell lysates, it was not possible to detect the protein isoforms (55KDa and 63KDa) expressed by the Staufen1 gene. Instead two non-specific protein bands were detected at 50KDa and 75KDa. The Staufen1 antibody was also tested using protein lysates obtained from Huh7 cells that had been transfected either with a pool of Staufen1 siRNAs or a negative control non-targeting siRNA (**Fig. 4.17b**). Protein band intensity did not alter in the presence of the Staufen1 siRNAs; this confirmed that the protein bands detected were non-specific, and that the antibody does not allow detection of the Staufen1 protein by western blotting.

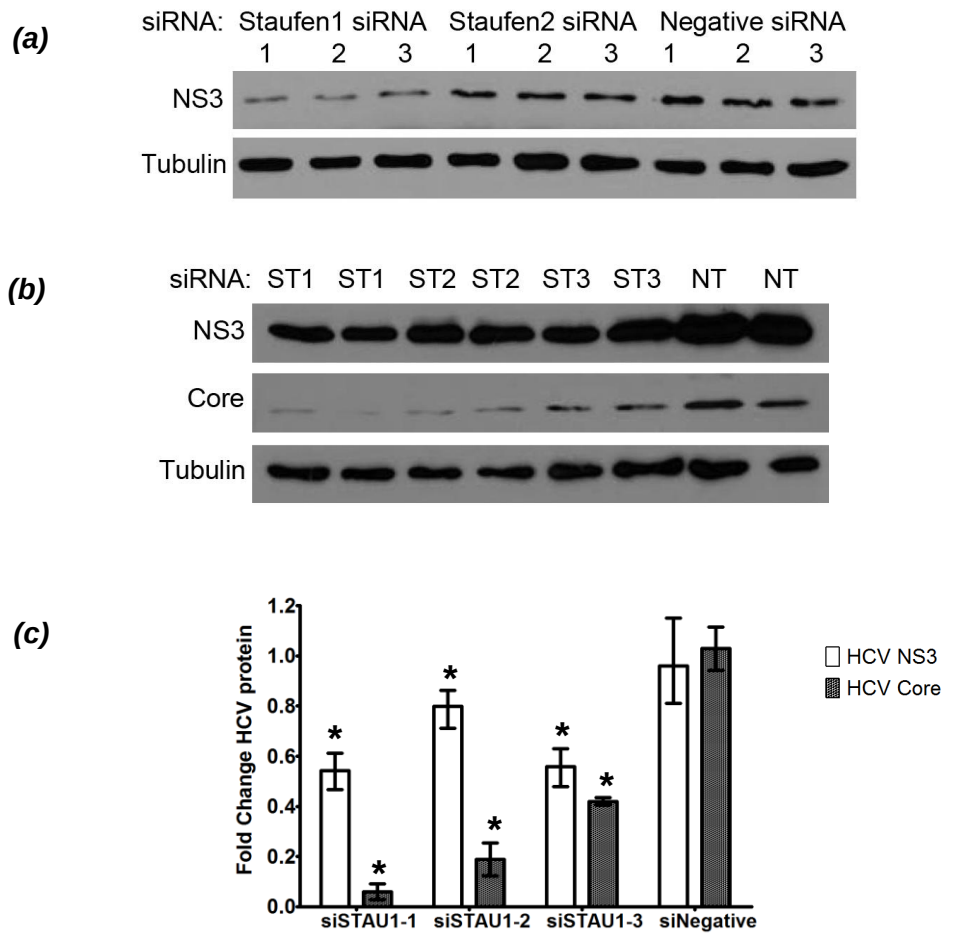
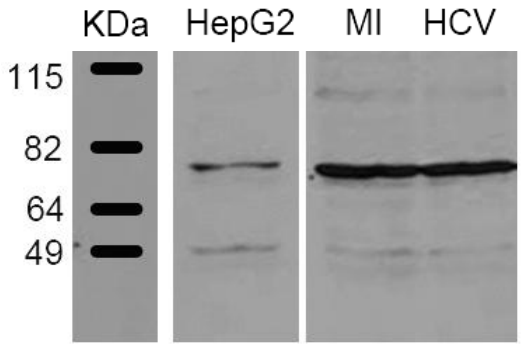


Figure 4.16 Staufen1 protein knockdown reduces JFH-1 protein abundance

(a) *Western blot analysis of JFH-1 NS3 following transfection of JFH-1 infected Huh7 cells with Staufen1 siRNAs. Huh7 cells were transfected with 50nM of pooled Staufen1 siRNAs (siSTAU1-1 and siSTAU1-2), 50nM of a Staufen2 siRNA and 50nM of a negative control non-targeting siRNA for 48 hours. Transfected cells were infected with JFH-1 (MOI = 3) for 48 hours and lysed using 0.5% Triton X-100 lysis buffer. Western blot analysis was performed with 25µg of each protein lysate.* ***(b)*** *Western blot analysis of JFH-1 core and NS3 proteins following transfection of JFH-1 infected Huh7 cells with individual Staufen1 siRNAs. Huh7 cells were transfected with 25nM of Staufen1 siRNAs (siSTAU1-1 (ST1), siSTAU1-2 (ST2) or siSTAU1-3 (ST3)) and 25nM of a negative control non-targeting siRNA (NT) for 48 hours. Transfected cells were infected with JFH-1 (MOI = 3) for 48 hours and lysed using 0.5% Triton X-100 lysis buffer. Western blot analysis was performed with 25µg of each protein lysate.* ***(c)*** *Fold change in JFH-1 core and NS3 protein abundance following Staufen1 knockdown in JFH-1 infected cells. Fold change was calculated by comparing protein band intensities quantified for JFH-1 infected Huh7 cells transfected with individual Staufen1 siRNAs to JFH-1 infected Huh7 cells transfected with a negative control siRNA. Protein band intensities were quantified using Image J, and normalised using tubulin. Fold change in protein abundance represents mean fold change (and replicate range) calculated using repeat band intensity quantifications of duplicate protein bands on blot (b). All Staufen1 siRNAs caused a statistically significant knockdown (p value ≤ 0.05) of JFH-1 protein abundance (indicated by an asterisk (*)). P values were calculated using a two-tailed unpaired T test in Graphpad prism.*

(a) *Staufen1 blotting in JFH-1 infected Huh7 cells and HepG2 cells*



(b) *Staufen1 blotting in STAU1 siRNA transfected Huh7 cells*

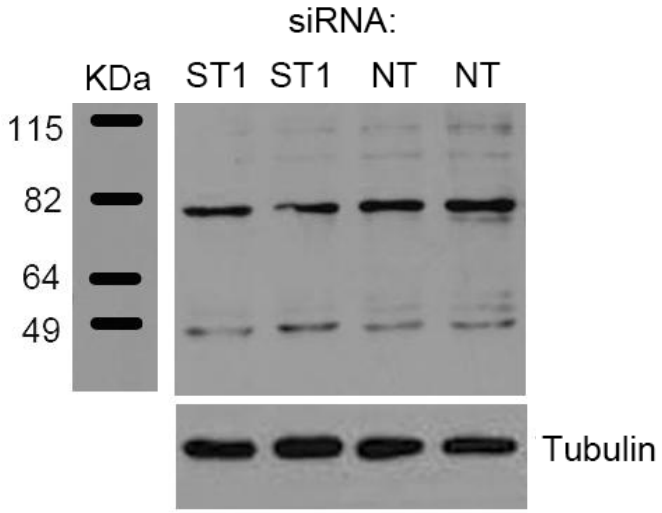


Figure 4.17 Anti-Staufen1 antibody does not detect Staufen1 isoforms

(a) *Western blotting of Staufen1 protein using cell lysates isolated from untreated HepG2 cells and JFH-1 infected Huh7 cells. Huh7 cells were infected with JFH-1 (MOI = 3) (HCV) or mock medium (MI) for 48 hours and the cells were lysed using 0.5% Triton X-100 lysis buffer. Untreated HepG2 cells were also lysed using 0.5% Triton X-100 lysis buffer. Western blot analysis was performed with 75µg of each protein lysate and the membrane was probed using the rabbit anti-Staufen1 antibody. Proteins bands detected at 50KDa and 75KDa do not correspond to Staufen1 isoforms (55KDa and 63KDa).* ***(b)*** *Western blotting of Staufen1 protein using cell lysates isolated from Huh7 cells transfected with Staufen1 siRNAs. Huh7 cells were transfected with 50nM of pooled Staufen1 siRNAs (siSTAU1-1 and siSTAU1-2) (ST1) and 50nM of a negative control non-targeting siRNA (NT) for 48 hours. The cells were lysed using 0.5% Triton X-100 lysis buffer. Western blot analysis was performed with 75µg of each protein lysate and the membrane was probed using antibodies that detect Staufen1 and tubulin. Proteins bands detected at 50KDa and 75KDa do not correspond to Staufen1 isoforms (55KDa and 63KDa).*

Chapter 4: Discussion

Optimisation of an siRNA knockdown assay to test the role of host factors in the HCV replication cycle

The protocol used for siRNA transfection of Huh7 cells was optimised using a positive control siRNA targeting GAPDH expression. This demonstrated that Lipofectamine 2000 was an effective transfection reagent for the Huh7 cell line (**Fig. 4.1**). Positive control siRNAs targeting the HCV genome and the RAB1B GTPase gene were also tested for their effects on JFH-1 replication and secretion. The siRNA targeting the HCV genome significantly reduced the replication and secretion of JFH-1 validating the protocols for the siRNA knockdown assay and quantification of JFH-1 RNA and JFH-1 virus titres (**Fig. 4.2**). The siRNA molecules targeting RAB1B had much more variable effects on the HCV replication cycle (**Fig. 4.5**). Although, RAB1B knockdown has previously been shown to reduce the replication of a J6/JFH-1 chimera by 85% [128], less significant effects were observed on the replication of JFH-1 when RAB1B silencing was performed. In general, RAB1B siRNAs that reduced RAB1B expression to the greatest extent had the most significant effect on JFH-1 RNA replication. This indicated that it is very important to achieve a high level of target knockdown and that small differences in the efficiency of knockdown can affect the results obtained. However, even the most effective siRNA which reduced RAB1B expression by 86% only reduced intracellular JFH-1 RNA levels by 50%. The inconsistency observed between the two studies may be attributable to the design of the experiment, as the cells were infected for 48 hours in this study compared to 72 hours in the previous study, and the virus strain used in this study was the genotype 2a JFH-1 virus compared to the genotype 2a J6/JFH-1 chimeric virus used in the previous study [128]. The J6/JFH-1 chimeric virus is known to have different replication kinetics to JFH-1 and this might affect the results obtained [138]. Different cell types were also used, as Huh7 cells were used in this study and Huh7.5 cells were used in the previous study; this may have further contributed to the differences observed. Despite these differences, the siRNA, siRAB1B3, used in this study had the same sequence as the most effective siRNA (duplex 9) used in the previous study [128].

The effect of siRNA knockdown on JFH-1 replication and secretion

To investigate the effect of host gene silencing on JFH-1 replication and secretion, each target gene was initially silenced using a pool of two siRNAs at a final concentration of 50nM (except for PGC1α, RIP140, CIDEB and CIDEC, which were targeted using a single siRNA). This concentration of siRNA was high enough for efficient knockdown of most target genes, with the exception of TIA1, TIAL1, CYP1A1 and ABLIM3 (**Fig. 4.6b, 4.7b and 4.8b**). The concentration of siRNA used in each pool was not raised above 50nM (or 25nM for a single siRNA molecule), as off-target effects can occur at high concentrations of siRNA. By comparison, most other published siRNA studies use between 25 and 75nM of siRNA to achieve maximal target knockdown without inducing off-target effects [30, 114, 116].

The effect of siRNA silencing was investigated using both Huh7 and Huh7.5 cells to test whether the host factor requirements of the HCV replication cycle differed between the two cell lines. The cells were also infected for different periods of time (24 versus 48 hours) to investigate whether a difference in the effect of host target knockdown could be observed. Several host targets were identified that had significant effects on JFH-1 replication and secretion. The siRNAs showing the most significant effects on the JFH-1 replication cycle included those targeting RAB2B, RAB4A, RAB11B, Staufen1 (**Fig. 4.6**), RAB27A/B, RAB33B, TXNIP, CYP1A1, ABLIM3 (**Fig. 4.7**) and CIDEC (**Fig. 4.8**). For most of the targets tested, consistent effects were observed with the assays performed in Huh7 and Huh7.5 cells indicating that the host factors involved in the HCV replication cycle do not differ between the two cell lines. However, in many cases greater effects were observed on JFH-1 replication and secretion in the cells infected for 24 hours compared to the cells infected for 48 hours. This finding did not reflect variation in the efficiency of host gene knockdown, as greater target knockdown was often observed at 48 hours post-infection than at 24 hours post-infection.

When comparing the effects of the different siRNA molecules on the JFH-1 replication cycle, two different patterns were observed. Firstly, some of the siRNA molecules significantly reduced both JFH-1 RNA and JFH-1 virus levels indicating that the host factors targeted may be required during an early phase of the JFH-1 replication cycle either for virus entry, genome translation or genome replication. The siRNA molecules with these effects included those targeting the expression of

RAB2B, RAB4A, RAB11B, RAB33B, CYP1A1, ABLIM3 and TXNIP. Secondly, some of the siRNA molecules reduced the levels of extracellular JFH-1 virus more significantly than the intracellular levels of JFH-1 RNA; this included the siRNAs targeting RAB27A/B, Staufen1 and CIDEC. The knockdown of these targets might have affected the processes of virus assembly or virus secretion rather than the rate at of genome replication. However, the siRNAs targeting Staufen1 and RAB27B also had a considerable effect on the intracellular JFH-1 RNA levels, indicating that these factors may play multiple different roles in the HCV replication cycle.

To further investigate the host genes that showed significant effects on the JFH-1 replication cycle, the siRNAs used in the siRNA pool were individually transfected (**Fig. 4.9**). For the majority of siRNAs tested, similar effects were observed on the levels of JFH-1 replication and secretion when the siRNAs were transfected individually or as a pool; this validated the target specific effects observed in the siRNA knockdown assay. However, there were some siRNAs that had inconsistent effects on the JFH-1 replication cycle when tested individually including the siRNAs targeting RAB11B and TXNIP. In both cases, little difference was observed in the efficiency of target knockdown with the individual siRNAs, although the siRNAs causing the greatest reduction in JFH-1 RNA and virus levels also reduced target expression by the greatest amount. It is possible that the rate of target knockdown may vary between the individual siRNAs tested, and this may alter the rate at which JFH-1 replication and secretion is suppressed. Further investigation into target mRNA abundance at 24, 48, 72 and 96 hours post-transfection would provide greater insight into the rate of target knockdown with each individual siRNA.

Several of the siRNA molecules tested for their effects on the JFH-1 replication cycle targeted host factors that belong to the Rab GTPase gene family. Most of the Rab proteins targeted have several isoforms such as RAB2A and RAB2B, RAB4A and RAB4B, RAB11A and RAB11B and RAB27A and RAB27B. Previously, these isoforms were thought to have overlapping functions; however, recent evidence suggests that many Rab GTPase isoforms may have distinct intracellular roles [294-296]. For this reason, the siRNA molecules targeting each Rab isoform were tested individually for their effects on the JFH-1 replication cycle. In support of this approach, the data obtained indicated that the siRNA

molecules targeting different Rab isoforms had very different effects on the JFH-1 replication cycle. For example, silencing the expression of RAB2A and RAB4B did not affect JFH-1 replication or secretion, whilst RAB2B and RAB4A silencing significantly reduced JFH-1 RNA levels and JFH-1 virus titres, indicating that specific Rab isoforms may be required during the HCV replication cycle.

Although different Rab protein isoforms often have variable intracellular roles, there are still examples of isoforms with overlapping functions [301, 302]. There are also several examples of Rab effector proteins that have a very broad specificity and can be activated by multiple different Rab GTPases [293]. Given the functional overlap observed between some Rab isoforms, the approach used in this siRNA knockdown assay may not have permitted identification of all HCV cofactors. If some of the Rab isoforms tested functionally overlap with others, then silencing the expression of these isoforms individually may not have effectively depleted Rab protein function in the transfected cells. In order to determine whether functionally overlapping Rab isoforms are required during the HCV replication cycle, it is necessary to simultaneously silence all the isoforms of each Rab protein. In this study, silencing RAB6A had little effect on the JFH-1 replication cycle. To confirm this finding, it will be important to investigate the effect of simultaneously silencing RAB6A, RAB6B and RAB6C genes. A recent study investigating the role of Rab proteins in the formation of the HCV membranous web indicated that a dominant negative RAB6 mutant reduced the correct formation of NS4B containing replication complexes; indicating a potential role for RAB6 in the HCV replication cycle [303]. Furthermore, other viruses have been shown to incorporate RAB6 into their replication cycles including HIV [304] and HMCV [305]. This illustrates the importance of performing further studies to investigate the effect that a combination isoform silencing approach would have on the HCV replication cycle.

Testing siRNA molecules for non-specific effects on JFH-1 replication

Before continuing to investigate the potential HCV cofactors identified, each siRNA was tested for its ability to stimulate a non-specific antiviral response that might account for the effects observed in the siRNA knockdown assay. The majority of the siRNAs tested did not affect cellular viability or induce a dsRNA interferon response. For those siRNA molecules that did reduce cellular viability (e.g. siRNAs targeting RAB2A, CIDEB, Staufen1 and TXNIP) the reduction observed never

exceeded 20%. A 20% reduction in viability is unlikely to significantly affect the rate of HCV replication; this is illustrated by the observation that several siRNAs which reduced cellular viability by 20% had no effect on either JFH-1 replication or JFH-1 secretion (e.g. siRNAs targeting RAB2A and PGC1α) (**Fig. 4.10 and 4.11**). Several of the siRNAs tested also induced minor increases in the expression of interferon stimulated genes (ISG) (e.g. siRNAs targeting Staufen1). However, the effect was generally inconsistent across the genes tested and expression was only ever stimulated by a maximum of 2 fold, which was much smaller than the fold change observed in the positive controls (**Fig. 4.13**).

To ensure accurate testing of the interferon response, Huh7 and Huh7.5 cells were also treated with IFNα and poly (I:C). When treating the Huh7 cells with these controls, IFNα induced a stronger increase in ISG expression than the poly (I:C). This may be due to direct stimulation of PKR and MX1 expression following activation of the JAK-STAT pathway by IFNα [299]. When the cells are treated with poly (I:C), the expression of PKR and MX1 is not directly stimulated. Instead, poly (I:C) must first activate the dsRNA recognition molecule, melanoma differentiation associated 5 (MDA5), which stimulates the production and secretion of IFNα and IFNβ [306]. Secreted IFNα and IFNβ are then able to bind to cell surface interferon receptors to stimulate the JAK-STAT pathway and activate transcription of PKR and MX1. Toll-like receptor 3 (TLR3) is another dsRNA recognition molecule that responds to poly (I:C) treatment [306]; however, its expression has been observed to be low [140, 307] or even absent [308] in Huh7 cells, indicating that it is unlikely to contribute to the poly (I:C) interferon response observed. In addition, the dsRNA recognition molecule, RIG-I may also respond to poly (I:C) in the Huh7 cells. Activated RIG-I has been shown to signal through the phosphate starvation-1 adaptor protein (IPS-1) (also known as MAVS, CARDIF or VISA), which is also activated by MDA5, allowing the two recognition molecules to converge into one signalling pathway [309]. Whether RIG-I is able to respond to poly (I:C) in Huh7 cells is unclear at present, as conflicting findings have been observed in studies investigating the ability of RIG-I to stimulate IFNβ expression in the presence of poly (I:C) [310-313].

When investigating ISG expression in Huh7.5 cells, poly (I:C) treatment had little effect on the expression of PKR and MX1. This may be due to a mutation in the RIG-I gene of the Huh7.5 cells, which has a dominant negative effect on the RIG-I

signalling pathway [140]. If RIG-I is able to respond to poly (I:C), as indicated by some studies [312, 313], the dominant negative effect of the RIG-I mutation would prevent activation of the RIG-I pathway by poly (I:C). This will reduce signalling through IPS-1 and reduce the extent to which IFNα and IFNβ expression is stimulated. If RIG-I is not able to respond to poly (I:C), as indicated by other studies [310, 311], it is possible that the dominant negative effect of the RIG-I mutation on RIG-I signalling may block the activity of IPS-1. Since MDA5 and RIG-I signals converge at IPS-1 [309], this would also result in a block on the signalling downstream of MDA5, which may be the only poly (I:C) recognition molecule present in Huh7 and Huh7.5 cells. Failure to activate IPS-1 downstream of poly (I:C) would prevent the production of IFNα and IFNβ, and block upregulation of the interferon stimulated genes. Previous studies comparing the effect of poly (I:C) treatment on ISG expression have also demonstrated that in comparison to Huh7 cells, Huh7.5 cells are unable to mount an effective interferon response following poly (I:C) treatment [140, 261].

Quantification of JFH-1 protein abundance following host gene knockdown

Several of the siRNA molecules tested in the siRNA knockdown assay significantly reduced both JFH-1 RNA levels and secreted virus titres. When these siRNAs were tested for their effects on JFH-1 protein abundance, the majority of molecules tested also significantly reduced JFH-1 NS3 and core proteins. This included the siRNAs targeting RAB2B, RAB11B, CYP1A1 and TXNIP (**Fig. 4.14 and 4.15**). These findings supported the observation that silencing the expression of these genes may have altered the ability of the cell to support processes occurring during an early phase of the HCV replication cycle. Although good consistency was observed in the western blot results obtained for the individual siRNAs targeting RAB2B, RAB11B and CYP1A1, greater variation was observed when testing the individual siRNAs targeting TXNIP. All three TXNIP specific siRNA molecules silenced the expression of TXNIP efficiently; however, siTXNIP-1 reduced JFH-1 NS3 protein abundance more significantly than siTXNIP-2 and siTXNIP-3. These findings reflect those observed for the effects of TXNIP silencing on JFH-1 RNA abundance (**Fig. 4.9**). There were no obvious differences in the effect of the three siRNAs on cellular viability or stimulation of an interferon response that might explain the variation in the effects observed. Instead it is

possible that siTXNIP-1 may have suppressed TXNIP expression more rapidly than siTXNIP-2 and siTXNIP-3.

Although, siRNAs targeting RAB2B, RAB11B, CYP1A1 and TXNIP had consistent effects on the HCV replication cycle, siRNA molecules targeting the expression of RAB4A did not reduce JFH-1 protein abundance as significantly as expected, given the effects of RAB4A knockdown on JFH-1 RNA levels and virus titres (**Fig. 4.9 and 4.14**). The western blotting experiment used to analyse JFH-1 protein abundance following RAB4A knockdown was performed only once, so further testing of JFH-1 protein abundance following RAB4A knockdown is required.

In addition to identifying potential HCV cofactors involved in an early phase of the HCV replication cycle, several host factors were also identified as potential cofactors involved in a later stage of the replication cycle (e.g. RAB27B and Staufen1). The siRNA molecules targeting these factors were observed to reduce the extracellular JFH-1 virus titres more significantly than the intracellular JFH-1 RNA levels, although some reduction in JFH-1 RNA abundance was also observed with all the siRNAs tested (**Fig. 4.9**). When investigating the effect of these siRNAs on JFH-1 protein abundance, variable effects were observed. For the siRNA molecules targeting RAB27B expression, good consistency was observed between the effects of siRNA transfection on JFH-1 RNA levels, JFH-1 virus titres and JFH-1 protein abundance (**Fig. 4.14**), as RAB27B knockdown had little effect on the intracellular abundance of JFH-1 protein and RNA, but a more significant effect on the extracellular JFH-1 virus titres. This indicates a potential role for RAB27B in the processes of HCV assembly or secretion. However, when silencing the expression of Staufen1, significant reduction was observed in the JFH-1 protein levels present in the infected cells, even though less significant effects had been observed in the intracellular JFH-1 RNA levels compared to the extracellular virus titres (**Fig. 4.16**). These findings indicate that Staufen1 may be involved in an early stage of the HCV replication cycle, or in multiple stages, which might explain why JFH-1 virus titres were reduced to a greater degree than the intracellular JFH-1 RNA levels.

For some of the siRNAs tested (e.g. siRAB2B-1/-2, siCYP1A1-1/-2 and siSTAU1-1/-2), much more significant fold decrease values were observed in the levels of the JFH-1 core protein compared to the levels of JFH-1 NS3. These findings may reflect an increased rate of core protein turnover in the siRNA transfected, JFH-1

infected cells, if the silenced host factor is usually required for core protein stabilisation during infection. Future experiments should further investigate these findings by quantifying the effect of target silencing on the abundance of other HCV structural and non-structural proteins. The western blot analysis performed should also be repeated to gain further evidence to support the data obtained.

For all siRNA transfected, JFH-1 infected cells analysed, it was also observed that the levels of HCV core protein detected by western blotting appeared to be lower than the levels of HCV NS3 protein. This is not a typical observation for cells expressing the JFH-1 genome, as HCV proteins are usually observed to be present at similar levels [135]. This finding most likely reflects variation in the signal intensity obtained for the two proteins on the western blot, which may be caused differences in the efficiency of protein transfer or differences in the affinity of the anti-core and anti-NS3 antibodies.

Summary of potential host factors involved in the HCV replication cycle

Using the information gathered from these siRNA silencing experiments, several host factors have been identified as potential novel HCV cofactors; these include:

- **RAB2B and RAB4A:** Rab GTPase proteins that control vesicle trafficking and membrane organisation at the Golgi body and ER (RAB2B) and recycling early endosomes (RAB4A) [178, 179]. Silencing the expression of these genes significantly reduced JFH-1 RNA replication, JFH-1 protein abundance and the titres of virus secreted (although RAB4A silencing had a less significant effect on JFH-1 protein abundance). This indicates that these proteins may be required during the early phases of HCV infection for virus entry, genome replication or genome translation. Other Rab GTPase genes, including RAB1B (ER) [128], RAB5 (early endosome) [30, 114, 253] and RAB7 (late endosome) [114, 303], which perform similar vesicle trafficking and membrane organisation functions as RAB2B and 4A, have recently been identified as essential cofactors for HCV replication. These proteins are thought to control the assembly of membrane associated replication complexes through manipulation of the intracellular membrane. RAB2B and RAB4A may play very similar roles in the HCV replication cycle facilitating the reorganisation of membrane during formation of the membranous web. Further evidence to support this hypothesis was recently observed in a study investigating host factors that co-fractionate with HCV

replication complexes. This study identified RAB4A and RAB2 as key proteins present within the membrane surrounding replication complexes alongside RAB1A, 5A, 5B, 6 and 7 [303], and demonstrated that RAB4 colocalises with HCV replication complexes in cells expressing a full-length HCV replicon, alongside RAB5 and RAB7 [30, 303]. Furthermore, this study also demonstrated that silencing the expression of RAB2 reduced the intracellular abundance of HCV RNA by 50% in cells expressing a full-length HCV replicon [303].

- **RAB11B:** Rab GTPase protein involved in the trafficking of proteins and vesicles between the *trans*-Golgi network, recycling endosomes and the plasma membrane. Previously, RAB11 has been shown to participate in the budding and morphogenesis of several viruses by facilitating the separation of viral and cellular membrane [183]. In this study, RAB11B silencing reduced the levels of JFH-1 RNA replication (although the effects were dependent on which siRNA was used), JFH-1 protein abundance and the titres of virus secreted. Given the effects of RAB11B on the intracellular levels of JFH-1 RNA and protein, rather than having a role in virus assembly it is possible that RAB11B may be involved in an early step of HCV infection. Due to its roles in the regulation of vesicle trafficking and membrane organisation, RAB11B may contribute to the formation of the HCV membranous web or it may facilitate the trafficking during the initial stages of the HCV replication cycle. A recent study investigating the role of Rab proteins in the formation of the NS4B HCV membranous web demonstrated that RAB11A and RAB11B cofractionated with intracellular membrane containing HCV replication complexes. However, dominant negative mutants of the Rab11 protein did not interfere with membranous web formation indicating that the requirement of RAB11B observed in this study may not be associated with membrane re-organisation during HCV replication complex formation [303].

- **Staufen1:** RNA binding protein that localises to the ER to control the processing of cellular mRNA molecules. Staufen1 has been shown to play a role in the assembly of several RNA viruses by facilitating the formation of viral ribonucleoprotein complexes that direct packaging of the nucleocapsid structure [197, 198]. Staufen1 has also previously been shown to bind to the HCV genome [155, 156]. In this study, Staufen1 silencing reduced the levels of JFH-1 RNA, JFH1 protein abundance and secreted virus titres, although the effects observed on the rate of virus secretion were greater than the effects observed on genome

replication. Given the results observed, it is possible that Staufen1 is important for a process occurring during the early phases of the HCV replication cycle. The ability of Staufen1 to bind directly to the HCV genome indicates that this protein may be important for promoting genome translation, replication and/or trafficking. Considering that Staufen1 silencing has a stronger effect on the secretion of virus from cells, it is also possible that Staufen1 may play an additional role in the incorporation of the HCV genome into the nucleocapsid during assembly. It is not uncommon for Staufen1 to possess multiple roles in the replication cycle of viruses, as during the HIV replication cycle, Staufen1 plays a role in both the translation of the HIV genome and virus particle assembly [196]. Recently, an siRNA screen investigating host cellular factors involved in the endocytosis of HCV identified Staufen1 as a factor required for effective entry of HCV into host cells and production of infectious HCV particles [254]. This indicates that the function of Staufen1 may act at an even earlier stage in the HCV replication cycle than first thought.

- **RAB27A and RAB27B:** Rab GTPase proteins that control the trafficking of secretory vesicles towards the cellular periphery [265, 267]. Silencing the expression of these genes significantly reduced the secreted JFH-1 virus titres observed with less of an effect on the intracellular levels of JFH-1 RNA and JFH-1 proteins. Given the key role that these proteins play in the trafficking of vesicles towards the plasma membrane it is possible that these proteins are required during HCV secretion. Recently, a study investigating the Human Cytomegalovirus (HMCV) demonstrated that HCMV not only increased RAB27A expression, but also utilised RAB27A as part of its replication cycle during the process of virus assembly. The intracellular localisation of RAB27A was investigated during HMCV infection and was observed to relocalise to the site of HMCV assembly. Furthermore, knockdown of RAB27A expression did not alter HMCV entry or protein expression but did reduce the levels of cell associated and secreted HMCV particles; indicating a role for RAB27A in the process of HMCV virus production [314]. Further investigation into the cellular localisation of RAB27A and RAB27B during HCV infection would provide greater insight into whether these proteins are involved in the assembly and secretion of HCV.

- **RAB33B:** Rab GTPase protein involved in retrograde trafficking between the Golgi body and ER and in the formation of autophagosomes during the

process of autophagy [249, 252]. Silencing the expression of RAB33B reduced the levels of JFH-1 RNA and secreted virus titres indicating a potential role during the early stages of the HCV replication cycle. It is possible that RAB33B may be important for the retrograde trafficking of HCV proteins during replication complex formation or for the formation of autophagosomes which have recently been shown to play an important role in the formation of the HCV membranous web [28, 31, 113].

- **CYP1A1:** Effector of the AHR xenobiotic metabolism pathway and regulator of intracellular lipid metabolism [228, 276, 277]. Silencing the expression of CYP1A1 reduced the levels of JFH-1 RNA, JFH-1 proteins and secreted virus titres indicating a potential role during the early stages of the HCV replication cycle. CYP1A1 is involved in the production of intracellular eicosanoid molecules from long chain fatty acids e.g. 14-EET and 15-EET from arachidonic acid [228]. One of the downstream effects of these molecules is the activation of the PPARγ transcription factor that controls the expression of genes involved in lipid synthesis [278]. The upregulation of CYP1A1 observed during JFH-1 infection may be important for activation of PPARγ and accumulation of the key intracellular lipid metabolites required during the HCV replication cycle.

- **TXNIP:** Regulator of cellular defence mechanisms, intracellular glucose metabolism and intracellular lipid metabolism [239, 270, 275]. Silencing the expression of TXNIP significantly reduced the levels of JFH-1 RNA, JFH-1 proteins and secreted virus titres indicating a potential role during the early stages of the HCV replication cycle. TXNIP is a thioredoxin binding protein that has been shown to inhibit PPARα transcription factor activity [239]. The upregulation of TXNIP observed during JFH-1 infection may be important for inhibition of PPARα leading to reduction in the breakdown and oxidation of fatty acids. This may facilitate accumulation of essential lipid metabolites required during the HCV replication cycle.

- **ABLIM3:** Actin binding protein that localises to adherens junctions in hepatocytes providing an interaction between the junctional complex and the actin cytoskeleton [255]. Silencing of ABLIM3 reduced the JFH-1 RNA levels and secreted JFH-1 virus titres indicating a potential role during the early stages of the HCV replication cycle. Through its actin binding properties, ABLIM3 may act during the early stages of HCV infection to promote trafficking of endocytosed

HCV particles on the actin cytoskeleton to the ER for genome translation. The actin cytoskeleton has been shown to play a key role in the process of HCV particle endocytosis and several proteins regulating actin cytoskeleton dynamics have already been shown to act as important cofactors in the HCV replication cycle [254].

- **CIDEC:** Lipid droplet protein that controls the production of lipid droplets in adipocytes [284]. Silencing CIDEC expression had little effect on JFH-1 RNA levels but reduced the level of virus particles secreted from the infected cells. This indicates that CIDEC may be implicated in a late stage of the HCV replication cycle. Considering the role that CIDEC plays in lipid droplet production, it may be required for the process of HCV virion assembly, which has been observed to take place at the surface of intracellular lipid droplets [39].

Chapter 4: Conclusions

This chapter has presented data that provides an initial insight into host cellular factors that may be involved in the HCV replication cycle. Through the use of siRNA silencing, several host genes were shown to be essential for effective replication of the HCV genome, production of HCV proteins and secretion of nascent virus particles. This included a range of factors involved in vesicle trafficking (e.g. RAB2B, RAB4A, RAB11B, RAB27A/B and RAB33B), lipid metabolism (e.g. TXNIP, CYP1A1 and CIDEC), mRNA processing and transport (e.g. Staufen1) and regulation of the actin cytoskeleton (e.g. ABLIM3). At the same time, other host factors tested for potential HCV cofactor function had only minimal effects on the HCV replication cycle when their expression was silenced. This was a surprising observation for some of the factors tested; including RAB18, PGC1α, RIP140 and CIDEB, which all control essential components of intracellular lipid metabolism, a key cellular pathway involved in the HCV replication cycle.

To further investigate the role that these potential HCV cofactors might play in the HCV replication cycle, detailed analysis of the findings must be performed. Two of the most promising potential HCV cofactors initially chosen for further investigation were TXNIP and Staufen1.

Chapter 5: Characterising the Role of the Thioredoxin Interacting Protein (TXNIP) and Staufen1 (STAU1) in the HCV Replication Cycle

Chapter 5: Introduction

Investigation into the HCV replication cycle by siRNA silencing has enabled the identification of host factors that may be essential cofactors required during HCV infection. Two of the factors chosen for further investigation were TXNIP and Staufen1, which both demonstrated significant effects on the JFH-1 replication cycle when their expression was silenced. Previous studies investigating these factors have also indicated their involvement in the replication cycle of HCV and other RNA viruses [155, 156, 197, 198, 240].

The thioredoxin interacting protein (TXNIP)

TXNIP is a signalling protein involved in pathways regulating cellular defence and the metabolism of intracellular lipids and glucose.

The role of TXNIP in cellular defence

Studies investigating the role of TXNIP in cellular defence have demonstrated that TXNIP expression promotes cell cycle arrest, apoptosis, oxidative stress and inflammation [270-273]. In **Chapter 3**, microarray analysis of JFH-1 infected Huh7 cells demonstrated that the expression of TXNIP was significantly increased during HCV infection. This observation is supported by a previous study which demonstrated that Huh7 cells expressing elevated levels of TXNIP support higher levels of HCV genome replication [240]. If an increase in TXNIP expression also occurs in the infected hepatocytes of chronically infected patients, it may contribute to the pathogenesis of infection to increase the levels of hepatocyte cell death, oxidative stress and inflammation [168, 170, 231].

When trying to characterise the function of TXNIP that may be important for the HCV replication cycle, the role of TXNIP in cellular defence may not be directly relevant, and is more likely to facilitate the host response to clear HCV infection. Instead, the ability of TXNIP to regulate glucose and lipid metabolism may be important for the HCV replication cycle, as the metabolic demands of infection are high and intracellular lipids are essential metabolites required for HCV replication and secretion [150].

The role of TXNIP in cellular metabolism

Through the analysis of TXNIP knockout mice, TXNIP has been shown to play a role in the regulation of glucose and lipid metabolism and insulin secretion [239,

275, 315]. One of the key observations for TXNIP knockout mice is the occurrence of serum hypoglycaemia. Studies investigating this finding have demonstrated that TXNIP is a negative regulator of glucose uptake into fat and muscle tissue [316], and is required for hepatic gluconeogenesis [275]. Infection of cells with HCV is a metabolically demanding process [150] with increased rates of protein and lipid synthesis. To meet the energy demands of HCV infection, glucose metabolism may be adjusted through alterations in hepatic TXNIP signalling to provide greater access to a glucose rich energy supply.

TXNIP knockout mice also display elevated levels of serum triglyceride and insulin [239]. Further investigation of these findings demonstrated that TXNIP is an inhibitor of glucose-stimulated insulin secretion [315], and in the absence of TXNIP expression, an increase is observed in the rate of pancreatic insulin secretion. These studies have also indicated that elevated serum triglyceride levels most likely occur as a result of the increased insulin levels, through insulin-induced lipogenesis and activation of the SREBF1 transcription factor [239]. This was confirmed by microarray analysis of hepatocytes isolated from the TXNIP knockout mice, which demonstrated increased expression of SREBF1 target genes. An increase was also observed in the expression of genes controlled by the PPARα transcription factor, which promotes fatty acid oxidation in peroxisomes and mitochondria [237]. Further investigation demonstrated that TXNIP is able to negatively regulate the transcriptional activity of PPARα; indicating that TXNIP may regulate the abundance of fatty acids in the liver [239].

Many studies have already demonstrated that intracellular lipids play an essential role in the HCV replication cycle, supported by the observations in this study that infection stimulates an increase in the abundance of key lipid metabolites (**Fig. 3.21 and 3.23**). As a result, TXNIP expression during HCV infection may be required for regulation of PPARα activity to ensure that sufficient fatty acid metabolites are available for synthesis of essential lipids, such as triglycerides, sphingolipids and phospholipids. Several studies have already investigated the role of PPARα in the HCV replication cycle. These studies have reported that the expression of PPARα is often reduced during HCV infection [68, 238]; suggesting that its function may be unfavourable for progression through the replication cycle. Reduced expression of PPARα was also observed in this study following infection of Huh7 cells with JFH-1 (**Fig. 3.8**). In addition, treatment of cells with PPARα

agonists, that stimulate PPARα activity, has been shown to reduce the replication of HCV occurring in replicon expressing cells [159], indicating that PPARα activity may have inhibitory effects on the HCV replication cycle. However, other studies have generated conflicting results demonstrating that PPARα antagonists, which inhibit PPARα activity, induce an accumulation of intracellular lipids that disperse HCV replication complexes and reduce HCV replication [317]. Further investigation into the effect of PPARα signalling on the HCV replication cycle is required to fully understand the effects that TXNIP mediated inhibition of PPARα activity might have on the HCV replication cycle.

The thioredoxin-binding properties of TXNIP

One of the key properties of TXNIP is its ability to bind to the antioxidant protein, thioredoxin. The importance of TXNIP-thioredoxin binding in cellular metabolism has recently been tested using a non-thioredoxin binding TXNIP mutant. Both mutant and wild-type TXNIP were shown to inhibit glucose uptake indicating that thioredoxin binding may not be important for this process [318]. However, a separate study investigating the role of TXNIP in gluconeogenesis demonstrated that the non-thioredoxin binding TXNIP mutant could not rescue gluconeogenesis defects in TXNIP-knockout primary hepatocytes. By comparison, overexpression of normal TXNIP was able to restore glucose production in the TXNIP-knockout cells. These findings indicate that binding of thioredoxin by TXNIP may be essential for the role of TXNIP in hepatic gluconeogenesis [275].

The role of the alpha-arrestin family in cellular metabolism

TXNIP belongs to the alpha-arrestin gene family which encodes five other homologous alpha-arrestin genes (ARRDC1-5), with ARRDC4 showing the greatest level of sequence homology with TXNIP. Little is known about the function of these other alpha arrestin family members, although homologous genes in yeast are known to control endocytosis [318]. There is also evidence to suggest that the other alpha arrestin family members may control cellular metabolism, as ARRDC3 has been linked to obesity [275], and ARRDC4 inhibits glucose uptake [318]. TXNIP is the only alpha-arrestin that can bind thioredoxin, as the other alpha-arrestin proteins do not contain a conserved cysteine residue that mediates disulphide binding with thioredoxin [318]. The observation that ARRDC4 is not able to bind thioredoxin, but blocks glucose uptake, is consistent

with the ability of TXNIP to block glucose uptake independently of thioredoxin binding [318].

The role of TXNIP in disease

Due to its wide range of cellular functions, TXNIP has been associated with a number of pathological conditions. Elevated TXNIP expression has been implicated in the pathogenesis of type 2 diabetes, where initial increases in blood glucose levels stimulate an increase in TXNIP expression, which is responsible for significant progression of the disease [319, 320]. Increased expression of TXNIP has been shown to worsen the conditions of diabetes because of its ability to reduce pancreatic insulin secretion through apoptosis of pancreatic beta cells [319], increase the rate of liver gluconeogenesis [275] and reduce the uptake of glucose from the blood by skeletal muscle and fat tissue [275, 316]. Targeting the expression of TXNIP during type 2 diabetes is a potential therapeutic strategy that may reduce disease severity. This is supported by the observation that deficiency in TXNIP expression protects mice against streptozotocin-induced diabetes [320]. Interestingly, individuals chronically infected with HCV have an increased risk of developing type 2 diabetes [321]. The increased expression of TXNIP that occurs during HCV infection may contribute to this by increasing the rate of gluconeogenesis in the infected hepatocytes of the liver.

In addition to diabetes, TXNIP expression has also been associated with the development of non-alcoholic steatohepatitis (NASH). NASH is a chronic liver disease that occurs as a result of a glucose and lipid rich diet leading to the development of hepatic steatosis. Once steatosis develops in the liver, it stimulates an increase in the levels of inflammatory cytokines and reactive oxygen species resulting in the development of liver fibrosis and causing significant liver damage. TXNIP has been implicated in the progression of NASH due to its role in the promotion of oxidative stress, inflammation and apoptosis. Knockdown of TXNIP expression in a mouse model of NASH has been shown to reduce the rate at steatohepatitis develops [322]. These observations further demonstrate that an increase in the expression of TXNIP during HCV infection may contribute significantly to the pathogenesis of infection, the features of which are very similar to NASH.

Investigating the role of TXNIP in the HCV replication cycle

In the liver, TXNIP plays a role in the regulation of gluconeogenesis and has been shown to inhibit the activity of the PPARα transcription factor. Its role in these processes may be important for controlling the availability of important intracellular glucose and lipid metabolites and may account for the essential function of TXNIP in the HCV replication cycle. To fully understand the role of TXNIP during HCV infection, it is important to determine what might be responsible for increasing TXNIP expression during infection. Transcription factors controlling TXNIP expression include those activated in the presence of glucose (e.g. forkhead box O1 (FOXO1) [323], kruppel like factor 6 (KLF6) [324], MAX-like protein X (MLX), MLX interacting protein (MLXIP or MondoA) and MLX interacting protein like (MLXIPL or Chrebp) [325-327]), or fatty acids (e.g. PPARα [237]) and those induced during hypoxia (e.g. hypoxia-inducible factor 1α (HIF1α) [328]). To test whether these factors were responsible for increasing TXNIP expression during HCV infection, this chapter summarises work investigating the effect of JFH-1 infection on transcription factor expression and the effect of transcription factor silencing on the expression of TXNIP and the replication of JFH-1. To investigate whether the requirements for TXNIP expression during the HCV replication cycle were specific to the TXNIP protein, the effect of JFH-1 infection on the expression of ARRDC1-4 and the efficiency of HCV replication following knockdown of ARRDC4 (the most homologous alpha arrestin) was also tested.

To gain further insight into the requirements for TXNIP expression during HCV infection, this chapter also summarises an investigation into the effect of TXNIP knockdown on cellular metabolism, in particular the effects observed on PPARα activity and the expression of its target genes. Although many PPARα target genes are associated with fatty acid oxidation, a recent study indicated that PPARα target genes have a wide range of cellular functions, including lipogenesis, lipid droplet formation, biotransformation, transcription and the metabolism of lipoproteins, ketones, cholesterol, glucose, glycerol and amino acids (**Table 5.1**) [237, 329]. The diverse range of PPARα target genes identified makes it difficult to predict the effect that TXNIP mediated PPARα inhibition may have on the HCV replication cycle. To fully investigate the effect of TXNIP silencing on PPARα activity, the expression of many different PPARα target genes was investigated in Huh7 cells transfected with TXNIP siRNA molecules.

Cellular pathway	PPARα target gene
Mitochondrial fatty acid oxidation	ACAA2, ACADS, ACADM, ACADVL, CPT1A, CPT2, ETFA, ETFDH, HADHA, HADHB, HMGCS2, SLC25A20, SLC22A5 and TXNIP
Peroxisomal fatty acid oxidation	ACAA1, ABCD2, ABCD3, ACOX1, ALDH3A1, CYP4A11, CYP4X1, ECH1, HACL1 and HSC17B4
Acyl-CoA formation, hydrolysis and binding	ACSL1, ACSL3, ACSL5, ACSM3, FABP1 and FABP3
Lipogenesis	ACACB, AGPAT2, ELOVL6, FADS1, GPAM, MLYCD and MOD1
Lipases and lipid droplet associated	ADFP, CIDEC, PNPLA2 and S3-12
Lipoprotein uptake and metabolism	ANGPTL4, APOA1, APOA2, APOA5, APOCIII, LIPC, PCTP and VLDLR
Ketogenesis/ketolysis	FGF21 and HMGCS2
Cholesterol metabolism	ABCA1, ABCB4 and CYP7A1
Transcription	PPARα and PPARD
Glucose/Glycerol metabolism and transport	AQP3, G6PC, GYK and PDK4
Biotransformation	AKR1B10, AKR1C3, CYP1A2, CYP2B6, CYP2C8, CYP2C9, CYP2J2, CYP3A7, CYP3A5, CYP3A7, CYP3A11, EPHX2, MGST3 and UGT1A9
Amino acid metabolism	ABAT, AGXT2, ASL, CBS, CPS-1, GLS2, GPT, OAT, ODC1, OTC, PAH and PSAT1

Table 5.1 PPARα target genes in human hepatocytes [237, 329]

A wide range of PPARα target genes have been identified, with roles in multiple cellular functions including: mitochondrial fatty acid oxidation; peroxisomal fatty acid oxidation; acyl-CoA formation, hydrolysis and binding; lipogenesis; lipid hydrolysis; lipid droplet formation; lipoprotein uptake and metabolism; ketogenesis; ketolysis; cholesterol metabolism; transcription; glucose / glycerol metabolism and transport; biotransformation and amino acid metabolism.

Staufen1 (STAU1)

Staufen1 is an RNA-binding protein that controls the translation, trafficking and degradation of cellular mRNA molecules [190] (**Chapter 1: Introduction**). As a result of its RNA binding activity and its ability to form large ribonucleoprotein complexes, Staufen1 has been shown to facilitate virus particle assembly in the replication cycles of HIV and Influenza A [196, 198]. Staufen1 has also been shown to stimulate translation of the HIV genome [196]. Previous investigations to identify RNA binding proteins that interact with the HCV genome have also demonstrated that Staufen1 binds directly to the HCV genome, at the 3'NTR of the positive RNA strand and 5'NTR of the negative RNA strand [155, 156].

According to the role of Staufen1 in the replication cycle of HIV and Influenza A, it was initially proposed that Staufen1 might also facilitate the process of HCV virus particle assembly. If this was the case, silencing the expression of Staufen1 would be expected to reduce the levels of virus secreted, with little effect on the intracellular levels of virus RNA or protein. This was the effect observed on the Influenza A virus replication cycle when Staufen1 expression was silenced, reflecting the role of Staufen1 in the process of Influenza A virion particle formation [198]. However, the results observed in the siRNA silencing assay performed in **Chapter 4** demonstrated that Staufen1 knockdown reduced the levels of JFH-1 RNA, JFH-1 core and NS3 proteins, and the extracellular titres of JFH-1 virus (**Fig. 4.6, 4.9 and 4.16**). Although, for all three siRNAs tested, larger decreases were observed in the levels of extracellular virus than the levels of intracellular JFH-1 RNA (**Fig. 4.6 and 4.9**). These findings instead indicate that Staufen1 might play a role early on during the HCV replication cycle, which may be associated with the translation, replication or trafficking of the HCV genome due to the RNA binding function of Staufen1.

The ability of Staufen1 to bind to the 3' NTR region of the HCV RNA positive strand and the 5'NTR region of the negative RNA strand suggests that Staufen1 may be involved in the regulation of HCV genome replication. In general, binding of host proteins to the 3'NTR of the genome is associated with regulation of genome replication, as this is the position at which NS5B initiates RNA synthesis (e.g. PTB [330]). Other host proteins have been shown to bind the HCV genome to alter the rate of genome translation; however, these proteins usually bind to the

5’NTR of the genome where the IRES sequence is located (e.g. La autoantigen [19] and hnRNPL [331]).

Based on our current understanding of Staufen1, binding at the 3’UTR of cellular mRNA stimulates mRNA degradation by staufen-mediated decay [194], and binding to the 5’UTR stimulates mRNA translation [195]. Considering these typical functions of Staufen1, binding at the 3’NTR of the HCV genome might be expected to stimulate degradation of the HCV RNA molecule, not induce an increase in its translation, replication or trafficking. Recent studies investigating the function of RNA-binding proteins in the HCV replication cycle have demonstrated that these proteins do not always perform their typical cellular role when bound to the HCV RNA. For example, the RNA-binding proteins, p54, LSm1-7, and PatL1, usually involved in the deadenylated-dependent degradation of cellular mRNAs, have recently been shown to bind to the 5’ and 3’ ends of the HCV genome to facilitate its replication and translation [37].

Based on the RNA binding function of Staufen1, the most likely role of this protein in the HCV replication cycle is associated with the regulation of HCV genome function. However, an alternative function was recently indicated in a study investigating host factors involved in HCV endocytosis, which demonstrated that Staufen1 silencing reduced the entry of HCV pseudo-particles and reduced the production of HCV virions in cells infected with Jc1 HCV [254]. Whilst these results support the findings from the siRNA knockdown assay (**Fig. 4.6, 4.9 and 4.16**), they suggest that Staufen1 may play a role in HCV entry rather than regulating HCV genome function. The HCV pseudo-particle system uses HIV virus particles that have been modified to contain HCV envelope glycoproteins and an RNA genome that replaces the HIV genes with a luciferase or GFP marker. Infection of cells with HCV pseudo-particles relies upon efficient cellular entry via HCV E1 and E2, followed by endocytosis of the virus particle and translation of the reporter gene at the rough ER [332]. Staufen1 is typically an ER localised protein [333] and it seems unlikely that it would be involved in the process of HCV entry at the plasma membrane. Other possible explanations for these findings are that Staufen1 may facilitate pseudo-particle endocytic trafficking through its ability to bind to microtubule and actin filaments [191, 193], or it may facilitate translation of the pseudo-particle RNA at the ER.

Another possible explanation for the results observed following Staufen1 knockdown, both in the pseudo-particle system [254] and the siRNA knockdown assay (**Fig. 4.6, 4.9 and 4.16**), is that the effects of Staufen1 silencing on the HCV replication cycle may reflect a more general cellular response to Staufen1 knockdown. Staufen1 has been shown to control host gene expression through staufen-mediated decay [194]. Microarray analysis of Staufen1 knockout cells demonstrated that 124 host transcripts were upregulated and 115 host transcripts were downregulated as a result of Staufen1 silencing [334]. Therefore, Staufen1 silencing might reduce the expression of genes required during the HCV replication cycle or increase the expression of genes that negatively regulate HCV replication. Analysis of the Staufen1 knockout microarray data demonstrated that several host genes involved in HCV associated cellular pathways were downregulated; this included genes involved in vesicle trafficking (SNAP23 and SNX13), lipid metabolism (HSD17B12, INSIG1 and ACLY), amino acid metabolism (CTH) and even the gene encoding TXNIP [334]. Staufen1 silencing has also been shown to increase the rate of stress granule formation in cells, resulting in global repression of cellular translation. This may further reduce the expression of host genes required during the HCV replication cycle, or it may reduce translation of the HCV genome itself [335].

Given the range of potential functions for Staufen1 in the HCV replication cycle, it was important to further investigate the interactions that form between Staufen1 and the HCV genome, and to determine whether Staufen1 can interact with HCV encoded proteins. The following chapter summarises preliminary work investigating the intracellular localisation of Staufen1 during JFH-1 infection and its ability to colocalise with HCV proteins and the HCV genome.

Chapter 5: Results

5.1 Identifying transcription factors that induce TXNIP expression

5.1.1 The expression of TXNIP transcription factor genes during JFH-1 infection

To investigate which pathway was responsible for increasing the expression of TXNIP during JFH-1 infection, the expression of host factors controlling TXNIP transcription was investigated in JFH-1 infected cells. The microarray data collected for JFH-1 infected Huh7 cells in **Chapter 3** was re-examined to identify transcription factor genes altering in expression at 48 hours post-infection. To validate the gene expression data observed, qRT-PCR analysis of host gene expression was also performed on Huh7 cells infected with JFH-1 or mock medium for 48 hours (**Fig. 5.1**). As a result of JFH-1 infection, an increase was observed in the expression of FOXO1, MLXIPL, HIF1α and KLF6 and a decrease was observed in the expression of PPARα.

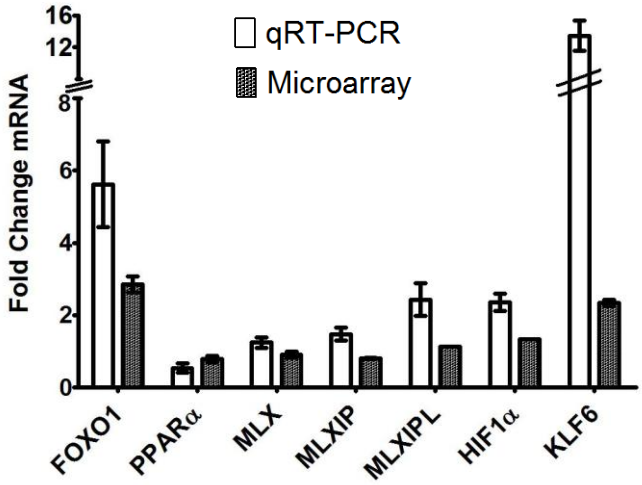


Figure 5.1 JFH-1 infection alters the expression of cellular transcription factors

Fold change in Huh7 cell host gene expression at 48 hours post-JFH-1 infection, quantified using microarray analysis and qRT-PCR. Huh7 cells were infected with JFH-1 (MOI = 3) or mock medium for 48 hours. Intracellular RNA was extracted and used for qRT-PCR analysis of host gene expression. The qRT-PCR data shown represents the mean (±SD) of triplicate infection samples (white bars). The corresponding microarray gene expression data is also shown (grey bars) and represents the mean fold change value calculated for triplicate infections at 48 hours post-infection. Confidence interval values calculated for the triplicate infection sample repeats of the microarray experiment can be found in the Appendix A.10. For some of the host genes investigated multiple probe sets were available on the microarray genechip, thus error bars are displayed for some of the microarray datapoints (grey bars) to represent the range of mean fold change values observed for the different gene probe sets.

5.1.2 Quantification of intracellular glucose levels in JFH-1 infected cells

Many of the transcription factors that control TXNIP expression are stimulated by high intracellular glucose conditions; including: FOXO1, MLX, MLXIP, MLXIPL and KLF6 [323-327]. The effect of JFH-1 infection on the abundance of intracellular glucose was investigated to determine whether an increase in glucose concentration was responsible for HCV induced upregulation of KLF6, FOXO1 and MLXIPL (**Fig. 5.1**). An assay to quantify intracellular glucose was optimised using protein lysate extracted from untreated Huh7 cells (**Fig. 5.2a**). The optimal amount of protein lysate chosen for the glucose quantification assay was 75µg. Higher amounts of lysate sample could have been used for the assay; however, restrictions on the availability of protein lysate meant that the smallest optimal amount of lysate was chosen. The effect of JFH-1 infection on intracellular glucose abundance was investigated comparing the glucose levels quantified in Huh7 cells infected with JFH-1 or mock medium for 48 hours (**Fig. 5.2b**). Little effect was observed on the intracellular glucose levels as a result of JFH-1 infection.

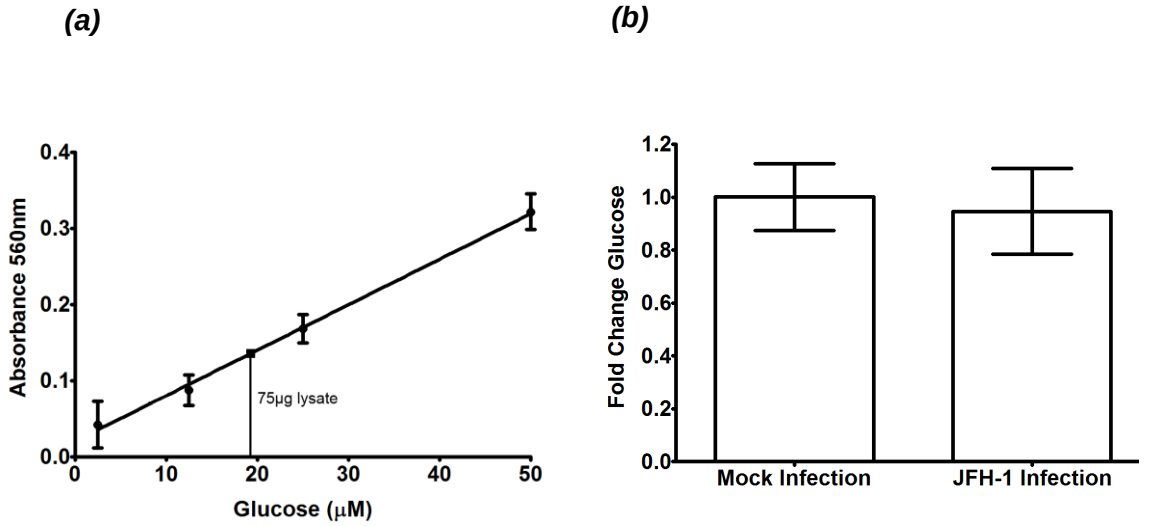


Figure 5.2 JFH-1 infection does not alter intracellular glucose levels

(a) *Optimisation of the glucose quantification assay using 75µg of Huh7 cell protein lysate. Huh7 cells lysed in 0.5% Triton X-100 lysis buffer were tested alongside a glucose standard curve (2, 12.5, 25 and 50µM glucose) in the Amplex Red glucose quantification assay. The standard curve absorbance readings represent the mean (±SD) of two standard curve assays performed in separate experiments.* ***(b)*** *Fold change in glucose levels during JFH-1 infection. Huh7 cells infected with JFH-1 (MOI = 3) or mock medium for 48 hours were lysed in 0.5% Triton X-100 and the intracellular glucose levels were quantified using the Amplex red glucose quantification kit. Glucose quantification data displayed represents the mean (±SD) of two independent experiments, each containing repeat infections performed in triplicate (N=6).*

5.1.3 The expression of glucose metabolism genes during JFH-1 infection

JFH-1 infection had little effect on the intracellular glucose levels present in Huh7 cells. To determine whether this finding was reflected in the host cell gene expression profile, the microarray gene expression data (**Chapter 3**) was re-examined to investigate the effect of JFH-1 infection on the expression of genes controlling glucose metabolism. Although the majority of genes involved in glucose metabolism did not alter in expression in the JFH-1 infected cells compared to the mock infected cells, several genes involved in the single step (**Fig. 5.3a**) and reversible reactions (**Fig. 5.3b**) of glycolysis and gluconeogenesis were transcriptionally regulated during infection. Despite the altered expression of these genes, the expression patterns observed were inconsistent, as genes involved in both pathways increased and decreased in expression. Furthermore, an increase was also observed in the expression of the rate-limiting enzymes for both gluconeogenesis (phosphoenolpyruvate carboxykinase 2 (PCK2)) and glycolysis (hexokinase 2 (HK2)) (**Fig. 5.3a**).

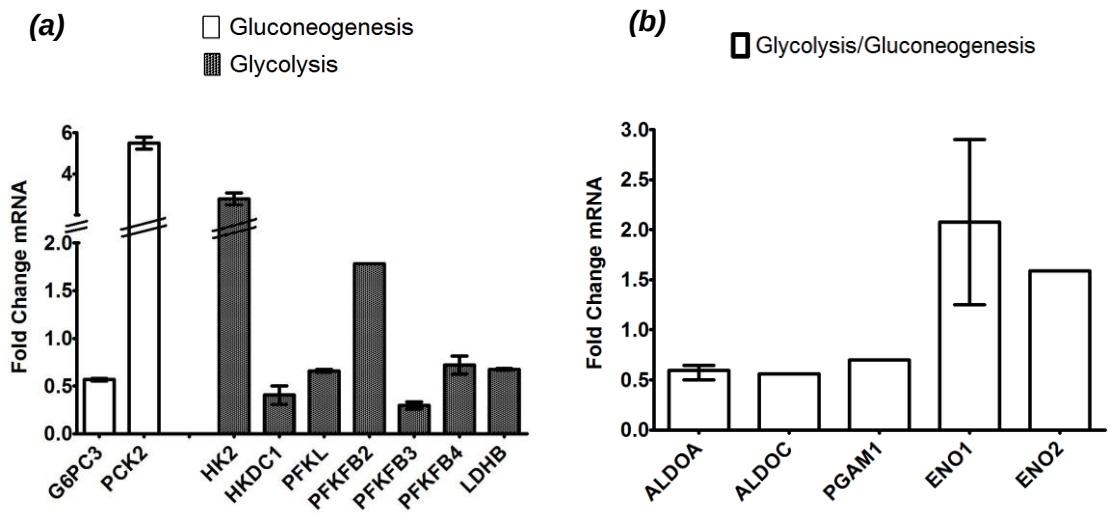


Figure 5.3 JFH-1 infection alters the expression of glucose metabolism genes

Fold change in Huh7 cell host gene expression at 48 hours post-JFH-1 infection, quantified using microarray analysis. The expression of genes involved in ***(a)*** *single step gluconeogenesis (white bars) and glycolysis reactions (grey bars) and* ***(b)*** *gluconeogenesis/glycolysis reversible reactions is shown. The microarray gene expression data shown represents the mean fold change value calculated for triplicate infections at 48 hours post-infection. Confidence interval values calculated for the triplicate infection sample repeats of the microarray experiment can be found in the Appendix A.10. For some of the host genes investigated multiple probe sets were available on the microarray genechip, thus error bars are displayed for some of the microarray datapoints to represent the range of mean fold change values observed for the different gene probe sets.*

5.1.4 Knockdown of transcription factors controlling TXNIP expression

To investigate transcription factors responsible for controlling TXNIP expression during JFH-1 infection, the effect of transcription factor knockdown on TXNIP expression and JFH-1 replication efficiency was tested. Huh7 cells transfected with siRNAs targeting the expression of FOXO1, MLX, MLXIP, MLXIPL and KLF6 were infected with JFH-1 for 48 hours. Intracellular RNA was extracted for qRT-PCR quantification of JFH-1 RNA, target mRNA and TXNIP mRNA. Extracellular medium was also collected for quantification of JFH-1 virus titres (**Fig. 5.4**).

Comparison of the TXNIP mRNA levels quantified in the siRNA transfected cells demonstrated that the knockdown of MLX, MLXIP and MLXIPL significantly reduced TXNIP expression. Silencing the expression of MLX, MLXIP and MLXIPL also reduced the intracellular levels of JFH-1 RNA and JFH-1 virus titres. For example, silencing MLX, MLXIP and MLXIPL expression reduced JFH-1 RNA by 40%, 50% and 53% and reduced JFH-1 virus titres by 47%, 90% and 83%, respectively. These findings are consistent with the reduced expression of TXNIP observed following knockdown of MLX, MLXIP and MLXIPL. Interestingly, the transcription factors encoded by MLXIP and MLXIPL act as cofactors for the MLX protein; together these transcription factors form two complexes: MLX/MLXIP and MLX/MLXIPL [326, 336, 337]. The data observed through the silencing of these factors indicated that both complexes (MLX/MLXIP and MLX/MLXIPL) may be required for upregulation of TXNIP expression in the JFH-1 infected Huh7 cells. By comparison, silencing the expression of FOXO1 had no effect on TXNIP expression and only minimal effects on the JFH-1 replication cycle; including a 20% reduction in JFH-1 RNA levels, and a 45% reduction in JFH-1 virus titres. Silencing the expression of KLF6 also had no effect on TXNIP expression; however, significant effects on the HCV replication cycle were observed including a 48% reduction in JFH-1 RNA levels, and a 75% reduction in JFH-1 virus titres. In all cases, target mRNA knockdown was successful with around 75% to 80% efficiency of host gene silencing. All siRNAs were tested for their effects on Huh7 cell viability and interferon stimulated gene (ISG) expression (**Appendix A.18**). None of the siRNAs had a major effect on cellular viability, except siMLXIP and siMLXIPL which reduced viability by 20% (**Appendix A.18a**). The majority of the siRNAs tested also had little effect on ISG expression, with the exception of the FOXO1 siRNA, which increased MX1 expression by 1.8 fold (**Appendix A.18b**).

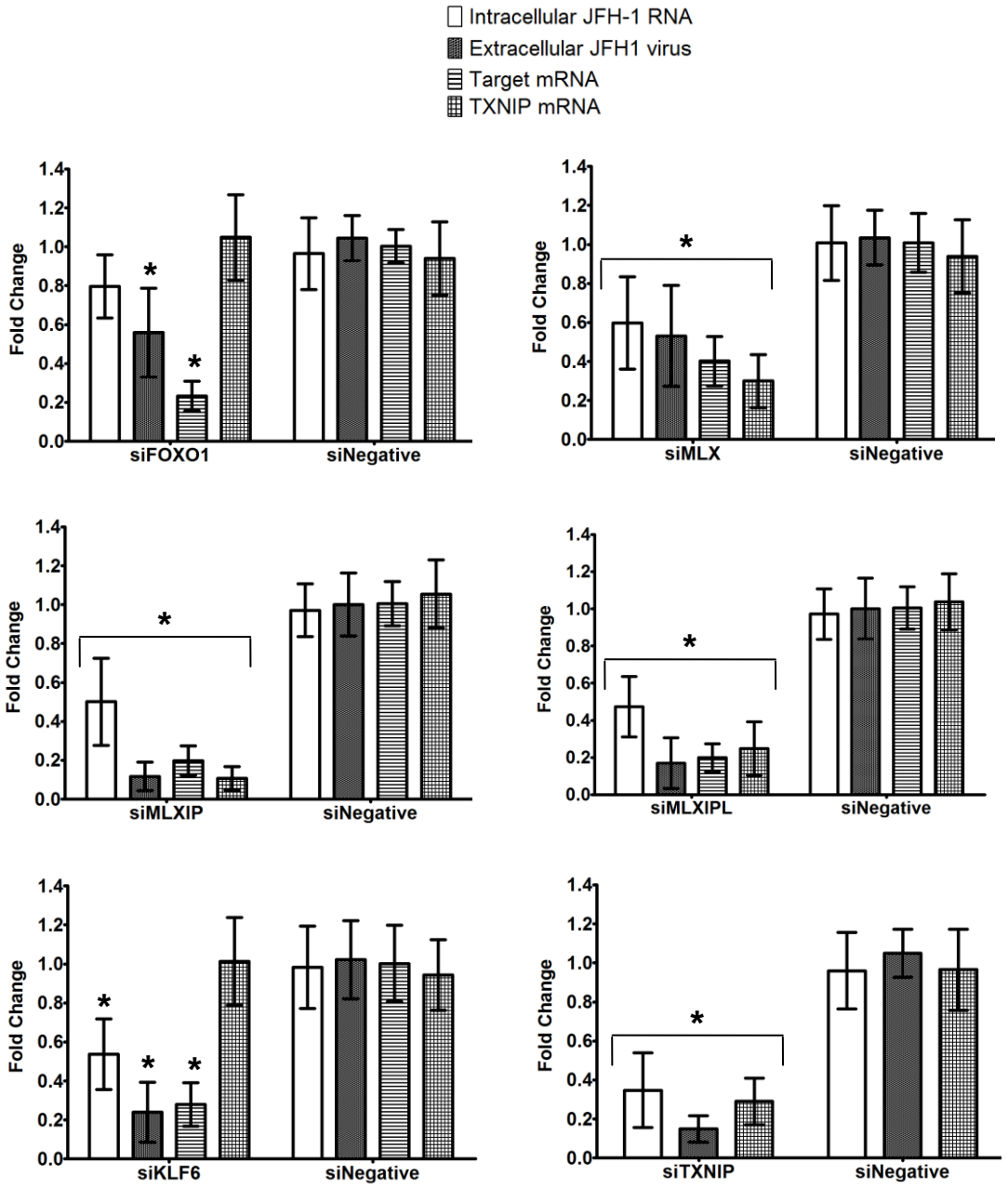


Figure 5.4 The effect of transcription factor knockdown on TXNIP expression and the JFH-1 replication cycle. *Fold change in JFH-1 RNA, JFH-1 virus titres, siRNA target mRNA and TXNIP mRNA following host gene knockdown in JFH-1 infected Huh7 cells. Huh7 cells were transfected with 50nM of individual target specific siRNA and 50nM of negative control non-targeting siRNA for 48 hours. Note: A 50nM pool of siRNAs was used to silence TXNIP (siTXNIP-1 and siTXNIP-2). The transfected cells were infected with JFH-1 (MOI = 3) for 48 hours. Intracellular RNA was extracted for qRT-PCR quantification of JFH-1 RNA, target mRNA and TXNIP mRNA. Media was also collected from the transfected cells for quantification of JFH-1 virus titres. Fold change data displayed represents the mean (±SD) of two independent experiments, each containing repeat siRNA transfections performed in triplicate (N=6). The target specific siRNAs causing a statistically significant knockdown (p value ≤ 0.05) of JFH-1 RNA, JFH-1 virus titres, siRNA target mRNA and TXNIP mRNA in comparison to the negative control siRNA are indicated by an asterisk (*). P values were calculated using a two-tailed unpaired T test in Graphpad Prism.*

5.1.5 TXNIP expression following knockdown of MLX complexes

To further investigate the role of the MLX transcription factor complexes in the regulation of TXNIP transcription, a time-course siRNA knockdown experiment was performed using siRNA molecules targeting MLX, MLXIP and MLXIPL. The expression of TXNIP was investigated by qRT-PCR at 24, 48, 72 and 96 hours post-transfection (**Fig. 5.5**). The expression of TXNIP was reduced in the presence of all three siRNA molecules at all time-points tested. MLXIP silencing had the greatest effect on TXNIP expression, with similar levels of TXNIP knockdown as the cells treated with the TXNIP siRNAs. The ability of all three factors to silence TXNIP expression is consistent with the formation of complexes between these factors and indicates that the MLX/MLXIP and MLX/MLXIPL complexes formed may both regulate TXNIP expression in Huh7 cells.

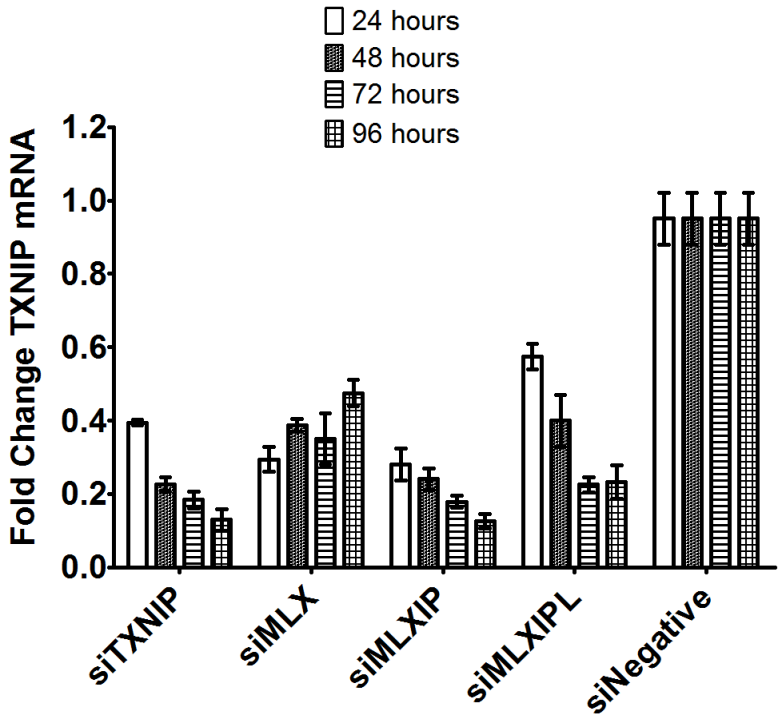


Figure 5.5 Knockdown of MLX, MLXIP and MLXIPL reduces TXNIP expression

Fold change in TXNIP expression following knockdown of TXNIP, MLX, MLXIP and MLXIPL in Huh7 cells. Huh7 cells were transfected with 50nM of siRNAs targeting TXNIP, MLX, MLXIP and MLXIPL and 50nM of a negative control non-targeting siRNA for 24, 48, 72 and 96 hours. Intracellular RNA was extracted for qRT-PCR quantification of TXNIP expression. Fold change data displayed represents the mean (±SD) of two independent experiments, each containing repeat siRNA transfections performed in triplicate (N=6). The knockdown of TXNIP achieved with the MLX, MLXIP, MLXIPL and TXNIP siRNAs compared to the negative control siRNA was statistically significant with a p value ≤ 0.05, calculated using a two-tailed unpaired T test in Graphpad Prism.

5.2 Investigating the role of alpha arrestins in the HCV replication cycle

TXNIP belongs to the alpha-arrestin gene family, which also contains ARRDC1, ARRDC2, ARRDC3, ARRDC4 and ARRDC5 [318]. To investigate whether JFH-1 infection also controlled the expression of other alpha-arrestin family members, the microarray data collected for JFH-1 infected Huh7 cells in **Chapter 3** was re-examined. A focus was placed on the identification of alpha arrestin genes altering in expression at 48 hours post-infection. To validate the gene expression data observed, qRT-PCR analysis of host gene expression was also performed on Huh7 cells infected with JFH-1 or mock medium for 48 hours (**Fig. 5.6a**). The expression of both ARRDC2 and ARRDC4 significantly increased during JFH-1 infection. It was not possible to detect an mRNA transcript from the ARRDC5 gene, even when several different primer pairs were tested.

The most homologous alpha arrestin to TXNIP is ARRDC4. To test whether this factor may also be important for efficient HCV infection, the effect of ARRDC4 knockdown on JFH-1 replication and secretion was investigated using the siRNA knockdown assay (**Fig. 5.6b**). TXNIP mRNA levels were also quantified to test whether ARRDC4 silencing affected TXNIP expression. Silencing the expression of ARRDC4 had little effect on JFH-1 RNA, JFH-1 virus titres, and TXNIP mRNA abundance. Knockdown of the ARRDC4 target gene was successful with around 70% reduction in ARRDC4 mRNA levels. The ARRDC4 siRNA did not significantly alter Huh7 cell viability or stimulate the expression of ISG when tested by the alamar blue assay and qRT-PCR, respectively (**Appendix A.18a and b**).

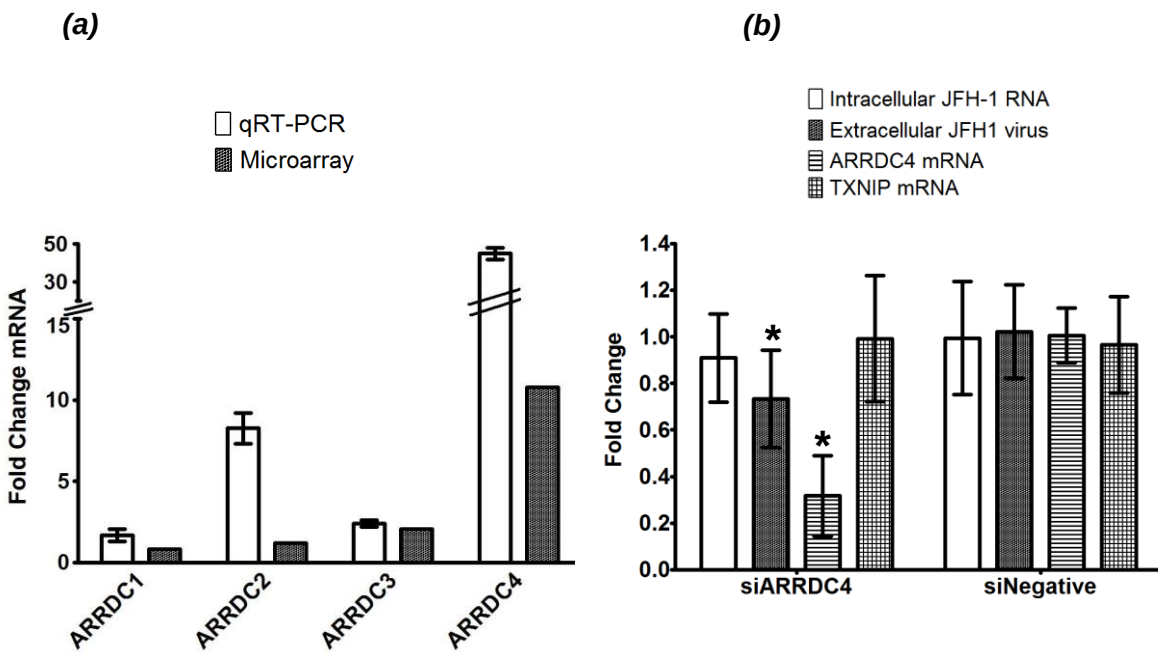


Figure 5.6 ARRDC4 is upregulated during JFH-1 infection but is not required for effective JFH-1 replication or secretion

(a) *Fold change in the expression of alpha arrestin genes 1-4 in JFH-1 infected Huh7 cells, quantified using microarray analysis and qRT-PCR. Huh7 cells were infected with JFH-1 (MOI=3) or mock medium for 48 hours. Intracellular RNA was extracted and used for qRT-PCR analysis of host gene expression. The qRT-PCR data shown represents the mean (±SD) of triplicate infection samples (white bars).The corresponding microarray gene expression data is also shown (grey bars) and represents the mean fold change value calculated for triplicate infections at 48 hours post-infection. Confidence interval values calculated for the triplicate infection sample repeats of the microarray experiment can be found in the Appendix A.10.* ***(b)*** *Fold change in JFH-1 RNA, JFH-1 virus titres, ARRDC4 mRNA and TXNIP mRNA following ARRDC4 silencing in JFH-1 infected Huh7 cells. Huh7 cells were transfected with 50nM of ARRDC4 siRNA and a negative control non-targeting siRNA for 48 hours. The transfected cells were infected with JFH-1 (MOI = 3) for 48 hours. Intracellular RNA was extracted for qRT-PCR quantification of JFH-1 RNA, ARRDC4 mRNA and TXNIP mRNA. Media was also collected from the transfected cells for quantification of JFH-1 virus titres. Fold change data displayed represents the mean (±SD) of two independent experiments, each containing repeat siRNA transfections performed in triplicate (N=6). The knockdown of ARRDC4 mRNA and extracellular JFH-1 virus titres achieved with the ARRDC4 siRNA compared to the negative control siRNA was statistically significant (p value ≤ 0.05) (indicated by an asterisk (*)). P values were calculated using a two-tailed unpaired T test in Graphpad Prism.*

5.3 The effect of TXNIP knockdown on the transcriptional activity of PPARα

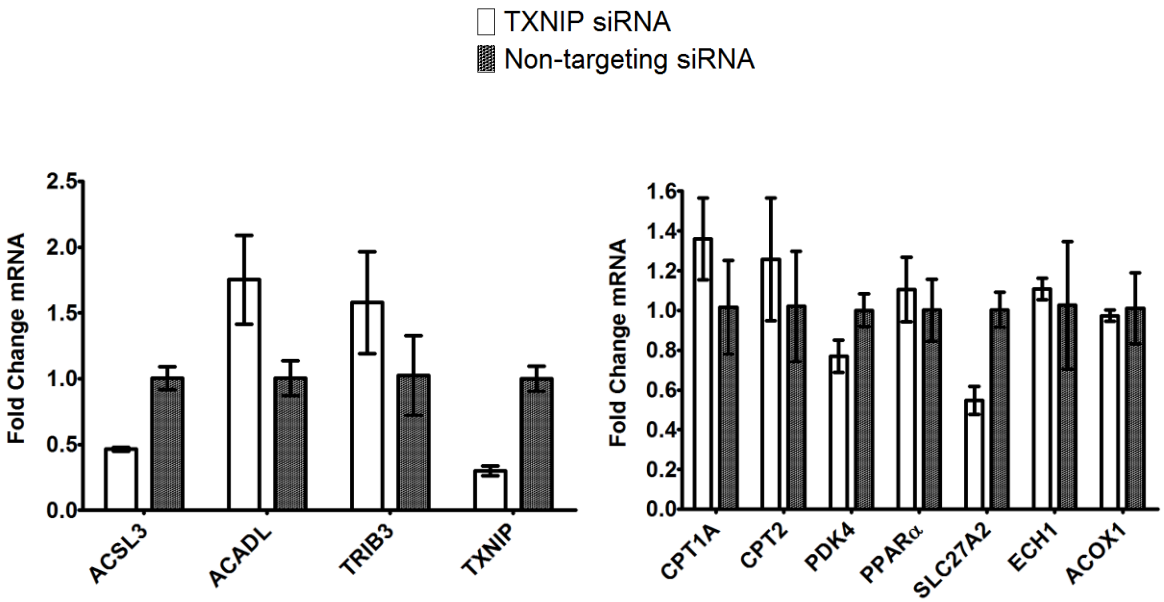
5.3.1 PPARα target gene expression following TXNIP knockdown

To investigate whether TXNIP knockdown altered PPARα activity, the expression of PPARα target genes was investigated following TXNIP silencing. Genes chosen for analysis were ACSL3, ACADL, TRIB3, CPT1A, CPT2, PDK4, PPARα, SLC27A2, ECH1 and ACOX1 [237, 329] (**Table 5.1**).

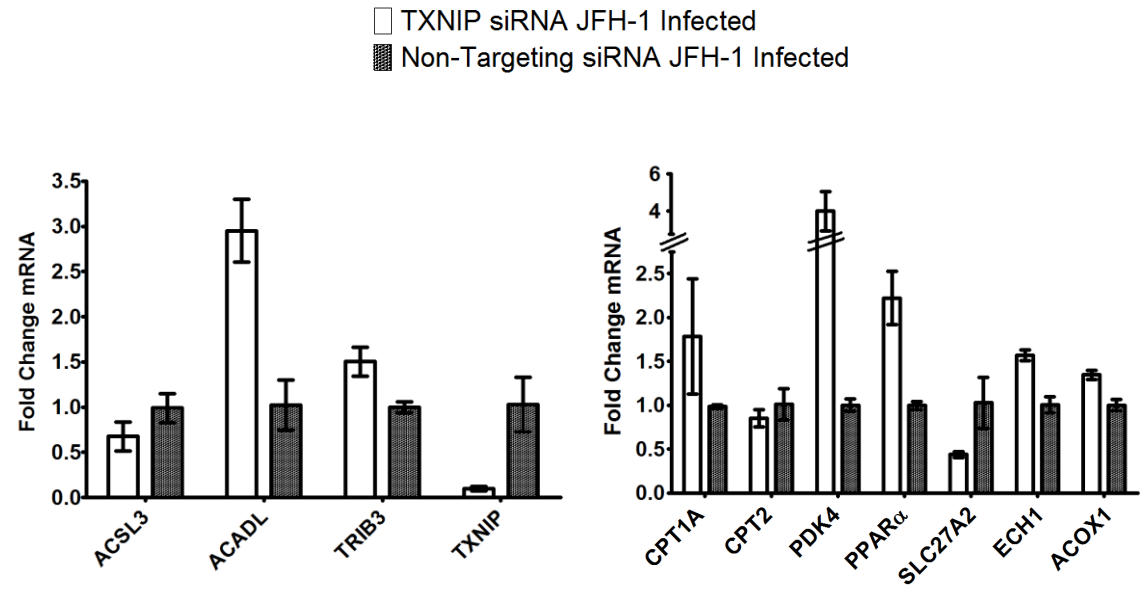
Initially, the effect of TXNIP silencing on PPARα target gene expression was investigated by qRT-PCR using Huh7 cells transfected for 48 hours with a pool of TXNIP siRNAs (siTXNIP-1 and siTXNIP-2) (**Fig. 5.7a**). The expression of TXNIP was efficiently reduced by 80% in the TXNIP knockdown cells, which also resulted in an increase in the expression of ACADL, TRIB3, CPT1A and CPT2, and a decrease in the expression of ACSL3, PDK4 and SLC27A2. The effect of TXNIP silencing on PPARα target gene expression was also investigated by qRT-PCR in Huh7 cells transfected with a pool of TXNIP siRNAs which were then infected for 48 hours with JFH-1 (**Fig. 5.7b**). The expression of TXNIP was efficiently reduced by 90% in the JFH-1 infected, TXNIP knockdown cells, which also resulted in an increase in the expression of ACADL, TRIB3, CPT1A, PDK4, PPARα, ECH1 and ACOX1, and a decrease in the expression of ACSL3 and SLC27A2. Finally, to facilitate interpretation of the gene expression data obtained, the effect of JFH-1 infection on PPARα target gene expression was also investigated using qRT-PCR and microarray analysis (**Fig. 5.7c**). Infection of Huh7 cells with JFH-1 for 48 hours induced an increase in the expression of ACSL3, ACADL, TRIB3, CPT1 and ACOX1, and a decrease in the expression of CPT2, PPARα and SLC27A2.

By comparing the different sets of gene expression data obtained, it is possible to see that TXNIP knockdown significantly alters the expression of PPARα target genes. Overlapping effects of TXNIP knockdown were observed in the uninfected Huh7 cells (**Fig. 5.7a**) and the JFH-1 infected Huh7 cells (**Fig. 5.7b**). This included a decrease in the expression of ACSL3 and SLC27A2, and an increase in the expression of ACADL, TRIB3 and CPT1A. Some of the expression changes observed in the JFH-1 infected, TXNIP knockdown cells were not observed in the uninfected TXNIP knockdown cells; including an increase in the expression of PDK4 and PPARα. These expression changes were also not observed in the Huh7 cells infected with JFH-1 for 48 hours (**Fig. 5.7c**).

(a) *Uninfected TXNIP knockdown Huh7 cells (48 hours post-transfection)*



(b) *JFH-1 infected TXNIP knockdown Huh7 cells (96 hours post-transfection)*



***(c)** JFH-1 and mock infected Huh7 cells (48 hours post-infection)*

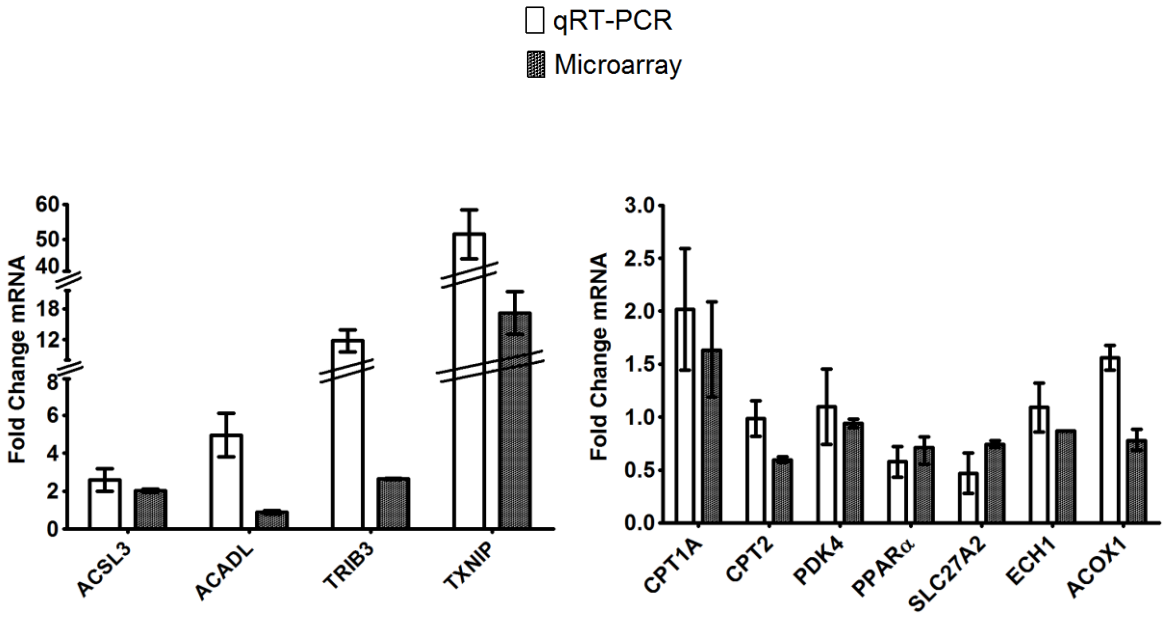


Figure 5.7 TXNIP knockdown alters the expression of PPARα target genes

*Fold change in PPARα target gene expression in **(a)** Huh7 cells transfected for 48 hours with 50nM of TXNIP siRNA (siTXNIP-1 and siTXNIP-2) or 50nM of a negative control non-targeting siRNA and **(b)** Huh7 cells transfected for 48 hours with 50nM of TXNIP siRNA (siTXNIP-1 and siTXNIP-2) or 50nM of a negative control non-targeting siRNA and infected for 48 hours with JFH-1 (MOI=3). Intracellular RNA was extracted for qRT-PCR quantification of host gene expression. Fold change data represents the mean (±SD) of one experiment with repeat siRNA transfections performed in triplicate (N=3). **(c)** Fold change in PPARα target gene expression in JFH-1 infected Huh7 cells. Huh7 cells were infected with JFH-1 (MOI=3) or mock medium for 48 hours. Intracellular RNA was extracted and used for qRT-PCR analysis of host gene expression. The qRT-PCR data shown represents the mean (±SD) of triplicate infection samples (white bars). The corresponding microarray gene expression data is also shown (grey bars) and represents the mean fold change value calculated for triplicate infections at 48 hours post-infection. Confidence interval values calculated for the triplicate infection sample repeats of the microarray experiment can be found in the Appendix A.10. For some of the host genes investigated multiple probe sets were available on the microarray genechip, thus error bars are displayed for some of the microarray datapoints (grey bars) to represent the range of mean fold change values observed for the different gene probe sets.*

5.3.2 ACSL3 gene expression following TXNIP knockdown

One of the PPARα target genes that altered in expression following TXNIP knockdown was ACSL3, which was recently identified as a key HCV cofactor required for secretion due to its role in VLDL synthesis [50]. Knockdown of TXNIP reduced ACSL3 expression in both uninfected and infected Huh7 cells (**Fig. 5.7a and b**). By comparison, ACSL3 expression was significantly increased during JFH-1 infection (**Fig. 5.7c**). Although these observations did not support the hypothesis that TXNIP knockdown may enhance PPARα activity; they did demonstrate that TXNIP knockdown was able to reduce the expression of key HCV cofactors. To further explore the effect of TXNIP knockdown on ACSL3 expression, individual TXNIP siRNAs were tested for their effects on ACSL3 expression in JFH-1 infected Huh7 cells (**Fig. 5.8**). TXNIP knockdown efficiency varied between the siRNAs tested reflecting previous observations (**Fig. 4.9**), with siTXNIP-1, siTXNIP-2 and siTXNIP-3 reducing TXNIP expression by 80%, 75% and 62%, respectively. ACSL3 expression was reduced in cells transfected with all three siRNAs, and the level of knockdown observed correlated roughly with the level of TXNIP knockdown achieved, as siTXNIP-1, siTXNIP-2 and siTXNIP-3 reduced ACSL3 expression by 75%, 40% and 55%, respectively.

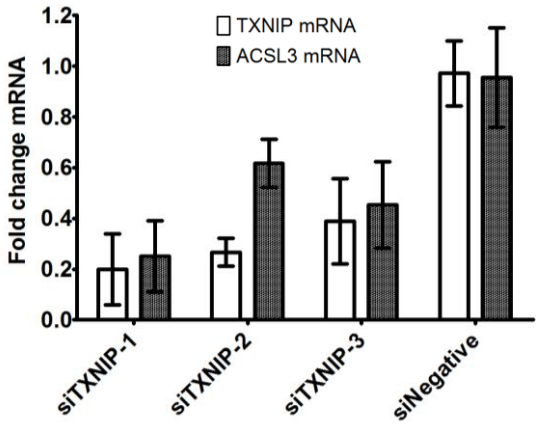


Figure 5.8 TXNIP knockdown reduces ACSL3 mRNA during JFH-1 infection

Fold change in TXNIP (white bars) and ACSL3 (grey bars) expression in JFH-1 infected Huh7 cells transfected with TXNIP siRNAs. Huh7 cells were transfected with 25nM of TXNIP siRNA (siTXNIP-1, siTXNIP-2 or siTXNIP-3) and 25nM of a negative control non-targeting siRNA for 48 hours. The cells were infected with JFH-1 (MOI=3) for 48 hours. Intracellular RNA was extracted for qRT-PCR quantification of TXNIP and ACSL3 expression. Fold change data displayed represents the mean (±SD) of one experiment with repeat siRNA transfections performed in triplicate (N=3). The knockdown of TXNIP and ACSL3 achieved with all three TXNIP siRNAs was statistically significant with a p value ≤ 0.05. P values were calculated using a two-tailed unpaired T test in Graphpad Prism.

5.4 Investigating the localisation of Staufen1 during JFH-1 infection

To further explore the role of Staufen1 in the HCV replication cycle, the intracellular localisation of the Staufen1 protein during JFH-1 infection was investigated.

The staining protocol for Staufen1 was optimised with an anti-Staufen1 antibody using untreated Huh7 cells (**Fig. 5.9a**). The Staufen1 antibody detected a protein that localised predominantly at the nuclear periphery, most likely in the ER where Staufen1 is known to localise [333]. To test whether the staining is specific to Staufen1, Huh7 cells transfected with either Staufen1 siRNAs or a non-targeting siRNA were stained for the Staufen1 protein. A reduction was observed in the intensity of Staufen1 staining in the Huh7 cells transfected with the Staufen1 siRNAs compared to cells transfected with the negative control siRNA (**Fig. 5.9b**), indicating that the antibody specifically stains the Staufen1 protein.

To investigate whether JFH-1 infection altered the localisation of Staufen1, Huh7 cells were infected with JFH-1 (MOI = 0.5) for 48 hours and costained for Staufen1 and the HCV core protein (**Fig. 5.10a**). When comparing the Staufen1 staining observed for the JFH-1 infected Huh7 cells (core-positive cells) and the uninfected Huh7 cells (core-negative cells), no obvious alterations in Staufen1 localisation were observed (**Fig. 5.10a**).

The ability of Staufen1 to interact with HCV proteins and HCV RNA was also investigated during JFH-1 infection. Huh7 cells infected with JFH-1 for 48 hours were costained for Staufen1 and the HCV core protein (**Fig. 5.10b**), Staufen1 and the HCV NS3 protein (**Fig. 5.10c**) and Staufen1 and dsRNA (representing the replicating viral genome) (**Fig. 5.10d**). A comparison was made between the intracellular localisation of Staufen1, HCV core, HCV NS3 and dsRNA in the JFH-1 infected cells. Although Staufen1 and the HCV core proteins localised very closely to one another during infection, the two proteins did not appear to overlap, indicating that Staufen1 may not localise to the core-coated lipid droplets (**Fig. 5.10b**). When comparing the localisation of Staufen1, NS3 and dsRNA, colocalisation was observed in some areas of the cell, although there were still areas where Staufen1 was found separately from both NS3 and dsRNA (**Fig. 5.10c and d**).

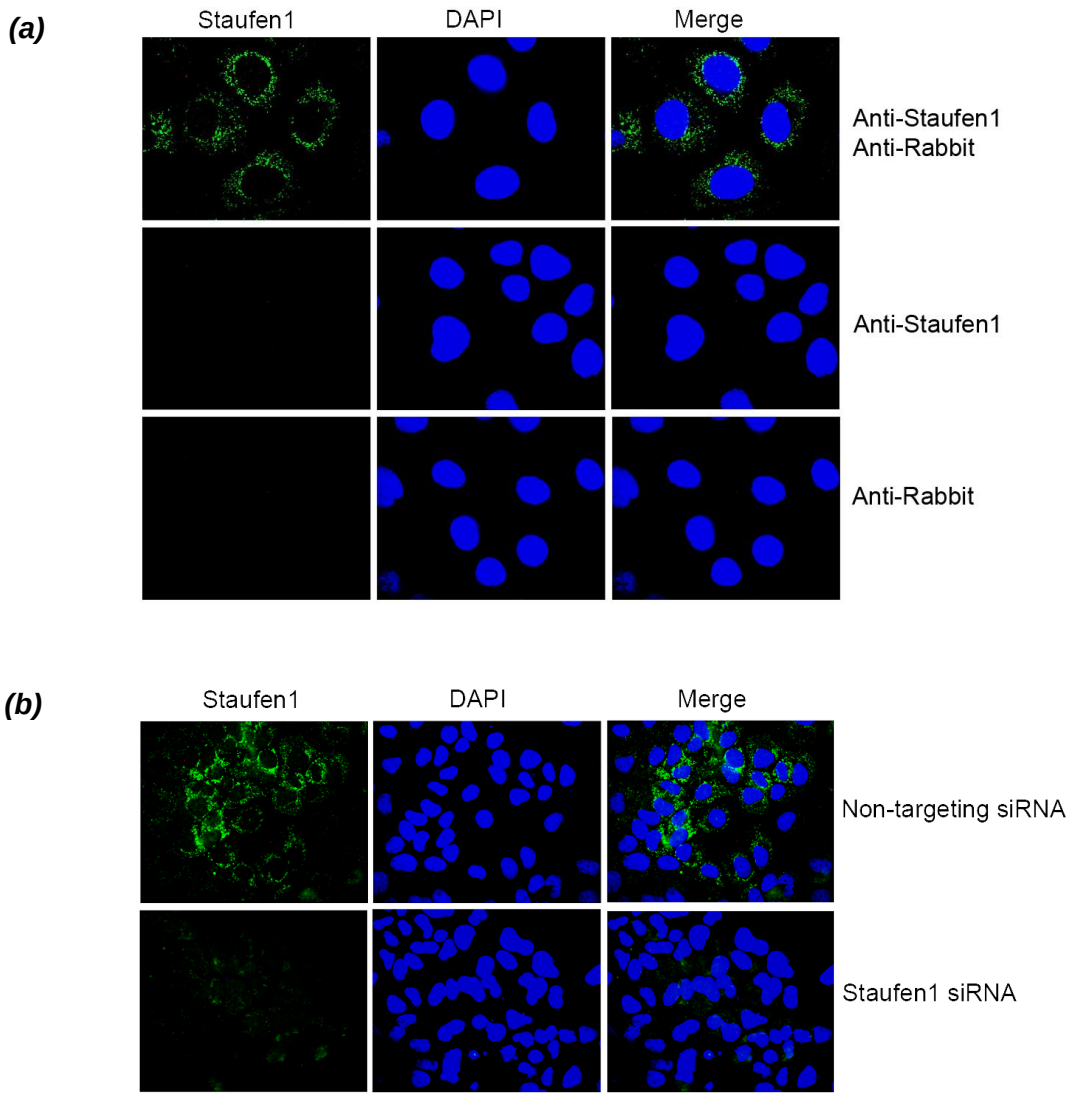
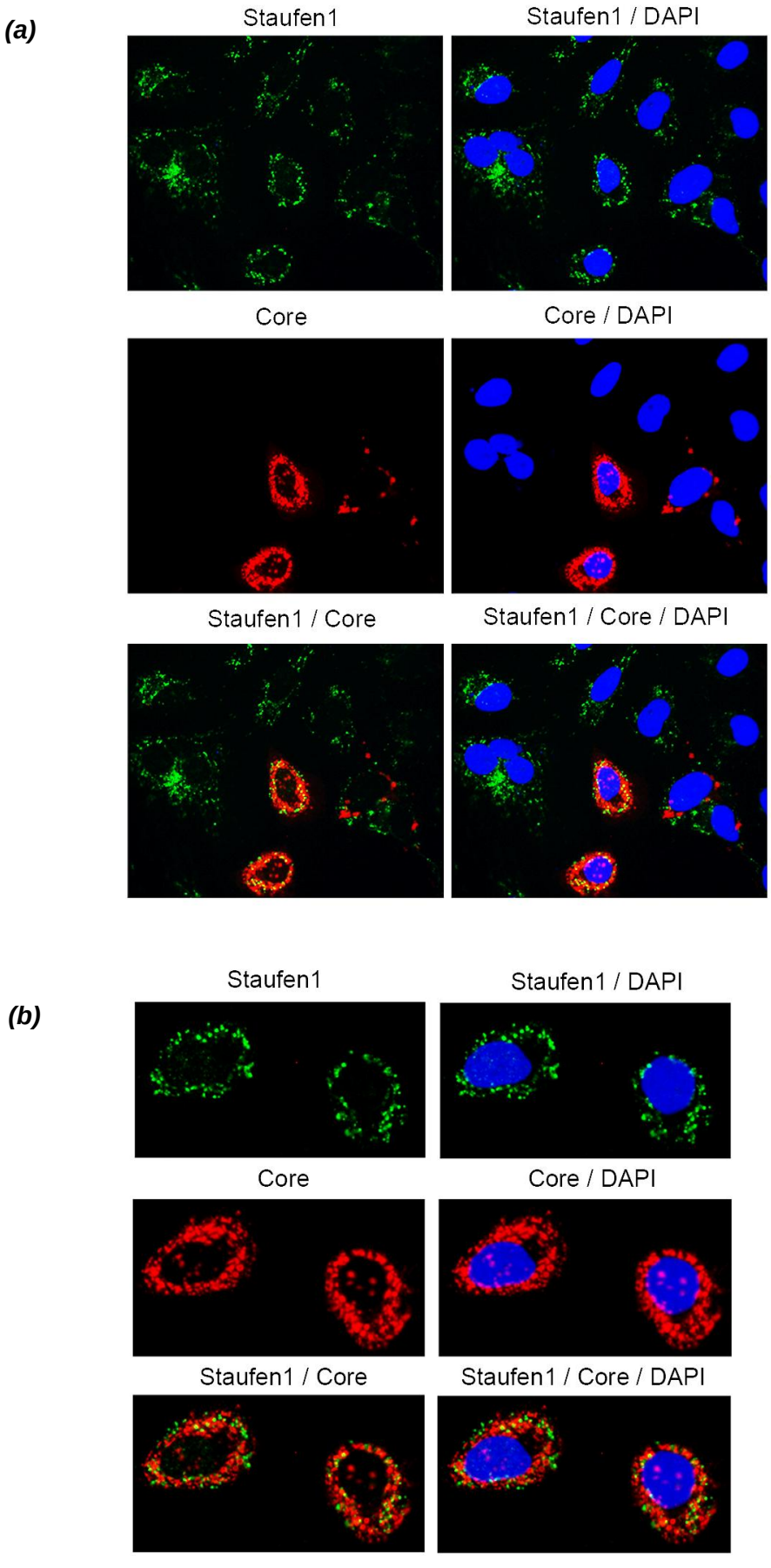


Figure 5.9 An anti-Staufen1 antibody detects a protein at the nuclear periphery

(a) *Staufen1 protein staining in uninfected Huh7 cells using a rabbit anti-Staufen1 antibody (green staining). The bound primary antibody was detected using a 488 Alexa Fluor-conjugated anti-rabbit antibody. Huh7 cells were also stained either with the anti-Staufen1 antibody alone (anti-Staufen1) or the Alexa Fluor anti-rabbit antibody alone (anti-Rabbit). Cell nuclei were stained with DAPI (blue staining). Images were captured using a Nikon Eclipse TE2000S fluorescence microscope at a magnification of 60x.* ***(b)*** *Staufen1 protein staining in Huh7 cells transfected with Staufen1 siRNA molecules. Huh7 cells were transfected with 50nM of Staufen1 siRNA pool (siSTAU1-1 and siSTAU1-2) or 50nM of negative control non-targeting siRNA for 48 hours. The cells were stained for Staufen1 protein using the anti-Staufen1 antibody (green staining) and cell nuclei were stained with DAPI (blue staining). Images were captured using a Nikon Eclipse TE2000S fluorescence microscope at a magnification of 40x. All images were taken using the same exposure time and gain settings to ensure accurate comparison of staining.*


(a)
Staufen1
Staufen1 / DAPI
Core
Core / DAPI
Staufen1 / Core
Staufen1 / Core / DAPI
(b)
Staufen1
Staufen1 / DAPI
Core
Core / DAPI
Staufen1 / Core
Staufen1 / Core / DAPI

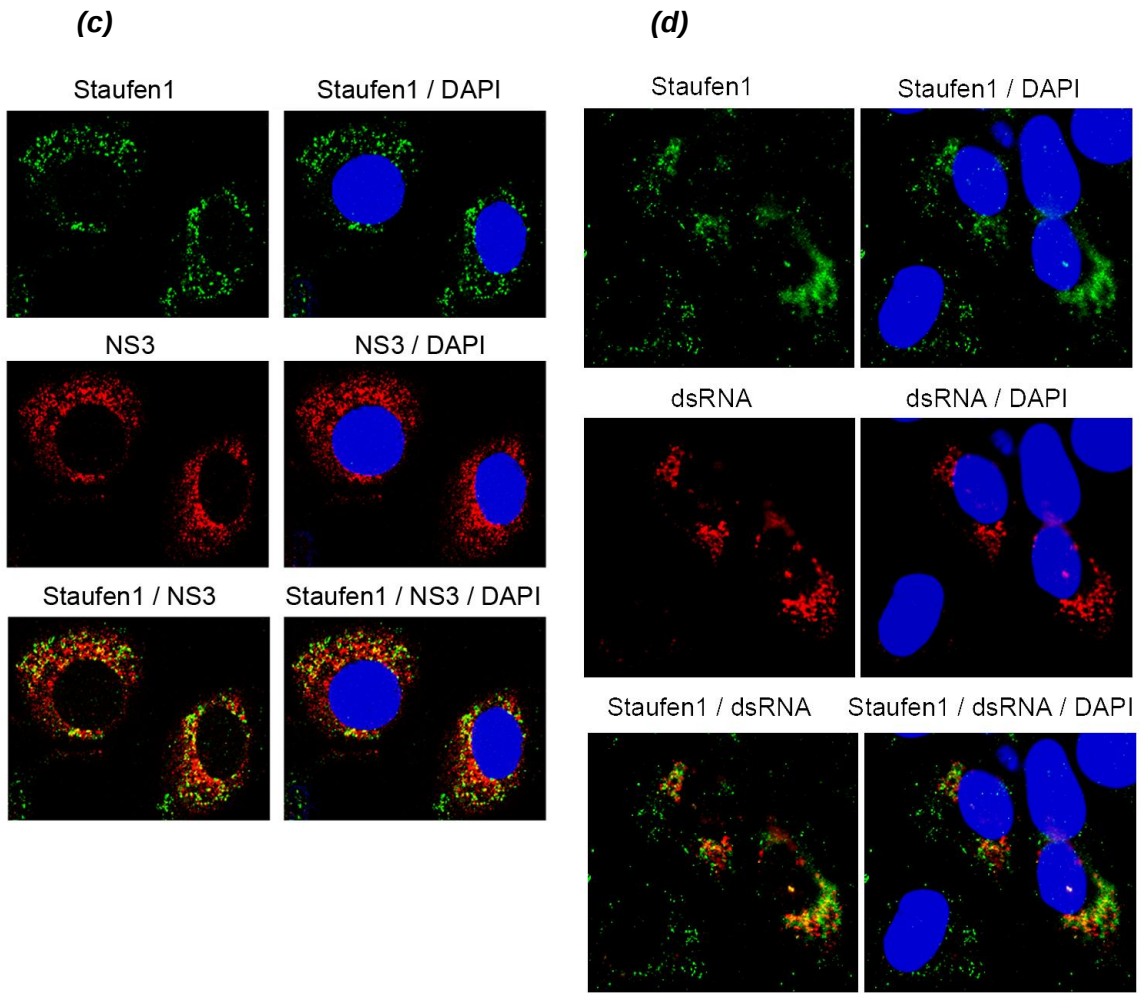


Figure 5.10 The intracellular localisation of Staufen1 during JFH-1 infection

Staining of Staufen1, HCV core, HCV NS3 and dsRNA in JFH-1 infected Huh7 cells. Huh7 cells were infected with JFH-1 (MOI = 0.5) for 48 hours and stained using the rabbit anti-Staufen1 antibody (green staining). Staining was also performed with ***(a/b)*** *the mouse anti-core antibody (red staining),* ***(c)*** *the mouse anti-NS3 antibody (red staining) and* ***(d)*** *the mouse anti-dsRNA antibody (red staining). Cell nuclei were also stained with DAPI (blue staining). Images were captured using a Nikon Eclipse TE2000S fluorescence microscope at a magnification of 60x and 100x. All images were taken using the same exposure time and gain settings to ensure accurate comparison of staining.*

Chapter 5: Discussion

The role of TXNIP in the HCV replication cycle

Why is TXNIP expression upregulated during JFH-1 infection?

Several host transcription factors that control TXNIP expression were upregulated during JFH-1 infection (e.g. FOXO1, MLXIPL, HIF1α and KLF6) indicating that these factors may contribute to the increased expression of TXNIP observed (**Fig. 5.1**). Other studies investigating the effect of HCV infection on host gene expression have also observed an increase in the expression of KLF6 [165] and MLXIPL [164], providing evidence to support these observations. However, when the effect of transcription factor silencing on TXNIP expression was investigated, the only factors shown to be essential for TXNIP transcription were those encoding the MLX transcription factor complexes (e.g. MLX, MLXIP and MLXIPL) (**Fig. 5.4**). The reduction observed in TXNIP expression when these factors were silenced was almost as significant as that observed when the cells were transfected with the TXNIP siRNA molecules; indicating that the MLX transcription factor complexes may directly stimulate TXNIP transcription during HCV infection. Silencing the expression of other factors, such as FOXO1 and KLF6, had no effect on the expression of TXNIP indicating that the effects observed when silencing the MLX transcription factor complexes were likely to be specific. Even though KLF6 silencing did not alter TXNIP expression, it did significantly reduce the replication and secretion of JFH-1; indicating that this factor may regulate the expression of additional host genes required during the HCV replication cycle.

The observation that knockdown of MLX, MLXIP and MLXIPL significantly reduced TXNIP expression indicated that both of the transcription factor complexes formed by these proteins (e.g. MLX/MLXIP and MLX/MLXIPL) may be required for activation of TXNIP transcription in Huh7 cells (**Fig. 5.4**). This is different to the findings observed in previous studies investigating TXNIP transcription, which often demonstrate that only one of the MLX transcription factor complexes is required for TXNIP transcription. For example, the MLX/MLXIP complex has been shown to stimulate TXNIP transcription in HeLa cells, L6 cells and U20S cells and is expressed predominantly in skeletal and muscle tissue, whilst the MLX/MLXIPL complex has been shown to stimulate TXNIP transcription in INS-1 cells and HepG2 cells and is expressed predominantly in liver tissue [338, 339].

Although MLXIPL was upregulated by two-fold during JFH-1 infection, MLX and MLXIP were not observed to alter in expression. This indicates that the upregulation of TXNIP during infection is unlikely to occur because of an increase in the expression of the factors that control TXNIP transcription. Instead, it is possible that post-transcriptional or post-translational alterations may occur in the cell to stimulate the activity of the MLX transcription factor complexes during JFH-1 infection. Studies investigating cellular conditions responsible for stimulating MLX transcription factor complex activity have demonstrated that high levels of intracellular glucose and lactic acid increase the expression of many MLX transcription factor complex target genes, including TXNIP [326, 339, 340]. Both of these conditions are associated with an increased rate of cellular glycolysis, as high glucose conditions promote glycolytic metabolism of excess glucose, and lactic acid accumulation occurs in cells following the process of anaerobic glycolysis. Recent studies investigating the effect of glycolysis on the activity of MLX transcription factor complexes have demonstrated that several of the early glycolytic intermediates (glucose-6-phosphate (G6P) and glyceraldehydes-3-phosphate (GAPD)) are able to directly stimulate the activity of the MLX transcription factor complexes [327, 339]. In particular, G6P has been shown to play a key role in the activation of TXNIP transcription by MLX/MLXIP, as it has been shown to promote nuclear accumulation, TXNIP promoter occupancy and transcriptional activation of the MLX/MLXIP complex [326, 339]. Together these findings indicate that there may have been an increase in the abundance of glycolytic intermediates during JFH-1 infection which may have stimulated the activity of the MLX transcription factor complexes to upregulate TXNIP expression.

Investigation into the intracellular abundance of glucose during JFH-1 infection demonstrated that glucose levels did not alter significantly at 48 hours post-infection (**Fig. 5.2**). In addition, investigation into the expression of glucose metabolism genes during JFH-1 infection demonstrated that there were no obvious alterations in glycolysis or gluconeogenesis, as genes involved in these pathways showed conflicting expression patterns with increases and decreases in gene expression taking place within each pathway (**Fig. 5.3**). These findings indicated that there was not a significant increase in the rate of glycolysis during JFH-1 infection that may account for an increase in the activity of the MLX transcription factor complexes. Despite these observations, other studies investigating the effect of HCV infection on the rate of cellular glycolysis have

instead demonstrated a significant increase in the abundance of proteins involved in glycolysis as a result of HCV infection, including significant increases in the lactate dehydrogenase enzyme (LDHA), which drives glycolysis towards the production of lactic acid [150]. An increase in the rate of glycolysis in HCV infected cells has also been observed to occur as a result of reduced cellular oxidative phosphorylation, which occurs following the onset of HCV-induced mitochondrial-mediated apoptosis [341]. These observations, therefore, provide evidence to indicate that there may have been an increase in the abundance of glycolytic intermediates during HCV infection. One reason that may account for the minimal effects observed on glycolysis as a result of JFH-1 infection in this study (**Fig. 5.2 and 5.3**) may be the focus of the investigation on the mRNA expression levels of the glycolytic genes (**Fig. 5.3**). Previous studies demonstrating increased abundance of glycolytic enzymes during HCV infection did not observe a concordant increase in the expression of the genes encoding these enzymes; and it was suggested that the expression changes taking place occurred as a result of post-transcriptional regulatory mechanisms [150]. To gain further insight into the mechanisms regulating TXNIP expression during HCV infection, future studies need to be performed to quantify the abundance of glycolytic intermediates during HCV infection and to investigate the effect of HCV infection on the trafficking of MLX transcription factor complexes.

In this study, the upregulation of TXNIP expression during JFH-1 infection has been shown to be dependent on the activity of the MLX transcription factor complexes (**Fig. 5.4**). However, many other MLX target genes either did not alter in expression or were observed to decrease in expression during JFH-1 infection (**Appendix A.19**). This included genes involved in glycolysis (PFKFB3), gluconeogenesis (G6PC3 and SLC37A4), fatty acid synthesis (ACYL, ACACA and FASN), and cholesterol metabolism (DHCR7) [326, 336, 337]. One exception to these findings was ARRDC4, an MLX target gene that is highly homologous to TXNIP [318], which was significantly upregulated during JFH-1 infection (**Fig. 5.6 and Appendix A.19**). These findings indicate that the increased transcriptional activity of the MLX transcription factor complexes during JFH-1 infection may be specific to the genes encoding TXNIP and ARRDC4. Further investigation by qRT-PCR into the effect of JFH-1 infection on the expression of other MLX transcription factor complex target genes is required to validate these findings.

What role does TXNIP play in the HCV replication cycle?

Silencing the expression of TXNIP significantly reduced the levels of JFH-1 replication and secretion observed in JFH-1 infected Huh7 cells (**Fig. 4.9**), indicating that TXNIP may be an important host factor involved in the HCV replication cycle. This finding was supported by the observation that silencing the expression of MLX, MLXIP and MLXIPL, which resulted in the knockdown of TXNIP expression, also reduced the replication and secretion of JFH-1 (**Fig. 5.4**). Furthermore, a recently published siRNA screen investigating host factors required during HCV infection also demonstrated that silencing MLXIPL reduced the replication and secretion of JFH-1 by an average of 73% and 78%, respectively [116].

To determine whether the potential role of TXNIP during the HCV replication cycle was specific to the TXNIP protein, or was associated with a more general function of the alpha-arrestin proteins, the requirement for ARRDC4 expression during HCV infection was investigated. ARRDC4 was chosen for further investigation because it shares the greatest level of homology with TXNIP [318, 342] and its expression was significantly upregulated during JFH-1 infection (**Fig. 5.6a**). However, despite the overlap in the functional properties of ARRDC4 and TXNIP, silencing the expression of ARRDC4 had minimal effects on the HCV replication cycle (**Fig. 5.6b**). This indicates that the function of TXNIP required during the HCV replication cycle may be specific to the TXNIP protein. Further investigation into the role of the other alpha-arrestin family members in the HCV replication cycle is required before it is possible to conclude that TXNIP is the only family member required during the HCV replication cycle. It would also be advisable to test additional anti-ARRDC4 siRNA molecules for their effects on the JFH-1 replication cycle, as the knockdown achieved with the siRNA used was only 70% effective (**Fig. 5.6b**).

Two of the potential TXNIP functions that may account for its role in the HCV replication cycle include its involvement in the process of hepatic gluconeogenesis [275], and its ability to alter the activity of the PPARα transcription factor [239]. Since the intracellular levels of glucose did not alter during JFH-1 infection (**Fig. 5.2**), initial analysis of TXNIP function was focused on the role of TXNIP in the regulation of PPARα activity.

The PPARα transcription factor is predominantly involved in the transcription of genes controlling fatty acid oxidation and transport. The ability of TXNIP to inhibit PPARα signalling [239] may be important for controlling the availability of lipids required during infection by altering the rate at which fatty acid uptake and oxidation takes place. As a result of this potential function, it was originally hypothesised that silencing TXNIP expression may increase PPARα activity and the expression of PPARα target genes and may induce an increase in the rate of intracellular fatty acid oxidation. This may lead to a reduction in the abundance of fatty acids available for synthesis of key lipid metabolites which may lead to a reduction in the rate of HCV replication. However, investigation into the effect of TXNIP silencing on the expression of PPARα target genes demonstrated that complex mechanisms may be involved in the regulation of PPARα signalling, as several target genes were observed to increase in expression following TXNIP knockdown, whilst others were observed to decrease in expression (**Fig. 5.7**). Out of the PPARα target genes investigated, those which increased in expression following TXNIP silencing included: ACADL, which is involved in mitochondrial beta-oxidation of fatty acids [343]; TRIB3, which has been implicated in the regulation of apoptosis [344] and degradation of acetyl-coenzyme A carboxylase (ACC), the rate-limiting enzyme for fatty acid synthesis [345]; and CPT1A / CPT2, which are involved in the transport of fatty acids across the mitochondrial membrane for fatty acid oxidation [346] (**Fig. 5.7a and b**). Simultaneous upregulation of these genes in Huh7 cells may increase the rate of fatty acid oxidation and decrease fatty acid synthesis reducing the availability of fatty acids for production of essential triglyceride, sphingolipid and phospholipid metabolites. The reduced replication and secretion of JFH-1 observed in the TXNIP knockdown cells may, therefore, have resulted from increased expression of these PPARα target genes. One factor that complicates the findings from this investigation was the observation that the genes encoding ACADL, TRIB3 and CPT1A were actually upregulated in the Huh7 cells infected with JFH-1 for 48 hours (**Fig. 5.7c**); indicating that increased expression of these genes may not necessarily compromise virus replication. However, it is possible that further increases in the expression of these genes following TXNIP silencing increased the rate of fatty acid oxidation to a level that reduced progression through the HCV replication cycle. Studies investigating overexpression of these proteins would provide some insight into the validity of these claims.

Alongside genes that increased in expression, other genes were observed to decrease in expression following TXNIP silencing including ACSL3, a host factor required during VLDL synthesis that is essential for HCV secretion [50]. These findings were confirmed for individual siRNAs targeting TXNIP expression (**Fig. 5.8**), and indicate that reduced JFH-1 secretion may occur in the TXNIP knockdown cells because of reduced ACSL3 expression. To avoid the possibility that changes in ACSL3 were entirely due to the level of JFH-1 replication, which independently upregulated ASCL3 expression and was reduced by TXNIP silencing, it was important to demonstrate that TXNIP knockdown reduced ACSL3 expression in both infected and uninfected Huh7 cells (**Fig. 5.7a and b**). The observation that ACSL3 expression was depleted following TXNIP silencing in uninfected cells confirmed that this was a direct effect of TXNIP knockdown, and not an indirect effect caused by changes in the intracellular JFH-1 level.

When comparing the results observed for the infected and uninfected TXNIP knockdown cells, several additional PPARα target genes were observed to be upregulated in the TXNIP knockdown infected cells. This included genes encoding: the PPARα transcription factor itself; PDK4, which is an inhibitor of pyruvate dehydrogenase: the enzyme required for metabolism of glucose to pyruvate for acetyl-CoA production [347]; ECH1, which is involved in an auxiliary step of fatty acid beta-oxidation [348]; and ACOX1, which is the first enzyme involved in peroxisomal fatty acid beta-oxidation [349] (**Fig. 5.7a and b**). The upregulation of these genes following TXNIP knockdown in the JFH-1 infected cells may further contribute to the reduced replication and secretion of JFH-1 observed because of their ability to promote fatty acid oxidation and inhibit production of acetyl-CoA, an essential component required for intracellular lipid synthesis. The differences observed in the expression of these genes in the infected and uninfected TXNIP knockdown cells may reflect the period of time for which the cells have been transfected, as the infected cells were harvested at 96 hours post-transfection and showed greater efficiency of TXNIP knockdown, compared to the uninfected cells, which were harvested at 48 hours post-transfection and had a lower efficiency of TXNIP knockdown (**Fig. 5.7a and b**). It is also possible that the presence of the virus in the infected cells had additional effects on the transcriptional regulation of genes. Although the expression of PPARα and PDK4 was not upregulated in the infected cells, and the expression of ACOX1 and ECH1 was only slightly upregulated during infection (**Fig. 5.7c**).

Investigation into the effects of TXNIP knockdown on PPARα target gene expression enabled identification of several expression patterns that may have been responsible for the reduction of JFH-1 replication and secretion in the TXNIP knockdown cells. However, much more detailed analysis of the gene expression patterns observed is required to validate these findings. In addition, it will also be important to investigate whether TXNIP knockdown actually alters the intracellular abundance of fatty acids and lipid metabolites. One technique that could be used to quantify intracellular lipids in the TXNIP knockdown cells may involve lipid droplet staining with BODIPY. Future experiments that compare lipid droplet abundance between TXNIP expressing and TXNIP knockdown cells may be performed to investigate the effect of TXNIP silencing on lipid droplet abundance.

The role of Staufen1 in the HCV replication cycle

Does Staufen1 interact with HCV proteins and HCV RNA during JFH-1 infection?

Staining of JFH-1 infected Huh7 cells for the Staufen1 protein demonstrated that the cellular localisation of Staufen1 does not appear to alter significantly during HCV infection (**Fig. 5.10a**). Further investigation of Staufen1 localisation during infection also indicated that Staufen1 does not appear to colocalise with the HCV core protein, but may partially colocalise with the HCV NS3 protein and the dsRNA replicative intermediate of the HCV genome (**Fig. 5.10b, c and d**). These findings suggest that Staufen1 may localise to the HCV replication complexes that contain the HCV NS3 protein and dsRNA intermediate, but not the core-coated lipid droplets which participate in virus assembly. This indicates that Staufen1 may facilitate the processes involved in replication, translation or trafficking of the HCV genome, but not the process of nucleocapsid assembly and supports the observation that Staufen1 knockdown reduced the extracellular titres of JFH-1 virus and the intracellular abundance of JFH-1 RNA and JFH-1 protein present in JFH-1 infected cells (**Fig. 4.6, 4.9 and 4.16**). It also supports the observation that Staufen1 interacts with the 3’ NTR of the HCV genome and the 5’NTR of the negative RNA strand, which are present in HCV replication complexes as the replicative intermediate form of the HCV genome [155, 156]. Together these findings indicate that the function of Staufen1 in the HCV replication cycle may be distinct from the function observed for Staufen1 in the replication cycles of HIV and Influenza A, where it has been shown to colocalise with virus nucleocapsid

proteins to facilitate nucleocapsid formation [196, 198] and has been shown to relocalise to virus assembly sites as a result of infection [197].

Although the colocalisation data observed supports the observation that Staufen1 silencing reduced JFH-1 replication and secretion, it does not explain why the rate of secretion was reduced more significantly than the rate of replication in the JFH-1 infected cells (**Fig. 4.6 and 4.9**). These findings initially indicated that Staufen1 is more likely to be required for the process of virion particle formation than the process of HCV genome replication. However, the lack of colocalisation observed between Staufen1 and the HCV core protein suggests that Staufen1 is unlikely to be present at the site of nucleocapsid formation or during the budding and secretion of nascent virus particles. One possible explanation that may account for the findings observed in both the siRNA knockdown assay and colocalisation study is that Staufen1 may be required for an early stage of the virus assembly process that is not associated with the HCV core protein. For example, Staufen1 may facilitate the switch from genome replication to assembly within the HCV replication complex, or it may be required for trafficking of the HCV genome to the lipid droplet surface for initiation of nucleocapsid formation. It is possible to envision a situation whereby Staufen1 may bind to the HCV genome as part of a larger ribonucleoprotein complex, which may also contain host factors required for the processes of HCV genome replication or translation. Therefore, knockdown of Staufen1 may not only reduce Staufen1-mediated assembly function, but it may also disrupt the correct formation of this ribonucleoprotein complex and may alter the binding of other essential HCV cofactors required for genome replication and translation. This type of effect may explain how Staufen1 silencing was able to reduce the extracellular levels of JFH-1 virus (e.g. 60% to 80% reduction) much more significantly than the intracellular levels of JFH-1 RNA (e.g. 30% to 40% reduction) in the JFH-1 infected Huh7 and Huh7.5 cells (**Fig. 4.6 and 4.9**).

Studies investigating the processes involved in the trafficking of the HCV genome to the lipid droplet surface for nucleocapsid formation have demonstrated that the HCV genome may be transported in a complex that contains NS3 alongside other HCV proteins (e.g. NS2, NS5A, P7, E1 and E2) [43]. It is possible that this complex may also contain the Staufen1 protein and may be responsible for the colocalisation observed between Staufen1 and NS3 during JFH-1 infection (**Fig. 5.10**). The NS3 helicase domain was also recently shown to interact directly with

the HCV core protein. This provides further evidence to indicate that NS3 containing ribonucleoprotein complexes may play an essential role in the trafficking of the HCV genome to the lipid droplet surface for initiation of virus particle assembly [350].

Alongside the observations in this study that suggest a potential role for Staufen1 in the regulation of HCV genome replication, translation and trafficking, a recent study investigating HCV endocytosis indicated that Staufen1 may be required during HCV particle entry [254]. The intracellular localisation observed for Staufen1 during JFH-1 infection indicates that Staufen1 is unlikely to play a role in the process of E1/E2 mediated cellular entry (**Fig. 5.10**). Instead, Staufen1 may facilitate actin and microtubule filament trafficking of the pseudo-particle RNA following endocytosis or translation of the RNA at the ER. It is also possible that the role of Staufen1 in the regulation of host translation may regulate the expression of a key host factor involved in the process of endocytosis [334].

The colocalisation data presented in this chapter provides a preliminary insight into the role of Staufen1 in the HCV replication cycle. Greater clarification of the findings observed may be provided using co-immunoprecipitation experiments to determine whether Staufen1 is able to bind directly to HCV proteins. Further investigation should also be performed to determine whether Staufen1 knockdown significantly alters the rate of HCV genome replication and translation using replication deficient HCV variants and subgenomic replicon expressing cells.

Chapter 5: Conclusions

Through microarray expression profiling and siRNA knockdown analysis (**Chapter 3 and 4)**, TXNIP was identified as a host factor upregulated during HCV infection with a potential cofactor role in the HCV replication cycle. Further investigation into the transcription factors that control TXNIP expression demonstrated that silencing MLX transcription factor complexes reduced TXNIP expression and the level of JFH-1 replication and secretion. This indicated that these factors may be responsible for upregulating the expression of TXNIP during infection. Other members of the alpha arrestin family, to which TXNIP belongs, were also upregulated during JFH-1 infection, including ARRDC4. However, this protein was shown to be non-essential for the HCV replication cycle. Attempts to understand the potential role of TXNIP in the HCV replication cycle have indicated that TXNIP silencing upregulates genes involved in fatty acid oxidation and inhibition of fatty acid synthesis, consistent with the inhibition of PPARα by TXNIP. Several PPARα target genes involved in fatty acid activation and lipid synthesis were also surprisingly downregulated as a result of TXNIP silencing. The gene expression patterns observed as a result of TXNIP knockdown provide some insight into why TXNIP silencing may affect the HCV replication cycle. However, detailed analysis of the transcriptional and metabolic effects of TXNIP knockdown are required to gain further insight into the potential HCV cofactor function of TXNIP.

Staufen1 protein has been shown to facilitate the process of virus particle assembly for HIV and Influenza A virus. Recent studies have also shown that Staufen1 can bind the HCV RNA genome indicating a potential role of Staufen1 in the HCV replication cycle. Investigation by siRNA knockdown demonstrated that silencing of Staufen1 reduced the ability of the host cell to support the replication and secretion of JFH-1 virus. Investigation of Staufen1 cellular localisation demonstrated partial overlap of the Staufen1 protein with HCV NS3 and dsRNA in JFH-1 infected cells. These observations indicate that Staufen1 may play a potentially important role in the HCV replication cycle during the early phases of infection prior to nucleocapsid formation, virion particle budding and secretion. Future experiments should be performed to investigate whether Staufen1 can directly interact with HCV proteins, and whether Staufen1 is required for specific processes during HCV infection such as genome replication, genome translation or the trafficking of HCV RNA to virus assembly sites.

Chapter 6: General Discussion and Future Work

6.1 Introduction

The replication cycle of HCV is a complex process that relies heavily upon interactions that form between the virus and the host cell. Understanding the molecular mechanisms involved in different stages of this replication cycle has become a key focus of research, as the hunt for novel therapeutic targets intensifies in the drive to develop next generation antiviral therapeutics [7].

Recent developments in the field of HCV research, such as the generation of the fully infectious JFH-1 clone [135], alongside significant advances in the field of genomics has provided an excellent set of tools that can be used to improve our understanding of the HCV replication cycle. As a result, the past few years has seen a rapid increase in the numbers of host cell factors identified as either key structural or functional components of the HCV replication cycle.

In 2007, when this research project began, the fully infectious JFH-1 clone had only recently been developed, many aspects of the HCV replication cycle had not been characterised, and only a limited number of host factors required during HCV infection had been identified. In addition, little work had been done to investigate the host cell response during the full HCV replication cycle. To try and build a greater understanding of the processes involved in HCV infection, an aim was established for the project to combine the use of the latest genomic expression profiling techniques with the recent developments in culturing infectious HCV to provide a thorough investigation of the host cell response to HCV infection. It was hypothesised that the data generated may facilitate an increased understanding of the mechanisms contributing to pathogenesis and may help to identify host factors with a role in the HCV replication cycle. At the same time, a more targeted approach to HCV research was also proposed to provide an alternative method for identifying host factors involved in the HCV replication cycle; this involved the analysis of candidate host proteins selected from the replication cycle of other RNA viruses.

6.2 The host cell response to HCV infection

The use of microarray expression profiling to investigate host gene expression in JFH-1 infected cells has provided invaluable insight into the host cell response to HCV infection. This study was the first genome-wide investigation to be published that analysed the Huh7 cell response to JFH-1 infection and was the second study

to be published analysing the host cell response to the entire HCV infection cycle [149, 215]. As a result of this study, HCV infection has been shown to alter the expression of many genes belonging to several key cellular pathways. As predicted, a number of the pathways significantly altered by infection provide potential insight into the mechanisms underlying HCV associated pathogenesis. This includes the pathways regulating interferon signalling, cellular proliferation and apoptosis, lipid metabolism and oxidative stress, which may contribute to the development of inflammation, hepatocyte cell death, hepatic steatosis and oxidative stress-induced damage that are frequently observed to occur in the livers of chronically infected patients (**Fig. 3.6**) [167, 168, 170]. Since the publication of these findings [215], a number of other microarray expression profiling experiments investigating HCV infection have been published and have demonstrated good consistency with the expression patterns observed in this study [149, 164, 165].

So far, the gene expression patterns observed through microarray analysis have been validated using qRT-PCR (**Fig. 3.8**). In addition, the increased expression of lipid synthesis genes has been shown to increase the protein levels of key lipid metabolism regulators (**Fig. 3.19**) and the abundance of intracellular lipid metabolites (**Fig. 3.21 and 3.23**), indicating that HCV infection may contribute directly to the development of hepatic steatosis. In order to determine whether the other expression patterns observed may also contribute to the pathogenesis of infection, further investigation should be performed to determine the effect of HCV infection on host protein abundance and intracellular signalling. Another PhD student in Dr McGarvey's laboratory, Fadhil Al-Hababi, recently investigated the effect of JFH-1 infection on cellular proliferation and demonstrated that an increase in the rate of cell cycle arrest and apoptosis was observed to occur as a result of infection [216]. These findings support the gene expression patterns identified and indicate that HCV may contribute directly to the increased levels of hepatocyte cell death observed in chronically infected patients. Other research groups have also observed that HCV infection increases the rate of apoptosis and cell cycle arrest [149] and induces an accumulation of intracellular lipid metabolites and reactive oxygen species [164] supporting the gene expression patterns observed in this study (**Fig. 3.6**). Future studies that might be performed to investigate the pathogenic consequences of the host gene expression patterns observed include detailed analysis of the intracellular lipid metabolites present

during infection using powerful techniques such as nuclear magnetic resonance (NMR) spectroscopy and mass spectroscopy. Our laboratory is currently in the process of establishing collaboration with Professor Elaine Holmes (Imperial College London) to perform detailed metabolic analysis of JFH-1 infected cells. These studies should provide greater insight into the abundance of a variety of lipid metabolites during HCV infection, including different phospholipid and fatty acid species. In addition, further investigation into the effect of HCV infection on the activity of the cellular anti-oxidant system could also be performed to investigate whether a decrease in antioxidant signalling occurs as a result of HCV infection.

Previous studies comparing the effect of HCV infection on host gene and protein expression have often found disconcordant results, as post-translational regulatory mechanisms can alter host protein abundance independently of cellular mRNA [150, 164]. As a result of these observations, much more detailed analysis of host protein expression during HCV infection is also required to determine whether the gene expression patterns observed are likely to impact host cell function.

In addition to validating the biological impact of the gene expression changes observed, another key consideration is how accurately they reflect the expression changes that take place in the liver hepatocytes of chronically infected patients. The microarray expression study described was performed using the Huh7 cell line, instead of the RIG-I deficient Huh7.5 cell line [140], which has been used for most other published genomic studies of HCV infection [149, 164, 165]. However, even with its intact RIG-I pathway, the Huh7 cell line is still a transformed cell line and has different properties to normal liver hepatocytes. Huh7 cells are not polarised and grow in a monolayer, unlike liver hepatocytes, which are polarised and grow in the 3D structure of the liver. In addition, Huh7 cells have many tumour-like properties including abnormal proliferation, deregulated gene expression and dysfunctional mitochondria. Huh7 cells also express high levels of α-fetoprotein, a marker of cellular dedifferentiation; have a mutated p53 gene; express elevated levels of glucose metabolism enzymes and overexpress the pituitary tumour transforming gene (PTTG) [147].

To determine how accurately the expression patterns observed reflect those occurring in infected liver hepatocytes, the host response to infection should be investigated in a system that better reflects the *in vivo* situation. A range of

different *in vitro* and *in vivo* systems for investigating the HCV replication cycle were highlighted in **Chapter 1.** One of the approaches that could be used to test the validity of the expression patterns observed is the analysis of *in vitro* cultured primary human hepatocytes, which can be successfully infected with cell culture grown HCV. Recent data comparing the virions produced by primary human hepatocytes and Huh7 cells infected with JFH-1 demonstrated that the virions produced by the primary hepatocytes were most similar to those observed in patients. Further research demonstrated that this was associated with the ability of primary hepatocytes to secrete virus particles in complex with ApoB containing triglyceride rich lipoproteins. By comparison, Huh7 cells do not secrete HCV particles in their natively assembled form, as particles are found in association with ApoE, but not ApoB. This defect in HCV particle assembly is due to the inability of Huh7 cells to secrete authentic VLDL particles, as ApoB containing pre-VLDL particles are not fully lipidated and cannot fuse with ApoE containing precursors [23, 145].

Further validation of expression patterns could also be performed using liver biopsy material isolated from chronically infected patients or the recently developed humanised immunocompetent mouse model for HCV infection [153]. Although, the heterogeneous nature of patient biopsy material can make it difficult to observe HCV induced expression changes, several studies have successfully characterised the gene and protein expression profiles of HCV infected hepatocytes using material isolated from patients [149, 150]. One recent study compared the results obtained following microarray analysis of *in vitro* infected Huh7.5 cells and patient biopsy tissue. This study demonstrated good consistency in the gene expression profiles observed indicating that *in vitro* cell culture systems provide an accurate representation of the events occurring in chronically infected patients [149]. Studies making comparisons such as these also highlight another important consideration for the data obtained in this study. This is the question of whether different HCV virus strains belonging to different HCV genotypes induce the same host cell response during infection. All microarray studies published to date that have performed analysis of *in vitro* infected cells utilise virus produced from the genotype 2a HCV clones: JFH-1 and Jc1 [149, 164, 165, 215]. Both of these HCV clones have an increased replication capacity in comparison to most serum derived HCV particles and studies have demonstrated that JFH-1 and Jc1 both induce a high level of cellular apoptosis [149, 351].

Comparison of the pro-apoptotic effect of HCV infection between different HCV genotypes indicates that high levels of apoptosis may be associated with genotype 2a HCV strains only [146, 352]. Furthermore, the JFH-1 clone was derived from a patient suffering from a rare fulminant HCV infection [353] compared to the slow progressing chronic HCV infection that usually occurs in patients. Together, these differences raise a valid concern for how accurately the JFH-1 and Jc1 replication cycles reflect those of other HCV virus strains that are found more frequently in patients. At present, it is not possible to easily investigate the answer to this question using cell culture grown virus, as the only other infectious HCV clone available is the H77S genotype 1a clone [352]. However, since serum derived HCV particles can be used to infect cultured primary human hepatocytes, it might be possible to investigate the host cell response to a variety of different serum derived HCV strains using this system [146, 147].

To further explore the data observed in the microarray profiling experiment, an investigation was also performed to characterise the gene expression patterns observed in cells expressing a genotype 2a (GT2a) subgenomic replicon (**Fig. 3.12 and 3.13**). The purpose of this was to determine whether HCV non-structural proteins were responsible for inducing the expression patterns observed during HCV infection. An attempt to create a core protein expressing cell line was also made to determine whether the HCV core protein significantly alters host gene expression. This type of work can be useful when trying to determine whether specific HCV proteins are responsible for the pathogenesis observed during infection. For example, the HCV core protein has been shown to play a particularly significant role in the development of hepatic steatosis [263]. This may be associated with the ability of HCV core to upregulate the expression of genes involved in lipid synthesis and its ability to inhibit the VLDL secretory pathway [66, 263]. Although a number of the expression patterns observed during infection were also observed in the replicon expressing cells, many of the host genes did not alter in expression in the presence of the non-structural proteins. In order to accurately determine whether specific HCV proteins contribute to the regulation of host gene expression, more thorough analysis of the effects that HCV proteins have on host gene expression is required. This might involve the expression of each HCV protein individually in cells and assessment of the gene expression profiles observed. The drawback to this type of investigation is that expression of individual proteins can create artefactual effects on host gene expression if the

level of protein expression is very high. Furthermore, the cooperative effect of expressing all the HCV proteins together in the cell during infection may alter host gene expression in different ways to when the HCV proteins are expressed individually.

Another recently developed approach being used to investigate the mechanisms responsible for the HCV induced gene expression patterns involves analysis of the cellular microRNA profile. MicroRNA (miRNA) molecules are non-coding RNA molecules transcribed from the genome to regulate host gene expression through sequence specific translational repression and degradation of mRNA. In total, around 30% of mammalian genes are regulated through the process of miRNA targeted mRNA degradation [354]. Recently, microarray studies of the miRNA profile during HCV infection have been performed in conjunction with experiments investigating host gene expression [165, 243, 354]. The purpose of these studies is to determine whether matching pairs of anti-correlative miRNA and mRNA regulated genes can be identified. The hypothesis of such studies is that mRNA molecules specifically regulated by miRNA may be altered during infection because of HCV induced changes in miRNA abundance. One study investigating JFH-1 infected Huh7.5.1 cells demonstrated that 5, 40, 63 and 108 miRNAs and 267, 262, 301 and 1208 mRNAs were regulated at 1, 2, 3 and 4 days post-infection, respectively. Comparison of the miRNA and mRNA profiles obtained demonstrated that the top 50 miRNA molecules altered by infection had the ability to regulate 31% of the HCV regulated genes identified [165]. Interestingly, comparison of the miRNA-mRNA pairs identified to the gene expression data obtained in our microarray study identified a number of overlapping patterns. For example, downregulation was observed in several miRNAs that target host genes observed to be upregulated in our study including: miR15a/b (ACSL1), miR181a (KLF6, ACSL1) and miR24 (AARS), miR130a/b (GADD45A) and miR30a/c/e (CARS) [165]. Further investigation into the miRNA profile of JFH-1 infected cells might facilitate identification of HCV regulated miRNA molecules that are responsible for the gene expression patterns observed in this study. It would also be interesting to investigate whether specific changes occur in the levels of the miRNA, miR122, during the early stages of infection, which might explain the complex expression pattern observed for the genes regulating cholesterol synthesis during JFH-1 infection (**Fig. 3.15**).

6.3 Host cell factors involved in the HCV replication cycle

One of the key reasons for performing microarray analysis of JFH-1 infected cells was to use the gene expression data collected to facilitate identification of host factors involved in the HCV replication cycle. This was based on the hypothesis that larger quantities of host factors may be required during HCV infection, which may be achieved through upregulation of gene expression by regulatory feedback mechanisms.

When analysing the gene expression data collected, it was possible to identify examples of host factors already shown to be essential HCV cofactors that were significantly upregulated during infection, e.g. RAB7L1 [253] and ACSL3 [50]. However, at the same time it was also possible to identify host factors that are essential HCV cofactors, but whose expression was downregulated during infection, e.g. regulators of VLDL production: MTTP and ApoB [42, 47]. There were examples of host factors that have inhibitory effects on the HCV replication cycle that were upregulated as part of the host cell antiviral response, e.g. OAS3, MX1 and IRF1. Finally, there are also likely to be many examples of host genes upregulated during infection, which do not have a cofactor function in the HCV replication cycle. Therefore, it was anticipated that identifying upregulated host genes which encode factors required during HCV replication may be a complicated task. In order to maximise our chances of identifying novel HCV cofactors, focus was placed on the upregulated genes involved in pathways significantly altered by infection that were highly relevant to the HCV replication cycle. This included genes controlling lipid metabolism, vesicle trafficking and cytoskeletal function, which are all pathways known to be important during HCV infection.

Using the factors selected from the microarray expression profiling experiment (**Fig. 3.6**), alongside factors chosen from the replication cycles of other RNA viruses (**Fig. 3.4**), the siRNA knockdown assay was performed to identify factors essential for HCV replication. The results obtained through the siRNA knockdown assay demonstrated that a proportion of the host factors chosen through both approaches were identified as potential HCV cofactors. This indicates that both of the approaches used provide valid methods for identifying novel cofactors that may be involved in the HCV replication cycle. A summary of the siRNA silencing data obtained is given in **Table 6.1**.

Cellular process	siRNA target	JFH-1 RNA knockdown	JFH-1 virus knockdown	NS3 protein knockdown	Core protein knockdown
Vesicle trafficking and intracellular transport	RAB2A*	+	+	N/T	N/T
	RAB2B*	++/+++	+++	++	++++
	RAB4A*	++/+++	+++	++	++
	RAB4B*	+	+/++	N/T	N/T
	RAB6A*	+	+	N/T	N/T
	RAB11A*	+	+	N/T	N/T
	RAB11B*	+++	+++	+++	+++
	RAB18*	+	+	N/T	N/T
	RAB27A	++	+++	N/T	N/T
	RAB27B	++	+++	+	++
	RAB33B	+++	+++	N/T	N/T
	RAB37	++	++	N/T	N/T
	ABLIM3	+++	+++	N/T	N/T

Cellular process	siRNA target	JFH-1 RNA knockdown	JFH-1 virus knockdown	NS3 protein knockdown	Core protein knockdown
RNA-binding proteins	TIA1*	+	+	N/T	N/T
	TIAL1*	+	+	N/T	N/T
	Staufen1*	++	+++	++	++++

Cellular process	siRNA target	JFH-1 RNA knockdown	JFH-1 virus knockdown	NS3 protein knockdown	Core protein knockdown
Lipid metabolism	TXNIP	+++	++++	+++	N/T
	CYP1A1	+++	+++	++	+++
	PGC1α	+	+	N/T	N/T
	CIDEB	++	+	N/T	N/T
	CIDEC	+	+++	N/T	N/T
	RIP140	++	+	N/T	N/T
	MLX	++	++	N/T	N/T
	MLXIP	+++	++++	N/T	N/T
	MLXIPL	+++	++++	N/T	N/T
	FOXO1	+	++	N/T	N/T
	KLF6	+++	++++	N/T	N/T
	ARRDC4	+	+	N/T	N/T

Table 6.1 Summary of siRNA knockdown data

***N/T** = Not tested*

**** =** Host targets chosen from the replication cycle of other RNA viruses*

Percentage Knockdown (at 48 hours post-infection):
***+** = 0% - 25%*
***++** = 25% - 50%*
***+++** = 50% -75%*
***++++** = 75% – 100%*

The results obtained from the siRNA knockdown study performed have highlighted a number of host factors involved in intracellular transport, RNA trafficking and lipid metabolism that can be further investigated as potential HCV cofactors. Whilst the siRNA knockdown assay in this study was being performed, a number of other studies were published that used a genome-wide siRNA silencing approach to identify host factors with essential roles either in HCV replication or secretion [114, 116, 253, 254, 298]. With the exception of Staufen1 [254] and MLXIPL [116], none of the other host factors identified in this study were characterised as key host factors for HCV infection by any of the published genome-wide siRNA screens. Comparing the data sets obtained for the different genome-wide studies demonstrated that only a proportion of the host factors identified as potential HCV cofactors were consistent between the different datasets generated. One study compared the degree of overlap observed and demonstrated that 11% (1/9) [298], 15% (15/96) [114], 23% (6/26) [355] and 28% (2/7) [253] of cofactors identified through other published genome-wide siRNA screens were consistent with the cofactors identified in their screen [116]. There are many factors that may contribute to the differences observed between genome-wide siRNA screens and may explain the low level of consistency observed with the findings in our study. Variation in the experimental protocol used may be largely responsible for the differences observed; including the use of different cell types (Huh7 versus Huh7.5 cells), different siRNA molecules (including sequence and concentration), different transfection methods, and different virus strains (JFH-1 versus Jc1 and replicon versus infectious virus). Furthermore, differences in the cut-off threshold values used to select host factors that significantly reduce HCV replication and secretion may also affect which factors are presented as potential cofactors [114, 116]. Most of the HCV genome-wide siRNA studies highlighted siRNAs that reduced the replication and secretion of HCV by at least 50% [114, 116], 60% [298] or 65% [253, 355].

To further investigate the results observed through the siRNA knockdown assay, each host factor identified as a potential cofactor must be further tested to explore the nature of its role in the HCV replication cycle. Several experiments have already been performed to check for non-specific effects of siRNA transfection on the JFH-1 replication cycle (**Fig. 4.10, 4.11, 4.13 and A.18**). The majority of siRNA molecules tested did not have a significant effect on cell viability or the interferon

response pathway. In addition, when several siRNAs were used to target each host gene, most had consistent effects on the HCV replication cycle.

In addition to testing the siRNA molecules for non-specific effects on the HCV replication cycle, it is also important to investigate the functional role of each target in the replication cycle using other methods. One approach that can be used is a loss-of-function experiment performed using dominant negative mutant proteins or enzymatic inhibitors that block host protein function. Host factors that may be investigated using dominant negative mutants include the Rab GTPase proteins, such as RAB2, RAB4, RAB6, RAB11 and RAB27B [303, 356-358] and transcription factors, such as MLX [359]. Other interesting mutant proteins that might be useful for further investigation are the TXNIP mutant proteins, which do not interact with thioredoxin [275]. These would allow determination of whether the thioredoxin bound or unbound form of TXNIP is important for the HCV replication cycle. Enzymatic inhibitors can also be used to perform loss-of-function experiments. One host factor that may be further investigated using this approach is CYP1A1, as several different inhibitors are available including galangin [360] and the trans-resveratrol analogues [361]. In addition to the use of loss-of-function experiments, an alternative approach that may be used to further investigate HCV cofactor function may involve over-expression of host factors during HCV infection to determine whether the rate of virus replication or secretion can be upregulated.

Alongside experiments that validate the functional requirements for host factors during HCV infection, it is also important to investigate the precise function of each host factor in the HCV replication cycle. Preliminary work has been performed to investigate the functional role of TXNIP and Staufen1 in the HCV replication cycle. The work performed for these targets needs to be extended to the other host factors identified to assess the potential function of these factors during infection. Experiments that can be performed include those that investigate the intracellular localisation of host factors during infection and their potential colocalisation with HCV proteins. This will be particularly important when investigating the function of Rab GTPase proteins, as they may be associated with the formation of the membranous web structure or the trafficking of vesicles containing nascent virus particles [30, 303]. Co-immunoprecipitation experiments would also provide greater insight into whether HCV proteins can directly interact with host factors during infection. This approach will be particularly useful when investigating

Staufen1 to determine whether it can interact directly with HCV proteins, in addition to the HCV RNA.

Other experiments that can be performed to investigate the role of potential cofactors during HCV infection include analysis of host cell function following host protein knockdown. This type of experiment has already been performed following TXNIP silencing and has indicated that TXNIP knockdown may affect the expression of key lipid metabolism genes to control intracellular abundance of lipid metabolites during infection. Other host factors, such as CYP1A1, may also play an important role in the regulation of lipid metabolism during infection. Further investigation into the effects of TXNIP and CYP1A1 silencing on the abundance of intracellular lipid metabolites would facilitate determination of whether HCV cofactor function of these proteins is associated with regulation of lipid metabolism. Lipid quantification techniques such as NMR and mass spectroscopy could be used to accurately determine the intracellular abundance of key lipid metabolites following host factor knockdown.

In addition to investigating the effect of host factor knockdown on host cell function, much more detailed analysis of the effects observed on HCV replication and secretion needs to be performed for each of the cofactors identified. Many of the host factors identified are thought to have a significant effect on the early stages of the HCV replication cycle. To determine the precise role of these host factors, several different HCV research tools are available. For example, the HCV pseudoparticle system can be used to identify host factors involved in HCV entry [332], HCV subgenomic replicons can be used to identify host factors involved in genome translation and replication [33] and replication deficient virus strains can be used to identify host factors involved specifically in genome translation [135, 362]. In addition, when investigating host factors with a potential role in membranous web or replication complex formation (e.g. as RAB2B and RAB4A), it may be interesting to investigate the effect of host factor knockdown on the intracellular localisation of non-structural HCV proteins to determine whether the replication complexes assemble correctly.

Through the use of these different experimental approaches, it should possible be to further explore the findings from the siRNA knockdown assay and gain further insight into the precise role that each host factor may play in the HCV replication cycle. Alongside these investigations, it will also be important to determine

whether other HCV strains have the same host factor requirements as JFH-1, and whether studies performed in a more *in vivo* environment generate similar findings. In this study, siRNA knockdown assays have only investigated the host factor requirements for JFH-1 in the immortalised Huh7 and Huh7.5 cells. Therefore, future studies should be performed to investigate the effect of siRNA knockdown on the HCV replication cycle in cultured primary human hepatocytes infected either with cell culture grown or serum derived virus. Furthermore, if any of the HCV cofactors identified become potential antiviral targets, it might also be useful to investigate the effect of host gene knockdown on HCV replication using the immunocompetent mouse model of HCV infection [153].

6.4 Conclusions

Microarray gene expression profiling of HCV infection has provided invaluable insight into the host cell response to the HCV replication cycle. Analysis of the HCV induced host gene expression profile observed has facilitated identification of expression patterns that may be associated with pathogenesis of infection. This includes an increase in the expression of genes controlling lipid synthesis, vesicle trafficking, cell cycle arrest, apoptosis and inflammation, and a decrease in the expression of genes controlling the protective anti-oxidant response and cytoskeleton function. These HCV-induced expression patterns may be responsible for the increased levels of steatosis, inflammation, apoptosis and oxidative stress that are frequently observed in the livers of chronically infected patients. Alongside an increase in the expression of genes controlling lipid synthesis, an increase has also been observed in the protein levels of key lipid metabolism regulators (TXNIP and PGC1α), the levels of triglyceride and cholesterol and the abundance of intracellular lipid droplets during HCV infection. These findings provide further evidence to indicate that the expression of HCV proteins during infection may be directly responsible for the development of hepatic steatosis in chronically infected patients. Studies investigating the HCV proteins responsible for lipid metabolite accumulation during HCV infection have also demonstrated that the non-structural HCV proteins (NS2-NS5B) and the HCV structural core protein may contribute to the increased intracellular lipid abundance observed.

Further investigation into the host factors upregulated by infection, along with host factors previously implicated in the replication of other RNA viruses, has enabled the identification of potential novel cofactors required during the HCV replication cycle. Host factors shown to significantly reduce the replication and secretion of HCV following siRNA mediated host protein knockdown included those involved in lipid metabolism (TXNIP, CYP1A1 and CIDEC), intracellular transport (RAB2B, RAB4A, RAB11B, RAB27A/B, RAB33B and ABLIM3), and mRNA regulation (Staufen1). Investigation into the HCV cofactor role of TXNIP and Staufen1 has demonstrated that TXNIP may control the activity of PPARα and the expression of genes involved in fatty acid metabolism, and Staufen1 may colocalise with HCV replication complexes to control HCV genome translation, replication or trafficking.

Future studies to investigate the findings observed should be now performed to further explore the host cell response to HCV infection and the role of the potential HCV cofactors identified. At present, collaborative plans have been made to further investigate the lipid metabolite profile of JFH-1 infected cells using NMR and mass spectroscopy. Other studies investigating the effect of HCV infection on the anti-oxidant response pathway may also provide greater insight into the mechanisms underlying oxidative stress induced damage, which is frequently observed as a result of chronic HCV infection. Initial studies have already been performed to characterise the potential cofactor role of TXNIP and Staufen1 during the HCV replication cycle. These studies need to be extended further to explore the effect of TXNIP silencing on intracellular lipid abundance and the ability of Staufen1 to interact directly with HCV proteins. Studies should also be performed to investigate whether Rab GTPase proteins (RAB2B, RAB4A, RAB11B, RAB33B and RAB27A/B) may be required for HCV replication complex formation and virion particle trafficking; CYP1A1 and CIDEC proteins may be required to control intracellular lipid metabolism and lipid droplet formation, and ABLIM3 may be required for regulation of the actin cytoskeleton during HCV particle trafficking. It will also be important to determine the relevance of the findings observed in the replication cycle of other HCV genotypes and in a range of different HCV infection cell culture systems, such as HCV infected primary human hepatocytes. Host factors found to be functionally relevant for several different HCV strains and in a variety of host cell systems may provide effective targets for the development of novel antiviral therapeutics.

Bibliography and Appendix

1. Neukam, K., et al., *A review of current anti-HCV treatment regimens and possible future strategies.* Expert Opin Pharmacother, 2009. **10**(3): p. 417-33.
2. Munir, S., et al., *Hepatitis C treatment: current and future perspectives.* Virol J, 2010. **7**: p. 296.
3. Jacobson, I.M., et al., *Manifestations of chronic hepatitis C virus infection beyond the liver.* Clin Gastroenterol Hepatol, 2010. **8**(12): p. 1017-29.
4. Torresi, J., D. Johnson, and H. Wedemeyer, *Progress in the development of preventative and therapeutic vaccines for hepatitis C virus.* J Hepatol, 2011. **54**(6): p. 1273-1285.
5. Baker, D.E., *Pegylated interferon plus ribavirin for the treatment of chronic hepatitis C.* Rev Gastroenterol Disord, 2003. **3**(2): p. 93-109.
6. Thomas, E., et al., *Ribavirin potentiates interferon action by augmenting interferon-stimulated gene induction in hepatitis C virus cell culture models.* Hepatology, 2011. **53**(1): p. 32-41.
7. He, Y., W. Duan, and S.L. Tan, *Emerging host cell targets for hepatitis C therapy.* Drug Discov Today, 2007. **12**(5-6): p. 209-17.
8. Vermehren, J. and C. Sarrazin, *New HCV therapies on the horizon.* Clin Microbiol Infect, 2011. **17**(2): p. 122-34.
9. Zeisel, M.B., et al., *Hepatitis C virus entry into hepatocytes: Molecular mechanisms and targets for antiviral therapies.* J Hepatol, 2011. **54**(3): p. 566-576.
10. Salem, M.L., M. El-Demellawy, and A.R. El-Azm, *The potential use of Toll-like receptor agonists to restore the dysfunctional immunity induced by hepatitis C virus.* Cell Immunol, 2010. **262**(2): p. 96-104.
11. Chang, D.Y. and E.C. Shin, *Immune-based therapy for chronic hepatitis C.* J Leukoc Biol, 2009. **86**(1): p. 33-9.
12. Lindenbach, B.D., H.J. Thiel, and C.M. Rice, *Flaviviridae; The viruses and their replication*, in *Fields Virology, 5th Edition*, M.K. D and M.H. P, Editors. 2007, Lippincott-Raven Publishers.
13. Gottwein, J.M., et al., *Development and characterization of hepatitis C virus genotype 1-7 cell culture systems: role of CD81 and scavenger receptor class B type I and effect of antiviral drugs.* Hepatology, 2009. **49**(2): p. 364-77.
14. Chayama, K. and C.N. Hayes, *Hepatitis C virus: How genetic variability affects pathobiology of disease.* J Gastroenterol Hepatol, 2011. **26 Suppl 1**: p. 83-95.
15. Bochud, P.Y., et al., *Genotype 3 is associated with accelerated fibrosis progression in chronic hepatitis C.* J Hepatol, 2009. **51**(4): p. 655-66.

16. Rubbia-Brandt, L., et al., *Hepatocyte steatosis is a cytopathic effect of hepatitis C virus genotype 3.* J Hepatol, 2000. **33**(1): p. 106-15.
17. Suzuki, T., et al., *Hepatitis C viral life cycle.* Adv Drug Deliv Rev, 2007. **59**(12): p. 1200-12.
18. Bartenschlager, R. and S. Sparacio, *Hepatitis C virus molecular clones and their replication capacity in vivo and in cell culture.* Virus Res, 2007. **127**(2): p. 195-207.
19. Pudi, R., P. Srinivasan, and S. Das, *La protein binding at the GCAC site near the initiator AUG facilitates the ribosomal assembly on the hepatitis C virus RNA to influence internal ribosome entry site-mediated translation.* J Biol Chem, 2004. **279**(29): p. 29879-88.
20. Aizaki, H., et al., *Polypyrimidine-tract-binding protein is a component of the HCV RNA replication complex and necessary for RNA synthesis.* J Biomed Sci, 2006. **13**(4): p. 469-80.
21. Rivas-Aravena, A., et al., *The Elav-like protein HuR exerts translational control of viral internal ribosome entry sites.* Virology, 2009. **392**(2): p. 178-85.
22. Sabahi, A., *Hepatitis C Virus entry: the early steps in the viral replication cycle.* Virol J, 2009. **6**: p. 117.
23. Herker, E. and M. Ott, *Unique ties between hepatitis C virus replication and intracellular lipids.* Trends Endocrinol Metab, 2011.
24. Harris, H.J., et al., *Claudin association with CD81 defines hepatitis C virus entry.* J Biol Chem, 2010. **285**(27): p. 21092-102.
25. Benedicto, I., et al., *The tight junction-associated protein occludin is required for a postbinding step in hepatitis C virus entry and infection.* J Virol, 2009. **83**(16): p. 8012-20.
26. Reynolds, G.M., et al., *Hepatitis C virus receptor expression in normal and diseased liver tissue.* Hepatology, 2008. **47**(2): p. 418-27.
27. Mee, C.J., et al., *Effect of cell polarization on hepatitis C virus entry.* J Virol, 2008. **82**(1): p. 461-70.
28. Ferraris, P., E. Blanchard, and P. Roingeard, *Ultrastructural and biochemical analyses of hepatitis C virus-associated host cell membranes.* J Gen Virol, 2010. **91**(Pt 9): p. 2230-7.
29. Quinkert, D., R. Bartenschlager, and V. Lohmann, *Quantitative analysis of the hepatitis C virus replication complex.* J Virol, 2005. **79**(21): p. 13594-605.
30. Stone, M., et al., *Participation of rab5, an early endosome protein, in hepatitis C virus RNA replication machinery.* J Virol, 2007. **81**(9): p. 4551-63.

31. Guevin, C., et al., *Autophagy protein ATG5 interacts transiently with the hepatitis C virus RNA polymerase (NS5B) early during infection.* Virology, 2010. **405**(1): p. 1-7.
32. Aizaki, H., et al., *Characterization of the hepatitis C virus RNA replication complex associated with lipid rafts.* Virology, 2004. **324**(2): p. 450-61.
33. Lohmann, V., et al., *Replication of subgenomic hepatitis C virus RNAs in a hepatoma cell line.* Science, 1999. **285**(5424): p. 110-3.
34. Li, K., et al., *Immune evasion by hepatitis C virus NS3/4A protease-mediated cleavage of the Toll-like receptor 3 adaptor protein TRIF.* Proc Natl Acad Sci U S A, 2005. **102**(8): p. 2992-7.
35. Meylan, E., et al., *Cardif is an adaptor protein in the RIG-I antiviral pathway and is targeted by hepatitis C virus.* Nature, 2005. **437**(7062): p. 1167-72.
36. Isken, O., et al., *Nuclear factors are involved in hepatitis C virus RNA replication.* Rna, 2007. **13**(10): p. 1675-92.
37. Scheller, N., et al., *Translation and replication of hepatitis C virus genomic RNA depends on ancient cellular proteins that control mRNA fates.* Proc Natl Acad Sci U S A, 2009. **106**(32): p. 13517-22.
38. Yu, K.L., S.I. Jang, and J.C. You, *Identification of in vivo interaction between Hepatitis C Virus core protein and 5' and 3' UTR RNA.* Virus Res, 2009. **145**(2): p. 285-92.
39. Miyanari, Y., et al., *The lipid droplet is an important organelle for hepatitis C virus production.* Nat Cell Biol, 2007. **9**(9): p. 1089-97.
40. McLauchlan, J., *Hepatitis C virus: viral proteins on the move.* Biochem Soc Trans, 2009. **37**(Pt 5): p. 986-90.
41. Masaki, T., et al., *Interaction of hepatitis C virus nonstructural protein 5A with core protein is critical for the production of infectious virus particles.* J Virol, 2008. **82**(16): p. 7964-76.
42. Bartenschlager, R., et al., *Assembly of infectious hepatitis C virus particles.* Trends Microbiol, 2010. **19**(2): p. 95-103.
43. Ma, Y., et al., *Hepatitis C virus NS2 protein serves as a scaffold for virus assembly by interacting with both structural and nonstructural proteins.* J Virol, 2011. **85**(1): p. 86-97.
44. Parent, R., et al., *The heat shock cognate protein 70 is associated with hepatitis C virus particles and modulates virus infectivity.* Hepatology, 2009. **49**(6): p. 1798-809.

45. Syed, G.H., Y. Amako, and A. Siddiqui, *Hepatitis C virus hijacks host lipid metabolism.* Trends Endocrinol Metab, 2009. **21**(1): p. 33-40.
46. Gastaminza, P., et al., *Cellular determinants of hepatitis C virus assembly, maturation, degradation, and secretion.* J Virol, 2008. **82**(5): p. 2120-9.
47. Huang, H., et al., *Hepatitis C virus production by human hepatocytes dependent on assembly and secretion of very low-density lipoproteins.* Proc Natl Acad Sci U S A, 2007. **104**(14): p. 5848-53.
48. Merz, A., et al., *Biochemical and morphological properties of hepatitis C virus particles and determination of their lipidome.* J Biol Chem, 2010. **286**(4): p. 3018-32.
49. Jiang, J. and G. Luo, *Apolipoprotein E but not B is required for the formation of infectious hepatitis C virus particles.* J Virol, 2009. **83**(24): p. 12680-91.
50. Yao, H. and J. Ye, *Long chain acyl-CoA synthetase 3-mediated phosphatidylcholine synthesis is required for assembly of very low density lipoproteins in human hepatoma Huh7 cells.* J Biol Chem, 2008. **283**(2): p. 849-54.
51. Matto, M., et al., *Role for ADP ribosylation factor 1 in the regulation of hepatitis C virus replication.* J Virol, 2011. **85**(2): p. 946-56.
52. Cun, W., J. Jiang, and G. Luo, *The C-terminal alpha-helix domain of apolipoprotein E is required for interaction with nonstructural protein 5A and assembly of hepatitis C virus.* J Virol, 2010. **84**(21): p. 11532-41.
53. Corless, L., et al., *Vps4 and the ESCRT-III complex are required for the release of infectious hepatitis C virus particles.* J Gen Virol, 2010. **91**(Pt 2): p. 362-72.
54. Wollert, T., et al., *Membrane scission by the ESCRT-III complex.* Nature, 2009. **458**(7235): p. 172-7.
55. Ariumi, Y., et al., *The ESCRT system is required for hepatitis C virus production.* PLoS One, 2011. **6**(1): p. e14517.
56. Amako, Y., G.H. Syed, and A. Siddiqui, *Protein kinase D negatively regulates hepatitis C virus maturation through phosphorylation of oxysterol binding protein and ceramide transfer protein.* J Biol Chem, 2011. **286**(13): p. 11265-11274.
57. Backes, P., et al., *Role of annexin A2 in the production of infectious hepatitis C virus particles.* J Virol, 2010. **84**(11): p. 5775-89.
58. Popescu, C.I. and J. Dubuisson, *Role of lipid metabolism in hepatitis C virus assembly and entry.* Biol Cell, 2009. **102**(1): p. 63-74.
59. Herker, E., et al., *Efficient hepatitis C virus particle formation requires diacylglycerol acyltransferase-1.* Nat Med, 2010. **16**(11): p. 1295-8.

60. Boulant, S., et al., *Hepatitis C virus core protein induces lipid droplet redistribution in a microtubule- and dynein-dependent manner.* Traffic, 2008. **9**(8): p. 1268-82.
61. Dubuisson, J., *Hepatitis C virus proteins.* World J Gastroenterol, 2007. **13**(17): p. 2406-15.
62. Wang, T., et al., *Role of Hepatitis C virus core protein in viral-induced mitochondrial dysfunction.* J Viral Hepat, 2009. **17**(11): p. 784-93.
63. Yoshida, T., et al., *Activation of STAT3 by the hepatitis C virus core protein leads to cellular transformation.* J Exp Med, 2002. **196**(5): p. 641-53.
64. Chen, W., et al., *HCV core protein interacts with Dicer to antagonize RNA silencing.* Virus Res, 2008. **133**(2): p. 250-8.
65. Hsieh, T.Y., et al., *Hepatitis C virus core protein interacts with heterogeneous nuclear ribonucleoprotein K.* J Biol Chem, 1998. **273**(28): p. 17651-9.
66. Kim, K.H., et al., *HCV core protein induces hepatic lipid accumulation by activating SREBP1 and PPARgamma.* Biochem Biophys Res Commun, 2007. **355**(4): p. 883-8.
67. Jackel-Cram, C., et al., *Hepatitis C virus genotype-3a core protein enhances sterol regulatory element-binding protein-1 activity through the phosphoinositide 3-kinase-Akt-2 pathway.* J Gen Virol, 2010. **91**(Pt 6): p. 1388-95.
68. Dharancy, S., et al., *Impaired expression of the peroxisome proliferator-activated receptor alpha during hepatitis C virus infection.* Gastroenterology, 2005. **128**(2): p. 334-42.
69. Mirandola, S., et al., *Hepatic steatosis in hepatitis C is a storage disease due to HCV interaction with microsomal triglyceride transfer protein (MTP).* Nutr Metab (Lond), 2010. **7**: p. 13.
70. Jhaveri, R., et al., *Specific polymorphisms in hepatitis C virus genotype 3 core protein associated with intracellular lipid accumulation.* J Infect Dis, 2008. **197**(2): p. 283-91.
71. Vieyres, G., et al., *Characterization of the envelope glycoproteins associated with infectious hepatitis C virus.* J Virol, 2010. **84**(19): p. 10159-68.
72. Li, H.F., et al., *Mutagenesis of the fusion peptide-like domain of hepatitis C virus E1 glycoprotein: involvement in cell fusion and virus entry.* J Biomed Sci, 2009. **16**: p. 89.
73. Clarke, D., et al., *Evidence for the formation of a heptameric ion channel complex by the hepatitis C virus p7 protein in vitro.* J Biol Chem, 2006. **281**(48): p. 37057-68.

74. Luik, P., et al., *The 3-dimensional structure of a hepatitis C virus p7 ion channel by electron microscopy.* Proc Natl Acad Sci U S A, 2009. **106**(31): p. 12712-6.
75. Griffin, S.D., et al., *The p7 protein of hepatitis C virus forms an ion channel that is blocked by the antiviral drug, Amantadine.* FEBS Lett, 2003. **535**(1-3): p. 34-8.
76. Jirasko, V., et al., *Structural and functional studies of nonstructural protein 2 of the hepatitis C virus reveal its key role as organizer of virion assembly.* PLoS Pathog, 2010. **6**(12): p. e1001233.
77. Wozniak, A.L., et al., *Intracellular proton conductance of the hepatitis C virus p7 protein and its contribution to infectious virus production.* PLoS Pathog, 2010. **6**(9): p. e1001087.
78. Tedbury, P., et al., *The sub-cellular localisation of the hepatitis C virus non-structural protein NS2 is regulated by an ion channel-independent function of the p7 protein.* J Gen Virol, 2011. **92**(4): p. 819-830.
79. Schregel, V., et al., *Hepatitis C virus NS2 is a protease stimulated by cofactor domains in NS3.* Proc Natl Acad Sci U S A, 2009. **106**(13): p. 5342-7.
80. von dem Bussche, A., et al., *Hepatitis C virus NS2 protein triggers endoplasmic reticulum stress and suppresses its own viral replication.* J Hepatol, 2010. **53**(5): p. 797-804.
81. Morikawa, K., et al., *Nonstructural protein 3-4A: the Swiss army knife of hepatitis C virus.* J Viral Hepat, 2011. **18**(5): p. 305-15.
82. Huang, Z.S., C.C. Wang, and H.N. Wu, *HCV NS3 protein helicase domain assists RNA structure conversion.* FEBS Lett, 2010. **584**(11): p. 2356-62.
83. Shiryaev, S.A., et al., *The acidic sequence of the NS4A cofactor regulates ATP hydrolysis by the HCV NS3 helicase.* Arch Virol, 2011. **156**(2): p. 313-318.
84. Ma, Y., et al., *NS3 helicase domains involved in infectious intracellular hepatitis C virus particle assembly.* J Virol, 2008. **82**(15): p. 7624-39.
85. Deng, L., et al., *NS3 protein of Hepatitis C virus associates with the tumour suppressor p53 and inhibits its function in an NS3 sequence-dependent manner.* J Gen Virol, 2006. **87**(Pt 6): p. 1703-13.
86. Khu, Y.L., et al., *Hepatitis C virus non-structural protein NS3 interacts with LMP7, a component of the immunoproteasome, and affects its proteasome activity.* Biochem J, 2004. **384**(Pt 2): p. 401-9.
87. Nomura-Takigawa, Y., et al., *Non-structural protein 4A of Hepatitis C virus accumulates on mitochondria and renders the cells prone to undergoing mitochondria-mediated apoptosis.* J Gen Virol, 2006. **87**(Pt 7): p. 1935-45.

88. Gouttenoire, J., F. Penin, and D. Moradpour, *Hepatitis C virus nonstructural protein 4B: a journey into unexplored territory.* Rev Med Virol, 2010. **20**(2): p. 117-29.
89. Gouttenoire, J., et al., *Amphipathic alpha-helix AH2 is a major determinant for the oligomerization of hepatitis C virus nonstructural protein 4B.* J Virol, 2010. **84**(24): p. 12529-37.
90. Park, C.Y., et al., *Hepatitis C virus nonstructural 4B protein modulates sterol regulatory element-binding protein signaling via the AKT pathway.* J Biol Chem, 2009. **284**(14): p. 9237-46.
91. Foster, T.L., et al., *All three domains of the hepatitis C virus nonstructural NS5A protein contribute to RNA binding.* J Virol, 2010. **84**(18): p. 9267-77.
92. Kim, S., et al., *Regulation of Infectious Genotype 1a Hepatitis C Virus Production by Domain III of NS5A.* J Virol, 2011.
93. Hughes, M., S. Griffin, and M. Harris, *Domain III of NS5A contributes to both RNA replication and assembly of hepatitis C virus particles.* J Gen Virol, 2009. **90**(Pt 6): p. 1329-34.
94. Amako, Y., et al., *Role of oxysterol binding protein in hepatitis C virus infection.* J Virol, 2009. **83**(18): p. 9237-46.
95. Huang, Y., et al., *Phosphorylation of hepatitis C virus NS5A nonstructural protein: a new paradigm for phosphorylation-dependent viral RNA replication?* Virology, 2007. **364**(1): p. 1-9.
96. Quezada, E.M. and C.M. Kane, *The Hepatitis C Virus NS5A Stimulates NS5B During In Vitro RNA Synthesis in a Template Specific Manner.* Open Biochem J, 2009. **3**: p. 39-48.
97. Hamamoto, I., et al., *Human VAP-B is involved in hepatitis C virus replication through interaction with NS5A and NS5B.* J Virol, 2005. **79**(21): p. 13473-82.
98. Fernandes, F., I.U. Ansari, and R. Striker, *Cyclosporine inhibits a direct interaction between cyclophilins and hepatitis C NS5A.* PLoS One, 2010. **5**(3): p. e9815.
99. Reiss, S., et al., *Recruitment and activation of a lipid kinase by hepatitis C virus NS5A is essential for integrity of the membranous replication compartment.* Cell Host Microbe, 2011. **9**(1): p. 32-45.
100. Appel, N., et al., *Essential role of domain III of nonstructural protein 5A for hepatitis C virus infectious particle assembly.* PLoS Pathog, 2008. **4**(3): p. e1000035.

101. Nordle Gilliver, A., S. Griffin, and M. Harris, *Identification of a novel phosphorylation site in hepatitis C virus NS5A.* J Gen Virol, 2010. **91**(Pt 10): p. 2428-32.
102. Lan, K.H., et al., *HCV NS5A interacts with p53 and inhibits p53-mediated apoptosis.* Oncogene, 2002. **21**(31): p. 4801-11.
103. He, Y., et al., *Subversion of cell signaling pathways by hepatitis C virus nonstructural 5A protein via interaction with Grb2 and P85 phosphatidylinositol 3-kinase.* J Virol, 2002. **76**(18): p. 9207-17.
104. Gale, M.J., Jr., M.J. Korth, and M.G. Katze, *Repression of the PKR protein kinase by the hepatitis C virus NS5A protein: a potential mechanism of interferon resistance.* Clin Diagn Virol, 1998. **10**(2-3): p. 157-62.
105. Piccininni, S., et al., *Modulation of the hepatitis C virus RNA-dependent RNA polymerase activity by the non-structural (NS) 3 helicase and the NS4B membrane protein.* J Biol Chem, 2002. **277**(47): p. 45670-9.
106. Chinnaswamy, S., et al., *Regulation of de novo-initiated RNA synthesis in hepatitis C virus RNA-dependent RNA polymerase by intermolecular interactions.* J Virol, 2010. **84**(12): p. 5923-35.
107. She, Y., et al., *Hepatitis C virus NS2/3 protease regulates HCV IRES-dependent translation and NS5B RdRp activity.* Arch Virol, 2009. **154**(9): p. 1465-73.
108. Shimakami, T., et al., *Effect of hepatitis C virus (HCV) NS5B-nucleolin interaction on HCV replication with HCV subgenomic replicon.* J Virol, 2006. **80**(7): p. 3332-40.
109. Goh, P.Y., et al., *Cellular RNA helicase p68 relocalization and interaction with the hepatitis C virus (HCV) NS5B protein and the potential role of p68 in HCV RNA replication.* J Virol, 2004. **78**(10): p. 5288-98.
110. Kim, S.J., et al., *Protein kinase C-related kinase 2 regulates hepatitis C virus RNA polymerase function by phosphorylation.* J Biol Chem, 2004. **279**(48): p. 50031-41.
111. Domitrovich, A.M., et al., *Role of La autoantigen and polypyrimidine tract-binding protein in HCV replication.* Virology, 2005. **335**(1): p. 72-86.
112. Shirasaki, T., et al., *La protein required for internal ribosome entry site-directed translation is a potential therapeutic target for hepatitis C virus replication.* J Infect Dis, 2010. **202**(1): p. 75-85.
113. Dreux, M., et al., *The autophagy machinery is required to initiate hepatitis C virus replication.* Proc Natl Acad Sci U S A, 2009. **106**(33): p. 14046-51.

114. Tai, A.W., et al., *A functional genomic screen identifies cellular cofactors of hepatitis C virus replication.* Cell Host Microbe, 2009. **5**(3): p. 298-307.
115. Berger, K.L. and G. Randall, *Potential roles for cellular cofactors in hepatitis C virus replication complex formation.* Commun Integr Biol, 2009. **2**(6): p. 471-3.
116. Li, Q., et al., *A genome-wide genetic screen for host factors required for hepatitis C virus propagation.* Proc Natl Acad Sci U S A, 2009. **106**(38): p. 16410-5.
117. Trotard, M., et al., *Kinases required in hepatitis C virus entry and replication highlighted by small interference RNA screening.* Faseb J, 2009. **23**(11): p. 3780-9.
118. Jangra, R.K., M. Yi, and S.M. Lemon, *Regulation of hepatitis C virus translation and infectious virus production by the microRNA miR-122.* J Virol, 2010. **84**(13): p. 6615-25.
119. Esau, C., et al., *miR-122 regulation of lipid metabolism revealed by in vivo antisense targeting.* Cell Metab, 2006. **3**(2): p. 87-98.
120. Norman, K.L. and P. Sarnow, *Modulation of hepatitis C virus RNA abundance and the isoprenoid biosynthesis pathway by microRNA miR-122 involves distinct mechanisms.* J Virol, 2009. **84**(1): p. 666-70.
121. Wilson, J.A., et al., *Human Ago2 is required for efficient microRNA 122 regulation of hepatitis C virus RNA accumulation and translation.* J Virol, 2010. **85**(5): p. 2342-50.
122. Goueslain, L., et al., *Identification of GBF1 as a cellular factor required for hepatitis C virus RNA replication.* J Virol, 2010. **84**(2): p. 773-87.
123. Kim, C.S., et al., *An RNA-binding protein, hnRNP A1, and a scaffold protein, septin 6, facilitate hepatitis C virus replication.* J Virol, 2007. **81**(8): p. 3852-65.
124. Spangberg, K., L. Wiklund, and S. Schwartz, *HuR, a protein implicated in oncogene and growth factor mRNA decay, binds to the 3' ends of hepatitis C virus RNA of both polarities.* Virology, 2000. **274**(2): p. 378-90.
125. Weinlich, S., et al., *IGF2BP1 enhances HCV IRES-mediated translation initiation via the 3'UTR.* Rna, 2009. **15**(8): p. 1528-42.
126. Wang, C., et al., *Identification of FBL2 as a geranylgeranylated cellular protein required for hepatitis C virus RNA replication.* Mol Cell, 2005. **18**(4): p. 425-34.
127. Zhang, Z., D. Harris, and V.N. Pandey, *The FUSE binding protein is a cellular factor required for efficient replication of hepatitis C virus.* J Virol, 2008. **82**(12): p. 5761-73.

128. Sklan, E.H., et al., *TBC1D20 Is a Rab1 GTPase-activating Protein That Mediates Hepatitis C Virus Replication.* J Biol Chem, 2007. **282**(50): p. 36354-61.
129. Yi, Z., et al., *Subproteomic study of hepatitis C virus replicon reveals Ras-GTPase-activating protein binding protein 1 as potential HCV RC component.* Biochem Biophys Res Commun, 2006. **350**(1): p. 174-8.
130. Taguwa, S., et al., *Human butyrate-induced transcript 1 interacts with hepatitis C virus NS5A and regulates viral replication.* J Virol, 2008. **82**(6): p. 2631-41.
131. Sakamoto, H., et al., *Host sphingolipid biosynthesis as a target for hepatitis C virus therapy.* Nat Chem Biol, 2005. **1**(6): p. 333-7.
132. Ye, J., *Reliance of host cholesterol metabolic pathways for the life cycle of hepatitis C virus.* PLoS Pathog, 2007. **3**(8): p. e108.
133. Lai, C.K., et al., *Association of hepatitis C virus replication complexes with microtubules and actin filaments is dependent on the interaction of NS3 and NS5A.* J Virol, 2008. **82**(17): p. 8838-48.
134. Roohvand, F., et al., *Initiation of hepatitis C virus infection requires the dynamic microtubule network: role of the viral nucleocapsid protein.* J Biol Chem, 2009. **284**(20): p. 13778-91.
135. Wakita, T., et al., *Production of infectious hepatitis C virus in tissue culture from a cloned viral genome.* Nat Med, 2005. **11**(7): p. 791-6.
136. Bukh, J., et al., *Mutations that permit efficient replication of hepatitis C virus RNA in Huh-7 cells prevent productive replication in chimpanzees.* Proc Natl Acad Sci U S A, 2002. **99**(22): p. 14416-21.
137. Yi, M. and S.M. Lemon, *Genotype 1a HCV (H77S) infection system.* Methods Mol Biol, 2008. **510**: p. 337-46.
138. Pietschmann, T., et al., *Construction and characterization of infectious intragenotypic and intergenotypic hepatitis C virus chimeras.* Proc Natl Acad Sci U S A, 2006. **103**(19): p. 7408-13.
139. Blight, K.J., J.A. McKeating, and C.M. Rice, *Highly permissive cell lines for subgenomic and genomic hepatitis C virus RNA replication.* J Virol, 2002. **76**(24): p. 13001-14.
140. Sumpter, R., Jr., et al., *Regulating intracellular antiviral defense and permissiveness to hepatitis C virus RNA replication through a cellular RNA helicase, RIG-I.* J Virol, 2005. **79**(5): p. 2689-99.

141. Koutsoudakis, G., et al., *The level of CD81 cell surface expression is a key determinant for productive entry of hepatitis C virus into host cells.* J Virol, 2007. **81**(2): p. 588-98.
142. Akazawa, D., et al., *Characterization of infectious hepatitis C virus from liver-derived cell lines.* Biochem Biophys Res Commun, 2008. **377**(3): p. 747-51.
143. Targett-Adams, P. and J. McLauchlan, *Development and characterization of a transient-replication assay for the genotype 2a hepatitis C virus subgenomic replicon.* J Gen Virol, 2005. **86**(Pt 11): p. 3075-80.
144. Fletcher, N.F., et al., *Hepatitis C virus infection of neuroepithelioma cell lines.* Gastroenterology, 2010. **139**(4): p. 1365-74.
145. Podevin, P., et al., *Production of infectious hepatitis C virus in primary cultures of human adult hepatocytes.* Gastroenterology, 2010. **139**(4): p. 1355-64.
146. Aly, H.H., et al., *Strain-dependent viral dynamics and virus-cell interactions in a novel in vitro system supporting the life cycle of blood-borne hepatitis C virus.* Hepatology, 2009. **50**(3): p. 689-96.
147. Buck, M., *Direct infection and replication of naturally occurring hepatitis C virus genotypes 1, 2, 3 and 4 in normal human hepatocyte cultures.* PLoS One, 2008. **3**(7): p. e2660.
148. Jo, J., et al., *Experimental models to study the immunobiology of hepatitis C virus.* J Gen Virol, 2010. **92**(Pt 3): p. 477-93.
149. Walters, K.A., et al., *Genomic analysis reveals a potential role for cell cycle perturbation in HCV-mediated apoptosis of cultured hepatocytes.* PLoS Pathog, 2009. **5**(1): p. e1000269.
150. Diamond, D.L., et al., *Temporal proteome and lipidome profiles reveal hepatitis C virus-associated reprogramming of hepatocellular metabolism and bioenergetics.* PLoS Pathog, 2010. **6**(1): p. e1000719.
151. Boonstra, A., et al., *Experimental models for hepatitis C viral infection.* Hepatology, 2009. **50**(5): p. 1646-55.
152. Walters, K.A., et al., *Host-specific response to HCV infection in the chimeric SCID-beige/Alb-uPA mouse model: role of the innate antiviral immune response.* PLoS Pathog, 2006. **2**(6): p. e59.
153. Washburn, M.L., et al., *A Humanized Mouse Model to Study Hepatitis C Virus Infection, Immune Response, and Liver Disease.* Gastroenterology, 2011. **140**(4): p. 1334-1344.

154. Shi, S.T., et al., *Hepatitis C virus RNA replication occurs on a detergent-resistant membrane that cofractionates with caveolin-2.* J Virol, 2003. **77**(7): p. 4160-8.
155. Harris, D., et al., *Identification of cellular factors associated with the 3'-nontranslated region of the hepatitis C virus genome.* Mol Cell Proteomics, 2006. **5**(6): p. 1006-18.
156. Tingting, P., et al., *Subproteomic analysis of the cellular proteins associated with the 3' untranslated region of the hepatitis C virus genome in human liver cells.* Biochem Biophys Res Commun, 2006. **347**(3): p. 683-91.
157. Basu, A., et al., *Microarray analyses and molecular profiling of Stat3 signaling pathway induced by hepatitis C virus core protein in human hepatocytes.* Virology, 2006. **349**(2): p. 347-58.
158. Budhu, A., et al., *Induction of a unique gene expression profile in primary human hepatocytes by hepatitis C virus core, NS3 and NS5A proteins.* Carcinogenesis, 2007. **28**(7): p. 1552-60.
159. Nishimura-Sakurai, Y., et al., *Comparison of HCV-associated gene expression and cell signaling pathways in cells with or without HCV replicon and in replicon-cured cells.* J Gastroenterol, 2009.
160. Abe, K., et al., *cDNA microarray analysis to compare HCV subgenomic replicon cells with their cured cells.* Virus Res, 2005. **107**(1): p. 73-81.
161. Bigger, C.B., et al., *Intrahepatic gene expression during chronic hepatitis C virus infection in chimpanzees.* J Virol, 2004. **78**(24): p. 13779-92.
162. Bigger, C.B., K.M. Brasky, and R.E. Lanford, *DNA microarray analysis of chimpanzee liver during acute resolving hepatitis C virus infection.* J Virol, 2001. **75**(15): p. 7059-66.
163. Su, A.I., et al., *Genomic analysis of the host response to hepatitis C virus infection.* Proc Natl Acad Sci U S A, 2002. **99**(24): p. 15669-74.
164. Woodhouse, S.D., et al., *Transcriptome sequencing, microarray, and proteomic analyses reveal cellular and metabolic impact of hepatitis C virus infection in vitro.* Hepatology, 2010. **52**(2): p. 443-53.
165. Liu, X., et al., *Systematic identification of microRNA and messenger RNA profiles in hepatitis C virus-infected human hepatoma cells.* Virology, 2009. **398**(1): p. 57-67.
166. Kim, K., et al., *Hepatitis C virus NS5A protein increases hepatic lipid accumulation via induction of activation and expression of PPARgamma.* FEBS Lett, 2009. **583**(17): p. 2720-6.

167. Negro, F., *Abnormalities of lipid metabolism in hepatitis C virus infection.* Gut, 2011. **59**(9): p. 1279-87.
168. Zeremski, M., L.M. Petrovic, and A.H. Talal, *The role of chemokines as inflammatory mediators in chronic hepatitis C virus infection.* J Viral Hepat, 2007. **14**(10): p. 675-87.
169. Ciccaglione, A.R., et al., *Microarray analysis identifies a common set of cellular genes modulated by different HCV replicon clones.* BMC Genomics, 2008. **9**: p. 309.
170. Farinati, F., et al., *Hepatitis C virus: from oxygen free radicals to hepatocellular carcinoma.* J Viral Hepat, 2007. **14**(12): p. 821-9.
171. Fang, C., et al., *Proteome analysis of human liver carcinoma Huh7 cells harboring hepatitis C virus subgenomic replicon.* Proteomics, 2006. **6**(2): p. 519-27.
172. Xun, M., et al., *Proteomic analysis of HuH-7 cells harboring in vitro-transcribed full-length hepatitis C virus 1b RNA.* Acta Pharmacol Sin, 2008. **29**(6): p. 720-7.
173. Mannova, P., et al., *Modification of host lipid raft proteome upon hepatitis C virus replication.* Mol Cell Proteomics, 2006. **5**(12): p. 2319-25.
174. Mankouri, J., et al., *Enhanced hepatitis C virus genome replication and lipid accumulation mediated by inhibition of AMP-activated protein kinase.* Proc Natl Acad Sci U S A, 2010. **107**(25): p. 11549-54.
175. Molina, H., et al., *Global proteomic profiling of phosphopeptides using electron transfer dissociation tandem mass spectrometry.* Proc Natl Acad Sci U S A, 2007. **104**(7): p. 2199-204.
176. Belov, G.A., et al., *Activation of cellular Arf GTPases by poliovirus protein 3CD correlates with virus replication.* J Virol, 2007. **81**(17): p. 9259-67.
177. Mas, A., et al., *Host deadenylation-dependent mRNA decapping factors are required for a key step in brome mosaic virus RNA replication.* J Virol, 2006. **80**(1): p. 246-51.
178. Schwartz, S.L., et al., *Rab GTPases at a glance.* J Cell Sci, 2007. **120**(Pt 22): p. 3905-10.
179. Stenmark, H., *Rab GTPases as coordinators of vesicle traffic.* Nat Rev Mol Cell Biol, 2009. **10**(8): p. 513-25.
180. Hutagalung, A.H. and P.J. Novick, *Role of Rab GTPases in membrane traffic and cell physiology.* Physiol Rev, 2011. **91**(1): p. 119-49.
181. Mari, M., et al., *The Rab4 effector Rabip4 plays a role in the endocytotic trafficking of Glut 4 in 3T3-L1 adipocytes.* J Cell Sci, 2006. **119**(Pt 7): p. 1297-306.

182. Krishnan, M.N., et al., *Rab 5 is required for the cellular entry of dengue and West Nile viruses.* J Virol, 2007. **81**(9): p. 4881-5.
183. Bruce, E.A., P. Digard, and A.D. Stuart, *The Rab11 pathway is required for influenza A virus budding and filament formation.* J Virol, 2010. **84**(12): p. 5848-59.
184. Martin, S. and R.G. Parton, *Characterization of Rab18, a lipid droplet-associated small GTPase.* Methods Enzymol, 2008. **438**: p. 109-29.
185. Ozeki, S., et al., *Rab18 localizes to lipid droplets and induces their close apposition to the endoplasmic reticulum-derived membrane.* J Cell Sci, 2005. **118**(Pt 12): p. 2601-11.
186. Yamasaki, S., et al., *T-cell intracellular antigen-1 (TIA-1)-induced translational silencing promotes the decay of selected mRNAs.* J Biol Chem, 2007. **282**(41): p. 30070-7.
187. Emara, M.M. and M.A. Brinton, *Interaction of TIA-1/TIAR with West Nile and dengue virus products in infected cells interferes with stress granule formation and processing body assembly.* Proc Natl Acad Sci U S A, 2007. **104**(21): p. 9041-6.
188. Li, W., et al., *Cell proteins TIA-1 and TIAR interact with the 3' stem-loop of the West Nile virus complementary minus-strand RNA and facilitate virus replication.* J Virol, 2002. **76**(23): p. 11989-2000.
189. Ariumi, Y., et al., *Hepatitis C Virus Hijacks P-body and Stress Granule Components Around Lipid Droplets.* J Virol, 2011.
190. Furic, L., M. Maher-Laporte, and L. DesGroseillers, *A genome-wide approach identifies distinct but overlapping subsets of cellular mRNAs associated with Staufen1- and Staufen2-containing ribonucleoprotein complexes.* Rna, 2008. **14**(2): p. 324-35.
191. Maher-Laporte, M., et al., *Molecular composition of staufen2-containing ribonucleoproteins in embryonic rat brain.* PLoS One, 2010. **5**(6): p. e11350.
192. Miki, T., K. Takano, and Y. Yoneda, *The role of mammalian Staufen on mRNA traffic: a view from its nucleocytoplasmic shuttling function.* Cell Struct Funct, 2005. **30**(2): p. 51-6.
193. Villace, P., R.M. Marion, and J. Ortin, *The composition of Staufen-containing RNA granules from human cells indicates their role in the regulated transport and translation of messenger RNAs.* Nucleic Acids Res, 2004. **32**(8): p. 2411-20.
194. Kim, Y.K., et al., *Mammalian Staufen1 recruits Upf1 to specific mRNA 3'UTRs so as to elicit mRNA decay.* Cell, 2005. **120**(2): p. 195-208.

195. Dugre-Brisson, S., et al., *Interaction of Staufen1 with the 5' end of mRNA facilitates translation of these RNAs.* Nucleic Acids Res, 2005. **33**(15): p. 4797-812.
196. Abrahamyan, L.G., et al., *Novel Staufen1 ribonucleoproteins prevent formation of stress granules but favour encapsidation of HIV-1 genomic RNA.* J Cell Sci, 2010. **123**(Pt 3): p. 369-83.
197. Milev, M.P., C.M. Brown, and A.J. Mouland, *Live cell visualization of the interactions between HIV-1 Gag and the cellular RNA-binding protein Staufen1.* Retrovirology, 2010. **7**: p. 41.
198. de Lucas, S., et al., *Human Staufen1 protein interacts with influenza virus ribonucleoproteins and is required for efficient virus multiplication.* J Virol, 2010. **84**(15): p. 7603-12.
199. Kumar, U., et al., *Cloning and sequencing of the structural region and expression of putative core gene of hepatitis C virus from a British case of chronic sporadic hepatitis.* J Gen Virol, 1992. **73 (Pt 6)**: p. 1521-5.
200. Kato, T., et al., *Cell culture and infection system for hepatitis C virus.* Nat Protoc, 2006. **1**(5): p. 2334-9.
201. Baillie, A., *Cellular and viral determinants for HCV replication*, in *PhD thesis: Department of Hepatology and Gastroenterology*. 2010, Imperial College London.
202. Osborn, M. and K. Weber, *Immunofluorescence and immunocytochemical procedures with affinity purified antibodies: tubulin-containing structures.* Methods Cell Biol, 1982. **24**: p. 97-132.
203. Ingenuity®Systems. Available from: www.Ingenuity.com
204. Thomas, P.D., et al., *PANTHER: a library of protein families and subfamilies indexed by function.* Genome Res, 2003. **13**(9): p. 2129-41.
205. Saeed, A.I., et al., *TM4: a free, open-source system for microarray data management and analysis.* Biotechniques, 2003. **34**(2): p. 374-8.
206. Support, Q.T., *Critical success factors and new technologies for PCR and RT-PCR*.
207. Pfaffl, M.W., *A new mathematical model for relative quantification in real-time RT-PCR.* Nucleic Acids Res, 2001. **29**(9): p. e45.
208. Asselah, T., et al., *Significant gene expression differences in histologically "Normal" liver biopsies: Implications for control tissue.* Hepatology, 2008. **48**(3): p. 953-62.

209. Chevalier, C., et al., *Inhibition of hepatitis C virus infection in cell culture by small interfering RNAs.* Mol Ther, 2007. **15**(8): p. 1452-62.
210. Nakayama, G.R., et al., *Assessment of the Alamar Blue assay for cellular growth and viability in vitro.* J Immunol Methods, 1997. **204**(2): p. 205-8.
211. Karlsson, G.B. and P. Liljestrom, *Delivery and expression of heterologous genes in mammalian cells using self-replicating alphavirus vectors.* Methods Mol Biol, 2004. **246**: p. 543-57.
212. Lyn, R.K., et al., *Dynamics of lipid droplets induced by the hepatitis C virus core protein.* Biochem Biophys Res Commun, 2010. **399**(4): p. 518-24.
213. Svaren, J., et al., *EGR1 target genes in prostate carcinoma cells identified by microarray analysis.* J Biol Chem, 2000. **275**(49): p. 38524-31.
214. Aizaki, H., et al., *Critical role of virion-associated cholesterol and sphingolipid in hepatitis C virus infection.* J Virol, 2008. **82**(12): p. 5715-24.
215. Blackham, S., et al., *Gene expression profiling indicates the roles of host oxidative stress, apoptosis, lipid metabolism, and intracellular transport genes in the replication of hepatitis C virus.* J Virol, 2010. **84**(10): p. 5404-14.
216. Al-Hababi, F., *Inhibition of HCV Replication by Host Cell Innate Antiviral Defences*, in *PhD thesis: Department of Hepatology and Gastroenterology.* 2011, Imperial College London.
217. Charo, I.F. and R.M. Ransohoff, *The many roles of chemokines and chemokine receptors in inflammation.* N Engl J Med, 2006. **354**(6): p. 610-21.
218. Ren, X., et al., *Mitogenic properties of endogenous and pharmacological doses of macrophage inflammatory protein-2 after 70% hepatectomy in the mouse.* Am J Pathol, 2003. **163**(2): p. 563-70.
219. Yoshimura, A., *Regulation of cytokine signaling by the SOCS and Spred family proteins.* Keio J Med, 2009. **58**(2): p. 73-83.
220. Persico, M., et al., *Elevated expression and polymorphisms of SOCS3 influence patient response to antiviral therapy in chronic hepatitis C.* Gut, 2008. **57**(4): p. 507-15.
221. Bode, J.G., et al., *IFN-alpha antagonistic activity of HCV core protein involves induction of suppressor of cytokine signaling-3.* Faseb J, 2003. **17**(3): p. 488-90.
222. Brown, K.S., et al., *Severe fibrosis in hepatitis C virus-infected patients is associated with increased activity of the mannan-binding lectin (MBL)/MBL-associated serine protease 1 (MASP-1) complex.* Clin Exp Immunol, 2007. **147**(1): p. 90-8.

223. Choi, J. and J.H. Ou, *Mechanisms of liver injury. III. Oxidative stress in the pathogenesis of hepatitis C virus.* Am J Physiol Gastrointest Liver Physiol, 2006. **290**(5): p. G847-51.
224. Chung-man Ho, J., et al., *Differential expression of manganese superoxide dismutase and catalase in lung cancer.* Cancer Res, 2001. **61**(23): p. 8578-85.
225. Hosakote, Y.M., et al., *Respiratory syncytial virus induces oxidative stress by modulating antioxidant enzymes.* Am J Respir Cell Mol Biol, 2009. **41**(3): p. 348-57.
226. Tao, X., et al., *Downregulated expression of metallothionein and its clinicopathological significance in hepatocellular carcinoma.* Hepatol Res, 2007. **37**(10): p. 820-7.
227. Rifkind, A.B., *CYP1A in TCDD toxicity and in physiology-with particular reference to CYP dependent arachidonic acid metabolism and other endogenous substrates.* Drug Metab Rev, 2006. **38**(1-2): p. 291-335.
228. Arnold, C., et al., *Cytochrome P450-dependent metabolism of omega-6 and omega-3 long-chain polyunsaturated fatty acids.* Pharmacol Rep, 2010. **62**(3): p. 536-47.
229. Kawano, Y., et al., *Activation of the aryl hydrocarbon receptor induces hepatic steatosis via the upregulation of fatty acid transport.* Arch Biochem Biophys, 2010. **504**(2): p. 221-7.
230. Lan, L., et al., *Hepatitis C virus infection sensitizes human hepatocytes to TRAIL-induced apoptosis in a caspase 9-dependent manner.* J Immunol, 2008. **181**(7): p. 4926-35.
231. Castello, G., et al., *HCV-related hepatocellular carcinoma: From chronic inflammation to cancer.* Clin Immunol, 2009. **134**(3): p. 237-50.
232. Yu, S., et al., *Adipocyte-specific gene expression and adipogenic steatosis in the mouse liver due to peroxisome proliferator-activated receptor gamma1 (PPARgamma1) overexpression.* J Biol Chem, 2003. **278**(1): p. 498-505.
233. Horton, J.D., J.L. Goldstein, and M.S. Brown, *SREBPs: activators of the complete program of cholesterol and fatty acid synthesis in the liver.* J Clin Invest, 2002. **109**(9): p. 1125-31.
234. Heikkinen, S., J. Auwerx, and C.A. Argmann, *PPARgamma in human and mouse physiology.* Biochim Biophys Acta, 2007. **1771**(8): p. 999-1013.
235. Fujino, T., et al., *Expression profile of lipid metabolism-associated genes in hepatitis C virus-infected human liver.* Hepatol Res, 2010. **40**(9): p. 923-9.

236. Jhaveri, R., G. Qiang, and A.M. Diehl, *Domain 3 of hepatitis C virus core protein is sufficient for intracellular lipid accumulation.* J Infect Dis, 2009. **200**(11): p. 1781-8.
237. Rakhshandehroo, M., et al., *Comparative analysis of gene regulation by the transcription factor PPARalpha between mouse and human.* PLoS One, 2009. **4**(8): p. e6796.
238. Yamaguchi, A., et al., *Hepatitis C virus core protein modulates fatty acid metabolism and thereby causes lipid accumulation in the liver.* Dig Dis Sci, 2005. **50**(7): p. 1361-71.
239. Oka, S.I., et al., *Thioredoxin Binding Protein-2 (TBP-2)/Txnip is a Critical Regulator of Insulin Secretion and PPAR Function.* Endocrinology, 2009. **150**(3): p. 1225-1234.
240. Inoue, Y., et al., *Transcriptomic comparison of human hepatoma Huh-7 cell clones with different hepatitis C virus replication efficiencies.* Jpn J Infect Dis, 2007. **60**(4): p. 173-8.
241. Pedersen, I.M., et al., *Interferon modulation of cellular microRNAs as an antiviral mechanism.* Nature, 2007. **449**(7164): p. 919-22.
242. Marquez, R.T., et al., *Correlation between microRNA expression levels and clinical parameters associated with chronic hepatitis C viral infection in humans.* Lab Invest, 2010. **90**(12): p. 1727-36.
243. Peng, X., et al., *Computational identification of hepatitis C virus associated microRNA-mRNA regulatory modules in human livers.* BMC Genomics, 2009. **10**: p. 373.
244. Otsuka, M., et al., *Interaction between the HCV NS3 protein and the host TBK1 protein leads to inhibition of cellular antiviral responses.* Hepatology, 2005. **41**(5): p. 1004-12.
245. Chan, E.Y., et al., *Dynamic host energetics and cytoskeletal proteomes in human immunodeficiency virus type 1-infected human primary CD4 cells: analysis by multiplexed label-free mass spectrometry.* J Virol, 2009. **83**(18): p. 9283-95.
246. Bernstein, H.B. and R.W. Compans, *Sulfation of the human immunodeficiency virus envelope glycoprotein.* J Virol, 1992. **66**(12): p. 6953-9.
247. Martina, J.A., et al., *Stonin 2: an adaptor-like protein that interacts with components of the endocytic machinery.* J Cell Biol, 2001. **153**(5): p. 1111-20.
248. Ford, M.G., et al., *Simultaneous binding of PtdIns(4,5)P2 and clathrin by AP180 in the nucleation of clathrin lattices on membranes.* Science, 2001. **291**(5506): p. 1051-5.

249. Starr, T., et al., *Rab33b and Rab6 are functionally overlapping regulators of Golgi homeostasis and trafficking.* Traffic, 2010. **11**(5): p. 626-36.
250. Wanschers, B.F., et al., *A role for the Rab6B Bicaudal-D1 interaction in retrograde transport in neuronal cells.* Exp Cell Res, 2007. **313**(16): p. 3408-20.
251. Valsdottir, R., et al., *Identification of rabaptin-5, rabex-5, and GM130 as putative effectors of rab33b, a regulator of retrograde traffic between the Golgi apparatus and ER.* FEBS Lett, 2001. **508**(2): p. 201-9.
252. Itoh, T., et al., *Golgi-resident small GTPase Rab33B interacts with Atg16L and modulates autophagosome formation.* Mol Biol Cell, 2008. **19**(7): p. 2916-25.
253. Berger, K.L., et al., *Roles for endocytic trafficking and phosphatidylinositol 4-kinase III alpha in hepatitis C virus replication.* Proc Natl Acad Sci U S A, 2009. **106**(18): p. 7577-82.
254. Coller, K.E., et al., *RNA interference and single particle tracking analysis of hepatitis C virus endocytosis.* PLoS Pathog, 2009. **5**(12): p. e1000702.
255. Matsuda, M., et al., *abLIM3 is a novel component of adherens junctions with actin-binding activity.* Eur J Cell Biol, 2010. **89**(11): p. 807-16.
256. Amsellem, V., et al., *The actin cytoskeleton-associated protein zyxin acts as a tumor suppressor in Ewing tumor cells.* Exp Cell Res, 2005. **304**(2): p. 443-56.
257. Dang, C., et al., *Identification of dysregulated genes in cutaneous squamous cell carcinoma.* Oncol Rep, 2006. **16**(3): p. 513-9.
258. Akgul, B., et al., *Proteomic analysis reveals the actin cytoskeleton as cellular target for the human papillomavirus type 8.* Virology, 2009. **386**(1): p. 1-5.
259. Alberts, B., D. Bray, J. Lewis, R. Martin, K. Roberts, and J. D. Watson, *Molecular biology of the cell*. Vol. 3. 1994, New York: ed. G. publishing.
260. Dahari, H., et al., *Mathematical modeling of subgenomic hepatitis C virus replication in Huh-7 cells.* J Virol, 2007. **81**(2): p. 750-60.
261. Sainz, B., Jr., N. Barretto, and S.L. Uprichard, *Hepatitis C virus infection in phenotypically distinct Huh7 cell lines.* PLoS One, 2009. **4**(8): p. e6561.
262. Anderson, G.R., et al., *Regulation of the CYP1A1 gene by 2,3,7,8-tetrachlorodibenzo-p-dioxin but not by beta-naphthoflavone or 3-methylcholanthrene is altered in hepatitis C virus replicon-expressing cells.* Mol Pharmacol, 2006. **70**(3): p. 1062-70.
263. Khan, M., et al., *Interaction of the hepatitis C virus (HCV) core with cellular genes in the development of HCV-induced steatosis.* Arch Virol, 2010. **155**(11): p. 1735-53.

264. Eng, F.J., et al., *Internal initiation stimulates production of p8 minicore, a member of a newly discovered family of hepatitis C virus core protein isoforms.* J Virol, 2009. **83**(7): p. 3104-14.
265. Mizuno, K., et al., *Rab27b regulates mast cell granule dynamics and secretion.* Traffic, 2007. **8**(7): p. 883-92.
266. Raposo, G., M.S. Marks, and D.F. Cutler, *Lysosome-related organelles: driving post-Golgi compartments into specialisation.* Curr Opin Cell Biol, 2007. **19**(4): p. 394-401.
267. Izumi, T., *Physiological roles of Rab27 effectors in regulated exocytosis.* Endocr J, 2007. **54**(5): p. 649-57.
268. Pereira-Leal, J.B. and M.C. Seabra, *Evolution of the Rab family of small GTP-binding proteins.* J Mol Biol, 2001. **313**(4): p. 889-901.
269. Masuda, E.S., et al., *Rab37 is a novel mast cell specific GTPase localized to secretory granules.* FEBS Lett, 2000. **470**(1): p. 61-4.
270. Saxena, G., J. Chen, and A. Shalev, *Intracellular shuttling and mitochondrial function of thioredoxin-interacting protein.* J Biol Chem, 2010. **285**(6): p. 3997-4005.
271. Nishiyama, A., et al., *Identification of thioredoxin-binding protein-2/vitamin D(3) up-regulated protein 1 as a negative regulator of thioredoxin function and expression.* J Biol Chem, 1999. **274**(31): p. 21645-50.
272. Yamaguchi, F., et al., *Rare sugar D-allose induces specific up-regulation of TXNIP and subsequent G1 cell cycle arrest in hepatocellular carcinoma cells by stabilization of p27kip1.* Int J Oncol, 2008. **32**(2): p. 377-85.
273. Schroder, K., R. Zhou, and J. Tschopp, *The NLRP3 inflammasome: a sensor for metabolic danger?* Science, 2010. **327**(5963): p. 296-300.
274. Okuyama, H., et al., *Thioredoxin binding protein 2 modulates natural killer T cell-dependent innate immunity in the liver: possible link to lipid metabolism.* Antioxid Redox Signal, 2009. **11**(10): p. 2585-93.
275. Chutkow, W.A., et al., *Thioredoxin-interacting protein (Txnip) is a critical regulator of hepatic glucose production.* J Biol Chem, 2008. **283**(4): p. 2397-406.
276. Androutsopoulos, V.P., A.M. Tsatsakis, and D.A. Spandidos, *Cytochrome P450 CYP1A1: wider roles in cancer progression and prevention.* BMC Cancer, 2009. **9**: p. 187.
277. Fallone, F., et al., *PPARalpha activation potentiates AhR-induced CYP1A1 expression.* Toxicology, 2005. **216**(2-3): p. 122-8.

278. Liu, Y., et al., *The antiinflammatory effect of laminar flow: the role of PPARgamma, epoxyeicosatrienoic acids, and soluble epoxide hydrolase.* Proc Natl Acad Sci U S A, 2005. **102**(46): p. 16747-52.
279. Leu, G.Z., T.Y. Lin, and J.T. Hsu, *Anti-HCV activities of selective polyunsaturated fatty acids.* Biochem Biophys Res Commun, 2004. **318**(1): p. 275-80.
280. Chen, Z., J.Y. Norris, and B.N. Finck, *Peroxisome proliferator-activated receptor-gamma coactivator-1alpha (PGC-1alpha) stimulates VLDL assembly through activation of cell death-inducing DFFA-like effector B (CideB).* J Biol Chem, 2010. **285**(34): p. 25996-6004.
281. Benton, C.R., D.C. Wright, and A. Bonen, *PGC-1alpha-mediated regulation of gene expression and metabolism: implications for nutrition and exercise prescriptions.* Appl Physiol Nutr Metab, 2008. **33**(5): p. 843-62.
282. Hallberg, M., et al., *A functional interaction between RIP140 and PGC-1alpha regulates the expression of the lipid droplet protein CIDEA.* Mol Cell Biol, 2008. **28**(22): p. 6785-95.
283. Gavrilova, O., et al., *Liver peroxisome proliferator-activated receptor gamma contributes to hepatic steatosis, triglyceride clearance, and regulation of body fat mass.* J Biol Chem, 2003. **278**(36): p. 34268-76.
284. Yonezawa, T., et al., *Which CIDE are you on? Apoptosis and energy metabolism.* Mol Biosyst, 2011. **7**(1): p. 91-100.
285. Ye, J., et al., *Cideb, an ER- and lipid droplet-associated protein, mediates VLDL lipidation and maturation by interacting with apolipoprotein B.* Cell Metab, 2009. **9**(2): p. 177-90.
286. Erdtmann, L., et al., *The hepatitis C virus NS2 protein is an inhibitor of CIDE-B-induced apoptosis.* J Biol Chem, 2003. **278**(20): p. 18256-64.
287. Fritah, A., M. Christian, and M.G. Parker, *The metabolic coregulator RIP140: an update.* Am J Physiol Endocrinol Metab, 2010. **299**(3): p. E335-40.
288. Ni, X., et al., *Molecular cloning and characterization of a novel human Rab (Rab2B) gene.* J Hum Genet, 2002. **47**(10): p. 548-51.
289. Tanaka, A.R., et al., *Formation of cholesterol-enriched structures by aberrant intracellular accumulation of ATP-binding cassette transporter A1.* Genes Cells, 2008. **13**(8): p. 889-904.
290. Uhlig, M., W. Passlack, and J. Eckel, *Identification and characterization of a novel variant in the highly conserved catalytic center of Rab11a.* Eur J Med Genet, 2006. **49**(1): p. 29-36.

291. Johnson, J.L., et al., *Rab27a and Rab27b regulate neutrophil azurophilic granule exocytosis and NADPH oxidase activity by independent mechanisms.* Traffic, 2010. **11**(4): p. 533-47.
292. Brighouse, A., J.B. Dacks, and M.C. Field, *Rab protein evolution and the history of the eukaryotic endomembrane system.* Cell Mol Life Sci, 2010. **67**(20): p. 3449-65.
293. Fukuda, M., et al., *Large scale screening for novel rab effectors reveals unexpected broad Rab binding specificity.* Mol Cell Proteomics, 2008. **7**(6): p. 1031-42.
294. Ostrowski, M., et al., *Rab27a and Rab27b control different steps of the exosome secretion pathway.* Nat Cell Biol, 2010. **12**(1): p. 19-30; sup pp 1-13.
295. Lapierre, L.A., et al., *Rab11b resides in a vesicular compartment distinct from Rab11a in parietal cells and other epithelial cells.* Exp Cell Res, 2003. **290**(2): p. 322-31.
296. Oehlke, O., et al., *Rab11b and its effector Rip11 regulate the acidosis-induced traffic of V-ATPase in salivary ducts.* J Cell Physiol, 2010. **226**(3): p. 638-51.
297. Robbins, M., A. Judge, and I. MacLachlan, *siRNA and innate immunity.* Oligonucleotides, 2009. **19**(2): p. 89-102.
298. Ng, T.I., et al., *Identification of host genes involved in hepatitis C virus replication by small interfering RNA technology.* Hepatology, 2007. **45**(6): p. 1413-21.
299. Takaoka, A. and H. Yanai, *Interferon signalling network in innate defence.* Cell Microbiol, 2006. **8**(6): p. 907-22.
300. Matsumoto, M. and T. Seya, *TLR3: interferon induction by double-stranded RNA including poly(I:C).* Adv Drug Deliv Rev, 2008. **60**(7): p. 805-12.
301. Junutula, J.R., et al., *Molecular characterization of Rab11 interactions with members of the family of Rab11-interacting proteins.* J Biol Chem, 2004. **279**(32): p. 33430-7.
302. Van Gele, M., P. Dynoodt, and J. Lambert, *Griscelli syndrome: a model system to study vesicular trafficking.* Pigment Cell Melanoma Res, 2009. **22**(3): p. 268-82.
303. Manna, D., et al., *Endocytic Rab proteins are required for hepatitis C virus replication complex formation.* Virology, 2010. **398**(1): p. 21-37.
304. Brass, A.L., et al., *Identification of host proteins required for HIV infection through a functional genomic screen.* Science, 2008. **319**(5865): p. 921-6.
305. Indran, S.V., M.E. Ballestas, and W.J. Britt, *Bicaudal D1-dependent trafficking of human cytomegalovirus tegument protein pp150 in virus-infected cells.* J Virol, 2010. **84**(7): p. 3162-77.

306. Watanabe, A., et al., *Raftlin is involved in the nucleocapture complex to induce poly(I:C)-mediated TLR3 activation.* J Biol Chem, 2011.
307. Khvalevsky, E., et al., *TLR3 signaling in a hepatoma cell line is skewed towards apoptosis.* J Cell Biochem, 2007. **100**(5): p. 1301-12.
308. Li, K., et al., *Distinct poly(I-C) and virus-activated signaling pathways leading to interferon-beta production in hepatocytes.* J Biol Chem, 2005. **280**(17): p. 16739-47.
309. Kawai, T., et al., *IPS-1, an adaptor triggering RIG-I- and Mda5-mediated type I interferon induction.* Nat Immunol, 2005. **6**(10): p. 981-8.
310. Kato, H., et al., *Length-dependent recognition of double-stranded ribonucleic acids by retinoic acid-inducible gene-I and melanoma differentiation-associated gene 5.* J Exp Med, 2008. **205**(7): p. 1601-10.
311. Kato, H., et al., *Differential roles of MDA5 and RIG-I helicases in the recognition of RNA viruses.* Nature, 2006. **441**(7089): p. 101-5.
312. Yoneyama, M., et al., *Shared and unique functions of the DExD/H-box helicases RIG-I, MDA5, and LGP2 in antiviral innate immunity.* J Immunol, 2005. **175**(5): p. 2851-8.
313. Ranjith-Kumar, C.T., et al., *Agonist and antagonist recognition by RIG-I, a cytoplasmic innate immunity receptor.* J Biol Chem, 2009. **284**(2): p. 1155-65.
314. Fraile-Ramos, A., et al., *Rab27a is required for human cytomegalovirus assembly.* PLoS One, 2010. **5**(12): p. e15318.
315. Rani, S., et al., *Decreasing Txnip mRNA and protein levels in pancreatic MIN6 cells reduces reactive oxygen species and restores glucose regulated insulin secretion.* Cell Physiol Biochem, 2010. **25**(6): p. 667-74.
316. Parikh, H., et al., *TXNIP regulates peripheral glucose metabolism in humans.* PLoS Med, 2007. **4**(5): p. e158.
317. Lyn, R.K., et al., *Direct imaging of the disruption of hepatitis C virus replication complexes by inhibitors of lipid metabolism.* Virology, 2009. **394**(1): p. 130-42.
318. Patwari, P., et al., *Thioredoxin-independent regulation of metabolism by the alpha-arrestin proteins.* J Biol Chem, 2009. **284**(37): p. 24996-5003.
319. Chen, J., et al., *Thioredoxin-interacting protein: a critical link between glucose toxicity and beta-cell apoptosis.* Diabetes, 2008. **57**(4): p. 938-44.
320. Masson, E., et al., *High beta-cell mass prevents streptozotocin-induced diabetes in thioredoxin-interacting protein-deficient mice.* Am J Physiol Endocrinol Metab, 2009. **296**(6): p. E1251-61.

321. Negro, F. and M. Alaei, *Hepatitis C virus and type 2 diabetes.* World J Gastroenterol, 2009. **15**(13): p. 1537-47.
322. Ahsan, M.K., et al., *Thioredoxin-binding Protein-2 Deficiency Enhances Methionine-Choline Deficient Diet-induced Hepatic Steatosis but Inhibits Steatohepatitis in Mice.* Antioxid Redox Signal, 2009.
323. Li, X., et al., *Up-regulation of thioredoxin interacting protein (Txnip) by p38 MAPK and FOXO1 contributes to the impaired thioredoxin activity and increased ROS in glucose-treated endothelial cells.* Biochem Biophys Res Commun, 2009. **381**(4): p. 660-5.
324. Qi, W., et al., *Transcription factors Kruppel-like factor 6 and peroxisome proliferator-activated receptor-{gamma} mediate high glucose-induced thioredoxin-interacting protein.* Am J Pathol, 2009. **175**(5): p. 1858-67.
325. Cha-Molstad, H., et al., *Glucose-stimulated expression of Txnip is mediated by carbohydrate response element-binding protein, p300, and histone H4 acetylation in pancreatic beta cells.* J Biol Chem, 2009. **284**(25): p. 16898-905.
326. Stoltzman, C.A., et al., *Glucose sensing by MondoA:Mlx complexes: a role for hexokinases and direct regulation of thioredoxin-interacting protein expression.* Proc Natl Acad Sci U S A, 2008. **105**(19): p. 6912-7.
327. Yu, F.X., et al., *Thioredoxin-interacting protein (Txnip) gene expression: sensing oxidative phosphorylation status and glycolytic rate.* J Biol Chem, 2010. **285**(33): p. 25822-30.
328. Baker, A.F., et al., *Identification of thioredoxin-interacting protein 1 as a hypoxia-inducible factor 1alpha-induced gene in pancreatic cancer.* Pancreas, 2008. **36**(2): p. 178-86.
329. Rakhshandehroo, M., et al., *Peroxisome proliferator-activated receptor alpha target genes.* PPAR Res, 2010. **2010**.
330. Chang, K.S. and G. Luo, *The polypyrimidine tract-binding protein (PTB) is required for efficient replication of hepatitis C virus (HCV) RNA.* Virus Res, 2006. **115**(1): p. 1-8.
331. Hwang, B., et al., *hnRNP L is required for the translation mediated by HCV IRES.* Biochem Biophys Res Commun, 2009. **378**(3): p. 584-8.
332. Bartosch, B., J. Dubuisson, and F.L. Cosset, *Infectious hepatitis C virus pseudo-particles containing functional E1-E2 envelope protein complexes.* J Exp Med, 2003. **197**(5): p. 633-42.

333. Wickham, L., et al., *Mammalian staufen is a double-stranded-RNA- and tubulin-binding protein which localizes to the rough endoplasmic reticulum.* Mol Cell Biol, 1999. **19**(3): p. 2220-30.
334. Kim, Y.K., et al., *Staufen1 regulates diverse classes of mammalian transcripts.* Embo J, 2007. **26**(11): p. 2670-81.
335. Thomas, M.G., et al., *Mammalian Staufen 1 is recruited to stress granules and impairs their assembly.* J Cell Sci, 2009. **122**(Pt 4): p. 563-73.
336. Sans, C.L., et al., *MondoA-Mlx heterodimers are candidate sensors of cellular energy status: mitochondrial localization and direct regulation of glycolysis.* Mol Cell Biol, 2006. **26**(13): p. 4863-71.
337. Ma, L., L.N. Robinson, and H.C. Towle, *ChREBP*Mlx is the principal mediator of glucose-induced gene expression in the liver.* J Biol Chem, 2006. **281**(39): p. 28721-30.
338. Yu, F.X. and Y. Luo, *Tandem ChoRE and CCAAT motifs and associated factors regulate Txnip expression in response to glucose or adenosine-containing molecules.* PLoS One, 2009. **4**(12): p. e8397.
339. Peterson, C.W., et al., *Glucose controls nuclear accumulation, promoter binding, and transcriptional activity of the MondoA-Mlx heterodimer.* Mol Cell Biol, 2010. **30**(12): p. 2887-95.
340. Chen, J.L., et al., *Lactic acidosis triggers starvation response with paradoxical induction of TXNIP through MondoA.* PLoS Genet, 2010. **6**(9).
341. Ripoli, M., et al., *Hepatitis C virus-linked mitochondrial dysfunction promotes hypoxia-inducible factor 1 alpha-mediated glycolytic adaptation.* J Virol, 2010. **84**(1): p. 647-60.
342. Patwari, P., et al., *The interaction of thioredoxin with Txnip. Evidence for formation of a mixed disulfide by disulfide exchange.* J Biol Chem, 2006. **281**(31): p. 21884-91.
343. Kurtz, D.M., R.J. Tolwani, and P.A. Wood, *Structural characterization of the mouse long-chain acyl-CoA dehydrogenase gene and 5' regulatory region.* Mamm Genome, 1998. **9**(5): p. 361-5.
344. Ohoka, N., et al., *TRB3, a novel ER stress-inducible gene, is induced via ATF4-CHOP pathway and is involved in cell death.* Embo J, 2005. **24**(6): p. 1243-55.
345. Qi, L., et al., *TRB3 links the E3 ubiquitin ligase COP1 to lipid metabolism.* Science, 2006. **312**(5781): p. 1763-6.

346. McGarry, J.D. and N.F. Brown, *The mitochondrial carnitine palmitoyltransferase system. From concept to molecular analysis.* Eur J Biochem, 1997. **244**(1): p. 1-14.
347. Sugden, M.C. and M.J. Holness, *Recent advances in mechanisms regulating glucose oxidation at the level of the pyruvate dehydrogenase complex by PDKs.* Am J Physiol Endocrinol Metab, 2003. **284**(5): p. E855-62.
348. Agnihotri, G. and H.W. Liu, *Enoyl-CoA hydratase. reaction, mechanism, and inhibition.* Bioorg Med Chem, 2003. **11**(1): p. 9-20.
349. Varanasi, U., et al., *Isolation of the human peroxisomal acyl-CoA oxidase gene: organization, promoter analysis, and chromosomal localization.* Proc Natl Acad Sci U S A, 1994. **91**(8): p. 3107-11.
350. Mousseau, G., et al., *Dimerization-driven interaction of hepatitis C virus core protein with NS3 helicase.* J Gen Virol, 2010. **92**(Pt 1): p. 101-11.
351. Sekine-Osajima, Y., et al., *Development of plaque assays for hepatitis C virus-JFH1 strain and isolation of mutants with enhanced cytopathogenicity and replication capacity.* Virology, 2008. **371**(1): p. 71-85.
352. Yi, M., et al., *Production of infectious genotype 1a hepatitis C virus (Hutchinson strain) in cultured human hepatoma cells.* Proc Natl Acad Sci U S A, 2006. **103**(7): p. 2310-5.
353. Kato, T., et al., *Sequence analysis of hepatitis C virus isolated from a fulminant hepatitis patient.* J Med Virol, 2001. **64**(3): p. 334-9.
354. Steuerwald, N.M., et al., *Parallel microRNA and mRNA expression profiling of (genotype 1b) human hepatoma cells expressing hepatitis C virus.* Liver Int, 2010. **30**(10): p. 1490-504.
355. Randall, G., et al., *Cellular cofactors affecting hepatitis C virus infection and replication.* Proc Natl Acad Sci U S A, 2007. **104**(31): p. 12884-9.
356. Chen, Y., et al., *Rab27b association with melanosomes: dominant negative mutants disrupt melanosomal movement.* J Invest Dermatol, 2002. **118**(6): p. 933-40.
357. McCaffrey, M.W., et al., *Rab4 affects both recycling and degradative endosomal trafficking.* FEBS Lett, 2001. **495**(1-2): p. 21-30.
358. Furman, C.A., et al., *Rab 11 regulates constitutive dopamine transporter trafficking and function in N2A neuroblastoma cells.* Neurosci Lett, 2009. **463**(1): p. 78-81.
359. Ma, L., N.G. Tsatsos, and H.C. Towle, *Direct role of ChREBP.Mlx in regulating hepatic glucose-responsive genes.* J Biol Chem, 2005. **280**(12): p. 12019-27.

360. Ciolino, H.P. and G.C. Yeh, *The flavonoid galangin is an inhibitor of CYP1A1 activity and an agonist/antagonist of the aryl hydrocarbon receptor.* Br J Cancer, 1999. **79**(9-10): p. 1340-6.
361. Mikstacka, R., et al., *Inhibition of human recombinant cytochromes P450 CYP1A1 and CYP1B1 by trans-resveratrol methyl ethers.* Mol Nutr Food Res, 2007. **51**(5): p. 517-24.
362. Kato, T., et al., *Efficient replication of the genotype 2a hepatitis C virus subgenomic replicon.* Gastroenterology, 2003. **125**(6): p. 1808-17.

Appendix

A.1 Quantitative real-time PCR primer sequences

Name	Forward primer sequence	Reverse primer sequence
GAPDH	5'cccaatacgaccaaatccg3'	5'tctctgctcctcctgttcgac3'
RPLPO	5'cgacctggaagtccaactac3'	5'atctgctgcatctgcttg3'
BETA ACTIN	5'aggtcatcaccattggcaa3'	5'cacttcatgatggagttgaaggtagtt3'
HCV	5'tctgcggaaccggtgagta3'	5'tcaggcagtaccacaaggc3'

Pathway	Name	Forward primer sequence	Reverse primer sequence
Genes selected from replication cycle of other RNA viruses	RAB1B	5'cagcgagaacgtcaataagc3'	5'gacattggtggcattcttgg3'
	RAB2A	5'ccagtgcatgaccttactattgg3'	5'tacgaccttgtgatggaacg3'
	RAB2B	5'aactgcaaatctgggatacg3'	5'tttcacgccttgtaatgtcg3'
	RAB4A	5'atgggctcaggtattcagtacg3'	5'aggttccaacgattgtgtcc3'
	RAB4B	5'ttgcccaggagaatgagc3'	5'ccgtactgaatgccagagc3'
	RAB6A	5'caattgaggagggagagagg3'	5'ttctgtcctgtgtgctttcc3'
	RAB11A	5'attggagattctggtgttgg3'	5'acctggatgcttcttgttgc3'
	RAB11B	5'gtactaccgtggtgcagtgg3'	5'cgcaggtcactcttgttgc3'
	RAB18	5'gctaaccaccctgaagatcc3'	5'tgcaagttctggatcaaacg3'
	STAU	5'gctcactcagacacattggg3'	5'ggtcacgctgagtaggaagc3'
	TIAL1	5' ccccggactctatacgtagg3'	5'gttgacccttctgctatcgg3'
	TIA1	5'gggaccaaattatggagtgc3'	5'cactccctgtagcctcaagc3'
Sphingo-lipid metabolism	SGMS2	5'caattccttgctgcttctcc3'	5'agctgatgcctttgttttgc3'
	SGPP1	5'cttctggatctggaacctgg3'	5'agacctccaacttgaccacg3'
	SGPL1	5'aagatggagaagcatgtgcc3'	5'ttgaaaaacaccatctcccc3'
	SPTLC1	5'actgattgaagagtggcaacc3'	5'acagttttgtggcttggagg3'
Cholesterol synthesis	FDFT1	5'ctcaagaggtttggagcagg3'	5' tgatgacatctgggatgtgg3'
	SQLE	5'aatctttaggttggggctgc3'	5'ttcagaggcttctttttccg3'
	EBP	5'agacagccgatacatcctgg3'	5'ctgtagaatgaagcggaggg3'
	MVD	5' gatgaagagctggttctgcc3'	5'gtgaagtccttgctgatgacg3'
	HMGCR	5' ataatcctggggaaaatgcc 3'	5' ttgacaagatgtcctgctgc3'
Fatty acid metabolism	ELOVL4	5'ctggtccatcgcagataagc3'	5'aggttctcggtccttcatcc3'
	ELOVL7	5'ctatggactttctgcattggg3'	5'aactggcttatgtggatggc3'
	TXNIP	5'ataaaagccctttgaacccc3'	5'gctcagtgctctgacacagg3'
	SREBF1	5'ggagagcctgtacagcttgg3'	5'tgggtcacacagttcagtgc3'
	PPARγ	5'tgcaggtgatcaagaagacg3'	5'tggaagaagggaaatgttgg3'
	PPARα	5'gcagaaacccagaactcagc3'	5'atggcccagtgtaagaaacg3'
	ACSL3	5' tgttgtgccaaatcaaaagg3'	5' ttgctgaaatagcagcttcg3'
Lipid droplet production	CIDEB	5' aagcggaccatccggaaa3'	5' gcagtagggtctccaatgcttt3'
	CIDEC	5' taagcacggcggatcgaa3'	5' cagagtgtcccggaccttga3'
	RIP140	5' gagaaaccagcccaaaatga3'	5' ctgggtctctgctcttccac3'
	PGC1α	5'tcaagccactacagacaccg3'	5'gcctctcgtgctgatattcc3'

Pathway	Name	Forward primer sequence	Reverse primer sequence
AHR Pathway	AHR	5'ctgcctttcccacaagatgt3'	5'agttatcctggcctccgttt3'
	CYP1A1	5’aactagccaaaccaggaccc3’	5’tagggtcagattgctcagcc3’
	CYP1B1	5’ccccagtctcaatctcaacg3’	5’ctcccactcgagtctcttgg3’
Intracellular transport	RAB6B	5’ctacaggcaggaaaaccagg3’	5’catttgttcacacacagggc3’
	RAB21	5’agtagcatttgccttttggg3’	5’aaattcaacatgagccaccc3’
	RAB27A	5’tggttgattgaagggtcagg3’	5’ctcatcgcaaataactcggc3’
	RAB27B	5’ aatctgacacctgctctccc3’	5’ agaaatgttgtcttccccacc3’
	RAB33B	5’gaaacgtctgctaaaaacccc3’	5’taattccattatcagggggc3’
	RAB37	5’gagcagcgaaagagtgatcc3’	5’cggtatttcagttccttggc3’
	RAB40B	5'catctcagatcccggttcc3'	5'caagagcttcatgcacatcc3'
	ABLIM3	5’gacccttccctctttcaagg3’	5’gctctggtgggaacattagc3
TXNIP transcription factors	FOXO1	5’gcgcttagactgtgacatgg3’	5’cttgacactgtgtgggaagc3’
	MLX	5’gtgtgtcttcagctggatcg3’	5’cctcttgttggctgttctcc3’
	MLXIP	5’tcattctcttggtgctcacg3’	5’gtctggctggattcatcagg3’
	MLXIPL	5’ggtgttcagcatcctcatcc3’	5’agggagttcaggacagttgg3’
	HIF1α	5’tgcaacatggaaggtattgc3’	5’ttcacaaatcagcaccaagc3’
	KLF6	5’acagccaggaagatctgtgg3’	5’gctgatgagagtgtcctctgg3’
Alpha Arrestins	ARRDC1	5’ ggcagacaaggggagcctgc3’	5’ aaccgtggcgtgtggatggc3’
	ARRDC2	5’ gactggaggctgggggcctt 3’	5’ gctcatgtcggggtcctgcg 3’
	ARRDC3	5’ ccactgagacgagcgggagc3’	5’ tgcaaaatgcttgcaggccg3’
	ARRDC4	5’ttggttttgtgagctgagagc3’	5’cagtattctgcaggggaagc3’
PPARα Signalling	ACADL	5’ctccaaccccgtttttaagc3’	5’ggggtttcaaggcagtaagg3’
	TRIB3	5’ctcctgcctctgaactgagc3’	5’gcatgtgtgtggaacaaagc3’
	CPT1A	5’ gcagtctcttgatgctgtgg3’	5’gagatttggcgtagctgtcc3’
	CPT2	5’ tgagcttcagcagatgatgg3’	5’gagctcaggcaagatgatcc3’
	PDK4	5’acgacagcaacgaaaactcc3’	5’gctggccatctgttaactcc3’
	SLC27A2	5’tcagcgcatatggtatggaa3’	5’caagagtagcaccagccaca3’
	ECH1	5’gaggtgtggaccttgtcacc3’	5’gctgcagtgttcctacatcg3’
	ACOX1	5’ctgtcatgatgctccagacg3’,	5’cagactgctacctgctgtgg3’
ISG	PKR	5’tctgactcctgtctctggttctt3’	5’ctgctcagaagtcaccttcagat3’
	MX1	5’tgaaggagcggcttgcacgg3’	5’gggggcagacagtgtgcgtg3’

A.2 pCR2.1 vector sequencing primers

Name	Forward primer sequence	Reverse primer sequence
M13	5’gtaaaacgacggccagt3’	5’caggaaacagctatgac3’

A.3 pIRES vector core protein PCR primers

Name	Forward primer sequence	Reverse primer sequence
Core	5’ccgctagcggatcctaagccaccatgagcacaaatcctaaa3’	5’accgttccggtctctgcttagacgcgtgc3’

A.4 PCR cycling conditions

qRT-PCR (SYBR Green)

PCR Step		Temperature	Time	Ramp rate	Acquisition mode
Activation step		95˚C	15 minutes	20˚C/s	None
4 step cycle x 40 cycles	Denaturation	94˚C	15 seconds	20˚C/s	None
	Annealing	58˚C	30 seconds	20˚C/s	None
	Extension	72˚C	30 seconds	2˚C/s	None
	Data acquisition	78˚C	5 seconds	20˚C/s	Single
Melt curve step 1		95˚C	0 seconds	20˚C/s	None
Melt curve step 2		65˚C	15 seconds	20˚C/s	None
Melt curve step 3		95˚C	0 seconds	0.1˚C/s	Continuous
Cooling		40˚C	30 seconds	20˚C/s	None

Note: One-step qRT-PCR has an additional reverse transcription step prior to the activation step which runs at 50˚C for 20 minutes with a ramp rate of 20˚C/s.

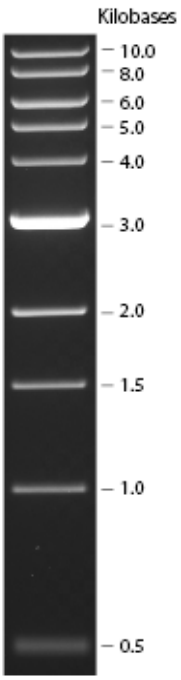
Standard PCR amplification

Bioline Red Taq polymerase			
PCR Step		**Temperature**	**Time**
Initial denaturation		94˚C	5 minutes
3 step cycle x 30 cycles	Denaturation	94˚C	45 seconds
	Annealing	55˚C	45 seconds
	Extension	72˚C	60 seconds
Final extension		72˚C	7 minutes
Cooling		4˚C	∞

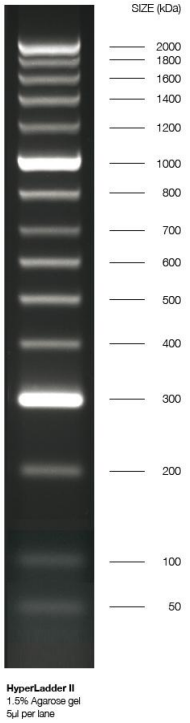
A.5 DNA and RNA molecular weight ladders

DNA ladders

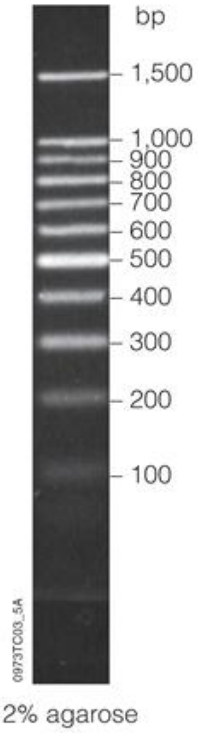
1KB DNA ladder (NEB)



Hyperladder II (Bioline)

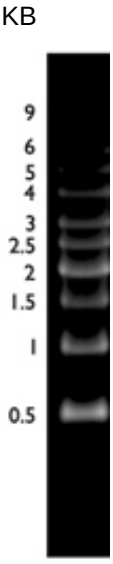


100bp DNA ladder (Promega)



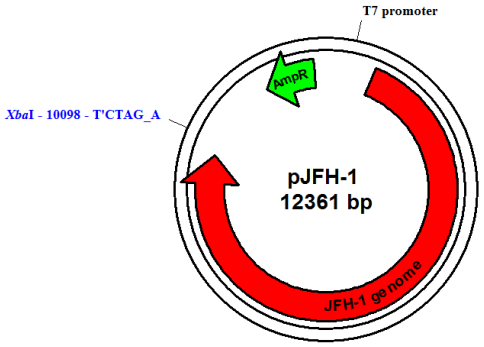
RNA ladder

Ambion Millennium RNA ladder

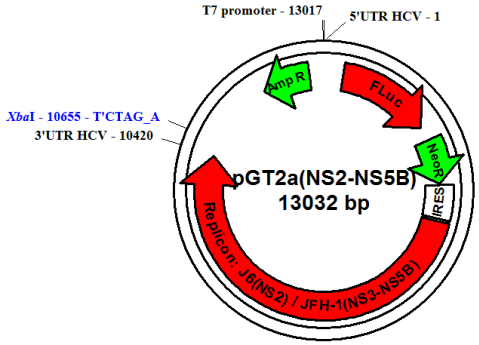


A.6 DNA plasmid maps

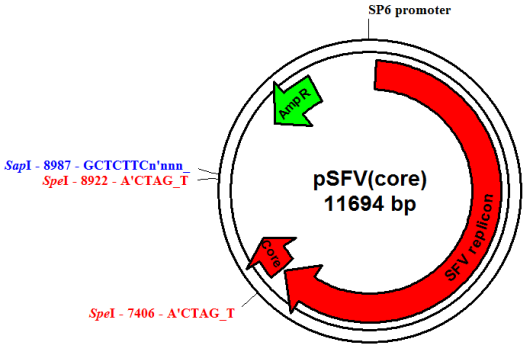
pJFH-1



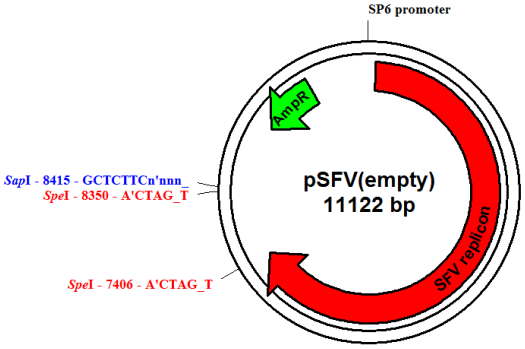
pGT2a(NS2-NS5B)



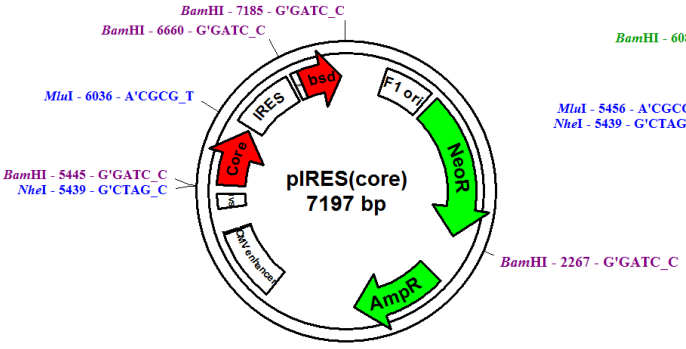
pSFV(core)



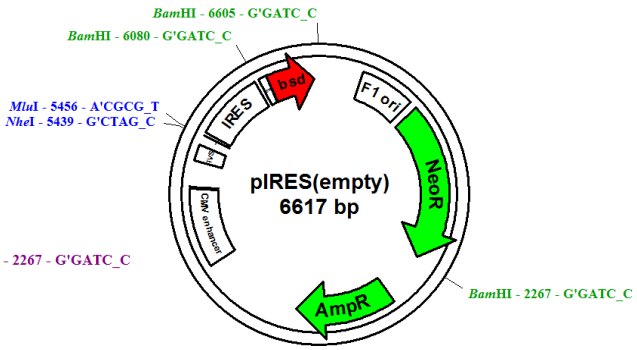
pSFV(empty)



pIRES(core)



pIRES(empty)



Amp R = Ampicillin resistance gene

NeoR = Neomycin resistance gene

bsd = Blasticidin resistance gene

FLuc = Luciferase reporter gene

IRES = EMCV IRES

A.7 siRNA molecule sequences

siRNA target gene	siRNA sense strand
HCV [209] (si313)	5’cccgggaggucucguagac[dt][dt]3’
Non-targeting (Sigma)	5’gaucauacgugcgaucaga[dt][dt]3’
RAB1B-1 (Sigma)	5’cacauggagugggacagga[dt][dt]3’
RAB1B-2 (Sigma)	5’gcaucaucgugguguauga[dt][dt]3’
RAB1B-3 [128] (duplex 9)	5’ugcaggagauugaccgcuauu3’
GAPDH (Sigma)	5’gguuuacauguuccaauau[dt][dt]3’
RAB2A-1 (Ambion)	5’gaaggagucuuugacauua[dt][dt]3’
RAB2A-2 (Ambion)	5’gagcuuuacuaguuuacga[dt][dt]3’
RAB2B-1 (Ambion)	5’gaauccuuccguucuauca[dt][dt]3’
RAB2B-2 (Ambion)	5’cgacauuacaaggcgugaa[dt][dt]3’
RAB4A-1 (Ambion)	5’ccuacaaugcgcuuacuaa[dt][dt]3’
RAB4A-2 (Ambion)	5’gaacgauucagguccguga[dt][dt]3’
RAB4B-1 (Ambion)	5’gcacuauccucaacaagau[dt][dt]3’
RAB4B-2 (Ambion)	5’agaauaaguucaaacagga[dt][dt]3’
RAB6A-1 (Ambion)	5’gagcugaauguuauguuua[dt][dt]3’
RAB6A-2 (Ambion)	5’aauucuucacgguaagaaa[dt][dt]3’
RAB11A-1 (Ambion)	5’caacaaugugguuccuauu[dt][dt]3’
RAB11A-2 (Ambion)	5’gagauuuaccgcauuguuu[dt][dt]3’
RAB11B-1 (Ambion)	5’cuaacguagaggaagcauu[dt][dt]3’
RAB11B-2 (Ambion)	5’gcaacgaguucaaccugga[dt][dt]3’
RAB18-1 (Ambion)	5’gguucacagaugauacguu[dt][dt]3’
RAB18-2 (Ambion)	5’ggaaaaucgugaagucgau[dt][dt]3’
TIA1-1 (Ambion)	5’gcgucagacuuuuucacca[dt][dt]3’
TIA1-2 (Ambion)	5’gauauucauuuguucgguu[dt][dt]3’
TIAL1-1 (Ambion)	5’cagaaguccuuauacuuca[dt][dt]3’
TIAL1-2 (Ambion)	5’ggauuuggaguagaucaau[dt][dt]3’
STAU1-1 (Ambion)	5’gaacgaauuuguaucucuu[dt][dt]3’
STAU1-2 (Ambion)	5’ggacuaguaauaaagagga[dt][dt]3’
STAU1-3 (Ambion)	5’ggcuguaggaguuagucaa[dt][dt]3’
STAU2 (Ambion)	5’gguuauaaagcauccacua[dt][dt]3’

RAB27A-1 (Ambion)	5'ggagagguuucguagcuua[dt][dt]3’
RAB27A-2 (Ambion)	5'gccucuacggaucaguuaa[dt][dt]3'
RAB27B-1 (Ambion)	5'gacuuaaucaugaagcgaa[dt][dt]3'
RAB27B-2 (Ambion)	5'ggaauagacuuucgggaaa[dt][dt]3'
RAB33B-1 (Ambion)	5'gaacgauucagaaagagca[dt][dt]3'
RAB33B-2 (Ambion)	5'ccuaccaucuuggauagaa[dt][dt]3'
RAB37-1 (Ambion)	5’ccagauccgagacuaugua[dt][dt]3’
RAB37-2 (Ambion)	5’ccagcuuccagauccgaga[dt][dt]3’
ABLIM3-1 (Ambion)	5’gcaaggaugguguuccaua[dt][dt]3’
ABLIM3-2 (Ambion)	5’gcgcuaaaguggauaauga[dt][dt]3’
CYP1A1-1 (Ambion)	5’cccucaucaguaaugguca[dt][dt]3’
CYP1A1-2 (Ambion)	5’guguaucggugagaccauu[dt][dt]3’
TXNIP-1 (Ambion)	5’cauccuucaaaggaaaaua[dt][dt]3’
TXNIP-2 (Ambion)	5’gaauauuccuuacugaucu[dt][dt]3’
TXNIP-3 (Ambion)	5’gaagaucaccgauuggaga[dt][dt]3’
PGC1α (Ambion)	5’ccuguuugaugacagcgaa[dt][dt]3’
CIDEB (Ambion)	5’gauucaccuuugacgugua[dt][dt]3’
CIDEC (Ambion)	5’ggcgacuuuuuaugauaca[dt][dt]3’
RIP140 (Ambion)	5’gcagcaguauucucgagaa[dt][dt]3’
FOXO1-1 (Ambion)	5’gcucaaaugcuaguacuau[dt][dt]3’
KLF6-1 (Ambion)	5’gcaggaaaguuuacaccaa[dt][dt]3’
MLX-1 (Ambion)	5’gaguaugccuacagcgaca[dt][dt]3’
MLXIP (Ambion)	5’ccacaagcggugaucauga[dt][dt]3’
MLXIPL (Ambion)	5’gacuacguccgaacccgua[dt][dt]3’
ARRDC4 (Ambion)	5’gggauacuguaauggagaa[dt][dt]3’

A.8 Fold change expression values on a log2 scale as represented in the heat map diagrams

Immunity and defence					
Host Gene	**FC 6 hours**	**FC 12 hours**	**FC 18 hours**	**FC 24 hours**	**FC 48 hours**
IFIT1	1.07	-0.21	0.07	-0.78	-0.81
MBL2	1.01	1.63	1.06	0.83	-0.94
MASP1	0.65	0.63	1.1	0.41	-0.27
IFIT5	0.13	0.71	0.12	0.85	1.02
CD55	-0.18	1.07	0.12	1.24	1.27
SOCS2	-0.69	0.54	-0.75	1.73	2.48
IRF9	0.52	1.19	1	2.08	2.55
SOCS4	0.01	0.52	0.29	0.74	1.01
IL8	-0.53	0.52	-0.12	0.8	1.52
IL6ST	-0.1	0.6	0.17	1.11	0.35
CXCL16	0.14	0.25	0.88	1.07	0.72
IRF1	-0.51	0.21	0	0.57	1.06
SOCS3	0.38	0.45	1.14	0.89	1.55
ISG20	-0.14	0.34	0.77	0.95	1.73
IL1RAP	-0.05	0.33	0.64	1	1.31
CEBPD	0.59	0.85	1.17	0.46	0.79
CXCL3	-0.33	1.44	1.04	0.33	0.83
CXCL1	-0.18	1.01	0.56	-0.12	0.32
CXCL2	0.16	1.96	1.56	1.34	1.95
CXCL5	0.4	1.2	0.8	0.95	0.91
CEBPB	-0.07	1.33	0.75	1.37	0.77
CEBPG	-0.07	1.14	0.56	1.22	0.81
CXCL6	-0.3	-0.75	-1.42	-1.34	-0.41
NCF2	-0.86	-1.71	-1.58	-1.26	-0.39
MX1	0.55	0.48	0.82	0.65	1.96
TRAF5	0.53	0.46	0.64	0.54	1.56
C2	0.3	0.22	0.67	0.71	1.76
IL6R	0.82	0.61	0.9	1.08	1.47
IL31RA	-0.51	-0.38	-0.65	-0.03	1.05
OAS3	0.29	0.03	0.1	0.51	1.3
GBP1	-0.84	-1.41	-1.54	-0.72	1.56

Oxidative stress and detoxification					
Host Gene	**FC 6 hours**	**FC 12 hours**	**FC 18 hours**	**FC 24 hours**	**FC 48 hours**
SOD2	0.02	2.03	0.73	1.02	0.96
AHR	0.55	1.57	0.52	0.84	0.75
CYP1A1	1.12	2.06	1.19	2.38	1.37
MAFF	-0.11	2.04	1	1.56	2.09
TXNIP	0.46	3.22	2.59	4.36	4.46
TXNL4B	0.31	1.09	0.64	1.56	1.69
CYP1B1	-0.15	1.03	0.45	1.92	1.94
NNMT	-0.13	1	0.3	1.28	2.05
FMO1	-0.36	-1.17	-1.62	-0.48	0.09
MAF	0.17	-0.02	0.25	0.24	1.25
TXNRD2	0.02	-0.31	0.03	0.18	1.07
DNAJC8	0.19	-0.05	0.29	0.25	0.78
AOX1	0.58	0.69	1.17	1.4	2.06
ESD	0.13	0.14	0.41	0.49	0.93
MAFK	-0.65	-0.36	-0.4	0.37	1.01
UGT2B4	-0.47	-0.39	-0.54	0.73	1.22
HSPB8	-0.62	-0.48	-0.64	-0.01	1
DDAH1	-0.01	0.06	0.12	0.45	1.14
GPX8	0.21	0.25	0.28	0.6	1.44
MT1M	-0.83	-0.98	-0.32	-2.03	0.07
MT1E	-0.69	-1.32	-0.21	-1.5	-0.69
MT1X	-0.67	-1.31	-0.13	-1.56	-0.7
MT1H	-0.7	-1	-0.11	-1.21	-0.44
MT1F	-0.76	-1.13	-0.31	-1.29	-0.54
MT1P2	-0.66	-1.08	-0.2	-1.25	-0.44
GLRX	-0.65	-1.21	-0.71	-1.3	-0.92
GPX3	0	-0.47	-0.6	-0.89	-1.41
NQO1	0.15	0.02	0.15	-0.33	-1.41
GSTM3	0.03	-0.46	-0.35	-0.83	-1.36
EPHX1	0.11	-0.26	-0.32	-0.4	-1.04
GSTM4	-0.16	-0.49	-0.91	-1.18	-1.74
GSTM1	-0.08	-0.41	-0.55	-0.95	-1.31
GSTM2	-0.02	-0.36	-0.51	-1	-1.45
TXNL1	-0.05	-0.1	-0.31	-0.73	-1.19
PON2	0.02	-0.1	-0.29	-0.53	-1.13
MGST3	-0.21	-0.5	-0.54	-1.09	-1.21
CAT	0.1	-0.44	-0.3	-1.38	-1.82
GPX2	0.49	-0.09	0.02	-1.56	-1.47
ATOX1	-0.32	-0.38	-0.03	-1.09	-1.36

Apoptosis					
Host Gene	**FC 6 hours**	**FC 12 hours**	**FC 18 hours**	**FC 24 hours**	**FC 48 hours**
BCL2L11	-0.66	-0.62	-0.59	-0.56	-0.77
DDIT3	0.17	1.55	0.81	0.8	0.53
MYC	0.77	1.31	1.16	0.88	0.76
DFFB	0.5	-0.36	0.63	-1.03	-0.49
NDRG4	-0.08	-0.62	-0.75	-1.13	-0.79
HLF	1.03	1.28	1.09	0.44	0.39
BCL2L12	0.15	-0.4	-0.17	-1	-1.2
TNFRSF11B	1.02	0.45	0.58	-0.2	-0.58
NDRG1	0.55	-0.04	0.02	-1.06	-1.01
BIRC5	0.19	-0.44	-0.31	-0.53	-1.2
IFT57	-0.05	-0.2	-0.2	-0.59	-2.12
NDRG2	0.15	-0.22	-0.49	-1.06	-2.05
BEX2	0.14	0.45	0.94	1.43	2.06
KLF10	-0.87	0.95	0.53	2.09	2.67
RASSF1	-0.01	0.72	0.52	1.19	1.3
JUNB	-1.48	-0.44	-0.36	0.2	0.53
ATF4	0.06	0.6	0.61	0.99	1.06
LTBP1	0.18	-0.05	0.26	0.25	1.19
HDAC4	1.22	1.41	1.56	1.56	2.05
TLE3	-0.35	-0.15	0.09	0.28	1.23
BEX1	0.24	0.11	1.21	1.19	2.92
WWOX	0.14	0.04	0.38	0.45	1.38
PRNP	0.12	0.09	0.58	1.14	3
PLAGL1	0.24	0.32	0.25	0.69	1.26
PPP1R13L	-1.07	-0.97	-0.83	0.03	1.29
PIK3CD	-1.09	-0.86	-1.19	-0.51	-0.1
TRIM69	0.38	0.61	0.31	1.04	1.54
BNIP1	-0.02	0.38	0.1	0.66	1.25
DPF2	-0.03	0.3	0.24	0.82	1.38
PMAIP1	-0.13	2.77	0.79	2.16	2.01
TRIB3	0.01	2.2	1.01	2.31	1.42

Apoptosis					
Host Gene	**FC 6 hours**	**FC 12 hours**	**FC 18 hours**	**FC 24 hours**	**FC 48 hours**
DDIT4	-0.23	3.68	2.26	3.45	2.18
SKIL	-1.09	0.03	-0.3	-0.21	-0.44
FOXO3	-0.08	0.88	0.12	1.2	1.06
TAF1A	0.14	0.94	0.4	1.13	1.11
BIRC3	-1.19	-0.1	-1.11	0.01	0.37
HDAC9	-1.43	1.64	-1.34	2.27	4.12
SIRT1	-0.1	0.6	0.14	0.72	1.11
RYBP	-0.39	0.41	0.04	0.63	1.12
TP53BP2	-0.59	0.28	-0.2	0.67	1.1
NEDD9	-1.14	-0.02	-0.56	0.59	1.21
PTPRH	-0.34	0.38	0.05	0.78	1.03
GADD45A	-0.38	1.02	0.16	0.75	1.56
PPP1R15A	-0.11	1.71	0.59	1.6	1.93
JUN	-1.01	0.07	0.04	0.02	0.44
GADD45B	-1.06	0.04	0.13	-0.07	0.52

Cell cycle					
Host Gene	**FC 6 hours**	**FC 12 hours**	**FC 18 hours**	**FC 24 hours**	**FC 48 hours**
CDKN1C	0.29	-0.49	0.11	-1.17	0.2
RFC3	0.2	-0.52	0.3	-1.34	-1.33
CCNG2	-0.17	0.16	-0.49	0.02	-1.25
CDC25C	0.14	0.2	-0.13	0.34	-1.2
CP110	-0.08	0.12	-0.31	-0.48	-1.26
CDC27	-0.03	0.04	-0.31	-0.16	-1.28
SFI1	0.15	0.31	0.09	-0.02	-1.01
CCNF	0.4	-0.4	-0.17	-0.15	-1.66
ESPL1	0.15	-0.25	-0.18	-0.16	-1.02
DLGAP5	0.15	-0.28	-0.3	-0.31	-1.29
SPC24	0.23	-0.17	-0.27	-0.26	-1.25
CCNE1	0.03	-0.09	0.18	-0.7	-1.08
MAP3K11	0.01	-0.39	-0.1	-0.68	-1.08
NCAPD2	0.13	-0.47	-0.14	-0.76	-1.47
CCNB1	0.09	-0.6	-0.3	-1.25	-2.39
CDKN3	0.01	-0.58	-0.37	-1.18	-2.35
HMG20B	0.02	-0.55	-0.23	-0.97	-2.06
CDK5	0.01	-0.41	-0.27	-0.84	-1.45
SPAG5	0.17	-0.21	-0.09	-0.63	-1.08
CDKN2C	0.48	-0.61	-0.27	-2.04	-2.78
ANAPC4	0.19	-0.14	-0.24	-0.91	-1.41
SMC1A	0.08	-0.27	-0.24	-0.79	-1.17
NDE1	-0.19	-0.26	-0.14	-0.6	-1.41
SKP2	0.51	0.04	0.05	-0.28	-1.21
KIF14	0.03	-0.41	-0.38	-0.72	-1.99
ASPM	0.29	-0.03	0.03	-0.72	-1.91
TFDP2	0.2	0.06	-0.1	-0.45	-1.12
RFC5	0.24	0.09	-0.07	-0.35	-1
CDK5R1	0.19	0.03	0.84	0.27	1.29
MOBKL2B	-0.23	0.37	0	0.63	1.49
CCNH	0.18	0.41	0.55	0.93	1.1
DOCK11	-0.56	-0.52	-0.3	0.42	1.29
NUBP1	-0.16	-0.13	0.04	0.49	1.01
CIP29	0.11	0.16	0.39	0.58	1.58
MIS12	0.08	0.33	0.38	0.65	1.27
PCM1	-0.02	0.31	0.25	0.49	1.17
CDK6	0.35	1.03	0.53	1.52	0.65
ANAPC10	0.22	0.76	0.32	0.66	1.03
INHBE	-0.83	2.84	1.28	4.52	4.17
STC2	0.63	3.11	2.23	4.2	4.36
TUBE1	0.43	2.18	0.89	2.31	1.81

Cholesterol metabolism					
Host Gene	**FC 6 hours**	**FC 12 hours**	**FC 18 hours**	**FC 24 hours**	**FC 48 hours**
GGPS1	-0.24	0.06	-0.01	0.37	1.31
PGGT1B	0	0.59	0.16	1.18	1.16
IDI1	-0.26	-0.64	-0.27	-1.05	-0.78
INSIG1	-0.42	-1.25	0.5	-2.17	-1.45
HMGCS2	0.63	0.04	-0.35	-1.41	-2.01
FDPS	-0.02	-0.4	-0.75	-1.33	-1.82
MVD	-0.2	-0.41	-0.63	-1.12	-1.79
DHCR7	-0.05	-0.3	-0.4	-1.22	-1.95
TM7SF2	-0.13	-0.33	-0.5	-0.82	-1.77
SQLE	-0.41	-0.69	0.01	-1.72	-1.02
HMGCR	-0.23	-0.36	0.1	-1.14	-0.73
HMGCS1	-0.23	-0.43	-0.05	-1.16	-0.91
SC4MOL	-0.22	-0.51	-0.22	-1.85	-1.49
NSDHL	-0.13	-0.5	-0.22	-1.07	-1.18
EBP	-0.04	-0.61	-0.06	-0.85	-0.83
CYP51A1	0.02	-0.18	-0.23	-1.37	-1.45
FDFT1	-0.19	-0.6	-0.72	-1.89	-2.01
MTTP	-0.31	-0.33	-0.34	-0.44	-0.87
APOB	-0.44	-0.64	-0.72	-1.2	-1.53

Sphingolipid and phospholipid metabolism					
Host Gene	**FC 6 hours**	**FC 12 hours**	**FC 18 hours**	**FC 24 hours**	**FC 48 hours**
SPTLC3	1.1	0.66	0.16	-1.03	-1.61
SPTLC2	-0.14	-0.05	-0.65	-0.63	-1.05
SGPP1	0.25	0.66	0.12	1.25	0.59
GULP1	0.28	1.01	0.05	0.88	0.93
LASS1	0.38	0.22	0.46	0.35	1.04
CHKA	0.32	-0.11	0.61	0.15	1
SPTLC1	0.16	0.21	0.65	1.24	1.7
KDSR	-0.16	0.03	0.4	0.72	1.19
SGMS2	-0.35	0.16	-0.3	0.42	1.76
SGPL1	-0.25	0.01	0.01	0.45	1.06
PPAP2B	0.23	0.77	0.47	0.98	1.41

Fatty acid metabolism					
Host Gene	**FC 6 hours**	**FC 12 hours**	**FC 18 hours**	**FC 24 hours**	**FC 48 hours**
FABP1	0.24	0.18	0.96	-0.56	-1.69
FADS2	0.07	-0.76	0.02	-0.93	-1.43
CES2	0.22	-0.41	-0.03	-1.09	-1.19
ABCD3	0.01	0.03	-0.37	0.12	-1.22
CPT2	0.18	0.25	-0.25	-0.26	-0.82
PPARα	0.14	-0.25	0.02	-0.63	-0.83
ACADSB	0.37	0.28	0.26	-0.63	-1.16
ACAT2	-0.14	-0.32	-0.55	-1.05	-1.3
CROT	0.31	-0.05	-0.07	-0.73	-1.01
FABP5	-0.1	-0.14	-0.25	-0.45	-1.21
ACLY	0.01	-0.27	-0.57	-1.02	-1.84
ACADVL	0.02	-0.21	-0.16	-0.18	-0.67
AHR	0.55	1.57	0.52	0.84	0.75
GPAM	0.93	1.7	1.43	1.48	0.71
ACSL5	0.32	0.56	1.17	1.1	0.87
SREBF1	0.09	0.46	0.42	1.09	0.41
ADFP	0.06	0.61	0.49	1.03	0.61
ACSL3	0.48	1.06	0.98	1.13	1.05
TXNIP	0.46	3.22	2.59	4.36	4.46
ACSL1	-0.61	-0.61	-0.38	0.87	1.4
ACOX3	-1.49	-1.63	-1.91	-0.7	0.09
ELOVL7	0.48	0.55	0.52	0.9	1.38
PGC1A	0.3	0.16	0.03	1.12	2.8
VLDLR	-0.86	0.27	-0.41	1.21	1.7
CPT1A	-0.28	-0.24	0.31	0.37	0.82
FABP3	0.17	-0.08	0.52	0.17	2.72
ELOVL4	0.25	0.13	0.14	0.42	1.28
BAAT	-0.11	-0.08	-0.16	0.13	1.61

Lipid metabolism (not included in heat-map diagrams)					
Host Gene	**FC 6 hours**	**FC 12 hours**	**FC 18 hours**	**FC 24 hours**	**FC 48 hours**
PPARγ	0.2	0.2	0.18	0.2	-0.21
RIP140	0.15	0.68	0.19	0.27	0.29
CIDEA	-0.02	-0.01	0.16	0.04	0.09
CIDEB	0.32	0.16	0.32	0.28	0.13
CIDEC	0.03	-0.06	0.18	-0.08	0.04

Protein synthesis and post-translational modification					
Host Gene	**FC 6 hours**	**FC 12 hours**	**FC 18 hours**	**FC 24 hours**	**FC 48 hours**
UBE3C	-0.02	-0.12	-0.42	-0.17	-1.15
UBE3B	0.12	-0.06	-0.57	0.08	-1.07
HUWE1	-0.07	-0.03	-0.23	0.38	-1
PSMA1	0	-0.41	-0.38	-0.9	-1.13
EIF4A1	0.47	-0.07	0.24	-0.58	-1.01
EIF2AK1	-0.07	-0.37	-0.48	-0.87	-0.99
PSMC1	0.06	-0.23	-0.41	-0.76	-1.05
PSMD3	0.02	-0.33	-0.47	-1.45	-1.3
PSMD1	0.07	0.04	-0.24	-0.49	-0.89
UBE2F	0.07	-0.03	-0.03	-0.39	-0.89
EIF4A2	0.19	0.09	0.19	-0.07	-1.1
CTSC	0.2	0.01	0.09	-0.14	-1.03
SULT1E1	0.27	0.42	1.54	0.96	0.05
OTUD7B	0	0.62	0.06	0.93	1.05
AARSD1	-0.43	-1.29	-1.51	-1.32	0.54
CTSH	-0.72	-0.73	-1.1	-0.78	-0.38
PSAT1	0.37	1.32	1.37	1.42	1.21
CTH	0.53	2.81	2.12	2.89	2.27
PSPH	0.49	1.03	0.78	1.08	0.77
AARS	0.23	0.79	0.77	1.15	0.65
SHMT2	0.16	1.02	1.18	1.46	0.43
BCAT1	0.23	1.08	2.06	1.79	1.56
MARS	0.14	0.67	0.86	1.46	1.07
WARS	0.06	0.31	0.78	1.01	0.87
CBS	0.35	0.68	1.36	1.87	1.79
PHGDH	0.21	0.47	1.14	1.37	1.42
EIF4EBP1	0.1	0.73	1.19	1.7	1.58
USP25	0.24	1.29	-0.03	1.06	0.83
USP37	0.21	1.06	0.61	0.91	1.19
CARS	0.02	0.92	0.67	1.34	1.11
RBM39	0.14	0.83	0.36	1.05	1.01
EPRS	0.07	0.67	0.52	1.03	0
GTPBP10	0.24	0.97	0.74	1.47	1.54
EIF1	-0.03	0.71	0.36	1.04	1.06
TXNL4B	0.31	1.09	0.64	1.56	1.69
ZCCHC8	-0.01	1.05	0.22	1.04	0.89

Protein synthesis and post-translational modification					
Host Gene	**FC 6 hours**	**FC 12 hours**	**FC 18 hours**	**FC 24 hours**	**FC 48 hours**
SENP6	0.12	1.12	0.6	1.2	1.06
SARS	0.07	0.56	0.58	1.52	1.55
LARS	0.17	0.51	0.43	1.01	0.89
TWISTNB	0.49	0.62	0.56	0.99	1.07
HNRPLL	-0.02	0.34	-0.06	0.82	1.01
GARS	0	1.02	0.99	1.6	1.39
CLK1	0.04	0.32	0.14	1.43	1.21
TARS	0.11	0.8	0.43	1.26	0.71
OGT	0.21	0.55	0.29	1.19	0.61
POLR1B	0.51	0.68	0.61	0.62	1.05
POLR3A	0.22	0.26	0.3	0.32	1.12
SLU7	-0.02	0.64	-0.05	0.87	1.32
SYNCRIP	0.06	0.65	0.23	0.69	1.08
WARS2	-0.36	0.27	-0.24	0.38	1.31
PAIP1	-0.08	0.37	-0.06	0.49	1.05
CLK4	-0.02	0.29	0	1.08	1.44
LSM5	-0.12	0.38	0.61	0.68	1.1
USP31	-0.29	0.02	0.42	0.39	1.2
EIF6	0.04	0.06	0.31	0.79	1.18
MRPL15	0.12	0.37	0.53	0.95	1.34
POLR3D	0.19	0.39	0.47	0.77	1.01
QKI	-0.22	0.22	-0.02	0.37	1.1
EIF4E	0.01	0.28	0.16	0.61	1.22
RNMT	0.11	0.37	0.32	0.61	1.1
INTS7	-0.04	0.45	0.23	0.78	1.27
OTUD1	-1.28	-0.21	-0.4	0.25	1.32
WDSOF1	0.23	0.38	0.44	0.57	1.22
GAD1	-0.94	-0.41	0.06	0.72	2.3
USP15	0.02	0.13	0.55	0.95	2.23
PLRG1	0.3	0.4	0.36	0.6	1.05
MGAM	0.15	0.27	0.25	1.01	2.23
EIF1AD	-0.15	-0.19	0.34	0.38	0.91
HNRNPH3	0.07	-0.03	0.39	0.49	0.74
RPL37	0.31	0.22	0.47	0.65	1.34
PCF11	0.2	0.18	0.47	0.53	1.05
SULT1C2	0.54	0.44	0.93	0.77	1.99
RPL13	0.43	-0.12	0.72	0.29	1.11
RPL28	0.18	-0.19	0.32	0.06	1.09
USP36	0.16	0.23	0.65	0.24	1.14
SULT2A1	0.69	0.66	1.39	0.8	1.36

Vesicle trafficking					
Host Gene	**FC 6 hours**	**FC 12 hours**	**FC 18 hours**	**FC 24 hours**	**FC 48 hours**
RAB40B	0.39	-0.07	-0.14	-1.05	-0.39
RAB8B	0.27	0.78	0.06	1.05	-0.15
SEC31A	0.51	1.4	0.67	0.93	1.06
SYNJ2BP	0.55	0.01	0.14	-0.09	1.07
TRAPPC2L	0.61	0.1	0.46	0.36	1.13
RAB27B	1.35	1.32	1.78	1.28	2.38
GOSR2	0.23	0.32	0.24	0.17	1.1
SEC11C	0.11	-0.01	0.61	0.55	0.89
USE1	-0.06	0.13	0.7	0.78	1.38
CPLX1	-0.02	0.06	0.99	0.78	1.81
RAB37	0.62	0.33	0.7	1.05	1.32
SYNPO	-0.77	-0.82	-0.51	0	1.31
RAB3IL1	0.25	0.02	0.3	0.6	1.25
STX3	0.2	0.19	0.4	0.67	1.21
ICA1	-0.3	-0.41	0.12	0.55	1.28
RAB7L1	0.65	0.33	0.71	0.72	1.77
VAT1	0.18	-0.18	0.18	0.32	1.2
SNX12	-0.02	-0.17	0.07	0.19	1.09
SYT1	0.45	0.58	0.1	0.82	1.04
RAB33B	-0.33	0.58	0.01	0.82	1.18
SYNCRIP	0.06	0.65	0.23	0.69	1.08
STX11	-0.83	-0.01	-0.38	0.31	1.03
STON2	0.24	0.76	0.53	0.86	1.21
RAB27A	0.34	0.59	0.47	0.88	1.62
RAB6B	-0.42	-0.07	-0.12	0.23	1.18
SCAMP1	0.06	0.38	0.21	0.54	1.02
RABIF	-0.01	0.25	-0.06	0.82	1.51
RAB21	0.09	0.35	0.08	0.8	1.11
SNX16	0.16	0.59	0.16	1.01	1.59
ARFGEF1	-0.18	0.09	0.05	0.67	1.14
PICALM	-0.22	0.14	0.12	0.6	1.04
GOLSYN	0.01	0.53	0.28	1.1	1.7
ARFGEF2	0.21	0.47	0.45	0.78	0.91

Microtubule binding proteins					
Host Gene	**FC 6 hours**	**FC 12 hours**	**FC 18 hours**	**FC 24 hours**	**FC 48 hours**
KIF5C	0.03	0.12	-0.18	0.42	1.09
TUBA1A	-0.48	-0.82	-1.34	-1.05	0.83
MICAL2	-0.78	-0.7	-1.33	-0.87	-1.22
MAP1A	0.24	-0.44	-0.68	-1.6	-1.19
KIF9	-0.17	-0.15	0	-0.75	-1.47
KIF18A	0.04	0.15	-0.13	-0.15	-1.21
DYNC2LI1	0.12	0.2	-0.24	-0.37	-1.34
KIF20A	0.32	-0.4	-0.03	-0.68	-1.39
KIF14	0.03	-0.41	-0.38	-0.72	-1.99
TBCD	0.19	-0.01	-0.28	-0.51	-1.01
MICALL2	-0.33	-0.51	-0.73	-1.48	-1.89
TUBA4A	0.07	-0.05	-0.1	-0.58	-1.08
EML1	-0.19	-0.26	-0.27	-0.76	-1.36

Actin binding proteins					
Host Gene	**FC 6 hours**	**FC 12 hours**	**FC 18 hours**	**FC 24 hours**	**FC 48 hours**
ITGA2	-0.89	-0.46	-0.7	-1.02	-1.07
EVL	-0.07	-0.45	-0.27	-1.04	-0.97
FSCN1	-0.52	-0.73	-0.99	-2.06	-2.29
GAS2L1	-0.04	-0.3	-0.31	-0.93	-1.07
LCP1	0.36	-0.27	-0.08	-0.95	-1.65
LIMCH1	-0.04	-0.35	-0.48	-0.82	-1.74
MAPKAP1	-0.05	-0.5	-0.56	-0.45	-1.1
ABLIM3	0.51	0.66	1.07	0.7	-0.45
DPYSL3	-1.3	-1.86	-2.58	-1.64	-1
MYL9	-0.29	-0.89	-1.4	-1.52	-0.26
TAGLN	-0.45	-1.13	-1.77	-1.59	0.28
AFAP1L1	0.22	0.62	0.89	0.74	1.61
SPTBN1	-0.09	0.51	0.05	1.22	1.46
SSFA2	0.04	0.39	0.42	1.15	1.62
DIAPH3	-0.22	-0.22	-0.36	0.5	1.19
TMOD1	-0.14	-0.1	-0.07	0.4	1

A.9 Functional role of host genes regulated by JFH-1 infection

Host pathway	Host function	Host genes
Immunity and defence	Type I and II interferon response	IRF1, IRF9, ISG20, OAS3, MX1, IFIT1, IFIT5, TRAF5, SOCS4, SOCS3, SOCS2
	Complement cascade	MASP1, CD55, C2, MBL2
	Inflammatory chemokines and cytokines	IL8, IL6ST, IL6R, CXCL6, CXCL3, CXCL2, CXCL5, CXCL16, CXCL1, IL1RAP, IL31RA, CEBPB, CEBPD, CEBPG, GBP1

Host pathway	Host function	Host genes
Oxidative stress and detoxification	NRF2 signalling	EPHX1, CAT, NQO1, MAFF,MAFK, GPX2, GPX3, AOX1, DNAJC8
	Metallothionein family	MT1E, MT1F, MT1M, MT1X, MT1H, MT1P2
	Glutathione-s-transferase family	GSTM1, MGST3, GSTM3, GSTM4, GSTM2
	Antioxidant response	GLRX, PON2, GPX8, ATOX1, SOD2, FMO1, TXNIP, TXNRD2, TXNL1
	Xenobiotic metabolism	AHR, CYP1A1, CYP1B1, ESD, NNMT, UGT2B4

Host pathway	Host function	Host genes
Cellular survival	Pro-apoptotic factors	TXNIP, DDIT3, DDIT4, TRIB3, WWOX, TRIM69, BEX1, BEX2, RYBP, PTPRH, BCL2L12, BCL2L11, DFFB, TNFRSF11B, IFT57, NDRG1, NDRG2, PPP1R15A, BNIP1
	Pro-apoptotic transcription factors	FOXO3, ATF4, DPF2
	P53 and TGFβ signalling	GADD45A, GADD45B, PMAIP1, SIRT1, NEDD9, TP53BP2, MYC, KLF10, LTBP1, JUN, JUNB, SKIL, PPP1R13L
	Anti-apoptotic factors	BIRC3, BIRC5, PRNP, BNIP1
	Cell-cycle arrest	RASSF1, INHBE, CDKN3, CDKN2C, CDKN1C
	Cell-cycle progression and cytokinesis	CCNE1, CCNB1, CCNG2, CCNH, CCNF, CDC25C, CDC27, SKP2, TFDP2, CDK6, STC2, ASPM, CP110, DLGAP5, ESPL1, ANAPC4, ANAPC10 /// ANAPC10P, HMG20B, KIF14, NCAPD2, NDE1, SPC24, SPAG5, SMC1A, SFI1, MIS12, MOBKL2B, PCM1, DOCK11, TUBE1
	S-phase DNA synthesis	RFC3, RFC5

Host pathway	Host function	Host genes
Lipid metabolism	Cholesterol metabolism	SQLE, HMGCR, HMGCS2, HMGCS1, MVD, FDPS, DHCR7, EBP, SC4MOL, CYP51A1, IDI1, INSIG1, NSDHL, TM7SF2, GGPS1, PGGT1B, FDFT1
	Sphingolipid metabolism	LASS1, SGMS2, SGPL1, SGPP1, SPTLC3, SPTLC1, SPTLC2, GULP1, KDSR, PPAP2B
	Fatty acid degradation and oxidation	CPT1A, ACOX3, ACADSB, ACADVL, CROT, CES2, CPT2, ABCD3, PPARα, TXNIP, ACSL3, ACSL1, ACSL5
	Fatty acid production, elongation and activation for triglyceride and phospholipid synthesis	ACAT2, ACLY, FADS2, ELOVL4, ELOVL7, GPAM, ACSL3, ACSL1, ACSL5, CHKA
	Lipid droplet production	PGC1A, RIP140, CIDEB, CIDEC
	Lipid metabolism gene transcription	SREBF1, PGC1A, PPARγ
	Lipid transport	FABP5, FABP1, FABP3, VLDLR, MTTP, APOB

Host pathway	Host function	Host genes
Intracellular transport	Endosomal trafficking	PICALM, STON2, SNX12, SNX16
	ER and Golgi trafficking	RAB6B, RAB7L1, RAB21, RAB33B, RAB40B, ARFGEF1, ARFGEF2, SEC31A, STX11, GOSR2, TRAPPC2L, USE1
	Secretory vesicle trafficking/ exocytosis	RAB27A, RAB27B, RAB37, CPLX1, STX3, ICA1, VAT1, GOLSYN, SYT1
	Microtubule formation and binding proteins	KIF20A, KIF18A, KIF9, KIF5C, KIF14, DYNC2LI1, MAP1A, MICAL2, MICALL2, TUBA1A, TUBA4A, TBCD, EML1
	Actin binding proteins	MYL9, TAGLN, EVL, FSCN1, GAS2L1, ITGA2, LCP1, LIMCH1, ABLIM3, AFAP1L1, DIAPH3, SPTBN1, SSFA2, TMOD1

Host pathway	Host function	Host genes
Protein synthesis and post-translational modification	Amino acid metabolism	CTH, PSAT1, PSPH, BCAT1, CBS
	tRNA synthesis	AARSD1, AARS, CARS, GARS, TARS, SARS, LARS, WARS2, WARS, MARS, EPRS
	Ribosome production	RPL37, RPL13, RPL28, MRPL15, POLR1B, WDSOF1, GTPBP10
	mRNA splicing and processing	HNRPLL, INTS7, PLRG1, QKI, RBM39, RNMT, SLU7, SYNCRIP, TXNL4B, ZCCHC8, PCF11, LSM5, CLK1, CLK4, HNRNPH3
	Protein translation	EIF1AD, EIF4A2, EIF4E, EIF6, EIF1, EIF4A1, EIF2AK1, EIF4EBP1, PAIP1
	Protein glycosylation	MGAM, OGT
	Protein sulphation	SULT1E1, SULT1C2, SULT2A1
	Proteasome function	PSMA1, PSMC1, PSMD1, PSMD3
	Lysosomal enzymes	CTSC, CTSH
	Ubiquitin removal	USP36, USP25, USP37, USP15, USP31, OTUD1, OTUD7B
	Ubiquitin addition	UBE3C, UBE3B, UBE2F, HUWE1

A.10 Microarray confidence interval values at 48 hours post-infection

Sphingolipid metabolism				
Gene	**Affymetrix ID**	**Fold Change**	**95% CI Lower**	**95% CI Upper**
SGMS2	227038_at	3.39	2.81	4.08
SGMS2	242963_at	1.23	1.04	1.46
SGMS2	243141_at	1.35	1.18	1.54
SGPP1	221268_s_at	1.51	1.27	1.79
SGPP1	223391_at	1.41	1.20	1.66
SGPL1	212321_at	2.08	1.88	2.31
SGPL1	212322_at	1.73	1.55	1.95
SPTLC1	1554053_at	3.25	2.66	3.94
SPTLC1	202277_at	1.23	1.13	1.36
SPTLC1	202278_s_at	1.12	0.99	1.27

Cholesterol synthesis				
Gene	**Affymetrix ID**	**Fold Change**	**95% CI Lower**	**95% CI Upper**
FDFT1	208647_at	0.25	0.23	0.27
FDFT1	210950_s_at	0.22	0.20	0.23
FDFT1	241954_at	0.41	0.35	0.49
SQLE	209218_at	0.46	0.41	0.50
SQLE	213562_s_at	0.37	0.32	0.44
SQLE	213577_at	0.49	0.39	0.62
SQLE	1557352_at	0.44	0.33	0.57
EBP	213787_s_at	0.54	0.50	0.57
EBP	202735_at	0.45	0.41	0.51
MVD	203027_s_at	0.29	0.25	0.33
HMGCR	202539_s_at	0.48	0.44	0.53
HMGCR	202540_s_at	0.60	0.55	0.66

Fatty acid metabolism				
Gene	**Affymetrix ID**	**Fold Change**	**95% CI Lower**	**95% CI Upper**
SREBF1	1558875_at	1.38	1.22	1.56
SREBF1	202308_at	1.33	1.16	1.52
PPARγ	208510_s_at	0.86	0.79	0.94
PPARα	206870_at	0.68	0.61	0.76
PPARα	223437_at	0.55	0.49	0.64
PPARα	223438_s_at	0.70	0.57	0.85
PPARα	226978_at	0.69	0.57	0.84
PPARα	244689_at	0.82	0.67	1.00
PPARα	1558631_at	0.77	0.65	0.92
PPARα	1560981_a_at	0.74	0.60	0.90
ACSL3	201660_at	1.96	1.75	2.19
ACSL3	201661_s_at	2.07	1.85	2.33
ACSL3	201662_s_at	1.45	1.31	1.61
ELOVL4	219532_at	2.43	1.95	3.05
ELVOL7	227180_at	2.60	2.39	2.81
TXNIP	201008_s_at	15.35	12.38	19.03
TXNIP	201009_s_at	14.32	12.91	15.89
TXNIP	201010_s_at	22.01	19.97	24.25

Lipid droplet production				
Gene	**Affymetrix ID**	**Fold Change**	**95% CI Lower**	**95% CI Upper**
PGC1A	219195_at	6.96	5.78	8.34
RIP140	202599_s_at	1.22	1.11	1.34
RIP140	202600_s_at	1.17	1.01	1.37
CIDEB	221188_s_at	1.09	0.97	1.23
CIDEC	219398_at	0.80	0.72	0.88

Cellular detoxification				
Gene	**Affymetrix ID**	**Fold Change**	**95% CI Lower**	**95% CI Upper**
AHR	202820_at	1.68	1.49	1.91
CYP1A1	205749_at	2.58	2.39	2.77
CYP1B1	202434_s_at	1.14	0.88	1.48
CYP1B1	202435_s_at	3.58	2.87	4.47
CYP1B1	202436_s_at	3.84	3.05	4.82
CYP1B1	202437_s_at	3.78	2.87	4.99

Intracellular transport				
Gene	**Affymetrix ID**	**Fold Change**	**95% CI Lower**	**95% CI Upper**
RAB6B	210127_at	1.66	1.33	2.08
RAB6B	221792_at	1.59	1.34	1.91
RAB6B	225259_at	2.27	1.96	2.60
RAB21	226268_at	2.16	1.87	2.50
RAB21	203885_at	2.04	1.91	2.19
RAB27A	209514_s_at	2.23	2.00	2.50
RAB27A	209515_s_at	3.07	2.71	3.46
RAB27A	210951_x_at	2.30	2.10	2.53
RAB27B	228708_at	5.21	4.41	6.11
RAB27B	207017_at	1.25	1.05	1.47
RAB27B	207018_s_at	1.45	1.25	1.71
RAB33B	221014_s_at	2.27	1.92	2.68
RAB37	228113_at	2.50	2.16	2.89
RAB40B	204547_at	0.76	0.60	0.97
ABLIM3	205730_s_at	0.73	0.62	0.86

TXNIP transcription factors				
Gene	**Affymetrix ID**	**Fold Change**	**95% CI Lower**	**95% CI Upper**
FOXO1	202723_s_at	2.69	2.39	3.03
FOXO1	202724_s_at	3.01	2.62	3.48
MLX	213708_s_at	0.95	0.88	1.01
MLX	217909_s_at	0.87	0.80	0.95
MLX	217910_x_at	1.00	0.93	1.08
MLXIP	225157_at	0.80	0.71	0.90
MLXIP	202519_at	0.80	0.70	0.91
MLXIP	211789_s_at	0.81	0.65	1.01
MLXIPL	221163_s_at	1.13	0.95	1.37
HIF1α	200989_at	1.34	1.22	1.46
KLF6	208960_s_at	2.23	1.99	2.50
KLF6	208961_s_at	2.43	2.23	2.62
KLF6	224606_at	2.38	2.22	2.55
KLF6	1555832_s_at	2.33	2.03	2.69

Alpha arrestin family				
Gene	**Affymetrix ID**	**Fold Change**	**95% CI Lower**	**95% CI Upper**
ARRDC1	226405_s_at	0.74226179	0.664343	0.835088
ARRDC3	224797_at	2.04202425	1.670176	2.496661
ARRDC4	225283_at	10.7778686	9.317869	12.46663

Glucose metabolism				
Gene	**Affymetrix ID**	**Fold Change**	**95% CI Lower**	**95% CI Upper**
G6PC3	221759_at	0.57834409	0.524858	0.63728
G6PC3	44654_at	0.55478474	0.517632	0.598739
PCK2	202847_at	5.20536742	4.823231	5.656854
HK2	222305_at	1.12505848	0.926588	1.36604
HK2	202934_at	3.05251842	2.770219	3.386981
HKDC1	220585_at	0.28717459	0.243164	0.339151
HKDC1	227614_at	0.30992692	0.266093	0.358489
HKDC1	237323_at	0.48971015	0.406126	0.590496
PFKL	201102_s_at	0.65067093	0.590496	0.716978
PFKL	211065_x_at	0.66896378	0.615572	0.732043
PFKFB2	226733_at	1.77768536	1.515717	2.084932
PFKFB3	202464_s_at	0.26061644	0.22688	0.29937
PFKFB4	228499_at	0.62850669	0.550953	0.712025
LDHB	213564_x_at	0.66434291	0.598739	0.737135
LDHB	201030_x_at	0.68302013	0.619854	0.752623
ALDOA	214687_x_at	0.64617642	0.598739	0.692555
ALDOA	238996_x_at	0.48971015	0.435275	0.554785
ALDOA	200966_x_at	0.6328783	0.586417	0.68302
ALDOC	202022_at	0.55864357	0.50698	0.615572
PGAM1	200886_s_at	0.69737183	0.655197	0.742262
ENO1	201231_s_at	1.24833055	1.189207	1.301342
ENO2	201313_at	1.59107297	1.148698	2.20381

PPARα signalling				
Gene	**Affymetrix ID**	**Fold Change**	**95% CI Lower**	**95% CI Upper**
ACADL	206068_s_at	0.93	0.75	1.16
TRIB3	218145_at	2.68	2.50	2.89
TRIB3	1555788_a_at	2.64	2.31	3.01
CPT1A	203633_at	2.08	1.77	2.46
CPT1A	203634_s_at	1.77	1.38	2.28
CPT1A	210688_s_at	1.47	1.15	1.89
CPT2	204263_s_at	0.62	0.54	0.72
CPT2	204264_at	0.57	0.50	0.64
SLC27A2	205768_s_at	0.71	0.61	0.82
SLC27A2	205769_at	0.77	0.64	0.94
ECH1	200789_at	0.87	0.81	0.93
ACOX1	207656_s_at	0.96	0.82	1.13
ACOX1	209600_s_at	0.72	0.65	0.81
ACOX1	213501_at	0.68	0.61	0.77
ACOX1	227962_at	0.81	0.67	0.99

A.11 Microarray confidence interval values for the time-course infection

PGC1α				
Affymetrix ID	**Hours post-infection**	**Fold Change**	**95% CI Lower**	**95% CI Upper**
219195_at	6	1.23	0.98	1.55
219195_at	12	1.12	0.93	1.35
219195_at	18	1.02	0.85	1.23
219195_at	24	2.17	1.80	2.62
219195_at	48	6.96	5.78	8.34

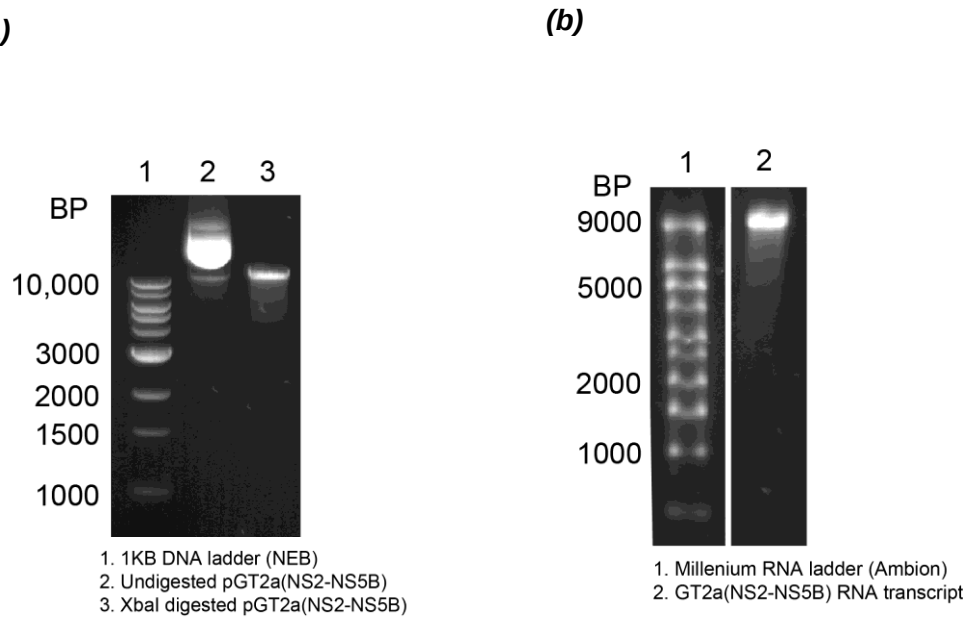
TXNIP				
Affymetrix ID	**Hours post-infection**	**Fold Change**	**95% CI Lower**	**95% CI Upper**
201008_s_at	6	1.30	1.00	1.68
201008_s_at	12	8.40	6.77	10.41
201008_s_at	18	5.28	4.26	6.50
201008_s_at	24	20.11	16.22	24.93
201008_s_at	48	15.35	12.38	19.03
201009_s_at	6	1.15	1.01	1.30
201009_s_at	12	6.54	5.94	7.26
201009_s_at	18	4.99	4.50	5.50
201009_s_at	24	13.55	12.21	15.03
201009_s_at	48	14.32	12.91	15.89
201010_s_at	6	1.38	1.22	1.55
201010_s_at	12	9.32	8.46	10.27
201010_s_at	18	6.02	5.46	6.63
201010_s_at	24	20.53	18.64	22.63
201010_s_at	48	22.01	19.97	24.25

CYP1A1				
Affymetrix ID	**Hours post-infection**	**Fold Change**	**95% CI Lower**	**95% CI Upper**
205749_at	6	2.17	2.00	2.38
205749_at	12	4.17	3.89	4.50
205749_at	18	2.28	2.13	2.45
205749_at	24	5.21	4.82	5.58
205749_at	48	2.58	2.39	2.77

RAB27A				
Affymetrix ID	**Hours post-infection**	**Fold Change**	**95% CI Lower**	**95% CI Upper**
209514_s_at	6	1.09	0.95	1.24
209514_s_at	12	1.20	1.07	1.34
209514_s_at	18	1.32	1.18	1.46
209514_s_at	24	1.87	1.67	2.08
209514_s_at	48	2.23	2.00	2.50
209515_s_at	6	1.27	1.09	1.47
209515_s_at	12	1.51	1.34	1.69
209515_s_at	18	1.39	1.22	1.56
209515_s_at	24	1.84	1.64	2.08
209515_s_at	48	3.07	2.71	3.46
210951_x_at	6	1.11	0.99	1.25
210951_x_at	12	1.24	1.13	1.36
210951_x_at	18	1.27	1.16	1.40
210951_x_at	24	1.82	1.65	1.99
210951_x_at	48	2.30	2.10	2.53

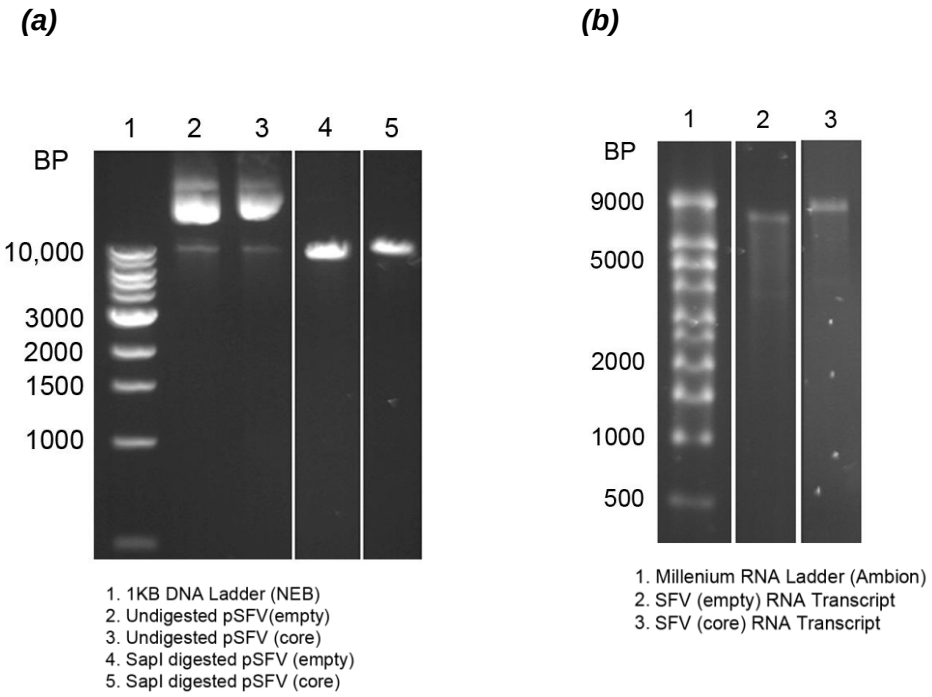
RAB37				
Affymetrix ID	**Hours post-infection**	**Fold Change**	**95% CI Lower**	**95% CI Upper**
228113_at	6	1.54	1.28	1.83
228113_at	12	1.26	1.09	1.45
228113_at	18	1.62	1.40	1.88
228113_at	24	2.07	1.79	2.39
228113_at	48	2.50	2.16	2.89

A.12 *In vitro* RNA transcription of the genotype 2a replicon RNA



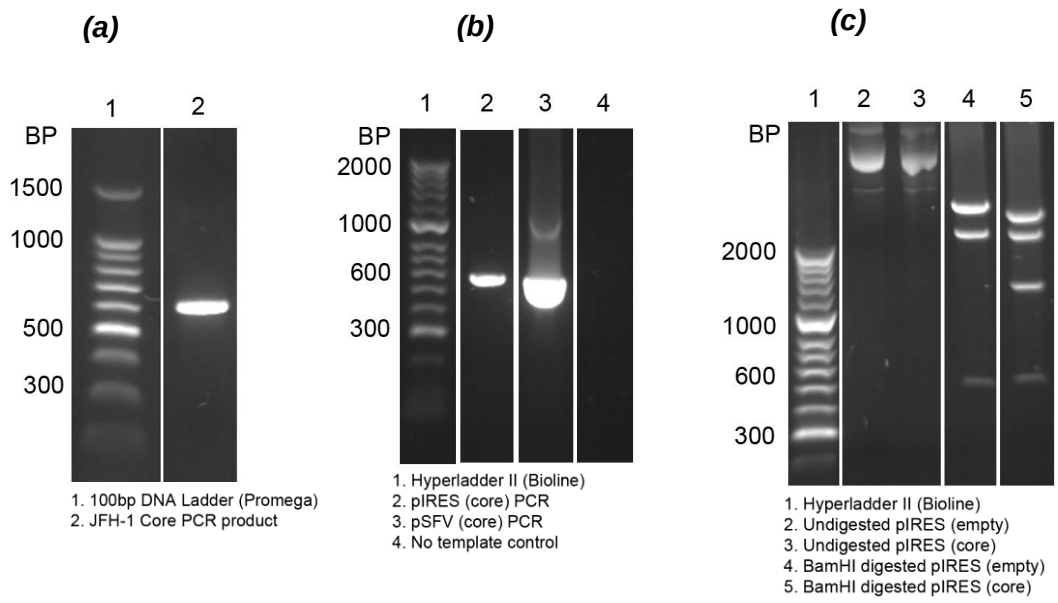
(a) *XbaI digestion of the pGT2a(NS2-NS5B) DNA plasmid encoding the genotype 2a subgenomic replicon. Digestion with XbaI was performed for 4 hours at 37˚C. 1µl of undigested plasmid DNA (lane 2) and digested plasmid DNA (lane 3) were run on a 0.8% agarose gel stained with SYBR safe. 1KB DNA ladder (New England Biosciences) was used for DNA size estimation (lane1).* ***(b)*** *In vitro RNA transcription of the subgenomic RNA molecule. 1µg of XbaI digested plasmid DNA was used for in vitro RNA transcription and 1µl of the RNA transcript was run on a 0.8% agarose non-denaturing gel stained with SYBR safe (lane 2). Millennium RNA ladder (Ambion) was used for RNA size estimation (lane 1). Diagrams representing DNA and RNA ladders used can be found in the Appendix A.5.*

A.13 *In vitro* RNA transcription of the SFV replicon (JFH-1 core) RNA



(a) *SapI digestion of the pSFV(core) and pSFV(empty) plasmid DNA. SapI digestion was performed for 2 hours at 37˚C. 1µl of undigested pSFV(empty) plasmid (lane2), undigested pSFV(core) plasmid (lane3), digested pSFV(empty) plasmid (lane4) and digested pSFV(core) (lane5) plasmid was run on a 0.8% agarose gel stained with SYBR safe. A 1KB DNA ladder (New England Biosciences) was used for DNA size estimation (lane1).* ***(b)*** *In vitro RNA transcription of SFV(core) and SFV(empty) RNA. 1µg of SapI digested plasmid DNA was used in an in vitro RNA transcription reaction to generate SFV(core) and SFV(empty) RNA. 1µl of the SFV(empty) RNA (lane2) and SFV(core) RNA (lane 3) was run on a 0.8% agarose non-denaturing gel stained with SYBR safe. Millennium RNA ladder (Ambion) was used for RNA size estimation (lane 1). Diagrams representing DNA and RNA ladders used can be found in the Appendix A.5.*

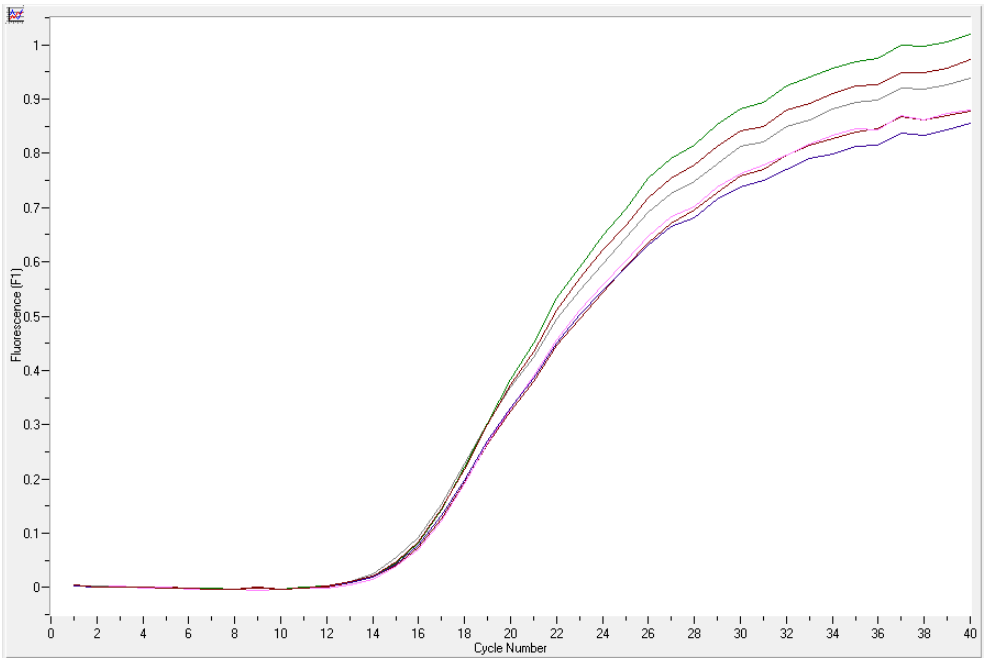
A.14 Cloning the JFH-1 core sequence into the pIRES vector



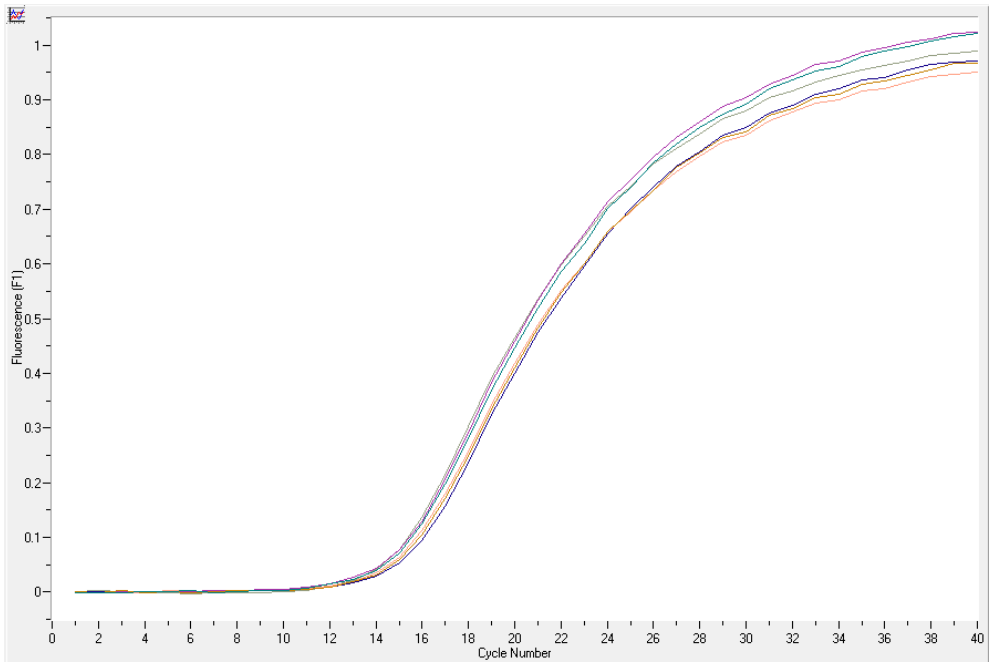
(a) *PCR amplification of the JFH-1 core sequence using pSFV(core) plasmid DNA and core PCR primers. The PCR product was run on a 1% agarose gel stained with SYBR safe (lane 2). A 100bp DNA ladder (Promega) was used for DNA size estimation (lane 1).* ***(b)*** *Diagnostic PCR analysis of the pIRES(core) plasmid DNA generated following ligation of the JFH-1 core PCR product with an empty pIRES/Blasicidin resistance vector. The PCR product produced following amplification of the pIRES(core) plasmid DNA with the JFH-1 core PCR primers was run on a 1% agarose gel stained with SYBR safe (lane 2). PCR amplification was also performed using the pSFV(core) plasmid DNA as a positive control (lane 3). A negative control PCR reaction was included with no DNA template (lane 4). DNA Hyperladder II was included for DNA size estimation (lane 1).* ***(c)*** *Diagnostic BamHI digestion performed using the pIRES(empty) and pIRES(core) plasmid DNA. The undigested pIRES(empty) plasmid (lane 2), undigested pIRES(core) plasmid (lane 3), digested pIRES(empty) plasmid (lane 4) and digested pIRES(core) plasmid (lane 5) were run on a 1% agarose gel stained with SYBR safe. DNA Hyperladder II was included for DNA size estimation (lane 1). Correct digestion of the pIRES(core) plasmid generated fragments of: 525bp, 1215bp, 2279bp and 3178bp. Correct digestion of the pIRES(empty) plasmid generated fragments of: 525bp, 2279 and 3813bp. A map of the pIRES(core) and pIRES(empty) plasmids can be found in the Appendix section A.6. Diagrams representing DNA ladders used can be found in the Appendix section A.5.*

A.15 qRT-PCR GAPDH curves for JFH-1 and mock infected samples

(a) Huh7 cells



(b) Huh7.5 cells



(c)

cDNA sample	CT value Huh7	CT value Huh7.5
JFH-1 infected 1	15.15	15.25
JFH-1 infected 2	14.93	14.61
JFH-1 infected 3	15.30	14.97
Mock infected 1	15.40	14.84
Mock infected 2	15.09	15.07
Mock infected 3	15.21	14.87

(a and b) *qRT-PCR amplification profile for the GAPDH gene in* ***(a)*** *Huh7 cells infected with JFH-1 or mock medium for 48 hours and* ***(b)*** *Huh7.5 cells infected with JFH-1 or mock medium for 48 hours. Each profile contains triplicate JFH-1 infected samples and triplicate mock infected samples.* ***(c)*** *CT (cycle threshold) values extracted from the qRT-PCR amplification profile for the GAPDH gene in JFH-1 infected and mock infected Huh7 and Huh7.5 cells.*

A.16 NS2 protein sequence homology of JFH-1 and J6 HCV clones

JFH-1 NS2 protein sequence

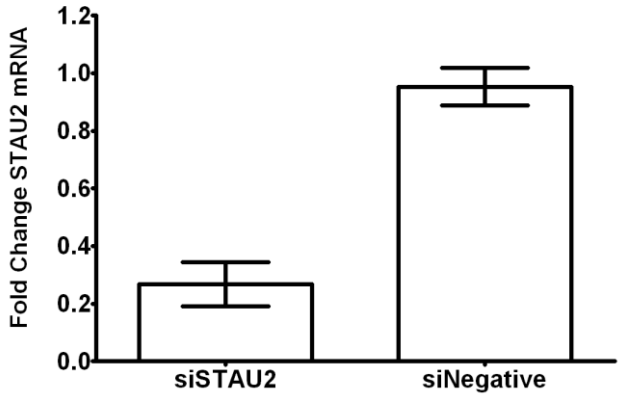
YDA*P*VHGQIG*VG*LL*I*LITLFTLTPGYKTLL*GQC*LWWLCYLLTL*G*EAM*I*QEW*V*PPMQVRGGRDGI*A*W AV*T*IFCPGVVFDITKWLLA*L*LGPAYLL*RA*ALT*H*VPYFVRAHAL*I*R*VC*A*LVKQ*LAGGRYVQ*VA*LLALG RWTGTYIYDHLTPMSDWAA*S*GLRDLAVAVEPIIFSPMEKKVIVWGAETAACGDILHGLPVSARLG*Q* E*I*LLGPADGYTSKGW*KL*L

J6 NS2 protein sequence

YDA*S*VHGQIG*AA*LL*V*LITLFTLTPGYKTLL*SRF*LWWLCYLLTL*A*EAM*V*QEW*A*PPMQVRGGRDGI*I*W AV*A*IFCPGVVFDITKWLLA*V*LGPAYLL*KG*ALT*R*VPYFVRAHAL*L*R*M*C*TMVRH*LAGGRYVQ*MV*LLAL GRWTGTYIYDHLTPMSDWAA*N*GLRDLAVAVEPIIFSPMEKKVIVWGAETAACGDILHGLPVSARLG *R*E*V*LLGPADGYTSKGW*S*LL

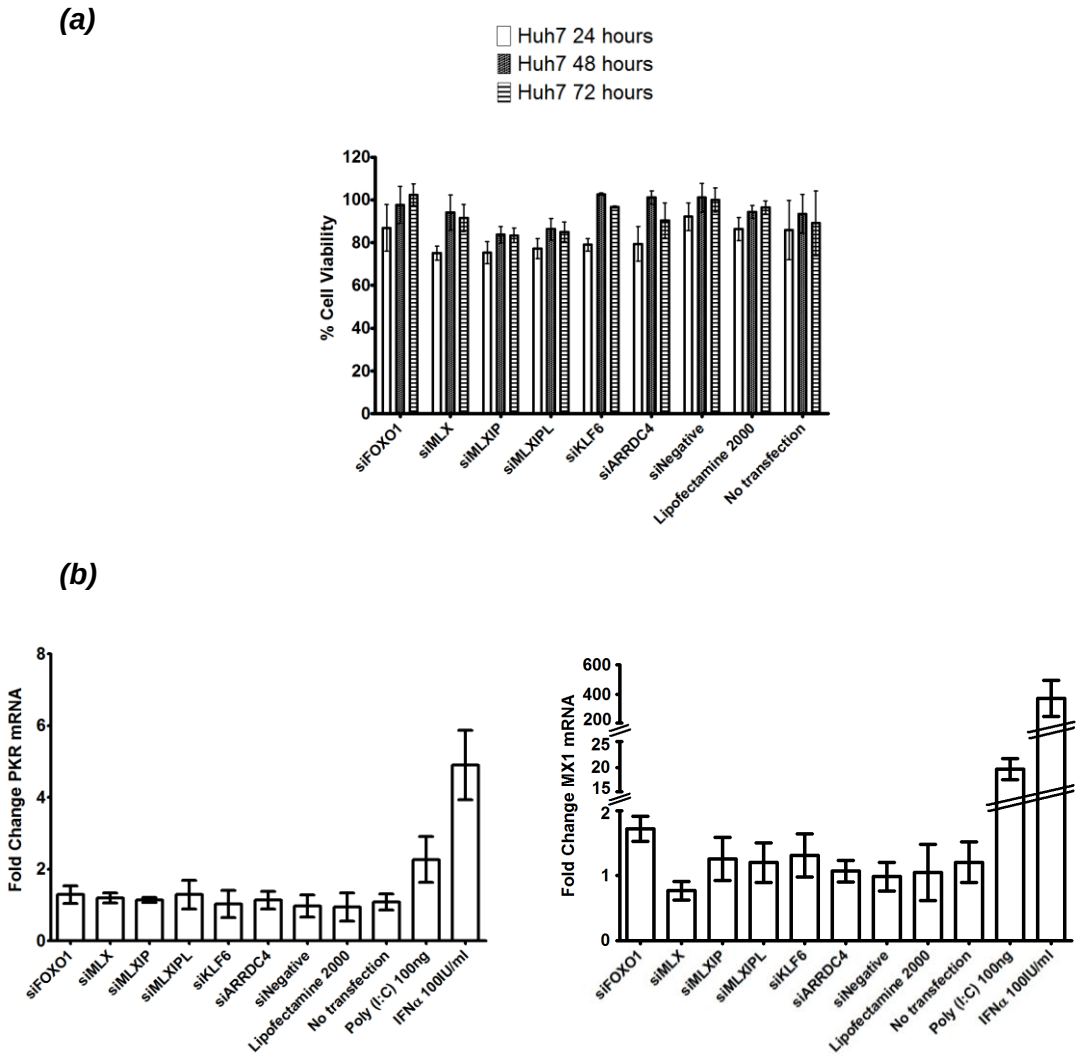
The amino acid differences in the NS2 protein sequence of JFH-1 and J6 are underlined and italicised. Number of identical amino acids = 187/217 (86% homology)

A.17 Knockdown of Staufen2 expression by siRNA silencing



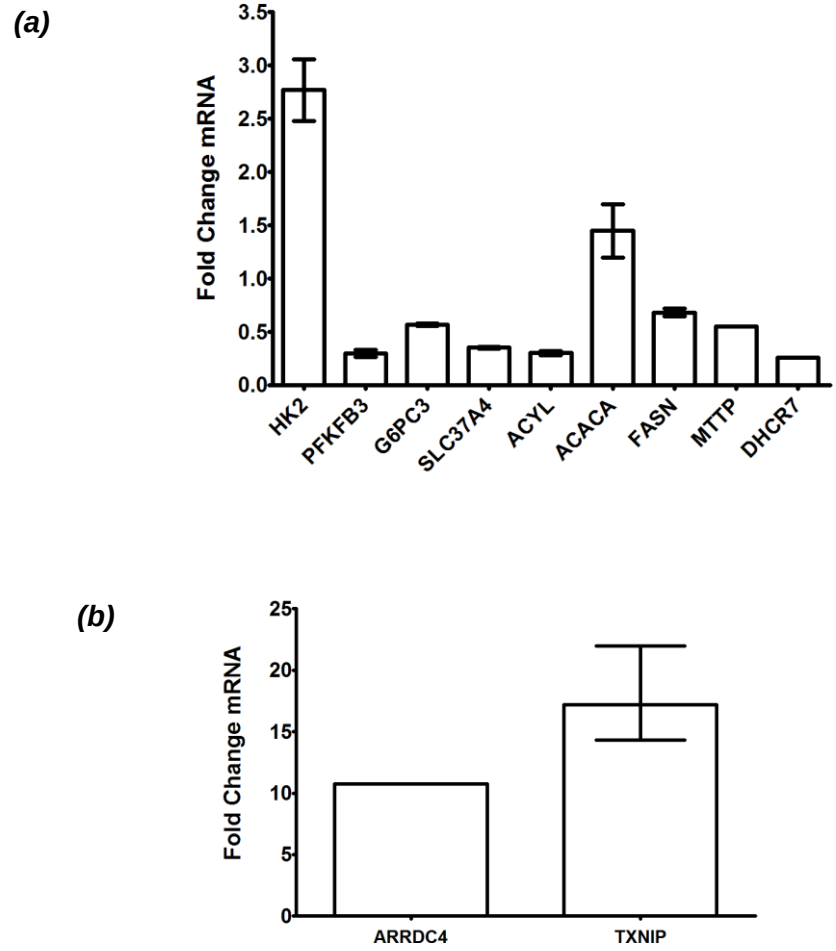
Fold change in Staufen2 mRNA abundance in Huh7 cells transfected with a Staufen2 targeting siRNA molecule. Huh7 cells were transfected with 50nM of a Staufen2 targeting siRNA and 50nM of a negative control non-targeting siRNA. At 48 hours post-transfection, intracellular RNA was extracted from the cells for qRT-PCR quantification of Staufen2 mRNA. Fold change data displayed represents the mean (±SD) of a single experiment with repeat siRNA transfections performed in triplicate (N=3). The knockdown of Staufen2 mRNA achieved with the Staufen2-specific siRNA was statistically significant with a p value ≤ 0.05, calculated using a two-tailed unpaired T test in Graphpad Prism.

A.18 siRNA transfection does not alter cell viability or ISG expression



(a) *Percentage viability of Huh7 cells transfected with target specific siRNA molecules. Huh7 cells were transfected with 50nM of individual target specific siRNAs, a negative control non-targeting siRNA, Lipofectamine 2000 reagent only or transfection medium only. Cell viability was measured at 24, 48 and 72 hours post-transfection using the alamar blue assay.* ***(b)*** *Fold change in ISG expression following transfection of Huh7 cells with target specific siRNA molecules. Huh7 cells were transfected with 50nM of target-specific siRNAs, 50nM of negative control non-targeting siRNA, Lipofectamine 2000 reagent only or transfection medium only. Cells were also treated with 100IU/ml IFNα and 100ng poly (I:C) as positive controls. At 48 hours post-transfection, intracellular RNA was extracted from the cells for qRT-PCR quantification of PKR and MX1 expression. Percentage viability and fold change expression data displayed represents the mean (±SD) of two independent experiments, each containing repeat siRNA transfections performed in triplicate (N=6).*

A.19 Expression of MLX target genes at 48 hours post-infection



(a/b) Fold change in Huh7 cell host gene expression at 48 hours post-JFH-1 infection, quantified using microarray analysis. The expression of genes involved in (a) glycolysis (HK2 and PFKFB3), gluconeogenesis (G6PC3 and SLC37A4), fatty acid synthesis (ACYL, ACACA and FASN), triglyceride formation (MTTP), cholesterol metabolism (DHCR7) and (b) glucose uptake (ARRDC4 and TXNIP) is shown. The microarray gene expression data shown represents the mean fold change value calculated for triplicate infections at 48 hours post-infection. Confidence interval values calculated for the triplicate infection sample repeats of the microarray experiment can be found in the Appendix A.10. For some of the host genes investigated multiple probe sets were available on the microarray genechip, thus error bars are displayed for some of the microarray datapoints to represent the range of mean fold change values observed for the different gene probe sets.